IAEA-SMR-68/I

NUCLEAR THEORY FOR APPLICATIONS – 1980

PROCEEDINGS OF THE INTERREGIONAL ADVANCED TRAINING COURSE ON APPLICATIONS
OF NUCLEAR THEORY TO NUCLEAR DATA CALCULATIONS FOR REACTOR DESIGN
HELD AT TRIESTE, 28 JANUARY – 22 FEBRUARY 1980
DURING THE WINTER COLLEGE ON NUCLEAR PHYSICS AND REACTORS
JOINTLY ORGANIZED BY THE
INTERNATIONAL ATOMIC ENERGY AGENCY
AND THE
INTERNATIONAL CENTRE FOR THEORETICAL PHYSICS
AND HELD AT THE
INTERNATIONAL CENTRE FOR THEORETICAL PHYSICS, TRIESTE
22 JANUARY – 28 MARCH 1980

INTERNATIONAL CENTRE FOR THEORETICAL PHYSICS, TRIESTE, 1981

NUCLEAR THEORY FOR APPLICATIONS – 1980

THE INTERNATIONAL CENTRE FOR THEORETICAL PHYSICS (ICTP) in Trieste was established by the International Atomic Energy Agency (IAEA) in 1964 under an agreement with the Italian Government, and with the assistance of the City and University of Trieste.

The IAEA and the United Nations Educational, Scientific and Cultural Organization (UNESCO) subsequently agreed to operate the Centre jointly from 1 January 1970.

Member States of both organizations participate in the work of the Centre, the main purpose of which is to foster, through training and research, the advancement of theoretical physics, with special regard to the needs of developing countries.

NUCLEAR THEORY FOR APPLICATIONS – 1980

PROCEEDINGS OF THE INTERREGIONAL ADVANCED TRAINING COURSE ON APPLICATIONS
OF NUCLEAR THEORY TO NUCLEAR DATA CALCULATIONS FOR REACTOR DESIGN
HELD AT TRIESTE, 28 JANUARY – 22 FEBRUARY 1980
DURING THE WINTER COLLEGE ON NUCLEAR PHYSICS AND REACTORS
JOINTLY ORGANIZED BY THE
INTERNATIONAL ATOMIC ENERGY AGENCY
AND THE
INTERNATIONAL CENTRE FOR THEORETICAL PHYSICS
AND HELD AT THE
INTERNATIONAL CENTRE FOR THEORETICAL PHYSICS, TRIESTE
22 JANUARY – 28 MARCH 1980

INTERNATIONAL CENTRE FOR THEORETICAL PHYSICS, TRIESTE, 1981

NUCLEAR THEORY FOR APPLICATIONS – 1980, IAEA, VIENNA, 1981

Printed by the IAEA in Austria
November 1981

FOREWORD

The International Centre for Theoretical Physics has maintained an interdisciplinary character in its research and training programmes in different branches of theoretical physics. In pursuance of this objective, the Centre has organized extended research courses and workshops, including topical conferences, with a comprehensive and synoptic coverage in varying disciplines. The first of these – on Plasma Physics – was held in 1964 and then repeated in 1977; the second, in 1965, was concerned with the Physics of Particles. Between then and now, the following courses were organized; five on Nuclear Theory (1966, 1969, 1971, 1973, 1978), six on the Physics of Condensed Matter (1967, 1970, 1972, 1974, 1976, 1978), three on Atomic Physics (1973, 1977, 1979), two on Geophysics (1975, 1977), one on Control Theory and Functional Analysis (1974), one on Complex Analysis (1975), one on Applications of Analysis to Mechanics (1976), one on Mathematical Economics (1978), one on Systems Analysis (1978), two on Teaching of Physics at tertiary level (in English in 1976, in French in 1977), and three on Solar Energy (1977, 1978, 1979). Most of the Proceedings of these courses have been published by the International Atomic Energy Agency (Vienna, Austria).

The present volume forms part of the Proceedings of the Winter College on Nuclear Physics and Reactors, conducted from 22 January to 28 March 1980. This volume contains the Proceedings of the Interregional Advanced Training Course on Applications of Nuclear Theory to Nuclear Data Calculations for Reactor Design, held at Trieste, 28 January to 22 February 1980. A separate volume contains the Proceedings of the Course on Operational Physics of Power Reactors, held from 3 to 28 March 1980. The Winter Courses were held in response to the growing need of developing countries which plan to establish a nuclear power programme to familiarize themselves with the nuclear and reactor physics foundations of nuclear energy and their applications in the design of nuclear reactors.

The programme of lectures and working sessions was organized by Drs. J.J. Schmidt and J.B. Dee (International Atomic Energy Agency, Vienna, Austria), Dr. M.K. Mehta (Bhabha Atomic Research Centre, Bombay, India), Professor U. Farinelli (Italian Council for Nuclear Energy (CNEN), Casaccia-Rome, Italy), and Professor L. Fonda (ICTP, University of Trieste).

Abdus Salam

PREFACE

This volume contains the text of the invited lectures presented during the Interregional Advanced Training Course on Applications of Nuclear Theory to Nuclear Data Calculations for Reactor Design which was held at the International Centre for Theoretical Physics (ICTP) in Trieste, Italy, from 28 January – 22 February 1980, within the framework of the nuclear physics activities of the ICTP during the winter of 1980. This Course was jointly organized by the IAEA Nuclear Data Section and ICTP. The Course was attended by 73 participants from 26 developing countries and 8 participants from five developed countries.

The purpose of this Course was, pursuant to a similar course held in 1978, to offer nuclear scientists from developing countries who are implementing a nuclear science and technology programme a review of advances in contemporary low-energy nuclear reaction theory and a training on an advanced level in the application of this theory to the interpretation and prediction of neutron nuclear data needed for nuclear reactor calculations and in the evaluation and processing of such data. The Course was also to provide a review of the experimental and theoretical methods used in the generation of 14 MeV neutron cross section data.

The Course comprized lectures, special seminars and workshop sessions on the following major topics:

1. Recent advances in the understanding of reaction mechanisms for fast neutron-nuclear interactions;
2. Recent advances in nuclear fission theory; both topics 1 and 2 included applications to the computation of neutron nuclear data;
3. Generation and computer processing of evaluated neutron nuclear data;
4. 14 MeV neutron cross sections in experiment and theory.

A special workshop held during the last week of the Course, 18–22 February 1980, developed the scientific and technical basis for a new IAEA Interregional Project (TA/INT/1/018) for the Training of Nuclear Scientists from Developing Countries using the Expertise available in the Nuclear Data Field; the findings of this workshop have been published separately by the IAEA as report INDC(NDS)-122/L.

The lectures given at this Course built upon those given at the Course on Nuclear Theory for Applications held at the ICTP in Trieste in 1978 and published as report IAEA-SMR-43. They are expected to be of interest to nuclear scientists both from developing countries where the interest in nuclear data and reactor physics research is steadily growing and from developed countries where such research is in an advanced stage. They can be used as reference in the field or as an advanced textbook for postgraduate study.

The organizers wish to express their deep appreciation to the lecturers and workshop leaders for their very active engagement and co-operation in the objectives of the Course. The excellent collaboration of the Training Section of the IAEA Division for Technical Assistance and of the staff of the ICTP as well as the generous financial support by the IAEA Division for Technical Assistance were indispensable for the successful organisation and conduct of this Course and are most gratefully acknowledged.

CONTENTS

STATISTICAL THEORY OF NEUTRON-NUCLEAR REACTIONS

P.A. MOLDAUER
Applied Physics Division,
Argonne National Laboratory,
Argonne, Illinois,
United States of America

ABSTRACT

In addition to the topics dealt with by the author in his lectures at the Joint IAEA/ICTP Course held at Trieste in 1978, recent developments in the statistical theory of multistep reactions are reviewed as well as the transport theory and intranuclear cascade approaches to the description of nuclear multi-step processes.

The lectures on this topic followed in substance the 1978 lectures[1] of the same title with the following topics added.

1. Statistical theory of multistep reactions.[2] Here the Hilbert space is divided into states belonging to different classes of complexity, arising from some model Hamiltonian. One example [3] is the exciton model of states with various numbers of particle-hole pairs in the independent particle shell model. Regardless of the specific model, it is assumed that the residual interaction (difference between true and model Hamiltonian) causes transitions only between states belonging to successive classes of complexities (e.g. differing by one in the number of particle-hole pairs). The model states are further classified into those belonging to the model continuum and discrete spectra. The reaction is described as proceeding from the entrance channel continuum state through either a succession of model continuum states (multistep direct reaction), or a succession of model discrete states (multistep compound reaction) to the exit channel.

In the case of the compound reactions, all processes belonging to different conserved quantum numbers (total angular momentum, parity, etc.) are added incoherently, leading to symmetric cross sections in the center-of-mass system. In the direct processes, matrix elements for transitions which do not change the momentum of the continuum particle are added coherently, so as to produce a characteristic forward peak in the cross section.

The expression for the multichannel compound cross section is of the form of the Hauser-Feshbach formula, where the exit channel width is replaced by a product of transition strengths between different classes of states. The latter calculated by combinatorial formulas based upon optical model and level density information as well as more detailed assumptions regarding the statistical properties of the various classes of states. Similarly the multichannel direct cross section is expressed as a multiple integral over transitions between successive steps.

2. Transport Theory.[4] Earlier, Agassi, Weidenmüller and Mantzouranis had devised a theory based upon physical assumptions quite similar to the above multistep compound processes, but had treated the transitions between classes of states as a transport phenomenon. The result is a formula in which transmission factors for the entrance and exit channels surround a probability matrix in the space of classes of states which satisfies a probability balance equation that describes the transport of the system among the various classes of states.

3. Intranuclear Cascade.[5-7] This is a numerical method in which the course of a highly energetic projectile is followed through the nucleus in coordinate space a large number of times. Each time a sequence of interactions between nucleons is selected at random and the ultimate state resulting from that sequence is weighted according to the cross sections for all the nuclear processes involved. The composite results of a large number of such runs yield cross sections for all processes initiated by the impact of a very energetic nucleon or other particle on a nucleus.

References

1. P. A. Moldauer, Nuclear Theory for Applications, IAEA-SMR-43, p. 165 (1980).
2. H. Feshbach A. Kerman, S. Koonin, Ann. Phys., 125, 429(1980).
3. J. J. Griffin, Phys. Rev. Lett. 17, 478(1966), Phys. Let. 24B, 5(1967).
4. D. Agassi, H. A. Weidenmüller and G. Mantzouranis, Phys. Let. 22C, 145(1975).
5. N. Metropolis et al., Phys. Rev., 110, 185,204(1958).
6. H. W. Bertini, Phys. Rev., 131, 1801(1963).
7. R. G. Alsmiller, Jr. and J. Barish, Nucl. Sci. Eng., 69, 378(1979).

RECENT RESULTS IN THE THEORETICAL DESCRIPTION OF PRE-EQUILIBRIUM PROCESSES

E. GADIOLI, E. GADIOLI ERBA
Istituto di Fisica dell'Università,
Milan,
and
I.N.F.N., Sezione di Milano,
Milan,
Italy

ABSTRACT

The main assumptions underlying the phenomenological pre-equilibrium models are reviewed. A special attention is given to the discussion of the different approaches suggested to reproduce the yield and spectral distribution of fast complex particles and the angular distribution of reaction products emitted during the fast stage of the reaction process.
A number of successful applications of these models to the description of reactions induced by fast neutrons are summarized.

1. *PRE-EQUILIBRIUM PROCESSES AND PHENOMENOLOGICAL MODELS.*

At not too high excitation energies a natural way to classify nuclear reactions seems to be according to the time scale on which they occur. At the two extremes of this time scale there are the fast or direct interactions and the compound nucleus processes.

Direct interactions are processes which involve few nucleons. Typical processes are inelastic scattering, stripping and pick-up. In these processes the emitted particle comes out in a time of the order the time it takes for the projectile to go through the nucleus. The most important features of such a kind of interactions are the diffraction structure of the angular distributions, usually forward peaked, and the high selectivity which manifests itself in the excitation of particular levels of residual nucleus.
The great importance of such a kind of reactions as spectroscopic tools comes just from the selectivity which favours transitions to states of the residual nucleus in a simple structural relationship with ground state of target nucleus. From the analysis of data, if the dynamics of the process is well understood one obtains useful information concerning the static properties of nuclei.

On the other hand, once the long lived compound nucleus state is reached, the emission of particles is governed by statistical laws and provided that spin, parity and energy are conserved the decay appears to be independent of the way the compound nucleus has been created. The decay probability is governed by the phase space which is accessible to the reaction products. The particles are emitted from the compound nucleus with symmetric or isotropic angular distributions and with a Maxwellian spectrum. The basic information concerning the nuclear properties which one obtains from the analysis of the experimental data concerns the density of levels of the residual nucleus which depends little upon the properties of the particular nucleus considered (except in the vicinity of magic numbers) but mainly upon the size of the nucleus and the total number of nucleons.

In between these two extreme processes, intermediate processes are likely to occur. A series of complicated collisions inside the nucleus can follow the initial interaction and there is a certain probability amplitude that a particle be emitted after each one of these collisions.

In a quantum mechanical description of this process, emissions from each stage of the cascade are expected to contribute coherently; however the experimental data accumulated during the last twenty years showed striking regularities. In a typical

experiment, at incident energies of the order of a few ten MeV, the spectra of emitted particles show a low energy peak which is to be attributed to evaporative contributions, and at the highest energies the selective population of low energy levels of residual nucleus, inbetween a smooth distribution. It seems natural to attribute this contribution to the intermediate processes described above which here-after will be referred to as pre-equilibrium emissions. In these processes the high selectivity of direct interactions is lost, on the other hand few degrees of freedom are involved, i.e. the number of excited particles and holes which shared the excitation energy of the intermediate system, when the particles contributing to the smooth measured distribution were emitted, is small. This feature can be proved by an analysis, like the one usually utilized in the case of the evaporation, which shows that the nuclear temperature of the residual nucleus is much higher than the one expected in a compound process. In addition, this temperature and the measured cross sections are practically independent from the particular nucleus considered. The absence of marked fluctuations in the measured spectrum, which should be apparent if interference effects are important, prompted the different authors to try to describe the process by semiclassical approaches by adding incoherently the contributions from each stage of the cascade.

These models have now become very useful tools for the analysis and interpretation of nuclear reactions at energies greater than approximately ten MeV. A formal theory of the processes previously described has been recently developed by Feshbach et al. [1]. This theory predicts the existence of two distinct processes: one, which should dominate near the evaporation end of the spectrum of emitted particles, is referred to as the statistical multi-step compound reaction; the other should dominate the highest energy part of the spectrum and is referred to as direct multi-step reaction. At present only a very few analyses of experimental data on the basis of the first mechanism have been reported [1,2]; the formalism describing the second process is yet at a stage which does not allow an immediate application to the analysis of data. In recent years, introducing suitable averaging procedures, also direct reaction theories have been applied with some success to the analysis of continuous part of the spectra [3,4].

The importance of pre-equilibrium phenomena is today fully recognized. They are extensively investigated and their relevance in practical and technological applications has been indicated by several authors. The need for an accurate reproduction of these processes has been stated in domains like: a) Fusion reactor design and radiation damage investigations. The need for data concerning nuclear reactions induced by 10-40 MeV neutrons has intensified in recent years. Due to the sparsity of experimental data in this energy range, model calculations are expected to play an important role in meeting the data requirements [5]; b) Radiotherapy. The fluxes of primary and secondary particles determine the biological damage in tissue. The energy spectra of these particles contribute essentially to the distribution of the absorbed dose and its localization and, as a consequence, to the relative biological effectiveness and the oxygen enhancement ratio of the radiation field [6]; c) Space explorations. Accurate calculations of fast neutron production are of importance to the shielding of space exploring vehicles from the highly abundant low energy protons in solar flares and in Van Allen belts [7]; d) Astrophysics. A systematic study of the yields of nuclides produced by cosmic ray irradiation (in particular protons of energy in the 10-100 MeV region and non-zero energy pions), which is only possible if one understands the mechanism of pre-equilibrium emission, is of interest in understanding the nuclear transformations produced during the exposure in space to high energy cosmic rays and solar flare particles, of meteorites, the surface of the moon and asteroids [8].

Different experimental techniques have been employed to investigate processes to which pre-equilibrium decay is supposed to contribute: I) Measurement of inclusive spectra of particles emitted in reactions induced by a given projectile. Differential energy spectra of p, d, t, τ, α particles can be measured simultaneously over a wide dynamical range (See as an example ref. 9). Precise measurements of neutron spectra have been reported by several groups (see e.g., ref. 10-12). Coincidence measurements of neutron spectra in (n, 2n) reactions have also been reported.[13] The experimental techniques utilised for the study of secondary particle energy spectra in reactions induced by 14 MeV neutrons will be reviewed by profs. Seeliger and Vonach; II) Measurement by activation techniques of the yield of radioactive residuals. Though remarkable differences in results obtained in past experiments are reported in literature, present-day techniques and knowledge of decay schemes allow accurate measurements. Cross sections as low as ten µbarns can be measured if one utilises radiochemical methods. In properly designed experiments the yield of several final products can be simultaneously detected and varying the incident projectile energy the excitation functions of several reactions measured (see, e.g., ref. 14). Though in general the sum of measured yields amounts only to a small fraction of the projectile reaction cross-section, at a given energy, the simultaneous reproduction of all the yields utilising a unique set of parameters constitutes a severe test of a theory; III) In beam measurement of γ - rays which identify the reaction products. In this case the residual nuclei identified can also be stable. A fraction of the total reaction cross section of the projectile much greater than the one measured by activation techniques can be detected [15]. The accuracy is, however, much smaller. Only cross sections greater than approximately 1mb can be measured and with a fair accuracy only in the case of even-even final nuclei, though also in this case the cross sections corresponding to processes which populate directly the ground state of the residual nucleus cannot be measured. In the case of odd residual nuclei several γ lines have to be detected and the decay scheme must be accurately known. Also in this case the reproduction of all the measured yields constitutes a severe test of a theory; IV) Recent experiments utilise in-beam and off-beam γ-ray spectroscopy to identify the final products. In this case a substantial fraction of the total reaction cross section of the projectile is measured[16];
V) Finally one can measure the spectrum of a particle in coincidence with a γ-ray which identifies a given final nucleus thus detecting only particles emitted in a particular process. This very recent technique is the most apt to visualize pre-equilibrium processes [17,18]. Also particle-particle coincidences are a powerful means of investigation.
Other techniques involve the use of particular detectors, e.g., a 4π liquid scintillator (by this technique several beautiful measurements of (n,xn) reactions have been performed [19]).

All the phenomenological models that we shall call, broadly speaking, pre-equilibrium models - e.g., the Intranuclear Cascade Montecarlo (I C M) model, the Exciton model (E M), the Harp-Miller-Berne Master Equation approach, the Hybrid and Geometry Dependent Hybrid models (including their Quasi Free version) - while differing in specific and even important points, introduce certain common hypotheses to describe the generic nuclear process [20-23]. These hypotheses are, briefly, the following: (a) The projectile or one of its constituent nucleons if the projectile is a complex particle, interacts with a nucleon, (or possibly with a small number of correlated nucleons) of the target giving rise to states of a simple configuration.
(b) The particles and the holes excited in the first stage of the process originate a cascade of two-body interactions that brings about the distribution of the excitation energy among an ever increasing number of particles and holes. In this second stage of the process fast particles may be emitted which, by retaining (at least partly) a memory of the direction of the incident projectile,

have asymmetric (forward peaked) angular distributions. Emissions during this stage are the ones we call pre-equilibrium emissions. (c) The statistical equilibrium is finally reached between all the states corresponding to a given energy, parity and angular momentum. Now the mean energy of the excited particles is low (assuming that the residual excitation energy is small in comparison to the total binding energy of the nucleus), and the subsequent emission of particles takes place through the well known evaporation mechanism.

In respect to the differences among the various models, we shall limit ourselves to a few remarks. In the I C M model the interaction cascade is calculated by following explicitly the trajectories of the excited nucleons inside the nuclei. An extraction of random numbers decides where inside a nucleus an interaction (which is assumed, except for limitations due to Pauli principle, identical with the free interaction) can take place, and it likewise decides the direction and momentum of the struck nucleon as well as the direction and energy of the particles after the collision. The calculation follows all the nucleons, excited in the course of the cascade, that are emitted if - on reaching the nuclear surface - they are not reflected there, and it terminates when the energy of every nucleon drops below a predetermined value.
The most sophisticated version of I C M is the one (the VEGAS code) described by Chen et al [24]. In this calculation the target nucleus is taken to be a Fermi gas with a step function density distribution chosen to approximate the Fermi distribution and one takes account of the effect of the refraction of the cascade particles as they move through the nucleus and of the possibility that particles with enough energy to escape from the nucleus may be reflected back into the interior while on their way out. In a further refinement of the calculation the effect of the velocity dependence of the nuclear potential [25] and of the granular structure of the nucleus-by imposing a minimum distance between successive nucleon collisions [26] have been considered. Though this model was originally intented to apply to the analysis of reactions induced by projectiles with energy exceeding some hundred MeV it has been utilised in the analysis of data at much lower energy [27]. As a result of the analysis of angle-integrated (p, p') spectra in reactions induced by 39 and 62 MeV protons on nuclei ranging from ^{12}C to ^{209}Bi, Bertini et al.[28] concluded that the inclusion of refractions and reflection effects suppresses the escape of fast particles to the extent that serious discrepancies were introduced for the elements considered at the lower incident energies and for the heavier elements at all the energies. Much better results were obtained by the use of a different code due to Bertini [29] in which the effect of refractions and reflections has been suppressed. In this case the calculation reproduced the shapes of the measured spectra satisfactorily and the absolute cross section within 25-30%.
It has been shown that a much better estimate of the yield of fast particles with Vegas code is obtained when in the calculation a mean free path for the cascade particles substantially longer than the one originally calculated is utilised [30].
Numerical calculations demonstrated, in the case of reactions induced by 60 MeV protons, that the effect of suppressing refractions and reflections is - to some extent - equivalent to an increase of the mean free path of the cascade particles[30, 31].
The Bertini code has been utilised for analysing reactions induced by protons of energies even lower than the ones previously considered and comparable to those of neutrons for fusion reactor studies (14-18 MeV). In this case the reproduction of the data was rather poor [7].
A code similar to the Bertini one has been developed at Dubna [32]. The I C M models assume that all interactions take place between nucleons. A preliminary calculation has been reported by Bertrand & Peelle [27], in the case of proton-induced reactions, which is based on a modification of Bertini code to allow for interactions of the primary proton and the cascade nucleons with correlated pair of nucleons. This calculation

showed a much increased yield of fast protons at backward angles.
In conventional versions of the I C M models one takes into account only the interactions that involve excited particles. It has to be mentioned that in a recent version by Iljinov et al. [33] account is taken, although in a rather schematic and artificial way, also of the interactions that involve excited holes.

In the other mentioned models the probability of a given process taking place is calculated with the methods of quantum statistical mechanics and is expressed by means of decay rates.
As an example we will sketch the approach one follows in the Exciton model [21]. In this section we will discuss the theory proposed to deal with angle-integrated particle emission. The modifications to be introduced to predict the angular distribution of the reaction products will be discussed in section 3. The states of the excited nucleus, the "composite" nucleus, are grouped into classes characterized by the number (n) of excited particles (p) and holes (h) referred to as the excitons; and the total excitation energy, E. A state of a given class can decay either by means of a residual two-body interaction (these decay rates, which can lead to states having a number of excitons $m = n, n\pm2$, hereafter will be referred to as internal transition decay rates and indicated as $W_{n\to m}(E)$) or by emitting a particle of a certain energy in the continuum (these decay rates will be indicated as $W_c^{n,\nu}(E,\epsilon_\nu)$, where ν identifies the particle which is emitted; the total decay rate for emissions in the continuum is $W_c^n(E)=\sum_\nu \int W_c^{n,\nu}(E,\epsilon_\nu)d\epsilon_\nu$).

The internal transition decay rates can be calculated, at low excitation energy where the average squared matrix element for two-body residual interaction $\overline{|M|^2}$ can be considered approximately energy-independent [34], by means of first order perturbation theory as [35]

$$W_{n\to n,n\pm2}(E)=\frac{2\pi}{\hbar}\,\overline{|M|^2}\,\rho_f^{n,n\pm2} \qquad (1)$$

where $\rho_f^{n,n\pm2}$ is the density of accessible final states (for a calculation of this quantity see refs. 36, 37)). Formula (1) has been extensively employed also at higher energies when $|M|^2$ can no more be considered energy-independent. In this case following Kalbach [38] one assumes

$$\overline{|M|^2}=K\,A^{-3}\,E^{-1} \qquad (2)$$

where A is the excited nucleus mass and E is its excitation energy.
For K, values in the interval 190-700 MeV^{+3} have been proposed [39-43].

At sufficiently high energies and in the case of not too light nuclei, for n values lower than $\bar{n}=\sqrt{2gE}$, where g is the single nucleon state density,

$$W_{n\to n+2}(E)\gg W_{n,n}(E),\ W_{n\to n-2}(E).$$

Then it has been proposed that the energy and exciton number dependence of the decay rate $W_{n\to n+2}(E)$ be calculated as

$$W_{n\to n+2}(E)=p\,\overline{W}_{1p}(p,h,E)+h\,\overline{W}_{1h}(p,h,E) \qquad (3)$$

where $\overline{W}_{1p}$ and $\overline{W}_{1h}$ are the values of particle and hole collision probabilities per unit time (collision probabilities per unit time of a particle above (hole below) the Fermi energy, ϵ_f, with a particle below (a hole above) the Fermi energy) averaged over all possible particle (hole) energies in states or class (n, E). The particle and hole collision probabilities per unit time are evaluated as $v\,\rho\,\bar{\sigma}$, where v is the nucleon velocity, ρ the nuclear density and $\bar{\sigma}$ the average nucleon-nucleon cross section in nuclear matter.
It has been shown in ref. (34), to which the reader interested in a detailed discussion of this point is referred, that $v\rho\bar{\sigma}$, at low nucleon energies, has an energy dependence equal to the one foreseen by the first order perturbation theory.
The absolute value of $W_{n\to n+2}(E)$ is obtained by the analysis of appropriate experimental data. In Table I, values of

$W_{n\to n+2}(E)$ for exciton numbers encountered in the case of nucleon-induced reactions are reported as a function of the excitation energy.

The decay rates, corresponding to the emission of a particle of a certain energy in the continuum, is evaluated by means of the expression

$$W_c^{n,\nu}(E,\epsilon_\nu)\,d\epsilon_\nu = P_{p,h}(\epsilon_\nu+B_\nu)\,\lambda_c(\epsilon_\nu)\,d\epsilon_\nu \qquad (4)$$

The quantity $P_{p,h}(\epsilon_\nu+B_\nu)$ is the product of the number of particles of type ν times the density of probability that the excited nucleus with energy E, in a state of a class characterized by $n=p+h$ excitons, has a configuration with one particle ν with energy in the interval $\epsilon_\nu+B_\nu \to \epsilon_\nu+B_\nu+d\epsilon_\nu$, where B_ν is the binding energy of particle ν and ϵ_ν its energy outside the nucleus. The assumption that all the states of a given class are equiprobable is often introduced and, as a consequence, $P_{p,h}(\epsilon_\nu+B_\nu)$ is expressed as

$$P_{p,h}(\epsilon_\nu+B_\nu) = \frac{\omega_{p-p_\nu,h}(U_R)\,g_\nu(\epsilon_\nu+B_\nu)}{\omega_{p,h}(E)} \qquad (5)$$

where $\omega_{p,h}(E)$ and $\omega_{p-p_\nu,h}(U_R)$ are, respectively, the state densities of the composite and residual nucleus (a detailed list of papers devoted to the calculation of the state densities can be found in ref. 21); further work relevant to the problem is due to Betak and Dobes [44]) and $g_\nu(\epsilon_\nu+B_\nu)$ is the single state density for particle ν.

In recent calculations $P_{p,h}(\epsilon_\nu+B_\nu)$ has been evaluated by means of an explicit calculation of the energy partition resulting from the dynamics of particle-particle interactions inside the nucleus [23, 45, 46].

In the nucleon case, this more complex procedure leads to results substantially coincident with expression (5); in the case of α - particle emission, in nucleon-induced reactions, if one supposes that the emitted α's were preformed in the nucleus and are knocked on by the incident nucleon or a cascade nucleon, a calculation based on nucleon-α dynamics indicates that expression (5) is a rather poor approximation. This case will be explicitly discussed in the next section.

$P_{p,h}(\epsilon_\nu+B_\nu)$ has been also evaluated by means of recursion relations which keep track of the exciton flux explicitly [47]. The quantity $\lambda_c(\epsilon_\nu)$ is the decay rate for the emission of particle ν in the continuum and is given by

$$\lambda_c(\epsilon_\nu) = \frac{\sigma_{inv}(\epsilon_\nu)\;v_\nu\;\omega_c(\epsilon_\nu)}{g_\nu(\epsilon_\nu+B_\nu)\,V} \qquad (6)$$

where $\sigma_{inv}(\epsilon_\nu)$ is the inverse cross section of particle ν, v_ν its velocity, $\omega_c(\epsilon_\nu)$ the density of translational states of particle ν in the continuum, V an arbitrary volume which cancels out with an identical quantity in $\omega_c(\epsilon_\nu)$.

Two different procedures have been proposed to calculate the cross-sections for particle emission in the framework of the exciton model. One is based on the solution of a system of master equations which determine the time-dependent occupation probability $P(n,t)$ of the n-exciton states of the composite nucleus [48 - 51]. Another resorts to closed-form expressions [34, 39, 40, 52-57].

a) Master equation approach. The function $P(n,t)$, which must satisfy the boundary conditions

$$P(n,0) = \delta(n,n_o), \quad P(n,t\to\infty) = 0$$

with n_o = number of excitons of the initial configuration, is determined by solving a system of equations like

$$\frac{dP(n,t)}{dt} = P(n+2,t)\,W_{n+2\to n}(E) + P(n-2,t)\,W_{n-2\to n}(E) - P(n,t)\left\{W_{n\to n+2}(E) + W_{n\to n-2}(E) + W_c^n(E)\right\} \qquad (7)$$

The time spent by the nucleus in a generic n-exciton configuration is

$$\tau_n = \int_0^\infty P(n,t)\,dt \qquad (8)$$

The energy spectrum of the particles ν emitted in the de-excitation process of the composite nucleus in a reaction induced by a particle b is given by:

$$\sigma(b,\epsilon_\nu) = \sigma_c^b(E_i) \sum_{\substack{n=n_0 \\ \Delta n=+2}}^{\bar{n}} W_c^{n,\nu}(E,\epsilon_\nu)\,\tau_n\,d\epsilon_\nu \qquad (9)$$

To this spectrum contribute both pre-equilibrium emissions and evaporations from the compound nucleus. $\sigma_c^b(E_i)$ denotes the cross-section for absorption of the incident particle. Finally, the cross-section of any given process x (e.g., the emission of particles ν with energy between E_1 and E_2) is obtained by integrating eq. (9):

$$\sigma(b,x) = \int_{E_1}^{E_2} \sigma(b,\epsilon_\nu)\,d\epsilon_\nu \qquad (10)$$

The connection between a random matrix model for the nuclear Hamiltonian and this statistical theory has been established by Weidenmüller and cow.[51]

Betak and Dobes[58] have shown that it is possible, utilising fast iterative procedures, to evaluate, with reasonable computing times, multiparticle emission probabilities. In addition these authors included also γ - emission (which usually is neglected) as a competing channel.

A generalisation of the system of master equations (7) in order to predict the angular distribution of particles emitted during the pre-equilibrium phase has been proposed by Weidenmüller et al.[59] and will be discussed in section 3.

A system of master equations to be utilised if one differentiates between neutrons and protons, neutron holes and proton holes, has been proposed by Gudima et al.[60, 61], however, it has not yet been applied to the analysis of experimental data.

b) Closed form expression.

If n is noticeably smaller than $\bar{n} = \sqrt{2gE}$, $W_{n\to n+2} \gg W_{n\to n}$, $W_{n\to n-2}$. This relation is satisfied for the states at the beginning of the de-excitation cascade in the case of not too light nuclei for excitation energies exceeding ten MeV and holds also in the case of light nuclei if the excitation energy is sufficiently high.

Then, one can express in a closed form the cross section of a given process. For instance the cross section given in the master equation approach by relation (9) in closed form is written

$$\sigma(b,\epsilon_\nu) = \sigma_c^b(E_i) \sum_{\substack{n=n_0 \\ \Delta n=+2}}^{\bar{n}} D_n \frac{W_c^{n,\nu}(E,\epsilon_\nu)\,d\epsilon_\nu}{W_c^n(E) + W_{n\to n+2}(E)} \qquad (11)$$

where D_n is a term representing the probability of reaching a state of class (n, E). $D_{n_0}=1$ if n_0 represents the exciton number of the states of the initial configuration; if $n>n_0$, differing by n_0 by an even integer number, :

$$D_n = \prod_{\substack{j=n_0 \\ \Delta j=+2}}^{n-2} \frac{W_{j\to j+2}(E)}{W_c^j(E) + W_{j\to j+2}(E)} \qquad (12)$$

The use of closed-form expressions, instead of the system of master equations, remarkably simplifies cross section calculations and yields very satisfactory results since pre-equilibrium emissions mainly occur from states with low values of n and the summation on the right hand of equation (11) usually converges rapidly. The probability that the sequence of two-body exciton-exciton interactions leads to the long-lived state of statistical equilibrium called compound-nucleus state can also be expressed in a closed form by means of the decay rates $W_{n\to n+2}(E)$ and $W_c^n(E)$. In fact, even if from a phenomenological point of view, it may be convenient to consider pre-equilibrium emission as distinct from evaporation, - and in fact they develop over quite different time scales, - it is essential

to keep in mind that the attainment of equilibrium is the conclusion of the equilibration process.
The cross-section for compound-nucleus formation $\sigma^{b}_{CN}(E_i)$ takes a suitably simple form

$$\sigma^{b}_{CN}(E_i) = \sigma^{b}_{c}(E_i) \prod_{\substack{n=n_0 \\ \Delta n=+2}}^{\bar{n}} \frac{W_{n\to n+2}(E)}{W_{n\to n+2}(E) + W^{n}_{c}(E)}$$

Once the compound nucleus state is created, its decay can be easily described by utilising well-known procedures. A generalisation of this approach in order to evaluate the angular distributions of particles emitted in the PE phase has been proposed [45, 62] and will be discussed in section 3.
Also the Hybrid model formalism resorts to closed-form expressions [22]. In that case, in the denominator of the fraction appearing in expression (11) the decay rate for emission of whatever particle of any possible energy, $W^{n}_{c}(E)$, is substituted by the decay rate for emission of particle ν with energy ϵ_ν ; the decay rate for internal transitions, $W_{n\to n+2}(E)$, by the collision probability per unit time $W_{1p}(\epsilon_\nu)$, referring again to particle ν, with energy $\epsilon_\nu + B_\nu$. The different physical assumptions underlying the Exciton and Hybrid models have been amply debated in literature. This discussion will not be repeated here, the reader is adressed to references (47, 63, 64).
The use of both the system of master equations and closed-form expressions is of little benefit when very complicated reactions are analysed, due to the need of evaluating all the possible reaction paths contributing to a given process. To treat these cases, in the framework of the E M, a Monte Carlo approach has been reported and widely employed in the analysis of data [45, 65-67].
The method of calculation is simply a generalisation of the well-known Dostrovski et al. [68] procedure, proposed to evaluate the de-excitation of a compound nucleus. In this approach the probability of a given process taking place is evaluated by simulating a great number of possible sequences of emissions. At any given stage of the reaction the probability of a given decay of the excited nucleus is evaluated as the ratio of the decay rate corresponding to that particular decay and the total decay rate. Once, by means of the extraction of a random number, the emission of a given particle has been settled, its energy ϵ is estimated by assuming that the probability of its occurence is given by the ratio between the values of the theoretical energy distribution at ϵ and at the maximum. Some examples of results obtained by means of calculations of this kind will be given later.

A great number of authors are convinced that in most cases the initial interaction of the projectile is localized in the peripheral region of the nucleus [20]. In fact it has been demonstrated that, in I C M calculations, the simplest reactions occur in the diffuse edge of the nucleus [24]. Detailed calculations of particle-particle collision probabilities per unit time, $W_{1p}(\epsilon_\nu, r)$, as a function of r, utilising a local density approximation and realistic matter density distributions $\rho(r)$ also show that the outer regions of the nucleus greatly contribute to the absorption of the incident particles (see ref. (69) and reference therein). A modification of the Hybrid model referred to as the Geometry-dependent hybrid model has been proposed by Blann to describe processes mainly occurring at the nuclear surface.[70,71] Blann argues that in a local-density approximation, due to the small depth of the potential well, no energy is supplied to the holes in this nuclear region. The density of the excited nucleus states in the initial configuration, in the case of nucleon-induced reactions, resembles $\omega_{p=2,h=0}(E) \div g^2 E$ and the residual nucleus density becomes equal to the density of single particle states g. In this model the emitted particle spectrum is almost flat, while processes occurring inside the nucleus would be characterised by a softer emitted particle energy distribution decreasing with the energy. In practice an effect of this kind has been observed only in the case of some (p, p') reactions,[71, 72]

while neutron spectra in (p,n) reactions are satisfactorily fitted by calculations which do not take explicitly into account the geometry of the process [55, 72, 73]. It has to be mentioned that calculations based on the use of direct reaction theory and Random Phase Approximation [4] and experimental results like the ones reported by Cohen et al. [74], show that in (p, p') reactions most likely low-energy collective states of the residual nucleus are excited. This process that hardly one could expect to be reproducible, in the framework of the models here described, could be responsible of the observed hardening of proton spectra.
Finally the argument that the intervention of peripheral interactions would be indicated by the fact that certain cross sections - like the total cross section for the emission of one fast proton in (p, p') processes - vary as $A^{1/3}$ is not conclusive since the same dependence is, e.g., foreseen by the Exciton model without implying peripheral interactions.

The pre-equilibrium models have been employed with increasing success as their sophistication grew and the knowledge of the required parameters became more precise, in the study of reactions induced by light particles (n, p, d,α) and less usual projectiles (γ,$\pi^{\pm}$,μ) as well. Here we will not attempt to give a complete list of the enormous amount of papers - appeared in the last years - reporting the results of analyses of experimental data. The reader is referred to the literature already quoted. The main results obtained in the case of neutron-induced reactions will be briefly summarized in Section 4. Just as an example we can show in Figs. 1-3 and Table II, the results of some recent calculations with the Hybrid, the Exciton and the I C M models at excitation energies up to $\approx$ 200 MeV (16, 67,75,76). These results indicate that by means of such models it is possible now to reproduce with quite good precision, using a well-defined set of parameters, the yield of the great majority of the reaction channels contributing to the total cross section of one of the projectiles previously mentioned, for nuclei spreading the entire mass table. This statement holds also in the case of low-probability processes with cross sections of 1 mb or less.

The probability of emissions during the pre-equilibrium stage rises with the excitation energy, so that, e.g., in the case of proton-induced reactions, for incident energies exceeding 50 MeV, in the majority of the reactions one gets the emission of at least one particle from the pre-equilibrium stage (see as an example Fig. 4). Such emissions lower considerably the excitation energy of the excited nucleus which afterwards decays through evaporation. Also if normally the average number of particles emitted during the pre-equilibrium stage is much lower than the one of the evaporated particles, the average energy dissipated during the pre-equilibrium stage is comparable or even greater (at the highest energies) than the one dissipated during evaporations.
To conclude this summary exposition, we would like to remark that although at comparatively lower energies the phenomena taking place during the equilibration are on the whole less relevant, still certain processes can occur only because there is a pre-equilibrium stage. Such is the case, e.g., of the emission of charged particles in reactions induced in heavy nuclei at comparatively low excitation energies.

2. α PARTICLE EMISSION IN NUCLEON-INDUCED PRE-EQUILIBRIUM PROCESSES.

The detailed study of α - emission in nucleon-induced reactions begins in the early fifties with activation measurements of cross-sections of (n,α) reactions at a neutron energy of about 14 MeV [77]. About ten years later sufficient material was collected to allow systematic analyses of this process. The result of these investigations was that calculations based on the statistical model satisfactorily reproduced the experimental cross-sections in the case of quite light nuclei (A$\lesssim$80),

while for heavier target nuclei the experimental cross sections greatly exceeded the calculated ones [78].
In subsequent years several measurements of continuous spectra and angular distributions of α's emitted in reactions produced by low-energy neutrons and protons have been reported.
The measured spectra indicated that a sizeable amount (in the case of heavy nuclei the greatest amount) of the α's emitted in low-energy nuclear reactions have an energy greatly exceeding the Coulomb barrier and a structureless distribution. Their angular distribution is also forward-peaked.
In the last few years, finally, a big amount of experimental measurements of the yield and energy distribution of α's emitted in processes induced by protons of energy exceeding 20 MeV have been reported.

The main features of the processes involving α-emission can be summarized as follows. The shape of the inclusive α-spectra clearly shows the presence of two different contributions. In the case of a light nucleus one observes a peak at low energy due to the evaporations from the compound nucleus; at higher energies a structureless shoulder which has to be attributed to a different reaction mechanism. This contribution becomes the predominant one in the case of heavy target nuclei and not too high bombarding energies when the evaporative contribution is greatly reduced or, in some cases, absent.
The non-evaporative contribution is concentrated at forward angles.

However, also at backward angles the non evaporative contribution is far from negligible; e.g., a comparison between the C.M. spectra of α-particles emitted at a backward angle under 90 MeV proton bombardment of nuclei ranging from Al to Bi, indicates that the slope of these spectra, corresponding to a temperature of 2-3 MeV, is identical for all target nuclei [79].
This feature clearly indicates that also at backward angles the hardest part of the α-spectra is not due to an evaporation process.

Theoretical analysis of backward-angle spectra on the basis of the statistical model is in full agreement with this finding[80].
The yield and energy distribution of these energetic α's depend little on the mass of target nucleus; their angular distribution has a shape which is practically the same for all the emitting nuclei [81].

In the framework of I C M model and Harp-Miller-Berne master equation approach, no attempt has been made to account for the emission of fast alphas.
In the framework of the other models, we mentioned, various suggestions have been advanced to account for their emission. A first attempt is based on the hypothesis that the α is formed from among the excited nucleons during the equilibration cascade which follows the interaction of the projectile with a nucleon of the target. To describe this process an expression for the decay rate, for α emission, of the same structure as the ones which are utilised to describe nucleon emission has been proposed:

$$W_c^{n,\alpha}(E,\epsilon_\alpha)\,d\epsilon_\alpha = \left[\frac{\omega_{p\text{-}p_\alpha,h}(U_R)\,g_\alpha(\epsilon_\alpha+B_\alpha)}{\omega_{p,h}(E)}\right] R_\alpha \left[\frac{\sigma_{inv,\alpha}(\epsilon_\alpha)\,v_\alpha\,\omega_c(\epsilon_\alpha)}{g_\alpha(\epsilon_\alpha+B_\alpha)V}\right] =$$

$$= \frac{1}{\pi^2\hbar^3}\,\mu_\alpha\,\epsilon_\alpha\,\sigma_{inv,\alpha}(\epsilon_\alpha)\,\frac{\omega_{p\text{-}p_\alpha,h}(U_R)}{\omega_{p,h}(E)}\,R_\alpha \qquad (13)$$

(R_α gives the probability that the p_α particles have the right combination of protons and neutrons to form the outgoing α).
The calculated α-yields greatly underestimate the experimental ones (especially at the highest α energies). [49]

Another expression which has been shown to reproduce successfully the experimental distribution is the following:

$$W_c^{n,\alpha}(E,\epsilon_\alpha)\,d\epsilon_\alpha = \left[\frac{\omega_{p-p_\alpha,h}(U_R)}{\omega_{p,h}(E)}\,\omega_{p_\alpha,0}(\epsilon_\alpha+B_\alpha)\right] R_\alpha \gamma_\alpha^* \cdot$$

$$\cdot\left[\frac{\sigma_{inv,\alpha}(\epsilon_\alpha)\,v_\alpha\,\omega_c(\epsilon_\alpha)}{g_\alpha(\epsilon_\alpha+B_\alpha)V}\right] d\epsilon_\alpha \qquad (14)$$

Now $\omega_{p_\alpha,0}(\epsilon_\alpha+B_\alpha)$ represents the number of ways p_α excited particles can statistically share the energy $\epsilon_\alpha+B_\alpha$, assuming all the partitions of the energy as equiprobable; γ_α^* is indicated as "the formation probability for the α in the composite nucleus to have the right momentum to undergo emission as an entity"; $g_\alpha(\epsilon_\alpha+B_\alpha)$ is the single-particle density for the α (usually assumed to be constant or a weak function of $(\epsilon_\alpha+B_\alpha)$ [79,82,83]. The quantity in the first square bracket should give the density of probability $P_{p,h}(\epsilon_\alpha+B_\alpha)$ that the energy E of the composite nucleus, in a (p,h) configuration, be partitioned between p_α particles with total energy $(\epsilon_\alpha+B_\alpha)$ and $(p-p_\alpha+h)$ excitons with energy U_R (to have exactly this meaning this quantity should be multiplied by $\frac{(p-p_\alpha)!\,p_\alpha!}{p!}$). $P_{p,h}(\epsilon_\alpha+B_\alpha)R_\alpha\gamma_\alpha^*$ should then have the meaning of density of probability that the energy E of the composite nucleus in a (p,h) configuration be partitioned between an α-particle with energy $(\epsilon_\alpha+B_\alpha)$ within the nucleus and $(p-p_\alpha+h)$ other excitons. The last quantity within square bracket represents the emission rate into the continuum for an α with energy outside the nucleus $\epsilon_\alpha = E-U_R-B_\alpha$ (B_α is the α binding energy). This approach leads to a reasonable reproduction of the α-spectra in reactions induced by protons of energy 30-90 MeV. The quantity γ_α^* was found to be energy-independent. It varies with the mass of target nucleus, from about unity for A~12 to less than 10^{-3} for A~200. The same approach with obvious generalisations and employing different values for the γ^* can be and has been applied for the analysis of spectra of d, t, τ. Despite the satisfactory agreement between experimental and calculated spectra [79] a serious question can be raised against this approach.

In expression (14) the quantity $\omega_{p_\alpha,0}(\epsilon_\alpha+B_\alpha)R_\alpha\gamma_\alpha^*$ has been utilized to evaluate the partition of the excitation energy between $(p-p_\alpha)$ particles, h holes and four excited particles clustered into one α. Then - in our opinion - it has the meaning of the density of α-states. The same quantity, instead of g_α, should then appear in the denominator of the emission rate [84,85]. This substitution would lead to an expression like (13) which has already proved unsatisfactory.

Different approaches based on the assumption of the existence of "preformed" α-particles in target nucleus, first proposed by L. Milazzo Colli et al. [86], have been reported [23,46]. Here we will describe the calculation of ref. (46) in which - by improving previous treatments based on the equiprobability assumptions - [65,66,86] the α-energy distribution is evaluated on the basis of nucleon - α scattering dynamics inside the nucleus. A similar approach - referrred to as Quasi-free scattering model - was previously considered by Blann et al. [23]. Though the basic idea underlying the two calculations and several of the assumptions introduced are the same, the two treatments differ in many aspects and - what is more important - in their quantitative conclusions. Obviously the main difference consists in the fact that while the approach by Blann et al. is a generalisation of the Hybrid model, the one here discussed constitutes a generalisation of the E M . Let us consider the case of nucleon-induced reactions. It is assumed that, in the interaction of the incident nucleon with the target nucleus, states of a simple configuration are excited. In most cases the configuration is of the 2p-1h type, but in a few cases the incident nucleon may interact with a "preformed" α-particle exciting $1N-1\alpha-1\alpha$ hole states. These initial states can decay either by particle emission or by exciton-exciton interactions (including interactions involving preformed α-particles). Both in the case of the excited residual system after a particle emission and in the case of the composite system in a more complex configuration, the competition between the two different decay modes continues. Eventually the nucleus reaches a state of statistical equi-

librium which further decays by evaporation. In evaluating the various possibilities some approximations are introduced. The most important are the following: i) at each stage of the process, states characterized by a configuration in which an excited α-particle is present are thought to represent a small minority of the total number of possible states. Then, the lifetime of the excited composite nucleus, at a given stage of the equilibration cascade, should be only slightly affected by their presence. In actual calculations the possibility of interactions of excited α's both with nucleons and preformed α's is neglected; (ii) the density of probability that the nucleus be in a configuration with an α-particle of a given energy, at each stage of the de-exciting cascade, is considered to be the one evaluated on the basis of nucleon - α scattering dynamics inside the nucleus.
In the initial configuration, this quantity is expressed as

$$P_3(E,\epsilon'_\alpha) = \frac{\phi_\alpha \lambda^+(E,\epsilon'_\alpha)}{\phi_\alpha \lambda^+_T(E) + W_{1p}(E)} \qquad (15)$$

where $\lambda^+(E,\epsilon'_\alpha)$ is the A-independent probability per unit time and unit energy that, due to the interaction with a proton (neutron) of energy, outside the nucleus, $E_i = E - B$ (B is the nucleon binding energy) a preformed α be excited in the energy interval ϵ'_α, $\epsilon'_\alpha + d\epsilon'_\alpha$ (ϵ'_α is the α-energy in excess of Fermi energy, which coincides with $(\epsilon_\alpha + B_\alpha)$ of formulae (13), (14)).
The quantity

$$\lambda^+_T(E) = \int_{\epsilon'_{\alpha min}}^{\epsilon'_{\alpha Max}} \lambda^+(E,\epsilon'_\alpha)\, d\epsilon'_\alpha \qquad (16)$$

is the total proton (neutron)- α' collision probability per unit time. $W_{1p}(E)$ is the total proton (neutron)-nucleon collision probability per unit time. $\phi_\alpha = N_\alpha / A$ is the density of α's within the nucleus in terms of nuclear density.
Since the absolute value of $W_{1p}(E)$ we used in the calculation is deduced from the analysis of experimental data and is noticeably smaller than the one evaluated on the basis of free nucleon-nucleon scattering [34], we assume that the second addendum of the denominator of expression (15) is an effective quantity which already takes into account the possible presence of preformed α's and we did not introduce the factor $(1-4\phi_\alpha)$ that otherwise would be necessary. A similar assumption is made in writing expression (23) (see later):

$$\lambda^+(E,\epsilon'_\alpha) = G(E,\epsilon'_\alpha)\, v\, \rho \qquad (17)$$

$G(E,\epsilon'_\alpha)$ is the angle integral of $\frac{d\sigma_L(\vec{P}^\alpha_f)}{d\vec{P}^\alpha_f} m_f P_f$, v the incident nucleon velocity in nuclear matter, ρ the nuclear density. The cross section $\left(d\sigma_L(\vec{P}^\alpha_f)/d\vec{P}^\alpha_f\right) d\vec{P}^\alpha_f$ is given by

$$\frac{d\sigma_L(\vec{P}^\alpha_f)}{d\vec{P}^\alpha_f} d\vec{P}^\alpha_f = \frac{m_1}{P_1} \int v_{Rel} \frac{dn(P_2)}{d\vec{P}_2} \frac{d\sigma_{CM}(\vec{k}_1, \vec{k}^\alpha_f)}{d\hat{k}^\alpha_f} d\hat{k}^\alpha_f\, d\vec{P}_2 \qquad (18)$$

here $\vec{P}^\alpha_f$ and $\vec{P}_1$ are, respectively, the final α momentum and the incident proton momentum within the nucleus in the Lab. system, which coincides, for sufficiently heavy nuclei with the C M system for proton-nucleus scattering. v_{Rel} is the relative nucleon-α velocity. $d\sigma_{CM}(\vec{k}_1, \vec{k}^\alpha_f)/d\hat{k}^\alpha_f$ is the free nucleon-α cross section in C M system of the two colliding particles and the $\vec{k}$'s are their momenta in this system.
The quantity $dn(P_2)/d\vec{P}_2$ is the momentum distribution of the preformed α's within the nucleus (normalized to one α). A detailed

description of the integration technique of (18) can be found in ref. (46). The $d\sigma_{CM}(\vec{k}_1,\vec{k}_f^{\alpha})/d\hat{k}_f^{\alpha}$ can be given in terms of $\theta = \hat{\vec{k}_1\vec{k}_f^{\alpha}} - \pi$ by

$$\frac{d\sigma_{CM}(\vec{k}_1,\vec{k}_f^{\alpha})}{d\hat{k}_f^{\alpha}} = A(\cos\theta)^{n_1} + B(1+\cos\theta)^{n_2} + C|\cos\theta|^{n_3} \qquad (19)$$

being $A \neq 0$ for $0 \leq \theta \leq \pi/2$, zero otherwise, and $C \neq 0$ for $\theta \geq \pi/2$, zero otherwise. The parameters A, B, C, n_1, n_2, n_3 are functions of the relative nucleon-α energy. Their values, at a given energy, are obtained by means of a logarithmic interpolation of values deduced, at several energies, by a best fitting of the experimental nucleon-α scattering angular distribution.

For the momentum distribution of preformed α's various expressions have been considered. The dynamics of nucleon-α scattering, due to the great mass of the α, hinders the transfer to the α particle of a great fraction of the energy at disposal. Therefore it is found that in order to reproduce quantitatively the measured yield of high energy α's it is necessary to assume that already before the interaction the α possesses a sizeable amount of energy (an amount, e.g., greater than the one foreseen by Harmonic Oscillator model, which predicts

$$\frac{dn(P)}{d\vec{P}}\,d\vec{P} \div P^{2L}\exp(-P^2/2P_L^2)\,d\vec{P} \qquad (20)$$

at least for reasonable values of L and P_L). Satisfactory results can be obtained if one utilises ad hoc α-momentum distribution like a Fermi Gas model one:

$$\frac{dn(P)}{d\vec{P}}\,d\vec{P} \div d\vec{P} \qquad (21)$$

or even better, an arbitrary distribution which greatly favours α-momenta near in modulus to the maximum available. In the calculations described from now on a distribution like

$$\frac{dn(P)}{d\vec{P}}\,d\vec{P} \div P^6\,d\vec{P} \qquad (22)$$

has been used. $P_\alpha \leq P_M = \sqrt{2m\epsilon_f^{\alpha}}$. For ϵ_f^{α}, the α Fermi energy, a value of 80 MeV, four times the value of the nucleon Fermi energy utilised in nucleon-nucleon collision probability calculations, was chosen. The integration limits in expression (16) represent the minimum and the maximum energies of the α after the nucleon-α scattering. $\epsilon'_{\alpha Max}$ is easily evaluated on the basis of energy conservation. The choice of $\epsilon'_{\alpha min}$ is somewhat arbitrary. Since an α within the nucleus is constituted by four correlated fermions, each of these after the scattering should occupy a state of energy greater than the nucleon Fermi energy ϵ_f^N. It is then to be expected (see the considerations by Blann et al. in Ref. (23) that nucleon-α scattering processes producing α-particles with energy slightly in excess of ϵ_f^{α} be strongly hindered by the Pauli principle. Since the effect of Pauli principle should disappear with increasing the α-particle energy, we arbitrarily assumed that its effect is negligible if the α final energy exceeds $\epsilon'_{\alpha min}$, while all those interactions leading to final α-states of energy smaller than $\epsilon'_{\alpha min}$ are suppressed. The arbitrariness of this procedure is temperated by the consideration that $\lambda_T^{+}(E)$ in (15) or $\lambda^{+}_{(n-2)T}(E)$ in (23) (see later) are, for reasonable values of $\epsilon'_{\alpha min}$, much smaller than $W_{1p}(E)$ or $W_{n-2\to n}(E)$. In all our calculations it was assumed $\epsilon'_{\alpha min} = B_\alpha + C_\alpha$ where B_α and C_α are, respectively, the α-binding energy and the Coulomb barrier. To evaluate $G(E,\epsilon'_\alpha)$ it has been also assumed that, after the interaction, the scattered proton momentum must exceed the Fermi momentum P_f^N. By far, and not too high incident nucleon energy, the greatest contribution to emitted α-spectra is due to the emissions from states of the initial configuration. In order to evaluate the α-energy distribution at the next stage of the equilibration cascade we introduce some simplifying assumptions. Possible improvements to the procedure here described will be indicated.

On the basis of the results of analyses of α-particle-induced reactions which seem to indicate that in most cases the incident α-particle divides into its constituents in the nuclear and Coulomb field of the struck nucleus [57] one hypothesizes that, if it is not emitted, an α does not survive. In this hypothesis, at a

given stage of the equilibration cascade, the α-energy distribution is the one which results from the interaction of one already excited nucleon with a preformed α. If we retain the usual assumption that, at the previous (n-2) exciton stage of the equilibration cascade, the density of states was the one corresponding to the partition of the excitation energy in all the possible and equiprobable ways among (p-1) excited nucleons and (h-1) nucleon holes (a good approximation in the case of nucleon-nucleon interactions [45]) and we neglect those few states in which an α was excited and divided subsequently into its constituents, the α-energy distribution in a n(=p+h) exciton configuration is given by:

$$P_m(E,\epsilon'_\alpha) = \frac{(p-1)\,\phi_\alpha\,\lambda^+_{(n-2)}(E,\epsilon'_\alpha)}{(p-1)\,\phi_\alpha\,\bar{\lambda}^+_{(n-2)T}(E) + W_{n-2\to m}(E)} \qquad (23)$$

where

$$\lambda^+_{(n-2)}(E,\epsilon'_\alpha) = \frac{1}{(p-1)\,\omega_{p-1,h-1}(E)} \int_{\epsilon'_\alpha}^{E} \omega_{p-2,h-1}(E-\epsilon'_p)\,g(\epsilon'_p)\,\lambda^+(\epsilon'_p,\epsilon'_\alpha)\,d\epsilon'_p \qquad (24)$$

$$\bar{\lambda}^+_{(n-2)T}(E) = \int_{\epsilon'_{\alpha\,min}}^{\epsilon'_{\alpha\,Max}} \lambda^+_{(n-2)}(E,\epsilon'_\alpha)\,d\epsilon'_\alpha \qquad (25)$$

and $W_{n-2\to n}(E)$ is the decay rate for exciton-exciton interaction in the (n-2) stage. ϵ'_p is the proton energy in excess of Fermi energy. It has to be explicitly noted that the assumption leading to expression (23) is a tentative one. In fact an α-particle excited at the j-th stage of the equilibration cascade, in a certain percentage of cases, could survive-without interacting with other nucleons or α-particles - for a time greater than the lifetime of the excited nucleus in the j-th configuration and could be emitted at a next stage. Since the energy distribution of the α-particles emitted in such a case is equal to the one of the α's at a previous stage, the assumption introduced tends to underestimate the yield of high energy α's; on the other hand it is counteracted by the implicit assumption - in the approach described - that the probability of α-break-up while on its way out is negligible.

The α-particle excited at a given stage could also suffer a further interaction with a nucleon or a preformed α being subsequently emitted. This effect is likely to occur in processes initiated by nucleons of sufficiently high energy. Once the energy distribution of the excited α's is known, it is an easy matter to write the expression for the decay rate for α emission:

$$W^c_\alpha(p,h,E,\epsilon_\alpha)\,d\epsilon_\alpha = P_m(E,\epsilon'_\alpha)\left(\frac{G_{inv,\alpha}(\epsilon_\alpha)\,v_\alpha\,\omega_c(\epsilon_\alpha)}{g_\alpha V}\right)d\epsilon_\alpha = \qquad (26)$$

$$= \frac{1}{\pi^2\hbar^3}\,\mu_\alpha\,\epsilon_\alpha\,\sigma_{inv,\alpha}(\epsilon_\alpha)\,\frac{P_m(E,\epsilon'_\alpha)}{g_\alpha}\,d\epsilon_\alpha$$

The decay rates for neutron and proton emission, neglecting in the evaluation of the state densities the few (p-1) nucleon-1α-(h-1) nucleon holes-1 α hole states, is approximately given by

$$W^c_{\nu(\pi)}(p,h,E,\epsilon_{\nu(\pi)})\,d\epsilon_{\nu(\pi)} = \frac{(2S+1)}{\pi^2\hbar^3}\,\mu_{\nu(\pi)}\,\epsilon_{\nu(\pi)}\,\sigma_{inv,\nu(\pi)}(\epsilon_{\nu(\pi)})\cdot \qquad (27)$$

$$\cdot\,\frac{\omega_{p-1,h}(U_R)}{\omega_{p,h}(E)}\,K_{\nu(\pi)}(p,h)\,d\epsilon_{\nu(\pi)}$$

The coefficients $K_{\nu(\pi)}(p,h)$ take into account that, both in residual and composite nucleus, a number of states can be excited which is lower than the one evaluated by counting all the possible ways of partitioning a given energy between p particles and h holes (their numerical value is tabulated in ref.(65)). The single α state density g_α was assumed to be constant and equal to $(2\pi V(2\mu_\alpha)^{3/2}\epsilon_f^{\alpha\,1/2})/h^3$, if $\epsilon_f^\alpha = 4\epsilon_f^N$, $g_\alpha = 4g$. We assumed ϵ_f^α =80 MeV and ϵ_f^N =20 MeV. Also the value of all the other parameters except ϕ_α, was fixed a priori. Their values are the ones

utilised in the extensive calculations made in recent years by our group [65]. In Ref. (46) it was shown that - by this procedure - it was possible to reproduce satisfactorily the measured intensity and energy dependence of the α-spectra (their strong similarity with nucleon spectra at low incident nucleon energy, their decreasing intensity at the increase of the projectile energy) for proton energies in the 20-45 MeV interval. A satisfactory reproduction of the spectra was achieved by using for all the considered nuclei and energies $\phi_\alpha \sim 0.19$.

However, it has to be stressed that only the ratio ϕ_α / g_α is determined by a best fit of the experimental spectra; consequently the value here quoted for ϕ_α should be modified if a different value for g_α would be chosen.

It was also shown that a variation of the Fermi energy of preformed α's, ϵ_f^α, within reasonable limits ($20 \leq \epsilon_f^\alpha \leq 80$ MeV) did not substantially modify the spectrum shape. A reasonable reproduction of spectral shape could also be obtained by employing a Fermi momentum distribution for the α's. However, in this case a value of ϕ_α / g_α greater than the one here reported would be needed.

A typical result is shown in Fig. 5.

The calculation here described was utilised also in the analysis of spectra of α - particles emitted in (p,α) reactions at higher proton energy (72 MeV) [81]. Also in this case the data were reproduced reasonably well (see Fig. 6).

For the time being, the approach described has to be considered chiefly as a method for evaluating α-emission yields utilising a completely defined set of parameters. In fact, the α-momentum distribution which was utilised lacks a physical interpretation. On the other hand it should be emphasized that the calculation discussed allows to reproduce satisfactorily - at the same time - the spectral shape, the angular distribution (see next section) and the yield of emitted α's as a function of incident nucleon energy in a rather wide incident energy ($\sim 14 \leq E \leq \sim 70$ MeV) and target mass range ($Al \leq A \leq Th$).

These agreements are a rather convincing suggestion that α-emission should really be governed by the dynamics of proton (neutron) - α scattering.

An independent estimate of the density of preformed α's could be based on the analysis of α-spectra in (α, α') reactions.

Chevarier et al. [87] found, at incident energies of 55 MeV, that the emitted α-spectrum, for nuclei with mass less than 115, presents a low energy evaporation peak followed by a flat continuous spectrum extending up to the region of low excitation energy of residual nucleus where discrete levels are selectively populated.

The heavier nucleus spectra do not exhibit the evaporative peak, or , at least, it is strongly reduced in intensity.

The continuous energy distribution of high energy α's, in this case, starting from threshold, increases in absolute value with the increase of outgoing α-energy, reaching a maximum at an α-energy near to the maximum attainable.

These general trends are confirmed by the results reported by other authors [88, 89].

A satisfactory explanation of these spectra is still lacking.

Chevenert et al. suggested that part of the spectrum could be attributed to nucleon pick-up followed by break-up of outgoing (^5He or ^5Li) particles [92].

Blann et al. [23] in the framework of Q F S model presented detailed calculations which - especially in the case of lighter nuclei - gave a poor reproduction of the data.

The harder part of calculated spectrum increases - for all considered nuclei - with the α-energy, peaking to a value near to the maximum kinetic energy of outgoing α's.

As a consequence, in the case of lighter nuclei, the superposition of the evaporative component and the Q F S spectrum originates a valley - at variance with experimental data.

In the case of Chevarier data, the valley occurs for $E_\alpha \simeq 25$ MeV and there the experimental yield is underestimated by a factor of the order of - but sometimes greater than - two [23].

The failure of these calculations, at least partially, could be due to the fact that Blann et al. considered only the possibility of interactions of the incoming α's with nucleons of target nucleus. Being the mass of the α much greater than the nucleon mass, the α preserves most of its energy. If, on the other hand, the incident α could interact with preformed α's, the energy distribution of outgoing α's would peak to a smaller energy (in the case of Chevarier data approximately 25 - 30 MeV).

A contribution of this kind of interactions to the α-spectrum would certainly help in reducing the discrepancy between experimental data and theoretical predictions.
α-induced processes are far more complicated than nucleon ones, so that one should be cautious before stating that such a suggestion is the only one which could allow to resolve the discrepancy above noted.
However, we can, at least, state that the consideration of (α,α') spectra does not seem to afford clues against the interpretation which has been given to the (nucleon - α) process.

In the case of proton-induced reactions, several calculations rest on the hypothesis that the pick-up of a triton might contribute to the highest energy portion of the α spectra.
L. Milazzo Colli et al. have noticed (in the case of double magic nuclei where their EM calculations have failed to account for the intensity and the shape of the measured spectra) the presence of a selective population of low excited states in residual nuclei. According to these authors, the α angular distributions and the individual transition intensities are satisfactorily reproduced by calculations based on the hypothesis of triton pick-up in the framework of the semi-microscopic model of Smits.[91] The hypothesis of triton pick-up is also at the basis of calculations in the framework of the multistep direct reaction approach by Tamura et al.[3] which reproduces satisfactorily the energy and the angular distribution of the high-energy part of the continuous α-spectra.

Kalbach[42] too, assumes that the pick-up of a triton can give rise to a spectrum that is continuous and structureless, whose intensity per MeV should be essentially proportional to the density of 3 hole states of the residual nucleus.
She suggests that the pick-up mechanism could effectively supply the predominant contribution to the α-spectrum in the highest energy region.

Her approach is, for the time being, founded on quite arbitrary assumptions with no attempt at theoretical justification, so that it is difficult to form an opinion on its reliability.

3. ANGULAR DISTRIBUTIONS

The calculation of the angular distribution of nucleons emitted during the pre-equilibrium phase can be carried out in a most natural way within the framework of the Intranuclear Cascade Model . The most comprehensive comparison between experimental results and model prevision - at not too high excitation energies - has been made by Bertrand et al.[27,28]
These authors analysed the spectra of protons emitted at different angles in (p,p') reactions induced on nuclei ranging from C to Bi by 39 and 62 MeV protons. Their conclusion was that the theoretical predictions compare reasonably well with the measured spectra for angles in the range 20°- 90°; serious discrepancies were noted in the very forward and the backward direction (analogous conclusions are reached by Galonsky et al.[92] after the analysis of (p,n) spectra at $25 \lesssim E_p \lesssim 45$ MeV). At very forward angles, the spectra predicted by Bertini code[24] show a quasi-elastic peak (which in the case of reactions induced by 62 MeV protons extends from ≈ 50 to ≈ 60 MeV) which is in serious conflict with experimental results. This quasi-elastic peak is removed when the effects of refraction are included. However in this case - expecially when heavy target nuclei are considered - the predicted cross section is too low.

This quasi-elastic peak arises in the calculation from a single scattering of the incident particle in the diffuse edge of the nucleus; refraction diminishes this class of events dramatically.[20]

At backward angles the predicted cross section was by far too low but it was shown that the predictions were greatly improved by allowing proton scattering from nucleon pairs - more generally clusters - within the model nucleus.
It has, however, to be noticed that also neutron spectra in (p, n) reactions are greatly underestimated at backward angles[92] and in this case it does not seem that the previous effect could eliminate the discrepancy.

The conclusions were quite distressing: because of the effect of solid angle, comparisons between calculated and experimental angle-integrated energy spectra could give a misleading impression of the overall validity of the considered model, also if marked discrepancies between predictions and experimental results exist.
It has to be honestly admitted that the same conclusion could often apply to other phenomenological models we consider in this report.

As regards the EM, the first attempt to reproduce not only the energy but also the angular distribution of the emitted fast particles is due to Weidenmüller et al.[59] Their theory has been improved by Akkermans et al. [41] in a recent article. The procedure of Weidenmüller et al. has been extended to the Hybrid model by Mantzouranis. [93]
In this theory the hypothesis is made that the configurations of the nucleus, during the de-excitation, can be characterized both by the number n of excited particles and holes and by the direction Ω that a fast particle (either the incident one retaining most of its energy or a struck one gaining a sizeable energy) has with respect to the incident direction. Then, the states of the excited nucleus are grouped into classes labelled by (n,Ω). (Herefrom the notation Ω,Ω' refers to directions in the projectile - target CM system).

The occupation probability of class (n,Ω) at time t, $P(n,\Omega,t)$ is evaluated by means of a generalized master equation

$$\frac{dP(n,\Omega,t)}{dt}=\sum_{\substack{m=n-2\\ \Delta m=2}}^{n+2}\int W_{m\to n}(E,\Omega'\to\Omega)P(m,\Omega',t)\,d\Omega' - P(n,\Omega,t)\cdot$$
$$\cdot\Big[W_c^n(E)+\sum_{m=n-2}^{n+2}\int W_{n\to m}(E,\Omega\to\Omega')\,d\Omega'\Big] \qquad (28)$$

It has to be explicitly noted that transitions with $\Delta n=0$ have to be included in (28) in contrast to the case of equation (7) since each collision contributes to the loss of correlation with the incident direction, irrespective whether the exciton number has been changed after the collision or not. [41]

It is further assumed that the decay rate corresponding to the transition from states of the class (n,Ω) to states of the class (m,Ω') can be factorized in the product of the usual decay rate to transit from an n to an m exciton configuration (adopting for this rate the William's expression, [36]) by a quantity supposed to depend only on the angle between the direction of fast particle before and after the transition:

$$W_{n\to m}(E,\Omega\to\Omega')=W_{n\to m}(E)\,G(\Omega,\Omega') \qquad (29)$$

$G(\Omega,\Omega')$ is independent of the classes m, n considered and is expressed by means of the free differential nucleon - nucleon cross - section $d\sigma/d\Omega$

$$G(\Omega,\Omega')=\frac{d\sigma}{d\Omega}(\Omega'\to\Omega)\Big/\Big[\frac{d\sigma}{d\Omega}(\Omega'\to\Omega)\,d\Omega\Big] \qquad (30)$$

Because $\frac{d\sigma}{d\Omega}$, is nearly isotropic in CM system of colliding particles, at not too high incident energies, it is assumed that:

$$\frac{d\sigma}{d\Omega}\approx\frac{d\sigma}{d\Omega_{LAB}}\frac{d\Omega_{LAB}}{d\Omega}\approx\frac{1}{\pi}\cos\theta_{LAB}\,\Theta\Big(\frac{\pi}{2}-\theta_{LAB}\Big)\frac{d\Omega_{LAB}}{d\Omega} \qquad (31)$$

where θ_{LAB} is the angle in LAB system - and Θ is the Heaviside function.
Using relations (29) and (30), equation (28) reads:

$$\frac{dP(n,\Omega,t)}{dt}=\sum_{\substack{m=n-2\\ \Delta m=2}}^{n+2}W_{m\to n}(E)\int d\Omega' G(\Omega,\Omega')P(m,\Omega',t)-$$
$$-P(n,\Omega,t)\Big[W_c^n(E)+\sum_{m=n-2}^{n+2}W_{n\to m}(E)\Big] \qquad (32)$$

Carrying out a solid angle integration the terms $\Delta n = 0$ cancel and the usual master equation (7) which holds when no account is taken of the direction of the fast particle is obtained.
Equation (32) has been solved by Weidenmüller et al. by nume-

rical methods; Akkermans et al. have shown how it can be reduced to a form similar to equation (7) of which, moreover, an analytical solution is presented.
To do that, one expands P(n,Ω,t) into a Legendre polynomial series

$$P(n,\Omega,t) = \sum_\ell \eta_\ell(n,t) P_\ell(\cos\theta) \tag{33}$$

and one demonstrates that the integral operator occurring in (32) can be diagonalized according to

$$\int d\Omega' G(\Omega,\Omega') P_\ell(\cos\theta') = \mu_\ell P_\ell(\cos\theta) \tag{34}$$

The eigenvalues μ_ℓ are given (in the approximation of an infinitely heavy nucleus) by:

$$\mu_\ell = \begin{cases} 1 & \ell = 0 \\ 2/3 & \ell = 1 \\ 0 & (\ell \text{ odd}, \ell \neq 1) \\ \dfrac{(-1)^{(\ell+2)/2}\,\ell!}{2^{\ell-1}(\ell-1)(\ell+2)\left[(\ell/2)!\right]^2} & (\ell \text{ even}) \end{cases} \tag{35}$$

Making use of relations (33), (34) and of the orthogonality of the Legendre polynomials equation (32) reduces to

$$\frac{d}{dt}\eta_\ell(n,t) = \mu_\ell \eta_\ell(n+2,t) W_{n+2\to n}(E) + \mu_\ell \eta_\ell(n-2,t) W_{n-2\to n}(E) - \eta_\ell(n,t)\left[W_{n\to n+2}(E) + W_{n\to n-2}(E) + (W_c^n(E) + (1-\mu_\ell) W_{n\to n}(E))\right] \tag{36}$$

We are thus led to a set of linear differential equations, one for each ℓ, whose form is identical to the one of equation (7).
The double-differential cross section corresponding to a process b + T → ν + R is given by:

$$\frac{d^2\sigma(b,\epsilon_\nu,\theta_\nu)}{d\Omega\, d\epsilon_\nu} = \sigma_c^b(E_i) \sum_{\substack{n=n_0 \\ \Delta n=+2}}^{\bar{n}} W_c^{n,\nu}(E,\epsilon_\nu)\, \tau(n,\Omega) \tag{37}$$

where

$$\tau(n,\Omega) = \int_0^\infty P(n,\Omega,t)\, dt \tag{38}$$

Also $\tau(n,\Omega)$ can be expanded into a Legendre polynomial series

$$\tau(n,\Omega) = \sum_\ell \xi_\ell(n) P_\ell(\cos\theta) \tag{39}$$

Akkermans et al. have been able to present an explicit expression for $\xi_\ell(n)$:

$$\xi_\ell(n) = \eta_\ell(n_0,t=0)(\mu_\ell)^{\frac{n-n_0}{2}} T_\ell(n) h_\ell(n) \cdot \left(\prod_{\substack{m=n_0 \\ \Delta m=2}}^{n-2} W_{m\to m+2}(E) T_\ell(m) \cdot h_\ell(m)\right)\left\{1 + \sum_{\substack{s=n+2 \\ \Delta s=2}}^{\bar{n}} \left[\prod_{\substack{K=n \\ \Delta K=2}}^{s-2} \mu_\ell^2 W_{K\to K+2}(E) T_\ell(K) h_\ell(K) W_{K+2\to K}(E) T_\ell(K+2) h_\ell(K+2)\right]\right\} \tag{40}$$

where

$$T_\ell(n) = \left[W_{n\to n+2}(E) + W_{n\to n-2}(E) + W_c^n(E) + (1-\mu_\ell) W_{n\to n}(E)\right]^{-1} \tag{41}$$

$$h_\ell(n) = \left[1 - \mu_\ell^2 W_{n-2\to n}(E) T_\ell(n-2) W_{n\to n-2}(E) T_\ell(n) h_\ell(n-2)\right]^{-1} \tag{42}$$

The first product within parenthesis in equation (40) represents a depletion factor (it must be replaced by unity if $n = n_0$). The second term within parenthesis keeps track of the many possible paths to reach the n - th exciton state, due to the inclusion of both $n \to n$ and $n \to n-2$ transitions.
A much more detailed discussion of the procedure can be found in the original papers by Akkermans et al. [41]

To solve equations (32) or (36), the initial condition is given as

$$P(n,\Omega,t=0) = \delta_{n,n_0} \frac{\cos\theta_{LAB}}{\pi} H\left(\frac{\pi}{2} - \theta_{LAB}\right) \frac{d\Omega_{LAB}}{d\Omega} \qquad (43)$$

or

$$\eta_\ell(n,t=0) = \delta_{n,n_0} \frac{(2\ell+1)M\ell}{4\pi} \qquad (44)$$

The higher order contributions to expansion (39) fastly decrease with respect to the isotropic part even for low n, so that in most of the cases it will be sufficient to consider only a few Legendre polynomials.

The above described theory has been applied in the analysis of (p,n) and (n,n') reactions. It has been found that in several instances a reasonably good agreement is obtained at forward angles but the angular distribution is underpredicted at the backward angles. Akkermans et al. [41] found, analysing the angular distributions of neutrons emitted in (n,n') reactions measured by Hermsdorf et al. [10] on nuclei ranging from Be to Bi at E_n = 14.6 MeV, that a much more satisfactory fit to experimental results could be obtained by multiplying the theoretical coefficients for ℓ = 1 and ℓ = 2 Legendre polynomials by, respectively, 0.87 and 1.74. Though this result can prove to be useful in calculations for practical purposes like fusion reactor design, no theoretical justification for it has been suggested.

The theory has been also applied in the analysis of (α,p) reactions [59] though, in this case, further assumptions have to be introduced.
A generalisation to the case of (p, complex particle) reactions has been discussed by Machner. [94]

The assumptions on which the whole treatment is based are attractive on account of their simplicity, however it has to be remarked that some of them are not devoid of arbitrariness and cannot be justified on the basis of calculations relying upon the nucleon - nucleon scattering inside the nucleus.
Of these, one of the most criticizable is assumption (29). It leads to the quite unphysical consequence (see expression (37)) that, according to this theory, the angular distribution of the particles emitted from states of a given class turns out to be independent of their energy, while one would expect that the more energetic a particle is, the more it should retain the memory of the direction of the incident particle. In itself the concept of fast particle - expecially at not toohigh energies of outgoing particles and not toolow n - is a quite drastic schematism.
Moreover, effects that are relevant expecially when the energies involved are not very high, like the refraction of the wave associated to the incident and to the emitted particle, when it enters and leaves the nucleus, or the Fermi motion of the struck nucleon, are neglected.

It has also been suggested that the angular distribution of particles emitted in (p,p'), (p,n), (p,α) reactions could be evaluated by utilising closed-form expressions like (11) and by substituting - in the expression of the decay rate for particle emission (see expression (4)) - the product of the number of particles of type ν times the density of probability that a particle of a given configuration has a given momentum (i.e. a given energy and direction of motion), $P_{p,h}(\epsilon_\nu + B_\nu, \Omega_\nu)$, for the quantity $P_{p,h}(\epsilon_\nu + B_\nu)$ previously defined.
Restricting ourselves to nucleon and α-particle emission and assuming that the α pre-exists in target nucleus, $P_{p,h}(\epsilon_\nu + B_\nu, \Omega_\nu)$ can be evaluated starting from nucleon - nucleon or nucleon - α interactions inside the nucleus. [45,62,81]

In practice the calculation of $P_{p,h}(\epsilon_\nu + B_\nu, \Omega_\nu)$ is feasible for states of the initial configuration but becomes immediately complicated as soon as subsequent configurations are considered, unless the approximation of the fast particle is adopted.

Therefore we will limit ourselves to the case of emissions from the first configuration and thus to the angular distribution of the highest energy particles.

Let us consider explicitly the case of (nucleon, α) reactions in order to utilise some formulae already discussed (the result concerning (nucleon, nucleon) reactions is obtained by a straight forward modification of the formulae here considered).

In this case, if Ω_α is the direction of the struck α-particle after collision, with respect to the direction of the nucleon before the collision,

$$P_{2,1}(E,\epsilon_\alpha+B_\alpha,\Omega_\alpha)=\frac{\phi_\alpha v \rho \frac{d\sigma_L(\vec{p}_f^{\,\alpha})}{d\vec{p}_f^{\,\alpha}} m_f p_f}{\phi_\alpha \lambda_T^+(E)+W_{1p}(E)} \qquad (45)$$

$$W_c^{3,\alpha}(E,\epsilon_\alpha,\Omega_\alpha)d\epsilon_\alpha d\Omega_\alpha=\frac{1}{\pi^2\hbar^3} p_\alpha \epsilon_\alpha \sigma_{inv,\alpha}(\epsilon_\alpha)\frac{P_{2,1}(E,\epsilon_\alpha+B_\alpha,\Omega_\alpha)}{g_\alpha} \cdot d\epsilon_\alpha d\Omega_\alpha \qquad (46)$$

and

$$\frac{d^2\sigma(b,\epsilon_\alpha,\Omega_\alpha)}{d\epsilon_\alpha d\Omega_\alpha}=\sigma_c^b(E_i)\frac{W_c^{3,\alpha}(E,\epsilon_\alpha,\Omega_\alpha)}{W_c^3(E)+W_{3\to5}(E)} \qquad (47)$$

If the incident and outgoing particle energies are not too high $d^2\sigma/d\epsilon d\Omega$, as given by (47), is not directly comparable to the experimental cross section due to refraction effects.

These effects which always lead to a smoothing of the angular distributions evaluated according (47) can be computed in a classical way assuming that the target nucleus - assumed as infinitely heavy - acts on the incoming or outgoing particle as a potential well of depth V_o. (95)

Incoming particles:

a) neutrons

The refracted particles are always in the plane defined by the incident direction and the centre of the nucleus (see fig. 7a). Due to axial symmetry one needs only to consider what occurs in a given plane.

The angle θ between the direction of the refracted and incident particle is given by

$$\theta=\hat{i}-\hat{r} \qquad (48)$$

Assuming that the tangential component of the particle momentum is unchanged-as the particle enters the nucleus - the relation holds

$$\frac{\sin\hat{i}}{\sin\hat{r}}=\sqrt{\frac{E_i+V_o}{E_i}}=n \qquad (49)$$

being E_i the incident particle energy and n the refraction index; $\hat{i}$ is related to the impact parameter q by the relation

$$\sin\hat{i}=\frac{q}{R} \qquad (50)$$

where R is the nuclear radius.

By means of (48),(49),(50) it is then possible to establish a relation connecting q to θ :

$$q^2=\frac{R^2n^2\sin^2\theta}{n^2-2n\cos\theta+1} \qquad (51)$$

Now the probability $P_R(\theta)$ that the incident neutron be refracted at an angle θ is easily calculated

$$P_R(\theta)2\pi\sin\theta d\theta=P(q)dq=\frac{2\pi q\,dq}{\pi R^2} \qquad (52)$$

$$P_R(\theta) = \frac{q}{\pi R^2} \frac{1}{\sin\theta} \frac{dq}{d\theta} \qquad (53)$$

and using relation (51) one obtains

$$P_R(\theta) = \frac{n^2}{\pi} \frac{[(n^2+1)\cos\theta - n(\cos^2\theta+1)]}{(n^2-2n\cos\theta+1)^2} \qquad (54)$$

b) Charged particles

In this case (see fig. 7b)

$$\theta = \eta - \hat{r} \qquad (55)$$

The trajectory of the incident particle is a branch of hyperbola - being the particle - nucleus force a repulsive Coulomb force - and the equations of an hyperbola in polar coordinates - if the origin is in the focus (the center of the nucleus) and φ is the angle between the polar vector ρ and the incidence direction (one asymptote of the hyperbola) - is given by

$$\rho = \frac{A}{-1+\epsilon\cos(\varphi-\gamma)} \qquad (56)$$

being $A = mc^2/K$; $c = \sqrt{\ell(\ell+1)}\hbar/m = \sqrt{2mE_i}\, q/m$; $K = ZZ_T e^2$; m the mass of the projectile; Z and Z_T the projectile and target nucleus charge in terms of elementary charge e ; ϵ is the eccentricity $\left(\epsilon = \sqrt{(2mc^2E_i + K^2)}/K\right)$ and $\gamma = \arccos(1/\epsilon)$.
Then $\eta = \arccos\varphi < \gamma$ is one of the two solutions of the equation which is obtained from (56) putting $\rho = R$, the nuclear radius,:

$$\sin\eta = -\frac{1}{\epsilon}\sqrt{1-\left(\frac{A+R}{R\epsilon}\right)^2} + \frac{A+R}{R\epsilon}\sqrt{1-\frac{1}{\epsilon^2}} \qquad (57)$$

Also in this case we assume that the tangential component of the particle momentum is conserved.

Then

$$\frac{P_T^{(t)}}{P_N^{(t)}} = \frac{P_T^{(i)}}{P_N^{(t)}} = tg\,\hat{r} \qquad (58)$$

being $P_T^{(i)}$ and $P_T^{(t)}$ the tangential component of the particle momentum before and after the refraction and $P_N^{(t)}$ the normal component of the refracted particle momentum.
Due to angular momentum conservation:

$$P_T^{(i)} R = P_T^{(t)} R = P_\infty\, q = \sqrt{2mE_i}\, q \qquad (59)$$

where P_∞ is the incident particle momentum at infinite distance.

$$P_N^{(t)} = \sqrt{P^{(t)2} - P_T^{(t)2}} = \sqrt{2m(E_i - C + V_0) - 2mE_i q^2/R^2} \qquad (60)$$

where C is the Coulomb barrier. Using (59) and (60), (58) can be written

$$\frac{q}{\sqrt{(1+\frac{V_0-C}{E_i})R^2 - q^2}} = tg\,\hat{r} \qquad (61)$$

By means of relations (57) and (61) , relation (55) - once the incident energy E_i is known - relates the deflection angle θ to the impact parameter q.

The maximum value of the impact parameter q_{Max} is the one corresponding to a grazing trajectory.
Then

$$q_{Max}\, P_\infty = R\, P^{(i)} = R\sqrt{2m(E_i - C)}$$

or

$$q_{Max} = R\sqrt{1 - \frac{C}{E_i}} \qquad (62)$$

It can be shown that - depending on the value of the various parameters entering (55) - while q varies from 0 to q_{Max}, θ can assume positive and negative values and a same value of θ can correspond to two different values of q. Due to axial simmetry we are simply interested in the modulus of θ.
Now

$$P_R(\theta) = \sum_i \frac{q_i}{\pi q_{Max}^2} \frac{1}{|\sin\theta|} \left|\frac{dq_i}{d\theta}\right| \qquad (63)$$

where q_i are the different values of the impact parameter leading to the same θ or to the same modulus of θ. $P_R(\theta)$ is -in this case- computed numerically by means of relations (55), (57), (61).

Outgoing particles.

To evaluate the refraction of particles leaving the nucleus, one has to note that - due to the reversibility of the optical path- the probability that the direction of a particle be changed by an angle θ approaching and entering the nucleus is equal to the one that the direction of the same particle be changed by the same angle when it reverses its path, i.e., leaves the nucleus and gets away.
For this reason the formulae already discussed apply.
The calculation is, however, more time consuming because the particles leaving the nucleus have a broad energy distribution instead of a fixed energy.
Finally, double differential cross section of α particles emitted in the (nucleon, α) process is given by

$$\frac{d^2\sigma(b,\epsilon_\alpha,\Omega_\alpha)}{d\epsilon_\alpha d\Omega_\alpha} = \frac{\sigma_c^b(E_i)}{W_c^3(E)+W_{3\to5}(E)} \iint P_R^b(\Omega'') W_c^{3,\alpha}(E,\epsilon_\alpha,\Omega''\to\Omega'_\alpha) P_R^\alpha(\epsilon_\alpha,\Omega'_\alpha\to\Omega_\alpha) \cdot d\Omega'' d\Omega'_\alpha \qquad (64)$$

In figs (8) and (9) the experimental angular distributions of α-particles emitted in the reactions ^{149}Sm (n,α) ^{146}Nd at E_n = 14.1 MeV and ^{165}Ho (p,α) ^{162}Dy at proton energies varying from ∿ 26 to ∿ 44 MeV are compared to the theoretical prediction. The same parameters and the same momentum distribution for the preformed α particles which have been utilised in calculations discussed in the previous Section have been used.

The agreement is satisfactory. Equally satisfactory agreement between experimental data and theoretical predictions has been obtained in the analysis of (p,α) reactions at $E_p \cong 70$ MeV.[81] These results add our confidence in the substantial correctness of the hypothesis that the emitted α's were preformed in the nucleus, and in the theoretical calculation described in previous Section.
In fact, it has to be noted that, in all the considered cases, the modulus of the incident nucleon momentum inside the nucleus was considerably smaller than the one of the struck α (from 3 to 2 times smaller).
Though one can qualitatively understand that the fact that the α-particle cannot lose energy in the collision and the increase of (nucleon - α) cross section at the lowering of relative nucleon - α energy favours the interaction of nucleons and α's having the same direction of motion, and thus the emission of α's in the forward direction, the quality of the agreement between experimental data and theoretical predictions is gratifying.

Examples of comparison of experimental data and theoretical results in the case of (p,p') reactions can be found in ref. (62). It has been noted that also in this case the calculation underestimates the emission at backward angles. It has been suggested that an increased emission at these angles could be obtained by allowing for the reflection of the outgoing particle at the nuclear boundary.

We have not discussed calculations of angular distributions in pre-equilibrium processes based (i) on the non-equilibrium statistical operator formalism of Zubarev and (ii) the use of state densities which depend on the total linear momentum of the exciton gas, re-

cently reported by Mädler et al. [98] These calculations presumably will be discussed by Prof. Seeliger in his lectures.

4. ANALYSIS OF PRE-EQUILIBRIUM PROCESSES IN NEUTRON-INDUCED REACTIONS.

We will briefly summarize the main conclusions reached in the analysis of fast neutron-induced reactions. No attempt will be made to present an exhaustive survey, and several papers published on the subject will not be cited.

On the other hand we believe that the most significant conclusions will be reported.

Values of $|M|^2$ deduced by various authors will be compared. In order to reduce as much as possible differences in absolute values of this quantity due to a different choice of the single particle level density, g, all the values we quote correspond - if it is not otherwise stated - to $g = \frac{A}{13.16}$ MeV^{-1}.

(n,n') reactions.

Time-of-flight measurements of (n,n') reaction cross sections have been reported by several Labs. As an example, we quote the results by Dresden group, which measured the differential inelastic scattering cross sections for 14.6 MeV neutrons on more than thirty elements ranging from Be to Bi [10].

Extensive analysis of these data have been later reported by Hermsdorf et al. [40] and Akkermans et al. [41]
The analysis of these data indicates that, at energies exceeding ≈ 6 MeV, the secondary neutron spectrum is fed almost completely by pre-equilibrium emissions.
The influence of pre-equilibrium emissions is not negligible also at lower energies. Hermsdorf et al. showed that the level density parameter a obtained from the analysis of neutron spectra in a narrow excitation energy range centered around ≈ 10.5 MeV (ϵ_n ≈ 3.6 - 4.6 MeV), without subtraction of the pre-equilibrium contribution, was greatly underestimated (often by a factor of two).
These authors found that the energy distribution of neutrons emitted during the pre-equilibrium phase (whose energy integrated cross section was found to vary with A according to the law $\sigma_{n,n'} \approx (130 \pm 30)A^{1/3}$mb) was satisfactorily reproduced in shape and absolute value by a calculation based on a simplified version of equation (11).
The analysis of the highest energy tail of neutron spectra gave for the square of the two-body residual interaction matrix element, $|M|^2$, the value (537 ± 60 MeV^3) A^{-3} E^{-1}.
These data have been recently re-analysed by Akkermans et al., who utilised the more approximate theory we discussed in Section 3. These authors obtained a good reproduction of integrated spectra using for $|M|^2$ the noticeably smaller value (181 MeV^3) A^{-3} E^{-1}.

It is not easy to understand - from a quantitative point of view - the reason for such a marked discrepancy which cannot be entirely due to the approximations on which the Hermsdorf treatment is based (these authors assumed that the main contribution to high-energy tail of the spectrum is due to emission from states of the initial n = 3 configuration and neglected $w_{3\to3}$ and $w_{3\to1}$ decay rates in comparison to $w_{3\to5}$ and w_c^3).
Akkermans et al. analysed also double-differential spectra with notably less satisfactory results (for a discussion of their results we refer to Section 3).

(n,p) reactions.

Accurate determinations of cross sections of (n,p) reactions at ≈ 14 MeV are of great importance in fusion reactor technology studies. Data prior 1969 have been collected by Csikai et al. [99] ; from that time on several other measurements have been reported (see refs. (39), (100) and references therein).
In the case of A > 100 target nuclei, the (n,p) cross sections cannot be accounted for by calculations based on the statisti-

cal model. The calculated cross sections are smaller than experimental ones by a factor varying from 10 to 10^3 at the increase of target nucleus mass. [101]

A comprehensive analysis, in the framework of Exciton Model, of data existing in literature up to 1972 has been pubblished by Braga Marcazzan et al.[39] who utilised an approximate version of relation (11) (the depletion factor was taken to be equal to unity, w_c^n was neglected in comparison to $w_{3\to5}$, for $w_{3\to5}$ the expression calculated using the first-order perturbation theory expression was utilised).

These authors were able to reproduce the data with an accuracy comparable to the experimental one (cross section measured in two or more different experiments often differed by a factor of two or even more) using for the square of the matrix element for residual two-body interactions the value $|M|^2 \approx (485\ \mathrm{MeV}^3)\ A^{-3}\ E^{-1}$ in a notable accord with the value found by Hermsdorf et al. [40] in their analysis of (n,n') reactions.

Since 1972 a number of new results, characterized by a greater accuracy, have appeared. A new evaluation utilising these new data would be worthwhile.

(n,α) reactions.

As in the case of (n,p) reactions, the statistical model predictions of the cross sections of (n,α) reactions induced by ∿ 14 MeV neutrons on heavy nuclei are an order of magnitude, or more, smaller than the experimental ones.
In addition the predicted energy distribution of emitted α's is too soft, at variance with the experimental results.

Analyses by L. Milazzo Colli et al. [101], Čaplar et al.,[102] Głowacka et al. [103] show that the exciton model allows one to reproduce satisfactorily the measured α particle energy distribution if one assumes that an α preformed in target nucleus has been knocked on by the incident neutron. In these calculations the further assumption is introduced that the energy distribution of the α is the one resulting from the statistical partition of the excitation energy among the neutron, the α and the α-hole assuming as equiprobable all the possible states.

Recently, as discussed in Section 2, detailed calculations of α-energy distributions resulting from the dynamics of nucleon - α scattering inside the nucleus have been reported. Analyses of (p,α) reactions - at energies varying from ≈ 20 to 70 MeV - based on the mentioned approach have been pubblished, but, at our knowledge, this theory has not been extensively applied in the analysis of (n,α) reactions. Nevertheless the few comparisons made up to now between experimental data and calculations based on this approach show a remarkable accord.
To give an example, in fig.(10) the experimental energy distribution of α's emitted in the reaction ^{149}Sm (n,α)^{146}Nd at En ∿ 14.1 MeV is compared to the one calculated according to the theory discussed in detail in Section 2; the comparison between experimental and calculated angular distributions has been already shown in fig.(8).

Comparison between (n,α) spectra and calculations based on the Quasi Free Scattering model have been published by Głowacka et al. [103]

A detailed analysis of the existing (n,α) data using such improved calculations in order to deduce the best fit parameters could be useful.

(n,xnyp) reactions.

A great number of experimental results concerning (n,xn) reactions have been recently published (see as an example refs. (13), (104)-(106)).
Cindro and Holub [107] and K. Seidel et al.[108] by analysing the angle and energy-integrated cross sections of (n,2n) reactions at En ≈ 14-15 MeV have shown that the calculated cross sections are systematically higher than the experimental ones. Cindro et al. have carefully investigated the influence of the level density parameter and neutron cross sections on the cal

culations and analysed (n,2n) cross sections for about 80 nuclei ranging from A = 45 to 209 at neutron energies which satisfy the condition $E_n + Q_{n,2n} = (6 \pm 1)$ MeV ($E_n \sim 14$-15 MeV), using a single set of input parameters.

The calculated cross sections were found - on the average - ≈ 10% greater than the measured ones.
This discrepancy was removed taking into account the possibility that the first neutron is emitted in a pre-equilibrium process. If this happens, the first neutron spectrum becomes harder and the probability of further neutron emissions decreases.
Recently Holub and Cindro [43] analysed the excitation functions of (n,2n) and (n,3n) reactions at neutron energies varying from ∼ 4 to 24 MeV on 12 nuclei ranging from A ≈ 45 to 209, using the Exciton Model.

They used for the $w_{3\to5}$ decay rate the first order perturbation theory expression and found (employing for the single particle level density parameter the values suggested by Gilbert and Cameron [109]) $|M|^2 \approx (700\ \mathrm{MeV}^3)$.

Calculations of the same kind [108] predict cross sections for the (n, n p) + (n, p n) reaction greater than the ones estimated on the basis of the statistical model.
In fact during the pre-equilibrium stage the proton emission competes much more favorably with neutron emission than during the evaporation stage, thus increasing the probability of occurrence of (n, n p) + (n, p n) reactions.

It has to be explicitly noted that second chance pre-equilibrium emissions give a noticeable contribution to the cross sections of these reactions.

References

1 - H.Feshbach, Rev. Mod. Phys. 46 (1974) 1; Proc. of the International Conference on Nuclear Reactions at Munich, vol. II, North Holland Publ. Co. (Amsterdam) 1973; Proc. of the International Conference on Nuclear Reaction Mechanisms, Varenna, Italy, Clued (Milano) 1977; Fizika 11 (1979) 37.

2 - A. De Rosa, G. Inglima, E. Perillo, E. Rosato, M. Sandoli, R. Bonetti, L. Milazzo Colli, Proc. of the International Conference on Nuclear Reaction Mechanisms, Varenna, Italy, Clued (Milano) 1977; J. Phys. G. 4 (1978) L 21

3 - T. Tamura et al., Phys. Lett. B66 (1977) 109; B71 (1977) 273; B78 (1978) 189; Phys. Rev. Lett. 41 (1978) 1770

4 - G. Bertsch, Proc. of the Int. Workshop on Reaction Models for Continuous Spectra of Light Particles, Bad Honnef, Institut für Strahlen - und Kernphysik der Universität Bonn, 1978.

5 - Report BNL-NCS-50681, 1977, unpublished

6 - U. Klein, G. Büche, W. Kluge, H. Matthäy and G. Mechtersheimer, Nucl. Phys. to be published

7 - V. Verbinski and W. R. Burrus, Phys. Rev. 177 (1969) 1671

8 - C.K. Garret and A. L. Turkevich, Phys. Rev. C8 (1973) 594

9 - J.R. Wu C.C.Chang and H.D. Holmgren, Phys. Rev. C19 (1979) 659

10 - D. Hermsdorf, A. Meister, S. Sassonov, D. Seeliger, K.Seidel and F. Shahin, Report ZfK-277, Zentralinstitut für Kernforschung, Rossendorf bei Dresden, 1977, unpublished.

11 - S.M. Grimes et al., Phys. Rev. C3 (1971) 645; C4 (1971) 607; C5 (1973) 1770; C7 (1973) 343

12 - M. Blann, R.R. Doering, A. Galonsky, D.M. Patterson, Nucl. Phys. A257 (1976) 15

13 - V. Schröder, W. Scobel, L. Wilde and M. Bormann, Z. Physik A287 (1978) 353

14 - M.V. Kantelo and J.J. Hogan, Phys. Rev. C13 (1976) 1095; C14 (1976) 64.

15 - M. Sadler et al., Phys. Rev. Lett. 38 (1977) 950

16 - H.S. Pruys et al., Nucl. Phys. A316 (1979) 365

17 - R. Legrain, Thesis, Université Paris VII, unpublished

18 - H. Ejiri et al., Nucl. Phys. A305 (1978) 167

19 - J. Frehaut and G. Mosinski, Rapport CEA-R-4627, Service de documentation, C.E.N. Saclay, 1974, unpublished

20 - J.M. Miller, Proc. of the International Conference on Nuclear Reactions at Munich, vol.II, North Holland Publ.Co. (Amsterdam) 1973

21 - E. Gadioli, Nukleonika 21 (1976) 385;
E. Gadioli, E. Gadioli Erba, L. Sajo Bohus and G. Tagliaferri, Nuovo Cim. Riv. 6 (1976) 1

22 - M. Blann, Ann. Rev. Nucl. Science, vol.25, 1975, E. Segrè, Edt.

23 - A. Mignerey et al., Nucl. Phys. A273 (1976) 125; W. Scobel et al., Nucl. Phys. A287 (1977) 301

24 - K. Chen et al., Phys. Rev. 166 (1968) 949

25 - K. Chen, G. Friedlander and J.M. Miller, Phys. Rev. 176 (1968) 1208

26 - K. Chen, G. Friedlander, G.D. Harp and J.M. Miller, Phys. Rev. C4 (1971) 2234

27 - F.E. Bertrand and R.W. Peelle, Phys. Rev. C8 (1973) 1045

28 - H.W. Bertini, G.D. Harp and F.E. Bertrand, Phys. Rev. C10 (1974) 2472

29 - H.W. Bertini, Phys. Rev. C5, (1972) 2118; C6 (1972) 631

30 - J.J. Hogan et al., Nuovo Cim. Lett. 23 (1978) 89;
23 (1978) 528

31 - J. Ginocchio, Private communication

32 - V.S. Barashenkov, K.K. Gudima and V.D. Toneev, Acta Phys. Pol. 36 (1969) 415

33 - A.S. Iljinov et al., Nucl. Phys. A268 (1976) 513

34 - E. Gadioli, E. Gadioli Erba and P.G. Sona, Nucl. Phys. A217 (1973) 589

35 - J.J. Griffin, Phys. Rev. Lett. 17 (1966) 478

36 - F.C. Williams jr., Phys. Lett. B31 (1970) 184

37 - I. Ribansky, P. Oblozinsky and E. Betak, Nucl. Phys. A205 (1973) 545; A226 (1974) 347

38 - C. Kalbach - Cline, Nucl. Phys. A210 (1973) 590

39 - G.M. Braga Marcazzan, E. Gadioli Erba, L. Milazzo Colli and P.G. Sona, Phys. Rev. C6 (1972) 1398

40 - D. Hermsdorf, A. Meister, S. Sassonov, D. Seeliger and K. Seidel, Nuclear Theory in Neutron Data Evaluation, vol. II, Technical Document IAEA-190, 1976

41 - J.M. Akkermans, H. Gruppelaar and G. Reffo, Submitted to Phys. Rev. C;
J.M. Akkermans, Phys. Lett. B82 (1979)20; Z.Physik A292 (1979) 57

42 - C. Kalbach, Z. Physik A283 (1977) 401

43 - E. Holub and N. Cindro, Proc. 2nd Int. Symp. on Neutron Induced Reactions, Smolenice (ČSSR), 1979, Fizika 11 (1979) 43

44 - E. Betak and J. Dobes, Z. Physik A279 (1976) 319

45 - E. Gadioli, E. Gadioli Erba and G. Tagliaferri, Proc. of the Int. Conference on Nuclear Reaction Mechanisms, Varenna, Italy, Clued (Milano), 1977

46 - A. Ferrero et al., Physik A293 (1979) 123

47 - J. Ernst and J. Rama Rao, Z. Physik A281 (1977) 129

48 - C.K. Cline and M. Blann, Nucl. Phys. A172 (1969) 225

49 - C. Kalbach-Cline , Nucl. Phys. A193 (1972) 417

50 - D. Agassi, H.A. Weidenmüller, Phys. Lett. B56 (1975) 305;

51 - D. Agassi, H.A. Weidenmüller and G. Mantzouranis, Phys. Reports C22 (1975) 147

52 - M. Blann, Phys. Rev. Lett. 21 (1968) 1357

53 - M. Blann and F.M. Lanzafame, Nucl. Phys. A142 (1970) 559

54 - E. Gadioli, Lett. Nuovo Cimento 3 (1972) 515

55 - C. Birattari et al., Nucl. Phys. A201 (1973) 579

56 - C. Birattari et al., Nuovo Cim. Lett. 7 (1973) 101

57 - E. Gadioli and E. Gadioli Erba, Acta Phys. Slov. 25 (1975) 126

58 - E. Betak and J. Dobes, Proc. 2nd Int. Symp. on Neutron Induced Reactions, Smolenice (ČSSR), 1979

59 - G. Mantzouranis, H.A. Weidenmüller and D. Agassi, Z. Physik A276 (1976) 145

60 - K.K. Gudima, G.A. Ososkov and V.D. Toneev, Yad. Fiz. 21 (1975) 260

61 - E. Betak and J. Dobes, Acta Phys. Slov. 29 (1979) 76

62 - E. Gadioli, E. Gadioli Erba and G. Tagliaferri, Proc. of the Int. Conference on Nuclear Reaction Mechanisms, Varenna, Italy, Clued (Milano), to appear,1979.

63 - M. Blann, Phys. Rev. C17 (1978) 1871

64 - E. Gadioli, E. Gadioli Erba and G. Tagliaferri, Phys. Rev. C17 (1978) 2238

65 - E. Gadioli, E. Gadioli Erba and J.J. Hogan, Phys. Rev. C16 (1977) 1404

66 - E. Gadioli, E. Gadioli Erba and J.J. Hogan, Nuovo Cim. A40 (1977) 383

67 - J.J. Hogan, E. Gadioli, E. Gadioli Erba and C. Chung, Phys. Rev. C20 (1979) 1831

68 - I. Dostrovsky, Z. Fraenkel and G. Friedlander, Phys. Rev. 116 (1959) 683

69 - E. Gadioli, E. Gadioli Erba and G. Tagliaferri, Phys. Rev. C 17 (1978) 1294

70 - M. Blann, Phys. Rev. Lett. 28 (1972) 757

71 - M. Blann, Nucl. Phys. A213 (1973) 570

72 - W. Scobel et al., Proc. of the Int. Workshop on Reaction Models for Continuous Spectra of Light Particles, Bad Honnef, Institut für Strahlen - und Kernphysik der Universität Bonn, 1978

73 - E. Gadioli, E. Gadioli Erba and G. Tagliaferri, Phys. Rev. C14 (1976) 573

74 - B.L. Cohen et al., Phys. Rev. C7 (1973) 331

75 - R. Michel, H. Weigel and W. Herr, Z. Physik A286 (1978) 393

76 - C.J. Orth et al., Phys. Rev. C18 (1978) 1426

77 - E.B. Paul and R.L. Clarke, Can. J. Phys. 31 (1952) 267

78 - U. Facchini et al., Nucl. Phys. 51 (1964) 460

79 - J.R. Wu, C.C. Chang and H.D. Holmgren, University of Maryland Report, NSF-3-78, unpublished

80 - E. Gadioli, I. Iori, N. Molho and L. Zetta, Phys. Rev. C4 (1971) 1412, Report INFN/BE 73/5 (1973), unpublished

81 - R. Wagner et al., Proc. of the Int. Conference on Nuclear Reactions Mechanisms, Varenna, Italy, Clued (Milano), to appear,1979.

82 - I. Ribansky and P. Oblozinsky, Phys. Lett. B45 (1973) 318

83 - J.R. Wu and C.C. Chang, Phys. Rev. C17 (1978) 1540

84 - A. Ferrero et al., Proc. of the XVII Int. Winter Meeting on Nuclear Physics, Bormio, Italy, Ed. I. Iori, Istituto di Fisica, Università di Milano, 1979.

85 - C. Kalbach, Phys. Rev. C19 (1979) 1547

86 - L. Milazzo Colli and G.M. Braga Marcazzan, Phys. Lett. B38 (1972) 155; Nucl. Phys. A210 (1973) 297; Nuovo Cim. Riv. 3 (1973) 535

87 - N. Chevarier, Thesis, C. Barnard University, Lyon, France, 1973

88 - G. Chevenert, Ph. D. Thesis, University of Washington,1969, unpublished

89 - J. Bisplinghoff, Ph.D. Thesis, University of Bonn, 1974, unpublished.

90 - G. Chevenert et al., Phys. Rev. Lett. 27 (1971) 434

91 - R. Bonetti et al., J. Phys. G : Nucl. Phys., 4 (1978) 1903

92 - A. Galonsky, R.R. Doering, D.M. Patterson and H.W. Bertini, Phys. Rev. C14 (1976) 748

93 - G. Mantzouranis, Phys. Lett. B63 (1976) 25

94 - H. Machner, Phys. Lett. B86 (1979) 129

95 - E. Gadioli and E. Gadioli Erba, to be published

96 - L. Głowacka, et al., Nucl. Phys. A329 (1979) 215; Proc. of the Int. Conference on Nuclear Reaction Mechanisms, Varenna, Italy, Clued (Milano) to appear,1979.

97 - A. Ferrero, I. Iori, N. Molho and L. Zetta, Report INFN/BE 78/6 (1978), unpublished

98 - P. Mädler and R. Reif, Proc. 2nd Int. Symp. on Neutron-Induced Reactions, Smolenice (ČSSR), 1979

99 - J. Csikai, M. Buczko, Z. Bödy and A. Demény, At. Energy Rev. 7 (1969) 93

100 - N.I. Molla and S.M. Qaim, Nucl. Phys. A283 (1977) 269

101 - L. Colli Milazzo and M.G. Braga Marcazzan, Phys. Lett. B36 (1971) 447

102 - R. Čaplar and P. Kulisic, Proc. of the Int. Conference on Nuclear Reactions at Munich, vol. I, North Holland Publ. Co. (Amsterdam), 1973

103 - L. Głowacka et al.,Munich Conference, vol. I, 1973; Nucl. Phys. A244 (1975) 117; A284 (1977) 257

104 - B.P. Bayhurst et al., Phys. Rev. C12 (1975) 451

105 - W. Augustyniak, M. Herman, A. Marcinkowski and B. Zwieglinski, Nucl. Phys. A285 (1977) 145

106 - J. Frehaut and G.M. Mosinski, Proc. of the Vth Int. Symposium on the Interactions of Fast Neutrons with Nuclei, Gaussig, 1975, Report ZFK-324, unpublished

107 - E. Holub, N. Cindro, O. Bersillon and J. Jary, Z.Physik A289 (1979) 421

108 - K. Seidel, D. Seeliger and A. Meister, Nuclear Theory in Neutron Data Evaluation, vol. II, Technical Document IAEA-190, 1976

109 - A. Gilbert and A.G.W. Cameron, Can. J. Phys. 43 (1965) 1446

TABLE I

Decay Rates, $W_{n\to n+2}(E)$ for Exciton-Exciton Interactions Utilised in Present Work
(The Unit of the Decay Rates is $10^{22}sec^{-1}$)

E (MeV)	$W_{3\to5}$	$W_{5\to7}$	$W_{7\to9}$	$W_{9\to11}$	$W_{11\to13}$	$W_{13\to15}$	$W_{15\to17}$	$W_{17\to19}$	$W_{19\to21}$	$W_{21\to23}$
3	0.022	0.018	0.012	0.010	0.008	0.006	0.005	0.004	0.003	0.002
5	0.054	0.040	0.034	0.031	0.027	0.022	0.019	0.016	0.014	0.011
10	0.17	0.13	0.11	0.092	0.080	0.072	0.061	0.052	0.044	0.038
15	0.34	0.26	0.22	0.19	0.16	0.15	0.13	0.12	0.11	0.10
20	0.55	0.43	0.35	0.30	0.27	0.24	0.22	0.21	0.20	0.19
25	0.74	0.63	0.52	0.45	0.39	0.35	0.32	0.30	0.29	0.28
30	0.91	0.84	0.71	0.61	0.54	0.48	0.43	0.41	0.39	0.38
35	1.04	1.03	0.91	0.79	0.70	0.63	0.56	0.52	0.50	0.48
40	1.17	1.22	1.12	0.99	0.88	0.79	0.71	0.66	0.62	0.59
45	1.26	1.37	1.31	1.19	1.07	0.96	0.88	0.81	0.75	0.71
50	1.35	1.54	1.51	1.40	1.27	1.15	1.06	0.97	0.90	0.85
55	1.41	1.65	1.67	1.58	1.46	1.34	1.26	1.15	1.07	1.00
60	1.48	1.80	1.86	1.79	1.67	1.55	1.48	1.35	1.25	1.17
65	1.52	1.87	1.99	1.96	1.86	1.74	1.70	1.56	1.44	1.35
70	1.58	2.00	2.16	2.16	2.07	1.95	1.93	1.78	1.65	1.54
75	1.60	2.05	2.26	2.30	2.24	2.14	2.15	2.01	1.86	1.74
80	1.65	2.16	2.41	2.49	2.45	2.35	2.38	2.23	2.09	1.95
85	1.66	2.20	2.49	2.60	2.59	2.52	2.59	2.46	2.31	2.17
90	1.70	2.29	2.63	2.77	2.79	2.73	2.80	2.68	2.54	2.39
95	1.71	2.31	2.68	2.86	2.91	2.88	3.00	2.90	2.76	2.62
100	1.74	2.40	2.81	3.03	3.10	3.09	3.19	3.11	2.98	2.84

TABLE II

Cross sections for proton-induced spallation of Cu at 200 MeV. The theoretical predictions are based on the Los Alamos version of VEGAS code (from ref.76).

RESIDUAL NUCLEUS	EXP. YIELD (mb)	TH. YIELD (mb)
62 Zn	2.4 ± 1.1	3.0 ± 0.9
61 Cu	25.0 ± 3.0	34.0 ± 3.1
57 Ni	1.7 ± 0.2	5.44± 1.23
55 Co	2.0 ± 0.2	6.4 ± 1.4
56 Co	12.4 ± 1.3	21.7 ± 2.5
57 Co	37.5 ± 4.0	37.3 ± 3.1
58 Co	44.6 ± 5.0	28.5 ± 2.8
61 Co		2.8 ± 0.9
52 Fe	0.1 ± 0.02	0.5 ± 0.37
59 Fe	1.3 ± 0.13	1.43± 0.66
52 Mn	5.56± 0.6	12.3 ± 2.0
54 Mn	17.4 ± 1.8	16.4 ± 2.1
56 Mn	2.3 ± 0.3	3.7 ± 1.0
48 Cr	0.07± 0.01	0.03± 0.09
49 Cr	0.74± 0.08	1.65± 0.75
51 Cr	12.2 ± 1.3	14.7 ± 1.0
48 V	2.4 ± 0.3	2.8 ± 0.9
44 Sc	0.33± 0.04	0.25± 0.26
46 Sc	0.61± 0.07	0.06± 0.13
47 Sc	0.36± 0.04	0.03± 0.09

Figure Captions

Fig. 1. Experimental excitation functions for (p, 2pxn) reactions on Ni and predictions of the Hybrid model (from ref. 75).

Fig. 2. Experimental excitation functions for (p,3pxn) reactions on Th (black dots with error bars) and predictions of the Exciton model (open points and line through them). (from ref. 67)

Fig. 3. Yield of isotopes produced after π^- absorption in ^{59}Co. Black dots are the experimental values,(16) the histograms the results of Exciton Model calculations (the expected uncertainty in theoretical estimate is indicated).

Fig. 4. Calculated pre-equilibrium emission fraction - ratio between the cumulative cross section of processes in which at least one particle is emitted during the pre-equilibrium stage and the reaction cross section-for the composite nucleus obtained in proton bombardament of ^{51}V. Dashed, dot-and-dash and solid curves represent proton, neutron and total emission fractions, respectively. (from ref. 21).

Fig. 5. Comparison between the measured (black points and triangles) and calculated (histograms) spectra of α-particles emitted in the reaction ^{118}Sn (p,α...) reaction at different proton energies.(46)

Fig. 6. Comparison between the measured and calculated (thin histograms) spectra of α-particles emitted in the reaction ^{27}Al (p,α ....) at different proton energies.(81)

Fig. 7. Trajectories full lines of a) a 20 MeV neutron striking a ^{165}Ho nucleus with impact parameter q = 4.14 fm, b) a 20 MeV proton striking a ^{165}Ho nucleus with an impact parameter q = 2 fm.

Fig. 8. Comparison between the experimental [96] (black circles with error bars) and calculated (full line) angular distributions of α-particles emitted in the reaction ^{149}Sm (n,α....) ^{146}Nd at E_n = 14.1 MeV

Fig. 9 Comparison between the experimental (black circles with error bars) [97] and calculated (full lines) angular distributions of α-particles emitted in the reaction ^{165}Ho (p,α ....) at different proton energies. Each angular distribution corresponds to α-particles with energy in the interval ΔE_α.

Fig.10 Comparison between the experimental [96] (black circles with error bars) and calculated (histogram) spectra of α-particles emitted in the reaction ^{149}Sm (n,α) at E_n = 14.1 MeV.

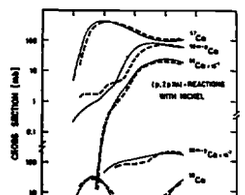

Fig. 1

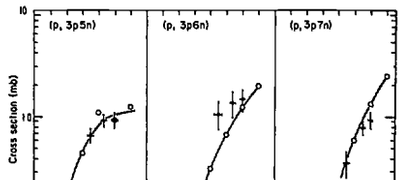

Fig. 2

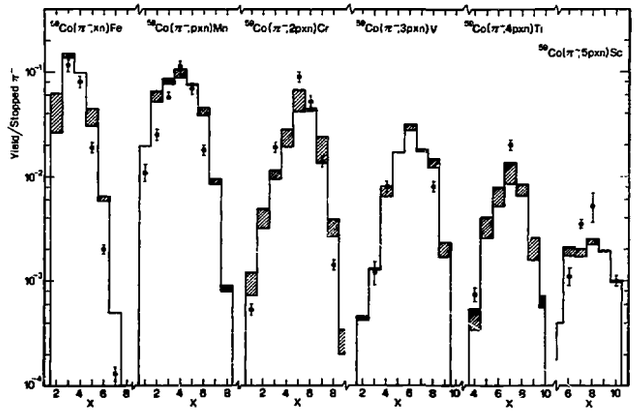

Fig. 3

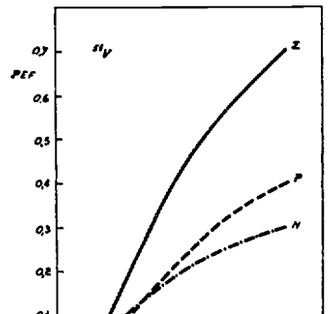

Fig. 4

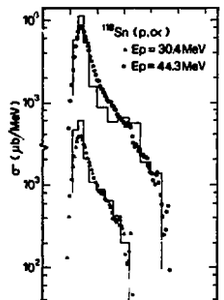

Fig. 5

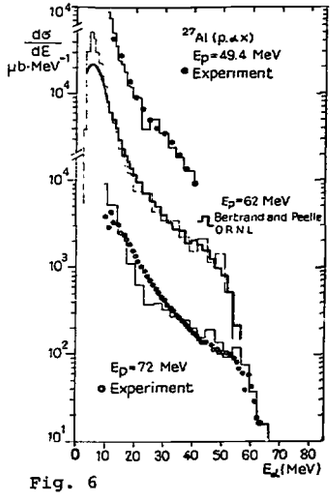

Fig. 6

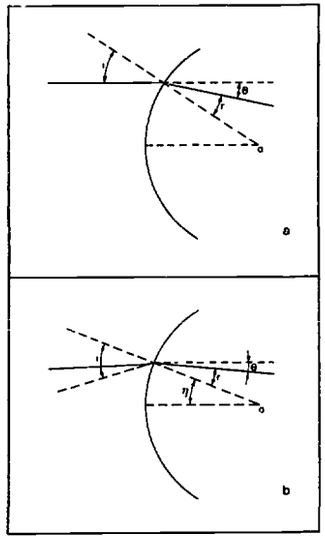

Fig. 7

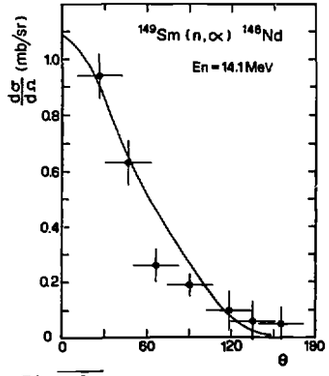

Fig. 8

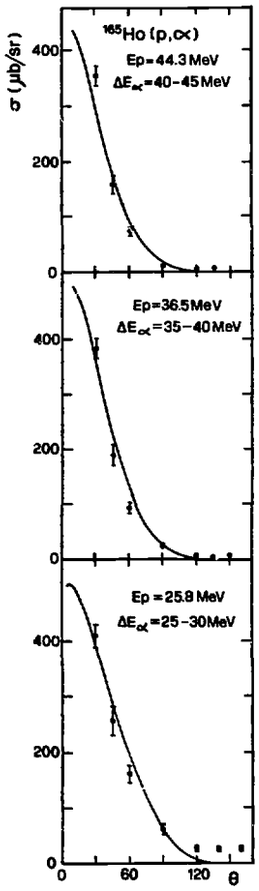

Fig. 9

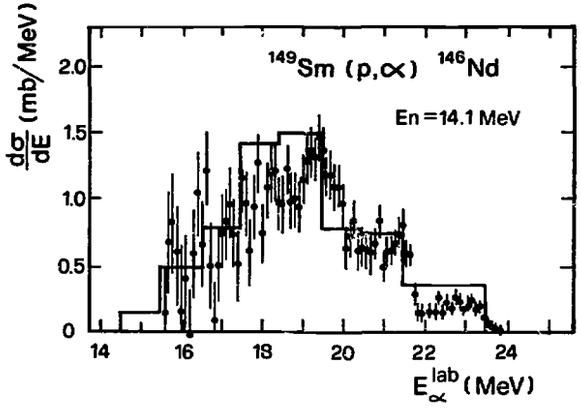

Fig. 10

DEVELOPMENT AND APPLICATIONS OF MULTI-STEP HAUSER-FESHBACH/PRE-EQUILIBRIUM MODEL THEORY

C.Y. FU
Oak Ridge National Laboratory,
Oak Ridge, Tennessee,
United States of America

ABSTRACT

A recently developed model that combines compound and precompound reactions with conservation of angular momentum is discussed. This model allows a consistent description of intermediate excitations from which tertiary reaction cross sections can be calculated for transitions to the continuum as well as to the discrete residual levels with known spins and parities. Predicted neutron, proton, and alpha-particle production cross sections and emission spectra from 14-MeV neutron-induced reactions are compared favorably with angle-integrated experimental data for 12 nuclides. The model is further developed to include angular distributions of outgoing particles. The random phase approximation used for the compound stage is partially removed for the precompound stages, allowing off-diagonal terms of the collision matrix to produce both odd and even terms in the Legendre polynomial expansion for the angular distribution. Calculated double-differential cross sections for the 14.6-MeV ^{23}Na(n,n'x) reaction are compared with experimental data.

I. INTRODUCTION

Development of fusion energy technology calls for substantial improvement in the knowledge of neutron cross sections in the energy range from a few MeV to about 40 MeV [1]. In this energy range, the multi-step Hauser-Feshbach model with precompound effects is the most versatile and is considered an indispensible theoretical tool for cross-section evaluations [2]. In analyzing cross sections such as hydrogen and helium production from 14-MeV neutron-induced reactions, we showed [3] that spin and parity effects are more important in the second step (tertiary reaction) of the calculation than in the first step, requiring conservation of angular momentum in the precompound stages in a manner consistent with the Hauser-Feshbach model used for the compound stage.

We have recently developed a model [4] that treats compound and precompound reactions consistently with conservation of angular momentum. The main features of this development are summarized in Section II.

The fact that angular momentum is conserved in both the precompound stages and the compound stage of our calculation provides the possibility of calculating angular distributions of outgoing particles. Progress in this respect is reported in Section III.

Our aim is to develop a model code, with ever-improving physics content, that can be used to calculate a large variety of nuclear cross sections over a wide energy range. Much work needs to be done, but in the meantime many uses of the code have been made. Some examples of applications are briefly discussed in Section IV.

II. THE CONSISTENT COMPOUND AND PRECOMPOUND MODEL WITH CONSERVATION OF ANGULAR MOMENTUM

Detailed derivation of the model will be published elsewhere [4]. Here we present the final formula and summarize its essential features. The cross-section formula for outgoing particle of type b and energy ε is given by

$$\sigma_b(E,\varepsilon)d\varepsilon = \pi \lambda^2 \sum_{J\pi} g_J \sum_{s\ell} T^J_{s\ell} \frac{d\varepsilon}{\sum_{J\pi} \sum_{s'\ell'} T^J_{s'\ell'}} \Omega_b(I,E,U), \quad (1a)$$

where

$$\Omega_b(I,E,U) = \sum_p D_b(p,E)\, \rho_b(p\text{-}1,h,I,U') + C(E)\, \rho_b(I,U') \quad (1b)$$

with

$$D_b(p,E) = \int_0^T P_b(p,h,t)dt/\omega(p,h,E) \quad (1c)$$

$$C(E) = \int_T^\infty P(p,h,t)dt/\omega(p,h,E) \quad (1d)$$

$$\rho_b(I,U') = \sum_p \rho_b(p\text{-}1,h,I,U') \quad . \quad (1e)$$

Equation (1a) has a form much like the Hauser-Feshbach formula except the quantity $\Omega_b(I,E,U)$ defined in Eq. (1b). E is the excitation energy of the composite nucleus. The quantity I [summed implicitly in Eq. (1a)] is the spin of a group of residual levels at excitation energy U. The effective excitation energy U' is related to U by $U' = U - U_{p,h}$ where $U_{p,h}$ accounts for the pairing effects. The righthand side of Eq. (1b) contains two terms, the first corresponds to the precompound component and the second the compound. Occupation probabilities P_b and P for the particle-hole pairs, (p,h), at time t are obtained from a set of new master equations which ensures consistency between the precompound and

the compound stages of the calculation. The equilibration time T is the time when all allowed states are equally populated. The level density $\rho_b(p\text{-}1,h,I,U)$ and the state density $\omega_b(p\text{-}1,h,I,U)$ are related by $\omega_b(p\text{-}1,h,I,U) = (2I+1)\,\rho_b(p\text{-}1,h,I,U)$.

The following features of Eq. (1) may be noteworthy.

1. Equation (1) reduces to the Hauser-Feshbach formula if instantaneous equilibration is assumed.

2. The occupation probabilities, P_b, for the precompound stages depend on the relative distribution of neutrons, protons, and alpha-particles in the excitons. This dependence is particularly strong for $t \ll T$ when the incident particle contributes predominantly to the particle-type distribution. On the other hand, there is no such dependence in the occupation probability, P, for the compound stage.

3. The spin dependences in ω, P_b, and P are assumed to be similar and therefore cancel in their ratios in Eqs. (1c) and (1d), allowing the use of spin-independent master equations for solving P_b and P. This assumption needs to be examined, but we do not expect it to cause a serious problem for nucleon-induced reactions above a few MeV.

4. The level density used for the compound stage of the calculation is obtained from summing those used for the precompound stages, removing a large source of uncertainty in defining the ratios of the precompound to compound cross sections often found in the literature.

5. Because (p,h) states have fewer high-spin stages than (p+1,h+1) states, conserving angular momentum in the precompound calculation results in spin populations different from those of the compound calculation, changing calculated cross sections accordingly.

Calculations of neutron, proton, and alpha-particle production spectra for 14.6-MeV neutrons incident on thirteen isotopes have been compared with experimental data [4]. Our calculated results for ^{56}Fe are compared in Fig. 1 with the (n,xn) spectrum measured by Hermsdorf *et al.* [5] and the (n,xp) and (n,xα) spectra measured by Grimes *et al.* [6]. The histograms in the calculated (n,xn) spectrum in Fig. 1 represent OWBA calculations for some discrete levels [7]. These cross sections correspond to rotational and vibrational excitations which are very weakly taken into account by the compound and precompound calculations. The dashed curves in Fig. 1 include calculated results from the binary step only. Twelve other comparisons similar to that shown in Fig. 1 can be found in reference 4.

III. ANGULAR DISTRIBUTIONS

The use of Eq. (1) in our multi-step Hauser-Feshbach code for the calculation of angular distributions yields front-back symmetry in the center-of-mass coordinates. This is of course incorrect because the random phase approximation used for the compound stage is invalid for the precompound stages.

We know that an incident particle enters a nucleus as a single particle. After initiating a certain number of collisions, creating h holes, the incident particle as well as any excited particles will have lost all traces of the incoming single-particle coherent motion and the random phase approximation becomes valid. On the other extreme, if an incident particle traverses the nucleus without suffering a collision, fully correlated phases for any connected pairs of the collision matrix elements should be assumed instead.

Knowing the two extremes at $h = 0$ and $h = \bar{h}$, we may be able to guess what happens in between by examining some experimental data. This is done in two steps. First we derive a formula for differential cross sections that assumes random phases for the compound stage but fully correlated phases for the precompound stages. Then a weighting function that depends on the number of collisions is used to require the formula to satisfy the two extreme cases. We obtain the following:

$$\frac{d\sigma}{d\Omega} = \frac{\lambda^2}{4(2I_0+1)(2i+1)} \sum_L (B_L+B'_L)\, P_L(\cos\theta) \tag{2a}$$

$$B_L = \sum_{s_a\, s_b\, J\, \ell_a\, \ell_b} (-1)^{s_a-s_b}\, Z(\ell_a\, J\, \ell_a\, J;\, s_a\, L)\, Z(\ell_b\, J\, \ell_b\, J;\, s_b\, L)\, T^J_{s_a\ell_a}\, T^J_{s_b\ell_b}\, \Omega_b(I,E,U)/D_{J\pi} \tag{2b}$$

$$B'_L = \sum_{s_a s_b\, J\, J'\, \ell_a\, \ell'_a\, \ell_b\, \ell'_b} (-1)^{s_a-s_b}\, (J\neq J' \text{ and/or } \ell_a\neq\ell'_a \text{ and/or } \ell_b\neq\ell'_b)\, i^{\ell_a-\ell'_a-L}\, Z(\ell_a\, J\, \ell'_a\, J';\, s_a\, L)\, i^{\ell_b-\ell'_b-L}\, Z(\ell_b\, J\, \ell'_b\, J';\, s_b\, L)\, (T^J_{s_a\ell_a}\, T^{J'}_{s_a\ell'_a}\, T^J_{s_b\ell_b}\, T^{J'}_{s_b\ell'_b})^{1/2}\, (D_{J\pi}\, D_{J'\pi'})^{-1/2} \sum_{p\ (h<\bar{h})} Y(h)\, D_b(p,E)\, \rho_b(p\text{-}1,h,I,U') \tag{2c}$$

where

$$Y(h) = \left(\frac{\bar{h}-h}{\bar{h}}\right)^y . \tag{2d}$$

Here the Z's are the Z coeffients defined by Biedenharn, Blatt, and Rose [8]. The phase correction due to Huby [9] corrects an error in the derivation given by Blatt and Biedenharn [10]. The collision matrix elements in the formula given by Blatt and Biedenharn [10] have been replaced by transmission coefficients in the manner described by Satchler [11]. The first term in Eq. (2a) produces even Legendre coefficients L = 0, 2, 4, ... The second term gives L = 1, 2, 3, 4, ... and is present for $h < \bar{h}$ and $t < T$. For $h \geq \bar{h}$ and $t \geq T$, the random phase approximation is valid and the second term approaches zero. This is achieved by using the weighting function Y(h) which we tentatively assume to take the form of Eq. (2d).

Calculated results using Eq. (2) for the 14.6-MeV ^{23}Na(n,n'x) are compared in Fig. 2 with the data of Hermsdorf *et al.* [5]. For this calculation, $\bar{h}$ was taken to be the most probable hole number in the excited composite nucleus and is equal to 2.7 for ^{24}Na. This number of course increases with increasing excitation energy and increasing mass number of the composite nucleus. The parameter y was determined to be 2.0 from fitting the data but can probably be derived from a theoretical model. From Fig. 2 it is clear that the model did what we wanted it to do — a forward peaking that increases with increasing outgoing particle energy and a backward peaking that exhibits angular momentum effects. Such backward peaking cannot be obtained from calculations that ignore angular momentum effects.

Extensive tests of the model are planned. Refinements of the model are anticipated.

IV. APPLICATIONS

While development of our model theory and code continues, many applications have been made. A summary of rather broad applications was given previously [3]. Here we describe our latest efforts.

A critical review of neutron emission spectra induced by 14-MeV neutrons from ENDF/B-V files was made by Hetrick *et al.* [12]. It became clear from this review why advanced nuclear model codes need to be developed and applied to cross-section evaluations. In 14-MeV neutron-induced reactions, several neutron-producing reactions compete. These reactions usually include (n,n'γ), (n,2n), (n,np), (n,nα), (n,pn), and (n,αn). Barring a sudden advancement in experimental techniques, cross sections of these competing reactions as well as the secondary particle and gamma-ray energy distributions can only be evaluated in a consistent fashion through the use of multi-step Hauser-Feshbach codes with precompound effects. The fact that such codes were not available several years ago explains the poor agreement of many ENDF/B-V neutron emission spectra with available experimental data shown in the review.

We have started to redo some of our evaluations for ENDF/B-V that were made without the aid of an advanced nuclear model code. An example is given here for the reevaluation of neutron and gamma-ray-production cross sections for calcium from 8 to 20 MeV [13]. The original evaluation [14] made extensive use of a multi-step Hauser-Feshbach code that had no precompound effects. For this reason, the neutron emission spectrum shown in the review [12] is typical of a pure compound component. We have made new calculations using our present model for all reaction cross sections of ^{40}Ca from 8 to 20 MeV. The same parameters as determined previously were used. The parameters required for the precompound mode of calculation were those determined in reference 4. Our calculated 14.6-MeV ^{40}Ca(n,xn) spectrum is compared in Fig. 3 with the data measured by Hermsdorf *et al.* [5]. The calculation is in much better agreement with the experiment than those used for ENDF/B-V.

Simultaneous calculations of neutron and gamma-ray-production cross sections will ensure consistency between the two and ensure energy balance between the incident neutron and the outgoing particles and gamma rays. For this reason, gamma-ray-production cross sections and spectra need also be calculated at the same time and be used for the new evaluation. Two such calculations, induced by 8.75- and 15.5-MeV neutrons respectively, were compared in Figs. 4 and 5 with the data measured by Dickens [15]. These calculated results deviate somewhat from those obtained previously for ENDF/B-V but remain in good agreement with the experimental data.

V. SUMMARY AND CONCLUSIONS

A model that treats compound and precompound reactions consistently with conservation of angular momentum is summarized. This model was extended, also in a consistent manner, to calculate angular distributions of outgoing particles from combined compound and precompound reactions. The importance of including spins in the precompound mode of calculation became apparent from the agreement between the calculated and the observed backward peaking in the angular distributions. The practical need of advanced nuclear model theory and code was reiterated.

Further developments in both theory and code are needed. Tests of the angular distribution method should be made for (n,xp) and (n,xα) reactions and more (n,xn) reactions. A scheme is needed to extrapolate the precompound effects in the angular distributions from the continuum to the discrete levels. Radiative capture should be incorporated in a consistent manner as one of the competing precompound reactions.

ACKNOWLEDGEMENT

Research sponsored by the Division of Basic Energy Sciences, U. S. Department of Energy, under contract W-7405-eng-26 with the Union Carbide Corporation.

REFERENCES

1. M. R. BHAT and S. PEARLSTEIN, editors, "Symposium on Neutron Cross Sections from 10 to 40 MeV," in BNL-NCS-50681, Brookhaven National Laboratory, Upton, New York (1977).
2. L. STEWART and E. D. ARTHUR, "Neutron Cross-Section Evaluation at High Energies — Problems and Prospects," *ibid.*, 435.
3. C. Y. FU, "Multi-Step Hauser-Feshbach Codes with Precompound Effects: A Brief Review of Current and Required Developments and Applications up to 40 MeV," *ibid.*, 453.
4. C. Y. FU, "A Consistent Nuclear Model for Compound and Precompound Reactions with Conservation of Angular Momentum," ORNL/TM-7042 (1980) and submitted to Physical Review C.
5. D. HERMSDORF, A. MEISTER, S. SASSONOFF, D. SEELIGER, K. SEIDEL, and F. SHAHIN, Zentralinstitut für Kernforschung, Rossendorf Bei Dresden, ZfK-277 (U), (1975).
6. S. M. GRIMES, R. C. HAIGHT, K. R. ALVAR, H. H. BARSCHALL, and R. R. BORCHERS, Phys. Rev. C19, 2127 (1979). R. C. HAIGHT and S. M. GRIMES, Lawrence Livermore Laboratory Report UCRL-80235 (1977) and private communication.
7. C. Y. FU, in Nuclear Cross Sections and Technology, Proceedings of a Conference, Vol. I, p. 328, National Bureau of Standards Special Publication SP-425, Washington, DC (1975).
8. L. C. BIEDENHARN, J. M. BLATT, and M. E. ROSE, Rev. Mod. Phys. 24, 249 (1952).
9. R. HUBY, Proc. Phys. Soc. (London) A67, 103 (1954).
10. J. M. BLATT and L. C. BIEDENHARN, Rev. Mod. Phys. 24, 258 (1952).
11. G. T. SATCHLER, Phys. Rev. 94, 1304 (1954); 104, 1198 (1956); 111, 1747 (1958).
12. D. M. HETRICK, D. C. LARSON, and C. Y. FU, in Proc. Conf. on Nucl. Cross Sections for Technology, Knoxville, Tennessee, October 22-26, 1979.
13. C. Y. FU and D. M. HETRICK, "Reevaluation of Neutron and Gamma-Ray-Production Cross Sections for Calcium from 8 to 20 MeV," ORNL/TM (to be published).
14. C. Y. FU, Atomic Data and Nucl. Data Tables 17, 127 (1976).
15. J. K. Dickens, Nucl. Sci. Eng. 48, 78 (1972).

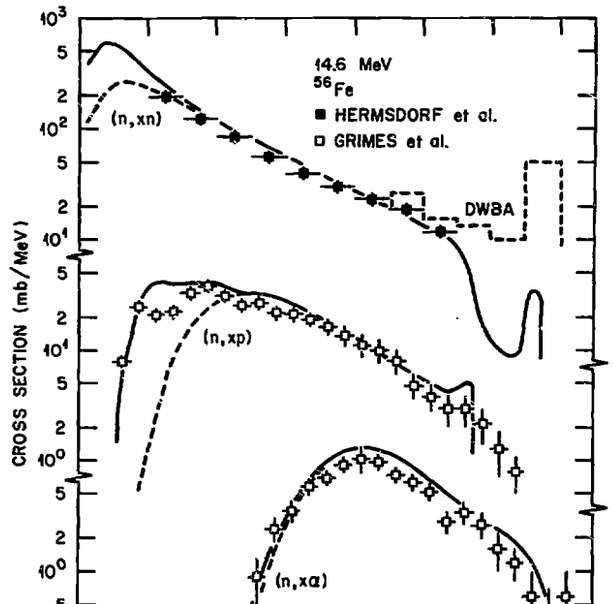

Fig. 1. Calculated and experimental angle-integrated neutron, proton, and alpha-particle production spectra from 14.6-MeV neutrons on ^{56}Fe. The solid curves are calculations. The dashed curves include calculated contributions from the binary step only. The histograms represent DWBA calculations of (n,n') cross sections for 15 discrete levels.

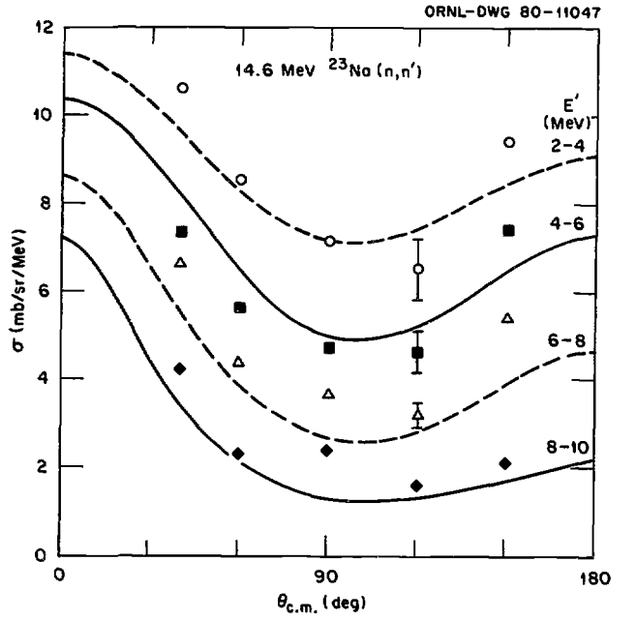

Fig. 2. Calculated and experimental double differential cross sections of the 14.6-MeV ^{23}Na(n,n'x) reaction. The data are due to Hermsdorf *et al.* [5]. Backward peaking in the calculated and observed angular distributions exhibits angular momentum effects.

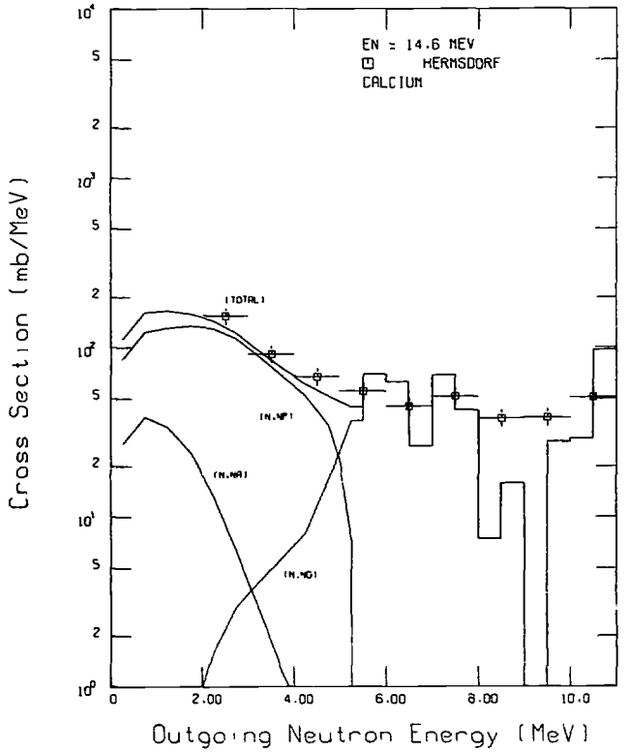

Fig. 3. The sum of partial neutron emission spectra calculated from various competing reactions for calcium is compared with the data measured by Hermsdorf *et al.* [5]. Correction due to DWBA calculations for the discrete levels has been applied.

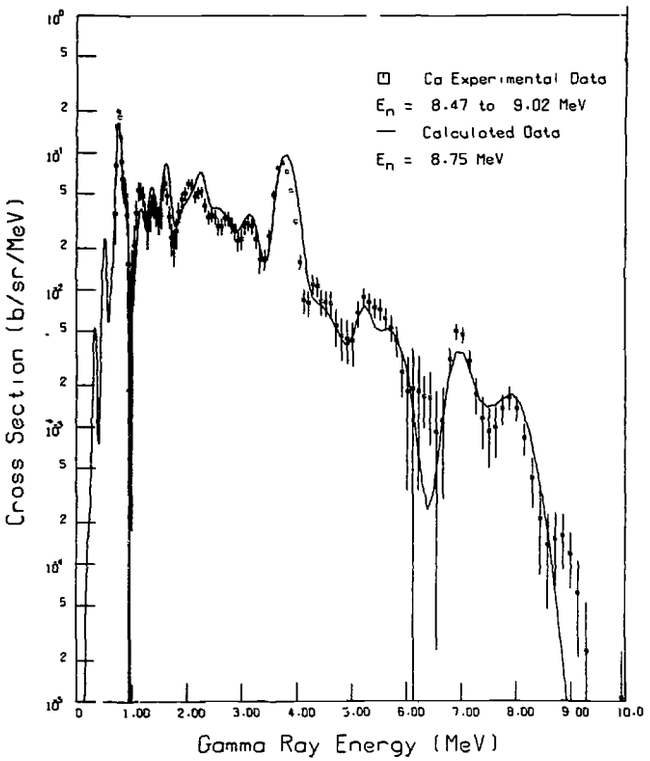

Fig. 4. Comparison of calculated and experimental [15] gamma-ray production spectra from 8.75-MeV neutrons on calcium. The calculation was done for ^{40}Ca while the observed 1.158-MeV gamma ray was produced in $^{44}Ca(n,n'\gamma)$ reaction.

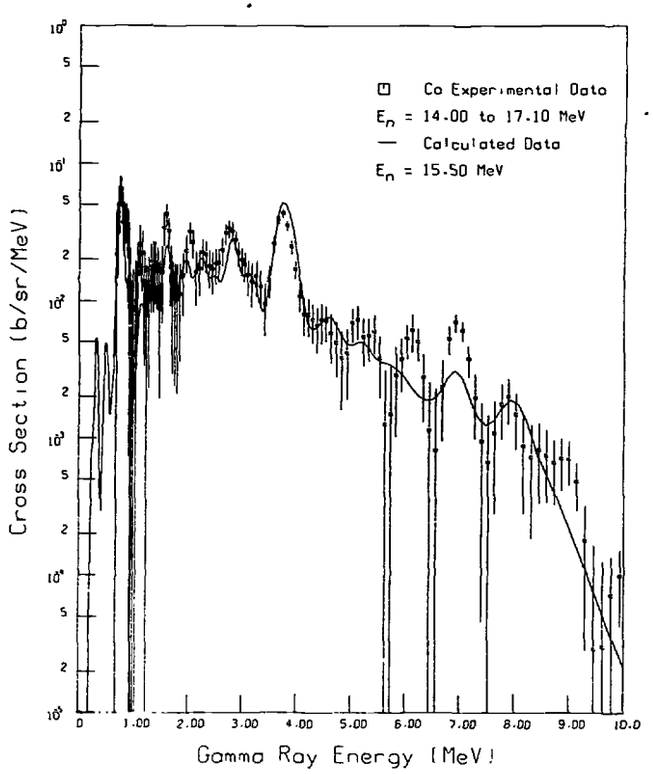

Fig. 5. Comparison of calculated and experimental [15] gamma-ray production spectra from 15.5-MeV neutrons on calcium. Some of the observed discrete gamma rays have not yet been identified.

A CRITICAL REVIEW ON SOME ASPECTS OF THE THEORY OF FISSION

H.C. PAULI
Max-Planck-Institutefür Kernphysik,
Heidelberg,
Federal Republic of Germany

Lecture notes by Drs. V.S. Ramamurthy and S.K. Kataria

Abstract. The lecture notes display briefly some of the facets which eventually will be part of a theory for the fission process. They cover some important aspects of our present understanding in a qualitative fashion and complement the existing review articles rather than replacing them. The notes include sections on (I) The Bohr-Wheeler Fission of a Drop, (II) The Strutinsky-Swiatecki Quantum Droplet, (III) The Question of Inertias of a Fluid in Motion, (IV) Some Selected Aspects of the Distributions of Mass and Kinetic Energy, and (V) Possible Relations Between the Phenomenological Models and Self-Consistent Field Approximations.

I. Introduction

Fission is the process in which a heavy nucleus splits into two fragments of nearly equal masses, either spontaneously or as a result of a reaction. It was discovered by Hahn and Strassmann (Ref. 144) in 1939, and in analogy to the division of a biological cell the term "fission" was coined by Meitner and Frisch (Ref. 254) soon after. These authors also gave the first qualitative interpretation of Hahn and Strassmann's observations, and in particular mentioned the possibility of a large energy release in this type of reaction. The foundations for understanding the mechanisms were laid by N. Bohr and J.A. Wheeler, and many of the concepts we use up to the present day can be found in their work (Ref. 50).

The general picture of this process is as follows: When a nucleon, say a neutron, impinges on a heavy nucleus like uranium, it is absorbed. The nucleus gains some energy as a result of this reaction, and goes through a series of complicated intermediate states about which we have little information. One refers to this entity of states as the compound nucleus (Ref. 51, 248), an idealized concept introduced by N. Bohr (Ref. 52). After some time long as compared to all other characteristic times, say after 10^{-18} seconds, the nucleus eventually fissions. The deexcitation by fission is accompanied by or is in competition with other reactions such as the emission of beta or gamma radiation or the emission of particles, mostly neutrons.

The emission of two to three neutrons on the average per fission event is particularly important. They maintain the chain reaction, and allow for the burning of the nuclear fuel. The economic, sociological, and environmental implications of this reaction are known, and cause the practical interest in this process. On the other hand,

> "The fission process has occupied a unique place in the development of nuclear physics, but should be recognised as part of a wider range of phenomena involving large-scale nuclear deformations and collective flow that are now becoming accessible in the study of reactions produced by accelerated heavy ions." (Ref. 47).

It might seem surprising that even four decades after the discovery of the process a complete and consistent description of the fission process does not exist. Almost uniquely in nuclear physics, one is faced with the full complexity of the many-body problem, which in turn makes fission an ideal testing ground for the various methods and descriptions. The models developed in the past to stress the various aspects such as collective and single particle motion, fluid dynamics, and single particle motion often contradict each other. All of them find some support in different classes of experiments, but for the further progress it seems a

necessity and a challenge to disentangle their mutual relations and possible overlap.

Any presentation of the theory of fission - the present one included - must suffer from these facts, and cannot give more than an unsatisfactory enumeration of the models. Also the litterature reflects the situation. Only two monographs deal with nuclear fission (Ref. 1, 2). The books of Hyde (Ref. 169) deal with many aspects of fission. The booklet of Wilets - despite being outdated slightly by some of the newer developments - is still worth reading, because of its succinct account of the essential ideas. A rather complete account of the various developments can be found in the proceedings of the IAEA symposia on the physics and chemistry of fission (Ref. 3, 5, 8). The proceedings of the Nobel symposium on superheavy nuclei (Ref. 6) contain many numerical results. The bulk of information can also be found in more recent review articles (Ref. 55, 59, 85, 302, 319).

The aim of the lectures is to complement the existing literature by presenting the essential concepts with a minimum of formal definitions and to accompany them with critical comments. This should facilitate the orientation of the scholar and pave the way for future improvement, but it cannot replace a careful study of the relevant literature.

In supporting this study, special care was taken in the List of References. Quite unusually it contains the title of the contribution, which should facilitate the orientation. Despite 432 citations, the list is not complete. Virtually all references to experimental work are omitted; some of these can be found in Weigmann's lecture (Ref. 418). Only published work was included. Contributions to Letter Journals, which were followed by extensive articles on the same subject, have been omitted. Questions of priority therefore cannot be decided by this list! Although I strived for completeness in the aspects of fission, I have to apologize for having missed possible important contributions.

The present lecture notes are arranged in five sections, which contain less material in more condensed form than did the oral presentation. The rather extensive reproduction of Bohr and Wheeler's fundamental concepts (Section II) seemed a necessary prerogative for the description of subsequent developments. The modification of the potential energy is treated in Section III. The questions related to the collective inertia (Section IV) are tightly interwoven with the problematics of nuclear collective motion. Attempts to understand some aspects of the multidifferential fission cross sections are presented in Section V. For an eventual reaction theory of the fission process, one seemingly needs ideas which go beyond the usual concepts. The phenomenological aspects are collected in Sections II to V. One can relate some of them to the less phenomenological self-consistent field methods. The need for an almost stenographic shortness of these notes becomes particularly obvious in the last section. Most of the formal apparatus had to be omitted and the comparison with experiment is less extensive than would correspond to good tradition and the taste of the author.

II. The Bohr-Wheeler Fission of a Drop

The concepts which allow for a qualitative understanding of the fission process have been developed by Bohr and Wheeler (Ref. 50). Even today, they are basic ingredients of our understanding, and, therefore, their salient features will be briefly displayed.

1. Saturation and the Nuclear Binding Energy

The volume occupied by the nucleons in a nucleus is roughly proportional to their number. This empirical fact is called saturation: The density in the central region is roughly independent of the nucleon number A. Since the volume is finite, the density must drop to zero relatively fast in a surface region. Empirically, the thickness of the surface layer does not depend on A either. Figure 1 shows a typical nuclear density in a commonly accepted parameterization.

Saturation leads to a characteristic behavior of the binding energy of a nucleus B (understood as the absolute difference between the physical mass and the sum of masses of the constituents).

The (nuclear part of the) binding energy per particle must tend to a constant in the limit of large particle number. Corrections for finite systems can come only for particles in the surface layer. Their number relative to the total is proportional to $A^{-1/3}$, and since this is a small quantity, it can be used as ordering parameter in a series (Ref. 287).

In practice, one restricts oneself mostly to the first two terms, called the volume and surface energy, $E_V = a_V A$ and $E_S(o) = a_S A^{2/3}$, respectively. Adding the electrostatic Coulomb energy $E_C(o) = c_3 Z^2/A^{1/3}$, one writes for the series

$$-B = A(a_V + a_S A^{1/3}) + E_C(o)$$

and determines the coefficients (a_V, a_S, and c_3) by a fit to the nuclear masses. Saturation leads thus to a kind of Weizsäcker's semiempirical mass formula (Ref. 420). One particular mass fit is shown in Figure 2. It may serve as an example for the general properties:

(i) Semiempirical mass formulas are smooth functions of neutron and proton numbers and describe binding energies very well on the mean;

(ii) Deviations from the mean are not statistical, but are regular structures peaked at the so-called magic numbers.

The nuclear binding energy is one of the central and long-standing themes in nuclear physics (Ref. 33, 34, 39, 40). The above arguments, based on the existence of a nuclear surface (Ref. 222, 360, 367, 385, 387, 388, 422) or a "thin skin" (Ref. 286, 287, 288) can and have been modified in various versions of liquid drop (Ref. 39, 403) or droplet models (Ref. 229, 247, 286-290). Often they are related to the many-body problem by the Thomas-Fermi (Ref. 38, 41, 57, 90, 91, 138, 139, 147, 162, 191) or other semiclassical approximations to the self-consistent field approximation (see Section VI). Some of the properties of mass formulas are related directly to properties of the nucleonic interaction. For example, because of charge symmetry, one expects the coefficients a_V and a_S to depend weakly and in second order on proton (Z) and neutron (N) number, i.e., $a_i = c_i(1 + \kappa_i I^2)$ with $I = (N - Z)/(N + Z)$ (Ref. 40, 291).

2. The Static Stability Against Fission

The binding energy per particle shows a pronounced maximum for mass numbers A around A ~ 60 (see Figure 2). For lighter masses a division of the nucleus would be endothermic, but heavier nuclei are potentially unstable against division. What prevents the fission of these nuclides?

It is remarkable that this question was raised only after fission was detected. Bohr and Wheeler answer this question by means of a deformation energy and argue in the following way: The transition from one dropletlike structure of the fissioning nucleus to the two of the fission fragments does not occur abruptly, but the density proceeds continuously through a sequence of shapes. This is possible by a deformation of the surface layer, while the central density remains essentially unchanged because of saturation. The deformations change the binding energy of the systems. Its deformation-dependent part, called deformation energy, has at least one maximum in between the two limiting deformations which correspond to the shape of the fissioning nucleus and to the fission fragments. This conclusion is based on a rather general consideration: Because of the constant central density, the particles in the interior cannot contribute much to the nuclear part of the deformation energy, in contrast to the particles in the changing surface layer. For increasing deformation, their number and thus the surface energy increases at first and tends to a constant when the density has reached the shape of the fission fragments. The third major contribution to the binding energy, the electrostatic energy, however, decreases continuously for the corresponding deformations, and reaches its asymptotic value only at very large distances. The maximum in the deformation energy, called the fission barrier or the fission threshold, provides the observed stability and plays a crucial role in the theory.

Bohr and Wheeler concretize these general concepts by replacing the nucleus by a droplet with a sharp boundary endorsed with a

surface tension and a homogeneously distributed charge. This liquid drop model has about similar properties as required by the general concepts, but has the advantage of being sufficiently simple. The deformation energy, for example, can be written down in the parameterization

$$W_{LD}(\alpha) = E_S(o)\left(B_S(\alpha) - 1\right) + E_C(o)\left(B_C(\alpha) - 1\right) \qquad (1)$$

where $E_S(o)$ and $E_C(o)$ refer to the surface and Coulomb energy of a sphere, respectively. All deformation dependence - symbolized by the argument α - is contained in the coefficients $B(\alpha)$ which take the value 1 for a sphere of radius R_o and do not depend on Z or N. They can be calculated once the contour of the surface is well defined, for example by assuming axial symmetry and expanding the radius vector of the surface in terms of Legendre polynomials

$$R(\theta,\phi) = R_o\left[\alpha_o + \sum_{i=2}^{N} \alpha_i P_i(\cos\theta)\right]$$

and terminating the sum at the appropriate order N.

Figure 3 shows one of the early calculations of liquid drop "deformation energy landscapes" as an example (Ref. 114). The figure shows clearly the appearance of the fission barrier as a saddle point in such a landscape. Its position and its height (in units of $E_S(o)$) depend on Z and A only through the dimensionless fissility parameter x. This parameter, defined as

$$x = \frac{E_C(o)}{2E_S(o)} \approx \frac{Z^2}{A} \Big/ \left(\frac{Z^2}{A}\right)_{\text{critical}}, \qquad (2)$$

is convenient, because the liquid drop barrier disappears for x = 1, the corresponding threshold shape being a sphere. The absolute height of the fission barrier depends sensitively on the coefficients of the mass formula, and for a particular case is given in Figure 4. As the figure shows, the fission barrier rarely exceeds 60 MeV, and for a typical heavy nucleus has the value 5-10 MeV.

The fission threshold energy is small as compared to other characteristic energies such as the volume energy (~3500 MeV), the surface energy (~650 MeV), or the Coulomb energy (~1000 MeV) in a heavy nucleus (A ~ 220), and is a result of a delicate cancellation. This cancellation is the reason for the enormous difficulties in calculating quantitatively the fission barriers by methods different from the liquid drop or similar approaches.

The determination of the deformation energy in the liquid drop model is not at all a simple technical problem. A particular difficulty is an economically and physically reasonable parameterization of the nuclear surface. The expansion in terms of Legendre polynomials is convenient only for smaller deviations from a sphere, and breaks down for the description of separated shapes. An accurate description of fission threshold shapes had to include polynomials up to order 18 (Ref. 73, 74). In the literature many different attempts to parameterize the surface and many different liquid drop energy surfaces can be found, for example Ref. 148, 190, 227, 229, 304, 306-308, 408. A parameter-free description of the surface can be given (Ref. 402), at the cost of solving an integrodifferential equation.

3. The Dynamic Stability Against Division

The existence of a nonzero fission barrier ensures classically that the nucleus is stable against shape deformations. However, quantum-mechanically, there is a finite probability of the nucleus tunnelling through this barrier.

The transmission of a quantum-mechanical particle with mass m through a barrier of potential energy W(x) is given by transmission coefficient $T = |\exp(-S/\hbar)|^2$ and governed by the action integral

$$S = \int_{x_1}^{x_2} dx\sqrt{2m(E - W(x))}$$

in between the two classical turning points x_1 and x_2, provided $S \gg \hbar$. The transmission coefficient multiplied with a character-

istic frequency ("number of assaults") gives an estimate for the probability per unit time of the particle to tunnel through the barrier.

By analogy Bohr and Wheeler estimate the probability per unit time for subthreshold fission as

$$\lambda_f = \frac{\Gamma_f}{\hbar} \quad . \tag{3}$$

The fission width Γ_f was taken as the product of the transmission coefficient multiplied with a characteristic energy $\hbar\omega_f$, i.e.,

$$\Gamma_f = \frac{\hbar\omega_f}{2\pi} \exp(-2S/\hbar) \quad . \tag{4}$$

The number of assaults per unit time was identified with a characteristic vibrational frequency ω_f ~ 1 MeV/$\hbar$ and the "fission action integral" as

$$S = \int_{\alpha_1}^{\alpha_2} \left| 2(W(\alpha) - E) \sum_i m_i \left(\frac{dx_i}{d\alpha}\right)^2 \right| d\alpha \quad , \tag{5}$$

i.e., as the sum of action integrals of the individual nucleons with mass m_i in between the two turning points α_1 and α_2 of the deformation energy $W(\alpha)$. The integral is estimated in the following way: The contributions of all the nucleons are set equal by the argument that they move in a collective fashion. The integral itself is approximated by the maximum of the integrand which is set equal to the threshold energy B_f times the thickness of the barrier $(\alpha_2 - \alpha_1)$, the latter set equal by order of magnitude to the nuclear radius R_o. For a fissioning nucleus (A ~ 240) and a threshold energy of B_f ~ 6 MeV, the action integral takes the estimated value $S \sim (2 \cdot m \cdot A \cdot B_f)^{1/2} R_o \sim 50\ \hbar$. The probability for spontaneous fission by tunnelling through the barrier or its inverse, the half-life for spontaneous fission $\tau_f = 1/\lambda_f \sim 10^{32}$ years is thus even longer than the half-life for α-decay, provided that the fission threshold does not become too small. This mechanism accounts for the large stability of most heavy nuclei against spontaneous fission.

4. Induced Fission as a Monomolecular Reaction

In the case of fission induced by a reaction such as the absorption of a neutron, one has to consider the decay by fission in competition with the other modes of decay such as neutron or gamma emission. In the compound model of Bohr the probability for the decay is independent of the probability for the formation. To determine the probability of fission from the compound state, Bohr and Wheeler treat the process as a monomolecular reaction and apply the transition state theory.

Consider a microcanonical ensemble of nuclei all having excitation energies between E and E + dE, the number of nuclei in the ensemble being exactly equal to the number $\rho(E)dE$ of levels in this energy interval. If Γ_f is the fission width, the number of nuclei which undergo fission per unit time in this ensemble will be $\rho(E)dE\Gamma_f/\hbar$. This number should also be equal to the number of nuclei in the transition state which pass outward over the fission barrier per unit time. In a unit distance measured in the direction of fission, there will be $(dp/\hbar)\rho^*(E - B_f - K)dE$ quantum states of the ensemble for which the momentum and kinetic energy in the fission degree of freedom have values in the intervals dp and dK = vdp, respectively.

ρ^{**} is the density of states of the transition state nucleus arising from all nonfission degrees of freedom. Assuming one nucleus in each state, the number of fissioning nuclei per unit time is $dE/v(dp/\hbar) \cdot \rho^*(E - B_f - K) = dEN^*/\hbar$ where N^* is the number of transition states available to the nucleus with the given excitation energy. Comparing this with the original expression for the number of fissioning nuclei in the ensemble, one gets

$$\Gamma_f = \frac{N^*}{2\pi\rho(E)} = \frac{d}{2\pi} N^* \quad , \tag{6}$$

where d is the level spacing of the compound nucleus. One can derive a similar expression for the probability of decay of the compound nucleus by neutron emission by considering the same microcanonical ensemble. The transition state in this case will be a

spherical shell of unit thickness just outside the nuclear surface and the density ρ^{**} of the transition state is given by the density of levels of the residual nucleus. The number of quantum states in the microcanonical ensemble which lie in the transition region and for which the neutron momentum lies in the range p and p + dp and in the solid angle $d\Omega$ is given by $(4\pi R^2 p^2 dp \cdot d\Omega/\hbar^3) \cdot \rho^{**}(E - B_n - K)dE$, where B_n is the neutron binding energy. Multiplying this by the normal velocity v cos θ = (dK/dp) cos θ and integrating, one obtains for the number of nuclei decaying per unit time $dE(4\pi R^2 2\pi m/\hbar^3) \int \rho^{**}(E - B_n - K)KdK$.

Identifying this with the number $\rho(E)dE\Gamma_n/\hbar$ of compound nuclei decaying by neutron emission per unit time, we obtain for the neutron width

$$\Gamma_n = \frac{1}{2\pi\rho}\left(\frac{2mR^2}{\hbar^2}\right) \int \rho^{**}(E - B_n - K)KdK$$

or

$$\Gamma_n = \frac{d}{2\pi} \frac{A^{2/3}}{K'} \sum_i K_i \ . \qquad (7)$$

The summation is taken over all available states of the residual nucleus, K_i denoting the corresponding kinetic energy $E - B_n - E_i$ which will be left for the neutron. For heavy compound nuclei with excitation energies of the order of a few MeV, fission and neutron emission represent the two predominant modes of decay and all other decay modes have few relative probabilities. Thus, once the fission and neutron widths are known, it is easy to calculate the respective branching ratios. However, for a calculation of the absolute fission yield, or the fission cross section, one should also know the formation probability of the compound nucleus. In the case of neutron-induced fission, the probability of absorption of the neutron by the nucleus to form a compound nucleus is proportional to the inverse probability $\Gamma_{n'}/\hbar$ of a neutron emission process which leaves the residual nucleus in its ground state. The resulting expression for the fission cross section at low neutron energies is

$$\sigma_f = \pi\lambda\!\!\!^{-2} \Gamma_{n'} \Gamma_f / (\Gamma_f + \Gamma_n) \frac{2\pi}{d} \ , \qquad (8a)$$

where $\lambda\!\!\!^{-}$ is the wavelength of the neutron divided by 2π. For high energies of the neutron when $\lambda\!\!\!^{-}$ becomes smaller than the radius R of the nucleus

$$\sigma_f = \pi R^2 \frac{\Gamma_f}{(\Gamma_f + \Gamma_n)} \ . \qquad (8b)$$

On the basis of the simple picture described above, Bohr and Wheeler draw the following conclusion: If the height of the fission barrier is comparable to or greater than the excitation energy of the compound nucleus resulting from the neutron capture, one can expect very low fission cross section. As the energy of the neutron is increased, one expects a steep rise, which, however, is governed by the competition between fission and neutron emission. Once the excitation energy of the compound nucleus exceeds the fission barrier height, the fission cross section becomes independent of the compound nucleus energy. It exhibits a plateau structure, since the probability for neutron emission and for fission varies with energy in nearly the same way except that the entire fission curve is shifted relative to the neutron curve, according to the relative values of the fission barrier and the neutron binding energy. This behavior is illustrated in Figure 5.

One should, however, bear in mind that the derivation given above for the fission width is valid only when the number of fission channels is sufficiently large, as in the case of overlapping resonances. When the compound nucleus excitation energy exceeds the fission barrier height only marginally or falls below it, specific quantum-mechanical tunnelling effects will become important and the mathematical expressions for the reaction rate essentially go over to a quantum-mechanical penetration formula. This is the belief, at least.

In conclusion we should stress a point which implicitly already resides in the above concept: The fact that we experimentally observe fission at all is primarily not a question of the excitation energy nor one of the existence of a fission barrier;

it is solely a consequence of the large number of states allowing for fission, is only a question of level density. To make this point clear let us construct an artificial system with only one state at a sufficiently high energy, which allows for fission, but many others, say N, at the same energy which have no fission width at all. Let us suppose that the reaction occupies this one, single state. The randomization property of the compound concept will distribute the strength of this one state over all the other N states after a very short time with equal probability; the fission state will be emptied, down to the value $1/(N+1)$. The number of states, however, can be large, say 10^6, 10^{10} or so, and instead of observing a fission probability "1" we get something of the order of 10^{-10}, which is zero for all practical purposes.

Therefore, any analysis of the fission cross section [illegible] to a point where level densities become important. We shall come back to this very important question but very briefly in Section III.

5. Some Critical Comments

The concept of deformation energy combined with the compound model can account for the order of magnitude of the energy release, the question of stability of most of the nuclei against fission, and last but not least for the characteristic plateau behavior of cross sections for nucleon-induced fission, which is closely related to the existence of a fission threshold.

The picture, however, is deficient in many respects, as was brought out by later experiments which were not available at the time of the proposal by Bohr and Wheeler.

One of the earliest deficiencies noted was the systematics of fission threshold energies obtained by an analysis of experimental fission cross sections. For nuclei in the actinide region, the experimental fission barrier heights are almost constant as a function of the mass number, whereas the liquid drop model predicts a rather sharp decrease of the fission barrier with increasing value of the fissility parameter. The experimental fission barrier heights were consistent with a value of $(Z^2/A)_{crit} \approx 60$, while the general trend of the barriers over a broader region of nuclei and fits to nuclear ground state masses leads to a value of $(Z^2/A)_{crit} \approx 45\text{-}48$. Since the fission barrier heights are determined as the energy difference between two stationary shapes, namely the ground state and the transition state shapes, this discrepancy does not depend on the still poorly understood dynamical features of the fission process. Thus the above discrepancy must be taken as an indication that something essential is missing in the liquid drop model.

Another experimental feature bringing out the inadequacy of the simple liquid drop model was the observed systematics of the ground state spontaneous fission half-lives of heavy nuclei. In the picture of the Bohr-Wheeler liquid drop model, all measured spontaneous fission half-lives plotted logarithmically against the parameter (Z^2/A) should fall on a universal line. While such a systematics was indeed followed by the available experimental data over orders of magnitude changes in the lifetimes, systematic discrepancies remained.

Other experimental observables like the angular distributions of fission fragments, or the distribution of the fragment's kinetic energy or its mass, or last but not least the existence of fission isomers in a wide range of heavy nuclei, intermediate structure resonances in subbarrier neutron-induced fission and gross structure resonances in (n,f) and (d,pf) studies add to the list of inadequacies of Bohr and Wheeler's description. The quantitative formulation of shell effects (see below) only partly removes the difficulties.

The concepts so far developed cannot replace a proper reaction theory of fission and constitute only a crude idealization. It is hard to believe that all physical observables are determined completely by the bottleneck, the fission threshold, especially since it is virtually impossible to give a clear definition of this quantity in terms of experimental observables.

Fig.

Fig.

Fig.

Fig.1

F

The work of Bohr and Wheeler provides an extremely useful frame for the discussion of many experimental facets. But its contact with the many-body problem is almost impossible to visualize. Even on the level of phenomenology, severe problems remain unsolved. For example, the deformations are treated as the canonical coordinates in a classical theory. But Bohr and Wheeler do not define their equations of motion, nor do they specify, at least operationally, how one should associate an inertia to them. Last but not least it is an open question how many true collective variables exist and how a "fission variable" could be selected among them. These questions become insurmountable difficulties, once one wishes to go beyond the simple order of magnitude estimates (see Section IV), and the theory of fission suffers from all these open problems up to the present day.

Later we shall see how through all those years after Bohr and Wheeler the main effort was expended on the problem of how their fundamental concepts could be substantiated by sound operational procedures which do not obviously contradict the facts established in the other fields of nuclear experience.

III. The Strutinsky-Swiatecki Quantum Droplet

As obvious from Figure 2, saturation cannot account completely for the nuclear binding energies. The regular deviations from a semiempirical mass formula - being peaked at the so-called magic numbers - are a strong argument in favor of a nuclear shell model. They were brought up rather early, but taken seriously only after the invention of an abnormally strong spin-orbit interaction (Ref. 124, 152). Shells in nuclei - as well as in atoms - give a contribution to the binding energy. Consequently, the deformation energy should depend on shell structure (Ref. 153, 184, 234, 278, 279, 300); it should contain a "shell correction energy" $\delta U(\alpha)$,

$$W(\alpha) = W_{LD}(\alpha) + \delta U(\alpha) \ , \qquad (9)$$

up to and beyond the "liquid drop contribution" $W_{LD}(\alpha)$. The question was how it could be done.

The development went mostly along two similar lines. The one advocated by Myers and Swiatecki (Ref. 291) was the formulation of the empirical fact that the bunching of single particle states in spherical nuclei leads to an increased binding energy. It was assumed that this bunching effect was less strong in deformed nuclei, that shell effects fade out. A suitable parameterization of these bunching effects and its subsequent adaption to the empirical masses did improve the quality of the mass formula and remove the long-standing discrepancy between liquid drop parameters for masses and those for the barriers. Moreover, these authors were led to the conclusion that the increased energy in magic nuclei could lead to stable nucleides, even if the "liquid drop" threshold energies were substantially smaller than the neutron binding energy. The result of their work was shown in Figure 3. The so-generated speculation on the possible existence of superheavy elements (Ref. 6) has never stopped since, but has calmed down in recent years because of the lack of experimental evidence.

The other line was due to the argument of Strutinsky (Ref. 397, 400, 401) that "shells" should be interpreted not as degeneracies of single particle states but as large-scale nonuniformities in the spectral distribution of states. As seen in an actual calculation given in Figure 6, such shells appear in spherical and in deformed potentials. In fact, because of the fingerprintlike patterns which appear as a function of deformation (Ref. 300) the density of states around the last occupied state orbit is an oscillatory function of deformation. Correspondingly, the shell correction energy should be an undulatory function. Albeit similar in spirit to considerations of Myers and Swiatecki, the shell correction approach of Strutinsky leads to a number of qualitatively (Ref. 45, 46, 364, 365, 398, 399) different conclusions, which are indicated in Figure 7. Instead of having one minimum and one maximum as in Bohr and Wheeler's or in Myers and Swiatecki's approach, the deformation energy in the shell correction approach may have several of them. Their number depends on the relative

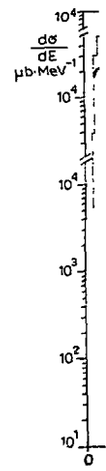

Fig. 6

strength of liquid drop and shell contributions. The minima of the deformation energy must be interpreted as local ground states of the nuclear matter; the fact that one may have several opens up the possibility for shape isomers (Ref. 325, 257, 411); ground state spontaneous fission is supplemented by isomeric spontaneous fission. Instead of one fission barrier, one may have two (or more) - the "double-humped" fission barrier. Last but not least, the shell correction approach gives deformed ground state shapes as due to shell effects.

The above qualitative considerations are complemented by a quantitative procedure, the shell correction method. Its principal aspects are the following: Consider the distribution of single particle states in the energy scale, $g(\varepsilon) = \sum_\nu \delta(\varepsilon - \varepsilon_\nu)$. One may regard this as a function which fluctuates around some average $\bar{g}(\varepsilon)$. Remembering the above definition of shells, only the fluctuations around the average $\delta g(\varepsilon) = g(\varepsilon) - \bar{g}(\varepsilon)$ can be of relevance for the "shell effects." Only they can give a contribution to a shell correction energy

$$\delta U(\varepsilon) = \int^{\varepsilon} d\varepsilon' \delta g(\varepsilon') \varepsilon' \ . \tag{10}$$

One may view this expression as the difference of two large numbers, the sum of single particle energies U and the sum "on the average," i.e.,

$$\delta U = U - \bar{U} \ ; \quad U = \sum_\nu n_\nu \varepsilon_\nu \quad \text{and} \quad \bar{U} = \langle \sum_\nu n_\nu \varepsilon_\nu \rangle \ . \tag{11}$$

The occupation number n_ν of each state is either zero or one in an independent particle model, and reflects the exclusion principle. The particular prescription of how to take the average $\bar{g}$ or $\bar{U}$ can be found in the original work (Ref. 400, 401, 64). Its mechanism becomes particularly clear in the notation of average occupation numbers $\tilde{n}_\nu$, in terms of which the average energy can be written as $\bar{U} = \sum_\nu \tilde{n}_\nu \varepsilon_\nu$ (Ref. 63, 64). The shell correction energy depends then only on $\delta n_\nu = n_\nu - \tilde{n}_\nu$. This function, visualized as a function of the energy and displayed in Figure 8, is mostly zero except in a region of width γ around the Fermi energy. The bulk of the shell correction energy comes from single particle states very close to the Fermi energy, or, in other words, from an energy region for which "single particle excitations" are physically meaningful and reproduced by phenomenological shell models (Ref. 300, 349, 432, 32). In this sense, the shell correction energies are rather model-independent. Their value depends less on the position of individual states than on the "gross shell structure" (Ref. 64, 432).

Strutinsky's shell correction method is by no means canonical. A number of alternative methods for extracting shell effects from independent particle models (Ref. 31, 42, 78, 137, 172, 175, 215, 270, 281, 334, 335, 379-384) have been proposed. In fact, the philosophy of the method is closely related to the question of the distribution of single particle energies in a three-dimensional potential well (Ref. 14-17, 353, 362, 391-393), which can be approached by semiclassical methods (Ref. 171-174). Such approaches are very helpful for the understanding of shell structures and the origin of shell structures in general (Ref. 393).

The shell correction method has provoked a number of serious criticisms (Ref. 24-27, 43, 154, 206, 223, 242, 313, 326, 333, 346, 347, 410). Part of the criticism concerns the question of whether single particle energies can be the carriers of shell energies at all. This will be treated in greater detail in Section VI. Some of the criticism concerns the method of taking averages, which indeed is not a trivial problem. Strutinsky's original method is developed for an unlimited spectrum, i.e., one whose range is limited neither from below nor from above. He averages the spectrum over a finite energy interval γ, which by an order of magnitude is equal to the mean intershell distance and fulfills the two major requirements of a sensible averaging procedure: (i) The average is independent of the averaging interval γ; (ii) The average of the average is again the average. However, the condition of unlimited spectra is not met in reality. The spectrum is limited either from below (e.g., harmonic oscillator), or from below and above (e.g., Woods-Saxon or similar potentials).

This defect has been considered, but so far not been applied on a larger scale (Ref. 192-194, 394). The identification of the smooth average with the liquid drop energy generates the following problem. In any drop or droplet model, the nuclear density is parameterized; in the shell model one parameterizes the deformation of the potential. No theorem exists to relate the two deformations neatly, except the somewhat vague belief that the density follows the potential "on the average." In practice, one identifies the deformation of an equipotential line with an equidensity line of the droplet (Ref. 64, 395).

Finally, the shell correction approach is cooked down to the simple "Strutinsky recipe"; (i) Define a single particle Hamiltonian which (in addition to a kinetic energy and a spin-orbit interaction) contains an average potential. (ii) The average potential can be deformed, its deformation being described by one or several formal parameters α_i. (iii) One calculates the "shell correction energy δU" as a function of the deformations α_i, and (iv) adds them to a suitably defined average or liquid drop energy $W_{LD}(\alpha_i)$. The so-generated deformation energy $W(\alpha) = W_{LD}(\alpha) + \delta U(\alpha)$ plays the role of a potential energy in a "collective model" (see below).

The conceptual and methodological simplicity of the shell correction approach has initiated a large number of calculations (Ref. 19, 20, 23, 99, 101, 119, 125, 146, 158, 167, 187, 188, 221, 225, 226, 263, 265, 266, 267, 274, 275, 298, 321, 331, 352, 369, and further references below). As a by-product, effective computer algorithms and single particle models have been developed, by use of which the single particle problem can be treated even for very large and exotic deformations (Ref. 77, 126, 159, 189, 253, 321, 345). Unfortunately, in the present context a detailed and complete account of the various contributions cannot be given. The major development took place in the years 1967-1973 and came to a certain saturation in the year of the third IAEA symposium on the physics and chemistry of fission (Ref. 5).

The various approaches differ, for example, in the particular way the radial dependence of the average potential is chosen.

The models cover the modified harmonic oscillator of the familiar Nilsson model, e.g., Ref. 298, 331, and 352; two-center oscillators, e.g., Ref. 10, 11, 159, 185, and 368, either joined smoothly by inverted parabolas or not; or finite size potentials of Woods-Saxon shape (Ref. 187, 188, 321) or of the similar "folded Yukawa" type (Ref. 53, 167, 265). Contrary to common belief, the latter two approaches cover two-center potentials as well. The various models and approaches differ as well in the way the deformation is formally introduced. Some of them parameterize equipotential lines by expansion in terms of spherical harmonics, up to and including order 6; some of them parameterize the geometry of these surfaces according to "generalized spheroids," "fission threshold shapes," "spheroids connected by hyperboloids of revolution," or similar approaches. A classification of deformation other than by the formal parameters is difficult if not impossible, because one has no guiding principle other than imagining what could be important. In some of the calculations, one has replaced the formal parameterization of equipotential lines with the spatial moments of the density (Ref. 80, 230, 260, 261). This does not remove all of the problem, but it at least allows for direct comparison of different models, including self-consistent field calculations. In order to avoid an all too obvious dependence on the particular parameterization, a serious shell correction calculation should work with three or four independent and qualitatively different formal deformation parameters.

They should be related to the most important aspects of deformation, i.e., (i) elongation, (ii) constriction in the middle, (iii) left-right asymmetry of an axially symmetric density, and (iv) axial asymmetry. All of them are important in certain regions of deformations.

Qualitatively, the various calculations based on different models agree in one respect: they give a deformation energy like the one presented in Figure 7. All of them thus have at least four stationary points in the energy landscape. Two of them are stable against deformation (E_I and E_{II}) and can be identified

with local ground states; two of them are unstable in the "fission mode" and can be identified with "fission barriers" (E_A and E_B). Taken with a grain of salt they can be compared with experimental data.

The comparison is restricted below to a few characteristic aspects and results. A broader discussion in view of empirical data is reserved to the lectures of H. Weigmann (Ref. 418) in this school.

The binding energy or rather the difference between empirical masses and a semiempirical mass formula, is given in Figure 9. The small discrepancies detectable in Figure 2 are drastically enlarged in the top part of Figure 9. These large "shell effects" are qualitatively reproduced by a shell correction calculation as given in the middle part, but some significant deviations (lower part of the figure) remain which albeit being small (1-2 MeV on the average) expose some regular and smooth structure. This is in some conflict with the philosophy of the shell correction approach according to which all smooth dependence should be contained in the "liquid drop background." Whether these deviations are due to the shell correction method, or due to the phenomenological average potential, or due to a nonoptimal semiempirical mass formula is unclear. To this level of accuracy it is equally unclear whether or not one should add some mystical zero-point energy, i.e., whether the formal deformation parameters α_i are quantum-mechanical coordinates; but this is another story.

In the ground state deformations (Ref. 83, 140, 263, 297, 329), the underlying liquid drop energy is almost irrelevant. They are almost entirely a shell effect. As seen in Figure 10 the agreement with experiment is satisfactory though not complete in all of the cases. But one should remember the uncertainty of how to relate "deformation parameters" to the experimental B(E2) values. Quadrupole moments have been measured directly by reorientation measurements and agree with the calculated quadrupole moments within the limits of error so far.

The energy of the second minimum is about 1-3 MeV above the ground state, depending somewhat on the nuclear charge. This is displayed in Figure 11, and compared with experimental numbers extracted from excitation functions for isomeric fission. In view of the above-quoted theoretical uncertainty, the agreement for elements heavier than uranium is satisfactory, but for thorium the discrepancy is obvious. Whether or not this discrepancy can be removed by the existence of a third, but shallow minimum in the potential energy (Ref. 44) or whether other causes are possible is still under debate (Ref. 12, 8).

The deformation at the second minimum is about twice as large as for the ground state. Values for various heavy nucleides are tabulated in the literature (Ref. 61, 321). A first but indirect experimental evidence of its size was found by Specht and collaborators, identifying members of a rotational band with an abnormally small rotational constant (Ref. 366). Direct evidence was brought by the experiment of Metag, Habs, and others, as a result of which they could measure the quadrupole moment of the isomerically fissioning state of ^{239}Pu to be Q = 36 barn (Ref. 141, 256). This largest quadrupole moment ever measured demonstrates without any need of calculations the large deformations involved with isomeric fission and gives strong evidence for the interpretation of the fission isomers as shape isomers as advocated by Strutinsky. The calculations of the quadrupole moment (Ref. 61), preceding the experiment in time, agree with these findings.

The energies of the two fission barriers (Ref. 187, 258, 264, 265, 273, 298, 302, 322) have been calculated and tabulated by many authors. In Figure 11 the results of Nix and Möller (Ref. 265) are plotted. The Z^2/A dependence of the underlying liquid drop energy is completely masked by the shell corrections. In fact the calculated fission barriers are almost independent of Z and A (in certain regions of the periodic table), very much in line with the old experimental findings (see also the discussion above). A detailed comparison with the experiment is difficult (Ref. 419), because the extraction of fission barriers from the excitation function for fission relies strongly on Bohr and Wheeler's model of a transition state, a concept which is not dramatically changed by the existence of two or more fission barriers.

Combining experimental results on intermediate structure and model calculations of level densities with the fission cross sections in a suitable manner, one may extract "experimental fission barriers" with sufficient accuracy to permit a meaningful comparison with calculations. As a rule, calculation and experiment agree much better for the outer barrier than for the inner barrier. For some of the calculations this has the following reason. The liquid drop deformation energy is extremely sensitive to the ratio of the surface to Coulomb energy at spherical shape, much more so than the binding energies. As it turned out, it is possible to enforce agreement between experiment and calculation by adjustment of this ratio at the barrier, without changing the binding energy. Because the inner barrier with its smaller deformations depends much less on the liquid drop energy, its discrepancy with experiments must be related to shell structure. It is unclear whether the obviously wrong trend with (N - Z) has the same cause as the discrepancy noted for the ground state shell corrections, whether the relation between calculation and experiment is obscured by the appearance of a third minimum (Ref. 44), whether dynamic barriers (Ref. 320) would be more relevant than the static one for these particular nucleides, or whether so far unknown reasons are responsible.

The deformation at the fission barriers is usually not tabulated, but resides in the unpublished material, or in drawings of deformation energy surfaces for selected nucleides (Ref. 267, 268, 321). Perhaps due to Hill and Wheeler's (Ref. 153) statements it came as a surprise (Ref. 268) that shell effects cause the outer barrier to appear at left-right asymmetric shapes. In fact their inclusion is crucial for a quantitative agreement with experiments. The asymmetry of shape at the outer barrier has been brought immediately in connection with the empirically asymmetric distribution of fission fragment masses. Its peak-to-peak ratio correlates with the shape asymmetry at the barrier almost quantitatively, as shown in Figure 12. The mass distribution being decided at the (outer) barrier is in certain conflict with the statistical interpretation of Fong to be discussed below (Section V).

On the other hand, the shape asymmetry is maintained between the barrier and scission in practically all of the calculations. This is particularly obvious in Figure 13, taken from the work of Mosel (Ref. 285). The inclusion of axial asymmetry leaves the outer barrier unchanged but improves the agreement between experiment and calculation for the inner barrier to some extent. The effect is however considerably weaker than for axial left-right asymmetry; also it does not persist for larger deformations (Ref. 125, 187, 265).

In a rotating nucleus the fission barriers can be substantially lowered (Ref. 72). Sufficiently fast rotations can also change the shell structure appreciably with additional impact on the fission barriers. The shell correction approach can be adapted to rotations (Ref. 94, 95, 100, 284, 389), but we must decline to go into the details.

The shell correction approach was particularly useful for calculating the deformation energy of the hypothetical superheavy nuclei (Ref. 30, 54, 69, 102, 166, 186, 211, 212, 246, 255, 262, 276, 281, 301-303, 305, 348, 357, 407), which are supposed to be stable against fission almost exclusively due to shell structure.

The above-reported calculations deal with the lowest possible energy of a deforming nucleus. But a fissioning compound nucleus (Ref. 170, 351) can be regarded as a hot, intrinsically excited system. At sufficiently high intrinsic excitation, shell effects disappear gradually with temperature (Ref. 128, 178, 270), which is of particular importance for the second barrier, where the asymmetry is entirely a shell effect.

Shell structure modifies the Bohr-Wheeler picture primarily in one respect: the liquid drop deformation energy is replaced by a more complicated function. But shell structure also influences the other ingredient needed for the analysis of fission cross section: the density of states in an excited nucleus (Ref. 168). The evaluation of the number of states per unit energy interval as a function of the energy is a problem of its own with a vast field of activity (Ref. 88, 127-129, 168, 174, 180, 181, 205, 332, 409, 424), which we may only touch on in passing. In the inde-

pendent particle model, it can be obtained by enumeration, but the combinatorial problem becomes increasingly prohibitive for the higher excitations, and approximation methods must be used. In part of the work, evaluation of the density of states by a renormalization method similar to the shell correction approach was suggested (Ref. 128).

IV. Fission Dynamics I: Spontaneous Fission and the Question of Collective Inertia

In Bohr and Wheeler's approach to fission, the density of nucleons - more precisely their one-body density - is characterized by a number, the fission coordinate α. It is a function of time. They associate a potential energy with this coordinate and identify it with the deformation energy. For treating induced fission in the transition state model only one point of this function, the fission threshold, is really needed. It is irrelevant at what time the system passes over the saddle, and in this sense their approach is static. The modification of the deformation energy by the shell correction approach does not change the concept: the highest of the fission barriers is to be identified with the threshold.

Bohr and Wheeler use the same picture for spontaneous fission, which is interpreted as barrier penetration. But this cannot be done without certain statements on the dynamics. The following steps seem compulsory. (i) Associate with the fission coordinate not only a potential $W(\alpha)$ but also a kinetic energy $K = (1/2)B(\alpha)\dot{\alpha}^2$; the classical equations of motion conserve the energy

$$\tilde{H} = \tfrac{1}{2}B(\alpha)\dot{\alpha}^2 + W(\alpha) \quad . \tag{12}$$

(ii) Rewrite this function in terms of the canonically conjugate momentum $\pi = \partial K/\partial\dot{\alpha}$ and replace α and π by operators, subject to the appropriate commutation relations. Finally, (iii) apply the WKB approximation. Because α describes the collective motion of all the nucleons, one refers to $\dot{\alpha}$ as the collective velocity, to $B(\alpha)$ as the collective inertia, and to $\tilde{H}$ as the collective Hamiltonian.

The collective model of nuclei (Ref. 47-49, 51), i.e., the reduction of the nuclear many-body problem to a collective Hamiltonian of low dimension N,

$$\tilde{H} = \frac{1}{2}\sum_{i,j=1}^{N} B_{ij}(\beta_1,\ldots,\beta_N)\dot{\beta}_i\dot{\beta}_j + W(\beta_1,\ldots,\beta_N) \quad , \tag{13}$$

continues to be a central problem in nuclear theory. Many different versions of collective models (Ref. 350) can be found in the literature (Ref. 29, 36, 37, 149, 176, 228, 280, 318, 342, 350, 374, 375), and many different ways of calculating the tensor of effective mass B_{ij} (Ref. 151, 164, 177, 201, 259, 327, 328, 361, 371, 390, 412, 421) or moments of inertia for rotations (Ref. 358, 405, 406). The generator coordinate method (Ref. 18, 104, 105, 121, 135, 343, 431) and the cranking model (Ref. 182, 183, 195, 196, 204, 243, 244, 299, 315, 324) for cold and excited nuclei (Ref. 271, 272, 386) have been applied in various versions, not to speak about other approaches related to self-consistent fields (Section VI). But whether the reduction to Eq. (13) is possible at all and, in particular, whether the formal deformation parameters β_i are the true canonical variables subject to quantization and how (Ref. 156, 157, 309), cannot be rigorously answered and will not be pursued for the moment. Instead we suppose the existence of a collective Hamiltonian ad hoc and ask ourselves how we can cope with the multidimensionality in penetration calculations (Ref. 68, 75, 155, 210, 283, 320, 338, 344), and in particular how (i) Bohr and Wheeler's fission degree of freedom α' could possibly be related to the set of formal deformations β_i, and (ii) how the "collective inertia tensor" B_{ij} is obtained in the cranking model.

In the good old times of Bohr and Wheeler, both questions did not need to be answered explicitly, because for the description of the one fission decay constant it is possible to absorb the fission coordinate and its inertia into the numerical values of the fission barrier and its "thickness." In the presence of two (or more) fission barriers, one has, however, (at least) three decay constants in one and the same nucleus: (i) the "traditional"

decay constant for ground state spontaneous fission, (ii) the decay constant for isomeric fission, and (iii) the decay constant from the second into the first well. If one wants to maintain the concept of penetration even for this case, one has to make sure that the three penetration integrals are evaluated consistently.

The fission trajectory. Suppose a space of sufficiently many formal deformation parameters $\{\beta_1,\ldots,\beta_N\}$. One may create a whole manifold of "fission coordinates" by various trajectories

$$\alpha(t):\ \{\beta_1(t),\ldots,\beta_N(t)\} \tag{14}$$

embedded in the multidimensional space of the $\{\beta_i\}$. For fixed end points, each of these trajectories has an associated action integral

$$S = \int_{\alpha_1}^{\alpha_2} d\alpha \left[2|E - W| \sum_{ij} B_{ij} \frac{d\beta_i}{d\alpha} \frac{d\beta_j}{d\alpha}\right]^{1/2} , \tag{15}$$

being the transcription of Eq. (5) for one particular trajectory, and consequently has its own decay constant in WKB approximation. In order to remove this ambiguity, one may search for the particular trajectory which minimizes S and around which

$$\delta_\alpha S = 0 \tag{16}$$

holds with respect to variations in the trajectory. This procedure should not be confused with the least action principle of classical mechanics, nor with stationary phases in semiclassical approximations to path integrals; it merely serves as an operational prescription for α.

The cranking model has been the most popular for the calculations of collective inertias B_{ij} (Ref. 182). In the following we shall follow the procedure of Wilets (Ref. 2). Assume first the nucleons moving in a time-independent average potential $V(x,\beta)$, whose deformation and orientation in space is fixed by the formal parameters $\{\beta_i\} = \beta$. This is the same assumption as made above for the calculation of deformation energy. The many-body state

for this problem, $|\phi_\mu(\beta)\rangle$, is a solution of the deformation-dependent Hamiltonian $H(\beta)$

$$H(\beta) = \sum_i \hat{p}_i^2/2m + V(\hat{x}_i,\beta) , \tag{17}$$

i.e.,

$$E_\mu(\beta)|\phi_\mu(\beta)\rangle = H(\beta)|\phi_\mu(\beta)\rangle . \tag{18}$$

H is a one-body operator, and the eigenvalue E_μ is the sum of single particle energies of the occupied orbits. One of the E_μ is the lowest, say E_{μ_o}, and can be identified with the potential energy $W(\beta) \equiv E_{\mu_o}(\beta)$. Suppose now that someone sets this potential in motion, i.e., induces a given time dependence $\beta(t) = \{\beta_i(t)\}$. The state of the system then develops according to the Schrödinger equation

$$i\hbar \frac{\partial}{\partial t}|\psi(t)\rangle = H(\beta(t))|\psi(t)\rangle , \tag{19}$$

with an explicitly time-dependent Hamiltonian $H(\beta(t))$. One may write the amplitude $|\psi(t)\rangle$ in terms of the above $|\phi_\mu(\beta(t))\rangle$, taken as the eigenstates of a parametrically time-dependent Hamiltonian $H(\beta) = H(\beta(t))$, i.e.,

$$|\psi(t)\rangle = \sum_\mu C_\mu(t) \exp\{\tfrac{1}{i\hbar}\int_{t_o}^{t} E_\mu(\beta(t'))dt'\}|\phi_\mu(\beta(t))\rangle . \tag{20}$$

Specifying the initial condition as $C_\mu(t_o) = \delta_{\mu\mu_o}$, the problem is completely determined. It is solved as soon as the coefficients $C_\mu(t)$ are known functions of the time. They are solutions of the first order and linear differential equation

$$\dot{C}_\mu(t) = \sum_{\ell=1}^{N} (-i\dot{\beta}_\ell) \sum_{\mu'} \langle\phi_\mu(\beta)|\frac{\partial}{\partial\beta_\ell}|\phi_{\mu'}(\beta)\rangle C_{\mu'}(t) \cdot$$

$$\exp\{\tfrac{1}{i\hbar}\int_{t_o}^{t} (E_\mu(t') - E_{\mu'}(t'))dt'\} , \tag{21}$$

being obtained by substitution of Eqs. (20) and (18) into (19). Because of the explicit time dependence of the Hamiltonian, the energy $E = \langle\psi(t)|H(\beta(t))|\psi(t)\rangle$ is not a constant of motion, and

takes the form

$$E = \sum_{\mu} |C_{\mu}(t)|^2 E_{\mu}(\beta(t)) \ .$$

Using conservation of norm,

$$\langle \Psi(t) | \Psi(t) \rangle = \sum_{\mu} |C_{\mu}|^2 = 1 \ ,$$

it can be split into the above defined potential energy W and a rest K, i.e.,

$$E = W(\beta(t)) + K \ , \quad K = \sum_{\mu} |C_{\mu}(t)|^2 (E_{\mu}(t) - E_{\mu_o}(t)) \ . \tag{22}$$

The energetic response to the cranking resides in K, and depends only on the size of the $\dot{\beta}(t)$. Being strictly zero for $\dot{\beta}_i = 0$, it is quadratic

$$K = \frac{1}{2} \sum_{ij} B_{ij}(\beta(t)) \dot{\beta}_i(t) \dot{\beta}_j(t) \tag{23}$$

in lowest order of approximation, i.e., has the structure of a kinetic energy.

The last step only is an approximation. It is obtained from Eq. (21) by setting at $t - t_o$ all coefficients C_{μ} zero, except $C_{\mu_o} \sim 1$, and treating the time dependence of all terms small except at the upper limit of the phase integral. Under this assumption, Eq. (22) can be solved

$$C_{\mu}(t) = \sum_{\ell} i\hbar \dot{\beta}_{\ell} \sum_{\mu} \frac{\langle \phi_{\mu} | \partial / \partial \beta_{\ell} | \phi_{\mu_o} \rangle}{E_{\mu} - E_{\mu_o}} \cdot$$

$$\exp\left\{\frac{1}{i\hbar} \int_{t_o}^{t} (E_{\mu}(t') - E_{\mu_o}(t')) dt'\right\} \tag{24}$$

and upon insertion into the expression for K, Eq. (23), leads to an explicit expression for B_{ij}, i.e.,

$$B_{ij}(\beta) = 2\hbar^2 \sum_{\mu \neq \mu_o} \frac{\langle \phi_{\mu} | \partial / \partial \beta_i | \phi_{\mu_o} \rangle \langle \phi_{\mu_o} | \partial / \partial \beta_j | \phi_{\mu} \rangle}{E_{\mu} - E_{\mu_o}} \ . \tag{25}$$

A similar consideration can be performed for quasiparticles. It amounts to replacing the Slater determinants by $|\phi_{\mu_o}\rangle$ by BCS states in order to account for parts of the residual interactions. This modification does not affect the approximation scheme in general, but makes the final expressions somewhat less transparent. They can be found in the literature.

In the above derivation, certain terms have been dropped by an argument of smallness. But it remains unclear as compared to what they are small. Sometimes referred to as "adiabasy condition," it is therefore very difficult to judge and discuss its validity (Ref. 350). However, these questions are not specific to the theory of fission, but to the collective model in general, and will not be pursued in detail.

The moments of inertia (Ref. 61, 95, 361, 363) against rotations are obtained by taking the formal parameter $\beta(t)$ as the rotation angle of the $\phi(t)$ of the average potential, i.e., $K = (1/2)\Theta\dot{\phi}^2$. Figure 14 displays such a moment of inertia as a function of deformation. It is an additional assumption to identify this number with the moment of inertia Θ appearing in the energies of rotational spectra $E_I \sim (\hbar^2/2\Theta) I(I+1)$. If one does so for the ground state band in ^{240}Pu as well as for Specht's band (Ref. 366) associated with the isomer state, and inserts them at the respective theoretical equilibrium deformations, one obtains an almost perfect agreement between theory and experiment, as seen in the figure. This agreement is disquieting in view of what was said above, but it seems a general feature that cranking model moments of inertia agree with experiment in wide regions of the periodic table.

The mass parameters (Ref. 21, 322, 361) against changes of shape are obtained by identification of the β_i with the respective formal deformation parameters. With lack of knowledge of normal modes of vibrations, one has to deal in general with a mass tensor, B_{ij}. In practice, this tensor is far from being diagonal, its components being complicated functions of the deformations. They show strong dependence on shell structure, an example being given in Figure 15 for a particular case. As compared to

some average they are relatively small at the deformations corresponding to local minima in the deformation energy, indicated by arrows in the figure, and relatively large in the barrier regions. Depending on the deformation they are larger by a factor of 4-10 than the inertias obtained from a fluid dynamical picture with irrotational flow. Contrary to the moments of inertia, mass parameters for changes in shape cannot be compared to experiments without explicit use of the curvatures in the deformation energy, and without additional assumptions on the nature of collective motion. But it seems as if the cranking model mass parameters are too small by at least a factor of 2 to account for the characteristic vibrational frequencies in nuclei (Ref. 89).

If one applies the cranking model mass parameters to the problem of ground state spontaneous fission in the way outlined above, it turns out that the calculated lifetimes are much too large. These lifetimes can be shortened by an ad-hoc reduction of the calculated inertias by roughly a factor of 2, i.e., by a correction in the opposite direction than for the spectra. This apparent inconsistency has not yet been resolved.

In some of the calculations (Ref. 233) the reduction of the penetration integral was achieved by treating the fissility parameter as a free parameter subject to reach agreement between calculated and measured decay constants for spontaneous fission. This procedure merely changes the thickness of the barriers, but leaves the minimal action trajectories as well as the dynamic fission barriers almost unchanged. The so obtained results are displayed in Figures 16 and 17. The agreement for ground state spontaneous fission, of course, is a consequence of the procedure, but the agreement for isomeric fission (Ref. 257) by order of magnitude is unsolicited. The decay constant for the decay from the second into the first well has about the right order of magnitude (Ref. 320).

In other calculations (Ref. 338-340) the problem of too large cranking model mass parameters is solved by an overall reduction factor. This leads to an agreement with the experimental half-lives to within a factor of 20, although the deviation is sometimes appreciably larger. The most recent calculations with the cranking model report an agreement within a factor of 50 (Ref. 21). Quite significant discrepancies occur in the systematics of fission half-lives.

In conclusion, it is not clear whether the reported discrepancies between calculation and experiment are due to the particular model of cranking or due to some deeper problematics related to the collective model in general. Although the problem of spontaneous fission seems to be solved qualitatively, the disagreement remains worrisome.

V. Fission Dynamics II: Selected Aspects on Mass and Kinetic Energy Distributions

If a slow neutron is absorbed by a heavy nucleus, say ^{240}Pu, inducing it to fission, one does not observe fission fragments with a particular mass and a particular relative kinetic energy, but a whole distribution. As an example, one of the earliest doubly differential cross sections measured is presented in Figure 18. This cross section is peaked at the most probable mass and at the most probable kinetic energy of the fission fragments, i.e., at 100 (140) amu and 180 MeV, respectively. The distributions in fragment masses and their energies are not independent statistically, and, therefore, the reduction to the one-dimensional mass-distribution kinetic energy distributions destroys part of the information. Often, these distributions are characterized by their moments, for example their centroid and their variances. The distributions are functions of the projectile energy, but mass and kinetic energy behave differently. The peaks at the most probable masses are washed out comparatively fast and grow into broad distributions, quite opposed to the mean kinetic energy and its variance which vary much less. A collection of more recent experimental material can be found in the IAEA proceedings.

The mass distribution of the fission fragments is asymmetric. The most probable fission event occurs for unequal masses. This is in conflict with the liquid drop picture of fission, and has challenged a respectable number of models, e.g. Ref. 113, 149,

185, 213, 370. Shell structure at the fission thresholds was denied in the beginning (Ref. 153), but reconsidered later (Ref. 184, 234), but only with the advent of the shell correction approach was it possible to isolate its impact: the shape at the outer barrier is left-right asymmetric (Ref. 268) in the actinide region (see also Section III).

This interpretation is supported by three kinds of model considerations: (i) The asymmetry is maintained between saddle and scission (see for example Figure 13); (ii) The trajectory calculations reported in Section IV prefer the asymmetric shapes even beyond the saddle, the shape asymmetry is relevant also dynamically; (iii) Shell effects fade out with increasing excitation energy; one expects, therefore, a trend toward the more symmetric droplet fission in accordance with the data. But these arguments account only for the peak values of the distributions; the mechanism for their broadness is largely unclear. Attempts to interpret them as quantal zero-point fluctuations in the mass-asymmetry collective coordinate agree with the data on spontaneous fission at and around the peaks, but fail at the valleys of the distribution (Ref. 241, 251, 252). It is unclear how this mechanism can be extrapolated to high excitation energies. At a first glance, this interpretation is in conflict with the former, the statistical interpretation of Fong (Ref. 92, 97, 98, 110-113). For the former the shell effects at the barrier, i.e., at strongly overlapping densities, are decisive, while Fong works with the phase space available for the separated fragments. The formation of the fragmentary shells at the barriers and their maintenance between saddle and scission could be an element of connection eventually; see also Ref. 149, 150, 158, 423.

The kinetic energy distribution has been the goal of much theoretical effort, but its origin is even less clear than the distribution of masses. Of particular interest was the question of why the mean value of the kinetic energy is so appreciably lower than the Q value of the reaction. This indicates that some of the available energy goes into degrees of freedom other than the relative kinetic energy of the fragments. The other degrees of freedom can be of collective nature, like rotations of vibrations of the fragments, or of single particle nature resulting in an intrinsic excitation, or most likely both of them. The problem is once more, how these qualitatively different types of excitation can be separated.

The most straightforward model is of geometrical nature and based on the peculiarities of the liquid drop energy surface. As pointed out by Strutinsky et al. (Ref. 402), this surface has an additional barrier between the simply connected and the separated shapes. This barrier disappears at characteristic elongations, at a mean center distance of the fragments of $\rho^* = 1.16\ R_o$. This number holds for almost all of the nuclei. Behind this "exit deformation" (Ref. 64) strong forces arise which tend to disrupt the density. If one assumes the prescission kinetic energy to be small such that all kinetic energy results from the Coulombic repulsion beyond this point, one obtains a fair agreement with the experimental data.

This simple result allows for two different conclusions. Either virtually all of the energy available at the exit deformation converts into collective modes perpendicular to relative kinetic energy motion, or dissipation into intrinsic degrees of freedom is so strong that the fragments remain essentially at rest until they are fully separated. An answer to this question can be found by model calculations (Ref. 70, 79, 82, 145, 203, 219, 224, 310, 355).

Nix and co-workers have performed a number of calculations (Ref. 81, 356, 357) in which dissipation was treated in terms of Rayleigh's dissipation function

$$F = \frac{1}{2}\frac{dE}{dt} = \frac{1}{2}\sum_{i,j}\eta_{ij}\dot{\beta}_i\dot{\beta}_j \ . \qquad (26)$$

With the Lagrangian $L = K - W$, the difference of collective kinetic and potential energy, the equations of motion for the collective variables $\beta_i(t)$ are given by

$$\frac{d}{dt}\left(\frac{\partial L}{\partial \dot{\beta}_i}\right) - \frac{\partial L}{\partial \beta_i} = -\frac{\partial F}{\partial \dot{\beta}_i} \ . \qquad (27)$$

The collective inertias were obtained from an irrotational flow model, and the viscosity tensor η_{ij} was evaluated for two models: (i) for two-body viscosity and (ii) for the wall-and-window formula (Ref. 217, 218, 336, 337, 354). The results for the first are shown in Figure 19, but with suitable adjusted parameters the latter agrees equally and almost indiscernably well with the mean kinetic energies. Obviously they are not very sensitive to the mechanism of dissipation. Whether the energy is dissipated by two-body collisions or by collision of particles with a moving wall seems irrelevant.

The mechanism of single particle excitation (Ref. 376-378) as the source of dissipation has been studied by solving the cranking model equations numerically, at finite collective velocities. The respective equations are given in Section IV, and by means of them, the elementary modes of quasiparticle-quasihole excitations can be treated properly. To some extent this model of "dynamic excitation" is the quantal analog to the "wall-and-window formula" - the particles gain additional momentum by collisions with the moving walls of the potential - and agrees with it in the main conclusion: Most of the energy available at the scission configuration is absorbed into intrinsic excitation. A further common feature is the necessity to preselect a "fission trajectory." No element in these models permits judgment of the "best" of all possible ones. The model of dynamic excitation, however, is hampered by additional difficulties: On top of the very complicated numerics, it converges very slowly - if at all - with the number of particle-hole channels included in the calculations. For additional approaches we refer to the literature (Ref. 120, 231, 232, 314, 372).

Based on these model calculations one concludes with little doubt that the collective motion in the fission mode is slowed down by the coupling to single particle degrees of freedom. Albeit this coupling is not understood in detail, it acts as if *frictional terms are present in the equations of motion*, tractable for example by Rayleigh's dissipation function. Obviously, the mean kinetic energies of fission fragments are not sensitive to further details.

The models so far discussed deal with the most probable kinetic energy, the peak of the distribution. The distribution itself has been generated in the past by solving the equations of motion for the collective coordinates $\beta_i(t)$ for different initial velocities at the barrier and weighting the resulting kinetic energies according to an initial thermal velocity distribution. This procedure executed for a nonviscous irrotational flow could be extended eventually for viscous motion according to Eq. (27) and includes all possible effects due to "amplifying modes" (Ref. 269). The so obtained distributions have variances, which are too small by a factor of 2 as compared to experiment. One may speculate that the variances for viscous motion rather are smaller than larger, thus increasing the discrepancy with experiment. The inclusion of friction seems necessary to enforce agreement with experiment for the mean kinetic energy.

But if one agrees on <u>friction</u>, one must conclude on <u>diffusion</u> in the sense that the sharp and well-defined trajectories associated with a particular initial condition should spread into bundles and be replaced by distributions. This follows from the "fluctuation-dissipation theorem." Such a mechanism becomes tractable replacing the equations of motion (Eq. (27)) by transport equations for the distributions. The recent and very simple model calculations seem to indicate a substantial change in the distribution of kinetic energies. The variances are increased due to <u>thermal fluctuations</u> in addition to and opposed to the "collective variances" mentioned. Eventually, they could improve comparison between theory and experiment (Ref. 131, 132).

Transport equations of this kind are conceptually very close to an old and almost forgotten idea of Kramers (Ref. 220) that fission might be interpreted as a <u>diffusion phenomenon</u>, and tractable similar to a chemical reaction. The relevance of transport phenomena in heavy ion collisions (Ref. 136, 417) - which in many ways are similar to or complementary to fission - make such an

interpretation more likely than in all the years before. In a first attempt (Ref. 130) - slightly different from Kramers' approach - the diffusion over a barrier was tackled in a one-dimensional model, a kind of energy representation. In thermal equilibrium, one has a small but finite probability for the occupation of states being energetically over the fission barrier. These may leak out. The friction term works in toward reoccupation of these states. The delicate balance between the feeding and decay of the states above the barrier is not discussed in detail in this short account, but one should stress the point that the Bohr-Wheeler cross section for fission is obtained in the limit of large friction. At finite values of the friction constant the fission cross section deviates from the Bohr-Wheeler formula toward a better agreement with the experiment. Eventually this will allow for an alternative determination of the friction constant.

Perhaps the even more important aspect of transport phenomena is the possibility of overcoming the quasistatic picture of Bohr and Wheeler's transition state and replacing it by dynamic developments. It seems unlikely that only one point in the deformation energy landscape should determine all the aspects of the fission process, in particular the "distributions," i.e., the multidifferential cross sections, which after all are the only quantities of interest, as they can be measured.

VI. Selected Relations to the Many-Body Problem by Self-Consistent Field Approximations

In one way or the other the phenomenological methods can be justified only if they turn out as approximative solutions to the nuclear many-body problem. For this one may admit a nonrelativistic approach, as the binding energies are sufficiently small. On top of the operator for the kinetic energy such a Hamiltonian should contain <u>at least</u> the pairwise interactions V(i,j) of any two particles labelled i and j, respectively, i.e.,

$$H = \sum_{i=1}^{A} \vec{p}_i^{\,2}/2m + \frac{1}{2} \sum_{i=1}^{A} \sum_{j=1}^{A} V(i,j) \ . \qquad (28)$$

The interactions do not appear in the above phenomenological models. One may conclude from this that they reside implicitly in the model parameterizations. The establishment of such relations is a difficult and widely unsolved problem. In view of a multitude of partially conflicting models, such relations are a necessity up to and beyond the intellectual satisfaction.

Some aspects of the models can be made plausible, at least. For example, the shell correction approach of Section III can be understood as an approximation to constraint, self-consistent field equations, and in particular, one can learn in which sense single particle energies can be the carrier of a shell correction energy. This is demonstrated further below.

First, we recall a few elements of the nuclear many-body problem in a very condensed form. This seems necessary in view of the more formal arguments to be presented below. We shall deal first with the time-dependent problem, and only later with the stationary one, but this is more a question of personal preference.

In the self-consistent field approximation, one substitutes the problem of finding a solution to the <u>many-body</u> state $|\Psi(t)\rangle$,

$$i\hbar \frac{\partial}{\partial t}|\Psi(t)\rangle = H|\Psi(t)\rangle \ , \qquad (29)$$

or of constructing the many-body density N(t) by

$$\frac{\partial}{\partial t} N(t) = \frac{1}{i\hbar}(HN - NH) \equiv \{H,N\} \ , \qquad (30)$$

where

$$N(t) = |\Psi(t)\rangle\langle\Psi(t)| \ , \qquad (31)$$

by the much simpler problem of finding a solution to the <u>single particle</u> state $|\psi_i(t)\rangle$, i.e., to

$$i\hbar \frac{\partial}{\partial t}|\psi_i(t)\rangle = h(t)|\psi_i(t)\rangle \ , \qquad (32)$$

or to the one-body density $\rho(t)$,

$$\frac{\partial}{\partial t} \rho(t) = \{h(t),\rho(t)\} \ , \qquad (33)$$

which in its diagonal form is defined by

$$\rho(t) = \sum_i n_i |\psi_i(t)><\psi_i(t)| \ . \qquad (34)$$

The (one-body) Hamiltonian h is the sum of kinetic and potential energy

$$h(t) = p^2/2m + \Phi(t) \ , \qquad (35)$$

of any one particle (i), as usual, but the potential is obtained from the pair interaction V(i,j) by an average over all particles, i.e.,

$$\Phi(t;i) = tr_j \rho(t;j) V(i,j) \ . \qquad (36)$$

One speaks of a "self-consistent" generation of the potential Φ.

The first attempt to derive a one-body equation like (34) was made by Dirac (Ref. 86, 87); see also Ref. 404. By the nature of his arguments (maintenance of proper normalization and antisymmetry), Dirac was compelled to an idempotent density matrix, i.e.,

$$\rho^2 = \rho \ , \qquad (37)$$

or in other words, to occupation numbers $n_i = 0$ or $n_i = 1$ (see Eq. (34)). This in turn is identical with the statement (Ref. 404) that the many-body state $|\Psi(t)>$ is the antisymmetrized product of single particle states $|\psi_i(t)>$ (Slater determinant). For a Slater determinant, the energy can be expressed in closed form by the one-body density (matrix), i.e.,

$$E \equiv <\Psi(t)|H|\Psi(t)> = tr\rho p^2/2m + \frac{1}{2} tr_1 tr_2 \rho(1) V(1,2) \rho(2) \ . \qquad (38)$$

Provided that $\rho(t)$ is a solution to Eq. (34), E is a constant of motion ($\dot{E} = 0$). The requirement of a stationary density (matrix) ρ, i.e., $\dot{\rho} = 0$, gives an eigenvalue equation for the single particle state,

$$h|\psi_i> = \varepsilon_i |\psi_i> \ , \qquad (39)$$

the so-called Hartree-Fock equation.

This way one is confronted with the statement of a Slater determinant being an eigenstate to the (many-body) Hamiltonian H. Its failure is obvious immediately, and one has fought about it by methods which essentially replace true pair interaction by effective interactions (Ref. 7, 67, 76, 93, 277, 293, 295, 296) of various natures but still maintaining the concept of a Slater determinant. The relevant arguments were given for the stationary (Ref. 294, 295), but not - and this should be stressed - for the time-dependent version of the one-body equation. A careful analysis of the time-dependent problem has recently led to a one-body equation with a collision term (Ref. 249), but in which the collision term and the effective interaction are not independent of each other. The variational approach (Ref. 22) reverts the hierarchy of the argument. One assumes for all times a Slater determinant to begin with, and searches for the "best set" of single particle states by variation of the action integral I

$$I(t_1,t_2) = \int_{t_1}^{t_2} dt <\Psi(t)| H - i\hbar \frac{\partial}{\partial t} |\Psi(t)> \qquad (40)$$

with respect to $|\psi_i>$. The first variation gives back Eq. (33); the second variation has been investigated recently (Ref. 235-237). The variational approach does not provide additional insight; one simply assumes what has to be proven (the relevance of the Slater determinant), but it is a powerful tool for treating further approximations.

The one-body equation (33) is often called the "time-dependent Hartree-Fock equation" (TDHF), although historically it rather is another Dirac equation. Nowadays numerical solutions are available (Ref. 103). Thanks to admirable efforts one has been able to cope with the utter (numerical) complexity of such equations for different effective interactions (Ref. 6, 7, 9, 103, 105, 165, 198-200, 207, 214, 216, 239, 240). Among various other aspects, one may have learned from such calculations how the (one-body) density can change in time, generating a coherent motion of all particle states. Thus, one may regard Eq. (33) as a kind of master equa-

tion for collective or for fluidlike motion. In the detail, the relations to standard fluid dynamics, or to the standard collective model (Ref. 47) are not clear. The various attempts to work out fluid dynamical models (Ref. 35, 118, 133, 134, 160, 161, 202, 316, 317, 425-429) or the "adiabatic time-dependent Hartree-Fock" (ATDHF) approximations (Ref. 22, 115, 116, 323, 416) all suffer by ad-hoc assumptions, which are very difficult to judge a priori. A posteriori one has the difficulty that they mostly lead to an irrotational flow pattern, which cannot be brought into consistency with the experimental evidence from the low-energy spectra of "collective" nature. Similarly, the Thomas-Fermi approximation (Ref. 38, 41, 57, 90, 91, 138, 139, 147, 162, 191) and thus all kinds of drop or droplet models must be understood as a particular approximation to some mean field equation, although this relation is not stated often in the literature.

The stationary version of the one-body equation (39) combination with the definition of the energy, Eq. (38), can account for the single particle spectra and the binding energy of nuclei (Ref. 330). It is progress that simple effective interactions could have been found which account almost quantitatively for these two aspects over wide regions of the periodic table (Ref. 208, 209, 245, 329, 330, 413-415). In view of the complexity of the calculations, it is still worthwhile to develop approximation methods, and the shell correction approach has turned out to be a very quantitative one. The arguments for the latter will be given briefly (Ref. 64).

A self-consistent density operator ρ, i.e., one which is a solution to Eq. (39), certainly contains shell effects. Suppose that the shell part $\delta\rho$ is sufficiently small as compared to the complementary smooth part $\bar{\rho}$, i.e.,

$$\rho = \bar{\rho} + \delta\rho \ , \quad \delta\rho \ll \bar{\rho} \ . \tag{41}$$

The total energy, Eq. (38), being a functional $E[\rho]$ of the density ρ, can be split according to the powers of $\delta\rho$,

$$E[\rho] = E[\bar{\rho}] + \mathrm{tr}\,\delta\rho\left[\frac{p^2}{2m} + \bar{\Phi}\right] + \frac{1}{2}\,\mathrm{tr}_1\mathrm{tr}_2\,\delta\rho(1)V(1,2)\delta\rho(2) \ . \tag{42}$$

The smooth part of this energy $E[\bar{\rho}]$ can be understood as the quantum mechanical definition of the bulk or the liquid drop part of the energy W_{LD},

$$E[\bar{\rho}] = W_{LD} \ . \tag{43}$$

Terms linear in $\delta\rho$ can be understood as the shell correction energy $\delta U \sim \delta_1 E$,

$$\delta_1 E \equiv \mathrm{tr}\,\delta\rho\left[\frac{p^2}{2m} + \bar{\Phi}\right] = \sum_\nu \delta n_\nu e_\nu \ , \tag{44}$$

provided that the e_ν are not the self-consistent eigenvalues, but eigenvalues to a smoother, quasiphenomenological potential $\bar{\Phi}$,

$$e_\nu|\phi_\nu\rangle = \left(\frac{p^2}{2m} + \bar{\Phi}\right)|\phi_\nu\rangle \ ; \quad \bar{\Phi} = \mathrm{tr}\,\bar{\rho}V \ . \tag{45}$$

The last term is quadratic in the small $\delta\rho$,

$$\delta_2 E \equiv \frac{1}{2}\,\mathrm{tr}_1\mathrm{tr}_2\delta\rho(1)V(1,2)\delta\rho(2) \sim O(\delta\rho^2) \ , \tag{46}$$

and be dropped by an argument of smallness. What remains is the energy theorem of Section III:

$$E = E[\bar{\rho}] + \delta_1 E + \delta_2 E \sim W_{LD} + \delta U \ . \tag{47}$$

Properly said, these arguments hold for the self-consistent ground state. In order to obtain a deformation energy, one must move the density out of its equilibrium configuration. This can be achieved by external, constraining potentials $U(x)$, i.e., by searching solutions to

$$(h + U)|\psi_\nu\rangle = \varepsilon_\nu|\psi_\nu\rangle \tag{48}$$

and calculating the energy according to Eq. (38) or (47) as functions of the parameters appearing in U, or by equivalent spatial moments of the density like the quadrupole moment.

A more precise but lengthier argument can be found in the literature (Ref. 56, 58, 62, 66, 395, 396). The resulting equations were checked numerically by extensive comparison with the available fully self-consistent field calculations (Ref. 106-109).

Figure 20, as an example, shows the quality of the agreement. In this figure, the self-consistent deformation energy E_{HF}, calculated for an effective interaction of the Skyrme type (Ref. 359), is plotted versus the quadrupole moment Q_2 and compared to another calculation ($\tilde{E} + \delta\tilde{E}$) in which the term corresponding to $\delta_2 E$ was omitted.

The above considerations and the extensive numerical calculations make the shell correction appear as a rather accurate approximation to constraint self-consistent field equations. This statement is helpful not only with respect to its economical impact. It provides the insight that the notion of a liquid drop energy does not imply literally the identification of a nucleus with a water droplet. It rather stands for a very simple, overall substitution of the parameters of the interaction by another and equivalent set, the liquid drop parameters. Indeed, the various versions of effective interactions have their "own liquid drop" parameters (Ref. 71). Attempts to take the short cut, and to express the liquid drop parameters directly as closed-form expressions of the coupling constants have been made but have not been very successful (Ref. 13).

We return once more to the constraint self-consistent field equation (48). It can be viewed as the solution to a variational problem (Ref. 26, 28, 123, 163, 330), i.e., finding those single particle states which minimize the energy, Eq. (38), subject to the condition of fixed particle number $N = \mathrm{tr}\ \rho$ and some fixed spatial moments $Q_i = \mathrm{tr}\ \rho\ Q_i(x)$. One solves this variational problem with constraints by the method of Lagrange multipliers (λ_i and ε). This allows a free variation, i.e.,

$$\delta E - \varepsilon\delta N - \sum_i \lambda_i \delta Q_i = 0 \ , \tag{49}$$

with respect to the single particle states and leads straightforwardly to Eq. (48) with the external field U(x) as

$$U(x) = \sum_i \lambda_i Q_i(x) \ . \tag{50}$$

The energy, calculated with Eq. (38), can be expressed as a function of the Q_i,

$$E = W(Q_i) \ . \tag{51}$$

Taking partial derivatives with respect to any particular Q_i and comparing with Eq. (49) identifies the Lagrange multipliers as the generalized forces

$$\lambda_i = \frac{\partial W}{\partial Q_i} \ . \tag{52}$$

The unconstrained equation (39) gives the equilibrium, since all forces disappear ($\lambda_i = 0$).

Straightforwardly, the so obtained potential energy W has been identified with the phenomenological potential energy, as defined for example by the shell correction approach. The quoted numerical agreement between the two supports such an identification. But there are some problems. It implies the identification of the Q_i with the phenomenological deformation parameters β_i. They are functions of the time, subject to obeying the well-known classical equations of motion. Thus with $Q_i \leftrightarrow \beta_i$,

$$\sum_{i,j} B_{ij}(Q)\dot{Q}_i\dot{Q}_j + W(Q) = \text{const.} \tag{53}$$

If this were true, one should be able to derive them from the only available dynamic equation, the time-dependent mean-field equation (33). So far, this was not possible without further ad-hoc assumptions like the conditions of "slow motion" or "small amplitude motion," concepts which are defined only vaguely (Ref. 22, 23, 65, 115-117, 122, 143). Moreover, the simplest of these approaches yields mass parameters for irrotational flow characteristics (Ref. 316, 317). Those, however, are in conflict with the spectral aspects of collective motion.

It might well be possible that the theories both of collective motion and of fission rest on an inadequate surmise, the existence of a "collective Hamiltonian" which must be "quantized" subsequently. The recently developed mean field approximations for

spontaneous fission (Ref. 235-237) might turn out as a workable alternative, if the necessary numerics can be mastered to also treat sufficiently heavy nuclei.

But the familiar mean-field approximations rely on the fundamental assumption that the many-body state of the system is a Slater determinant for all times. This might be justified at low excitations, but certainly not for the fission of highly excited nuclei (Ref. 60), or for the later stages of the fission process. Indeed a careful reduction of the many-body equation to an equation closed in the one-body density does not lead directly to a mean-field equation like Eq. (33), but to one which includes "collision terms" (Ref. 249, 311, 430). Eventually, equations of such structure might be useful to derive simplified diffusion models for the theory of induced fission.

As a conclusion one should state that a self-consistent description of the fission process is still in its infancy. Many problems are not understood. The difficulties we meet are closely related to our inability to formulate collective motion in quantal many-body systems in general.

VII. Concluding Remarks

A more or less complete presentation of our ideas on the mechanism of the fission process and a careful discussion of the rather different concepts developed in the past would provide sufficient material for a monograph of several volumes. On these few pages not more can be given than a bird's-eye view of the problem. Most of the topics had to be omitted, in particular those of interest for the experimenter, the many different partial cross sections. We mention in particular the angular distribution of fission products (Ref. 341), which is a wide field of activity and has provided much insight into the mechanism. We mention also the distribution of fission neutrons, which are so important for maintaining the chain reaction. Last but not least we have omitted such interesting topics as for example muon- or pion-induced fission (Ref. 250, 282), Coulomb fission (Ref. 238, 312), or any discussion of odd-even fission (Ref. 84, 373).

They were omitted because these lectures have another aim. Starting from the concept of Bohr and Wheeler, in Section II, I have tried to show that much of the later development is just to put "flesh on the bones." The shell correction method of Section III, for example, modifies Bohr and Wheeler's concept only marginally by substituting the liquid drop energy surface by some more complicated function. Spontaneous fission, as treated in Section IV, was considered as a barrier penetration problem already by Bohr and Wheeler, only that the modern penetration calculations are infinitely more complicated (numerically). The aim was rather to show how one gets into difficulties if one tries to calculate the only relevant objects, the cross sections for mass, energy, angles, and so on, based on these simple concepts alone. Almost every class of experiments needs its own phenomenological concepts with arbitrarily adjusted parameters (see Section V). If one tries to relate the phenomenological concepts to the many-body problem, one admittedly is able to establish some relations, as for example the relation between the shell correction energy and constrained field calculations (Section VI), but the dynamical aspects get more confusing, the more one goes into depth.

So the aim of the lecture is to encourage the students to have new ideas on the problem; not much is really solved and clear in the wide field of nuclear dynamics, and fission provides an ideal testing ground for checking new developments.

References

Monographs on Fission

1 R. Vandenbosch and J.R. Huizenga, Nuclear Fission, Academic Press, New York, 1973.

2 L. Wilets, Theories of Nuclear Fission, Clarendon Press, Oxford, 1964.

Conferences and Symposia

3 Vienna 1969: Physics and Chemistry of Fission 1969, IAEA, Vienna, 1969.

4 Trieste 1971: The Structure of Nuclei, IAEA, Vienna, 1972.

5 Rochester 1973: Physics and Chemistry of Fission 1973, IAEA, Vienna, 1974.

6 Ronneby 1974: Physica Scripta 10A (1974).

7 Trieste 1975: Nuclear Self-Consistent Fields, North-Holland, Amsterdam, 1975.

8 Jülich 1979: Physics and Chemistry of Fission 1979, IAEA, Vienna, 1980.

9 Erice 1979: published as: Progress in Particle and Nuclear Physics, Vol. 4 (1980), Pergamon, New York, 1980.

Articles in Journals, Review Articles and Other Citations

10 K. Albrecht, D. Scharnweber, W. Greiner, and U. Mosel, Phys.Lett. 32B(1970)229.
Nuclear deformation energy in the two-center shell model.

11 B.L. Andersen, F. Dickmann, and K. Dietrich, Nucl.Phys. A159(1970)337.
Potential landscape for fissioning nuclei. (I) General method, symmetric shapes.

12 M. Ashgar, Z.Phys. A286(1978)299.
The subbarrier photo-fission and the ^{232}Th fission barrier profile.

13 N.L. Balazs and H.C. Pauli, Z.Phys. A281(1977)395.
Short range forces and surface tension in nuclei.

14 R. Balian and C. Bloch, Ann.Phys. (N.Y.) 69(1972)76.
Distribution of eigenfrequencies for the wave equation in a finite domain: III. Eigenfrequency density oscillations.

15 R. Balian and C. Bloch, Ann.Phys. (N.Y.) 64(1971)271.
Distribution of eigenfrequencies for the wave equation in a finite domain: II. Electromagnetic field. Riemannian spaces.

16 R. Balian and C. Bloch, Ann.Phys. (N.Y.) 63(1971)592.
Asymptotic evaluation of the Green's function for large quantum numbers.

17 R. Balian and C. Bloch, Ann.Phys. (N.Y.) 60(1970)401.
Distribution of eigenfrequencies for the wave equation in a finite domain: I. Three dimensional problem with smooth boundary surface.

18 B. Banerjee and D.M. Brink, Z.Phys. 258(1973)46.
A Schrödinger equation for collective motion from the generator coordinate method.

19 A. Baran, A. Superson, and K. Pomorski, Z.Phys. A299(1980)299.
New estimates for the parameters of the modified oscillator potential of the rare earth nuclei.

20 A. Baran and K. Pomorski, Z.Phys. A291(1979)175.
New modified oscillator potential for nuclei in the actinide region.

21 A. Baran, K. Pomorski, S.E. Larsson, P. Möller, S.G. Nilsson, J. Randrup, A. Łukasiak, A. Sobiczewski, Jülich 1979, p. 143.
Dynamical calculations of spontaneous fission half-lives.

22 M. Baranger and M. Véneroni, Ann.Phys. (N.Y.) 114(1978)123.
An adiabatic time-dependent Hartree-Fock theory of collective motion in finite systems.

23 M. Baranger, Journal de Physique C5(1972)61.
A microscopic view of nuclear collective properties.

24 W.H. Bassichis, A.K. Kerman, and D.R. Tuerpe, Phys.Rev. C8(1973)2140.
Analysis of the Strutinsky-Nilsson shell correction.

25 W.H. Bassichis and A.K. Kerman, Phys.Rev. C6(1972)370.
Note on self-consistent calculations of shell effects.

26 W.H. Bassichis and L. Wilets, Phys.Rev.Lett. 27(1971)1451.
Solution to a problem in constrained Hartree-Fock and other calculations.

27 W.H. Bassichis and L. Wilets, Phys.Rev.Lett. 22(1969)799.
Validity of nuclear deformation energies obtained from single-particle levels.

28 M. Beiner, H. Flocard, N.V. Giai, and P. Quentin, Nucl.Phys. A238(1975)29.
Nuclear ground-state properties and the self-consistent calculations with the Skyrme interaction.

29 S.T. Belyaev, in: Developments and borderlines of nuclear physics (1972) 'III Corso, Academic Press, Inc.-New York, p.60.
Collective excitations and their microscopic models.

30 C.E. Bemis and J.R. Nix, Comments Nucl.Part.Phys. 7(1977)65.
Superheavy elements - The quest in perspective.

31 R. Bengtson, Nucl.Phys. A198(1972)591.
Shell correction energies derived from statistical entropy calculations.

32 J. Bennewitz and P.K. Haug, Z.Phys. 212(1968)295.
Einzelteilchenberechnungen zur Kernspaltung.

33 R.A. Berg and L. Wilets, Phys.Rev. 101(1956)201.
Nuclear surface effects.

34 R.A. Berg and L. Wilets, Proc.Phys.Soc.Lon. A68(1955)229.
On the validity of the Weizsäcker inhomogeneity correction term.

35 G.F. Bertsch, Nucl.Phys. A249(1975)253.
Nuclear hydrodynamics.

36 D. Bès, K.Dan.Vidensk.Selsk., Mat.-Fys.Medd 33(1961) No.2.
A study of nuclear potential energy surfaces and gamma vibrations.

37 D.R. Bès and Z. Szymański, Nucl.Phys. 28(1961)42.
The ground-state equilibrium deformation in rare earth nuclei.

38 H.A. Bethe, Phys.Rev. 167(1968)879.
Thomas Fermi theory of nuclei.

39 H.A. Bethe, Rev.Mod.Phys. 9(1937)69.
Nuclear physics.

40 H.A. Bethe and R.F. Bacher, Rev.Mod.Phys. 8(1936)82.
Nuclear physics.

41 R.K. Bhaduri, Phys.Rev.Lett. 39(1977)329.
Turning point in the Thomas-Fermi approximation.

42 R.K. Bhaduri and S. Das Gupta, Phys.Lett. 47B(1973)129.
The equivalence of the Strutinsky type smoothing and the temperature averaging method.

43 R.K. Bhaduri and C.K. Ross, Phys.Rev.Lett. 27(1971)606.
Shell corrections in the independent particle model.

44 B.S. Bhandri, Phys.Rev. C19(1980)1820.
Three-hump fission barrier in ^{232}Th.

45 S. Bjørnholm, J.Phys. 33(1972)C5-33.
Intermediate structures in fission - Spectroscopy of shape isomers.

46 S. Bjørnholm and V.M. Strutinsky, Nucl.Phys. A136(1969)1.
Intermediate states in fission.

47 A. Bohr and B. Mottelson, Nuclear Structure, Benjamin, New York, Vol.I, 1969; Vol.II, 1975.

48 A. Bohr and B. Mottelson, Mat.Fys.Medd.Dan.Vid.Selsk. 27(1953)No.16.
Collective and individual-particle aspects of nuclear structure.

49 A. Bohr, K.Dan.Vidensk,Selsk., Mat.-Fys.Medd. 26(1952)No.14.
The coupling of nuclear surface oscillations to the motion of individual nucleons.

50 N. Bohr and J.A. Wheeler, Phys.Rev. 56(1939)426.
The mechanism of nuclear fission.

51 N. Bohr and F. Kalckar, K.Dan.Vidensk.Selsk., Mat.-Fys.Medd. 14(1937)No.10.
On the transmutation of atomic nuclei by impact of material particles.

52 N. Bohr, Nature 127(1936)351.
The compound nucleus.

53 M. Bolsterli, E.O. Fiset, J.R. Nix, and J.L. Norton, Phys.Rev. C5(1972)1050.
New calculation of fission barriers for heavy and super-heavy nuclei.

54 M. Bolsterli, E.O. Fiset, J.R. Nix, and J.L. Norton, Phys.Rev.Lett. 27(1971)681.
Shape of the island of superheavy nuclei.

55 M. Brack, Trieste, 1978; p.327.
Fundamentals of the double-humped fission barrier.

56 M. Brack, Phys.Lett. 71B(1977)239.
An improved approximation to constrained Hartree-Fock calculations.

57 M. Brack, B. Jennings, and Y.H. Chu, Phys.Lett. 65B(1976)1.
On the extended Thomas-Fermi approximation to the kinetic energy density.

58 M. Brack and P. Quentin, Phys.Lett. 56B(1975)421.
Self-consistent average density matrices and the Strutinsky energy theorem.

59 M. Brack, Jülich 1979; p.227.
Static deformation energy calculations. From microscopical to semiclassical theories.

60 M. Brack and P. Quentin, Phys.Lett. 52B(1974)159.
Self-consistent calculation of highly excited nuclei.

61 M. Brack, T. Ledergerber, H.C. Pauli, A.S. Jensen, Nucl.Phys. A234(1974)185.
Deformations and moments of inertia of actinide nuclei in the ground and shape isomeric states.

62 M. Brack and P. Quentin, Rochester 1973; p.231.
Test of Strutinsky's method using Hartree-Fock-results.

63 M. Brack and H.C. Pauli, Nucl.Phys. A207(1973)401.
On Strutinsky's averaging method.

64 M. Brack, J. Damgaard, H.C. Pauli, A.S. Jensen, V.M. Strutinsky, and C.Y. Wong, Rev.Mod.Phys. 44(1972)320.
Funny Hills: The shell correction approach to nuclear shell effects and its application to the fission process.

65 D.M. Brink, M.J. Giannoni, and M. Véneroni, Nucl.Phys. A258 (1976)237.
Derivation of an adiabatic time dependent Hartree-Fock formalism from a variational principle.

66 G.G. Bunatyan, V.M. Kolomietz, and K.M. Strutinsky, Nucl.Phys. A188(1972)225.
A foundation to the shell correction method.

67 X. Campi and D.W. Sprung, Nucl.Phys. A194(1972)401.
Spherical nuclei in the local density approximation.

68 B.V. Carlsson, K.W. McVoy, M.C. Nemes, Nucl.Phys. A331 (1979)117.
Fission widths and multi-dimensional barrier penetration.

69 R.R. Chasman, Phys.Rev.Lett. 33(1974)544.
Superheavy elements and the Strutinsky prescription.

70 R.K. Choudhury and V.S. Ramamurthy, Phys.Rev. C18(1978)2213.
Scission point configuration of ^{252}Cf from trajectory calculation.

71 Y.H. Chu, B.K. Jennings, and M. Brack, Phys.Lett. 68B(1977)407.
Nuclear binding energies and liquid drop parameters in the exterded Thomas-Fermi approximation.

72 S. Cohen, F. Plasil, and W.J. Swiatecki, Ann.Phys.(N.Y.) 82(1974)557.
Equilibrium configurations of rotating charged or gravitating masses with surface tension.II.

73 S. Cohen and W.J. Swiatecki, Ann. Phys. 22(1963)406.
The deformation energy of a charged drop. Part V: Results of electronic computer studies.

74 S. Cohen and W.J. Swiatecki, Ann.Phys. 19(1962)67.
The deformation energy of a charged drop: IV. Evidence for a discontinuity in the conventional family of saddle point shapes.

75 J.D. Cramer, J.R. Nix, Phys.Rev. C2(1970)1048.
Exact calculation of the penetrability through two-peaked fission barriers.

76 R.Y. Cusson, H.P. Trivedi, H.P. Meldner, M.S. Weiss, and R.E. Wright, Phys.Rev. C14(1976)1615.
Self-consistent K-matrix-model calculation for finite and superheavy nuclei.

77 J. Damgaard, H.C. Pauli, V.V. Pashkevich, and V.M. Strutinsky, Nucl.Phys. A135(1969)432.
A method of solving the independent-particle Schrödinger equation with a deformed average field.

78 S. Das Gupta and S. Radhakant, Phys.Rev. C9(1974)1775.
Aspects of thermodynamic calculations of shell correction energies.

79 K.T.R. Davies, R.A. Managan, J.R. Nix, and A.J. Sierk, Phys.Rev. C16(1977)1890.
Rupture of the neck in nuclear fission.

80 K.T.R. Davies and J.R. Nix, Phys.Rev. C11(1976)1977.
Calculation of moments, potentials, and energies for an arbitrary shaped diffuse-surface nuclear density distribution.

81 K.T.R. Davies, A.J. Sierk, and J.R. Nix, Phys.Rev. C13 (1976)2385.
Effect of viscosity on the dynamics of fission.

82 H.H. Deubler, K. Lekkas, P. Sperr, K. Dietrich, Z.Phys. 284(1978)237.
Kinetic energy and angular distributions of instantaneous fission fragments in a classical model.

83 F. Dickmann, V. Metag, and R. Repnow, Phys.Lett. 38B(1972)207.
Predicted region of oblate deformation around ^{72}Kr.

84 K. Dietrich and E. Werner, J. de Physique 37(1976)435.
On low energy fission of odd nuclei.

85 K. Dietrich, Trieste 1971, p.373.
Nuclear fission.

Combi
calcu
in a
riers
with
much
some
uid d
of th
than
enfor
of th
Becau
much
ments
the o
discr
the r
appea
(Ref.
parti
spons
Th
lated
defor
321).
came
barri
inclu
ments
broug
distr
corre
tativ
cided
tisti

86 P.A.M. Dirac, Proc. Cambridge Phil.Soc. 26(1930)376.
Note on the exchange phenomena in the Thomas atom.

87 P.A.M. Dirac, Proc. Cambridge Phil.Soc. 27(1931)240.
Note on the interpretation of the density matrix in the many electron problem.

88 T. Døssing and A.S. Jensen, Nucl.Phys. A222(1974)493.
Nuclear level densities with collective rotations included.

89 J. Dudek, W. Dudek, E. Ruchowska, and J. Skalski, Z.Phys. A294(1980)341.
Systematically too low values of the cranking model collective inertial parameters.

90 M. Durand, P. Schuck, and M. Brack, Z.Phys. A296(1980)87.
Partial resummation of the h-expansion of the Bloch-density for non local potentials.

91 M. Durand, M. Brack, and P. Schuck, Z.Phys. A286(1978)381.
A semiclassical density matrix valid beyond the classically allowed region.

92 E. Erba, U. Facchini, and E. Saetta-Menichella, Nucl.Phys. 84(1966)595.
Statistical analysis of low-energy fission.

93 D. Ehlers and S.A. Moskowski, Phys.Rev. C6(1972)217.
Hartree-Fock calculations for double-closed-shell nuclei using the modified delta interaction.

94 M. Faber, M. Ploszajczak, and A. Faessler, Nucl.Phys. A326 (1979)129.
Fission instability of nuclei at very high angular momenta.

95 M. Faber, Phys.Lett. 77B(1978)18.
Moments of inertia of fissioning isomers.

96 W. Fabian, G.E.W. Horlacher, and K. Albrecht, Nucl.Phys. A190(1972)533.
Potential energy surfaces in the two-center shell model.

97 U. Facchini and G. Sassi, J.de Phys. G3(1977)269.
A statistical approach to the scission mechanism.

98 U. Facchini and E. Saetta-Menichella, J.de Phys. A7(1974)975.
A statistical model for excitation energy distributions in actinide fission.

99 A. Faessler, J.E. Galonska, U. Götz, and H.C. Pauli, Nucl.Phys. A230(1974)302.
Ground-state deformations for neutron-rich nuclei in the A ≈ 100 region.

100 A. Faessler, M. Ploszajczak, and H. Toki, Phys.Lett. 70B (1977)399.
The fission barrier of actinide nuclei at very high angular momentum.

101 A. Faessler, B. Slavov, Phys.Lett. 31B(1970)350.
How to calculate the nuclear deformation-energy surface from a single-particle potential.

102 E.O. Fisset and J.R. Nix, Nucl.Phys. A193(1972)647.
Calculation of half-lives for superheavy nuclei.

103 H. Flocard, Nucleonika 24(1979)19.
Nuclear dynamics by self-consistent methods: TDHF and ATDHF.

104 H. Flocard and D. Vautherin, Phys.Lett. 55B(1975)259.
Generator coordinate calculations of monopole and quadrupole vibrations with Skyrme interaction.

105 H. Flocard and D. Vautherin, Phys.Lett. 52B(1974)399.
Derivation of collective potentials and mass parameters from the generator coordinate method.

106 H. Flocard, P. Quentin, D. Vautherin, M. Vénéroni, and A.K. Kerman, Nucl.Phys. A231(1974)176.
Self-consistent calculation of the fission barrier of ^{240}Pu.

107 H. Flocard, J.Phys. 34(1973)87.
Calculs Hartree-Fock sphérique avec interaction effective.

108 H. Flocard, P. Quentin, A.K. Kerman, and D. Vautherin, Nucl.Phys. A203(1973)433.
Nuclear deformation energy curves with the constrained Hartree-Fock method.

109 H. Flocard, P. Quentin, and D. Vautherin, Phys.Lett. 46B (1973)304.
Self-consistent calculation of the ground state properties of some rare-earth nuclei.

110 P. Fong, Phys.Rev. C19(1979)868.
Dynamical interpretation of the statistical theory of fission.

111 P. Fong, Phys.Rev. C13(1976)1259.
Dynamical theory of nuclear fission.

112 P. Fong, Phys.Rev.Lett. 34(1975)697.
Equivalence of the Maruhn-Greiner theory and the statistical theory of fission.

113 P. Fong; Gordon and Breach, New York, 1969.
Statistical theory of nuclear fission.

114 S. Frankel and N. Metropolis, Phys.Rev. 72(1947)914.
Calculations in the liquid drop model of fission.

115 M.J. Giannoni and P. Quentin, Phys.Rev. C21(1980)2060.
Mass parameters in the adiabatic time-dependent Hartree-Fock approximation: I. Theoretical aspects; the case of a single collective variable.

116 M.J. Giannoni and P. Quentin, Phys.Rev. C21(1980)2076.
Mass parameters in the adiabatic time-dependent Hartree-Fock approximation: II. Results for the isoscalar quadrupole mode.

117 M.J. Giannoni, F. Moreau, P. Quentin, D. Vautherin, M. Véneroni, and D.M. Brink, Phys.Lett. 65B(1976)305.
A method for calculating adiabatic mass parameters: Application to isoscalar quadrupole modes in light nuclei.

118 M.J. Giannoni, D. Vautherin, M. Véneroni, and D.M. Brink, Phys.Lett. 63B(1976)8.
Variational derivation of nuclear hydrodynamics.

119 H. Gick, D. Glas, U. Mosel, Z.Phys. A282(1977)417.
Shell corrections for highly asymmetric systems.

120 D. Glas and U. Mosel, Nucl.Phys. A294(1976)268.
Microscopic description of nuclear friction in heavy ion collisions.

121 K. Goeke and P. G. Reinhard, preprint: KFA Jülich 1980.
The generator coordinate method and its relation to quantized ATDHF.

122 K. Goeke, Phys.Rev.Lett. 38(1977)212.
Collective masses by time-dependent Hartree-Fock: Application to monopole vibrations.

123 K. Goeke, Nucl.Phys. A265(1976)301.
Theories for large amplitude collective motion and constrained Hartree-Fock.

124 M. Goeppert-Mayer, Phys.Rev. 75(1949)1969.
On closed shells in nuclei.

125$_1$ U. Götz, H.C. Pauli, K. Junker, K. Alder, Nucl.Phys. A192(1972)1.
Ground state deformations in the rare earth nuclei.

125$_2$ U. Götz, H.C. Pauli, and K. Junker, Phys.Lett. 39B (1972)436.
Influence of axially asymmetric distortions on fission barriers.

126 U. Götz, H.C. Pauli, K. Alder, Nucl.Phys. A175(1971)481.
Single-particle states in a non-axially symmetric average field.

127 P.A. Gottschalk and T. Ledergerber, Nucl.Phys. A278 (1977)16.
Shell correction approach to nuclear state densities and the competition between fission and the neutron emission of ^{210}Po.

128 P.-A. Gottschalk and T. Ledergerber, Z.Phys. A276(1976)367.
Level densities for nuclei near A = 60 based on realistic single-particle level spectra.

129 P.-A. Gottschalk, Z.Phys. 267(1974)157.
Der Zustandsdichteparameter für ein diffuses Kernpotential

130 P. Grangé and H.A. Weidenmüller, Phys.Lett. 96B(1980)26.
Fission probability and the nuclear friction constant.

131 P. Grangé, H.C. Pauli, and H.A. Weidenmüller, Z.Phys. A296(1980)107.
Suzuki's scaling limit and the theory of statistical fluctuations in nuclear fission.

132 P. Grangé, H.C. Pauli, and H.A. Weidenmüller, Phys.Lett. 88B(1979)9.
The influence of thermal fluctuations on the kinetic energy distribution of fission fragments.

133 J.J. Griffin, P.C. Lichtner, and M. Dworzecka, Nukleonika 24(1979)343.
Fermidynamics and commensurability; TDHF restructured into T.D.-S-H.F.

134 J.J. Griffin and K.-K. Kan, 1, Rev.Mod.Phys. 48(1976)467.
Colliding heavy ions: Nuclei as dynamical fluid.

135 J.J. Griffin and J.A. Wheeler, Phys.Rev. 108(1957)311.
Collective motions in nuclei by the method of generator coordinates.

136 D.H.E. Gross and H. Kalinowski, Phys.Lett. C45(1978)175.
Friction model of heavy ion collisions.

137 D.H.E. Gross, Phys.Lett. 42B(1972)41.
The statistical model of nuclei and its relation to the Strutinsky averaging method.

138 C. Guet and M. Brack, Z.Phys. A297(1980)247.
Validity of the semiclassical kinetic energy density functional for deformed nuclear shapes.

139 G. Gumpertsberger and P. Schuck, Phys.Lett. 66B(1977)219.
Semi-classical approximation to the single-particle and spectral density.

140 C. Gustafson, I.L. Lamm, B. Nilsson, and S.G. Nilsson, Arkiv för Fysik 36(1966)No.69.
Nuclear deformabilities in the rare-earth and actinide regions with excursions off the stability line and into the super-heavy region.

141 D. Habs, V. Metag, H.J. Specht, and G. Ulfert, Phys.Rev.Lett. 38(1977)387.
Quadrupole moment of the 8-μs fission isomer in ^{239}Pu.

142 D. Habs et al., Z.Phys. 267(1974)149.
The spherical to asymmetric shape transition in the mass region with 50 < (N,Z) < 82.

143 P.K. Haff and L. Wilets, Phys.Rev. C7(1973)951.
Microscopic theory of nuclear collective motion.

144 O. Hahn and F. Strassmann, Naturwissenschaften 27(1939)11.
Über den Nachweis und das Verhalten der bei der Bestrahlung des Urans entstehenden Erdalkalimetalle.

145 R.W. Hasse, J.Math.Phys. 16(1975)2005.
On the quantum mechanical treatment of dissipative systems.

146 R.W. Hasse, Nucl.Phys. A229(1974)141.
A two-nucleus shell model with pairing for the calculation of molecular heavy-ion or fission potentials.

147 R.W. Hasse and W. Stocker, Phys.Lett. 44B(1973)26.
Temperature effects in the liquid drop description of nuclear fission.

148 R.W. Hasse, Ann.Phys. (N.Y) 68(1971)377.
Studies in the shape dependence of the droplet model of nuclei (curvature and compressibility effects).

149 R.W. Hasse, Nucl.Phys. A128(1969)609.
Dynamic model of asymmetric fission.

150 R.W. Hasse, Nucl.Phys. A118(1968).
Ground-state and saddle-point properties of heavy nuclei for a dynamic fission model.

151 R.W. Hasse, R. Ebert, and G. Süssmann, Nucl.Phys. A106 (1968)117-128.
Effective masses for nuclear fission.

152 O. Haxel, J.H.D. Jensen, and H.E. Suess, Phys.Rev. 75 (1949)1766.
On the "magic numbers" in nuclear structure.

153 D.L. Hill and J.A. Wheeler, Phys.Rev. 89(1953)1102.
Nuclear constitution and the interpretation of fission phenomena.

154 M. Hillmann, Phys.Rev. C7(1973)2037.
Normalisation of shell-model nuclei to liquid-drop-model nuclei.

155 H. Hofmann, Nucl.Phys. A224(1974)116.
Quantum mechanical treatment of the penetration through a two dimensional barrier.

156 H. Hofmann, Z.Phys. 250(1972)14.
On the quantisation of a kinetic energy with variable inertia.

157 H. Hofmann and K. Dietrich, Nucl.Phys. A165(1971)1.
Effects of variable inertia on collective dynamics.

158 R. Holub, M.G. Mustafa, and H.W. Schmitt, Nucl.Phys. A222(1974)252.
Calculation of charge vibration in fission with Strutinsky shell correction.

159 P. Holzer, U. Mosel, and W. Greiner, Nucl.Phys. A138(1969)241.
Double-center-oscillator and its application to fission.

160 G. Holzwart and G. Eckarth, Nucl.Phys. A325(1979)1.
Fluid-dynamical approximation for finite-Fermi systems.

161 G. Holzwarth, Z.Phys. A284(1978)291.
Nuclear fluid dynamics.

162 G. Holzwarth, Phys.Lett. 66B(1977)29.
Static and dynamical Thomas-Fermi theory for nuclei.

163 G. Holzwarth and T. Yukawa, Nucl.Phys. A219(1974)125.
Choice of the constraining operator in the constrained Hartree-Fock method.

164 G. Holzwarth, Nucl.Phys. A207(1973)545.
Four approaches to the function of inertia in a solvable model.

165 P. Hoodbhoy and J.W. Negele, Nucl.Phys. A288(1977)23.
Solution of Hartree-Fock equations in coordinate space for axially symmetric nuclei.

166 W.M. Howard and J.R. Nix, Nature 247(1974)17.
Production of superheavy nuclei by the multiple capture of neutrons.

167 W.M. Howard and J.R. Nix, Rochester 1973, p. 145.
Calculation of fission barriers for heavy neutron-rich nuclei.

168 J.K. Huizenga and L.G. Moretto, Ann.Rev.Nucl.Sci. 22(1972)427.
Nuclear level densities.

169 E.K. Hyde, Nuclear Properties of the Heavy Elements,
Prentice Hall, Englewood Cliffs, New Jersey, 1964; Vols.
I,II,III.

170 A. Jägare, Nucl.Phys. A137(1969)241.
On the fissioning hot compound nucleus.

171 B.K. Jennings, R. Bhaduri, and M. Brack, Nucl.Phys. A253
(1975)29.
Semiclassical approximation in a realistic one-body potential.

172 B.K. Jennings and R. Bhaduri, Nucl.Phys. A237(1975)149.
Smoothing methods for the independent particle model.

173 B.K. Jennings, R.K. Bhaduri and M. Brack, Phys.Rev.Lett.
34(1975)228.
Semiclassical approximation in a one-body potential.

174 B.K. Jennings, Ann.Phys. (N.Y.) 84(1974)1.
The semiclassical single-particle density of states.

175 B.K. Jennings, Nucl.Phys. A207(1973)538.
Strutinsky smoothing and the partition function approach.

176 A.S. Jensen and S.M. Larsen, Phys.Lett. 94B(1980)280.
Dynamics of collective parameters.

177 A.S. Jensen and A. Miranda, Nucl.Phys. A244(1975)93.
Pairing effects on the mass rensor for spontaneous fission.

178 A.S. Jensen and J. Damgaard, Nucl.Phys. A210(1973)282.
The shell structure and the asymmetry of nuclear fission for
^{240}Pu in a statistical model.

179 A.V. Ignatyuk, N.S. Rabotnov, G.N. Smirenkin, A.S. Soldatov,
and Yu.M. Tsipenyuk, Sovj.Phys.JETP 34(1972)684.
Subbarrier photo fission of even-even nuclei.

180 A.V. Ignatyuk, V.S. Stavinskii, and Y.N. Shubin, Sov.J.Nucl.
Phys. 11(1970)563.
Density of levels of near-magic nuclei.

181 A.V. Ignatyuk and V.S. Stavinskii, Sov.J.Nucl.Phys. 11
(1970)674.
Spin dependence of the density of excited states of nuclei.

182 D.R. Inglis, Phys.Rev. 103(1956)1786.
Nuclear moments of inertia due to motion in a rotating well.

183 D.R. Inglis, Phys.Rev. 96(1954)1059.
Particle derivation of nuclear rotation properties associated
with a surface wave.

184 S.A.E. Johansson, Nucl.Phys. 22(1962)529.
Nuclear octupole deformation and the mechanism of fission.

185 T.A. Johansson, Nucl.Phys. A183(1972)33.
Single-particle energy levels in a two-centre shell model.

186 Th. Johansson, S.G. Nilsson, and Z. Szymanski, Ann.Phys. (N.Y.)
5(1970)377.
Theoretical predictions concerning superheavy elements.

187 K. Junker and J. Hadermann, Z.Phys. A282(1977)391.
Fission barriers for even-even actinide nuclei.

188 K. Junker, Acta Phys. Austriaca 43(1975)221.
A single-particle model with deformed average field, taking
into account simultaneously the various deformation degrees
of freedom.

189 K. Junker, Atomenergie (ATKE) 23(1974)57.
The axially asymmetric two-center shell model.

190 K. Junker, Acta Phys.Austr. 40(1974)335.
The liquid-drop model with inclusion of axial asymmetry.

191 Yu.B. Ivanov, Sov.J.Nucl.Phys. 28(2)(1978)177.
Influence of spin-orbit interaction on the surface energy
of a nucleus.

192 F.A. Ivanyuk and V.M. Strutinsky, Z.Phys. A293(1979)337.
Energy- and N-averagings in the shell correction method.

193 F.A. Ivanyuk and V.M. Strutinsky, Z.Phys. A290(1979)107.
Shell corrections for finite depth deformed potentials.

194 F.A. Ivanyuk and V.M. Strutinsky, Z.Phys. A286(1978)291.
Shell corrections for finite depth potentials.

195 A. Iwamoto and J.A. Maruhn, Z.Phys. A293(1979)315.
The behaviour of the temperature-dependent cranking mass
parameter.

196 A. Iwamoto and W. Greiner, Z.Phys. A292(1979)301.
The effect of a super-normal phase transition on the collec-
tive mass parameter.

197 P.B. Kahn and R. Rosenzweig, Phys.Rev. 187(1969)1193.
Theory of nuclear level density for periodic independent-particle energy-level schemes.

198 K.K. Kan, P.C. Lichtner, and J.J. Griffin, Nucl.Phys. A334 (1980)198.
Taylor series comparison of TDHF approximation and exact Schrödinger dynamics.

199 K.K. Kan, P.C. Lichtner, M. Dworzecka, and J.J. Griffin, Phys.Rev. C21(1980)1098.
TDHF dynamics and phase transition in Lipkin-Meshkov-Glick model.

200 K.K. Kan, J.J. Griffin, P.C. Lichtner, and M. Dworzecka, Nucl.Phys. A332(1979)109.
"TDHF-eigenstates": Gauge invariant periodic solutions.

201 K.K. Kan and J.J. Griffin, Nucl.Phys. A301(1978)258.
Independent particle Schrödinger fluid: Moments of inertia.

202 K.K. Kan and J.J. Griffin, Phys.Rev. C15(1977)1126.
The single-particle Schrödinger fluid I: Formulation.

203 K.K. Kan and J.J. Griffin, Phys.Lett. 50B(1974)241.
Quantized friction and the correspondence principle: Single particle with friction.

204 T. Kaniowska, A. Sobiczewski, K. Pomorski, and S.G. Rohozinski, Nucl.Phys. A274(1976)151.
Microscopic inertial functions for nuclei in the Barium region.

205 S.K. Kataria and V.S. Ramamurthy, Pramana 7(1976)407.
Nuclear level densities in self-consistent field approximation.

206 I. Kelson and Y. Shoshani, Phys.Lett. 40B(1972)58.
Lowering of calculated fission barriers of superheavy nuclei.

207 A.K. Kerman and S.E. Koonin, Ann.Phys. (N.Y.) 100(1976)332.
Hamiltonian formulation of time-dependent variational principles of the many-body system.

208 A.K. Kerman, J.P. Svenne, and F.M.H. Villars, Phys.Rev. 147(1966)710.
Hartree-Fock calculation for finite nuclei with a nonlocal two-body potential.

209 C.M. Ko, H.C. Pauli, M. Brack, and G.E. Brown, Nucl.Phys. A236(1974)269.
A microscopic, but not self-consistent approach to nuclear binding and deformation energies.

210 T. Kodama, P.A. Nazareth, P. Möller, and J.R. Nix, Phys.Rev. C17(1978)111.
Exact calculation of the penetrability for a simple two-dimensional heavy-ion fusion barrier.

211 D. Kolb, Z.Phys. A280(1977)143.
Shell structure in the mass region 250 $\leq$ A $\leq$ 500.

212 D. Kolb, Phys.Lett. 65B(1976)319.
Is triple fission predominant in $^{298}_{114}Z$?

213 D. Kolb, R.Y. Cusson, and H.W. Schmitt, Phys.Rev. C10 (1974)1529.
Asymmetric fission in a self-consistent K-matrix model.

214 D. Kolb, R.Y. Cusson, and M. Harvey, Nucl.Phys. A215(1973)1.
Realistic single-particle K-matrix for deformed and fissioning nuclei.

215 V.M. Kolomietz, Sov. J.Nucl.Phys. 18(1974)147.
Shell corrections for nuclear masses in the presence of pairing.

216 S.E. Koonin, Erice, p. 283.
The time-dependent Hartree-Fock description of heavy ion collisions.

217 S.E. Koonin and J. Randrup, Nucl.Phys. A289(1977)475.
Classical theory for one-body nuclear dynamics.

218 S.E. Koonin, R.L. Hatch, and J. Randrup, Nucl.Phys. A283 (1977)87.
One-body dissipation in a linear response approach.

219 S.E. Koonin and J.R. Nix, Phys.Rev. C13(1976)209.
Microscopic calculation of nuclear dissipation.

220 H.A. Kramers, Physica 7(1940)284.
Brownian motion in a field of force and the diffusion model of chemical reactions.

221 H.J. Krappe, J.R. Nix, and A.J. Sierk, Phys.Rev. C20(1979)992.
Unified nuclear potential for heavy-ion elastic scattering, fusion, fission, and ground-state masses and deformations.

222 H.J. Krappe and J.R. Nix, Rochester 1973; p. 159.
Modified definition of the surface energy in the liquid drop formula.

223 S.J. Krieger and C.Y. Wong, Phys.Rev.Lett. 28(1972)690.
Validity of Strutinsky's theory of renormalization.

224 T. Krogulski and J. Błocki, Nucl.Phys. A144(1970)617.
Model calculations of the energy and angular distributions of light nuclei accompanying fission.

225 S.E. Larsson and G. Leander, Nucl.Phys. A239(1975)93.
Potential energy surfaces for the doubly-even N = Z nuclei.

226 S.E. Larsson, G. Leander, S.G. Nilsson, I. Ragnasson, and R.K. Sheline, Phys.Lett. 47B(1973)422.
Axial asymmetry and the spectrum of ^{16}O.

227 J.N.P. Lawrence, Phys.Rev. 139(1965)B1227.
Static fission barrier calculations of a two-parameter liquid drop.

228 G. Leander, Nucl.Phys. A273(1976)286.
Solution of Bohr's collective Hamiltonian for transitional odd-mass nuclei.

229 G. Leander, Nucl.Phys. A219(1974)245.
The droplet model energy of axially asymmetric nuclei.

230 T. Ledergerber, H.C. Pauli, and Y.Yariv, Nucl.Phys. A280 (1977)241.
Description of nuclear deformations in fission and heavy ion reactions by moments of the density.

231 T. Ledergerber, Z. Paltiel, Z. Fraenkel, and H.C. Pauli, Nucl.Phys. A275(1977)280.
Dynamic excitation in fission.

232 T. Ledergerber, Z. Paltiel, H.C. Pauli, G. Schütte, Y. Yariv, and Z. Fraenkel, Phys.Lett. 56B(1975)417.
Dynamic excitation in the fission process.

233 T. Ledergerber and H.C. Pauli, Nucl.Phys. A207(1973)1.
On the dynamics of fission: The rôle of reflection asymmetry in the nuclear shape.

234 K. Lee and D.R. Inglis, Phys.Rev. 108(1957)774.
Stability of pear-shaped nuclear deformations.

235 S. Levit, J.W. Negele,and Z. Paltiel, Phys.Rev. C22(1980)1979.
Barrier penetration and spontaneous fission in the time-dependent mean field approximation.

236 S. Levit, J.W. Negele, and Z. Paltiel, Phys.Rev. C21 (1980)1603.
Time-dependent mean field theory and quantised bound states.

237 S. Levit, Phys.Rev. C21(1980)1594.
On the time dependent mean field approximation for nuclear dynamical problems.

238 S. Levit and U. Smilansky, Nucl.Phys. A315(1979)205.
A uniform semi-classical approach to the Coulomb fission problem.

239 P.C. Lichtner, J.J. Griffin, H. Schultheis, R. Schultheis, and A.B. Volkov, Phys.Rev. C20(1979)845.
Variational derivation of a time-dependent Hartree-Fock Hamiltonian.

240 P.C. Lichtner, J.J. Griffin, H. Schultheis, R. Schultheis, and A.B. Volkov, Nukleonika, 24(1979)359.
The time-dependent phases of TDHF solutions and the TDHF variational principle.

241 P. Lichtner, D. Drechsel, J. Maruhn, and W. Greiner, Phys.Lett. 45B(1973)175.
Fission mass asymmetry as a dynamic process described by collective coordinates.

242 W.F. Lin, Phys.Rev. C2(1970)871.
Validity of the Strutinsky shell correction theory.

243 S. Liran, H.J. Schaefer, W. Scheid, and W. Greiner, Nucl. Phys. A248(1975)191.
Theory of non-adiabatic cranking and nuclear collective motion.

244 K.F. Liu and G. Ripka, Nucl.Phys. A293(1977)333.
Matrix elements with cranked deformed oscillator wave function.

245 R.J. Lombard, Ann.Phys. (N.Y.) 77(1973)380.
The energy density formalism in nuclei.

246 A. Łukasiak, A. Sobiczewski, and W. Stepien-Rudzka, Acta Phys.Pol. B2(1971)535.
Theoretical estimates of lifetimes of superheavy nuclei.

247 S. Ludwig, H. von Groote, E. Hilf, A.G.W. Cameron, and J. Truvan, Nucl.Phys. A203(1973)627.
Droplet mass formula fit.

248 C. Mahaux and H.A. Weidenmüller, Ann.Rev.Nucl.Part.Sci. 29(1979)1.
Recent developments in compound-nucleus theory.

249 G. Mantzouranis and H.C. Pauli, Phys.Rev. C22(1980)1550.
Hot drops: The mean field approximation for collective and statistical properties in nuclei.

250 J.A. Maruhn, V.E. Oberacker, and V.Maruhn-Rezwani, Phys.Rev. 44(1980)1576.
Myon-induced fission as a probe for fission dynamics.

The
mode
(i)
mula
are
latt
kine
mech
two-
wall
T
the
mode
resp
them
can
exci
- th
movi
conc
rati
feat
elem
sibl
by a
ics,
part
tion.
314,
B
doub
down
beit
fric
able

251 J. Maruhn, W. Greiner, P. Lichtner, and D. Drechsel, Nukleonika 19(1974)237.
The asymmetric two-center shell model and the mass distribution in fission.

252 J. Maruhn and W. Greiner, Phys.Rev.Lett. 32(1974)548.
Theory of fission-mass distribution demonstrated for ^{226}Ra, ^{236}U, ^{258}Fm.

253 J. Maruhn and W. Greiner, Z.Phys. 251(1972)431.
The asymmetric two center shell model.

254 L. Meitner and O.R. Frisch, Nature 143(1939)239.
Disintegration of uranium by neutrons: A new type of nuclear reaction.

255 H. Meldner, Phys.Rev. 178(1969)1815.
Realistic nuclear single particle Hamiltonians and the proton shell 114.

256 V. Metag and G. Sletten, Nucl.Phys. A282(1977)77.
The quadrupole moment of the 40 ps fission isomer in ^{236}Pu.

257 V. Metag, Jülich 1979, p.153.
Spectroscopic properties of fission isomers.

258 P. Möller, Jülich 1979, p.283.
Macroscopic-microscopic calculation of fission barriers and masses for heavy elements with a Yukawa-plus-exponential model for the macroscopic energy.

259 P. Möller and J.R. Nix, Nucl.Phys. A296(1978)289.
Studies of the nuclear inertia in fission and heavy-ion reactions.

260 P. Möller and J.R. Nix, Nucl.Phys. A281(1977)354.
Potential-energy surfaces for asymmetric heavy-ion reactions.

261 P. Möller and J.R. Nix, Nucl.Phys. A272(1976)502.
Macroscopic potential-energy surfaces for symmetric fission and heavy-ion reactions.

262 P. Möller and J.R. Nix, Phys.Rev.Lett. 37(1976)1461.
Calculated half-lives of superheavy nuclei near $^{354}|126|$.

263 P. Möller, S.G. Nilsson, and J.R. Nix, Nucl.Phys. A229 (1974)292.
Calculated ground-state properties of heavy nuclei.

264 P. Möller and J.R. Nix, Nucl.Phys. A229(1974)269.
Calculation of fission barriers with the droplet model and folded Yukawa single-particle potential.

265 P. Möller and J.R. Nix, Rochester 1973; Vol.I, p.103.
Calculation of fission barriers.

266 P. Möller, S.G. Nilsson, and R.K. Sheline, Phys.Lett. 40B (1972)329.
Octupole deformations in the nuclei beyond ^{208}Pb.

267 P. Möller, Nucl.Phys. A192(1972)529.
Odd-multipole shape distortions and the fission barriers of elements in the region $84 \leq Z \leq 120$.

268 P. Möller and S.G. Nilsson, Phys.Lett. 31B(1970)283.
The fission barrier and odd-multipole shape distortions.

269 L.G. Moretto, Nucl.Phys. A247(1975)211.
Statistical emission of large fragments: A general theoretical approach.

270 L.G. Moretto, Phys.Lett. 38B(1972)393.
Note on the disappearance of shell effects with excitation energy and the Strutinsky smoothing procedure.

271 L.G. Moretto and R. Stella, Phys.Lett. 32B(1970)558.
Statistical approach to the deformation of excited nuclei.

272 U. Mosel, P.G. Zint, and K.H. Passler, Nucl.Phys. A236 (1974)252.
Self-consistent calculations for highly excited compound nuclei.

273 U. Mosel, Phys.Rev. C6(1972)971.
Fission barrier for nuclei lighter than Ra.

274 U. Mosel and H.W. Schmitt, Phys.Rev. C4(1971)2185.
Fragment-shell influences in nuclear fission.

275 U. Mosel and H.W. Schmitt, Nucl.Phys. A165(1971)73.
Potential energy surfaces for heavy nuclei in the two center shell model.

276 U. Mosel and W. Greiner, Z.Physik 222(1969)261.
On the stability of superheavy nuclei against fission.

277 S.A. Moskowski, Phys.Rev. C2(1970)402.
Nuclear surface properties with a simple effective interaction.

278 B.R. Mottelson and S.G. Nilsson, Mat.Fys.Skr.Dan.Vid.Selsk 1(1959) No.8.
The intrinsic states of odd-A nuclei having ellipsoidal equilibrium shape.

279 B. Mottelson and S.G. Nilsson, Phys.Rev. 99(1955)1615.
Classification of the nucleonic states in deformed nuclei.

280 E. Moya de Guerra and F. Villars, Nucl.Phys. A285(1977)297.
The coupling of a large amplitude collective motion to RPA excitations.

281 P. Mukherjee, K. Krishan, and G. Banerjee, Phys.Rev.Lett. 44(1980)1391.
Revised shell structure of ^{208}Pb and its effect on the magicity of superheavy nuclei.

282 N.C. Mukhopadhyay, J. Hadermann, and K. Tucker, Nucl.Phys. A319(1979)448.
Theory of nuclear fission by stopped pions.

283 M.G. Mustafa and R.L. Ferguson, Phys.Rev. C18(1978)301.
Calculation of spontaneous fission properties of very heavy nuclei: 98 ≤ Z ≤ 106 and 150 ≤ N ≤ 164.

284 M.G. Mustafa and K. Kumar, Phys.Lett. 49B(1974)405.
Angular momentum dependence of moments of inertia and fission barriers of ^{240}Pu.

285 M.G. Mustafa, U. Mosel, and H.W. Schmitt, Phys.Rev. C7 (1973)1519.
Asymmetry in nuclear fission.

286 W.D. Myers and H. v.Groote, Phys.Lett. 61B(1976)125.
The nuclear surface diffuseness.

287 W.D. Myers and W.J. Swiatecki, Ann.Phys.(N.Y.) 84(1974)186.
The nuclear droplet model for arbitrary shapes.

288 W.D. Myers, Nucl.Phys. A204(1973)465.
Geometric properties of leptodermous distributions with applications to fission.

289 W.D. Myers, Nucl.Phys. A145(1970)387.
Droplet model nuclear density distribution in single particle potential wells.

290 W.D. Myers and W.J. Swiatecki, Ann.Phys.(N.Y.) 55(1969)395.
Average nuclear properties.

291 W.D. Myers and W.J. Swiatecki, Nucl.Phys. 81(1966)1.
Nuclear masses and deformations.

292 F.W. Negele, S.E. Koonin, P. Möller, J.R. Nix, and A.F. Sierk, Phys.Rev. C17(1978)1098.
Dynamics of induced fission.

293 F.W. Negele and D. Vautherin, Phys.Rev. C11(1975)1031.
Density-matrix expansion for an effective nuclear Hamiltonian. II.

294 J.W. Negele and D. Vautherin, Phys.Rev. C5(1972)1472.
Density-matrix expansion for an effective nuclear Hamiltonian.

295 F.W. Negele, Phys.Rev. C1(1970)1260.
Structure of finite nuclei in the local-density approximation.

296 J. Nemeth and D. Vautherin, Phys.Lett. 32B(1970)561.
Study of finite nuclei in the local density approximation.

297 B. Nerlo-Pomorska, Z.Phys. A293(1979)9.
Microscopic quadrupole and hexadekapole moments of rare earth nuclei.

298 S.G. Nilsson, C.F. Tsang, A. Sobiczewsky, Z. Szymanski, S. Wychec, G. Gustafson, I.L. Lamm, P. Möller, and B. Nilsson, Nucl.Phys. A131(1969)1.
On the nuclear structure and stability of heavy and superheavy elements.

299 S.G. Nilsson and O. Prior, Mat.Fys.Medd.Dan.Vid.Selsk. 32, No.16(1960).
The effect of pair correlation on the moment of inertia and the collective gyromagnetic ratio of deformed nuclei.

300 S.G. Nilsson, Mat.Fys.Medd.Dan.Vid.Selsk. 29, No.16(1955).
Binding states of individual nucleons in strongly deformed nuclei.

301 J.R. Nix, S.Afr.J.Phys. 1(1978)103.
Superheavy elements.

302 J.R. Nix, Ann.Rev.Nucl.Sci. 22(1971)65.
Calculation of fission barriers for heavy and superheavy nuclei.

303 J.R. Nix, Phys.Today (April 1972)30.
Predictions for superheavy nuclei.

304 J.R. Nix, Nucl.Phys. A130(1969)241.
Further studies in the liquid drop theory of fission.

305 J.R. Nix, Phys.Lett. 30B(1969)1.
Predicted properties of the fission of super-heavy nuclei.

306 J.R. Nix, Ann.Phys.(N.Y.) 41(1967)52.
The normal modes of oscillation of a uniformly charged drop about its saddle-point shape.

307 J.R. Nix and E. Sassi, Nucl.Phys. 81(1966)61.
Estimates of the variation of nuclear fissilities throughout the periodic table.

308 J.R. Nix and W.J. Swiatecki, Nucl.Phys. 71(1965)1.
Studies in the liquid-drop theory of nuclear fission.

309 W. Nörenberg, Z.Phys. 260(1973)165.
Particle motion in guide potentials and the collective nuclear motion.

310 W. Nörenberg, Phys.Rev. C5(1972)2020.
Theoretical study on scission configuration of fissioning ^{240}Pu and ^{242}Pu.

311 H. Orland and R. Schaeffer, Z.Phys. A290(1978)191.
Two-body collisions and time dependent Hartree-Fock theory.

312 V. Oberacker, W. Greiner, H. Kruse, and W.T. Pinkstone, Phys.Rev. C20(1979)1453.
Characteristics of Coulomb fission.

313 S.R. Ofengenden, V.F. Zavarzin, and V.M. Kolomietz, Phys. Lett. 69B(1977)264.
Inclusion of the continuum effects in thermodynamical calculations of nuclear binding energy shell corrections.

314 Z. Paltiel and Z. Fraenkel, Phys.Rev. C19(1979)2274.
Dynamic excitation in the fission of ^{240}Pu.

315 K.H. Passler and U. Mosel, Nucl.Phys. A257(1976)242.
Self-consistent cranking calculations for ^{20}Ne.

316 H.C. Pauli, Nucl.Phys. A346(1980)397.
On the hydrodynamic limit of self-consistent field equations.

317 H.C. Pauli, Z.Phys. A295(1980)315.
On classical hydrodynamics and collective motion as approximation to the nuclear-many body problem.

318 H.C. Pauli and L. Wilets, Z.Phys. A277(1976)83.
Phase factors in bases for solutions of time-dependent Schrödinger equations.

319 H.C. Pauli, Nukleonika 20(1975).
Four lectures on fission. Fragments of a dynamic theory of collective motion in nuclei.

320 H.C. Pauli and T. Ledergerber, Rochester 1973; Vol.I, p.463.
The dynamics of fission in the subbarrier region of deformation.

321 H.C. Pauli, Phys.Lett. 7C(1973)36.
On the shell model and its application to the deformation energy of heavy nuclei.

322 H.C. Pauli and T. Ledergerber, Nucl.Phys. A175(1971)545.
Fission threshold energies in the actinide region.

323 R.E. Peierls and D.F. Thouless, Nucl.Phys. 38(1962)154.
Variational approach to collective motion.

324 R.E. Peierls and I. Yoccoz, Proc.Phys.Soc. A70(1957)381.
The collective model of nuclear motion.

325 S. Polikanov et al., JETP 15(1962)1016.
Spontaneous fission with an anomalously short period.

326 P.N. Pomorska, Nucl.Phys. A327(1979)1.
Discussion of fission barrier calculations by the shell correction method.

327 K. Pomorski, T. Kaniowska, A. Sobiczewski, and S.G. Rohozinski, Nucl.Phys. A283(1977)394.
Study of the inertial function of rare earth nuclei.

328 K. Pomorski, B. Nerlo-Pomorsko, I. Ragnarsson, R.K. Sheline, and A. Sobiczewski, Nucl.Phys. A205(1973)433.
Ground state moments of inertia of deformed nuclei around barium.

329 P. Quentin, I. Brissaud, and R. de Swiniarski, Z.Phys. A298 (1980)37.
The determination of hexadekapole deformation parameters in actinide nuclei and their variation near the nuclear surface.

330 P. Quentin and H. Flocard, Ann.Rev.Nucl.Sci. 28(1978)523.
Self-consistent calculations of nuclear properties with phenomenological effective forces.

331 I. Ragnarsson, S.G. Nilsson, and E.K. Sheline, Phys.Lett. C45(1978)1.
Shell structure in nuclei.

332 V.S. Ramamurthy, S.K. Kataria, and S.S. Kapoor, Nucl.Phys. A334(1980)477.
Analysis of fission excitation functions and fission barrier heights of preactinide nuclei.

333 V.S. Ramamurthy, M. Prakash, and S.S. Kapoor, Phys.Lett. 62B(1976)124.
On the uncertainties in the shell correction by Strutinsky smearing procedure for certain shapes relevant in fission.

334 V.S. Ramamurthy and S.S. Kapoor, Pramana 9(1977)613.
Evaluation of nuclear shell correction energies for realistic level schemes for temperature smearing method.

335 V.S. Ramamurthy and S.S. Kapoor, Phys.Lett. 42B(1972)399.
Statistical properties of excited nuclei and the determination of the ground-state shell correction energies.

336 J. Randrup, Ann.Phys. 112(1978)356.
Nuclear one-body proximity friction.

337 J. Randrup, Nukleonika 22(1977)1029.
Nuclear one-body dissipation.

338 J. Randrup, S.E. Larsson, P. Möller, S.G. Nilsson, K. Pomorski, and A. Sobiczewski, Phys.Rev. C13(1976)229.
(Further studies on) spontaneous-fission half-lives for even nuclei with Z ≥ 92.

339 J. Randrup, S.E. Larsson, P. Möller, A. Sobiczewski, and A. Lukasiak, Physica Scripta 10A(1974)60.
Theoretical estimates of spontaneous-fission half-lives for superheavy elements based on the modified-oscillator model.

340 R. Randrup, C.F. Tsang, P. Möller, and S.G. Nilsson, Nucl. Phys. A217(1973)221.
Theoretical predictions of fission half-lives of elements with Z between 92 and 106.

341 J.O. Rasmussen, W. Nörenberg, and H.F. Mang, Nucl.Phys. A136(1969)465.
A model for calculating the angular momentum distribution in fission.

342 P.G. Reinhard and D. Drechsel, Nucl.Phys. A295(1978)125.
A microscopic study of the dipole giant resonance in fissioning nuclei.

343 P. G. Reinhard and K. Goeke, J.Phys. G4(1978)L245.
The generator-coordinate-method with conjugate parameters and the unification of microscopic theories for large amplitude collective motion.

344 P. Ring, H. Massmann, and J.O. Rasmussen, Nucl.Phys. 296 (1978)50.
On the treatment of a two dimensional fission model with complex trajectories.

345 P. Röper, Z.Phys. 195(1966)316.
Einzelteilchen-Niveaus in einem deformierten energieabhängigen Kernpotential.

346 C.K. Ross and C.S. Warke, Phys.Rev.Lett. 30(1973)55.
Angular momentum conservation in the Strutinsky method.

347 C.K. Ross and R.K. Bhaduri, Nucl.Phys. A188(1972)566.
Continuum effects in Strutinsky calculations.

348 E. Rost, Phys.Lett. 26B(1968)184.
Proton shell-model potentials for lead and the stability of superheavy nuclei.

349 E. Rost, Phys.Rev. 154(1967)994.
Coupled channel calculations for nuclear bound states.

350 D.F. Rowe, Nuclear Collective Motion, Methuen and Co., Ltd., London, 1970.

351 G. Sauer, H. Chandra, and U. Mosel, Nucl.Phys. A264(1976) 221.
Thermal properties of nuclei.

352 R.K. Sheline, I. Ragnarsson, and S.G. Nilsson, Phys.Lett. 41B(1972)115.
Shell structure for deformed nuclear shapes.

353 P.J. Siemens and A. Sobiczewski, Phys.Lett. 41B(1972)16.
Asymptotic expansion for eigenvalue density.

354 A.J. Sierk, S.E. Koonin, and J.R. Nix, Phys.Rev. C17(1978) 646.
Modified one-body nuclear dissipation.

355 A.J. Sierk and J.R. Nix, Phys.Rev. C16(1977)1048.
Effects of the finite range of the nuclear force on the dynamics of fission and heavy-ion collisions.

356 A.J. Sierk and J.R. Nix, Phys.Rev. C21(1980)982.
Fission in a wall-and-window one-body-dissipation model.

357 A.J. Sierk and J.R. Nix, Rochester 1973, p.273.
Dynamics of fission and fusion with applications to the formation of superheavy nuclei.

358 T.H.R. Skyrme, Proc.Phys.Soc. A70(1957)433.
Nuclear moments of inertia.

359 T.H.R. Skyrme, Nucl.Phys. 9(1959)615.
The effective nuclear potential.

360 T.H.R. Skyrme, Phil.Mag. 1(1956)1043.
The nuclear surface.

361 A. Sobiczewski, Z. Szymanski, S. Wycech, S.G. Nilsson, J.R. Nix, C.F. Tsang, C. Gustafson, P. Möller, and B. Nilsson, Nucl.Phys. A131(1969)67.
Microscopic calculation of the inertial mass parameters for fissioning nuclei.

362 A. Sobiczewski, A. Gyurkovich, and M. Brack, Nucl.Phys. A289(1977)346.
An asymptotic form of the smooth part of the total single-particle energy.

363 A. Sobiczewski and S. Bjørnholm, Nucl.Phys. A202(1973)274.
The moment of inertia and the energy gap of fission isomers.

364 H. Specht, Nukleonika 20(1975)717.
The shape of the fission barrier.

365 H.J. Specht, Rev.Mod.Phys. 46(1974)773.
Nuclear fission.

366 H.J. Specht, J. Weber, E. Konecny, and D. Heunemann, Phys. Lett. 41B(1972)43.
Identification of a rotational band in the ^{240}Pu fission iscmer.

367 W.F. Swiatecki, Proc.Phys.Soc.London A64(1951)226.
The nuclear surface.

368 D. Scharnweber, W. Greiner, and U. Mosel, Nucl.Phys. A164 (1971)275.
The two-center shell model.

369 H.W. Schmitt and U. Mosel, Nucl.Phys. A186(1972)1.
Fission properties of heavy and superheavy nuclei.

370 H.W. Schmitt, Vienna 1969, p.67.
A model for fragment mass-versus-energy correlations in fission.

371 G. Schütte, Z.Phys. A296(1980)331.
Mass parameters for deformation process.

372 G. Schütte, P. Möller, J.R. Nix, and A.F. Sierk, Z.Phys. A297(1980)289.
Fission with microscopic energy dissipation.

373 G. Schütte, Jülich 1979, p.345.
Estimates of odd-even effects in nuclear fission.

374 G. Schütte, Phys.Lett. 89B(1979)11.
Fission: Adiabatic? Non-adiabatic!

375 G. Schütte, Z.Phys. A288(1978)161.
Lifetime of pair excitations in nuclear fission.

376 G. Schütte and L. Wilets, Z.Phys. A286(1978)313.
Excitation during collective deformation: How simple it is.

377 G. Schütte, Z.Phys. A283(1977)183.
Solution of the cranking model to all orders.

378 G. Schütte and L. Wilets, Nucl.Phys. A252(1975)21.
Dynamics and non-adiabaticity in the fission process.

379 H. Schultheis, R. Schultheis, and K. Wildermuth, Nukleonika 20(1975)423.
Shell energy in fission and its relation to the cluster structure of nuclei.

380 H. Schultheis and R. Schultheis, Lett.Nuovo Cim. 6 (1973) 169.
Deviations from axial symmetry at scission.

381 H. Schultheis and R. Schultheis, Nucl.Phys. A215(1973)329.
Axial asymmetry and mass asymmetry at the scission point.

382 H. Schultheis and R. Schultheis, Phys.Lett. 34B(1971)245.
Axial asymmetric fission-barrier distortions.

383 H. Schultheis and R. Schultheis, Phys.Lett. 37B(1971)467.
Secondary shells in a semi-empirical treatment.

384 H. Schultheis and R. Schultheis, Lett.Nuovo Cim. 3(1972) 313.
On a three-parameter description of the nuclear shape in fission.

385 W. Stocker, Nucl.Phys. A264(1976)244.
A spin-asymmetry term for the mass formula.

386 W. Stocker and J. Burzlaff, Nucl.Phys. A202(1973)265.
Liquid-drop description of the nuclear excitation energy.

387 W. Stocker, Nucl.Phys. A166(1971)205.
Nuclear surface properties and the nuclear compressibility in a statistical approximation.

388 W. Stocker, Nucl.Phys. A159(1970)222.
Two-body spin-orbit potentials and semi-infinite nuclear matter.

389 V.M. Strutinsky and V.M. Kolomietz, Z.Phys. A289(1978)77.
Macroscopic rotation of cold nuclei.

390 V.M. Strutinsky, Z.Phys. A280(1977)99.
Collective motion at large amplitudes and finite velocities.

391 V.M. Strutinsky, A.G. Magner, S.R. Ofengenden, and T. Døssing, Z.Phys. A283(1977)269.
Semiclassical interpretation of the gross-shell structure.

392 V.M. Strutinsky and A.G. Magner, Sov.J.Part.Nucl. 7(1976) 138.
Quasiclassical theory of nuclear shell structure.

393 V.M. Strutinsky, Nukleonika 20(1975)679.
Semi-classical theory of the nuclear shell structure.

394 V.M. Strutinsky and F.A. Ivanjuk, Nucl.Phys. A255(1975)405.
A new definition of shell corrections to the liquid drop energy.

395 V.M. Strutinsky, Nucl.Phys. A254(1975)197.
The shell correction and self-consistent deformation energies.

396 V.M. Strutinsky, Nucl.Phys. A218(1974)169.
Hartree-Fock distortion energy of the nucleus.

397 V.M. Strutinsky, Sov.J.Nucl.Phys. 3(1969)449.
Influence of nucleon shells on the energy of a nucleus.

398 V.M. Strutinsky, Riv.Nuovo Cim. 1(1969)442.
The fission process.

399 V.M. Strutinsky and S. Bjørnholm, Dubna 1968, p.431.
Intermediate states in fission.

400 V.M. Strutinsky, Nucl.Phys. A122(1968)1.
Shells in deformed nuclei.

401 V.M. Strutinsky, Nucl.Phys. A95(1967)420.
Shell effects in nuclear masses and deformation energies.

402 V.M. Strutinsky, N.Y. Lyashenko, and N.N. Popov, Nucl.Phys. 46(1962)639.
Symmetrical shapes of equilibrium for a liquid drop.

403 V.M. Strutinsky and A.S. Tyapin, JETP 45(1963)960.
Quasistatic drop model of the nucleus as an approximation to the statistical model.

404 D.F. Thouless, The quantum mechanics of many body systems, Academic Press, New York, 1961.

405 D.F. Thouless and F.G. Valatin, Nucl.Phys. 31(1962)211.
Time-dependent Hartree-Fock equation and rotational states of nuclei.

406 D.F. Thouless, Nucl.Phys. 21(1960)225.
Stability conditions and nuclear rotation in the Hartree-Fock theory.

407 F. Tondeur, Z.Phys. A297(1980)61.
Shell structure and stability of nuclei with 270 < A < 500 and the possible existence of primordial superheavy nuclei.

408 S. Trentalange, S.E. Koonin, and A.J. Sierk, Phys.Rev. C22 (1980)1159.
A new shape parametrization for liquid-drop studies.

409 A.S. Tyapin, Sov.F.Nucl.Phys. 14(1972)50.
A statistical estimate of the density of single particle states in a weakly deformed Nilsson potential.

410 A.S. Tyapin, Sov.F.Nucl.Phys. 11(1970)53.
The shell correction method.

411 R. Vandenbosch, Ann.Rev.Nucl.Sci. 27(1977)1.
Spontaneously fissioning isomers.

412 D. Vautherin, Phys.Lett. 57B(1975)425.
Mass parameters for quadrupole vibrations in the adiabatic approximation.

413 D. Vautherin, Phys.Rev. C7(1973)296.
Hartree-Fock calculations with Skyrme's interaction. II. Axially deformed nuclei.

414 D. Vautherin and D.M. Brink, Phys.Rev. C5(1972)626.
Hartree-Fock calculations with Skyrme's interaction. I. Spherical nuclei.

415 D. Vautherin and D.M. Brink, Phys.Lett. 32B(1970)149.
Hartree-Fock calculations with Skyrme's interaction.

416 F.M.H. Villars, Nucl.Phys. A285(1977)269-296.
Adiabatic time-dependent Hartree-Fock-theory in nuclear physics.

417 H.A. Weidenmüller, Prog.Part.Nucl.Phys. 3(1980)49-126.
Transport theories of heavy-ion reactions.

418 H. Weigmann, Winter College IAEA, Trieste, 1980.
Theory and phenomenology of neutron induced fission cross sections.

419 H. Weigmann and J.P. Theobald, Nucl.Phys. A187(1972)305.
Evaluation of fission barrier parameters from near-barrier fission and isomeric half life data.

420 C.F. von Weizsäcker, Z.Phys. 96(1935)431.
Zur Theorie der Kernmassen.

421 L. Wilets, D.R. Tuerpe, and P.K. Haff, Phys.Rev. C12(1975) 2088.
Calculation of the mass parameter in the theory of self-cranked generator coordinates.

422 L. Wilets, Rev.Mod.Phys. 30(1958)542.
Theories of the nuclear surface.

423 B.D. Wilkins, E.P. Steinberg, and R.R. Chasman, Phys.Rev. C14(1976)1832.
Scission-point model of nuclear fission based on deformed shell effects.

424 F.C. Williams, Jr., G. Chan, and J.R. Huizenga, Nucl.Phys. A187(1972)225.
The significance of shell corrections in the parametrization of numerical state density calculations.

425 C.Y. Wong and H.H.K. Tang, Phys.Rev. C20(1979)1419.
Dynamics of nuclear fluid V: Extended time-dependent Hartree-Fock approximation illuminates the approach to thermal equilibrium.

426 C.Y. Wong, Phys.Rev. C17(1978)1832.
Dynamics of nuclear fluid IV: Some spin and isospin properties in the hydrodynamical model.

427 C.Y. Wong and J.A. McDonald, Phys.Rev. C16(1977)1196.
Dynamics of nuclear fluid III: General considerations on the kinetic theory of quantum fluids.

428 C.Y. Wong, T.A. Welton, and J.A. Maruhn, Phys.Rev. C15 (1977)1558.
Dynamics of nuclear fluid II: Normal sound, spin sound, isospin sound and spin-isospin sound.

429 C.Y. Wong, J.A. Maruhn, and T.A. Welton, Nucl.Phys. A253 (1975)469.
Dynamics of nuclear fluid I.

430 C.Y. Wong and H.H.K. Tang, Phys.Rev.Lett. 40(1978)1070
Extended time-dependent-Hartree-Fock approximations with particle collisions.

431 C.W. Wong, Phys.Lett. 15C(1975)283.
Generator coordinate methods in nuclear physics.

432 Y. Yariv, T. Ledergerber, and H.C. Pauli, Z.Phys. A278 (1976)225.
Single particle models in the shell correction approach.

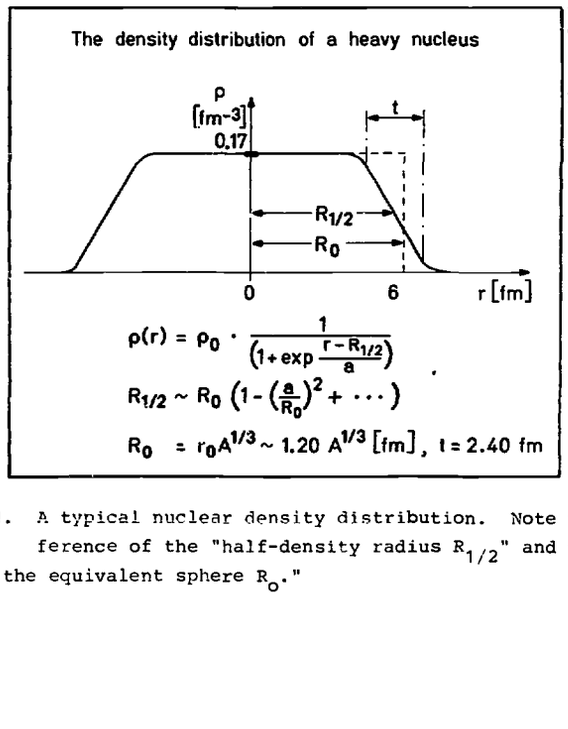

Figure 1. A typical nuclear density distribution. Note the difference of the "half-density radius $R_{1/2}$" and the "radius of the equivalent sphere R_o."

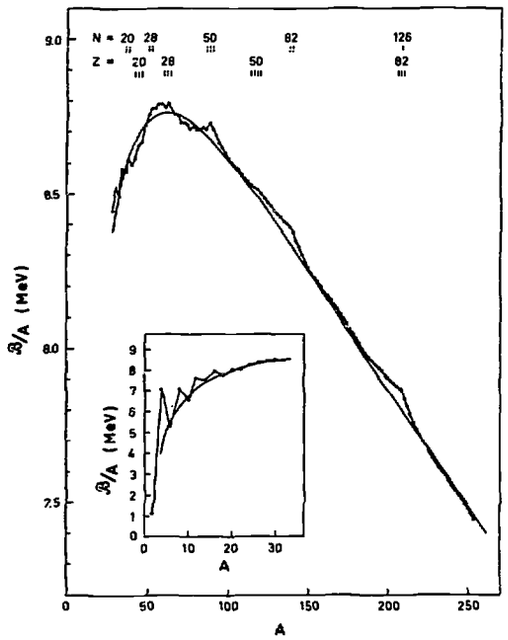

Figure 2. Binding energy per nucleon as a function of A, taken from the book of Bohr and Mottelson. The experimental binding energies were taken from the compilation by J.H.E. Mattauch, W. Thiele, and H.A. Wapstra, Nucl.Phys. 67 (1965) 1. The thin, smooth curve represents the semiempirical mass formula, with the constants given by A.E.S. Green and N.A. Engler, Phys.Rev. 91 (1953) 40.

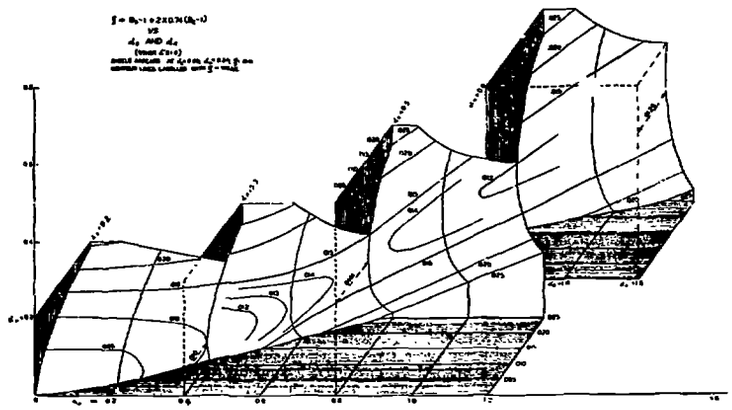

Figure 3. The deformation energy of a homogeneously charged drop with sharp boundary. The figure is taken from the work of S. Frankel and N. Metropolis, Phys.Rev. 72 (1947) 914. It shows the deformation energy in units of the surface energy of the drop at the value of the fissility parameter $x = 0.74$. Note the appearance of the characteristic saddle point at $\alpha_2 = 0.80$ and $\alpha_4 = 0.24$; for the definition of the α_i see text.

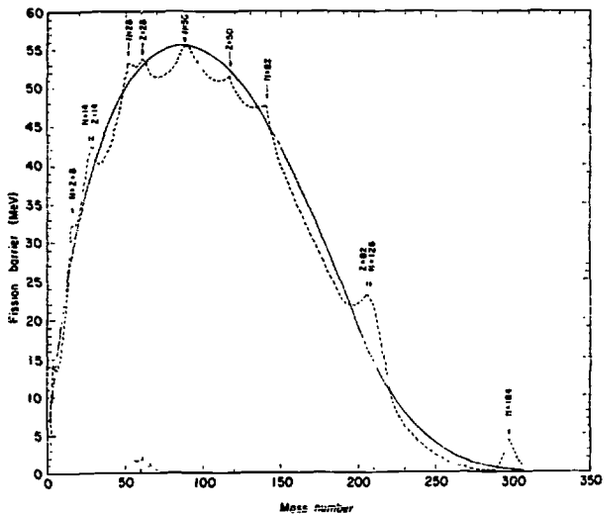

Figure 4. The fission barrier versus mass number. The figure was taken from W.D. Myers and W.J. Swiatecki, Nucl. Phys. 81 (1966) 1, and shows the fission threshold energies as obtained from their liquid drop fit to the binding energies and fission barriers. The dotted curve includes their way of treating the shell corrections; see also Section III.

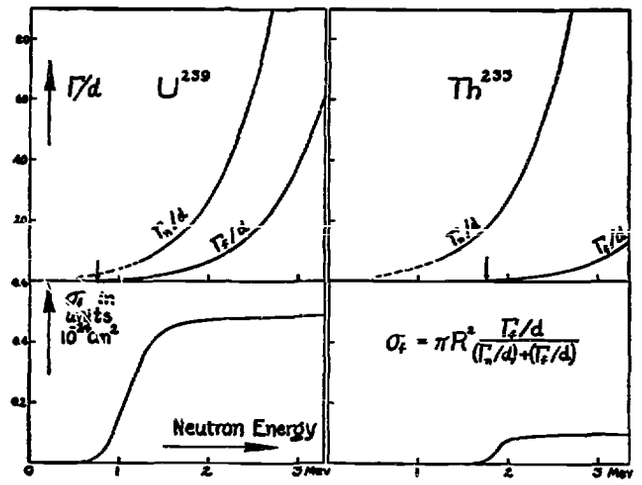

Figure 5. The threshold behavior of nucleon-induced fission cross section. Γ_n/d and Γ_f/d are the ratios of the neutron emission and fission probabilities (taken per unit of time and multiplied by $\hbar$) to the average level spacing in the compound nucleus at the given excitation. These ratios will vary with energy in nearly the same way for all heavy nuclei, except that the entire fission curve must be shifted to the left or right according as the critical fission energy E_f is less than or greater than the neutron binding E_n. The cross section for fission produced by fast neutrons depends on the ratio of the values in the two curves, and is given on the left for $E_f - E_n = (\frac{3}{4})$ Mev and on the right for $E_f - E_n = 1\frac{3}{4}$ Mev, corresponding closely to the cases of U^{239} and Th^{233}, respectively. (Figure and caption was taken from N. Bohr and J.A. Wheeler, Phys.Rev. 56 (1939) 426.)

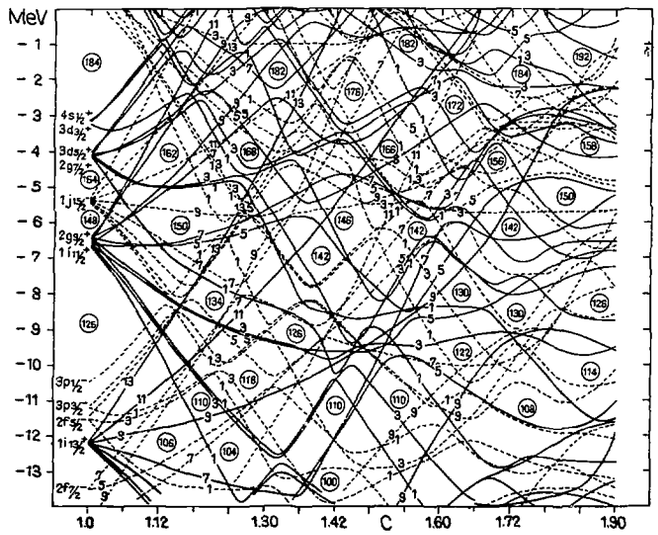

Figure 6. Single particle states in an axially deformed potential, taken from H.C. Pauli, Phys.Lett. C7 (1973) 36. The figure shows the single particle states for the neutrons in ^{240}Pu in an axially symmetric average potential plotted as a function of c, the longer axis in units of the equivalent radius of a sphere. c = 1.0 corresponds to spherical symmetry. Odd parity states are dotted, the number inserted correspond to twice the K value, the projection of angular momentum on the axis of symmetry. Note the regions of abnormally small density of states, marked by the circles, which include the corresponding neutron number.

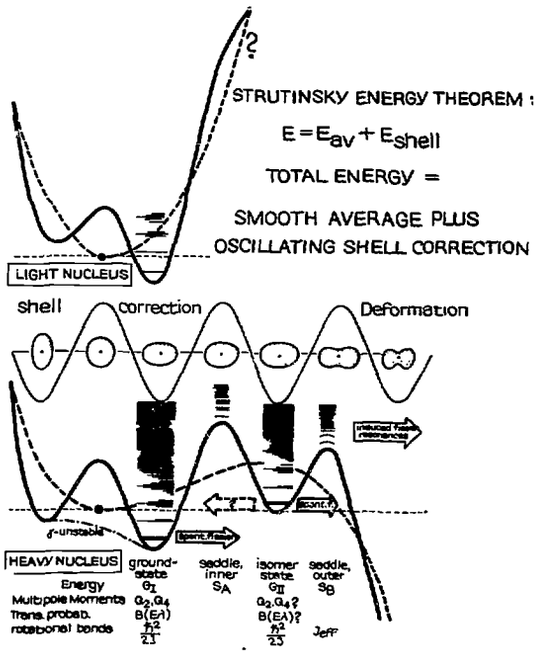

Figure 7. The modification of the drop's deformation energy by shell corrections for a light and a heavy nucleus, schematic.

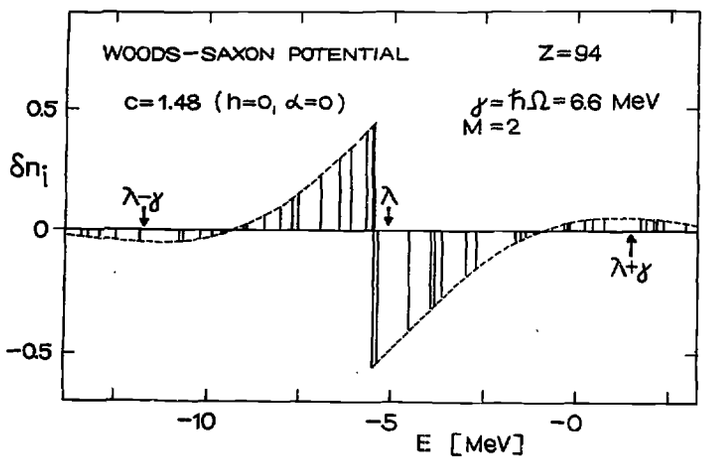

Figure 8. The function $\delta n_i = n_i - \overline{n_i}$ plotted as a function of single particle energies, taken from M. Brack, Nucl. Phys. A207 (1973) 401. The single particle states for protons in a deformed Woods-Saxon potential are indicated by the vertical lines, their length being equal to values of δn_i. The Fermi energy λ and the averaging interval γ are indicated in the figure.

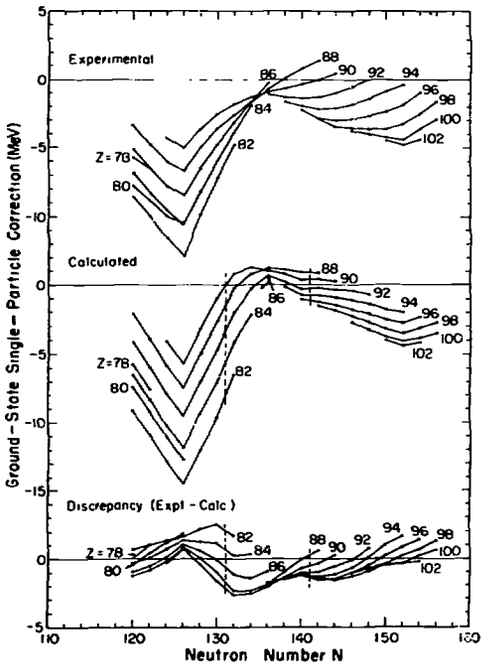

Figure 9. Shell corrections to the binding energies. The figure is taken from P. Möller and J.R. Nix, Rochester 1973, p. 103, where calculational details may also be found.

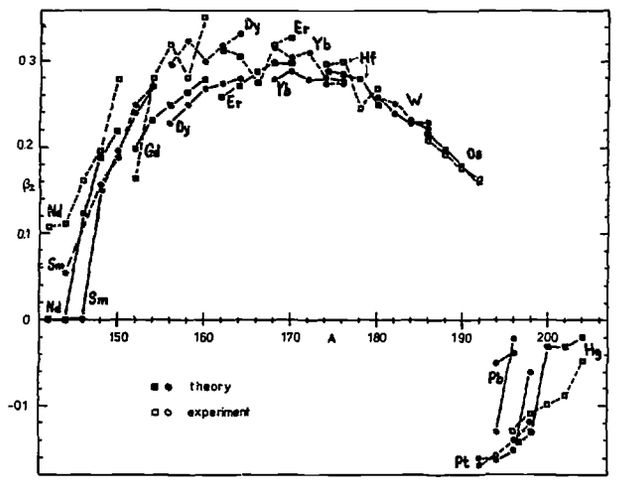

Figure 10. Ground state deformations in the rare earth region. The figure was taken from the work of U. Götz et al. Nucl.Phys. A192 (1972) 1.

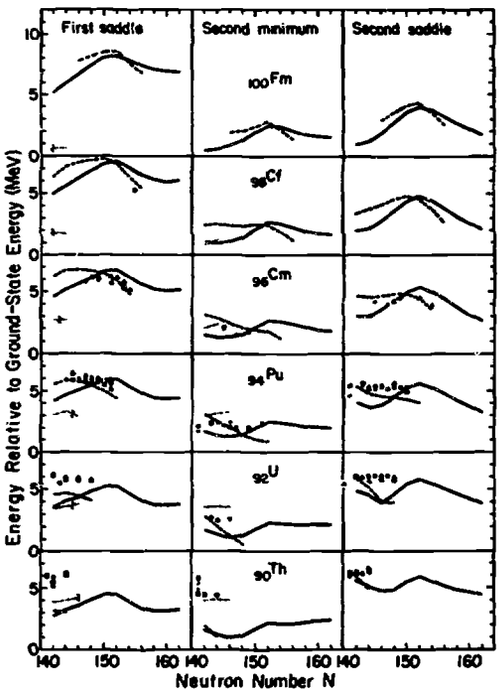

Figure 11. The energies of the first barrier, the second minimum, and the second barrier relative to the ground state. The figure was taken from the work of P. Möller and J.R. Nix, Rochester 1973, p. 103.

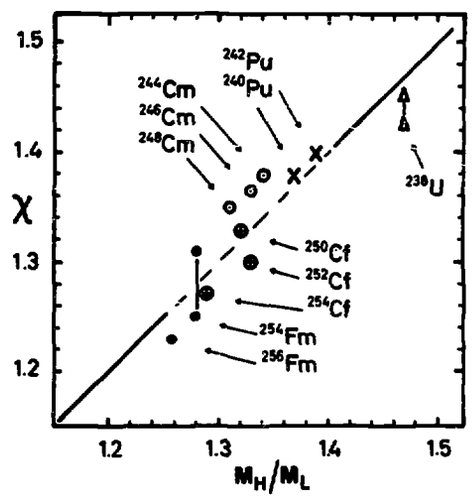

Figure 12. The asymmetry in the mass distribution of fission fragments. The figure, taken from the work of M. Brack, et al., Rev.Mod.Phys. 44 (1972) 320, correlates the calculated mass asymmetry χ at the second barrier with the experimental peak-to-peak ratio M_H/M_L of the mass distribution.

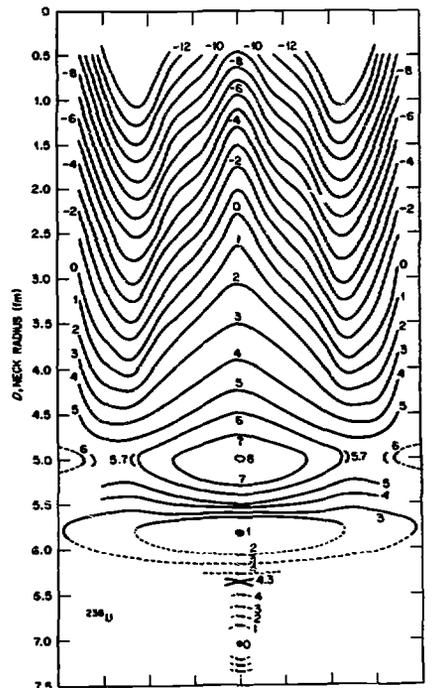

Figure 13. The deformation energy of ^{236}U versus mass asymmetry and neck radius of the density droplet. The figure, taken from the work of M.G. Mustafa, U. Mosel, and H.W. Schmitt, Phys.Rev. C7 (1973) 1519, demonstrates the maintenance of fragmentary shells between the second saddle at D = 5 fm and the scission point at D = 0 fm.

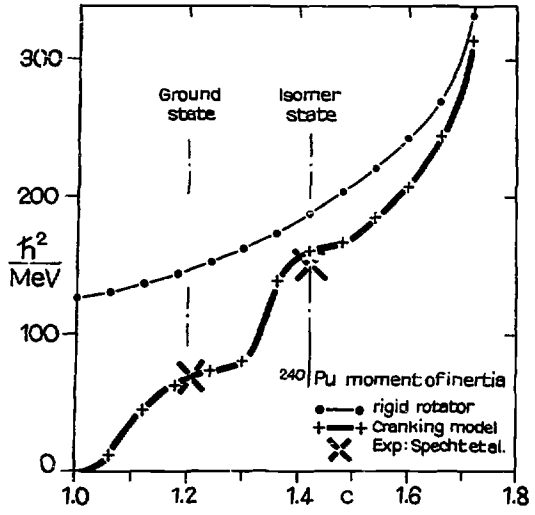

Figure 14. The moment of inertia versus deformation. The moment of inertia figure is prepared based on the material of M. Brack et al., Nucl.Phys. A234 (1974) 185, and shows the moment of inertia as calculated from the cranking model for ^{240}Pu (thick line). The rigid body value is indicated by the thin line. The deformation c refers to the longer axis of the droplet in units of the spherical radius. Experimental values refer to the work of Specht et al., Phys.Lett. 41B (1972) 43.

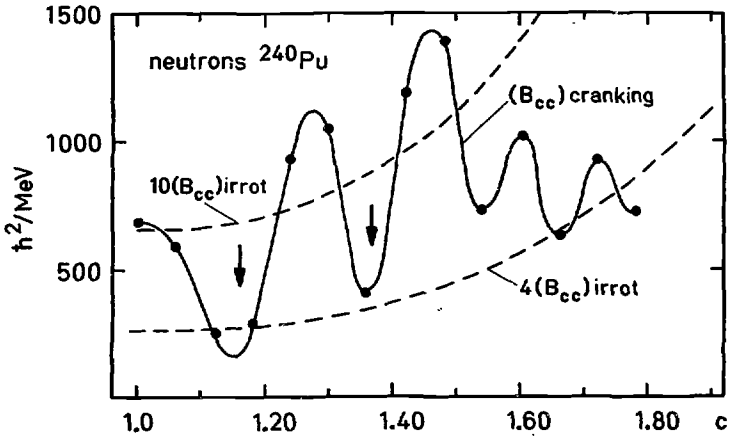

Figure 15. One component (B_{cc}) of the mass tensor versus deformation. The cranking model mass parameter B_{cc} is plotted versus deformation c in order to display its shell structure. The equilibrium deformations are indicated by the arrows and occur at comparatively low single particle level densities. The material for this figure has been taken from the work of Ledergerber, Nucl.Phys. A207 (1973) 1, and Pauli, Z.Physik A295 (1980) 315.

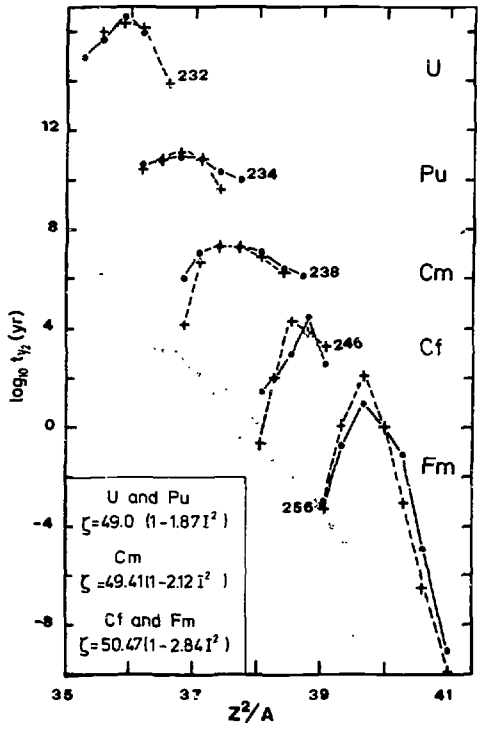

Figure 16. Lifetimes for spontaneous fission. The lifetimes (in years) for the spontaneous fission from the ground state are indicated by the dots and plotted versus Z^2/A. They are compared to the calculated values, indicated by the crosses. The figures was taken from the work of Pauli and Ledergerber, Rochester 1973, p. 463.

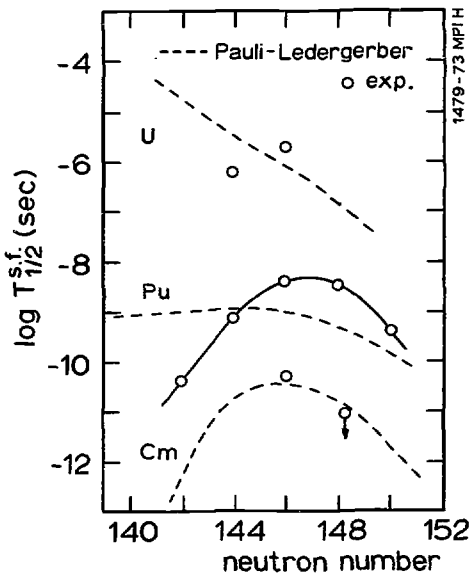

Figure 17. Lifetimes of fission isomers. The lifetime for spontaneous fission from the isomer state (in seconds) is plotted versus the neutron number. The figure is taken from the work of Pauli and Ledergerber, Rochester 1973, p. 463.

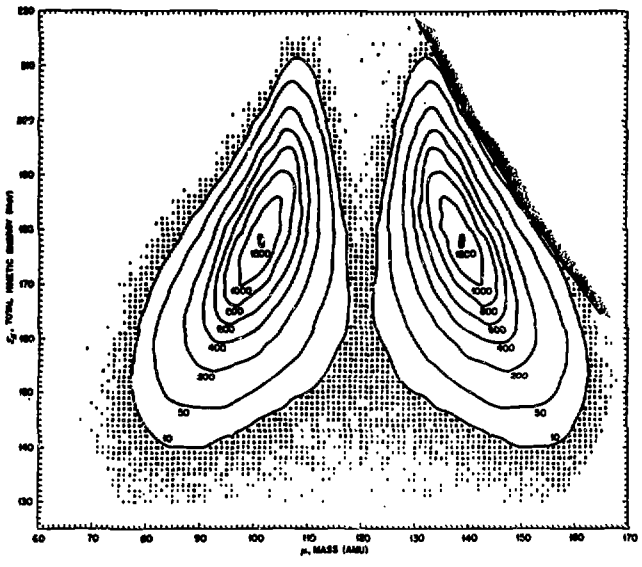

Figure 18. The double differential cross section for the fission of ^{239}Pu induced by thermal neutrons is given as a contour plot (in relative units) versus the total kinetic energy of the fission fragments and their mass. The figure was taken from the work of J.H. Neiler, F.J. Walter, and H.W. Schmitt, Phys. Rev. 149 (1966) 894.

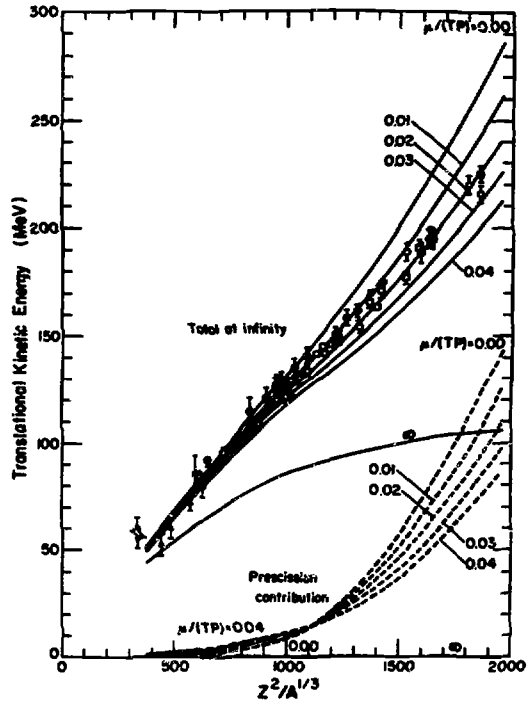

Figure 19. Comparison of the most probable fission-fragment kinetic energies with results calculated for different values of the viscosity coefficient μ (in Terapoise). The figure was taken from the work of K.T.R. Davies, A.J. Sierk, and J.R. Nix, Phys.Rev. C13 (1976) 2385.

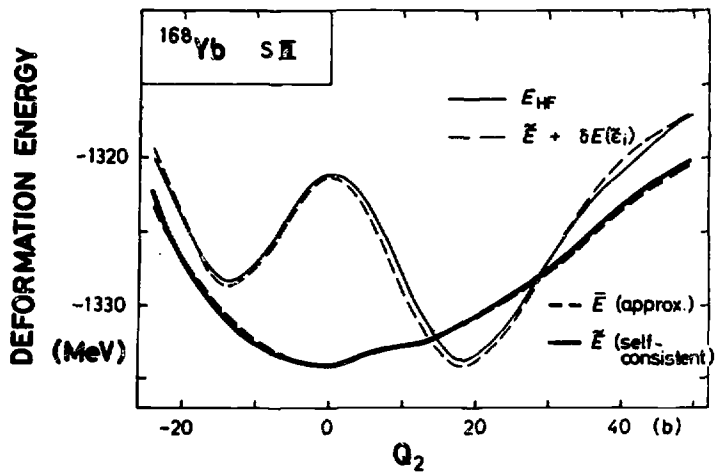

Figure 20. The deformation energy for ^{168}Yb plotted versus the quadrupole moment. The thin line denotes the fully self-consistent energy, as calculated for the SIII force. The dashed curve refers to the approximative calculation as described in the text. The figure was taken from the work of M. Brack and Ph. Quentin, Phys.Lett. 56B (1975) 421.

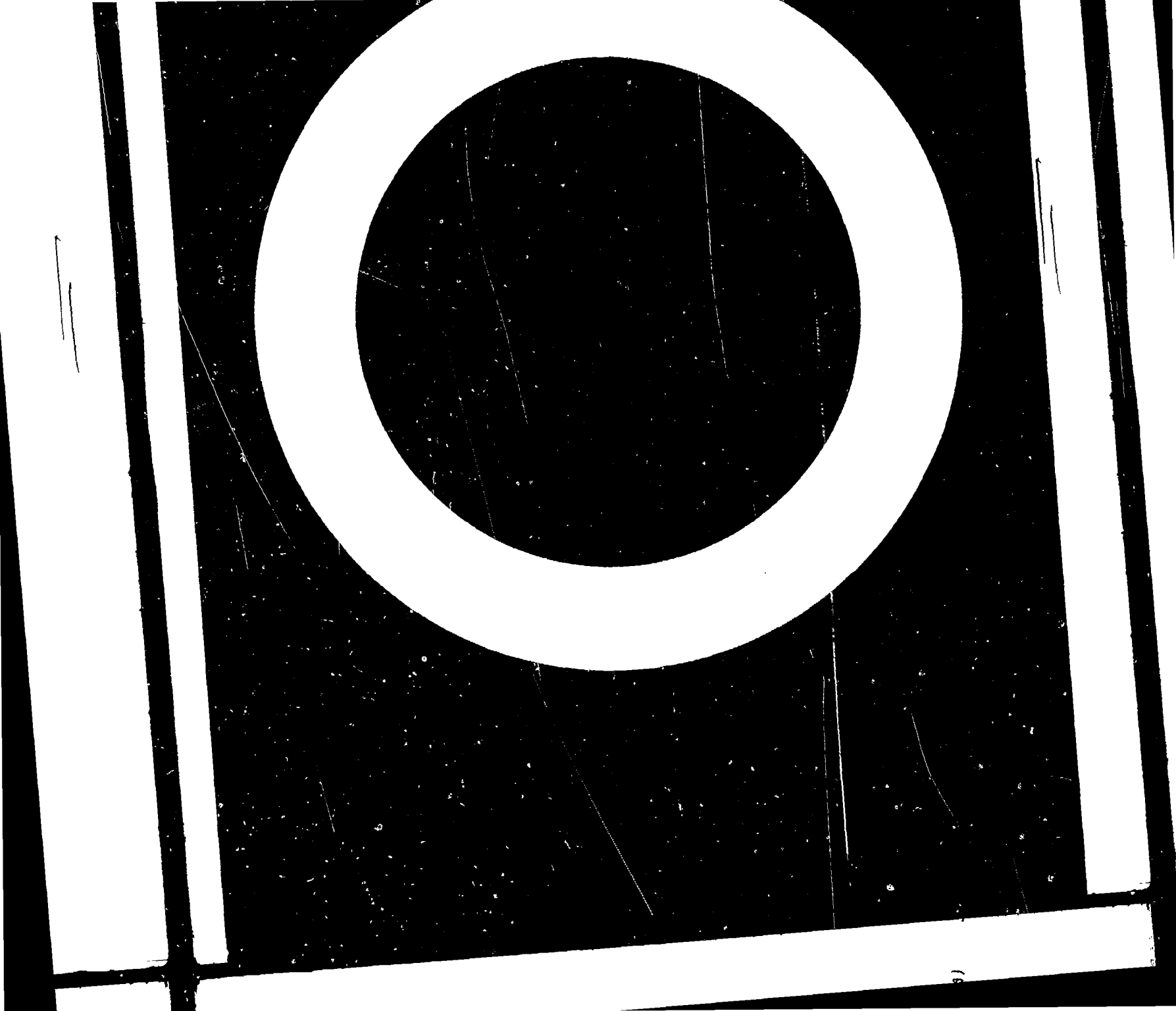

THEORY AND PHENOMENOLOGY OF NEUTRON INDUCED FISSION CROSS SECTIONS

H. WEIGMANN
Commission of the European Communities,
Joint Research Centre,
Central Bureau for Nuclear Measurements,
Geel, Belgium

Abstract

The lectures discuss the theory and phenomenology of neutron-induced fission cross sections. First, a brief summary of our knowledge of the potential energy surface in the deformation plane is given. Then the theory of neutron-induced fission reactions is discussed with special emphasis on structure effects related to the "double humped" fission barrier. The status of the experimental information is examined and recent developments are described. Finally, parametrizations and data used for actual calculations of unknown cross sections are discussed.

1. Introduction

The subject of these lectures is a review of the theory and phenomenology of cross sections for neutron-induced fission, in view of their application in the evaluation of fission data and the calculation of unknown fission cross sections. The discussion of actual evaluation procedures and of computer codes for cross section calculations will not be included, since these are the subject of a series of lectures given by S. Pearlstein and V. Konshin at this course. The purpose of the present lectures is rather to provide the necessary background for the lectures of Drs. Pearlstein and Konshin by the discussion of the basic properties of fission cross sections and their theoretical interpretation.

A very extensive series of lectures on the same subject has been given by E. Lynn [Ly78] during the preceding Course on Nuclear Theory for Applications at Trieste in 1978. The contents of the present lectures will overlap to a large degree with the 1978 lectures by Lynn : Although the present lectures will try to emphasise phenomenological aspects and especially the development during the past two years, a considerable amount of overlap is unavoidable in order to keep the present lectures self-consistent.

Among other recent reviews on the subject of neutron-induced fission we want to especially mention the very comprehensive article by A. Michaudon [Mi73] in "Advances in Nuclear Physics".

In chapter 2 we will briefly discuss the deformation potential of actinide nuclei. This will be done only very crudely, since the basic properties of the deformation energy and the fission process itself, including its dynamical aspects, will be extensively treated in the lectures by H.C. Pauli at the present course.

Chapter 3 will deal with the statistical theory of neutron-induced reactions and will include the fission degree of freedom in a preliminary, essentially macroscopic way.

In chapter 4, the fission decay of the compound nucleus will be discussed in detail in a microscopic way, including the various phenomena of intermediate structure. Some discussion of empirical data will also be included.

In chapter 5 the question of vibrational resonances will be addressed, and we will especially discuss recent data on the light actinides (Th- and Pa- isotopes) which may indicate additional structure (a third minimum) in the deformation potential of these nuclei.

Finally in chapter 6 we will briefly review our knowledge of empirical data needed as input for actual calculations of unknown cross sections.

2. The Deformation Potential

The questions of basic fission theory, including the various aspects of the potential energy as a function of deformation as well as the dymanics of the fission process, will be extensively treated in the lectures of H.C. Pauli at this course. Therefore, only a very crude reminder of the basic ideas underlying the determination of the deformation potential will be given here in order to keep the present lecture self-supporting.

2.1. The Liquid Drop Energy

For many years the process of nuclear fission had been interpreted in terms of the liquid drop model of the nucleus [BW39]. In this model, the total energy of the nucleus is expressed as the sum of a volume energy E_v proportional to the mass number, a surface energy E_s proportional to the surface area of the drop, and the Coulomb energy E_c :

$$E_{LDM} = E_v + E_s + E_c \qquad (2.1)$$

Since the volume energy is independent of deformation, the deformation dependence may be expressed by the deformation energy

$$E_D(\epsilon) = E_s(\epsilon) + E_c(\epsilon) - E_s(o) - E_c(o) \qquad (2.2)$$

where ϵ is the deformation parameter as defined, e.g. by Nilsson [Ni55]. For a nucleus around $A \approx 240$, for a small ϵ, $E_s(\epsilon)$ increases more quickly with ϵ than $E_c(\epsilon)$ decreases, such that a net increase of $E_D(\epsilon)$ results for small ϵ; but for $\epsilon \gtrsim 0.6$, the situation reverses and $E_D(\epsilon)$ decreases with increasing ϵ, with the consequence that the nucleus becomes unstable with respect to further deformation and finally fissions. Thus $E_D(\epsilon)$ exhibits a "fission barrier" which was expected to determine the properties of the nucleus with respect to fission.

During the past decade, the increased interest in the deformation energy has led not only to extensive investigations of single particle effects (see section 2.2 below), but also to improvements of the liquid drop model. The most important one is the droplet model of Myers and Swiatecki [MS69] which takes into account effects of the diffuseness of the nuclear surface, the redistribution of charge in the surface region, and effects of the finite compressibility of nuclear matter. The parameters of the droplet model are obtained from adjustment to experimental data and from statistical calculations.

However, in spite of refinements, the liquid drop model was clearly inadequate to explain some of the basic properties of actinide nuclei, like the predominantly asymmetric mass division in fission, and the fact that the actinides were deformed in their ground states. To explain these features obviously demanded inclusion of a more microscopic theory of the nucleus, i.e. the shell model.

2.2. Shell Corrections

The obvious alternative to the macroscopic liquid drop model, i.e. simply summing the energies e_ν of all occupied shell model single particle states according to

$$U = \sum 2 n_\nu e_\nu \qquad (2.3)$$

in order to obtain the total energy of the nucleus, was clearly inadequate, too: The neglect of residual interactions and inadequacies of the single particle potential would lead to errors which would accumulate; thus the final result would be much less accurate than the one obtained from the liquid drop model with its semi-empirically adjusted parameters.

The breakthrough came with Strutinsky's [St67] proposal to combine the virtues of both models. His "macroscopic - microscopic" method amounts to a renormalization of the sum equ. (2.3) of single particle energies according to

$$E = U - \tilde{U} + E_{LDM} = E_{LDM} + \delta U \qquad (2.4)$$

where $\tilde{U}$ is basically a sum similar to the one of equ.(2.3), but with the shell model single particle energies e_ν replaced by energies of pseudo-single particle states obtained from the original e_ν by an averaging procedure which washes out the actual shell effects. The quantity $\tilde{U}$ is expected to resemble the shell model analogue to the liquid drop energy, such that the difference $\tilde{U} - E_{LDM}$ represents the desired renormalization of the single particle energy sum U.

Besides the shell correction δU, also a correction δP has to be included which takes into account the different pairing energies for the true and the averaged single particle state densities. Thus, in place of equ.(2.4) we have :

$$E = E_{LDM} + \delta U + \delta P \qquad (2.5)$$

By taking the difference $U - \tilde{U}$, the systematic errors inherent to the shell model ought to cancel, and only effects associated with the local shell structure as a function of nucleon number and deformation will remain.

The effect of the shell correction on the deformation energy is examplified in figures 1 and 2 : Fig. 1 shows single neutron levels as a function of deformation

as calculated by Nilsson et al. [Ni69]. Also shown as the bold solid line is the highest level occupied for N = 152. For a nucleus with this neutron number, a low single neutron level density near to that line, as around $\epsilon \approx 0.55$, will lead to a negative contribution to δU, whereas a high single neutron level density (at $\epsilon \approx 0.4$ and $\epsilon \approx 0.75$) will yield a positive contribution to δU. Thus, seen as a function of deformation, the shell correction produces modulations on top of the smooth liquid drop model contribution to the deformation energy. The result is seen in fig. 2, which shows, for a typical actinide nucleus, the final deformation potential (solid line) and its liquid drop model part (broken line).

After the pioneering work of Strutinsky a large amount of effort has been put into the calculation of deformation potential surfaces. They differ in several aspects, e.g. in the choice of the single particle potential used to determine the shell correction : Many calculations have been done with the deformed modified oscillator potential [Ni69] and with the deformed Woods - Saxon potential which was also used in Strutinsky's original work [St67]. Other potentials used are the two-centre oscillator potential [Sc71] and the folded Yukawa potential [Bo72]. Many details of the Strutinsky method as well as its justification on the basis of Hartree - Fock theory can be found in a review paper by Brack et al. [Br72]. No further details will be discussed here, with the exception of the special question of asymmetric deformations which will prove to be very important for the analysis and prediction of fission cross sections (chapters 5 and 6).

2.3. Inclusion of Asymmetric Deformations

Until now we have been talking about the potential energy as a function of the deformation parameter ϵ [Ni35] which to first order describes pure quadrupole deformations. Of course, more complicated deformations have been considered : hexadecapole deformations have been included into Strutinsky-type calculations almost from the beginning; in fact, fig. 1 is for a value of the hexadecapole deformation parameter $\epsilon_4 = 0.04$. What really is calculated, is the potential energy in a multi-dimensional space of deformation coordinates. As an example, fig. 3 shows a contour plot of the potential energy in the (ϵ, ϵ_4) - plane. It also shows as the solid arrow marked ϵ_{24} the approximate path which the nucleus would be expected to go on its way to fission. Thus, the coordinate labelled "deformation" in fig. 2 (and in similar figures which will follow) should be understood as a measure of progress along such a path in a multi-dimensional space of deformation coordinates.

So far, the inclusion of additional deformation coordinates like ϵ_4 has mainly the consequence of a quantitatively more accurate prediction of the deformation potential. The inclusion of asymmetric deformations, however, has important consequences also on fission cross sections and other observables.

It had first been noted by Møller and Nilsson [MN70] that the inclusion of reflection-asymmetric (mass-asymmetric) deformations has the effect of strongly lowering the outer peak of the two-peaked fission barrier of fig. 2 (in fact, quantitatively fig. 2 is drawn to already include this effect): Without inclusion of mass-asymmetry, the outer barrier of common actinide nuclei like U- and Pu-isotopes usually came out to be much higher than the inner barrier, whereas with mass-asymmetry included, both barriers turn out to be about equally high. The effect is due to a strong depression with asymmetric deformation (only for symmetric deformations corresponding to the outer barrier) of Nilsson orbitals with $n_z = 0$. This result may offer an immediate explanation of the asymmetric mass devision in the fission of most actinides. It must be remembered, however, that dynamic effects on the descent from the second barrier to the scission point might still considerably change the final mass division.

The first barrier apparently is stable against mass asymmetric deformation [MN70]. However, as has first been found by Pashkevich [Pa69], it is unstable against non-axial (γ-) distortions. A systematic study of the effects of axially asymmetric deformations has been performed by Larsson and Leander [LL73]. They find that by inclusion of γ-deformation the height of the inner barrier is reduced by up to about 2 MeV. As will be discussed in section 6.3, the axially asymmetric deformation of the nucleus at the first barrier has an important effect on the density of barrier transition states and thereby on the magnitude of above-barrier fission cross sections.

To conclude this chapter, reference is made to a recent review paper by Brack [Bra79] which summarises and compares the different methods of calculating the deformation potential.

3. Statistical Theory of (n,f) Reactions

The statistical theory of nuclear reactions provides a description of reaction cross sections when averages over many compound nuclear levels are taken. The cross section for the formation of the compound nucleus by

absorption of a neutron in a target nucleus with spin I is

$$\bar{\sigma}_n\,(C.N.) = \pi\lambda^2 \sum_J g(I,J) \sum_{\ell s} T_{n\ell s}^{(J)} \qquad (3.1)$$

where the first sum on the right hand side is over the compound nuclear spins J, the second sum is over orbital angular momenta ℓ and channel spins s, and

$$g(I,J) = \frac{2J+1}{2(2I+1)} \qquad (3.2)$$

is the spin statistical factor.

If the cross sections are dominated by narrow resonances, as in the case for non-fissile nuclei at moderately low energies, the transmission coefficient $T_{n\ell s}^{(J)}$ is obtained from averaging neutron widths $\Gamma_{n\ell s}^{(J)}$ and spacings D_J over many resonances as

$$T_{n\ell s}^{(J)} = \frac{2\pi \langle \Gamma_{n\ell s}^{(J)} \rangle}{\langle D_J \rangle} \qquad (3.3)$$

The partial cross section for a reaction leading to exit channel c is then

$$\bar{\sigma}_{nc} = \frac{2\pi^2\lambda^2}{\langle D_J \rangle} \sum_J g(I,J) \sum_{\ell s} \left\langle \frac{\Gamma_{n\ell s}^{(J)} \Gamma_c^{(J)}}{\Gamma^{(J)}} \right\rangle \qquad (3.4)$$

Usually, the last factor on the right hand side is written as

$$\left\langle \frac{\Gamma_{n\ell s}^{(J)} \Gamma_c^{(J)}}{\Gamma^{(J)}} \right\rangle = \frac{\langle \Gamma_{n\ell s}^{(J)} \rangle \langle \Gamma_c^{(J)} \rangle}{\langle \Gamma^{(J)} \rangle} f_{n\ell s,c}^{(J)} \qquad (3.5)$$

such that

$$\bar{\sigma}_{nc} = \pi\lambda^2 \sum_J g(I,J) \sum_{\ell s} \frac{T_{n\ell s}^{(J)} T_c^{(J)}}{\sum_{c'} T_{c'}^{(J)}} f_{n\ell s,c}^{(J)} \qquad (3.6)$$

The factor $f_{n\ell s,c}^{(J)}$ is called the width-fluctuation correction, expressions for which are given by, e.g., Dresner [Dr59].

If, for fissile nuclei or at higher neutron energies, resonance widths approach their average spacings, such that resonance-resonance interference becomes important, expression (3.3) for the transmission coefficient should be replaced by [Mo67]

$$T_c^{(J)} = 1 - \exp\left[-\frac{2\pi \langle \Gamma_c^{(J)} \rangle}{\langle D_J \rangle}\right] \qquad (3.7)$$

3.1. The Entrance Channel

The magnitude of the transmission coefficient for the neutron entrance channel is mainly determined by the effect of the centrifugal barrier on neutrons with orbital angular momentum ℓ and kinetic energy E_n

$$\frac{\langle \Gamma_{n\ell s}^{(J)} \rangle}{\langle D_J \rangle} = 2 P_\ell(E_n) \frac{\langle \gamma_{n\ell s}^2 \rangle}{\langle D_J \rangle} = 2 P_\ell(E_n)\, s_{J\ell s}(E_n) \qquad (3.8)$$

where γ_{nJls}^2 is the reduced width and $s_{Jls}(En)$ is the neutron strength function for spin J and channel ℓs, and is only weakly dependent on E_n. The penetration factor is given as

$$P_\ell(E_n) = \rho\, v_\ell \qquad \rho = ka \qquad (3.9)$$

with

$$\begin{aligned} v_0 &= 1 \\ v_1 &= \rho^2/(1+\rho^2) \\ v_2 &= \rho^4/(9+3\rho^2+\rho^4) \\ v_3 &= \rho^6/(225+45\rho^2+6\rho^4+\rho^6) \end{aligned} \qquad (3.10)$$

where a is the "channel radius".

When a neutron is absorbed in the target nucleus to form the compound nucleus, there is no reason to assume a drastic change in the shape of the system during that process. Thus it is assumed that the compound nucleus is found in a state of deformation corresponding to the primary well of the deformation potential of fig. 2.

The compound nuclear states which are populated in the process of compound nucleus formation are expected to represent a large variety of degrees of freedom corresponding to a high nuclear temperature. There is no reason for preference of any particular degree of freedom, like β- deformation, i.e. the

degree of freedom ultimately leading to fission; rather, statistical equilibrium between all degrees of freedom is assumed, such that all exit channels are treated on an equal basis. This assumption is the justification for equ. (3.3).

3.2. Exit Channels other than Fission

The only exit channels besides fission which we have to consider are emission of neutrons (elastic and inelastic scattering) and γ-rays (radiative capture).

The transmission coefficient for neutron emission $T_n^{(J)}$ may be subdivided into two parts :

$$T_n^{(J)} = T_n^{(J)}\,(\text{discr.}) + T_n^{(J)}\,(\text{cont.}) \qquad (3.11)$$

The first term describes the emission of neutrons to the well-known low-lying states i of the target nucleus

$$T_n^{(J)}(\text{discr.}) = \sum_i \sum_{\ell s} T_{n\ell s}^{(J)}(E_n - \varepsilon_i)\,\delta(\pi\pi_i, (-1)^\ell) \qquad (3.12)$$

where ε_i is the excitation energy of the final state and the factor $\delta(\pi\pi_i, (-1)^\ell)$ serves for parity conservation (=0, if the product of the parities of compound - and final state is not equal to $(-1)^\ell$).

Above a certain value E_c of the excitation energy, not all states will be known individually. Here, an estimate of the level density as a function of ε and spin I, $\rho(\varepsilon, I)$, has to be found, and the second term of equ. (3.11) is then given as

$$T_n^{(J)}(\text{cont.}) = \int_{\varepsilon_c}^{E_n} d\varepsilon \sum_I \sum_{\ell s} T_{n\ell s}^{(J)}(E_n - \varepsilon)\,\rho(\varepsilon, I)\,\delta(\pi\pi_I, (-1)^\ell) \qquad (3.13)$$

In the case of neutron capture, the lowest states in the residual nucleus usually do not contribute significantly to the total radiative width. Therefore they are included into the continuum contribution. Furthermore, only electric dipole transitions are taken into account. Thus the transmission coefficient for radiative capture is written as

$$T_{\gamma\,\text{total}}^{(J)} = \frac{2\pi}{\langle D_J \rangle} \sum_{I=|J-1|}^{J+1} \int_0^{B_n + E_n} d\varepsilon\; \Gamma_{\gamma I}^{(J)}(B_n + E_n - \varepsilon)\,\rho(\varepsilon, I)\,\delta(\pi\pi_I, -1) \qquad (3.14)$$

B_n being the neutron binding energy. For the partial width $\Gamma_{\gamma I}^{(J)}$ for radiative transition from the compound state with spin J to a final state with spin I, two expressions are in use :

In the strong coupling dipole model

$$\Gamma_{\gamma I}^{(J)}(E_\gamma) = c_\gamma\, E_\gamma^{\,3} \qquad (3.15)$$

where the constant c_γ is adjusted to empirical data.

In the giant resonance model

$$\Gamma_{\gamma I}^{(J)}(E_\gamma) = C_\gamma \frac{E_\gamma^{\,4}}{(E_G^{\,2} - E_\gamma^{\,2})^2 + (\Gamma_G^{\,2} E_\gamma^{\,2})^2} \qquad (3.16)$$

where again the constant C_γ and the parameters of the giant resonance E_G and Γ_G , are taken from empirical data.

3.3. Fission Decay

According to the theory of fission by Bohr and Wheeler [BW39], the transmission coefficient for fission through the energetically lowest channel is given by the quantum mechanical penetrability P(E) of the fission barrier of fig. 2.

If the fission barrier is approximated by a single barrier of parabolic shape,

$$P_F(E) = \frac{1}{1 + \exp\left[-\frac{2\pi(E - E_f)}{\hbar\omega_f}\right]} \qquad (3.17)$$

where E_f is the peak height of the barrier and $\hbar\omega_f$ is related to the width of the barrier and the inertial parameter associated with the fission degree of freedom. The true fission barrier of fig. 2 has a very complicated shape, in particular it consists of two barriers with a deep minimum in between. It usually is approximated by two separate barriers of parabolic shape, as indicated in fig. 4, such that an equation of the form (3.17) is valid for the lowest fission channel at each of the two barriers A and B separately. It should be kept in mind, however, that the assumption of parabolic barrier shapes is a crude approximation, and that in particular the parameters $\hbar\omega_A$ and $\hbar\omega_B$ have meaning only as a crude parametrization of the respective barrier widths.

3.3.1. Fission channels

The fission barriers of figs. 2 and 4 represent the deformation potential, i.e. at each value of the deformation coordinates the internal structure of the nucleus has been assumed such as to minimise the total energy. Many other internal structures are possible which give rise to the existence of excited states on top of the barriers, characterised by quantum numbers K, J^π. These are the Bohr fission channels. The true transmission coefficient for each of the two barriers A and B is thus

$$T_X^{(J)} = \sum_i \frac{1}{1 + \exp\left[-\frac{2\pi(E - E_X - \epsilon_i)}{\hbar\omega_X}\right]} \quad , \quad X = A, B \qquad (3.18)$$

where ϵ_i is the excitation energy (with respect to the barrier top) of the fission channel i.

Essentially only for even-even fissioning nuclei are the lowest fission channels known individually. For higher excitation energies, and in general for odd and odd-odd fissioning nuclei, an estimate must be found for the density $\rho_X(\epsilon, J)$ of fission channels and the sum of equ. (3.18) be replaced by an integral. Thus, in general,

$$T_X^{(J)} = \sum_i \frac{1}{1 + \exp\left[-\frac{2\pi(E - E_X - \epsilon_i)}{\hbar\omega_X}\right]} + \int_0^\infty d\epsilon \; \rho_X(\epsilon, J) \frac{1}{1 + \exp\left[-\frac{2\pi(E - E_X - \epsilon)}{\hbar\omega_X}\right]} \qquad (3.19)$$

Approximations for the integral on the right hand side of equ. (3.19) which are obtained under the assumption of a constant temperature level density relation for $\rho_X(\epsilon, J)$ are given by Lynn [Ly74].

Equations (3.18) and (3.19) give expressions for the transmission coefficient of the barriers A and B separately. If the process of fission is looked at as a two-step process (first transmission of barrier A, then of barrier B), the final transmission coefficient for fission is

$$T_f^{(J)} = \frac{T_A^{(J)} \, T_B^{(J)}}{T_A^{(J)} + T_B^{(J)}} \qquad (3.20)$$

However, this equation is valid only if the excitation energy E is higher than the peak height of the lower one of the two barriers, i.e. if at least one of T_A and T_B is close to unity or greater. For true sub-barrier fission (energy E lower than both barrier peaks) intermediate structure effects change the picture drastically.

3.3.2. Transmission through a 2-humped barrier

In this and the following subsections sub-barrier fission will be discussed only superficially; a more detailed treatment will follow in sections 4 and 5.

For $E < E_X$ the individual terms in the sum over fission channels i in equ. (3.19) decrease rapidly with increasing ϵ_i, and a corresponding statement holds for the integral in equ. (3.19). Thus, in the case of sub-barrier fission, usually only a very small number of fission channels need to be considered for a given J^π, often only a single one. Thus, in the following, we will deal with the transmission through just one double-humped fission barrier of the kind of fig. 4, assuming the energy E to be smaller than both E_A and E_B, but greater than E_{II}.

3.3.3. Vibrational resonances.

Essentially two types of calculations of the penetrability of a double-humped barrier are available : Cramer and Nix [CN70] have exactly calculated the penetrability of a barrier constructed from three smoothly joined parabolas as indicated in fig. 5a. Ignatyuk et al. [Ig 69] have used the WKB approximation to calculate the penetrability of a double-humped barrier of more general shape.

The WKB approximation yields

$$P_F(E) = \frac{P_A P_B}{4}\left[\left(\frac{P_A + P_B}{4}\right)^2 \sin^2\varphi + \cos^2\varphi\right]^{-1} \qquad (3.21)$$

where the phase φ is given by

$$\varphi(E) = \int_{\epsilon_1}^{\epsilon_2} \left[\frac{2m}{\hbar^2}\left(E - V(\epsilon)\right)\right]^{1/2} d\epsilon \qquad (3.22)$$

The limits of integration ϵ_1 and ϵ_2 are the values of ϵ in the intermediate well at which the integrand vanishes.

Equ. (3.21) has been compared to the exact calculation for (among others) the barriers of fig. 5a by Cramer and Nix [CN70]. This comparison is shown in fig. 5b : It can be seen that only relatively small deviations occur at the minimum of $P_F(E)$ and in the exact position of the resonances.

According to equ. (3.21) the penetrability at the resonance peaks is

$$P_{max} = \frac{4\,P_A P_B}{(P_A+P_B)^2} \qquad (3.23)$$

and in the minima between the resonances it is

$$P_{min} = \frac{1}{4} P_A P_B \qquad (3.24)$$

The penetrability averaged over an interval of $\Delta\varphi = \pi$, i.e. an interval corresponding to the spacing of two resonances, is

$$\langle P_F \rangle = \frac{P_A\ P_B}{P_A + P_B} \qquad (3.25)$$

The energies at which the resonances of fig. 5b occur, correspond to eigenenergies of vibrational states in the intermediate well. If this well is sufficiently well described by a harmonic oscillator potential with curvature parameter $\hbar\omega_{II}$ the energies are

$$E_n = E_{II} + \left(n + \tfrac{1}{2}\right)\hbar\omega_{II} \qquad (3.26)$$

In the vicinity of these resonances, the penetrability has a Lorentzian energy dependence :

$$P_F(E) = \frac{\Gamma_A\,\Gamma_B}{(E_n - E)^2 + \frac{(\Gamma_A+\Gamma_B)^2}{4}} \qquad (3.27)$$

with

$$\Gamma_x = \frac{\hbar\omega_{II}}{2\pi} P_x \qquad x = A, B \qquad (3.28)$$

The widths Γ_A and Γ_B may be interpreted as partial widths of the vibrational resonance for decay through barrier A and B respectively, due to the fact that the wave function of the quasi-stationary state in the intermediate well has an exponentially decaying tail penetrating through the barriers.

A well-known example of a vibrational resonance of this kind occurs in the neutron-induced fission cross section of ^{230}Th. Results from a measurement of this resonance performed in 1972 by James et al. [Ja72] are shown in fig. 6.

3.3.4. Excitation in the second well

If the second well in the deformation potential of fig. 2 is sufficiently deep, as is expected to be the case for most actinide nuclei, there is a sufficient amount of energy available for intrinsic excitations of the nucleus at a deformation corresponding to the second well (with the total energy being smaller than E_A and E_B). This means that besides the vibrational states discussed in the preceding subsection, there is a much larger number of states present inside the second well, representing other degrees of freedom, just as is the case inside the primary well. The situation is illustrated in fig. 7. In fact, for not too low excitation energies the level density in either well may approximately be described by a Fermi-gas level density relation :

$$\rho(U, J^\pi) = \frac{2J+1}{48\sqrt{2}\,\sigma^3 a^{1/4} U^{5/4}}\, e^{-\frac{(J+1/2)^2}{2\sigma^2}}\, e^{2\sqrt{aU}} \qquad (3.29)$$

where the effective excitation energy U is

$$U_I = E - \Delta_p - \Delta_n \qquad (3.30)$$

in the primary well (Δ_p and Δ_n being corrections due to pairing), and

$$U_{II} = E - \Delta_p - \Delta_n - E_{II} \qquad (3.31)$$

in the second well. If it is assumed that the level density parameter a and the spin dispersion coefficient σ are the same in both wells,

$$\frac{\rho_I}{\rho_{II}} = \left(\frac{U_{II}}{U_I}\right)^{5/4} \exp 2\sqrt{a}\left(\sqrt{U_I} - \sqrt{U_{II}}\right) \qquad (3.32)$$

With, as a typical example to energy E close to neutron binding energy, U_I = 5 MeV, U_{II} = 3 MeV and a = 30 MeV^{-1}, $\rho_I / \rho_{II} \approx 132$.

The levels in the second well other than vibrational states would by themselves have no influence on the fission cross section. However, particle-vibration coupling mixes vibrational and other levels in either well such that

principally all levels acquire a certain amount of vibrational amplitude. Due to this mixing all the levels in the secondary well gain an influence on the fission cross section. This will be discussed in more detail in section 4.

A gross effect of the mixing of vibrational and other degrees of freedom is that the vibrational strength is spread over many levels. This has as a consequence that the vibrational resonances in the fission transmission coefficient discussed in subsection 3.3.3. are broadened and their peak height is reduced. This effect is often referred to a damping. The width of the vibrational resonance equ. (3.27) is now replaced by

$$\Gamma_\nu = \Gamma_A + \Gamma_B + \Gamma_D \qquad (3.33)$$

where Γ_D is called the damping width.

If the excitation energy U_{II} and thereby the level density ρ_{II} in the second well are sufficiently large, the damping width will become larger than the spacing of vibrational states. Structure in the fission cross section due to vibrational resonances now disappears, but narrower intermediate structure due to the "mixed" levels in the second well prevails as will be discussed in section 4. This situation is referred to as "complete damping" and is also characteristic of the situation in the primary well at energies close to or above neutron binding energy.

To conclude this section, the hierarchy of states as outlined above, is discussed on a slightly more formal basis. The Hamiltonian of the nucleus can be regarded as a sum of three terms :

$$\hat{H} = H_\eta + H_i + H_C \qquad (3.34)$$

H_η describes the motion with respect to the deformation degree of freedom. The potential energy part of it is the deformation potential of fig. 2. H_i is the Hamiltonian for all other ("intrinsic") degrees of freedom, and H_C describes the interaction between deformation and intrinsic degrees of freedom ("particle vibration coupling").

The eigenstates of H_η are denoted by Φ_ν and those of H_i are denoted by χ_μ :

$$H_\eta \Phi_\nu = E_\nu \Phi_\nu \qquad (3.35)$$

$$H_i \chi_\mu = E'_\mu \chi_\mu \qquad (3.36)$$

and the eigenstates of the full Hamiltonian H are to be described as expansions over products $\Phi_\nu \chi_\mu$.

For energies sufficiently below the maxima E_A and E_B of the deformation potential the vibrational states Φ_μ may be subdivided into two classes, $\Phi_{\nu I}$ $\Phi_{\nu II}$ depending on whether the main amplitude of the wave function falls in the primary or the second well of the deformation potential. However, as mentioned above, there is some tailing of the wave functions through the barriers which gives rise to an interaction. To be more specific, H_η of equ. (3.34) could be divided according to

$$H_\eta = H_\eta^0 + V_\eta \qquad (3.37)$$

where the potential energy part of H_η^0 would consist of two potential wells separated by an infinitely high wall, whereas V_η would be the difference between this potential and the true deformation potential of fig. 2. Now $\Phi_{\nu I}$ and $\Phi_{\nu II}$ are eigenfunctions of H_η^0 in the first and second well, respectively

$$H_\eta^0 \Phi_{\nu I} = E_{\nu I} \Phi_{\nu I}$$
$$H_\eta^0 \Phi_{\nu II} = E_{\nu II} \Phi_{\nu II} \qquad (3.38)$$

From these two types of vibrational states two sets of product sates can be constructed which are eigenstates of $\hat{H} - V_\eta$, and thus almost eigenstates of the full Hamiltonian $\hat{H}$:

$$\varphi_{\lambda I} = \sum_{\nu_I \mu} C^{\lambda I}_{\nu_I \mu} \Phi_{\nu I} \chi_\mu \qquad (3.39)$$

$$\varphi_{\lambda II} = \sum_{\nu_{II} \mu} C^{\lambda II}_{\nu_{II} \mu} \Phi_{\nu II} \chi_\mu \qquad (3.40)$$

They are usually called class I and class II states, respectively. The true eigenstates of $\hat{H}$ have to be obtained from a diagonalization of $\hat{H}$ over these two sets. The matrix elements $\langle \varphi_{\lambda I} | \hat{H} | \varphi_{\lambda II} \rangle$ coupling the two sets are very small, however, because of the small amount of tailing of the wave functions Φ_ν through the barrier A. This is the reason why the states $\varphi_{\lambda I}$ and $\varphi_{\lambda II}$ may be treated as almost eigenstates of the Hamiltonian $\hat{H}$.

4. Narrow Structure in Fission Cross Sections

In this section the most obvious consequences of the existence of the two types of states which have been called class I and class II states in section 3.3.4., will be discussed. These rather dramatic effects occur in neutron-induced fission cross sections at energies below the two barriers E_A and E_B, if these cross sections are studied with sufficiently high energy resolution. "Sufficiently" high means that individual levels of the highly dense class I type (average spacing at neutron binding energy of the order of 1 eV) are resolved.

Before we enter the discussion of structure due to the two classes of states, we will recall a few fundamental facts of basic reaction theory.

4.1. Basic Reaction Theory

For the sake of simplicity we will start this reminder of basic reaction theory by considering the simple case of pure (elastic and inelastic) scattering of a neutron from a target nucleus of mass A - 1. Reaction theory provides expressions for the transition probability from an entrance channel c to an exit channel c', either directly or via compound states where all A nucleons are *in bound orbitals of the compound nucleus.* The channels c may differ by the state (ground - or excited state) of the target nucleus and by quantum numbers like orbital angular momentum, channel spin, etc.

Out of the several different formulations of reaction theory, only two will be mentioned here, the so-called "shell model approach" [MW69] and "R-matrix" theory [LT58].

4.1.1. The shell model approach to reaction theory.

In the shell model approach of Mahaux and WeidenmÜller [MW69], the total Hamiltonian of the system of A particles is subdivided according to

$$H = H_0 + V_n \tag{4.1}$$

where H_0 is basically a shell model Hamiltonian (with a potential of finite depth). Eigenstates of H_0 are discrete shell model states Φ_i of the compound nucleus A

$$H_0 \Phi_i = E_i \Phi_i \tag{4.2}$$

and scattering states χ_E^c consisting of the target A - 1 plus a neutron in a channel c

$$H_0 \chi_E^c = E \chi_E^c \tag{4.3}$$

which form a continuous spectrum. The residual interaction V_n allows for transitions between the various states Φ_i and χ_E^c. The problem is to solve

$$H \Psi_E^c = E \Psi_E^c \tag{4.4}$$

with Ψ_E^c being expressed as an expansion in the Φ_i and χ_E^i.

From a study of the asymptotic behaviour of possible solutions of (4.4) for $r_c \to \infty$, r_c being the coordinate of separation between the scattered neutron and the target, the scattering matrix $S_{c'c}$ for scattering from channel c to channel c' is obtained [MW69]. It reads

$$S_{c'c} = \exp(i\delta_c + i\delta_{c'}) \left(\delta_{c'c} - 2\pi i \sum_{jk} V_j^c (D^{-1})_{jk} V_k^{c'} \right) \tag{4.5}$$

with

$$D_{lm} = (E - E_l)\delta_{lm} - V_{lm} - \sum_{c''} \left[\mathcal{P} \int dE' \frac{V_l^{c''} V_m^{c''}}{E - E'} - i\pi V_l^{c''} V_m^{c''} \right] \tag{4.6}$$

and the matrix elements of the residual interaction defined as

$$V_{jk} = \langle \phi_j | V_n | \phi_k \rangle \qquad V_j^c(E) = \langle \phi_j | V_n | \chi_E^c \rangle \tag{4.7}$$

A possible direct channel-channel coupling has been neglected. The δ_c are potential scattering phase shifts for channels c.

The scattering matrix equ. (4.5) has poles at

$$e_j = \varepsilon_j - \tfrac{i}{2} \Gamma_j \tag{4.8}$$

which are given by the roots of

$$\det(\underline{D}) = 0 \tag{4.9}$$

If $\underline{Q}$ is the complex orthogonal matrix which diagonalises $\underline{D}$ such that

$$(\underline{Q}\,\underline{D}\,\underline{Q}^{-1})_{jk} = (E - e_j)\,\delta_{jk}$$

the scattering matrix equ. (4.5) can be written

$$S_{c'c} = \exp(i\delta_c + i\delta_{c'}) \left(\delta_{c'c} - i \sum_j \frac{\Gamma_{jc}^{1/2} \Gamma_{jc'}^{1/2}}{E - \varepsilon_j + \frac{1}{2} i \Gamma_j} \right) \tag{4.10}$$

where the "partial width amplitudes" are defined by

$$\Gamma_{jc}^{1/2} = (2\pi)^{1/2} \sum_k \mathcal{O}_{jk} V_k^c \qquad (4.11)$$

They are in general complex quantities. Only in the case of "isolated" resonances, i.e. if the widths Γ_j finally attained by the resonances are much smaller than their average spacing d, they are real and

$$\Gamma_j = \sum_c \Gamma_{jc} \qquad (4.12)$$

In fact, if the matrix elements V_j^c are sufficiently small such that $\sum_c V_j^c V_k^c \ll d$, the equation det $(\underline{D}) = 0$ is not very different from det $(\underline{D}^R) = 0$, where $\underline{D}^R$ is the real matrix obtained from $\underline{D}$ by omitting the last term in equ. (4.6). Correspondingly, the matrix $\underline{\mathcal{O}}$ is not very different from the real orthogonal matrix $\underline{O}^R$ which diagonalises $\underline{D}^R$. This diagonalisation of $\underline{D}^R$ by a real orthogonal matrix $\underline{O}^R$ is the usual procedure of the bound state shell model.

The Γ_j and Γ_{jc} in equ. (4.10) may be interpreted as resonance parameters in the usual way only if they are sufficiently energy-independent. As discussed in [MW69], this is the case only if no thresholds or single particle resonances are in the vicinity of the energy interval under investigation. We will furtheron assume that this condition is fulfilled.

4.1.2 R-matrix theory

An alternative formulation of the scattering problem is given by R-matrix theory. Here, the configuration space is subdivided into an "internal" and an "external" region, separated by channel radii a_c defined such that for $r_c > a_c$ there is no nuclear interaction in channel c. In the internal region a set of eigenfunctions X_λ of the Hamiltonian H is defined by imposing definite boundary conditions at the surface :

$$H X_\lambda = E_\lambda X_\lambda \qquad (4.13)$$

The boundary conditions are expressed by parameters B_c defined as

$$B_c = \frac{\delta_{\lambda c}}{\gamma_{\lambda c}} \qquad (4.14)$$

Here, the $\gamma_{\lambda c}$ are projections of the eigenfunctions X_λ upon the surface of channel c

$$\gamma_{\lambda c} = \left(\frac{\hbar^2}{2 M_c a_c}\right)^{1/2} \int_{r_c = a_c} \varphi_c^* X_\lambda \, d s_c \qquad (4.15)$$

φ_c being the channel surface function for channel c, i.e. a product of a wave-function describing the target and one describing the angular dependence of the relative motion of target and projectile. Similarly, the projections of the radial derivatives of X_λ are

$$\delta_{\lambda c} = \gamma_{\lambda c} + \left(\frac{a_c \hbar^2}{2 M_c}\right)^{1/2} \int_{r_c = a_c} \varphi_c^* \, \mathrm{grad} X_\lambda \, d s_c \qquad (4.16)$$

As the functions X_λ form a complete set, any solution of the proper Schrödinger equation (4.4) may in the internal region be expanded in the X_λ, and in the external region it is determined from the condition that it is continuous and has a continuous derivative at the surface. This condition allows to express the scattering matrix in terms of the so-called R-matrix R [LT58] :

$$\underline{S} = \underline{\Omega} \, \underline{P}^{1/2} \left(1 - \underline{R} \underline{L}^0\right)^{-1} \left(1 - \underline{R} \underline{L}^{0*}\right) \underline{P}^{-1/2} \, \underline{\Omega} \qquad (4.17)$$

The other matrices occuring in the equ. (4.17) are diagonal matrices with elements

$$L_c^0 = L_c - B_c \qquad L_c = S_c + i P_c \qquad (4.18)$$

with S_c and P_c being shift- and penetration factors for channel c (see [LT58]), and for neutrons,

$$\Omega_c = \exp(-i \Phi_c) \qquad (4.19)$$

Φ_c being the hard sphere scattering phase shift in channel c.

The R-matrix is given by

$$R_{c'c} = \sum_\lambda \frac{\gamma_{\lambda c'} \gamma_{\lambda c}}{E_\lambda - E} \qquad (4.20)$$

Equation (4.17) for the S-matrix involves the inversion of the matrix $(1 - \underline{R}\underline{L}^0)$ which generally is of very large order. It is possible, however, to transform this equation into another form which involves the inversion of a level matrix instead [LT58]. This is advantageous in cases where only a small number of levels has to be considered in a given energy interval. This level matrix parameterisation of the scattering matrix reads :

$$S_{c'c} = \exp(i\phi_c + i\phi_{c'}) \left(\delta_{c'c} + 2i P_c^{1/2} P_{c'}^{1/2} \sum_{\lambda\mu} \gamma_{\lambda c} A_{\lambda\mu} \gamma_{\mu c'}\right) \qquad (4.21)$$

where the matrix $\underline{A}$ is the inverse of the level matrix $\underline{C}$ with

$$C_{\lambda\mu} = (E_\lambda - E)\,\delta_{\lambda\mu} - \sum_c \left(S_c^0 + i P_c\right) \gamma_{\lambda c}\,\gamma_{\mu c} \qquad (4.22)$$

Equations (4.21) and (4.22) show a strong formal analogy with equ. (4.5) and (4.6). However, the different quantities appearing in these two sets of equations have a different physical meaning and in general exhibit a different energy dependence. It is shown in [MW69], however, that the energy dependence is similar if no single particle resonance is present in any channel and if the energy interval considered is not too large.

In the simple case of "isolated" resonances (see above) the non-diagonal elements of the level matrix $\underline{C}$ may be neglected and equ. (4.21) can be cast into the form (4.10) with

$$\varepsilon_\lambda = E_\lambda - \sum_c S_c^0 \gamma_{\lambda c}^2 \qquad \Gamma_{\lambda c} = 2 P_c \gamma_{\lambda c}^2 \qquad \Gamma_\lambda = \sum_c \Gamma_{\lambda c} \qquad (4.23)$$

This is the so-called multi-level Breit-Wigner approximation to R-matrix theory.

From the scattering matrix element $S_{c'c}$ describing the scattering from channel c to channel c', one obtains the full cross section for the reaction $\alpha \to \alpha'$ (α now describing configurations with the target A - 1 being in a definite energy level, but without specification of orbital angular momentum ℓ and channel spin s) through compound levels of total angular momentum J

$$\sigma_{\alpha\alpha'}(J) = \pi\lambda^2 \frac{2J+1}{(2I+1)(2i+1)} \sum_{s=|I-i|}^{I+i} \sum_{s'=|I'-i'|}^{I'+i'} \sum_{\ell=|J-s|}^{J+s} \sum_{\ell'=|J-s'|}^{J+s'} \left| \delta_{\alpha\alpha'}\delta_{ss'}\delta_{\ell\ell'} - S_{\alpha' s' \ell', \alpha s \ell} \right|^2 \qquad (4.24)$$

I and i being the spins of target and projectile, respectively.

Within the multi-level Breit-Wigner approximation one then has for $\alpha \neq \alpha'$

$$\sigma_{\alpha\alpha'}(J) = \pi\lambda^2 \frac{2J+1}{2(2I+1)} \sum_{s=|I-i|}^{I+i} \sum_{s'=|I'-i'|}^{I'+i'} \sum_{\ell=|J-s|}^{J+s} \sum_{\ell'=|J-s'|}^{J+s'} \left| \sum_\lambda \frac{\Gamma_{\lambda\alpha s\ell}^{1/2}\,\Gamma_{\lambda\alpha' s'\ell'}^{1/2}}{E - \varepsilon_\lambda + \frac{i}{2}\Gamma_\lambda} \right|^2 \qquad (4.25)$$

Equ. (4.25) still contains, of course, an approximate description of resonance-resonance interference. If the resonances are even more isolated such that this interference may be neglected altogether, the single-level Breit-Wigner approximation is obtained :

$$\sigma_{\alpha\alpha'}(J) = \pi\lambda^2 \frac{2J+1}{2(2I+1)} \sum_\lambda \frac{\Gamma_{\lambda(\alpha)}\,\Gamma_{\lambda(\alpha')}}{(E-\varepsilon_\lambda)^2 + \frac{1}{4}\Gamma_\lambda^2}$$

$$\Gamma_{\lambda(\alpha)} = \sum_{s=|I-i|}^{I+i} \sum_{\ell=|J-s|}^{J+s} \Gamma_{\lambda\alpha s\ell} \qquad \Gamma_\lambda = \sum_\alpha \Gamma_{\lambda(\alpha)} \qquad (4.26)$$

4.1.3. Inclusion of fission

Until now, we have only considered elastic and inelastic scattering of neutrons. If fission is to be taken into account, the fission degree of freedom could principally be represented by additional channels f. Thus, in single-level Breit-Wigner approximation the fission cross section would be

$$\sigma_{nf}(J) = \pi\lambda^2 \frac{2J+1}{2(2I+1)} \sum_\lambda \frac{\Gamma_{\lambda(n)}\,\Gamma_{\lambda(f)}}{(E-\varepsilon_\lambda)^2 + \frac{1}{4}\Gamma_\lambda^2} \qquad (4.27)$$

Equ. (4.27) gives a satisfactory description of the fission cross section under the following conditions:

1) The resonances are sufficiently isolated such that the single level Breit-Wigner approximation may be applied,
2) the neutron energy is sufficiently above the lower one of the two barriers, and
3) the heights of the two barriers, E_A and E_B, are sufficiently different.

Under the last condition the fission width $\Gamma_{\lambda(f)}$ is given as a sum of partial widths,

$$\Gamma_{\lambda(f)} = \sum_f \Gamma_{\lambda f} \qquad (4.28)$$

corresponding to individual Bohr fission channels. An estimate for the expectation value of each partial width is given by the statistical model as (see equ. (3.18))

$$\Gamma_{\lambda f} = \frac{D_\lambda}{2\pi} \frac{1}{1 + \exp\left[-\frac{2\pi(E - E_X - \varepsilon_f)}{\hbar\omega_K}\right]} \qquad (4.29)$$

Figure 1

state ar
are comp
The figu
Rocheste

Here, E_x and $\hbar\omega_x$ refer to the higher one of the two barriers.

If, on the other hand, the two barriers are almost equally high, a better expression for the total fission width is

$$\Gamma_{\lambda(f)} = \frac{D_\lambda}{2\pi} T_f \qquad (4.30)$$

with T_f given by equations (3.20) and (3.19).

Unfortunately, conditions (1) and (2) above almost exclude each other : Indeed, for most of the fissile isotopes resonance - resonance interference effects are quite important. Thus, for the description of the fission cross sections of these isotopes, more accurate formulations of R-matrix theory ought to be used, e.g. the "Reich-Moore" - formalism [RM58]. However, these demand partial fission widths which are consistently defined only under condition (3).

For fission at energies below the barriers E_A and E_B, the existence of two classes of states (class I and class II of section 3.3.4) gives rise to structure effects which will be discussed in section 4.3. Before that, a more general description of the significance of so-called "doorway states" will be given in section 4.2.

4.2 General Description of Doorway States

In the preceding discussion all the compound nuclear levels Φ_i (or X_λ in the case of the R-matrix formulation) have been considered principally equal, i.e. the matrix elements $\langle \Phi_i | V_n | \chi_E^c \rangle$ (or the amplitudes $\omega_{\lambda m}$) fluctuate statistically, but none of these are larger than others by fundamental structure effects, apart from the strict selection rules of angular momentum and parity.

This is not necessarily the actual situation in nature. There are quantum numbers which are (in contrast to total angular momentum) almost conserved, with some residual interaction mixing states with different values of these quantum numbers. A formidable example is isobaric spin. Such almost-good quantum numbers may lead to a preferred coupling of certain ones of the states Φ_i to certain channels. This situation is illustrated in fig. 8 : Instead of the direct and basically equal coupling of all compound levels Φ_i to both entrance and exit channels (fig. 8 a) one or both of the situations of fig. 8 b and c may occur : Certain ones of the states Φ_i, called doorway states, may be preferably populated from the entrance channel, with some residual interaction allowing subsequent transitions to the rest of the states Φ_i (fig. 8 b); or (fig. 8 c) : certain ones of the Φ_i may act as doorway states to a given exit channel such that the decay of the majority of the Φ_i into this exit channel proceeds preferably or even exclusively via these doorway states.

4.3 Class II States as Doorways to Fission

Fig. 8 c has a very literal meaning in the case of sub-barrier fission : The role of the doorway states with respect to the fission channel is played by the class II states defined at the end of section 3. They are literally separated from the majority of the compound states Φ_i in configuration space, by the different value of the deformation coordinate η characteristic of class II states as opposed to the class I states. The (weak) residual interaction which allows for coupling between the class II doorways and the class I states is the interaction V_η of equ. (3.39).

The Hamiltonian relevant for the description of (sub-barrier) neutron induced fission reactions is thus

$$H = \hat{H} + V_n = H^0 + V_\eta + V_n \qquad (4.31)$$

with (see equ. (3.34) and (3.39))

$$H^0 = H_\eta^0 + H_i + H_c \qquad (4.32)$$

The eigenstates of H^0 are the class I and class II states of section 3.3.4. We now call them Φ_i, and for the sake of simplicity assume that in the energy range of interest are dealing with m class I states Φ_i (i = 1, ...,m) and only one class II state which we call Φ_0

$$\begin{aligned} H^0 \Phi_0 &= E_0 \Phi_0 \\ H^0 \Phi_i &= E_i \Phi_i \qquad (i = 1, \ldots, m) \end{aligned} \qquad (4.33)$$

The residual interaction V_n couples the class I states to the neutron channels and amongst themselves, but the state Φ_0 is unaffected. On the other hand, the interaction V_η couples the state Φ_0 to the Φ_i (i = 1, ...,m), and it also couples Φ_0 to the fission channel. As discussed in section 3.3.2, we assume that we are dealing with a single fission channel.

The scattering matrix is given by (see equ. (4.5)) :

$$S_{\ell} = -\exp\left(i\delta_\ell + i\delta_f\right) 2\pi i \sum_{j,k=0}^{m} V_j^f \left(\mathcal{D}^{-1}\right)_{jk} V_k^n \qquad (4.34)$$

with the matrix $\underline{D}$ given by equ. (4.6).

According to the preceding definitions the matrix elements of the residual interaction are given by :

$$V_{jk} = \langle \Phi_j | V_\eta | \Phi_k \rangle \qquad j,k = 1,\dots,m$$
$$V_{ok} = \langle \Phi_o | V_\eta | \Phi_k \rangle \qquad k = 1,\dots,m \qquad (4.35)$$
$$V_j^n(E) = \langle \Phi_j | V_n | \chi_E^n \rangle \qquad j = 1,\dots,m$$
$$V_o^f(E) = \langle \Phi_o | V_\eta | \chi_E^f \rangle$$
$$V_j^f = V_o^n = 0$$

Let $\underline{O}^n$ be the complex orthogonal matrix which would diagonalise $\underline{D}$ in the absence of V_η, i.e. essentially diagonalises the m x m submatrix D_{jk} (j,k = 1,...,m). With

$$\underline{V}^f \underline{D}^{-1} \underline{V}^n = \underline{V}^f (\underline{O}^n)^{-1} \underline{O}^n \underline{O}^{-1} (\underline{O}^n)^{-1} \underline{O}^n \underline{V}^n = \underline{v}^f \underline{d}^{-1} \underline{v}^n \qquad (4.36)$$

equ. (4.34) can be written

$$S_{nf} = -\exp\left(i\delta_n + i\delta_f\right) 2\pi i \sum_{j,k=0}^{m} v_j^f \left(d^{-1}\right)_{jk} v_k^n \qquad (4.37)$$

with

$$d = O^n D (O^n)^{-1} = \begin{pmatrix} E - \varepsilon_o + i\pi (v_o^f)^2 & v_{oj} \\ v_{ok} & (E - e_j)\,\delta_{jk} \end{pmatrix} \qquad (4.38)$$

$$\varepsilon_o = E_o - P\int dE' \frac{(V_o^f)^2}{E - E'}$$

and

$$v_j^c = \sum_k O_{jk}^n V_k^c \qquad (4.39)$$

that is

$$v_j^n = \langle \varphi_n | V_n | \chi_E^n \rangle \qquad (4.40)$$
$$v_o^f = V_o^f$$

with newly defined class I states

$$\varphi_j = \sum_k O_{jk}^n \Phi_k \qquad j,k = 1,\dots,m \qquad (4.41)$$

and

$$v_{ok} = \langle \Phi_o | V_\eta | \varphi_k \rangle \qquad k = 1,\dots,m \qquad (4.42)$$

The energies e_j are complex

$$e_j = \varepsilon_j - \tfrac{i}{2} \Gamma_{j(n)} \qquad (4.43)$$

with widths $\Gamma_{j(n)}$ which are due to the coupling to the neutron channels. If V_n is sufficiently weak such that one is dealing with "isolated" resonances, which is true in all practical cases, the v_j^n are real and (see the discussion following equ. (4.10)):

$$\Gamma_{j(n)} = 2\pi \sum_n (v_j^n)^2 \qquad j = 1,\dots,m \qquad (4.44)$$

where the summation is over all neutron channels n.

For later use we finally define the fission width of the class II state

$$\Gamma^\uparrow = 2\pi (V_o^f)^2 \qquad (4.45)$$

its spreading or coupling width

$$\Gamma^\downarrow = \frac{2\pi}{D_I} \overline{v_{ok}^2} \qquad (4.46)$$

and its total width

$$\Gamma_{II} = \Gamma^\uparrow + \Gamma^\downarrow \qquad (4.47)$$

D_I is the average spacing of the class I states.

The problem of evaluating equ. (4.37), or equivalently, diagonalising the matrix $\underline{d}$ of equ.(4.38), is very similar to the one-channel case treated comprehensively by Mahaux and Weidenmüller [MW69], the only difference being that in the present case the e_j are complex whereas in the one-channel case they are replaced by the real energies ε_j. Thus only a rough sketch of the analysis will be given here, and for details we refer to [MW69].

DEFORMATION ENERGY

Figure 2

self-con
dashed c
in the t
Ph. Quen

First, a sum rule is established. The diagonalisation of $\underline{d}$, once achieved by a complex orthogonal matrix $\underline{O}$, leads to a diagonal matrix with eigenvalues

$$\mathcal{E}_j = \eta_j - \tfrac{i}{2} \, \Gamma_j \qquad (4.48)$$

The invariance of the trace of $\underline{d}$ under complex orthogonal transformations leads to the sum rule

$$\sum_{j=0}^{m} \Gamma_j = \Gamma^{\uparrow} + \sum_{j(n)} \Gamma_{j(n)} \qquad (4.49)$$

In the limit $V_n \to 0$ the Γ_j are only due to the fission channel and

$$\sum_{j=0}^{m} \Gamma_{jf} = \Gamma^{\uparrow} \qquad (4.50)$$

Let us now subdivide the discussion according to the relative size of the quantities d, $\Gamma^{\uparrow}$ and $\Gamma^{\downarrow}$.

4.3.1 Narrow class II state ($\Gamma_{\text{II}} < D_I$)

If besides V_n also $\Gamma^{\uparrow} = 2\pi |v_{0k}|^2$ is sufficiently small, i.e. $\Gamma^{\uparrow} \ll D_I$, then, as discussed earlier in connection with equ. (4.10), the matrix $\underline{O}$ is similar to the real orthonogal matrix $\underline{O}^R$ which diagonalises

$$\underline{d}^R = \begin{pmatrix} E - \varepsilon_0 & v_{0j} \\ v_{0k} & (E - \varepsilon_j)\,\delta_{jk} \end{pmatrix} \qquad (4.51)$$

Let us call λ_j (j = 0, ..., m) the corresponding real eigenvalues.

In this subsection we will treat the case that also $\Gamma^{\downarrow} < D_I$. Then the diagonalisation of $\underline{d}^R$ may be achieved by a perturbation treatment. Excluding the case of an accidental degeneracy of Φ_0 and one of the φ_j, the perturbation treatment yields new states φ_j' and Φ_0' with energies close to ε_j and ε_0. Expanded in the φ_j and Φ_0, the new states are

$$\begin{aligned} \varphi_j' &= \left(1 - \tfrac{1}{2}\,(O_{0j}^R)^2\right) \varphi_j + O_{0j}^R \, \Phi_0 \\ \Phi_0' &= \left(1 - \tfrac{1}{2} \sum_{k=1}^{m} (O_{0k}^R)^2\right) \Phi_0 + \sum_{k=1}^{m} O_{0k}^R \, \varphi_k \end{aligned} \qquad (4.52)$$

with

$$O_{0k}^R = \frac{v_{0k}}{(\varepsilon_0 - \varepsilon_k)} \qquad (4.53)$$

If the transformation from the φ_j, Φ_0 to the φ_j', Φ_0' is introduced in equ. (4.37), the new states φ_j' acquire a fission width

$$\Gamma_{jf} = 2\pi \langle \varphi_j' | V_n | \chi_E^f \rangle^2 = \frac{v_{0j}^2}{(\varepsilon_j - \varepsilon_0)^2} \, \Gamma^{\uparrow} \qquad j = 1, \ldots, m \qquad (4.54)$$

The fission width of the state Φ_0' is

$$\Gamma_{0f} = \left(1 - \sum_{k=1}^{m} \frac{v_{0k}^2}{(\varepsilon_0 - \varepsilon_k)^2}\right) \Gamma^{\uparrow} \qquad (4.55)$$

such that the sum rule equ. (4.50) is fulfilled.

Likewise, the state Φ_0' acquires neutron widths

$$\Gamma_{0n} = 2\pi \langle \Phi_0' | V_n | \chi_E^n \rangle^2 = \left[\sum_{k=1}^{m} \frac{v_{0k}}{(\varepsilon_0 - \varepsilon_k)} \, \Gamma_{kn}^{1/2} \right]^2 \qquad (4.56)$$

4.3.2 Class II state with large coupling width ($D_I \ll \Gamma^{\downarrow} > \Gamma^{\uparrow}$)

Simple analytic expressions are obtained only for the so-called picket-fence model which assumes that all class I states are equally spaced and all v_{0j} are equal. In this model it is shown in [BM69] that the elements O_{0j}^R of the matrix $\underline{O}^R$ are distributed according to

$$\left(O_{0j}^R\right)^2 = \frac{D_I}{2\pi} \, \frac{\Gamma^{\downarrow}}{(\varepsilon_j - \varepsilon_0)^2 + \frac{1}{4}(\Gamma^{\downarrow})^2} \qquad (4.57)$$

When the transformation $\underline{O}^R$ is introduced in equ. (4.37) in the same manner as was done in equ. (4.36), the resulting secular equation

$$\det \left(\underline{O}^R \underline{d} (\underline{O}^R)^{-1}\right) = 0 \qquad (4.58)$$

has, to first order in $\Gamma^{\uparrow} / \Gamma^{\downarrow}$ and for sufficiently small $\Gamma_{j(n)}$, the roots

$$\mathcal{E}_j = \lambda_j - \tfrac{i}{2} \left(\Gamma_{j(n)} + \left(O_{0j}^R\right)^2 \Gamma^{\uparrow} \right) \qquad j = 0, \ldots, m \qquad (4.59)$$

with λ_j being the solutions of $\det(\underline{O}^R \underline{d}^R (O^R)^{-1}) = 0$ (equ. (4.51)). Thus the total width is now

$$\Gamma_j = \Gamma_{j(n)} + \frac{D_I}{2\pi} \frac{\Gamma^\downarrow \Gamma^\uparrow}{(\varepsilon_j - \varepsilon_o)^2 + \frac{1}{4}(\Gamma^\downarrow)^2} \qquad (4.60)$$

To the same approximation, the transformation

$$(v_b^c)' = \sum_k O_{jk}^R \; v_k^c \qquad (4.61)$$

yields new partial widths. For c = f, equ. (4.61) gives (only $v_0^f \neq 0$)

$$\Gamma_{jf} = \frac{D_I}{2\pi} \frac{\Gamma^\downarrow \Gamma^\uparrow}{(\varepsilon_j - \varepsilon_o)^2 + \frac{1}{4}(\Gamma^\downarrow)^2} \qquad j = 0, \ldots, m \qquad (4.62)$$

For c = n and j = 0 we obtain

$$\Gamma_{on} = \left[\sum_{k=1}^{m} O_{ok}^R \; \Gamma_{kn}^{1/2} \right]^2 \qquad (4.63)$$

The results obtained in subsection 4.3.1 and 4.3.2 are exactly equivalently obtained from R-matrix theory : Starting from the original set of R-Matrix states X_λ containing m class I and one class II states, new sets X_λ' are constructed; this is done by a transformation

$$X_\lambda' = \sum_\mu O_{\lambda\mu}^R \; X_\mu \qquad (4.64)$$

with the $O_{\lambda\mu}^R$ given by equ. (4.53) in the perturbation case and by equ. (4.57) in the case treated in section 4.3.2. For sufficiently "isolated" resonances such that the multi-level Breit-Wigner approximation applies, this leads to the same results for the S-matrix partial widths as given in equ. (4.54) to (4.56) and equ.(4.62) and (4.63), respectively. The assumption of "isolated" resonances in R-matrix theory is exactly equivalent to the approximations made in subsections 4.3.1 and 4.3.2.

4.3.3 Class II states with large fission width ($D_I \ll \Gamma^\uparrow \gg \Gamma^\downarrow$)

In contrast to the previous cases, this case is not easily dealt with in the framework of R-matrix theory. The reason is that with the fission width of the class II state being much larger than the class I spacing, strong interference effects occur such that the multi-level Breit-Wigner approximation is no longer valid. In fact, the procedure of R-matrix theory, namely first to diagonalise the complete set of internal states and only afterwards couple it to the channels, is not the most straight-forward one in a situation where the class II state is coupled much more strongly to the fission channel than to the other bound states.

Within the formalism of the shell model approach, however, some insight into the situation may be got in a simple manner. We start from equ. (4.37) and (4.38). The poles of the scattering matrix are given by the secular equation $\det(\underline{d}) = 0$ which can also be written

$$E - \varepsilon_o + i\pi (v_o^f)^2 = \sum_{k=1}^{m} \frac{v_{ok}^2}{E - \varepsilon_k} \qquad (4.65)$$

Thus from the beginning we take into account the coupling of the class II state to the fission channel (the term $i\pi (v_o^f)^2$). However, in order to obtain the pole which is close to the class I state energy ε_j, we approximate equ. (4.65) by replacing E on the left hand side by ε_j and by neglecting all terms of the sum on the right hand side except the one with k = j :

$$\varepsilon_j - \varepsilon_o + \frac{i}{2}\Gamma^\uparrow \approx \frac{v_{oj}^2}{E - \varepsilon_j + \frac{i}{2}\Gamma_{j(n)}} \qquad j = 1, \ldots, m \qquad (4.66)$$

Thus

$$\xi_j \approx \varepsilon_j - \frac{i}{2}\Gamma_{j(n)} + \frac{v_{oj}^2}{\varepsilon_j - \varepsilon_o + \frac{i}{2}\Gamma^\uparrow} \qquad j = 1, \ldots, m \qquad (4.67)$$

The imaginary part of (4.67) gives

$$\Gamma_j \approx \Gamma_{j(n)} + \frac{D_I}{2\pi} \frac{\Gamma^\downarrow \Gamma^\uparrow}{(\varepsilon_j - \varepsilon_o)^2 + \frac{1}{4}(\Gamma^\uparrow)^2} \qquad j = 1, \ldots, m \qquad (4.68)$$

where we have also used (4.46). The additional width

$$\Gamma_{jf} \approx \frac{D_I}{2\pi} \frac{\Gamma^\downarrow \Gamma^\uparrow}{(\varepsilon_j - \varepsilon_o)^2 + \frac{1}{4}(\Gamma^\uparrow)^2} \qquad j = 1, \ldots, m \qquad (4.69)$$

is due to the fission channel. The sum rule (equ. (4.49)) gives

$$\Gamma_0 \approx \Gamma^{\uparrow} - \sum_{j=1}^{m} \Gamma_{jf} \qquad (4.70)$$

Also, from equ. (4.64) we obtain

$$\sum_{j=1}^{m} \Gamma_{jf} \approx \Gamma^{\downarrow} \qquad (4.71)$$

The "fission width" Γ_{jf} of equ. (4.69) is a contribution to the total resonance width due to the fission channel. It is not a partial width in the sense of being the residue of S_{nf} at the pole ξ_j. As shown in [MW69], these residues are complex due to interference effects. However, equ. (4.69) still gives the absolute value of that residue.

4.4 Comparison to Data

The first experimental data which showed the intermediate structure effect due to class II states, as theoretically described in the previous subsections, were data on the low energy neutrons induced fission cross sections of ^{237}Np measured at Saclay [Fu68] and ^{240}Pu measured at Geel [MT68]. The measurements on ^{240}Pu are illustrated in fig. 9. The upper half of the figure shows the total neutron cross section of ^{240}Pu [KB68] in the neutron energy range between 0.5 and 3 keV. A dense population of resonances is seen which represents essentially all class I states with $J^{\pi}=1/2^{+}$ (only s-wave resonances are observed at these low neutron energies) in this energy region. In the lower half of fig. 9, the fission cross section is shown. Fission is observed only in clusters of resonances which acquire a fission width due to the coupling to a nearby class II state with the same J^{π}. Four class II states are observed in the neutron energy range covered by fig. 9.

The most interesting further examples of this kind of intermediate structure in sub-barrier fission cross sections have been found, besides ^{237}Np, in ^{234}U, ^{238}U and ^{242}Pu. They will be discussed in some detail below.

The formulae developed in the previous sub-sections may principally be used to analyse the fission cross section in the intermediate structure clusters. The aim of such an analysis is to determine the intermediate structure parameters, mainly $\Gamma^{\uparrow}$ and $\Gamma^{\downarrow}$ which in turn may give information on barrier penetrabilities. As will be seen in some of the cases to be discussed below, the analysis meets characteristic difficulties which we will discuss on a more general basis first.

In most cases the individual fine structure resonances within a sub-barrier fission cluster are sufficiently "isolated" such that they may be reasonably accurately described by the single-level Breit-Wigner approximation equ. (4.27). The experimental energy resolution, including the so-called Doppler-width due to thermal movement of the target atoms (both are dependent on neutron energy), is usually larger than the total width Γ of the resonances in heavy nuclei. Therefore, the experimentally observed quantities are the areas under the resonances in the fission cross section which are given by

$$A_{if} = 2\pi^2\lambda^2 \frac{2J+1}{2(2I+1)} \frac{\Gamma_{i(n)}\Gamma_{if}}{\Gamma_i} \equiv g \frac{\Gamma_{i(n)}\Gamma_{if}}{\Gamma_i} \qquad (4.72)$$

Whenever one level (labelled i = 0 in section 4.3) contains a predominant fraction of the original class II state, i.e. in the perturbation case (subsection 4.3.1) as well as in the case of subsection 4.3.3, its neutron width $\Gamma_{0(n)}$ will be rather smaller than the average class I neutron width which is of the order of 10 to 100 meV, depending on neutron energy; at the same time its fission width Γ_{of} will be a considerable fraction of $\Gamma^{\uparrow}$ and may therefore be much larger than $\Gamma_{o(n)}$. Under these circumstances A_{of} becomes almost independent of Γ_{of}, and therefore Γ_{of} and thus the major contribution to Γ is not or only very inaccurately determined.

The situation may even become worse. In order to see this let us assume that we are dealing with the perturbation case (subsection 4.3.1), and that $\Gamma^{\uparrow} \gg \Gamma_i$ $(i \neq 0) > \Gamma_{o(n)}$. Then

$$A_{if} = g \frac{\Gamma_{i(n)}\Gamma_{if}}{\Gamma_i} = g \frac{\Gamma_{i(n)}}{\Gamma_i} \left(\sigma_{0i}^{R}\right)^2 \Gamma^{\uparrow} \qquad \text{for } i \neq 0 \qquad (4.73)$$

and

$$A_{0f} \approx g\,\Gamma_{0(n)} = g \left(\sum_{i\neq 0} \sigma_{0i}^{R}\,\Gamma_{in}^{1/2}\right)^2 \qquad (4.74)$$

If $\Gamma^{\downarrow}$ is sufficiently small such that the sum in equ. (4.74) extends only over a very small number of terms, then, because of the assumption $\Gamma^{\uparrow} \gg \Gamma_i$ $(i \neq 0)$,

$$A_{if} \gg A_{of}$$

and it is not clear whether the resonance labelled i = 0 has at all been observed in the experiment. The same is true if accidental cancellations occur in the sum equ. (4.74), and it is certainly true in the case of a class II state with "large" fission width ($D_I \ll \Gamma^{\uparrow} \gg \Gamma^{\downarrow}$) treated in subsection 4.3.3. For the latter case an estimate of the neutron width $\Gamma_{o(n)}$ is given in [Wg68] as

$$\left(\frac{1}{\alpha} A_{of} \approx \right) \quad \Gamma_{o(n)} \approx \overline{\Gamma}_{i(n)} \frac{\Gamma^{\downarrow}}{\Gamma^{\uparrow}} \qquad (4.75)$$

whereas for the larger ones of the A_{if}

$$A_{if} = \alpha \frac{\Gamma_{i(n)} \Gamma_{if}}{\Gamma_i} \approx \alpha \frac{\Gamma_{i(n)}}{\Gamma_i} \frac{D_I}{\pi} \frac{\Gamma^{\downarrow}}{\Gamma^{\uparrow}} \qquad (4.76)$$

Moreover, in this case the already small area equ. (4.75) is spread over a large width of $\Gamma_{of} \approx \Gamma^{\uparrow}$ such that the peak cross section is extremely small and virtually undetectable.

Thus the question arises by what other means is it possible to decide whether the resonance which is observed to have the largest fission width within a cluster, really contains a correspondingly large fraction of the original class II state. In principle there are several possibilities which, however, all have difficulties of their own :

First of all, if in the case of a narrow class II state only very few fission resonances are observed, it may be checked whether equ. (4.54) to (4.56) are satisfied simultaneously. However, once five or more resonances are observed within a cluster, the ambiguity in the relative sign of the individual terms in the sum of equ. (4.56) allows far too broad a range of possible values for $\Gamma_{o(n)}$.

Secondly one may try to observe any effect on the γ-decay of the class II state inside the second well. This is illustrated in fig.*10*a. A resonance which contains a major fraction of the class II state has an appreciable width for γ-decay within the second well (see equ. (4.52))

$$\Gamma_{o\gamma(II)} = \left(1 - \sum_{k=1}^{m} \left(\sigma_{ok}^{R}\right)^2\right) \Gamma_{\gamma}(II) \qquad (4.77)$$

as compared to its width for γ-decay within the primary well

$$\Gamma_{o\gamma(I)} \approx \sum_{k=1}^{m} \left(\sigma_{ok}^{R}\right)^2 \Gamma_{\gamma}(I) \qquad (4.78)$$

(interference effects of the contributions from the different class I states k are expected to cancel for the many channel process of radiative decay). Here, $\Gamma_{\gamma}(II)$ is the width for radiative decay inside the second well of the original pure class II state and from statistical calculations is expected to be of the order of 20 to 30% of the normal class I radiative width $\Gamma_{\gamma}(I)$.

The most obvious way to experimentally search for the γ-decay within the second well is to try and detect a delayed fission fraction within a cluster of fission resonances, due to the subsequent decay of the shape isomer . The method is limited to cases where the shape isomer half life is in a suitable range ($\approx$ 10 nsec - 1 μ sec). It has been tried without success in the case of neutron-induced fission of ^{242}Pu [BB74].

Another way to detect a γ-decay branch within the second well is by its influence on the gross shape of the capture γ-ray spectrum. Indeed, this spectrum for a resonance with a large class II fraction, consists of two components with relative intensities $\Gamma_{o\gamma}(II)$ and $\Gamma_{o\gamma}(I)$ for decay within the second and primary well, respectively (fig. *10* b). The component $\Gamma_{o\gamma}(II)$ is much softer since the available decay energy is smaller by ~ 2 MeV. Thus, if resonance areas A_{γ} are measured in a radiative capture experiment, and different γ-ray energy bias values B_1 and B_2 (fig. *10* b) are applied in such measurements, the ratio

$$R = \frac{A_{\gamma}(\text{bias } B_2)}{A_{\gamma}(\text{bias } B_1)}$$

should be appreciably smaller for a resonance with a major class II fraction than for a normal class I resonance. Measurements of this kind have been done on target nuclei ^{237}Np and ^{238}U [Wg74]. Fig. *11* shows the expected R-values (open circles) for those resonances which are candidates to contain a major class II fraction under the assumption that no resonance has been missed in the intermediate structure pattern. The expectations are different for the individual cases due to the fact that the intermediate structure parameters, mainly the

O_{0j} as obtained from the fine structure fission widths, are different. The error bars shown for the expected R-values reflect the uncertainty in those parameters as well as the uncertainty due to theamount of prompt fission γ-rays unavoidably detected in the capture γ-ray detector. The presence of the prompt fission γ-rays limits the applicability of this method to cases where $\Gamma^{\uparrow}$ is sufficiently small, $\Gamma^{\uparrow} \leq$ 1 meV. Also, since the bias B_2 has to be set at 1.5 to 2 MeV below neutron binding energy, statistical fluctuations of the partial widths for the high energy γ-transitions within the first well may influence the detected class I component and thereby confuse the picture. As seen from the experimental data shown in fig. 11 , no effect was found in these measurements. The implications thereof will be discussed separately for the individual nuclei below.

In what follows, the most interesting cases of intermediate structure in sub-barrier fission will shortly be discussed individually.

4.4.1 ^{240}Pu + n

^{240}Pu was not only one of the first cases where intermediate structure has been detected, but also a typical example for the difficulties encountered in the analysis of the data. The early measurements [MT68] did not allow a determination of the largest fission width within each cluster due to the fact that for these resonances $\Gamma_{of} \gg \Gamma_{o(n)}$. Only a later measurement with improved neutron energy resolution done at ORNL [AW75] allowed a shape analysis of those resonances and showed that Γ_{of} was of the order of a few eV : Fig. 12 shows the data for the cluster around 780 eV neutron energy. The widths of the resonances at 791, 811 and 820 eV are determined by the resolution which (including Doppler width) at 800 eV is ~ 1.6 eV. It can be seen from the figure that the 782 eV resonance is slightly broader. The clusters at 782 eV and 1936 eV represent examples of the perturbation situation as treated in subsection 4.3.1. With the parameters given in [AW75], equ. (4.54) to (4.56) can be satisfied simultaneously. With the rather large values of $\Gamma^{\uparrow}$ and $\Gamma^{\downarrow}$ obtained, it is probable that most of the class II strength has been detected. The cluster around 1405 eV represents an excellent example of an almost degeneracy of a class II and a class I level. This is discussed in detail in [AW75]. For later discussion we note rough averages of the parameters $\Gamma^{\uparrow}$ and $\Gamma^{\downarrow}$:

$$\Gamma^{\uparrow} = 2.5 \text{ eV} \quad ; \quad \Gamma^{\downarrow} = 1.5 \text{ eV}$$

4.4.2 ^{238}U + n

An extremely comprehensive measurement of the ^{238}U sub-barrier fission cross section has been done at ORNL [Di79]. Fig. 13 which shows the first cluster around 722 eV neutron energy gives an impression of the quality of the data. Also ^{238}U presents an example of the perturbation situation, but with a much smaller value of $\Gamma^{\uparrow}$than in the case of^{240}Pu.The question whether the major class II strength has been observed in the individual clusters cannot be answered uniquely. Failure to observe abnormal γ-ray spectral shapes for the main fission resonances was interpreted [Wg74] as evidence that most of the class II strength was missed and $\Gamma^{\uparrow}$ might be much larger than determined from the observed resonances. Fig. 11 shows, however, that this conclusion was mainly based on the 1211 eV cluster, whereas for the 722 eV cluster the data are not really statistically significant. For the latter case, the fine structure parameters [Di79] show that equ. (4.54) to (4.56) can be simultaneously fulfilled. Moreover, recent accurate resonance parameter studies at Geel [Po80] do indicate a major class II component for the 722 eV resonance: These measurements consist of total cross section data yielding acccurate neutron widths and neutron capture measurements which determine the capture area

$$A_{i\gamma} = \alpha \frac{\Gamma_{i(n)} \Gamma_{i(\gamma)}}{\Gamma_i} \varepsilon_{i\gamma}$$

Since the capture γ-ray detector employed has a sensitivity $\varepsilon_{i\gamma}$ which is proportional to the total γ-ray cascade energy released, it is less sensitive for a resonance which has a major decay branch into the second well than for a normal class I resonance. For ^{238}U, $\Gamma_\gamma(I)$ = 23.6 meV and statistical calculations give $\Gamma_\gamma(II)/\Gamma_\gamma(I) \approx 0.2$; for the 722 eV cluster, the experimental fission widths [Di75] yield $\sum_{k=1}^{m} (\sigma_{ck}^{q})^2 \approx 0.12$, thus according to equ. (4.77) and (4.73), $\Gamma_{o\gamma(II)} \approx$ 4.1meV and $\Gamma_{o\gamma(I)} \approx$ 2.8 meV ; again fission γ-rays (Γ_{of} = 1.57 meV) are unavoidably detected; finally with $\varepsilon_\gamma(II)/\varepsilon_\gamma(I) \approx$ 0.6 and $\Gamma_{o(n)}$ = 1.9 meV, $A_{o\gamma}$ for the 722 eV resonance is predicted to be ≈ 20% smaller than $A_{i\gamma}$ for a normal class I resonance with identical neutron width. Fig. 14 shows the data around the 722 eV resonance : The two resonances at 722 eV and 732 eV show up equally strong in the transmission data, corresponding to almost equal neutron widths. In the capture data, however, the 722 eV resonance is weaker (by even ≈ 27% as inspection of the numerical data tells)

in rough agreement with the above expectation under the assumption that the 722 eV resonance has a class II component of $\Gamma_{of}/\Gamma^{\uparrow} = 0.88$. In contrast to the γ-spectral measurements, this comparison of transmission and capture data is not only sensitive to the "hardness" of the γ-ray spectrum (which, as mentioned above is also subject to statistical fluctuations in the class I partial radiative widths), but rather to the total γ-ray energy released, i.e. roughly speaking, to the product of "hardness" and γ-ray multiplicity; it is also sensitive to the absolute value of $\Gamma_{o(\gamma)} = \Gamma_{o\gamma(II)} + \Gamma_{o\gamma(I)}$ as long as it is not much larger than $\Gamma_{o(n)}$. We thus now assume that for the 722 eV cluster the major class II strength has indeed been detected.

For the 1211 eV cluster the situation is different, however: Firstly, the γ-ray spectral measurements [Wg74] seem to show statistically significant evidence against a major class II component for the 1211 eV resonance. Secondly, the comparison of transmission and total capture data [80] show no reduction of the total capture yield for the 1211 eV resonance, although the reduction factor predicted for the 1211 eV resonance under the assumption of a class II component of $\Gamma_{of}/\Gamma^{\uparrow} = 0.95$ [Di79] would be even 0.4, due mainly to the fact that in this case $\Gamma_{o(\gamma)} < \Gamma_{o(n)}$ and therefore the capture area $A_{o\gamma}$ is very sensitive to the absolute value of $\Gamma_{o(\gamma)}$ which is estimated (equ. (4.77) and (4.78)) to be only $\Gamma_{o(\gamma)} \approx 5.7$ meV. We thus conclude that for the 1211 eV cluster the major component of the class II level is still undetected.

For an estimate of $\Gamma^{\uparrow}$ and $\Gamma^{\downarrow}$ we thus only use the data for the 722 eV cluster :

$$\Gamma^{\uparrow} \approx 1.8 \text{ meV} \qquad \Gamma^{\downarrow} \approx 2 \text{ eV}$$

4.4.3 ^{242}Pu + n

The sub-barrier fission cross section has been measured by Auchampaugh et al. [Au71]. Resonance analysis has been done in the course of total cross section measurements [Au73]. They meet the characteristic difficulty that for the resonance with the largest fission width within each cluster, only a lower limit for the fission width is obtained from the fission area. In [Au73] an upper limit for $\Gamma^{\uparrow}$ is obtained from the measured neutron widths with the aid of equ. (4.49) and (4.51). This, of course, implies the assumption that the major part of the class II strength has been detected, which is doubtful because of the failure of Browne and Bowman [BB74] to observe a delayed fission component. The rough averages, obtained from the results of the resonance analysis [Au73], of

$$\Gamma^{\uparrow} \approx 300 \text{ meV} \qquad \Gamma^{\downarrow} \approx 30 \text{ eV}$$

can therefore be considered as tentative only. Also, the value of $\Gamma^{\downarrow}$ shows, that a perturbation treatment is no longer adequate.

The cluster around 762 eV has also been analysed in connection with resonance parameter studies at Geel [Po73]. Due to the inclusion of radiative capture data, a more precise value of the fission width of the 762 eV resonance could be obtained The data have been interpreted in the spirit of sub-section 4.3.3. as being due to a class II state with large fission width. Thus, as compared to the analysis of [Au73], the roles of $\Gamma^{\uparrow}$ and $\Gamma^{\downarrow}$ are interchanged, which would explain why a delayed fission component is unobservable. We thus tentatively adopt the parameters given by [Po73] for the 762 eV cluster :

$$\Gamma^{\uparrow} = 12 \text{ eV} \quad ; \quad \Gamma^{\downarrow} = 37 \text{ meV}$$

4.4.4 ^{234}U + n

An extensive study of the fission cross section of ^{234}U has been performed by James et al. [Ja77]. The width of the class II state is now much larger than the class I spacing. This width is assumed to be due to $\Gamma^{\downarrow}$, mainly on the basis of systematics : Potential energy calculations generally indicate that with decreasing mass number A the inner barrier decreases whereas the outer one increases. We thus expect to find the situation described in subsection 4.3.2, i.e. the fine structure fission widths to be distributed according to a Lorentzian distribution with width $\Gamma^{\downarrow}$(equ.(4.57)). Fig. 45 shows the fission widths of resonances below 1.5 keV neutron energy and a fit with a superposition of two Lorentzians corresponding to the presence of two class II levels at 550 eV and 1092 eV [Ja77]. The averages of the parameters given by James et al. (for $\Gamma^{\uparrow}$ this includes results for five additional clusters below 13.1 keV neutron energy) are

$$\Gamma^{\uparrow} = 152 \text{ meV} \qquad \Gamma^{\downarrow} = 115 \text{ eV}$$

4.4.5 $^{237}Np + n$

^{237}Np is the only odd target nucleus for which a marked intermediate structure has been found in the sub-barrier neutron-induced fission cross section. The s-wave neutron resonances in $^{237}Np + n$ have spin of either 2^+ or 3^+. However, within a specific sub-barrier fission cluster only those resonances should show enhanced fission which have a spin equal to the spin of the class II doorway. This has been nicely demonstrated by Keyworth et al. [Ke73]: They did total and fission cross section measurements, using polarized targets and a polarized neutron beam. Part of their results is shown in fig. 16: In the lower half of the figure the total fission cross section is plotted, whereas the upper half shows the difference between the cross section observed with target and neutron spins parallel and the one observed with spins antiparallel. The fact that this difference remains always positive, demonstrates that all fine structure resonances of this cluster have the same spin, $J^\pi = 3^+$.

For a long time it was believed that the resonance at 39.91 eV neutron energy contained a significant class II fraction, according to the early data [Fu68] about 65%. This was contradicted by the γ-spectral measurements [Wg74] which, as can be seen from fig. 11, showed that the 39.91 eV resonance behaved like a normal class I. Indeed, a new resonance at 39.69 eV has recently been detected in fission [Pl76] as well as total cross section [Au80] measurements performed with cooled samples in order to reduce the Doppler width. According to Plattard et al. [Pl76] it is this resonance which has the largest fission width and therefore is a candidate to contain a major class II fraction. The distribution of fission widths has been fitted [Pl76] by a Lorentzian with a width of $\Gamma_{II} = 4$ eV, thus $\Gamma_{II} > D_I$, but it is as yet unclear whether this width is due to the fission or the spreading width of the class II state. The smaller of the two widths would then be given by the sum of fine structure fission widths, $\sum \Gamma_{if} = 4.2$ meV.

4.5 Deductions with Respect to Barrier Parameters

Once the parameters $\Gamma^\downarrow$ and $\Gamma^\uparrow$ have been determined from the analysis of the intermediate structure pattern, the results can be used to determine the penetrabilities P_A and P_B of the two barriers at an energy corresponding to the excitation energies of the respective class II states, according to the statistical model estimates :

$$\Gamma^\downarrow = \frac{D_{II}}{2\pi} P_A \qquad \Gamma^\uparrow = \frac{D_{II}}{2\pi} P_B \qquad (4.79)$$

The use of equ. (4.79) implies the assumption of "complete damping", i.e. it implies that the strength of the class II vibrational states $\Phi_{\nu II}$ (see discussion below equ. (3.38)) which exclusively provide the coupling to class I and to the fission channel, are statistically distributed among the class II compound states $\varphi_{\lambda II}$. This can be seen by comparison to equ. (3.28). Furthermore, the statistical admixture of the class II vibrations among the $\varphi_{\lambda II}$ means that equ. (4.79) only gives the relationships for the expectation values of $\Gamma^\downarrow$ and $\Gamma^\uparrow$ in the sense that individual values may fluctuate around these expectation values according to Porter-Thomas distributions. Thus; if the experimental data are based on only a very small number (e.g. only one) of intermediate structure clusters, the resulting values of P_A and P_B are correspondingly uncertain.

In Table 4, experimental data on P_A and P_B for a few nuclei are compared : columns 5 and 6 give values for P_A and P_B deduced from the widths $\Gamma^\downarrow$ and $\Gamma^\uparrow$ (columns 2 and 3) which were obtained from the analysis of intermediate structure in sub-barrier neutron-induced fission cross sections (section 4.4; in the case of ^{238}Np we tentatively assume $\Gamma^\downarrow < \Gamma^\uparrow$). These penetrabilities correspond to (equ. (3.17)) barrier heights E_A and E_B as given in columns 7 and 8, assuming $\hbar\omega_A = 0.8$ MeV for the odd A compound nuclei and $\hbar\omega_A = 0.65$ MeV for ^{238}Np, and $\hbar\omega_B = 0.52$ MeV and 0.45 MeV, respectively, i.e. the same values as used by Lynn [Ly74]. Barrier heights and curvatures have, among others, also been obtained by Lynn [Ly74] from statistical model analysis of average neutron induced fission cross sections in the threshold region, and by Britt [Bri79] from the analysis of different charged particle fission data. Penetrabilities calculated from these barrier parameters for excitation energies slightly above neutron binding energy (corresponding to the energies of the class II states analysed for columns 2 and 3) are listed in columns 9 and 10, and 10 and 11, respectively (since no curvatures are given in [Bri79], those of Back et al. [Ba74] have been used for columns 11 and 12).

Comparison of the penetrabilities listed in Table 4 shows surprisingly large discrepancies. Of course, the penetrabilities obtained from the inter-

TABLE 1

Comparison of barrier penetrabilities obtained from sub-barrier intermediate structure and other sources

comp. nucl.	$\Gamma^{\downarrow}$ [eV]	$\Gamma^{\uparrow}$ [eV]	D_{II} [eV]	P_A	P_B	E_A [MeV]	E_B [MeV]	Lynn [Ly 74]		Britt [Bri 79]	
								P_A	P_B	P_A	P_B
^{235}U	115	0.152	2100	0.34	$4.5\cdot10^{-4}$	5.38	5.94	$6.0\cdot10^{-3}$(x)	$7.8\cdot10^{-3}$(x)	$5.6\cdot10^{-3}$	$5.2\cdot10^{-4}$
^{239}U	2	$1.8\cdot10^{-3}$	1000	0.0126	$1.13\cdot10^{-5}$	5.36	5.75	$2.3\cdot10^{-6}$	$8.0\cdot10^{-8}$	$3.0\cdot10^{-5}$	$1.8\cdot10^{-4}$
^{238}Np	$4.2\cdot10^{-3}$	4	46	$5.7\cdot10^{-4}$	0.55	6.26	5.47	$1.12\cdot10^{-3}$	$8.9\cdot10^{-4}$	$4.5\cdot10^{-3}$	0.156
^{241}Pu	1.5	2.5	480	0.021	0.035	5.73	5.52	$1.9\cdot10^{-3}$(x)	0.084(x)	$5.6\cdot10^{-3}$	$5.3\cdot10^{-3}$
^{243}Pu	0.037	12	550	$4.2\cdot10^{-4}$	0.137	6.03	5.19	$3.8\cdot10^{-4}$	$7.7\cdot10^{-3}$	$1.7\cdot10^{-3}$	$(1.6\cdot10^{-3})$

(x) used barrier as indicated for $J^{\pi} = 1/2^{+}$

mediate structure data are very uncertain due to Porter-Thomas fluctuations of the widths $\Gamma^{\downarrow}$ and $\Gamma^{\uparrow}$ (in most cases they are based on the analysis of only one cluster), and due to the assumption of complete damping, thus differences of up to a factor five or even ten could be understood if they were random. However, the observed discrepancies are often much larger (the worst case is P_A of ^{239}U), and they are too systematic : It is interesting to note that it is generally the larger one of P_A and P_B for which the large discrepancies occur in the sense that the penetrability indicated by the intermediate structure data is much larger than the one obtained from average cross sections.

A similar discrepancy also exists [Di79] between the measured fission widths of low energy resonances (far below the first intermediate structure cluster) in ^{238}U + n and those calculated from the barrier parameters of Back et al. [Ba74] for direct tunnelling through both barriers according to (see equ. (3.24)) :

$$\Gamma_{f,max} = \frac{D_{II}}{2\pi} \frac{P_A P_B}{4} \qquad (4.80)$$

If, however, one uses the penetrabilities of columns 5 and 6 (Table 1) deduced from the intermediate structure analysis, in equ. (4.80), fission widths for resonances away from intermediate structure clusters are obtained as given in column 3 of Table 2 . They compare reasonably well with the corresponding experimental data listed in column 4 of the Table.

A possible source of large differences between the observed penetrabilities lies in the fact that in the case of intermediate structure and low-energy resonance data one looks at the barrier for a specific spin (corresponding to s-wave neutron interaction), whereas the average cross section data are sensitive to a comparatively broad spectrum of spin values and essentially the lowest effective barrier is obtained. This fact could thus explain why much smaller penetrabilities may result from resonance data than from average cross sections. However, the observed discrepancies generally have the opposite sign.

Thus, there exists a discrepancy between resonance data and average cross section data with respect to barrier parameters, which at present is not understood.

Apart from barrier parameters, intermediate structure data may yield information on the depth of the secondary well of the deformation potential. Indeed, as already discussed in sub-section 3.3.4, the ratio of class I and class II level densities is expected to be roughly given by equ. (3.32), provided that the parameters a and σ may be assumed to be the same for both wells. Although this assumption is certainly very crude, values of the energy difference between the second and first well obtained from class II level spacings are generally in fair agreement with corresponding information from isomer excitation functions.

4.6 Unresolved Class II Clusters

As we have seen in section 4.4, individual values of $\Gamma^{\downarrow}$ and $\Gamma^{\uparrow}$ are usually obtained only for a very small number of sub-barrier fission clusters at low neutron energies where the fine structure due to the class I states is well resolved. At higher neutron energies, often a large number of additional class II states is observed in the fission cross section, but the individual fine structure resonances are not resolved, and the only experimental information is the total area integrated over the entire class II cluster. Thus the question arises how this area, A_{fII}, is related to the parameters $\Gamma^{\downarrow}$ and $\Gamma^{\uparrow}$. The question cannot be answered in general because the relation between A_{fII} and $\Gamma^{\downarrow}$ and $\Gamma^{\uparrow}$ depends strongly on the coupling condition, and, for narrow class II states, on the neutron widths of a few individual class I resonances. However, for broad class II states, $\Gamma_{II} >> D_I$, the picket fence approximation can be used to obtain an expression for A_{fII} :

Table 2

Comparison of fission widths of resonances outside intermediate structure clusters calculated with P_A and P_B of columns 5 and 6 of table 1, to experimental data.

comp nucl.	D_I [eV]	Γ_{fmin}(calc.) [eV]	Γ_{fmin}(exp.) [eV]	Ref.
^{239}U	22	$12 \cdot 10^{-8}$	$7 \cdot 10^{-8}$	[Di 79]
^{238}Np	1.5	$19 \cdot 10^{-6}$	$3 \cdot 10^{-6}$	[Pl 76]
^{241}Pu	13	$3.8 \cdot 10^{-4}$	$4 \cdot 10^{-4}$	[AW 75]
^{243}Pu	17.5	$4 \cdot 10^{-5}$	$5 \cdot 10^{-5}$	[BF 71]

$$A_{fII} = 2\pi^2 \lambda^2 g(I,J) \sum_i \frac{\Gamma_{i\downarrow} \Gamma_{i\uparrow}}{\Gamma_i} = 2\pi^2 \lambda^2 g(I,J) \overline{\Gamma}_{\downarrow} \sum_i P_{if} \qquad (4.81)$$

where the fission widths Γ_{if} are distributed according to a Lorentzian (see equ. (4.62) and (4.69) :

$$\Gamma_{if} = \frac{D_I}{2\pi} \frac{\Gamma^{\uparrow} \Gamma^{\downarrow}}{(\varepsilon_i - \varepsilon_o)^2 + \frac{1}{4}\Gamma_{\Sigma}^2} \qquad (4.82)$$

We write

$$\Gamma_i = \Gamma_{if} + \Gamma_i' \qquad \Gamma_i' = \frac{D_I}{2\pi} T' \qquad (4.83)$$

where Γ_i' stands for all decay channels other than fission. From equ. (4.82) and (4.83) we have the fission probability :

$$P_{if} = \frac{\Gamma_{if}}{\Gamma_i'} = \frac{\Gamma^{\uparrow}\Gamma^{\downarrow}}{\Gamma'} \frac{1}{(\varepsilon_i - \varepsilon_o)^2 + \frac{1}{4}\Gamma_{II}^2 + \frac{\Gamma^{\uparrow}\Gamma^{\downarrow}}{\Gamma'}} \qquad (4.84)$$

Summation of terms (4.84) gives

$$\sum_i P_{if} = \frac{\Gamma^{\uparrow}\Gamma^{\downarrow}}{2\Gamma_i'} X \qquad (4.85)$$

$$X = \sqrt{\frac{\Gamma'}{\frac{1}{4}\Gamma'\Gamma_{II}^2 + \Gamma^{\uparrow}\Gamma^{\downarrow}}}$$

Thus the total fission area of a class II cluster is

$$A_{fII} = \pi^{-1}\lambda^2 g(I,J) \frac{\overline{\Gamma_{in}}}{\overline{\Gamma_i'}} \Gamma^{\uparrow}\Gamma^{\downarrow} X \qquad (4.86)$$

4.7 Fissile Nuclei

For energies sufficiently above the (lower) barrier, intermediate structure effects disappear. The average fission cross section (averaged over many compound nuclear resonances) is then given by the statistical model expression equ. (3.1) with the fission transmission coefficient given by equ. (3.20) and (3.19). At lower neutron energies, individual compound nuclear resonances are resolved, and the detailed energy dependence of the fission cross section is given by the formulae of S- or R- matrix theory, e.g. in the (usually too crude) single-level approximation, by equ. (4.27) to (4.30).

The question is, however, what are "energies sufficiently above the barrier"? May, for low-energy neutron-induced fission of the usual fissile nuclei ^{235}U and ^{239}Pu, the effects of class II states be ignored?

4.7.1 $^{235}U + n$

In the case of ^{235}U intermediate structure effects are obviously not negligible, as has been shown most instructively by Moore et al. [Mo78] : From their analysis of fission cross sections for separate channel spins, obtained from measurements with a polarized neutron beam and a polarized target, they deduce sets of average resonance parameters as a function of energy; the averaging intervals are chosen such as to contain at least 100 resonances. The resulting resonance parameter sets are not unique : The data can be described by several different sets; but they all have in common that the average fission widths fluctuate to a degreee as shown in fig. 17 , and in particular all solutions reproduce the pattern shown in fig. 17 b for the average fission width for channel spin 4. The degree of fluctuation shown in the figure is much larger than the 10-15% expected for a χ^2 distribution for two or three open fission channels. One thus has to conclude that the fission cross section of ^{235}U, at least for channel spin 4, is still strongly influenced by intermediate structure due to class II states with an average spacing between 0.5 and 1 keV. Of course, as we are at energies close to or slightly above the relevant barrier transition states, we expect that the class II widths are much larger than the class I spacing, $\Gamma_{II} >> D_I$.

4.7.2 $^{239}Pu + n$

The case of $^{239}Pu + n$ is special due to the fact that the energies of barrier transition states for the two compound nuclear spins obtained by s-wave neutron interaction, $J^{\pi} = 0^+$ and 1^+, are very different : The 0^+ fission barrier is expected to be about 1.5 MeV lower than neutron binding energy, thus for channel spin 0^+ one is definitely dealing with above-barrier fission and would no longer expect to see any effect of class II states. Resonances of spin 1^+, on the other hand, may fission only via $K = 1^+$ transition states (Bohr channels). and these can be built up only by combinations of different collective excitations. The lowest $K = 1^+$ channel is expected at $\sim$ 1.5 MeV above the $K = 0^-$ barrier, i.e. approximately at neutron binding energy. Thus, we are dealing with fission close to the barrier top, and still may expect effects of intermediate structure. They have indeed been found by a correlation analysis of the average fission cross section of ^{239}Pu below 6 keV neutron energy, performed by James and Patrick [JP69]. These authors show that the average fission cross section (multiplied by $\sqrt{E_n}$) may be well described by a constant plus a sum of Lorentzians describing the intermediate structure contribution due to class II states with an approximate spacing of about 500 eV and an average width of about 275 eV.

The difference in the positions of 0^+ and 1^+ barrier transition states has an important practical consequence which should be mentioned here : Fission widths of $J^\pi = 0^+$ resonances are large, $\langle \Gamma_{(f)}^{0+} \rangle = 2.27$ eV [B170], thus 0^+ resonances contribute almost only to the fission cross section; they are broad and have a small peak cross section. $J = 1^+$ resonances, on the other hand, with $\langle \Gamma_{(f)}^{1+} \rangle = 35.5$ meV, contribute to both, the capture- and fission cross section; they are narrow and tall. Thus resonance self-shielding primarily influences the $J = 1^+$ resonances and thereby influences the effective capture-to-fission ratio. This is illustrated in fig. *18* . For this figure, a neutron energy region, 70 eV $< E_n <$ 110 eV has been selected which contains several typical resonances of both spins. The effective capture-to-fission ratio for neutron incident perpendicular to the surface of a disk sample, has been numerically calculated as a function of sample thickness (for an effective temperature of 300°K) from the resonance parameters of [B170] . The drastic resonance self-shielding effect for the $J = 1^+$ resonances is immediately obvious from fig. *18*.

4.8 Consequences for Average Cross Sections

The usual statistical model expressions equations (3.6) to (3.8) for the average fission cross section do not take into account any effects of intermediate structure. This will be quite correct as long as fission well above the barrier is concerned. However, at energies close to or below the barrier top, the existence of intermediate structure due to class II states, may considerably change the average fission cross section with respect to the one calculated from the simple statistical model. This comes about because the statistical model expressions are equivalent to the calculation of $\langle \Gamma_n \rangle \langle \Gamma_f \rangle / \langle \Gamma \rangle$, whereas the true average fission cross section is rather proportional to $\langle \Gamma_n \Gamma_f / \Gamma \rangle$, where the averages are to be taken over energy ranges larger than D_{II}. The width fluctuation factor $f^{(J)}_{nls,c}$ of equ. (3.5) deals only with fluctuations due to the statistical distributions of the widths, not with the systematic fluctuations due to intermediate structure. If the fission strength is concentrated in a relatively small number of resonances with large fission widths for which then $\Gamma \approx \Gamma_f$, whilst for most of the remaining resonances $\Gamma >> \Gamma_f$, the necessary correction may be very large.

Lynn and Back [LB74] have treated the problem in a picket-fence model approach : In this approximation neutron widths for a given channel are assumed constant (over an energy range of the order of D_{II}) and the average fission cross section can be written as (see equ. (3.4)) :

$$\bar{\sigma}_{nf} = \sum_J \bar{\sigma}^{(J)}(c.N.)\, \bar{P}_f^{(J)} \qquad P_f^{(J)} = \frac{\Gamma_f^{(J)}}{\Gamma^{(J)}} \qquad (4.87)$$

where

$$\bar{\sigma}^{(J)}(c.N.) = \pi\lambda^2 g(I,J) \sum_{\ell,s} T_{n\ell s}^{(J)} \qquad (4.88)$$

is the cross section for formation of the compound nucleus in a state with total angular momentum J. If we assume $\Gamma_{II} \gg D_I$, in the picket-fence approximation the fission probability is given by equ. (4.84). Averaging this Lorentzian distribution between $\varepsilon_o - D_{II}/2$ and $\varepsilon_o + D_{II}/2$ gives (the index J is omitted) :

$$\bar{P}_f = \frac{1}{\pi} \frac{T_A T_B}{T'} \tan^{-1}(\pi y) \qquad (4.89)$$

$$y = \frac{D_{II} X}{2\pi} = \sqrt{\frac{T'}{\frac{1}{4}T'(T_A+T_B)^2 + T_A T_B}}$$

where we have used

$$\Gamma^{\downarrow} = \frac{D_{II}}{2\pi} T_A \qquad \Gamma^{\uparrow} = \frac{D_{II}}{2\pi} T_B \qquad (4.90)$$

In the last two equations, if we assume complete damping of class II vibrational states, T_A and T_B are the transmission coefficients of barriers A and B, equ. (3.18). If the condition of complete damping is released, these equations must be re-interpreted as will be described in subsection 5.1.3.

An expression for $\bar{P}_f$ valid in the presence of many uniformly distributed class II levels (a picket fence model for the class II states) is given by Lynn

and Back [LB74] :

$$\bar{P}_f = \left[1 + \left(\frac{\bar{T}'}{\bar{T}_f} \right)^2 + 2 \left(\frac{\bar{T}'}{\bar{T}_f} \right) \coth \left[\tfrac{1}{2} \left(T_A + T_B \right) \right] \right]^{-1/2} \qquad (4.91)$$

where $\bar{T}_f$ is the average fission transmission coefficient equ. (3.20)

$$\bar{T}_f = \frac{T_A \, T_B}{T_A + T_B} \qquad (4.92)$$

Thus whenever intermediate structure effects are expected to be important in the average fission cross section, the fission transmission coefficient entering the statistical model expression equ. (3.6) should be replaced by an effective transmission coefficient

$$T_{f,\alpha}^{(J)} = \frac{\bar{P}_f^{(J)}}{1 - \bar{P}_f^{(J)}} \sum_{c'} T_{c'}^{(J)} \qquad (4.93)$$

where the sum over c' includes all non-fission channels.

It should be kept in mind that the equations of this section are valid only for $\Gamma_{II} \gg D_I$, which is, however, mostly true for neutron energies where average fission cross sections are of interest. In particular, we have assumed that the neutron widths of all resonances are equal to $\langle \Gamma_n \rangle$. For the case of narrow class II states, $\Gamma_{II} \lesssim D_I$, however, it has been shown in subsection 4.3.1., that the resonance with the largest class II fraction and thereby the largest fission width, has a much smaller neutron width. This fact then further reduces the fission probability. It is shown in [LB74] that under certain simplifying assumptions (constant matrix elements v_{ok} and neglect of cross terms in the square of the sum on the right hand side of equ. (4.56)), the effective fission probability for the case $\Gamma_{II} < D_I$ can be calculated in a straight forward manner from the equations of subsection 4.3.1.

4.9 Open Problems

During the discussions of this chapter we met a few open problems which we will briefly recall here.

In the last section we discussed the effects of intermediate structure on average fission cross sections. This was done in a pure picket-fence model : We assumed constancy of all class II and class I parameters, including class I neutron widths. A more rigorous treatment which combines both, the variation of fission width expectation values due to intermediate structure and statistical fluctuations of individual widths, is not readily available. Some insight into this problem might be gained by Monte-Carlo simulations for a few typical situations.

As discussed in subsection 4.1.3., for the detailed description of resonance - cross sections of fissile nuclei, a rigorous R-matrix formalism which includes resonance-resonance interference, should be used. However, partial fission widths which are required for this purpose, are defined by equ. (4.29) only for a situation where only one of the two fission barriers is important. In a situation where the two barrier heights are about equal, $E_A \approx E_B$, equ.(4.30) and (3.20) define an effective total fission width, but no consistent description of resonance-resonance interference is available. The definition of a partial fission width with the aid of equ. (3.20), where T_A and T_B would now be specialised to an individual Bohr channel, would neglect the possibility of K-mixing in the class II states.

In section 4.5 we encountered severe discrepancies between fission barrier parameters obtained from sub-barrier neutron resonance data on the one hand and average cross sections, including charged particle induced fission, on the other hand. This discrepancy is not understood; it should lead to a re-investigation of the interpretation of both types of data and possibly also to additional and more comprehensive experimental studies of resonance data.

5. Structure due to Vibrational Resonances

In the discussion of chapter 4 we have made a distinction between class I and class II states according to whether the equilibrium deformation of the nucleus corresponds to the first or second well of the deformation potential. But we have treated all members of each class on an equal basis. This has been done although at the end of chapter 3 we had made a distinction between vibrational levels Φ_ν and other levels χ_μ describing the state with respect

to the intrinsic degrees of freedom. In this chapter we will discuss structure effects related to the necessity of this further distinction.

5.1 Damped Vibrational Resonances

The fact that in chapter 4 we have ignored the distinction between vibrational and other degrees of freedom, is equivalent to the assumption of "complete damping", i.e. the assumption that the strengths of the vibrational states Φ_ν are statistically distributed among the product states φ_λ of equ. (3.39) and (3.40). This assumption will be correct, and we will continue to use it, for the first well of the deformation potential. But, as will be discussed in what follows, it may be incorrect for the secondary well.

As discussed at the end of chapter 3, it is really the tailing off of the vibrational wave functions through the barriers which, at sub-barrier energies, allows for both, fission of the class II states as well as their coupling to the class I states. In other words : As far as the class II states are concerned, the vibrational levels $\Phi_{\nu\,II}$ play the role of doorway states with respect to both, the fission channel as well as the coupling to class I. This means that the situation may be described in a similar fashion as has been done in the discussion of general class II doorways in section 4.3. Since the coupling between the vibrational and other levels is due to the strong particle vibration interaction, we will usually be dealing with "braod" doorways and a condition analogous to sub-section 4.3.2. will be fulfilled : The strength of the state $\Phi_{\nu\,II}$ will, in picket-fence approximation, be distributed among the $\varphi_{\lambda\,II}$ according to a Lorentzian distribution.

The vibrational state $\Phi_{\nu\,II}$ now has two possibilities of decay by tunnelling through the inner and outer barrier, and we will call the respective widths Γ_A and Γ_B. Consequently both, the widths $\Gamma^\downarrow$ and $\Gamma^\uparrow$ of the individual class II compound levels $\varphi_{\lambda\,II}$ will follow the Lorentzian distribution:

$$\Gamma_i^\downarrow = \frac{D_{II}}{2\pi} \frac{\Gamma_A \Gamma_D}{(E_i' - E_{\nu_{II}})^2 + \frac{1}{4}\Gamma_V^2} \qquad (5.1)$$

$$\Gamma_i^\uparrow = \frac{D_{II}}{2\pi} \frac{\Gamma_B \Gamma_D}{(E_i' - E_{\nu_{II}})^2 + \frac{1}{4}\Gamma_V^2} \qquad (5.2)$$

Here, E_i' is the energy of the class II compound level in question, and $E_{\nu\,II}$ the energy of the vibrational state $\Phi_{\nu\,II}$. The width of these distributions is

$$\Gamma_V = \Gamma_A + \Gamma_B + \Gamma_D \qquad (5.3)$$

where Γ_D is the damping width due to the particle vibration coupling.

Equ. (5.3) has already been mentioned in subsection 3.3.4. (equ.(3.33)). As has also been mentioned before, the magnitude of Γ_D depends on the density ρ_{II} of the class II compound levels, and it thereby depends strongly on the excitation energy in the second well. Usually Γ_D will be by far the largest contribution to Γ_V and will be considerably larger than D_{II}. Exceptions to this situation will be discussed in section 5.2.

The strong dependence of the damping width of the vibrational levels on the excitation energy is also the reason for our assumption of complete damping in the first well.

5.1.1. Experimental evidence for fragmented vibrational resonances.

The first, and still the most impressive example of a fragmented vibrational resonance, i.e. a damped vibrational resonance for which the fragmentation into individual class II levels is observed, has been found not in a neutron-induced reaction, but in ^{239}Pu(d,pf) by Specht et al. [Sp69]. Their results are shown in fig. *19* : The lower half represents the proton yield from the ^{239}Pu(d,p) reaction, whereas the upper half shows protons in coincidence with fission, thus essentially the fission probability. The number of individual peaks observed in the fragmented vibrational level at ~ 4.9 MeV excitation energy, roughly agrees with what is expected if the class II level spacing observed by James and Patrick [JP69] at neutron binding energy, $D_{II} \approx 500$ eV (subsection 4.6.2.), is extrapolated down to that excitation energy.

For neutron-induced fission, fragmented vibrational resonances are probably seen in ^{234}U + n and in ^{238}U + n.

In their study of ^{234}U + n, James et al. [Ja77] interprete an enhancement of fission strength at ~ 310 keV neutron energy as a fragmented vibrational resonance. Their data are shown in fig. *20* In their analysis, James et al.

use Monte-Carlo techniques to generate class II state parameters essentially according to equ. (5.1) to (5.3), and from these to generate class I fission widths according to equ. (4.62). In this way they show that the structure of the cross section around 310 keV is in qualitative agreement with what is expected from barrier parameters and level spacings deduced from the low-energy resonance data.

The sub-barrier fission cross section data on ^{238}U [Di79] are those of the highest quality of all. Part of the data are shown in fig. 21 . The enhancement of fission strength between 120 and 170 keV neutron energy might be interpreted as being due to one or several fragmented vibrational resonances. The data have not yet been thoroughly analysed, but at first sight the fission strength does not seem to follow a pattern expected from equations (5.1) and (5.2) for a single vibrational level: The distribution is rather broad, and the onset at 120 keV as well as the fall off at 170 keV are rather sudden. Therefore, an interpretation in terms of at least two overlapping fragmented vibrational resonances seems preferable; e.g. if we were dealing with p-wave neutron interaction, these could be due to spins $1/2^-$ and $3/2^-$.

The point that we could be dealing with overlapping fragmented vibrational levels would not mean that we are already approaching the situation of complete damping : The latter would be characterised by a damping width exceeding the average spacing of vibrational levels of a given spin, whereas in the case of the ^{238}U fission cross section around 150 keV we were thinking of overlapping vibrational resonances of different spin.

5.1.2. Consequences for class II state parameters

The primary consequence of finite damping of class II vibrational levels into the bulk of other class II states has already been discussed: The widths $\Gamma^{\downarrow}$ and $\Gamma^{\uparrow}$ of the class II states are expected to be distributed according to the Lorentzian distributions equ. (5.1) and (5.2). These distributions are hard to verify experimentally: Individual values for $\Gamma^{\downarrow}$ and $\Gamma^{\uparrow}$ are usually obtained only for a very small number of sub-barrier fission clusters within an energy range which is much smaller than the widths of the distributions equ. (5.1) and (5.2) are expected to be. At higher neutron energies only fission areas integrated over entire class II clusters are usually obtained, as e.g. in the case of ^{238}U [Di79]. As discussed in section 4.6., a relation between these areas and $\Gamma^{\downarrow}$, $\Gamma^{\uparrow}$, can only be given (equ. (4.86)) in picket-fence approximation for broad class II states ($\Gamma_{II} \gg D_I$). For narrow class II states like in the case of ^{238}U, the class II fission area depends too strongly on the accidental energy difference between the class II and its nearest class I neighbour and on the neutron width of the latter.

There is another consequence of finite damping which could be verified experimentally if a few sub-barrier fission clusters have been fully analysed, even in a very limited energy range : Equations (5.1) and (5.2) tell that $\Gamma^{\downarrow}$ and $\Gamma^{\uparrow}$ of different class II levels are strictly proportional:

$$\Gamma_i^{\downarrow} / \Gamma_i^{\uparrow} = \Gamma_A / \Gamma_B \qquad (5.4)$$

This proportionality still holds if we leave the picket-fence approximation : Fluctuations are due to fluctuations in the coefficients $C_{\nu_{\beta/\pi}}^{\lambda s}$ of equ. (3.40) and effect both $\Gamma^{\downarrow}$ and $\Gamma^{\uparrow}$ in the same way. If more than one vibrational level are important in a given energy region, the proportionality equ. (5.4) is lost, but if the effective number of vibrational levels is very small, the correlation between $\Gamma^{\downarrow}$ and $\Gamma^{\uparrow}$ will persist. This phenomenon of width correlations is typical for a mechanism where doorways common to two (or more) channels are involved. It has been described extensively by Lane [La72].

5.1.3. Consequences for average cross sections

As was the case for structure due to individual class II states, also structure due to class II vibrations exists only for energies close to and below the barrier tops, i.e. over an energy region of ~ 2 MeV at maximum. On the other hand, the widths of vibrational structures are of the order of 50 to 200 keV. Thus it is not reasonable to really average over vibrational structures especially not in the threshold region where the fission cross section changes strongly (~ factor of 2) anyhow within 100 keV intervals.

Thus, in order to incorporate the effect of vibrational resonances in the calculation of average cross sections, one may proceed in the following way: One may still use the equations of section 4.8., however the quantities T_A and T_B would now no longer be given by the simple barrier transmission expression equ. (3.18). They would rather be defined by equ. (4.90), with $\Gamma^{\downarrow}$ and $\Gamma^{\uparrow}$

being given by equ. (5.1) and (5.2), thus

$$\Gamma_X = \frac{\Gamma_X \Gamma_D}{(E - E_{\nu II})^2 + \frac{1}{4}\Gamma_\gamma^2} \qquad X = A, B \qquad (5.5)$$

In these equations the widths Γ_A and Γ_B of the vibrational resonance are now given by the barrier penetrability expression equ. (3.28) :

$$\Gamma_X = \frac{\hbar\omega_X}{2\pi} \frac{1}{1 + \exp\left[-\frac{2\pi(E - E_X)}{\hbar\omega_X}\right]} . \qquad (5.6)$$

The positions $E_{\nu II}$ of the vibrational resonances can be obtained from calculations of the penetrability of the double humped barrier, as discussed in subsection 3.3.3. The damping width Γ_D, finally, has to be obtained from phenomenology.

5.2. Undamped Vibrational Resonances

The fission cross sections of a few nuclei exhibit very strong and narrow resonances in the threshold region. One of the most distinct examples is the resonance at 720 keV neutron energy in the ^{230}Th(n,f) cross section which has been studied in detail by James et al.[Ja72]. From the small width of this resonance they concluded that it was due to an undamped vibrational level, i.e. a vibrational level which was not fragmented into any more complex class II excitations. The only complication which unavoidably had to exist was a rotational band built on the intrinsic vibrational state. Thus the observed peak in the fission cross section was interpreted by James et al. [Ja72] as a superposition of narrow, nearly Lorentzian shaped, resonances with a spin sequence according to a rotational band with K = 1/2; this K-value was deduced from data on the angular distribution of the fission fragments.

The fact that apparently no damping of the vibrational resonance occurred was interpreted by the hypothesis that the secondary well in the ^{231}Th was very shallow. Then the vibrational level would be at very low excitation energies in that well where there simply are no more complex class II states into which the vibrational level could be fragmented. In the extreme the observed vibrational resonance could even be the ground state (zero point vibration) in that well.

Similar strong and narrow resonances which probably have to be interpreted as undamped vibrational levels are observed in the fission cross sections of ^{232}Th and ^{231}Pa.

5.2.1. The Thorium "anomaly"

The interpretation of the strong narrow resonances in the fission cross sections of Th and Pa isotopes as undamped vibrational levels implies that the secondary well in these nuclei is very shallow. It also implies that the height E_A of the first barrier is considerably above neutron binding energy. Both these conclusions are in contradiction to essentially all calculations of the deformation energy potential by the Strutinsky - and related methods. The situation is illustrated in fig. 22 , where calculated heights of the first barrier, second minimum, and second barrier, are compared to values deduced from experiments. The calculations are those of Møller and Nix [MN73] based on the macroscopic - microscopic method with the droplet model and a folded Yukawa potential. The solid lines give the heights relative to the calculated ground state energy, the dashed lines those relative to the experimental ground state energy. Whereas in general there is reasonable agreement, at least if the heights calculated relative to the experimental ground states are considered, predicted and experimental values for the first barrier and second minimum in the Th-isotopes fall apart by 2.5 to 3 MeV. This fact has become known as the so-called Th-anomaly.

5.2.2. The third minimum hypothesis

Møller and Nix [MN74] have proposed the following solution to the problem of the Th-anomaly : In their calculations of deformation energy potentials, Møller and Nix include mass asymmetric deformations. It has already been noted in section 2.3 that the inclusion of mass asymmetric deformations has the general effect of lowering the height of the second barrier. According to the calculations of Møller and Nix, in the lighter actinide nuclei this effect goes so far that an asymmetric third minimum develops at deformations corresponding to the original second barrier. As an example, fig. 23 shows the deformation potential of ^{240}U in the region of the second barrier, in the form of a contour plot of the potential energy in a two-dimensional plain of deformation

coordinates; the vertical axis represents asymmetric deformations. As can be seen, a third asymmetric minimum has developed between two asymmetric saddle points of almost equal height.

The proposal of Møller and Nix is that the undamped vibrational resonances in the fission cross sections of the Th- and Pa- isotopes represent low-lying vibrational states in this third minimum rather than the second one. Likewise, what was believed to be the first barrier, is replaced by the (second) asymmetric saddle point in front of the third minimum. The heights of both, third minimum and second saddle point would roughly agree to what is required in order to explain the experimental facts. If the true first barrier is as low as predicted by the calculations, it would have no influence on the neutron-induced fission cross sections of these isotopes. This is schematically illustrated in fig. 24 , which shows the deformation potential finally felt by a light actinide nucleus on its path to fission.

5.2.3. The ^{230}Th(n,f) reaction

As mentioned above, James et al. [Ja72] had interpreted the 720 keV resonance in the fission cross section of ^{230}Th as an undamped K = 1/2 vibrational level with a rotational band built on top of it, although the individual rotational states were not resolved in their data. Therefore, a new high resolution (1.7 keV FWHM) measurement was recently performed by Blons et al. [Bl78]. The measured fission cross section in the region of the vibrational resonance is shown in fig. 25 . It exhibits more structure than can be explained by a single K = 1/2 rotational band.

The interpretation of these data given by Blons et al. [Bl80] follows the arguments of Møller and Nix [MN74] : Assume that the resonance is due to vibrational level in a shallow asymmetrically deformed minimum similar to the one of fig. 23 . In fact there are two such minima at positive and negative values of the deformation coordinate ϵ_3 describing mass asymmetric deformations. The wave functions of stationary states in such a potential can be even or odd with respect to reflections at $\epsilon_3 \approx 0$. In other words : Levels in the third minimum would exist as almost degenerate pairs of levels with opposite parities. Thus, instead of just one K = 1/2 rotational band, one would expect two bands with $K = 1/2^+$ and $K = 1/2^-$ superimposed upon each other. This is the way the data of fig. 25 have been interpreted. The spins of the individual components of the two rotational bands are indicated in the figure. The energies of the two rotational bands follow the relationship :

$$E(J) = E_0 + \frac{\hbar^2}{2\theta}\left[J(J+1) - K(K+1) + a\,(-1)^{J+1/2}(J+1/2)\right] \qquad (5.7)$$

with the same value for the rotational constant, namely

$$\frac{\hbar^2}{2\theta} = (2 \pm 0.1)\ keV \qquad (5.8)$$

Due to the symmetry properties of the rotational wave function of a nucleus with a stable octupole deformation, the decoupling parameter a ought to have opposite sign, but the same absolute value, for the two rotational bands with opposite parities [BM 75]. The a-values derived [Bl80] from the level positions as indicated in fig. 25 , fulfil this requirement :

$$a(K^\pi = 1/2^+) = 1.3 \pm 0.2 \qquad a(K^\pi = 1/2^-) = -1.5 \pm 0.2$$

The above value of $\hbar^2/2\theta$ is considerably smaller than the one obtained by Specht et al. [Sp72] for the second minimum in ^{240}Pu, i.e. $\hbar^2/2\theta(^{240}\text{Pu}) = 3.33$ keV; this implies a considerably larger deformation for the ^{230}Th case, thus supporting the hypothesis that in ^{230}Th we are dealing with the third minimum.

The analysis of Blons et al. [Bl80] also includes a statistical model calculation of the ^{230}Th(n,f) cross section, in order to check whether the interpretation of the observed structure in terms of the assumed rotational bands is consistent with physically reasonable reaction parameters (neutron strength functions, inelastic scattering competition, etc.). It is shown that the relative strengths of the individual components of the two rotational bands can be reproduced very nicely by the statistical model calculation.

Finally it is shown in [Bl80] that the assumed rotational bands are in agreement with the available data on fission fragment angular distributions. However, such data are scarce, and generally suffer from a relatively poorer energy resolution. Additional experimental work on this subject would be very useful.

5.2.4. Data on ^{232}Th(n,f)

Two experimental studies of the ^{232}Th(n,f) cross section have recently been performed [Pl79,Bl79]. Fig. 26 shows the fission cross section as measured [Bl79] with a resolution of ~ 2.3 keV at 1.6 MeV. Besides the strong vibrational resonances which were known for a long time, a considerable amount of structure is seen in fig. 26 . The number of individual peaks observed between 1.33 and 1.7 MeV neutron energy corresponds to a level spacing of about 8.5 keV. Assuming that not much more than half of the levels has been missed and that the observed levels are due to neutron interaction with orbital angular momenta of $\ell = 0, \ldots, 3$, the level spacing is explainable in terms of a well depth of ~ 1 MeV, i.e. an excitation energy of that well of ~ 5.3 MeV with respect to the first well. This again would agree to the predicted height of the third rather than the second well. Further, at an excitation energy of ~ 1 MeV K is still expected to be a good quantum number; thus it should be possible to identify individual rotational bands. However, seen the complexity of the structure in fig. 26 this is not an easy task. Detailed measurements of the fragment angular distribution would help very much here. The data available on the angular distribution [Bl75,Pl79] suffer from comparatively poorer energy resolution and statistics, but they at least show that most of the broad maximum at ~ 1.6 MeV neutron energy, is probably K = 3/2.

5.2.5. The case of ^{231}Pa(n,f)

A high resolution measurement of the fission cross section of ^{231}Pa has recently been performed by Plattard et al. [Pl79b]. Their data are shown in fig. 27 . The most remarkable feature is the strong narrow resonance at 157 keV neutron energy. It had been interpreted already earlier [Si76] as a $K^\pi = 3^+$ vibrational resonance. This interpretation would explain why additional rotational levels are apparently unobserved : They would have to be formed by $\ell = 3$ neutrons and therefore have peak cross sections of σ_f (max) $\lesssim$ 1 mb, whereas the $J^\pi = 3^+$ bandhead would be formed by $\ell = 1$ neutrons. If the asymmetric third minimum hypothesis is correct, two of the smaller peaks between 170 keV and 190 keV neutron energy would have to be associated with $K = 3^-$ and $J = 3^-$ and 4^- levels which would be formed by $\ell = 2$ neutrons and thus have peak cross sections of the order of σ_f(max) $\simeq$ 10 mb.

The $K^\pi = 3^+$ barrier responsible for the 157 keV vibrational resonance ought to have two maxima (the second and third, if we are dealing with the third minimum) of nearly equal height: This is necessary in order to simultaneously explain the small width of the resonance and a peak transmission value between 0.5 and 1, say. In contrast to this barrier, the one responsible for the broad maximum in the fission cross section between 180 and 200 keV neutron energy, assigned K = 0 by Sicre [Si76], may be due to a barrier with rather different maxima: A large transmission through one of the maxima would be responsible for the large width of that resonance, whereas a low transmission through the other barrier would explain the low peak cross section.

5.3. Open Problems

The most challenging experimental problems are measurements of the fission fragment angular distribution with energy resolutions equivalent to those of the cross section measurements of figures 25 , 26 and 27 , in order to verify the angular momentum assignments of the individual rotational levels. Further improvement of the energy resolution of fission cross section measurements would also be helpful : Individual rotational levels could possibly be better resolved, or their natural width due to barrier penetrabilities could eventually be determined. However, all these experiments would probably require a considerable improvement in the characteristics of pulsed neutron sources.

Another interesting problem is the following : Assume that the calculations [e.g. MN74] which led to the picture of the triple-humped barrier of fig. 24 with a low first maximum, are correct. Then there is a broad range of excitation energies, essentially from the top of the first barrier up to somewhat below the second barrier, for which population of the shape isomer within the second well is rather probable: Below neutron separation energy, the probability for decay to the isomeric state divided by the probability for decay to the ground state would roughly be given by

$$R = \frac{\rho_{II}}{\rho_{I}} \frac{\Gamma_\gamma(II)}{\Gamma_\gamma(I)} \qquad (5.9)$$

which would be of the order of a few times 10^{-3}. The shape isomer would decay by γ-emission with a half-life determined by the penetrability of the first barrier. The detection of the shape isomer , the measurement of its

half-life and excitation function would provide a valuable verification of the deformation energy potential as calculated by e.g. Møller and Nix [MN74].

6. Data needed for Actual Calculations

As has been seen from the discussion in the preceding chapters, actual calculations of unknown cross sections require the knowledge of several nuclear parameters, most of which are functions of the excitation energy :

For the calculation of fission transmission coefficients one needs to know the barrier parameters, i.e. barrier heights E_A and E_B and curvatures $\hbar\omega_A$ and $\hbar\omega_B$.

The most important parameters needed are nuclear level densities, of which at least three different kinds have to be known : the density of (class I) compound states; for the calculation of inelastic cross sections the density of low-lying states of the target nucleus; and for fission transmission coefficients the density of barrier transition states (Bohr channels).

Finally neutron transmission coefficients or, equivalently, strength functions as well as radiative widths have to be known.

It cannot be the intention here to give a recommended set of parameters. The aim of the discussion in this chapter rather is to draw attention to some important points which should be kept in mind when parameter sets are established.

Nuclear theory is far from being sufficiently accurate to directly yield the required parameters. They should rather be taken from experiment whenever possible. However, nuclear theory can and should be used to establish systematic trends and thereby extrapolate empirical parameter sets into regions unexplored by experiment, to the best of our knowledge.

Another general remark is necessary here : Parameters like barrier properties and transition state densities are generally obtained from the analysis of experimental data in an indirect way. There is usually no unique solution. In other words : Values obtained for a certain parameter type may depend on the assumption made about another one. It is therefore preferable to use parameter sets originating from the same source. At any rate, any attempt to calculate a cross section should include the calculation of and comparison to an experimentally well-known cross section for a neighbouring nucleus such that re-adjustment of critical parameters can be done.

6.1. Barrier Parameters

At present the most complete sets of barrier parameters are those of Britt [Br79] and of Lynn [Ly74]. The parameter set of Britt is based on the analysis of a large variety of charged particle induced fission data measured at Los Alamos. This analysis differs from the older ones of Back et al. [Ba73, Ba74] by the inclusion of more recent experimental data and by modified assumptions about the density of barrier states (see below).

The barrier parameters of Lynn are based partly in the same type of data including the older Los Alamos data, but neutron-induced fission data, essentially average cross sections, are also included.

Unfortunately, there are important and systematic differences between the barrier parameters as given by Britt and Lynn : For even-even compound nuclei Lynn's barriers are systematically lower, by up to 0.5 MeV, than those of Britt. For odd A nuclei, the discrepancies are less systematic, but sizeable in many cases.

These differences may be partly due to different assumptions made about barrier state densities and to different approximations used in the treatment of intermediate structure effects on average fission cross sections (see section 4.8).

Moreover, for the few cases where information from neutron resonance studies is available, there are the additional discrepancies discussed already in section 4.5.

It thus is apparent that no definite set of barrier parameters can be recommended at present, and that the barrier parameter sets of Britt [Br79] and Lynn [Ly74] should be used only in conjunction with barrier state densities and other parameters used by the same authors.

6.2. Density of States at Normal Deformation

Nuclear level densities for normal deformation i.e. densities of class I states, are required over a wide range of excitation energies : First of all, the density of compound nuclear levels is needed at the relevant excitation energy of the compound nucleus; but for the same nucleus the level density all the way down to zero excitation energy is needed to calculate radiative widths (see equ. 3.14). Further, the density of states at low excitation energies in the target nucleus is required for the calculation of the inelastic scattering cross section.

For the high excitation energies of the compound nucleus it is usually assumed that the Fermi-gas level density expression

$$\rho(U, J^{\pi}) = \frac{(2J+1)\, e^{-J(J+1)/2\sigma^2}}{\sqrt{8\pi}\ \sigma^3}\ \omega(U)$$

$$\omega(U) = \frac{\sqrt{\pi}}{12\ a^{1/4}\ U^{5/4}}\ e^{2\sqrt{aU}} \qquad (6.1)$$

$$U = E - \delta_E - \delta_N$$

gives a sufficiently accurate description of the level density. The level density parameter a, the spin cut-off factor σ and the pairing energy corrections δ_E , δ_N may be obtained from phenomenology and systematics, or they may be calculated with the aid of microscopic theories from the density of single particle states. However, they should be adjusted to the observed spacings of s-wave neutron resonances whenever these are available.

A warning should be added here with respect to "experimental" neutron resonance spacings : Only resonance spacings corrected for missed levels and admixtures of p-wave resonances should be used. Values for a number of actinide nuclei are given in [Wg78] and [Ro80].

At intermediate energies, i.e. roughly between 1 MeV and an energy somewhat below neutron binding energy (where the Fermi-gas expression becomes valid), a constant temperature level density is more appropriate. Due allowance of rotational levels must be made. At still lower energies it will be best to take into account individual experimentally known levels, or to use empirically known level schemes in order to estimate the level density. Level schemes at these low energies of course strongly depend on the even-odd character of the nucleus in question. Simple empirical expressions for the intermediate and low energy regions which smoothly join the Fermi-gas expression for the higher energies are given by Lynn [Ly74].

A more profound calculation of level densities is possible by the so-called microscopic methods, as described, e.g. by Moretto [Mo72]. Here the density of intrinsic states is calculated directly from realistic single particle level schemes or approximations thereof. The total level density is then obtained by addition of the proper rotational bands. Such calculations provide level densities for essentially all except very low excitation energies, but they involve considerable numerical work. A more handable analytic parametrization of microscopic level densities has been given by Jensen and Sandberg [JS78].

As long as the calculated level densities are adjusted to experimental neutron resonance spacings, the more empirical formulae may be not much worse than the microscopic theories. However, if extrapolation to nuclei for which no resonance data are available, is required, the microscopic theories may be more profound. A simple empirical extrapolation procedure applicable to the Fermi-gas approximation has recently been proposed by Rohr [Ro79].

6.3. Density of Barrier States

Our empirical knowledge about the density of barrier transition states is much poorer than it is for states at normal deformation. Essentially the only source of empirical information are the fission cross sections themselves.

For even-even nuclei the lowest barrier states are, of course, predictable : The lowest barrier will be $K^{\pi} = 0^{+}$ with its associated rotational band built on top of it. Since the outer barrier is assumed to be asymmetric with respect to reflections, a $K^{\pi} = 0^{-}$ band will be present at essentially zero excitation energy. For the axially asymmetric inner barrier the $K^{\pi} = 2^{+}$ γ-vibrational band is expected to occur at comparatively low excitation energies. With these considerations in mind, Lynn [Ly74] has proposed a level scheme for barrier states at low excitations (< 1 MeV) of even-even nuclei.

For odd nuclei, and for even-even nuclei at higher excitations, predictions must essentially come from microscopic theories. They seem to indicate [Br79] that the density of intrinsic states at the barriers is not very different from the one at normal deformations, for the same excitation energies : This is due to two compensating effects : The increased density of single particle states at barrier deformations has as a consequence an increased level density at comparable effective excitation energies, but also an increased pairing energy which roughly compensates the first effect.

An important difference arises when rotational states are included. As has been pointed out by Bjørnholm, Bohr and Mottelson [Bj73], the loss of axial symmetry at the first barrier leads to a drastic increase in the number of rotational levels, by a factor of about 7 to 8 as compared to the first

minimum. Thus the net level density at the first barrier is expected to be larger by almost an order of magnitude than at the first minimum.

The second barrier is believed to be axially symmetric again, but the reflection asymmetry is expected to lead to an enhancement of the level density by a factor of 2 due to the almost-degeneracy of positive and negative parity states. Thus the net level density at the second barrier may be only slightly above the density at normal deformations.

Simple constant temperature parametrizations of the barrier state densities as obtained from fits to a few typical fission cross sections, are again given by Lynn [Ly74]. The parameters of Lynn [Ly74] indicate a somewhat higher level density at the second barrier than would be expected from the above qualitative arguments. More accurate predictions for individual nuclei would have to be done by microscopic calculations.

6.4. Neutron Strength Functions

Empirical data are practically available only on s- and p-wave neutron strength functions, and even for these usually only the overall strength function $s(\ell)$ is obtained from

$$s(\ell) = \frac{1}{2\ell+1} \frac{\langle g \Gamma_n(\ell)/2P_\ell \rangle}{\langle D(\ell) \rangle} \qquad (6.2)$$

rather than the strength functions $s_{J\ell s}$ of equ. (3.1.1) for individual compound nuclear spins and channels. The relation between the two is :

$$s(\ell) = \frac{1}{2\ell+1} \sum_{J=|I-\frac{1}{2}|}^{I+\frac{1}{2}} \sum_{j=|\ell-\frac{1}{2}|}^{\ell+\frac{1}{2}} g(I,J)\, s_{J\ell j} \qquad (6.3)$$

In equ. (6.2) $D(\ell)$ is the spacing of resonances for given orbital angular momentum ℓ, irrespective of the compound spin J, as opposed to D_J entering equ. (3.8). Also, $\Gamma_n(\ell)$ may contain contributions from two channels, if the spin of the resonance in question can be obtained in two ways of combining the orbital angular momentum ℓ with the channel spins I -1/2 and I +1/2.

By convention, neutron strength functions are usually written as

$$S_\ell = \frac{1}{2\ell+1} \frac{\langle g \Gamma_n^{(\ell)} \rangle}{\langle D(\ell) \rangle} \qquad (6.4)$$

with the definition

$$\Gamma_n^{(\ell)} = \Gamma_n / v_\ell \sqrt{\frac{E_n}{1\,eV}} \qquad (6.5)$$

such that

$$s(\ell) = S_\ell \frac{v_\ell}{2P_\ell} \sqrt{\frac{E_n}{1\,eV}} = S_\ell \frac{1}{2\rho} \sqrt{\frac{E_n}{1\,eV}} \qquad (6.6)$$

The empirical data on strength functions are either due to the analysis of average cross sections or of neutron resonance parameters. Strength functions obtained from the analysis of average cross sections are often dependent on assumptions made about other nuclear parameters; in particular, the decomposition of the average cross section into contributions from individual orbital angular momenta is often not unique and leads to large uncertainties in the resulting strength function values.

On the other hand, strength functions deduced from resonance parameters represent "local" values, obtained from resonances within a limited energy interval. It has recently been recognised that short range energy dependences of strength functions are not uncommon, at least for medium weight nuclei (see, e.g. [Wg79] and [St 79]). As long as the origin of these structures is not understood, similarly energy-dependent strength functions cannot be excluded for the actinide nuclei, and care has to be taken in the use of strength functions deduced from the parameters of low-energy neutron resonances.

If no empirical data are available, as is the case for $\ell \gtrsim 2$ for almost all nuclei, neutron strength functions may be calculated from the optical model (see lectures of P.A. Moldauer at this course).

6.5. Radiative Widths

The excitation energy dependence of total radiative widths is obtained from equ. (3.14) where the partial widths $\Gamma_{\gamma I}^{(J)}(E_\gamma)$ are given either by the strong coupling dipole model, equ. (3.15) or by the giant dipole resonance model, equ. (3.16). In either case the parameters of the model should be adjusted to reproduce the observed radiative width of low-energy resonances. For nuclei where no such experimental values are available, equ. (3.14) must be used to calculate the absolute values of radiative widths, with the parameters deduced from systematics. Radiative widths calculated in this way from the giant

dipole resonance model for many actinide nuclei at neutron binding energy, are given by Lynn [Ly74].

6.6. Open Problems

The most severe problems encountered in this chapter were associated with the existing discrepancies between empirical values for barrier parameters, the remaining uncertainty and complication in the establishment of transition state densities, and in particular the interconnection between the uncertainties of these data sets. The recommendation given at the beginning of this chapter, namely to use parameter sets originating from a single source, can of course be regarded only as an ad-hoc solution taken in view of these problems. It is very desirable that further discussion and evaluation work lead to some consensus with respect to individual parameter sets and to recommendations for the establishment of level densities, especially of barrier transition states.

7. Summary

In these lectures we have discussed the present status of our understanding of the cross sections for neutron-induced fission. Apart from the basic theoretical interpretation of phenomenological data, we have been concerned with the establishment of a theoretical framework which could be used for extrapolations and calculations of experimentally unknown cross sections. We have recognised several areas where our understanding is insufficient, and further work, both experimentally and with respect to the interpretation of available data, is required in order to improve our knowledge and thereby the accuracy and reliability of predicted cross sections : The interpretation of the cross sections of the light actinides by the hypothesis of a third minimum in the deformation potential has to be verified. More generally, the uncertainty in fission barrier parameters should be reduced. Probably the most important problem is the one of barrier transition states : At higher excitation energies their densities, and at low excitation energies also their spin sequence should further be investigated.

References

Au 71 G.F. Auchampaugh, J.A. Farrell and D.W. Bergen, Nucl. Phys. A171 (1971) 31

Au 73 G.F. Auchampaugh and C.D. Bowman, Phys. Rev. C7 (1973) 2085

Au 8D G.F. Auchampaugh, J.D. Moses, J.A. Harvey and N.W. Hill, private communication

AW 75 G.F. Auchampaugh and L.W. Weston, Phys. Rev. C12 (1975) 1850

Ba 73 B.B. Back, O. Hansen, H.C. Britt and J.D. Garrett, Phys. Rev. C9 (1973) 1924

Ba 74 B.B. Back, H.C. Britt, D. Hansen, B. Leroux and J.D. Garrett, Phys. Rev. C10 (1974) 1948

BB 74 J.C. Browne and C.D. Bowman, Phys. Rev. C9 (1974) 1177

BF 71 D.W. Bergen and R.R. Fullwood, Nulcear Physics A163 (1971) 577

Bj 73 S. Bjørnholm, A. Bohr and B.R. Mottelson, "Physics and Chemistry of Fission 1973", Vol. I, p.367; IAEA, Vienna 1974

Bl 70 J. Blons, H. Derrien and A. Michaudon, "Nuclear Data for Reactors", IAEA, Vienna (1970) 513

Bl 75 J. Blons, C. Mazur and D. Paya, Phys. Rev. Lett. 35 (1975) 1749

Bl 78 J. Blons, C. Mazur, D. Paya, M. Ribrag and H. Weigmann, Phys. Rev. Lett. 41 (1978) 1282

Bl 79 J. Blons, C. Mazur, D. Paya, M. Ribrag and H. Weigmann, "Physics and Chemistry of Fission 1979", paper B9 IAEA, Vienna 1980

Bl 80 J. Blons, C. Mazur, D. Paya, M. Ribrag and H. Weigmann, Proc. XVIII Int. Winter Meeting on Nuclear Physics, Bormio, January 1980

BM 69 A. Bohr and B. Mottelson, "Nuclear Structure" Vol. I, p. 302; Benjamin Inc. New York 1969

BM 75 A. Bohr and B. Mottelson,
"Nuclear Structure" Vol. II, p. 17; Benjamin Inc. New York 1975

Bo 72 M. Bolsterli, E.O. Fiset, J.R. Nix and J.L. Norton,
Phys. Rev. C5 (1972) 1050

Br 72 M. Brack, J. Damgaard, A.S. Jensen, H.C. Pauli, V.M. Strutinsky and C.Y. Wong,
Rev. Mod. Phys. 44 (1972) 320

Bra79 M. Brack,
"Physics and Chemistry of Fission 1979", paper C1
IAEA, Vienna 1980

Bri79 H.C. Britt,
"Physics and Chemistry of Fission 1979", paper A1
IAEA, Vienna 1980

BW 39 N. Bohr and J.A. Wheeler,
Phys. Rev. 56 (1939) 426

CN 70 J.D. Cramer and J.R. Nix,
Phys. Rev. C2 (1970) 1048

Di 79 F.C. Difilippo, R.B. Perez, G. de Saussure, D.K. Olsen and R.W. Ingle,
report ORNL/TM - 6788

Dr 59 L. Dresner,
report ORNL - 2659 (1959)

Fu 68 A. Fubini, J. Blons, A. Michaudon and D. Paya,
Phys. Rev. Lett. 20 (1968) 1373

Ig 69 A.V. Ignatyuk, N.S. Rabotnov and G.N. Smirenkin,
Phys. Lett. 29B (1969) 209

Ja 72 G.D. James, J.E. Lynn and L. Earwaker,
Nucl. Phys. A189 (1972) 225

Ja 77 G.D. James, J.W.T. Dabbs, J.A. Harvey, N.W. Hill and R.H. Schindler,
Phys. Rev. C15 (1977) 2083

JP 69 G.D. James and B.H. Patrick,
"Physics and Chemistry of Fission",
IAEA, Vienna (1969), 391

JS 78 A.S. Jensen and J. Sandberg,
Physica Scripta 17 (1978) 107

KB 68 W. Kolar and K.H. Böckhoff,
"Neutron Cross Sections and Technology", Vol. I, p. 519
NBS Special Publication 299 (1968)

Ke 73 G.A. Keyworth, J.R. Lemley, C.E. Olsen, F.T. Seibel, J.W.T. Dabbs and N.W. Hill,
Phys. Rev. C8 (1973) 2352

La 72 A.M. Lane,
"Statistical Properties of Nuclei",
J.B. Garg, ed., Plenum Press, New York 1972

LB 74 J.E. Lynn and B.B. Back
J. Phys. A 7 (1974) 395

LL 73 S.E. Larsson and G. Leander,
"Physics and Chemistry of Fission 1973", Vol. I, p. 177
IAEA, Vienna 1974

LT 58 A.M. Lane and R.G. Thomas,
Rev. Mod. Phys. 30 (1958) 257

Ly 74 J.E. Lynn,
UKAEA report AERE - R7468 (1974)

Ly 78 J.E. Lynn,
"Fission Barrier Theory and its Application to the Calculation of Actinide Neutron Cross Sections",
Lectures given at the ICTP/IAEA-NDS Course on Nuclear Theory for Applications, Trieste 1978

Mi 73 A. Michaudon,
"Advances in Nuclear Physics",
M. Baranger and E. Vogt, ed., Vol. 6, Plenum Press, New York 1973

MN 70 P. Møller and S.G. Nilsson,
Phys. Lett. 31B (1970) 283

MN 73 P. Møller and J.R. Nix,
"Physics and Chemistry of Fission 1973", Vol. I, p. 103;
IAEA, Vienna 1974

MN 74 P. Møller and J.R. Nix,
Nuclear Physics A229 (1974) 269

Mo 67 P.A. Moldauer,
Phys. Rev. 157 (1967) 907

Mo 72 L.G. Moretto,
Nucl. Phys. A182 (1972) 641

Mo 78 M.S. Moore, J.D. Moses, G.A. Keyworth, J.W.T. Dabbs and N.W. Hill,
Phys. Rev. C18 (1978) 1328

MS 69 W.D. Myers and W.J. Swiatecki,
Ann. Phys. 55 (1969) 395

MT 68 E. Migneco and J.P. Theobald,
Nucl. Phys. A112 (1968) 603

MW 69 C. Mahaux and H.A. Weidenmüller,
"Shell-Model Approach to Nuclear Reactions"
North Holland Publishing Co. Amsterdam 1969

Ni 55 S.G. Nilsson,
Kgl. Dan. Vid. Selsk.,
Mat. - Fys. Medd. 29 (1955) No. 16

Ni 69 S.G. Nilsson, C.F. Tsang, A. Sobiczewski, Z. Szymanski, S. Wycech,
C. Gustafson, I.L. Lamm, P. Møller and B. Nilsson,
Nucl. Phys. A131 (1969) 1

Pa 69 V.V. Pashkevich,
Nucl. Phys. A133 (1969) 400

Pl 76 S. Plattard, J. Blons and D. Paya,
Nucl. Sci. Eng. 61 (1976) 477

Pl 79 S. Plattard, G.F. Auchampaugh, N.W. Hill, R.B. Perez and G. de Saussure,
"Physics and Chemistry of Fission 1979", paper B11
IAEA, Vienna 1980

Pl 79b S. Plattard, G.F. Auchampaugh, N.W. Hill, G. de Saussure, R.B. Perez and
J.A. Harvey,
Proc. Intern. Conf. on Nuclear Cross Sections for Technology,
Knoxville 1979, to be published

Po 73 F. Poortmans, G. Rohr, J.P. Theobald, H. Weigmann and G. Vanpraet,
Nucl. Phys. A207 (1973) 342

Po 80 F. Poortmans, E. Cornelis, L. Mewissen, G. Rohr, R. Shelley,
T. van der Veen, G. Vanpraet and H. Weigmann,
to be published

RM 58 C.W. Reich and M.S. Moore,
Phys. Rev. 111 (1958) 929

Ro 79 G. Rohr, L. Maisano and R. Shelley,
NEANDC Specialists' Meeting on Neutron Cross Sections of Fission
Product Nuclei,
Bologna 1979, to be published

Ro 80 G. Rohr, L. Maisano and R. Shelley,
to be published

Sc 71 D. Scharnweber, W. Greiner and U. Mosel,
Nucl. Phys. A164 (1971) 257

Si 76 A. Sicre, Ph.D. Thesis, University of Bordeaux, 1976
report CENBG 7603

Sp 69 H.J. Specht, J.S. Fraser, J.C.D. Milton and W.G. Davies,
"Physics and Chemistry of Fission",
IAEA, Vienna (1969) 363

Sp 72 H.J. Specht, J. Weber, E. Konecny and D. Heunemann,
Phys. Lett. B41 (1972) 43

St 67 V.M. Strutinsky,
Nucl. Phys. A95 (1967) 420

St 79 P. Staveloz, E. Cornelis, L. Mewissen, F. Poortmans, G. Rohr,
R. Shelley and T. van der Veen,
Proc. Intern. Conf. on Nuclear Cross Sections for Technology,
Knoxville 1979, to be published

Wg 68 H. Weigmann,
Z. Phys. 214 (1968) 7

Wg 74 H. Weigmann, G. Rohr, T. van der Veen and G. Vanpraet,
Second Int. Symp. on Neutron Capture Gamma Ray Spectroscopy and
Related Topics,
Petten, N.H., RCN 1974

Wg 78 H. Weigmann,
Proc. of Intern. Conf. on Neutron Physics and Nuclear Data,
Harwell 1978, p. 969

Wg 79 H. Weigmann, S. Raman, J.A. Harvey, R.L. Macklin and [illegible]slaughter,
Phys. Rev. C20 (1979) 115

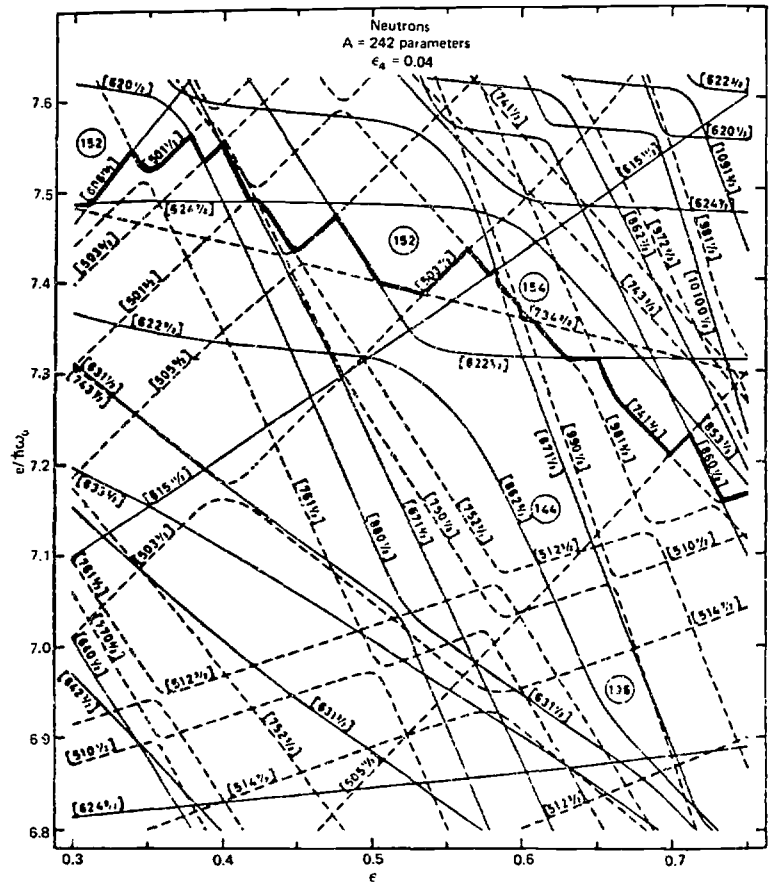

Fig. 1 : Nilsson diagram of single neutron levels as a function of the deformation parameter ϵ (for ϵ_4 = 0.04) as calculated by Nilsson et al. [Ni69]. The bold solid line indicates the highest level occupied for N = 152 ; figure taken from [Mi73].

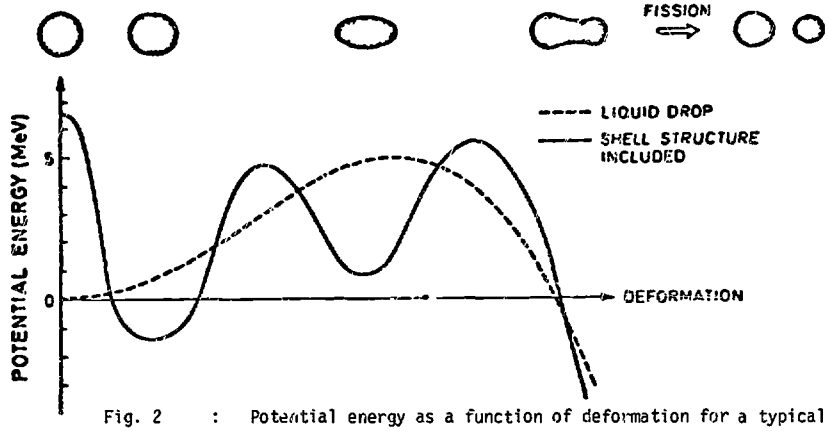

Fig. 2 : Potential energy as a function of deformation for a typical actinide nucleus.

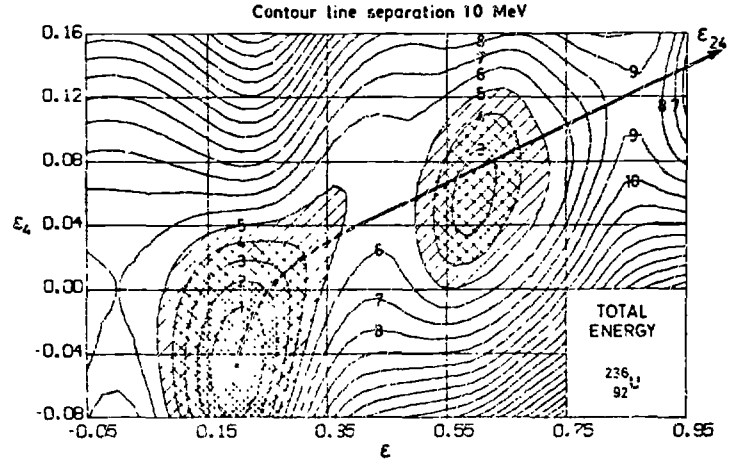

Fig. 3 : Contour plot of the potential energy in the (ϵ,ϵ_4)- plane of deformation coordinates, as obtained by Møller and Nilsson [MN70] ; figure taken from [LL73].

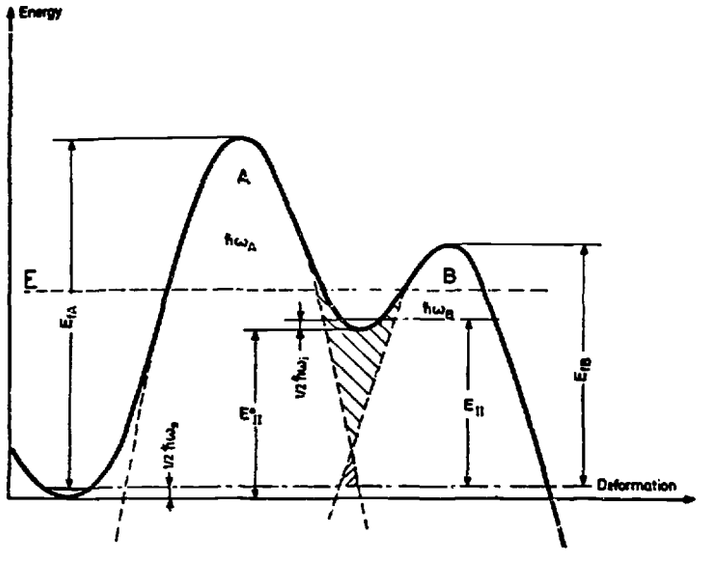

Fig. 4 : Parametrization of the double-humped fission barrier in terms of two parabolic barriers; figure taken from [Mi73].

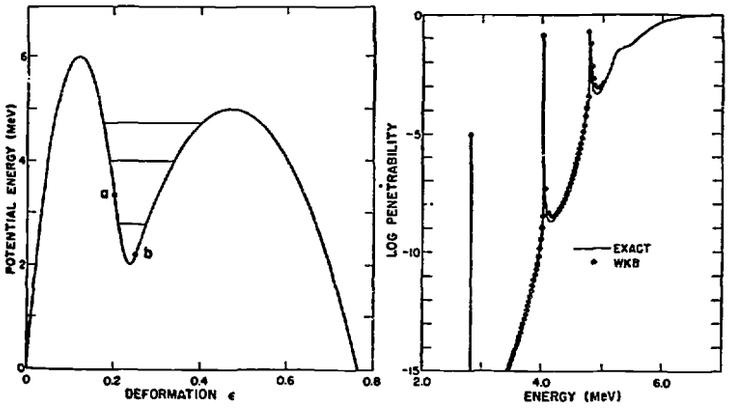

Fig. 5 : a) Fission barrier for which exact penetrability calculations have been performed by Cramer and Nix. The barrier is constructed of three paraboles joined at points a and b.

b) Comparison of exact calculations and WKB approximation (equ. (3.3.5)) of the penetrability for the barrier shown in fig. a. The energy shift at the 4.76 MeV resonance between the WKB and exact calculation is 20 keV. The penetrabilites in the minimum above the 4.76 MeV resonance are $8.4 \cdot 10^{-4}$ and $5.2 \cdot 10^{-4}$ for the WKB and exact calculation respectively.

After Cramer and Nix [CN70].

The diff
important p
of J^{π}
resonances
and have a
$< \Gamma_{(f)}^{I^+} >$
section; th
influences
to-fission
energy regi
typical res
neutron inc
numerically
temperature
resonance s
obvious fro

4.

The usual
average fiss
mediate stru
barrier is c
the existenc
change the a
the simple s
expressions
the true ave
where the av
width fluctu
due to the s
fluctuations
concentrate
widths for w
$\Gamma >> \Gamma_f$, th

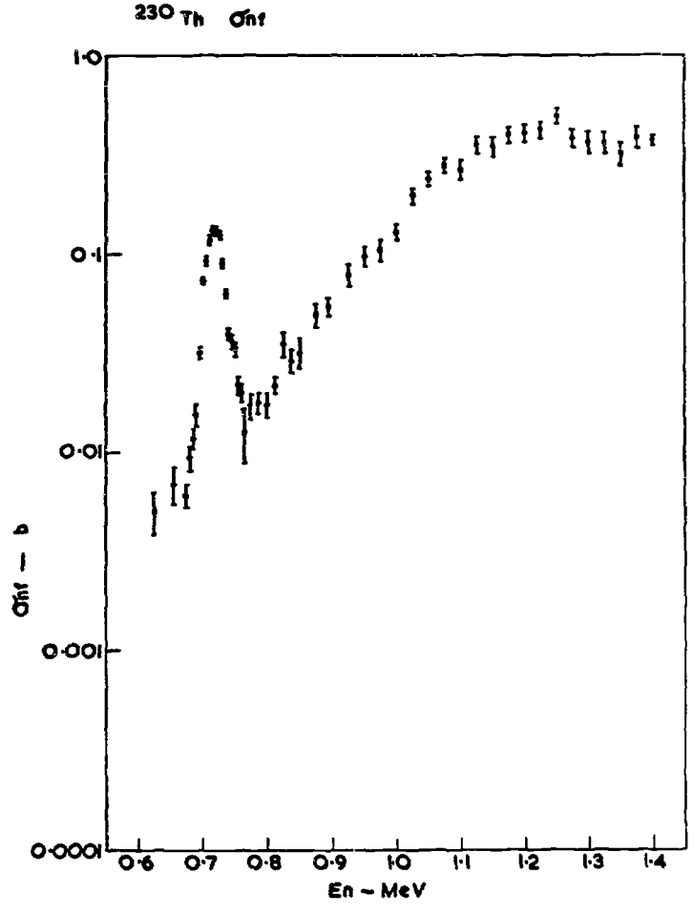

Fig. 6 : The neutron-induced fission cross section of ^{230}Th showing an isolated vibrational resonance. After James, Lynn and Earwaker [Ja72].

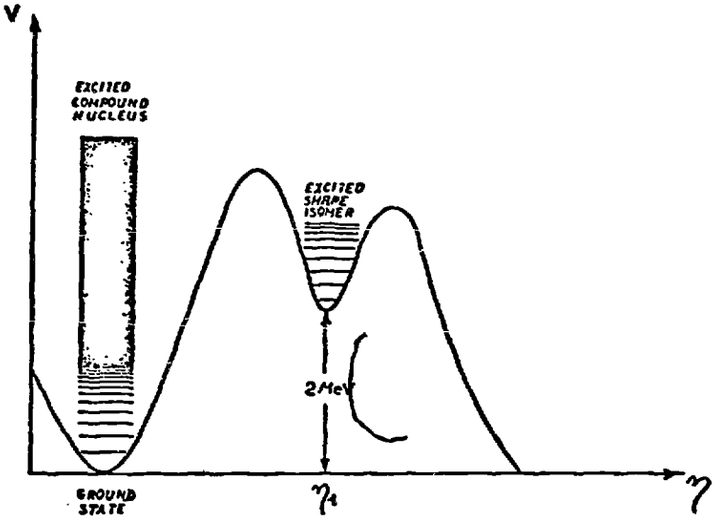

Fig. 7 : Excited states at deformation corresponding to the first and second well of the deformation potential.

and Back [LB74

$\overline{\rho}_f$

where $\overline{T}_f$ is th

$\overline{T}_f$

Thus whenever
the average fi
the statistica
transmission c

T_{f_i}

where the sum
It should b
for $\Gamma_{II} \gg D_I$,
fission cross
the neutron wi
narrow class I
4.3.1., that
largest fissio
reduces the fi
simplifying as
in the square
fission probab
forward manner

4.9

During the
will briefly r

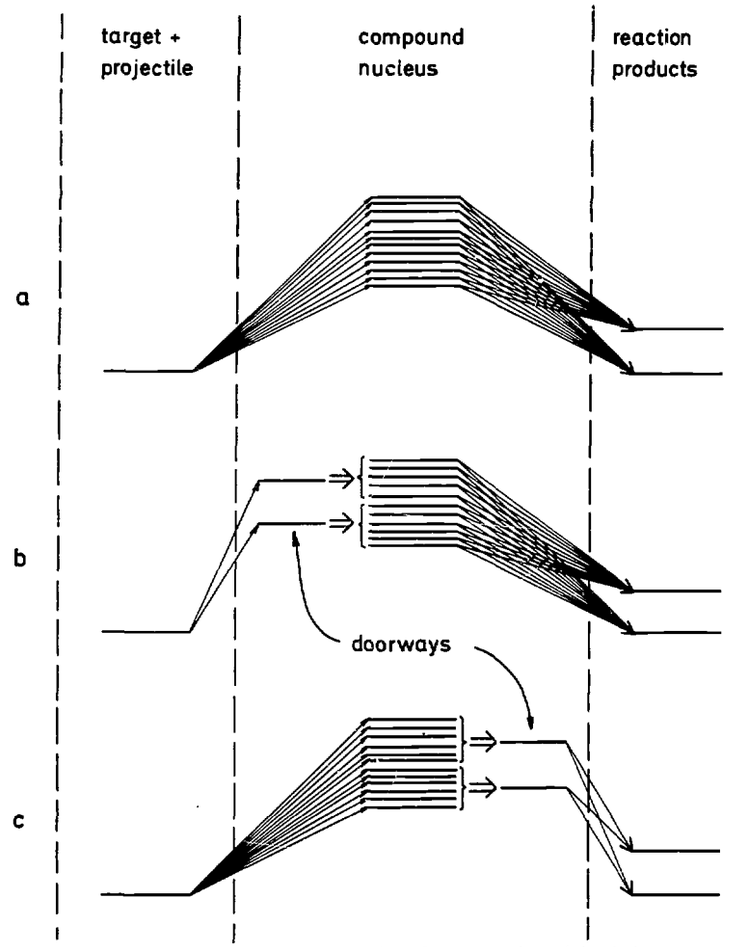

Fig. 8 : Illustration of a compound nuclear reaction without doorway states (a) and with doorway states with respect to the entrance (b) and exit (c) channels.

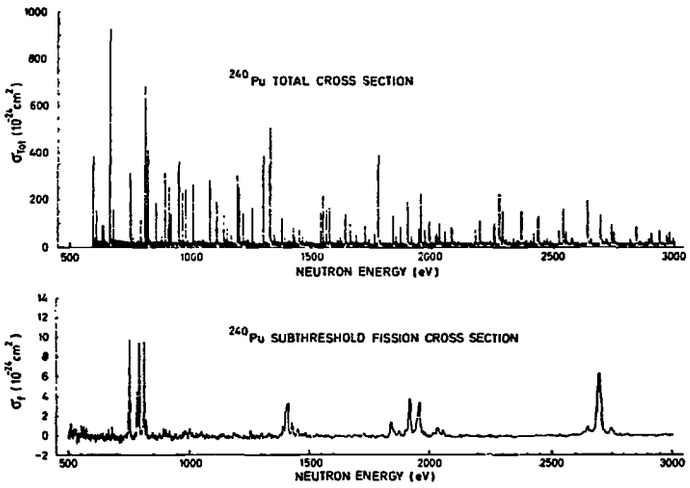

Fig. 9 : The neutron total [KB68] and sub-barrier fission [MT68] cross sections of ^{240}Pu as a function of neutron energy between 0.5 and 3 keV.

to the intr
effects rela

The fact
tional and
"complete da
states Φ_ν a
equ. (3.39)
to use it,
discussed i
As discus
vibrational
allows for
the class I
concerned,
respect to
means that
in the disc
coupling be
vibration i
condition a
the state Φ_ν
$\varphi_{\lambda II}$ accor
The vibra
through the
and Γ_B. Co
compound le

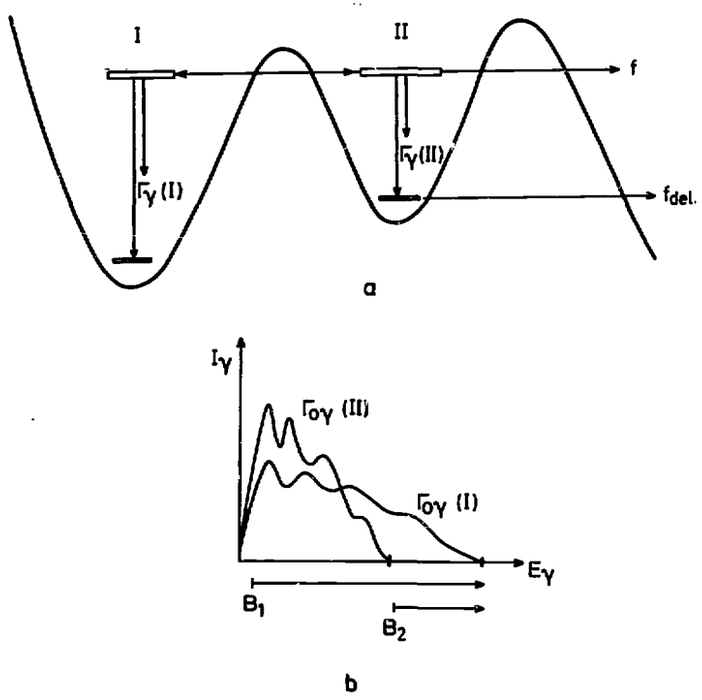

Fig. 10 : a) Various decay possibilities of a state with a major class II fraction.

b) Components of the capture γ-ray spectrum of that state due to decay within the primary and second wells.

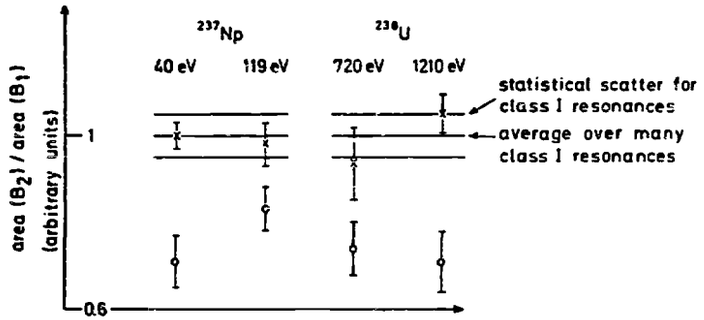

Fig. 11 : Ratios of capture areas for different bias values, normalized to 1 for class I resonances.

o values expected for two candidates for major class II admixture in each of the targets ^{237}Np and ^{238}U.

x measured values

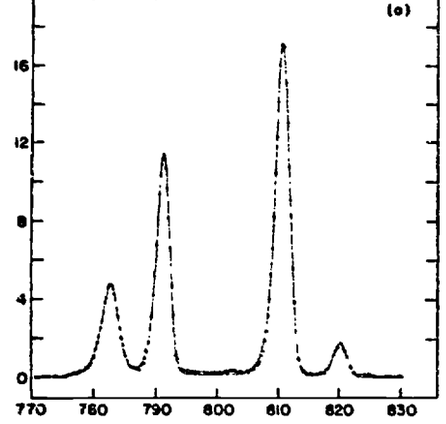

Fig. 12 : The neutron-induced fission cross section of ^{240}Pu in the region of the first sub-barrier fission cluster around 782 eV neutron energy; after Auchampuagh and Weston [AW75]

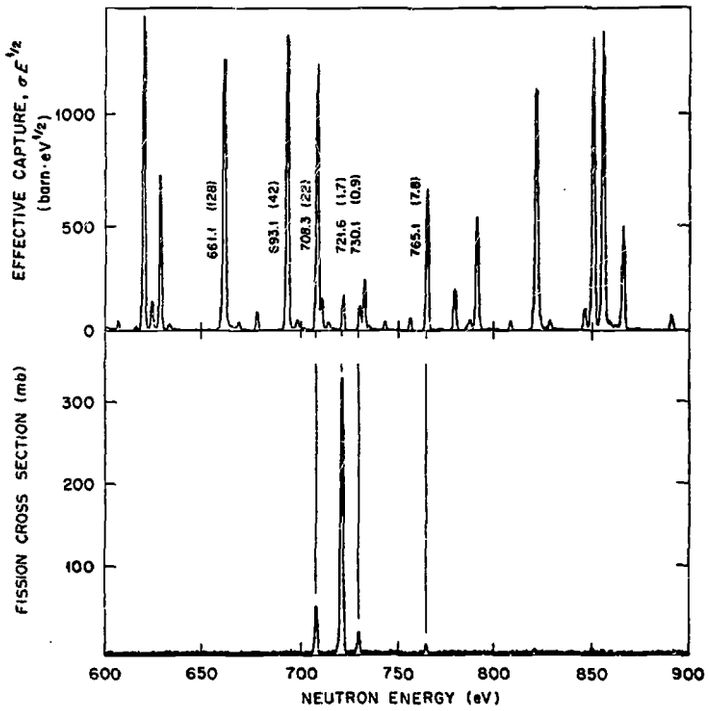

Fig. 13 : The $^{238}U(n,f)$ cross section (lower half) as compared to the $^{238}U(n,\gamma)$ cross section (upper half) between 600 and 900 eV neutron energy ; after Difilippo et al. [Di79]

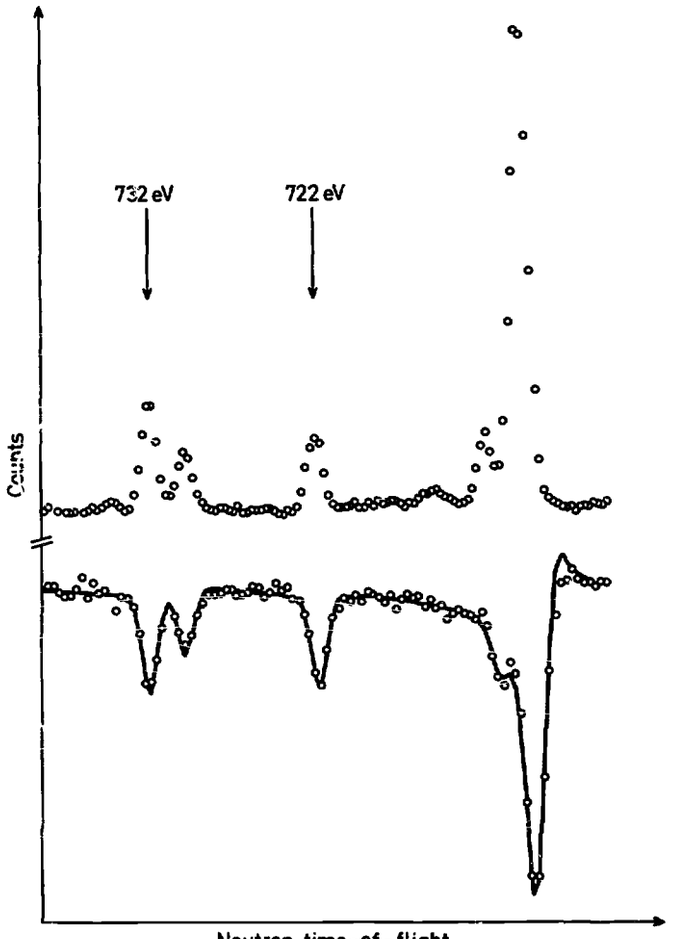

Fig. 14 : Comparison of neutron transmission (lower curve) and total capture (upper curve) data for resonances around 722 eV neutron energy in ^{238}U.

being giv

In these
given by

The posit
ations of
section 3
phenomen

The fi
resonance
resonance
studied i
they conc
tional le
The only
built on
cross sec
narrow, n
rotationa
distribut
The fa
was interp
shallow.
in that w
the vibra

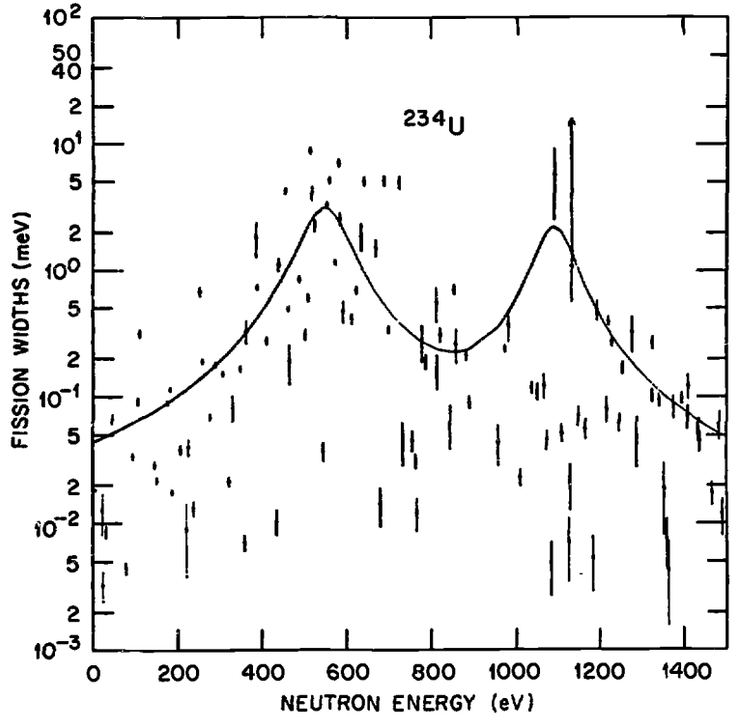

Fig. 15 : Distribution of fine structure fission widths of $^{234}U + n$ resonance and Lorentzian fit assuming class II levels at 530 eV and 1092.5 eV ; after James et al. [Ja77]

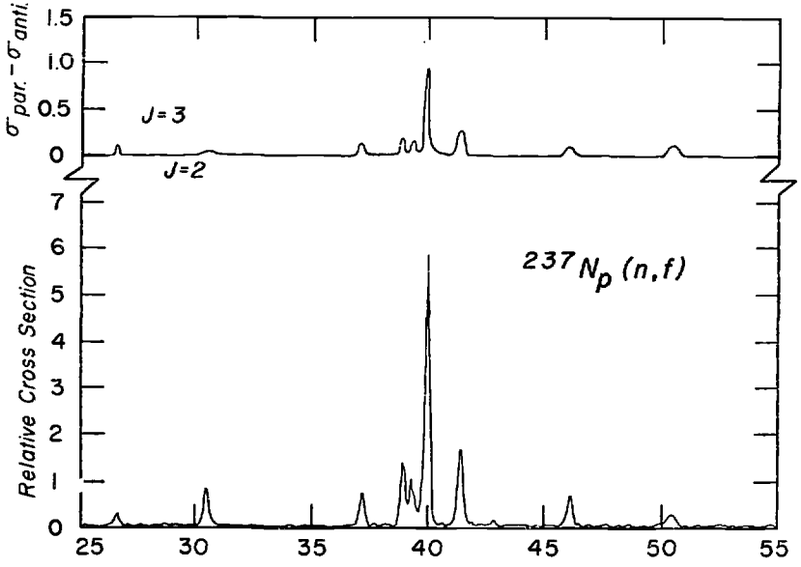

Fig. 16 : Relative fission cross section of ^{237}Np (lower part) and difference between cross sections observed with target and neutron spins parallel and antiparallel (upper part) ; The fact that the latter curve always remains positive, shows that $J = 3^+$ for all resonances within the cluster; after Keyworth et al. [Ke73]

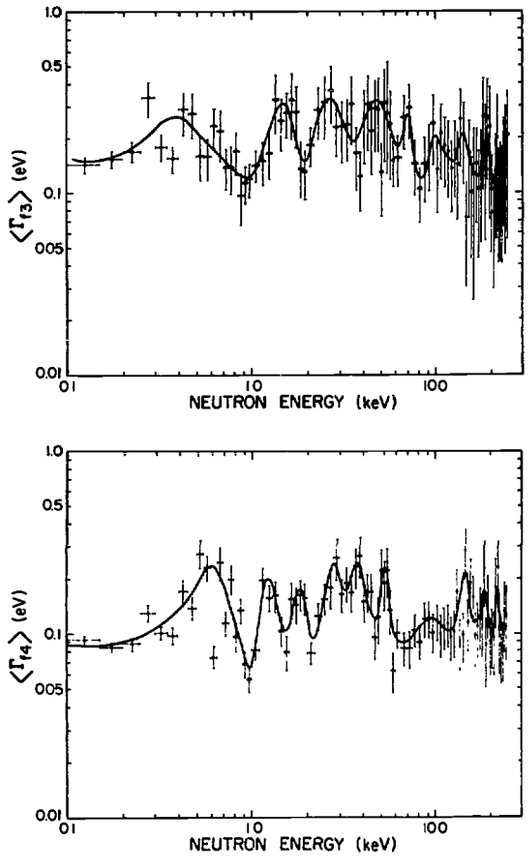

Fig. 17 : Average fission widths for ^{235}U + n as a function of neutron energy;
a) for channel spin 3 and
b) for channel spin 4 ;
after Moore et al. [Mo78]

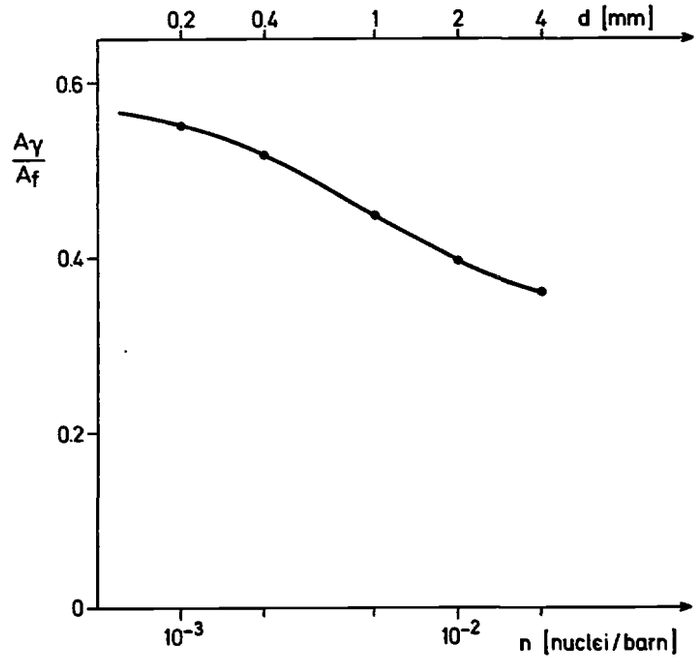

Fig. 18 : The effective capture-to-fission ratio for ^{239}Pu in the neutron energy range from 70 eV to 110 eV, calculated as a function of sample thickness (for sample thickness in mm assumed metallic Pu with ρ = 19.9 g/cm^3)

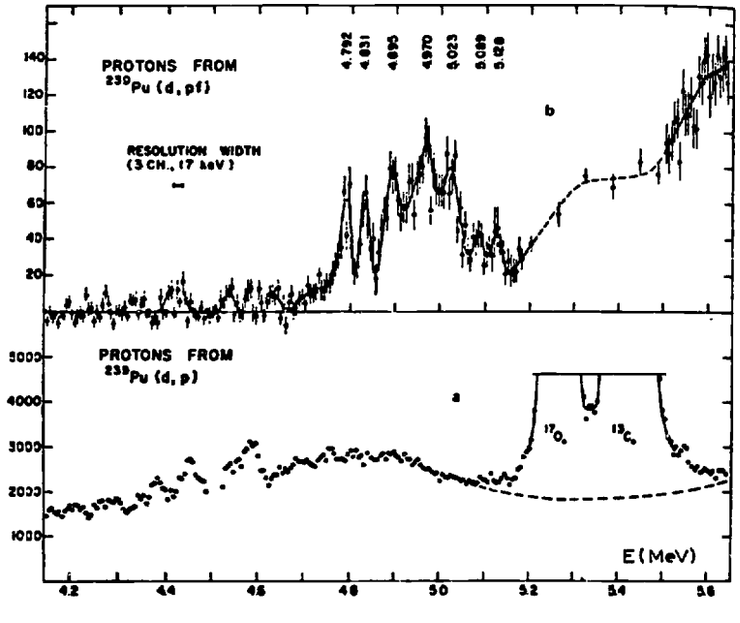

Fig. 19 : Spectra of proton singles (a) and protons in coincidence with fission (b) from the $^{239}Pu(d,p)$ and $^{239}Pu(d,pf)$ reactions as a function of the excitation energy in ^{240}Pu ; after Specht et al. [Sp69]

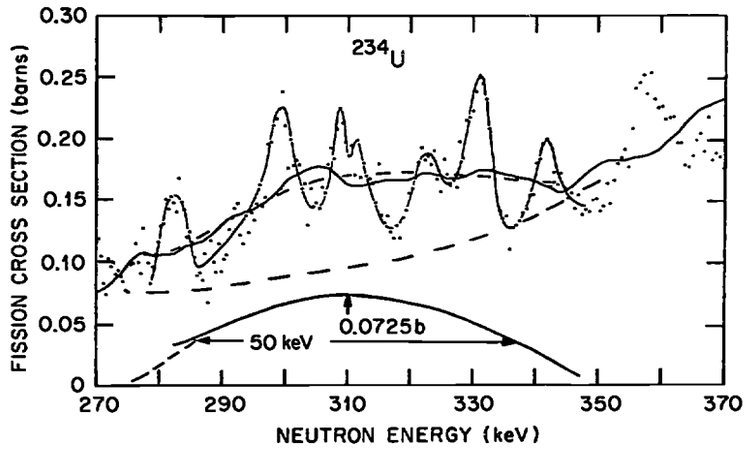

Fig. 20 : The fission cross section of ^{234}U around 310 keV neutron energy. The assumed contribution of the fragmented vibrational resonance is indicated by the two dashed lines and again by the diagram below the data ; after James et al. [Ja77]

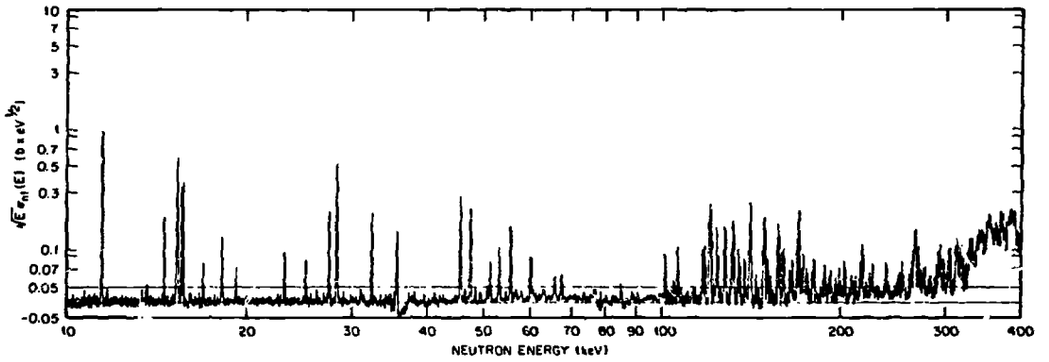

Fig. 21 : The neutron-induced fission cross section of ^{238}U, multiplied by E_n, between 10 and 400 keV neutron energy. The enhancement between 120 and 170 keV might be interpreted as being due to one or several fragmented vibrational levels ; after Difilippo et al. [Di79]

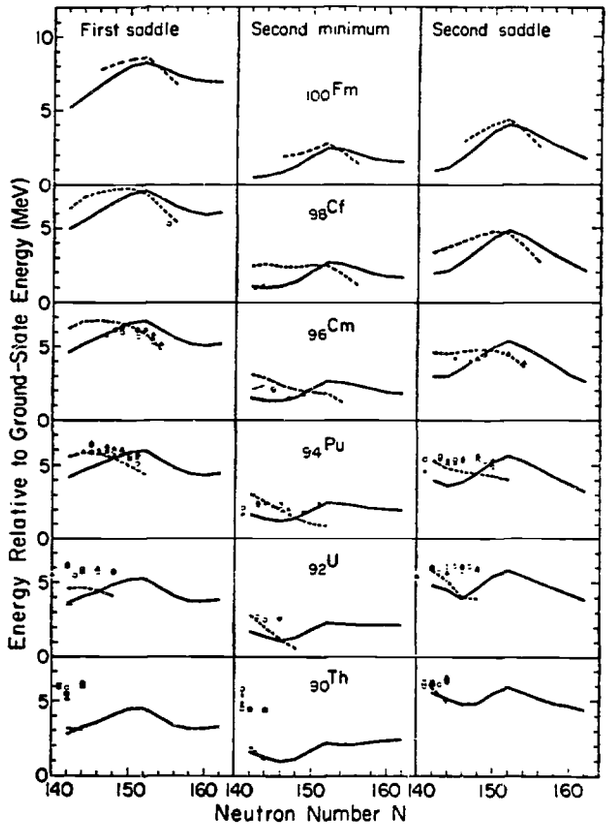

Fig. 22 : Heights of first barrier, second minimum and second barrier as calculated by Møller and Nix [MN73] are compared to values deduced from experiments; after [MN73]

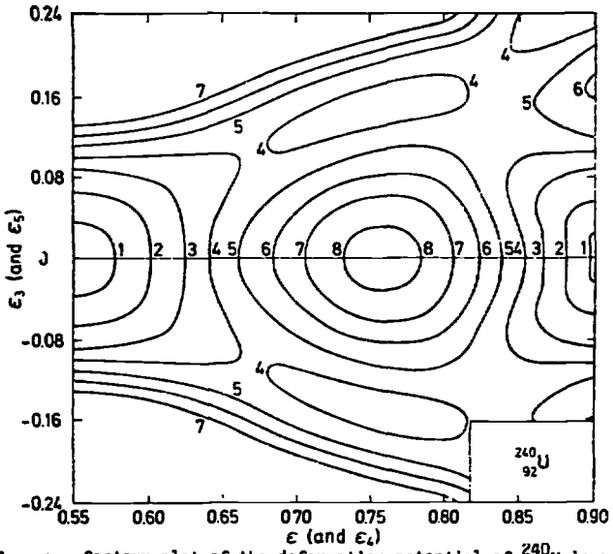

Fig. 23 : Contour plot of the deformation potential of ^{240}U in a two-dimensional plain of deformation coordinates. The curves are labelled in MeV relative to the spherical droplet model energy; after Møller and Nix [MN74]

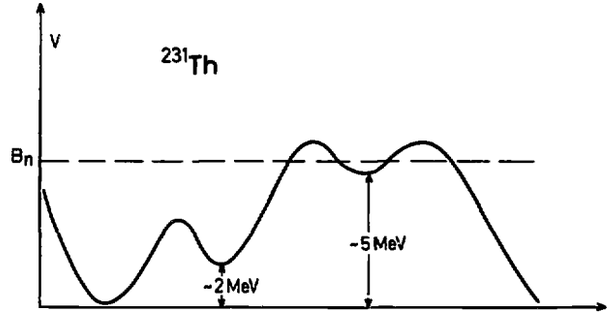

Fig. 24 : Schematic presentation of the deformation potential of Thorium isotopes with a low first barrier and a third minimum at the position of the original second barrier.

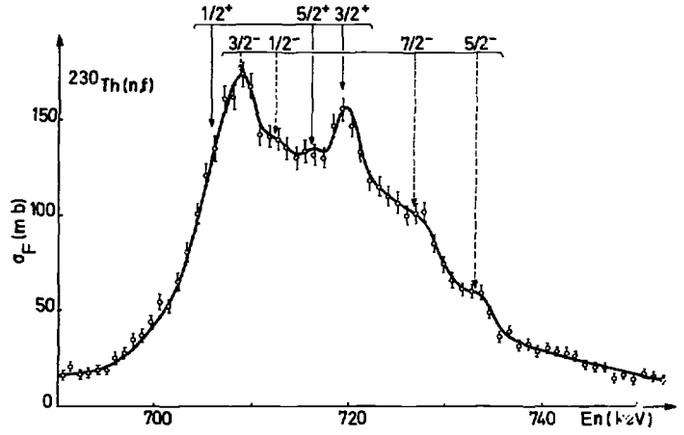

Fig. 25 : The measured fission cross section of ^{230}Th in the region of the vibrational resonance at 720 keV neutron energy; after Blons et al. [B178]

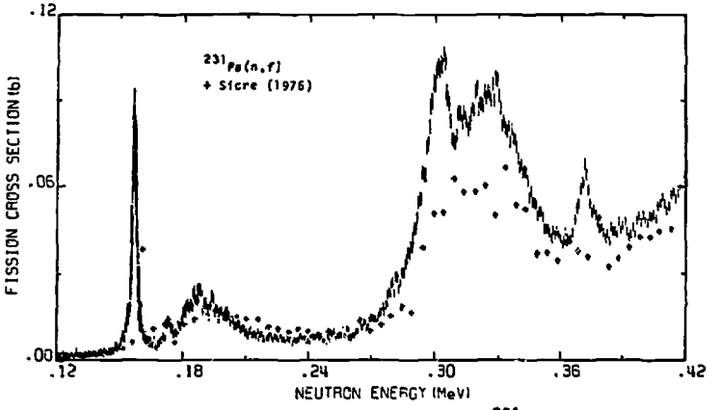

Fig. 27 : The measured fission cross section of ^{231}Pa showing the narrow vibrational resonance at 157 keV neutron energy ; after Plattard et al. [P179b]

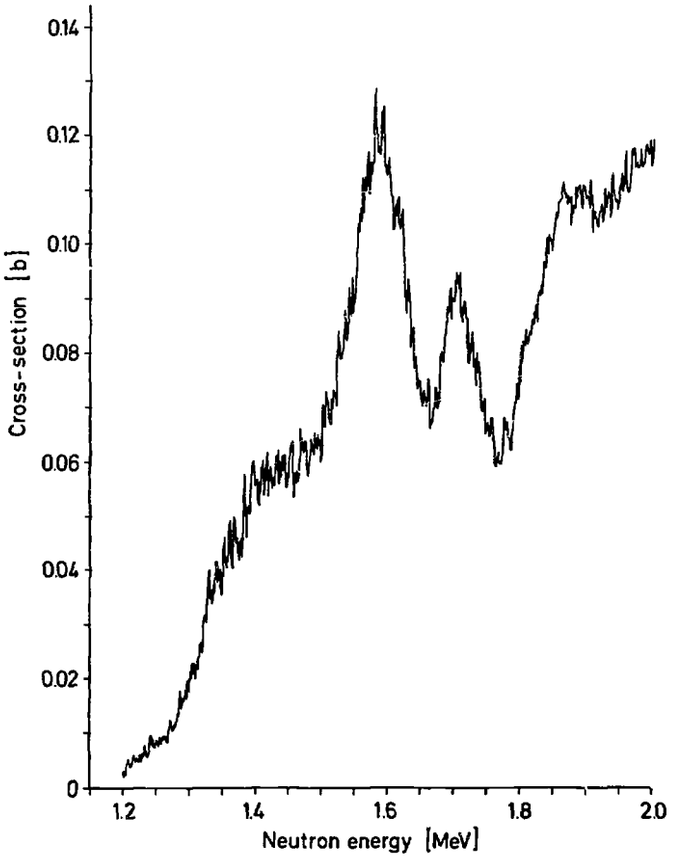

Fig. 26 : The measured [B179] fission cross section of ^{232}Th ; the strong vibrational resonances show a sub-structure possibly due to rotational states.

APPLICATIONS OF THE NUCLEAR THEORY TO THE COMPUTATION OF NEUTRON CROSS SECTIONS FOR ACTINIDE ISOTOPES

V.A. KONSHIN
Luikov Heat and Mass Transfer Institute,
BSSR Academy of Sciences,
Minsk,
Union of Soviet Socialist Republics

Abstract

Neutron cross section calculational methods for actinides in the unresolved resonance energy range (1-150 kev) are discussed, with a special emphasis on calculation of width fluctuation factors for the generalized distribution, as well as for a subthreshold fission. It is shown that the energy dependence of $\langle D \rangle_J$, the (n, n')-process competition and the structure in neutron cross section has to be taken into account in the energy range considered. Analysis of different approaches in the statistical theory for heavy nuclei neutron cross-section calculation is given, and it is shown to be important to allow for the $(n, \gamma f)$-reaction in neutron cross section calculations for fissile nuclei. The use of the non-spherical potential, the Lorentzian spectral factor and the Fermi-gas model involving the collective modes enables to obtain the self-consistent data for all neutron cross sections, including $\sigma_{n\gamma}$.

1. INTRODUCTION

Nuclear transactinide data are necessary to calculate the accumulation of these nuclei, to determine the changes in the reactor performances during long operation, to transport and process radiated fuel and to incinerate high actinides. It is natural that in the nearest future to get experimentally such a great amount of the data is extremely difficult. Therefore, in practice the acceptable way to obtain nuclear constants of nuclei, when there are no experimental data, is related to the theoretical methods of nuclear data evaluation involving carefully tested parameters used in the nuclear models.

The theoretical analysis of the experimental data enables to find parameters, e. g. such as optical model ones, that are required to calculate neutron cross sections for a wide scope of nuclei. To perform this task, it is necessary rather to analyse the systematic tendencies than to make specific calculations for a given nucleus. The modern state of art of the nuclear theory, when special models with carefully tested parameters are used, permits prediction of integral cross sections of heavy nuclei within 20-30%. The nuclear reaction theory should be considered as a means to obtain different parameters that may combine various experimental data. The main trend in nuclear data evaluation should be concentrated on the determination of a number of reliable parameters through the systematic self-consistent analysis of the experimental data accumulated.

Based on the statistical model, the formalism for neutron cross section calculations was developed long ago [1,2]. It may be considered that when the optical-statistical model is employed to calculate neutron cross sections for nuclei with middle A no difficulties arise, except some ones, due to several types of the nuclear potential that give a satisfactory agreement with the same experimental data and due to the nonunique choice of potential parameters. The contribution of correlation effects that are of importance but not yet sufficiently elaborated can lead to an increase in the reaction cross sections which may be larger than the one due to the direct reactions [3,4].

Some difficulties are associated with the optical-statistical model when used to calculate neutron cross sections for fissile nuclei since their evaluation is rather complex. The level of the nuclear fission theory developed at present is such that to predict

BM 75
Bo 72
Br 72
Bra79
Bri79
BW 39
CN 70
Di 79
Dr 59
Fu 68
Ig 69
Ja 72
Ja 77
JP 69
JS 78
KB 68

quantitatively fission cross sections is hardly possible. The theoretical predictions of fission barriers can be made within the 0.5-1.0 MeV accuracy [5] while the data evaluation requires the accuracy of about 100 keV. The fission process is the main competing process and should be thus allowed for in theoretical computations. The fission competition effect is very substantial and reaches about 80% at 50 keV for the inelastic scattering cross section, $\sigma_{nn'}$, for the first ^{239}Pu level. The correct account of the fission competition, especially for highly fissile nuclei, is a rather complex problem since the latter is associated with σ_f calculation.

Moreover, the heavy fissile nuclei possess a high density of the excited states which, as a result, can be resolved to relatively low energies. The low energy of the first level excitation requires to allow for the radiative capture competition in inelastic scattering cross section calculations.

One more circumstance is of importance here. If one type of a neutron cross section is calculated, then the agreement between the cross section of this type may be achieved due to the worse agreement between the cross sections of other processes, i. e. the information on the physics of a process may be lost. It is therefore necessary to make simultaneous calculation of all types of cross sections and to compare a greater number of the quantities in order to avoid the incorrect representation of the model accuracy.

2. NEUTRON ACTINIDE CROSS SECTION CALCULATIONS IN THE UNRESOLVED RESONANCE ENERGY RANGE (1-150 keV)

The unresolved resonance energy range for heavy nuclei is extending from several hundreds eV to a hundred keV. A knowledge of the average resonance parameters such as $\langle D\rangle_r$, $\langle\Gamma_n\rangle_r$, $\langle\Gamma_{n'}\rangle_r$, $\langle\Gamma_\gamma\rangle_r$, ν_{nr}, $\nu_{n'r}$, ν_{fr} in this range is necessary to correctly allow for the resonance self-screening and Doppler effects since this very range covers a considerable spectrum part of large fast breeders.

Average resonance parameters for the unresolved resonance region may be obtained in two ways: by averaging the parameters in the resolved resonance region with subsequent extrapolation to the unresolved one (the drawback of this method is associated with difficult spin and parity identification of levels) and by fitting the calculated average cross sections or transmissions to the experimental data in the unresolved resonance energy region (the shortcoming of this method is the introduction, into the defined parameters, of the error of the model used that requires a knowledge of the additional parameters). As a rule, the combined approach is advisable.

Usually the Hauser-Feshbach formalism [1] modified by Lane and Lynn [6] to allow for partial width fluctuations is used to calculate average cross sections in the unresolved resonance energy range and is valid in the case of no resonance interference and no correlations of widths for different processes. The expression for the average $\langle\sigma_{nx}\rangle_r$ cross section of the (n,x)-reaction and compound nucleus state r with the spin J and parity π is of the form:

$$\langle\sigma_{nx}\rangle_r = \frac{2\pi^2}{k^2}\,\frac{g_r}{\langle D\rangle_r}\,\frac{\langle\Gamma_n\rangle_r\,\langle\Gamma_x\rangle_r}{\langle\Gamma\rangle_r}\,S_{nxr} \qquad (1)$$

where g_r is the statistical factor of the state r, $\langle D\rangle_r$ the average distance between compound nucleus states, $\langle\Gamma_n\rangle_r$ the average neutron width, $\langle\Gamma_x\rangle_r$ the average (n,x)-reaction width, $\langle\Gamma\rangle_r$ the average total width of the state r and S_{nxr} the factor allowing for the partial width fluctuation effect.

Averaging in (1) is made in accordance with the accepted width distribution laws. For this purpose the Porter-Thomas distribution with ν degrees of freedom is usually used. In this case the number of ν_{xr} degrees of freedom corresponds to the number of the channels that contribute to the (n,x)-reaction width or to the effective quantity, $\nu_{eff\ xr}$, obtained by analysing the experimental resonance widths $\Gamma_{\lambda xr}$:

$$\nu_{eff\ xr} = 2\,\frac{\langle\Gamma_x\rangle_r^2}{\langle\Gamma_x^2\rangle_r - \langle\Gamma_x\rangle_r^2} \qquad (2)$$

or the channel transmissions:

$$\nu_{eff\ xr} = \frac{(\sum_k P_{kxr})^2}{\sum_k P_{kxr}^2} \qquad (3)$$

Schmidt [7] calculated the S_{nxr}-factor for neutron (ν_{nr}=1) and radiative ($\nu_{\gamma r} = \infty$) channels. This factor is typical for non-fissile nuclei in the energy region below the inelastic scattering threshold. Double (three reactions) or triple (four reactions) integration is to be made when the number of reactions becomes laroer. The expressions for the S-factor can be reduced to the tabular or analytical functions only in the limited number of reactions, namely, three processes [8]. So, it is more practical to use the exoressions for the S-factors that are convenient for computer calculations:

$$S_{\alpha\beta} = \langle\Gamma\rangle_r \int_0^\infty \frac{(\nu_\alpha+2\delta_{\alpha\beta})\nu_\beta \prod_{\alpha''} \nu_{\alpha''}^{\nu_{\alpha''}/2}\, d\lambda}{(\nu_\alpha+2\lambda\langle\Gamma_\alpha\rangle)^{\nu_\alpha} (\nu_\beta+2\lambda\langle\Gamma_\beta\rangle)^{\nu_\beta} \prod_{\alpha''} (\nu_{\alpha''}+2\lambda\langle\Gamma_{\alpha''}\rangle)^{\nu_{\alpha''}/2}} \qquad (4)$$

The calculations of the S-factor may be also performed by the numerical method proposed by Greebler and Hutchins [9].

Strictly speaking, when ν is defined as the number of channels, this definition is valid only in the case of equal relative contributions of the channels to an average width. The analysis of the experimental resonance width distributions (formula (2)) gives only the "effective" number of the freedom degrees, ν_{eff}, that contains very little information on the important characteristics of a process, namely, the number of channels and their relative contributions since one and the same value of ν_{eff} may be achieved by their different combinations. The analysis of average cross sections, due to the large number of the parameters, can give only the approximate ν-values which can effectively allow for a contribution of direct processes, especially for nuclei with middle A.

When relative channel contributions are not equal, the generalized distribution proposed in [10] should be adopted (the contributions of all k-channels to the average width are equal and the above distribution reduces to the Porter-Thomas one):

$$P(y,\alpha_1,\alpha_2,\ldots\alpha_\nu)dy = \left[\frac{y^{\nu-2}}{(2\pi)^\nu \alpha_1\cdot\alpha_2\cdots\alpha_\nu}\right]^{1/2} \exp\left(-\frac{y}{2\alpha_\nu}\right) \times$$
$$\times \int_0^1 z_1^{-1/2} \exp(-A_1 z_1 y)dz_1 \cdot$$
$$\int_0^{1-z_1} z_2^{-1/2} \exp(-A_2 z_2 y)dz_2 \cdots \int_0^{1-z_1-\cdots-z_{\nu-2}} [z_{\nu-2}(1-z_1-\cdots-z_{\nu-1})]^{-1/2} \times \qquad (5)$$
$$\times \exp(-A_{\nu-1} z_{\nu-1} y)dz_{\nu-1}dy$$

where $y = \frac{\Gamma_{xr}}{\langle\Gamma_x\rangle_r} = \sum_{k=1}^{\nu} \frac{\Gamma_{xrk}}{\langle\Gamma_x\rangle_{rk}} \frac{\langle\Gamma_x\rangle_{rk}}{\langle\Gamma_x\rangle_r} = \sum_{k=1}^{\nu} \chi_k\alpha_k$, $A_k = \frac{\alpha_\nu-\alpha_k}{2\alpha_\nu\alpha_k}$

The form of the generalized distribution may substantially differ from the Porter-Thomas one, $P_\nu(y)$ for ν being defired either as the number of channels or as the "effective" number of freedom degrees. The example of two channels (Fig. 1) illustrates that the difference between the Porter-Thomas distribution with ν=2 and the generalized one increases with increasing contribution difference (α_1-α_2).

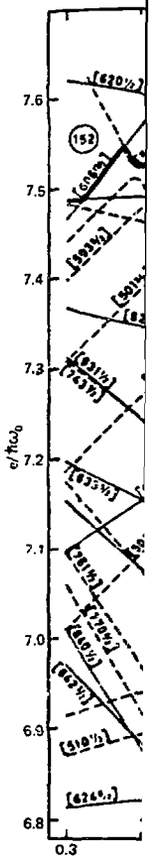

Fig. 1 :

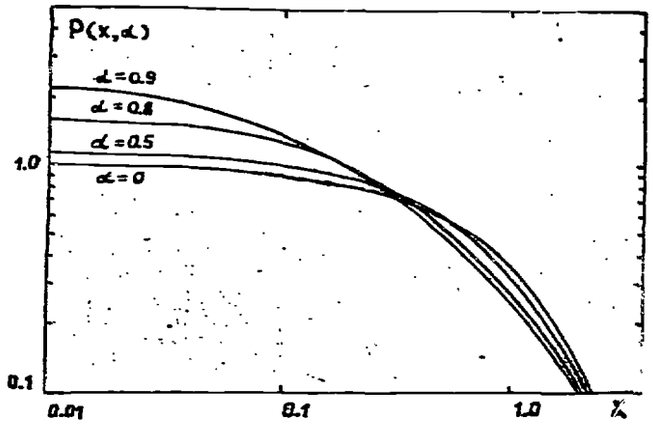

FIG. 1. Generalized Porter-Thomas distribution with k=2 at different values of channel contributions, $\alpha=|\alpha_1-\alpha_2|$

Figure 2 gives the generalized distribution with α_1=0.1 and α_2=0.9 and the Porter-Thomas distribution with ν_{eff} defined in terms of these relative contributions. At more close contributions the difference between the curves will decrease (Fig. 2).

The generalized distribution was proposed long ago [10] but was not widely used for evaluation purposes. Probably, this is caused by its more complicated form, as compared to the traditional Porter-Thomas distribution. We used the generalized distribution fo nuclear data evaluation [11].

It may be shown that for two channels the generalized distribution reduces to the form:

$$P(y,\alpha_1,\alpha_2)dy = \frac{1}{2(\alpha_1\alpha_2)^{1/2}} \exp(-\frac{y}{4\alpha_1\alpha_2}) I_0[\frac{y}{4}(\frac{1}{\alpha_2} - \frac{1}{\alpha_1})]dy \qquad (6)$$

where $I_0(z)$ is the Bessel function,

$$y = \frac{\Gamma_{rx}}{\langle\Gamma_x\rangle_r} = \sum_{k=1}^{\nu} \frac{\Gamma_{xrk}}{\langle\Gamma_x\rangle_{rk}} \frac{\langle\Gamma_x\rangle_{rk}}{\langle\Gamma_x\rangle_r} = \sum_{k=1}^{\nu} \chi_k\alpha_k.$$

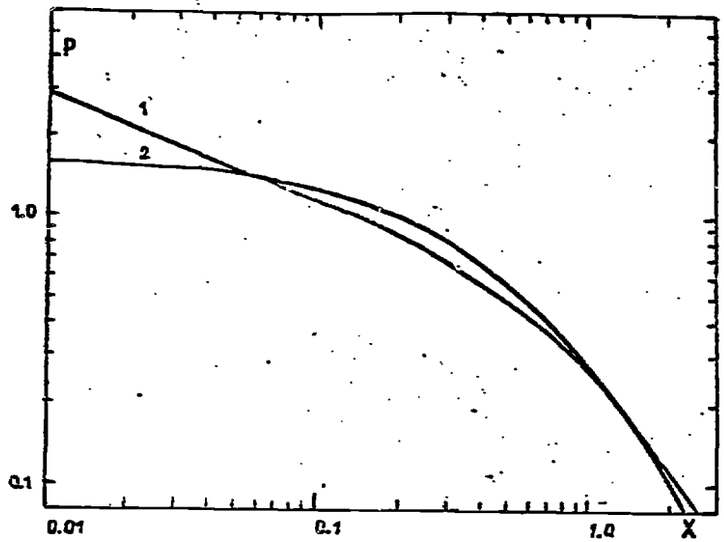

FIG. 2. Porter-Thomas distribution with ν_{eff}=1.22 (curve 1) and generalized distribution with ν=2, α_1=0.1 and α_2=0.9 (curve 2)

For the case of three fission channels one obtains the following expression:

$$P(y,\alpha_1,\alpha_2,\alpha_3)dy = \frac{\sqrt{y}}{2\sqrt{2}(\alpha_1\alpha_2\alpha_3)^{1/2}} \exp[-\frac{y}{4}(\frac{1}{\alpha_2} + \frac{1}{\alpha_3})] \times$$

$$\times \sum_{k=0}^{\infty} (\frac{A_2 y}{4})^{2k} \frac{1}{(k!)^2} \frac{\Gamma(2k+1)}{\Gamma(2k+3/2)} \Phi[\tfrac{1}{2}; 2k+\tfrac{3}{2}; y(\tfrac{1}{2}A_2 - A_1)]dy \qquad (7)$$

where $\Phi(\beta,\gamma,z)$ is the degenerated hypergeometric function [12].

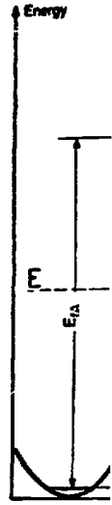

Fig. 4 :

When two fission channels have the same contribution to width (channels are either completely open or have the same transmission) expression (7) assumes the form:

$$P(y,\alpha,\alpha_3)dy = \sqrt{(2y/\pi)} \times \frac{1}{\alpha\alpha_3^{1/2}} \exp\left(-\frac{y}{2\alpha_3}\right)\Phi\left[1;\frac{3}{2};\frac{y}{2}\left(\frac{1}{\alpha_3}-\frac{1}{\alpha_1}\right)\right]dy \qquad (8)$$

where $\alpha=\alpha_1+\alpha_2$ and $\alpha_1=\alpha_2$.

When the number of the resonances analysed is not great, it is convenient to use the following distribution:

$$F(y\geq y_0,\ \alpha_1,\alpha_2,\ldots\ldots\alpha_k)=\int_{y_0}^{\infty} P(y,\alpha_1,\alpha_2,\ldots\ldots\alpha_k)dy \qquad (9)$$

defining the probability that the value of the variable y is less than that of y_0. In resonance width statistics, it means the number of resonance widths, whose values are larger than the given ones.

Figure 3 illustrates distribution (9) and comparison of the theoretical and experimental distributions for fission widths of ^{239}Pu 51 0^+-resonances. It is seen that the application of the generalized distribution improves an agreement between theory and experiment, as compared to the case when in the Porter-Thomas distribution ν coincides with the number of the channels equal to 2. The values $\alpha_1=0.77$ and $\alpha_2=0.23$ obtained from the width distribution dispersion agree with the transition state scheme proposed by Lynn [13].

The generalized distribution when applied to analyse the experimental data for fission widths enables to obtain the information about the relative contributions of the channels. Of special interest is the case of the small number of channels for fission resonance widths (ν=1÷4). In this case considerable deviations from the Porter-Thomas distribution should be expected. The generalized distribution makes it possible to relate the experimental width distributions to the structure of the transition states of a fissile nucleus.

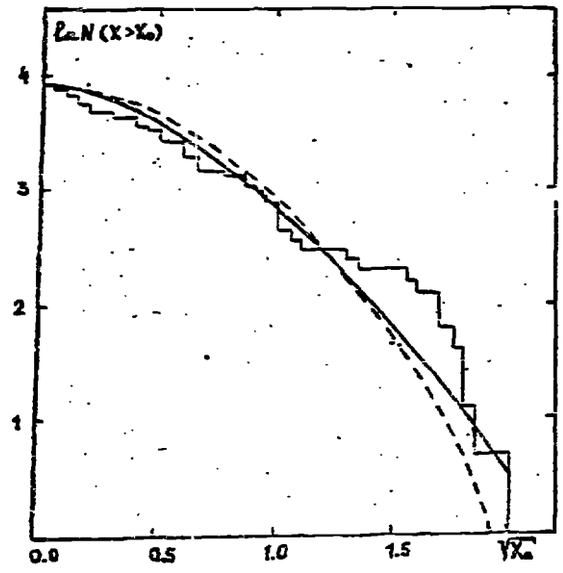

FIG. 3. Integral distribution of the fission widths of resonances for ^{239}Pu as a function of $\sqrt{X_0}=\Gamma_{\lambda c}/\langle\Gamma_c\rangle$: histogram, experimental data; -----, Porter-Thomas distribution with ν=2; _____, integral generalized distribution with $\alpha_1=0.77$ and $\alpha_2=0.23$

On one side, the transition state structure and fission barrier parameters may be found by analysing nucleus fissibility. On the other side, certain information on relative channel contributions may be

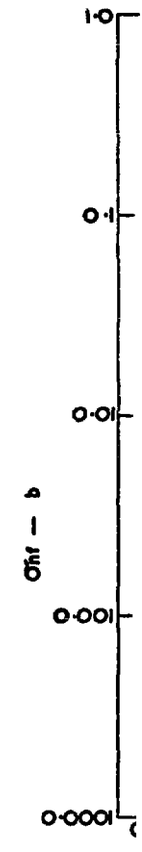

Fig. 6 :

obtained from the generalized distribution dispersion:

$$\frac{\langle\Gamma_c^2\rangle - \langle\Gamma_c\rangle^2}{\langle\Gamma_c\rangle^2} = 2\sum_{i=1}^{k}\alpha_k^2 \qquad (10)$$

and from the analysis of the correlation between the channel widths and the mean number of neutrons per fission [17]. The advances in spin resonance identification also stimulates to use the generalized distribution for analysing fission widths.

Compare the effects of the Porter-Thomas distribution and the generalized width distribution on average cross sections in the case of several channels. When the generalized distribution is adopted, the expression for the S_{nxr}-factor in the case of two channels is of the form:

$$S_{nxr} = \langle\Gamma\rangle_r \xi^{1/2} \int_0^\infty \frac{\exp(-\langle\Gamma_\gamma\rangle_r t)(\langle\Gamma_f\rangle_r t+\xi)^{\delta_{fx}} dt}{(1+2\frac{\langle\Gamma_n\rangle_r t}{\nu_{nr}})^{1+\delta_{nx}+\frac{\nu_{nr}}{2}} [(\langle\Gamma_f\rangle_r t+\xi)^2 - (\frac{\alpha_1-\alpha_2}{\xi})^2]^{\frac{1}{2}} + \delta_{fx}} \qquad (11)$$

where $\xi=(4\alpha_1\alpha_2)^{-1}$.

For three fission channels one may obtain:

$$S_{nxr} = \frac{\langle\Gamma\rangle_r}{2\sqrt{2}(\alpha_1\alpha_2\alpha_3)^{1/2}} \int_0^\infty \frac{\exp(-\langle\Gamma_\gamma\rangle_r t)}{(1+2\frac{\langle\Gamma_n\rangle_r t}{\nu_{nr}})^{1+\delta_{nx}+\frac{\nu_{nr}}{2}}} \times$$

$$\times \sum_{k=0}^{\infty} \frac{A_2^{2k}}{2^{4k+\delta_{fx}}} \times \frac{(2k+1)!}{(k!)^2} F^{1/2}(\frac{1}{2\alpha_1}) F^{2(k+1)-\delta_{fx}} [\frac{1}{4}(\frac{1}{\alpha_2}+\frac{1}{\alpha_3})] \times$$

$$\times [\frac{F(\frac{1}{2\alpha_2})}{F[\frac{1}{4}(\frac{1}{\alpha_2}+\frac{1}{\alpha_3})]} + 4k + 2]^{\delta_{fx}} dt \qquad (12)$$

where $F^q(\delta) = (\langle\Gamma_f\rangle_r t + \delta)^{-q}$.

Figure 4 gives the fluctuation factors S_{nn}^{0+}, $S_{n\gamma}^{0+}$ and S_{nf}^{0+} vs $(\alpha_1-\alpha_2)$ calculated by formulas (4) and (11) at 0.1 keV and 100 keV. The upper and lower straight lines correspond to the Porter-Thomas distribution with $\nu=2$ and $\nu=1$. Curve 4 stands for the generalized distribution while curve 3 denotes the Porter-Thomas distribution with $\nu_{fr}=\nu_{eff\ fr}$ where $\nu_{eff\ fr}$ is determined by the relative channel contributions from formula (2). These figures illustrate the considerable effect of different ways of the representation of the fission width distributions on the S-factors. This is especially pronounced in $S_{n\gamma}^{0+}$ and S_{nn}^{0+}. Comparison of curves 3 and 4 shows that the values of S_{nx}^{0+} differently depend on the channel contribution ratio despite the self-consistency between ν_{eff} and $(\alpha_1-\alpha_2)$, and the difference in S_{nn}^{0+} and $S_{n\gamma}^{0+}$ is about 18% and in S_{nf}^{0+}, about 5% at $(\alpha_1-\alpha_2)=0.7 \div 0.9$, as the energy increases, thereby causing a substantial growth of $\frac{\langle\Gamma_n\rangle^{0+}}{\langle\Gamma\rangle^{0+}}$ and a slight variation in $\langle\Gamma_\gamma\rangle^{0+}$ and $\langle\Gamma_f\rangle^{0+}$. The difference between the traditional way of allowing for fission width fluctuations with ν_{eff} and the one based on the two-channel distribution decreases. At 100 keV for S_{nn}^{0+} and $S_{n\gamma}^{0+}$ it decreases as much as 2-3 times and for S_{nf}^{0+}, 1.5-2.0 times.

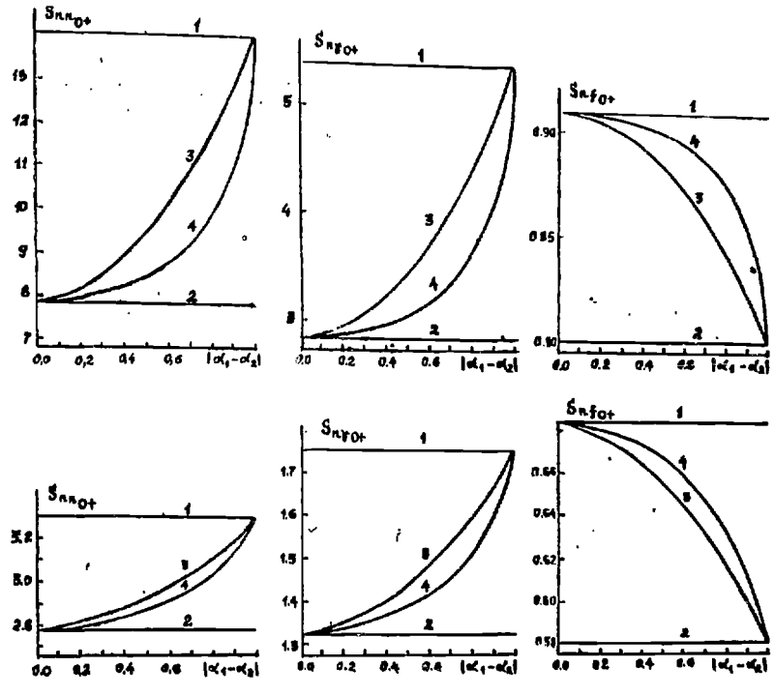

FIG. 4. S_{nn}^{0+} , $S_{n\gamma}^{0+}$ and S_{nf}^{0+}-factors vs the difference in relative contributions of two ^{239}Pu fission channels at E_n=0.1 keV (three upper figures) and at E_n=100 keV(three lower figures) (curves 1,2,3, Porter-Thomas distribution for ν=2, ν=1, $\nu=\nu_{eff}$:curve 4, generalized distribution)

Fig. 10 :

Note that the minimum error in the S-factors, when passing from $\nu=1$ to $\nu=2$, occurs at $(\alpha_1-\alpha_2)\approx 0.9$ and at $\nu_{eff}=1.35$. This circumstance should be borne in mind when use is made of the Porter-Thomas distribution with the integer freedom degrees. Also note that large values of S^{0+}_{nn} and $S^{0+}_{n\gamma}$ are caused by the strong fission competition and the small number of fission channels, which is consistent with the conclusions made in [15].

When three channels contribute to a mean width $\langle\Gamma_f\rangle_r$ (this case is implemented for 1^- state of the compound ^{240}Pu nucleus) the above differences for the case of two channels decrease and remain, however, noticeable for S^{1-}_{nn} and $S^{1-}_{n\gamma}$. At E=0-1 keV, the difference between curves 3 and 4 amounts to about 8% for S^{1-}_{nn} and $S^{1-}_{n\gamma}$ and about 0.5% for S^{1-}_{nf}. With increasing neutron channel competition, it decreases and does not exceed about 3% in S^{1-}_{nn} and $S^{1-}_{n\gamma}$.

From the aforesaid it follows that the generalized Porter-Thomas distribution rather than the traditional one should be used to calculate the average neutron cross sections in the unresolved resonance region, in particular, to take into account the fission width fluctuations with a small number of channels. The use of $\nu_{eff\ fr}$ and the Porter-Thomas distribution for Γ_{fr} fluctuations is justified only in the case of very weakly or very strongly differing relative channel contributions when the integer values of ν can be adopted.

Consider the method of calculating the S_{nf}-factor in the case of a more complicated fission width distribution that is valid for even-even fissile nuclei.

The presence of the structure in the subthreshold fission cross section of ^{240}Pu and ^{242}Pu may be explained within the framework of the double-humped fission barrier predicted by Strutinsky [17]. As is shown in [18,19], the existence of such a barrier does not practically affect the average fission width $\langle\Gamma_f\rangle$ but leads to a change in fission width distributions.

In the above distributions, it is implicitly assumed that fission barrier transmissions, P_{fr},

$$\Gamma_{fr} = 2\bar{\gamma}^2_{fr}\, P_{fr}(E) \qquad (13)$$

(where $\bar{\gamma}^2_{fr}$ is the reduced fission width) weakly depend on energy (do not fluctuate). In the single-humped fission barrier model, this assumption is valid, and fluctuations of Γ_{fr} as well as those of the widths γ^2_{fr} obey the same law.

The transmission of the double-humped fission barrier strongly depends upon energy, thereby achieving maximum at energies close to the quasi-stationary levels in the second well. The Porter-Thomas and generalized distribution (5) may thus be used only to describe the resonance width distributions for the channels, whose energy is above the second maximum of the fission barrier. As a rule, this case takes place for nuclei with negative fission thresholds.

The authors of [18] have proposed to calculate a fission width distribution in the subbarrier region in terms of the convolution of the Porter-Thomas distribution, that characterizes a fission width distribution with resoect to their local mean values, with the distribution of the average fission widths. Therefore, it may be assumed that the average fission widths can be fitted with the following distribution:

$$\omega(x)dx = \frac{1}{\pi x}(x-x_{min})^{-1/2}(x_{max}-x)^{-1/2}dx \qquad (14)$$

where $x=\dfrac{\Gamma_f}{\langle\Gamma_f\rangle}$, $x_{max}=\dfrac{\Gamma_{fmax}}{\langle\Gamma_f\rangle}$, $x_{min}=\dfrac{\Gamma_{fmin}}{\langle\Gamma_f\rangle}$ provided that $\sqrt{(\Gamma_{fmax}\Gamma_{fmin})}=\langle\Gamma_f\rangle$ and Γ_{fmax} and Γ_{fmin} are defined in terms of maximum and minimum transmissions.

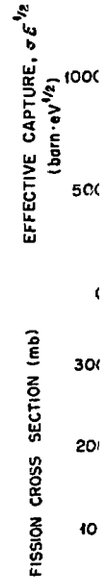

Fig. 13

It may be also assumed that, besides distribution (14), the widths Γ_f are subjected to local fluctuations relative to their average values that are governed by a χ^2-distribution

$P_\nu(\frac{\Gamma_{fr}}{\tilde{\Gamma}_{fr}})$ with the number of freedom degress being determined by the number of open fission channels. Then, the distribution for $z = \frac{\Gamma_{fr}}{\langle\Gamma_{fr}\rangle} = \frac{\Gamma_{fr}}{\tilde{\Gamma}_{fr}} \frac{\tilde{\Gamma}_{fr}}{\langle\Gamma_{fr}\rangle} = yx$ is determined by the convolution:

$$\phi(z) = \int_0^\infty P_\nu(y)\omega(\frac{z}{y})\frac{dy}{y} \qquad (15)$$

The average fission width $\langle\Gamma_f\rangle_r$ may be given as a sum of individual channel widths:

$$\langle\Gamma_f\rangle_r = \sum_{k=1}^{\nu} \langle\Gamma_f\rangle_{rk} = \sum_{k=1}^{\nu} \frac{\langle D\rangle_r}{2\pi} P_{frk} \qquad (16)$$

where P_{frk} is the transmission of a k-fission barrier for the state r and for the single-humped parabolic barrier it is determined by the Hill-Wheeler expression [20]. Different calculation procedures of double-humped barrier transmission coefficients are considered elsewhere in [18,21,22]. Comparison of the rigorous numerical calculation of the barrier transmission coefficients approximated by three parabolas [23] with quasi-classical approximation results [18] shows that the latter are substantially higher in the region near the peak of the smaller hump. However, the fission barrier parameters for even ^{240}Pu and ^{242}Pu nuclei-targets are such that in the energy range considered, P_A and P_B are much less than unity, which testifies the validity of the quasi-classical approximation.

In [21], the analytical expression for the barrier approximated by two convex parabolas is obtained which, unlike from the appropriate one in [18], is also valid in the near-barrier region. Maximum and minimum fission transmissions are defined as follows:

$$P_{\substack{max\\min}} = \frac{P_A P_B}{1 \pm \sqrt{(1-P_A)(1-P_B)}} \qquad (16)$$

Then, from (14) we have:

$$\langle\Gamma_f\rangle = \sqrt{\Gamma_{fmax}\cdot\Gamma_{fmin}} = \frac{\langle D\rangle}{2\pi} \frac{P_A P_B}{1-(1-P_A)(1-P_B)} \qquad (17)$$

$$x_{max} = \frac{1}{x_{min}} = \frac{1+\sqrt{(1-P_A)(1-P_B)}}{1-\sqrt{(1-P_A)(1-P_B)}} \qquad (18)$$

As is expected, at P_B=1 we deal with the single-hump case: $\langle\Gamma_f\rangle = \frac{\langle D\rangle}{2\pi} P_A$, $x_{max} = x_{min} = 1$, while in the subbarier region ($P_A, P_B << 1$) we have: $\langle\Gamma_f\rangle = \frac{P_A P_B}{P_A+P_B}$, $x_{max} = \frac{1}{x_{min}} = \frac{4}{P_A+P_B}$, which is consistent with the quasi-classical solution [18].

This more simple approach requires a knowledge of a smaller number of the parameters against the one described in [22] and is thus used to calculate ^{240}Pu fission width distribution. The algorithm used allows satisfactory calculation of ^{240}Pu and ^{242}Pu fission cross sections.

The quantity $\langle\frac{\Gamma_{nr}\Gamma_{xr}}{\Gamma_r}\rangle$ in this case cannot be calculated analytycally, and in the case of even-even nucleus-targets one of the methods for calculation of this value is the averaging of the values of $\frac{\Gamma_{nr}\Gamma_{xr}}{\Gamma_r}$ obtained using the Monte Carlo method, distribution (15)

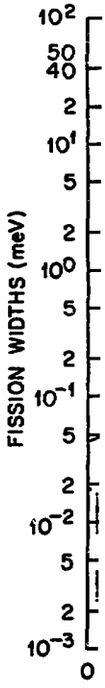

Fig. 15

and the Porter-Thomas distribution. The calculation is made until the statistical errors for each channel would not be less than 10^{-2}. It should be noted,however that the acceptable level of the accuracy in $\langle\sigma_f\rangle$ attained by this method requires considerable computer time.

This approach assumes that the nuclear states in the second well are pure vibrational. However, some experimental data point to the possible dissipation of the vibrational states in the second well into the intermediate compound nucleus states [24].

Probably, the analytical calculation of the S_{nf}-factors for even-even nuclei-targets may be performed using the fission width distribution in the form proposed in [22]. This calculation,however, faces great computational difficulties, and at present further studies are to use this approach for evaluation purposes.

In the case of odd nuclei-targets, the double-humped fission barrier concept should not be obligatorily adopted to calculate the S_{nf}-factors. Our calculations have shown that the greatest difference in the S_{nf}-factors for ^{239}Pu single- and double-humped fission barriers (about 2.5%) is observed at 40 keV for a large fission width state, which corresponds to the ^{239}Pu state 0^+. This difference is smaller (about 1%) for the states with small fission widths. The difference in the S_{nf}-factors for the ^{239}Pu single- and double-humped barriers decreases at 1 keV up to 0.6% and with an increase in neutron energy up to 200 keV the difference in the S_{nf}-factors disappears which is natural enough.

The difference in the S_{nf}-factors for single-and double-humped barriers for even-even nuclei-targets becomes very large. So, the difference in calculated ^{240}Pu σ_f and S_{nf} cross sections for single- and double-humped cases amounts to about 200% at 1 kev, about 30% at 20 keV and about 7% at 200 keV. The same difference in calculated ^{242}Pu cross sections is observed.

The average cross sections for fission, radiative capture and inelastic neutron scattering processes for actinides were calculated by formula (1). The values of $\langle\Gamma_\gamma\rangle$ and $\langle D\rangle_{obs}$ were obtained from the resolved resonance data and the remainder parameters, by fitting to the experimental results in the keV energy range. To allow for the structure, for instance, in ^{235}U σ_t and σ_f cross sections, the parameters $\langle\Gamma_n\rangle^{3^-}$ and $\langle\Gamma_n\rangle^{4^-}$ were obtained from the average $\langle\sigma_t\rangle$ and the parameter $\langle\Gamma_f\rangle^{4^-}$, from σ_f. Comparison of the calculated and experimental data for the independently measured value of α, i. e. the capture-to-fission cross section ratio, points to the validity of the average parameters and the methods used.

The theoretical models for the level density depending on spin, parity and excitation energy must be used to determine $\langle D\rangle_r$. For this purpose in the unresolved resonance energy region we used the independent particle model, whose main level density parameter "a" does not depend on energy and is determined from the observed resonance distance. This model assumes that $\langle D\rangle_J$ is independent of parity. For deformed heavy nuclei such as ^{235}U, ^{239}Pu and other actinides, the dependence of $\langle D\rangle_J$ on parity can be, probably, ignored [25].

Recently the nuclear level density theory has attained further development. It was shown how in the traditional Fermi-gas model to take into account a decrease in the shell effects due to increasing excitation energy [26] (energy dependence of the parameter "a"). The contribution of collectives modes to the level density was also calculated [27], which resulted in the improvement of the agreement between the systematics of the parameter "a" and its quasi-classical value. It should be noted that the account of these effects does not cause substantial changes in $\langle D\rangle_r$ in the unresolved resonance region. This is due to the nearness of this region to the normalization point (B_n-Δ) and due to the smallness of the shell correction,δW, in the mass formula, e. g. for ^{243}Pu, ^{241}Pu and other actinides. As compared to the Fermi-gas model, the superfluid nucleus model although allowing more correct calculation of the level density over the whole energy range does not greatly affect calculated cross sections in

the unresolved resonance region due to the nearness to the normalization point ($B_n-\Delta$).

As a rule, the energy dependence of $\langle D\rangle_r(E)$ is neglected in the unresolved resonance region. However, despite $E\ll B_n$, this dependence is substantial and leads to about 15% change in $\langle D\rangle_r$ at 100 keV. This fact naturally affects the average fissile nucleus cross sections, first, radiative capture cross section and then α. Our calculations show that the neglect of the energy dependence of $\langle D\rangle_r(E)$ for ^{241}Pu leads to about 15% decrease in $\langle\sigma_{n\gamma}\rangle$ and $\langle\alpha\rangle$ at 100 keV.

In our calculations we allowed for the energy dependence of $\langle D\rangle_J$ (outting $u=B_n+E-\Delta$) since for ^{240}Pu the mean distance is decreased as much as 20% at 140 keV.

Since the inelastic neutron scattering threshold for heavy nuclei is low, the (n,n')-reaction should be allowed for in the unresolved resonance region. Assume that the transmission coefficients, P_ℓ, for a nucleus in the excited state are determined similarly to those in the ground state, i. e. the difference between elastic and inelastic channels lies only in the value of energy. In this case the average inelastic width $\langle\Gamma_{n'}\rangle_r$ can be defined similarly to the elastic neutron width $\langle\Gamma_n\rangle_r$:

$$\langle\Gamma_{n'}\rangle_r = \langle D\rangle_r \sum_{q,\ \ell'} S_{\ell'}\varepsilon_q^{1/2}\ P_\ell(\varepsilon_q)\nu_{J\ell',q} \qquad (19)$$

where ε_q is the neutron energy in the inelastic channel characterized by the orbital moment, ℓ', and level energy excitation, $E_q(\varepsilon_q=E-E_q)$.

Summation in expression (19) is performed only over those levels and orbital moments ℓ' that contribute to this channel, r, i.e. those obeying the energy conservation law $E\geq E_q(A+1)/A$, total angular moment $\vec{I}+\vec{j}=\vec{J}=\vec{I}'+\vec{j}'$ and parity $(-1)^{\ell}\Pi=(-1)^{\ell'}\Pi_q$.

As a rule, when cross sections in the unresolved resonance region are calculated, the (n,n')-reaction is usually neglected. However, in a number of cases this gives a substantial difference in the neutron cross sections calculated. The calculations show that at 100 keV, the difference in $\sigma_f(^{235}U)$ with and without allowance for the (n,n')-reaction amounts to about 10%.

Further, a knowledge of the strength functions and average fission widths is required to calculate neutron cross sections. Strength functions may be obtained from the data for the resolved resonances and for average cross sections in the keV range. For this purpose the data for σ_t are more suitable since these can be calculated using a smaller number of other parameters. In principle, the strength functions can be determined from the transmission coefficients, $T_{\ell J}$, calculated using the optical model. However, the main difficulty in this case is associated with the choice of optical potential parameters since not sufficiently accurate input data (σ_p,σ_t,S_o) greatly affect the strength functions calculated. Using the fit to two experimental values of σ_p, Goldsmith [29] obtained such values of the parameters for ^{232}Th that give the values of S_1 differing almost 3 times. Therefore, the optical model calculation of the strength functions can be performed only in the case when other methods are inapplicable, i. e. when there are no necessary data.

In our calculations, average fission widths were obtained using the fission channel theory, and the values of fission barrier energies, E_{fk}, were chosen by fitting the calculated σ_f data to the experimental ones. These values were determined taking into account the approximate transition state scheme for fissile even-even nuclei [30].

This approach was adopted for the self-consistent calculation of neutron cross sections (σ_t,σ_f,$\sigma_{n\gamma}$,$\sigma_{nn'}$) for odd nuclei-targets up to 100 keV and for even nuclei up to 150-200 keV.

Figures 5 through 8 show the calculated average fission and radiative capture cross sections for ^{235}U. In these calculations, our evaluated σ_t and σ_f data averaged over the chosen energy inter-

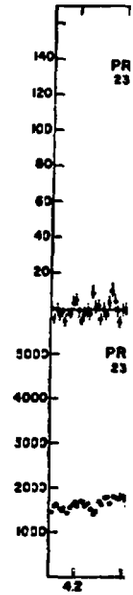

Fig. 19 :

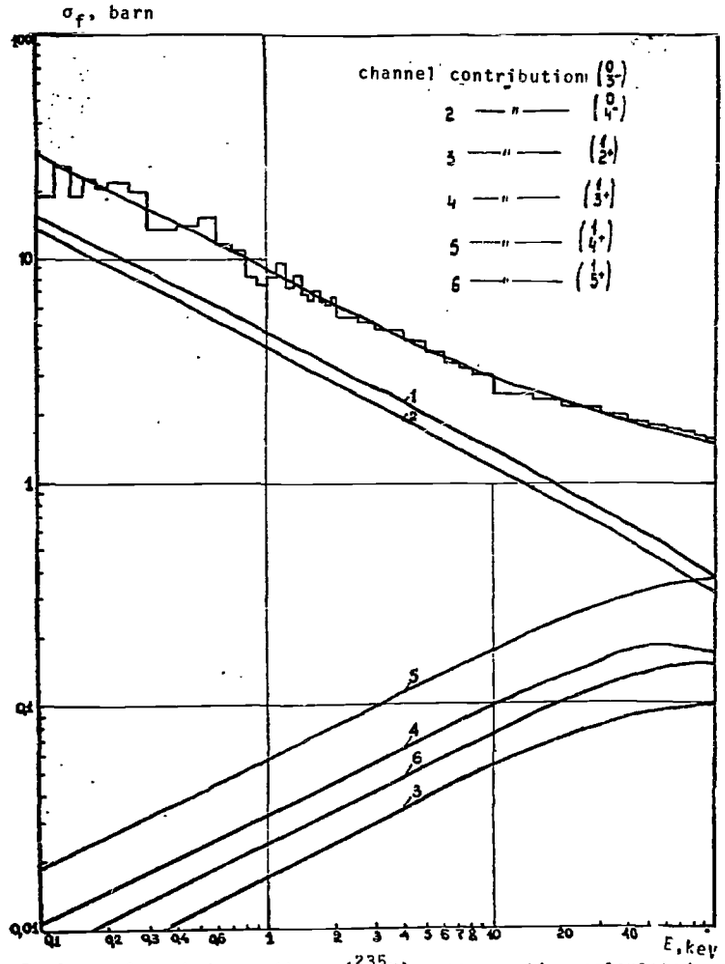

FIG. 5. Comparison between the $\sigma_f(^{235}U)$ cross section calculated (_____) in terms of the average parameters in the 0.1-100 kev range and the evaluated data (⎍⎍⎍)

vals served as the input information. The parameters obtained allowed reliable calculation of the (n,γ) and (n,n') cross sections in the energy range up to 100 keV.

Figure 5 shows the comparison between the experimental σ_f cross section and those calculated using the average parameters, which testifies the quality of the average fission widths, $\langle\Gamma_f\rangle_r$. Good agreement is achieved over the whole energy range. This figure also shows contributions of each channel for s- and p-waves. A contribution of d-waves is not essential and amounts to <3% σ_f at 100 keV. Figure 6 illustrates the effect of the (n,n')-reaction competition

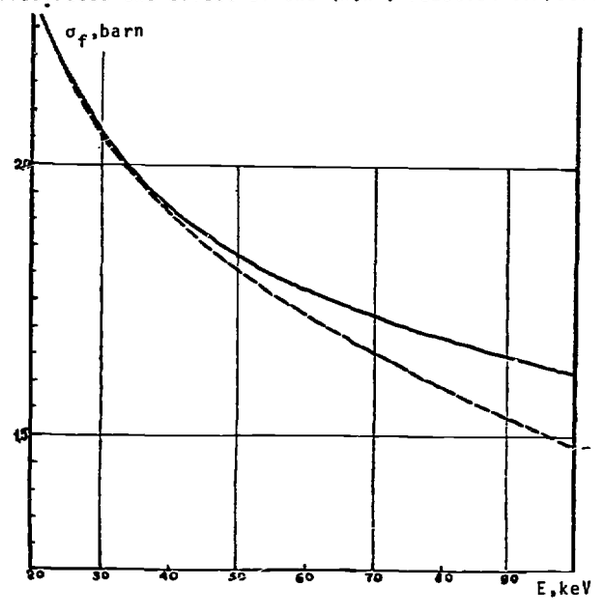

FIG. 6. Comparison of the $\sigma_f(^{235}U)$ cross section calculated with (---) and with no regard (____) for inelastic neutron scattering competition

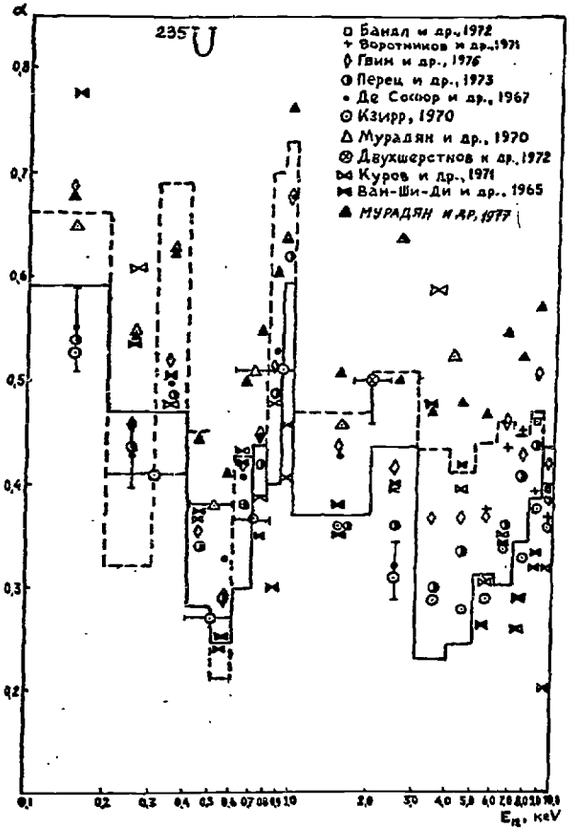

FIG. 7. Comparison of the calculated and experimental data for $\alpha(^{235}U)$ in the energy range 0.1-10keV:-----, calculation with $S_0=1.08.10^{-4}eV^{-1/2}$; _____, calculation with S_0 by fitting to σ_t in each energy interval

on fission cross section calculations. Here the dashed curve denotes the calculation with no allowance for the inelastic neutron scattering. This difference is substantial and amounts to about 10% at 100 keV.

Figure 7 shows the comparison of the experimental and calculated data for the capture-to-fission cross section ratio, $\alpha=(\sigma_{n\gamma}/\sigma_{nf})$. It is seen that a satisfactory agreement between the calculated and experimental values is observed, and the calculated structure in the α-value is in a general agreement with the experimental one. Comparison of the α-value calculated with the constant and fluctuating S_0 shows that below 10 keV, when fluctuations are allowed for, a somewhat better agreement between theory and experiment is attained, although this is not evident if the data of [31] and [32] are taken into account.

In the energy range 10-50 keV the calculations of the α-value made with the constant S_0 are in better agreement with experiment, and above 50 keV calculation results for the fluctuating and constant S_0 are close to each other, which is natural because with increasing energy the fluctuations in σ_t become smooth. In general, the not sufficient accuracy of the experimental data for α does not permit us to conclude that fluctuations in σ_t (and S_0) should be taken into account when calculating the α-value.

The direct comparison of the (n,n') cross sections for ^{235}U calculated in terms of the average resonance parameters with the experimental data for the unresolved resonance energy region (up to 100 keV) is impossible due to the absence of the experimental $\sigma_{nn'}$ data in this region. Comparison between the results obtained by this approach and those calculated by the statistical model using the optical model transmission coefficients shows a satisfactory agreement between the data obtained by these two methods (Fig. 8).

Fig. 22

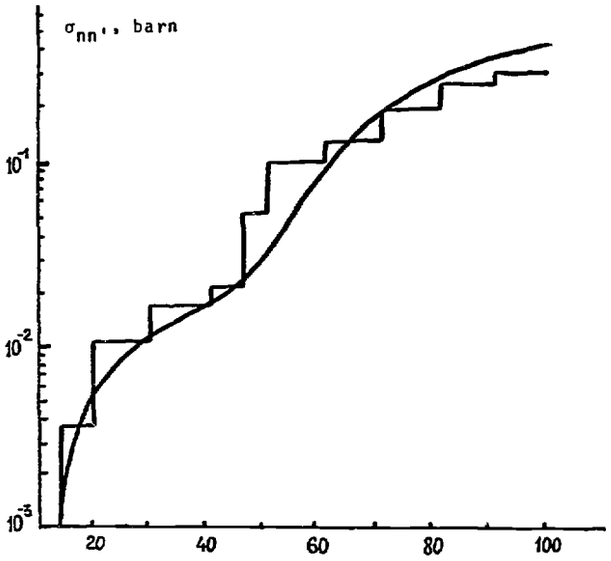

FIG. 8.

Comparison of the $\sigma_{nn'}(E)$ ^{235}U cross sections calculated using the optical transmission coefficients (_____) and average resonance parameters ($\int\Gamma$) up to 100 keV

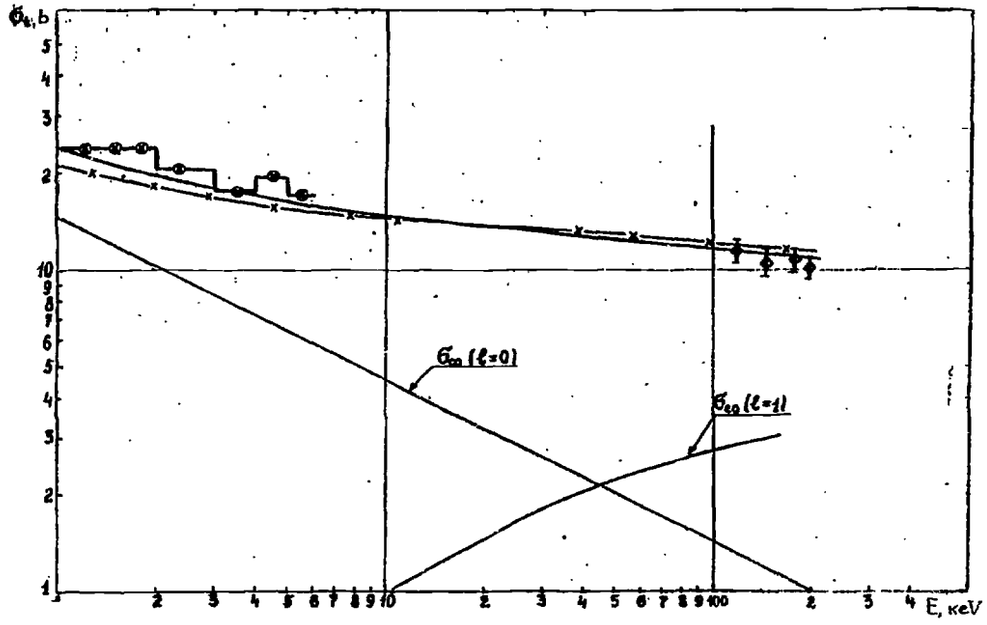

FIG. 9.

Comparison of the experimental and calculated $\sigma_t(^{240}Pu)$ in the energy region from 1 to 200 keV: _____, present evaluation; __x___x___, evaluation by Pitterle et al. [36].

Calculation results for average ^{240}Pu cross sections are presented in Figs. 9 through 11. These figures show that the calculated and experimental cross section are in good agreement. Of special interest is Fig. 10 which displays the calculation results for one of the most important reactor cross section, namely, $\sigma_{n\gamma}$. When our calculations were made, the experimental data for $\sigma_{n\gamma}$ [33] in the energy range 0.2 to 350 keV were unknown and appeared only in 1977. We could use only the data for $\sigma_{n\gamma}$ from [34] in the energy range from 6 to 28 keV. The solid line in Fig.10 stands for our self-consistent cross section calculations made in 1975. Later on, when Weston and Todd's data [33] were published, these were also plotted in Fig. 10. A good agreement between the calculated and experimental data is seen to be below 6 keV and above 30 keV where there were no experimental data at the moment of evaluation. This demonstrates the correctness of the approach used and the validity of the parameters chosen.

The ^{240}Pu σ_f cross section in the unresolved resonance region (Fig.11) was calculated using the double-humped fission barrier approach, which enabled to govern all the experimental data up to the peak near 1 keV that was found experimentally [36] and was absent in other evaluations [36].

The calculated and experimental data for ^{240}Pu σ_f, α and $\sigma_{n\gamma}$ are compared in Figs. 12 through 14, while the comparison of those for ^{242}Pu σ_t, $\sigma_{n\gamma}$, $\sigma_{nn'}$, and σ_f is given in Figs. 15 through 18. As is seen, the agreement is quite satisfactory.

Thus, the average parameters used ensure the agreement between the experimental and calculated neutron cross sections. Therefore, the calculation results may be taken as the evaluated values.

Hence, the method for calculating average cross sections in the unresolved resonance region was illustrated for nuclei ^{235}U, ^{240}Pu and ^{242}Pu. There are two important specific features in the methods used: 1) reaction widths have to be carefully determined using different approaches, especially those based on the experimental data for σ_t and σ_f and 2) the present method is an effective tool and can be, within a sufficient accuracy, applied only in the unresolved resonance energy range, i.e. for odd nuclei-targets up to 100 keV and for even nuclei-targets up to 150-200 keV. In the upper energy range, the limitations are associated with the facts that the strength function S_2 is not accurately known, the excitation cross sections of higher levels are not properly allowed for and the phase shifts, ϕ_ℓ, are not correctly calculated in the energy range above 200 keV. For odd nuclei-targets in the energy range considered, it is possible to allow for the contributions only of the s-and p-waves not only to $\langle\sigma_t\rangle$ but also to partial cross sections; in the case of even nuclei-targets account should be taken of s-, p- and d-waves.

When average resonance parameters are determined rather accurately, the accuracy in the $\sigma_{n\gamma}$ calculation by this method in the energy range considered is about 5-10%. For this purpose it is quite enough to know the average resonance parameters from the resolved resonance region and those for σ_t and σ_f, at least, in the limited energy range (keV region).

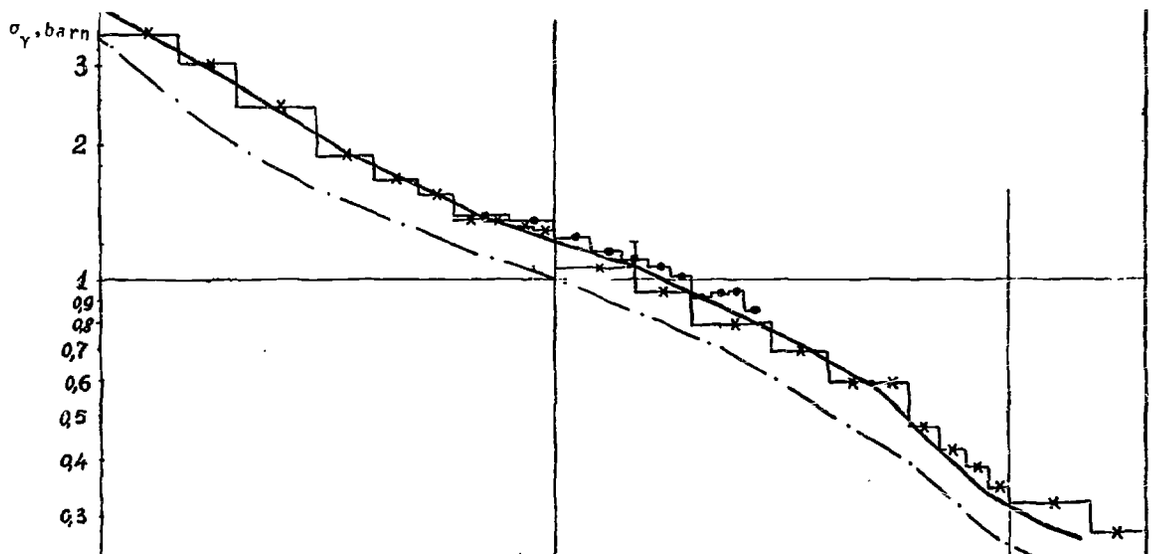

FIG. 10. Comparison of the calculated and experimental $\sigma_{n\gamma}(^{240}Pu)$ in the energy range 1 to 200 keV : _____, present calculation; -•-•-, experiment [34]; _x_x_, [33]; _._._._, evaluation by L'Heriteau, 1970

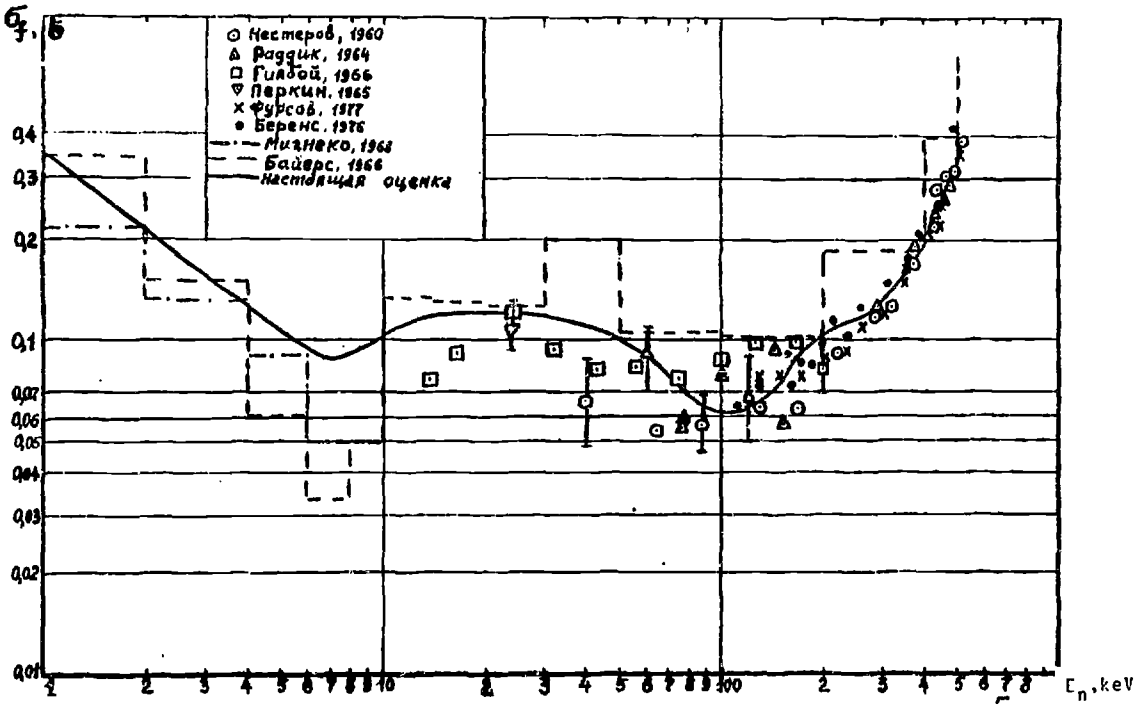

FIG. 11. Comparison of the experimental and calculated $\sigma_f(^{240}Pu)$ in the energy region 1 to 500 keV: _____, present calculation

or the channel

ν_{ef}

Schmidt [
radiative ($\nu_{\gamma r}$
nuclei in the
Double (three
to be made whe
sions for the
functions only
processes [8].
the S-factors

$S_{\alpha\beta} = \langle\Gamma\rangle_r$

The calcu
numerical meth
Strictly
this definitio
butions of the
perimental res
the "effective"
very little in
namely, the nu
one and the sa
combinations.

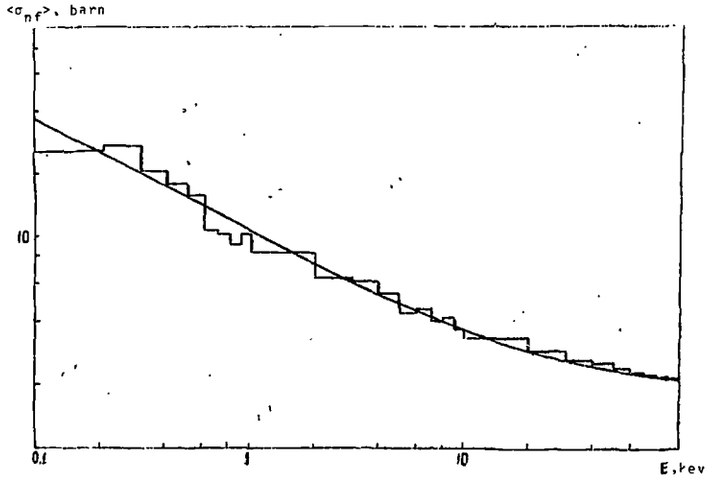

FIG. 12. Comparison of the experimental (⎍⎍) and calculated (____)$\langle\sigma_f\rangle$ (^{241}Pu)

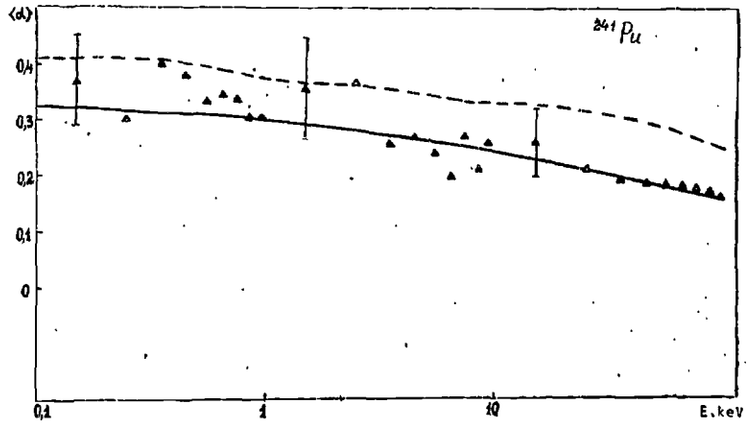

FIG. 13. Comparison of the calculated and experimental [37] data for α (^{241}Pu): ____, present calculation; ---, evaluation of [38]

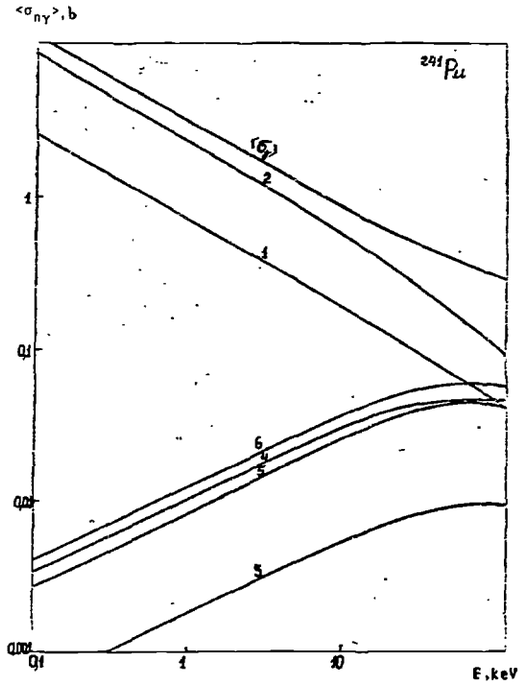

FIG. 14.

Calculated $\langle\sigma_{n\gamma}\rangle$ cross section for ^{241}Pu and its partial components: 1, channel contribution (2,0+); 2, (0,3+); 3, (1,1-); 4, (1,2-); 5, (1,3-); 6 (1,4-)

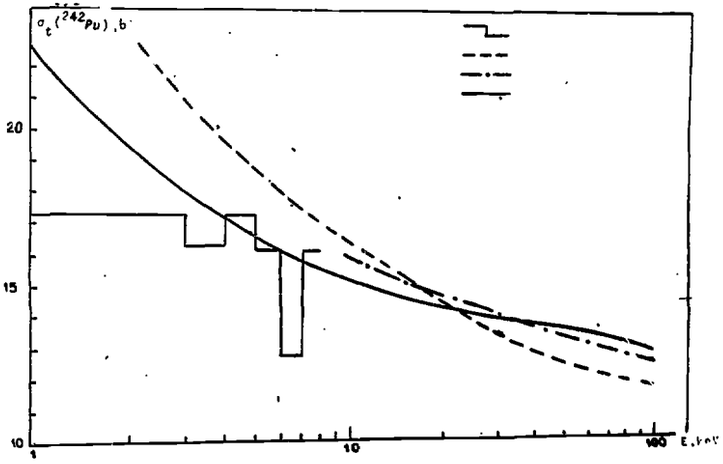

FIG. 15.

Comparison of the experimental and calculated $\langle\sigma_t\rangle$ for ^{242}Pu below 100 keV: ⎍⎍⎍, experimental data of [39]; ----, evaluation of [40]; -.-.-., calculation from [41]; _____ present calculation

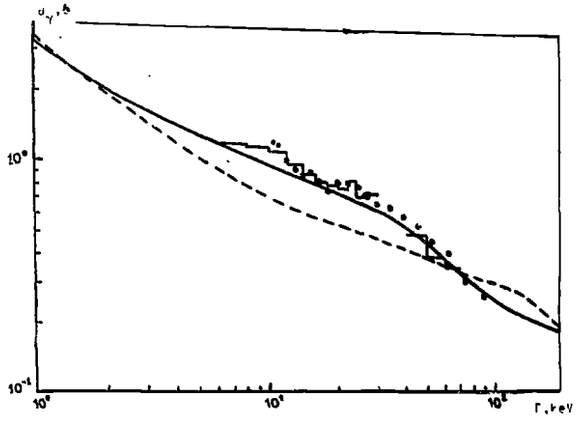

FIG. 16.

Comparison of the experimental and calculated $\sigma_\gamma(^{242}Pu)$: ⎍⎍⎍, experimental data from [42]; • , experimental data of [43]; ----, evaluation of [40];_____, present work

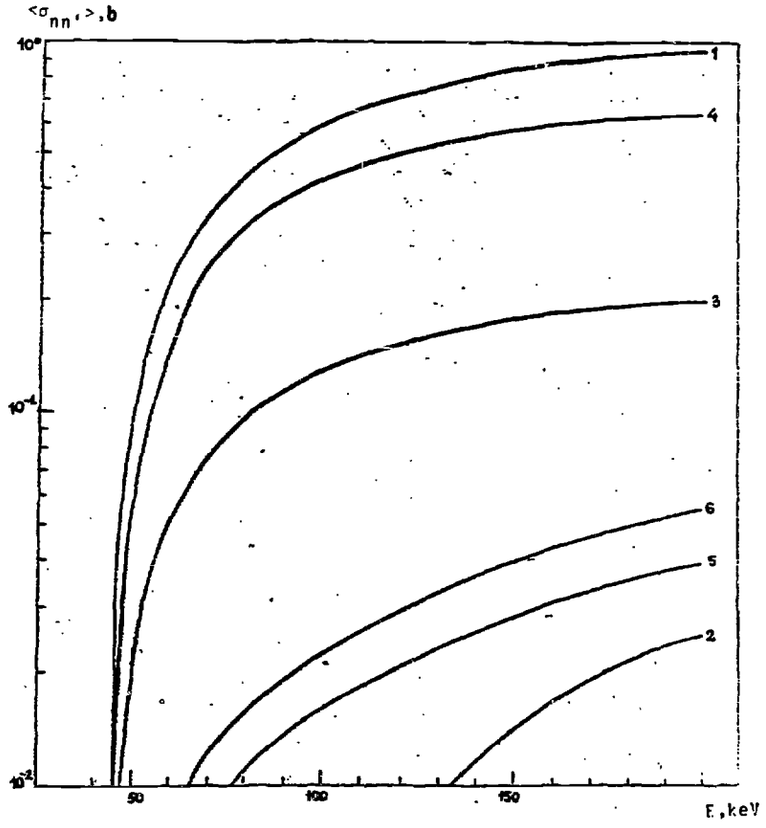

FIG. 17. Total (1) and partial (2-6)^{242}Pu inelastic scattering cross sections for the channels $1/2^+$, $1/2^-$, $3/2^-$, $3/2^+$ and $5/2^+$, respectively

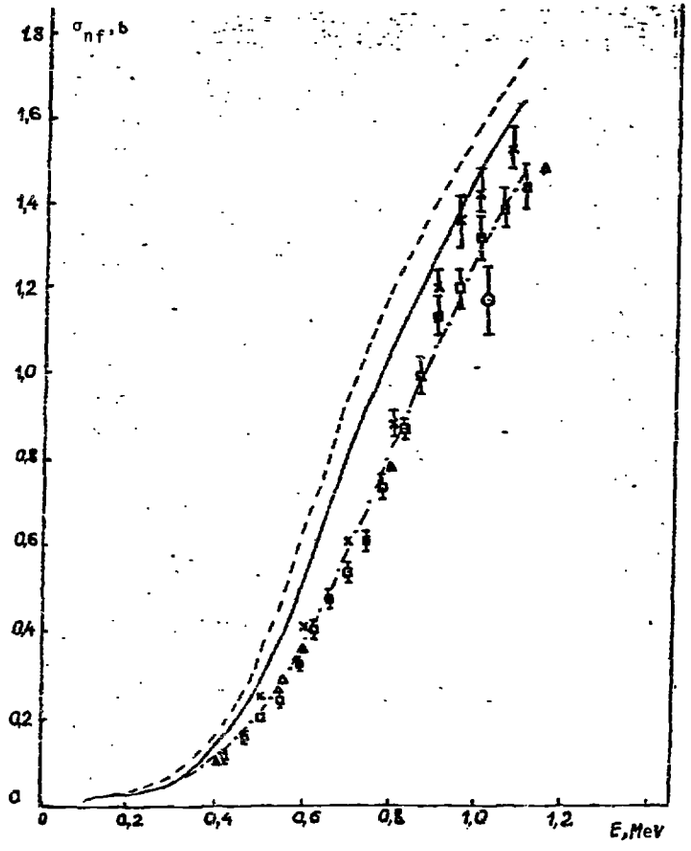

FIG. 18. Comparison of the experimental and calculated $\sigma_{nf}(^{242}Pu)$: ____, Tepel formalism; ---, Hauser-Feshbach formalism with no allowance for the S-factor; -.-.-., Hauser-Feshbach formalism with allowance for the S-factor

obtained fr

and from th
and the mea
spin resonar
distributior
Compare
generalized
of several c
the expressi
the form:

$S_{nxr}=\langle\Gamma\rangle_r\xi^{1/}$

where $\xi=(4\alpha_1$
For thr

S_{nxr} =

$\times \sum_{k=0}^{\infty}$ ~ ^{2}

3. STATISTICAL THEORY CALCULATION OF NEUTRON CROSS SECTIONS FOR FISSILE NUCLEI IN THE ENERGY RANGE FROM 1 keV to 5 MeV

Based on the statistical Hauser-Feshbach model [1], it is possible to develop an aporoach convenient for self-consistent calculation of neutron cross sections for fissile nuclei. The Hauser--Feshbach model assumes that the processes of compound nucleus formation and decay do not depend on each other, and this model thus ignores the effects associated with increasing cross section in the elastic channel that can be allowed for by the Tepel model [46].

The expression for the cross section of the level excitation, $E_{q'}$, with allowance for the competition of fission and radiative capture

$$\sigma_{nn'}(E,E_{q'}) = \frac{\pi}{k^2}\frac{1}{2(2i+1)}\sum_{\ell j}T_{\ell j}(E)\sum_{J}(2J+1)\times$$
$$\times\frac{\sum_{\ell' j'}T_{\ell' j'}(E-\frac{A+1}{A}E_{q'})}{T_{comp}+\sum_{\ell'' j'' q''}T_{\ell'' j''}(E-\frac{A+1}{A}E_{q''})}S_{\alpha\alpha'} \qquad (20)$$

where i is the soin of the ground state of a nucleus-target; ℓ, j the orbital and total moments of an incoming neutron; ℓ', j' the orbital and total moments of an outgoing neutron; J the compound nucleus spin.

The value of T_{comp} in (20) allows for the competitions of non--neutron decay channels permitted by the conservation laws and incorporates the transmission coefficients for radiative capture and fission:

$$T_{comp} = T_{\gamma J\pi}(\frac{A}{A+1}E + S_n) + T_{fJ\pi}(\frac{A}{A+1}E + S_n) \qquad (21)$$

Here $(\frac{A}{A+1}E + S_n)$ is the compound nucleus excitation energy; $T_{\gamma J\pi}$ and $T_{fJ\pi}$ are the "effective" transmission coefficients for radiative capture and fission.

The "effective" fission transmission coefficient, $T_{fJ\pi}$, in the transition state region can be calculated in the same way as in the case of the neutron one:

$$T_{fJ\pi} = 2\pi\frac{\Gamma_{fJ\pi}}{D_J} \qquad (22)$$

To determine the fission width, $\Gamma_{fJ\pi}$, use is usually made of the expression from [47]:

$$\Gamma_{fJ\pi} = \frac{D_J}{2\pi}\sum_k P(E_{fk}, \hbar\omega_k) \qquad (23)$$

where $P(E_{fk},\hbar\omega_k)$ is the penetrability of the kth fission barrier with a height E_{fk} and curvature parameter $\hbar\omega_k$ [20]:

$$P(E_{fk},\hbar\omega_k) = \frac{1}{1+\exp[-\frac{2\pi}{\hbar\omega_k}(E-E_{fk})]} \qquad (24)$$

Here E_{fk} are the energies of the transition states.

Summation in (23) is made over the transition states with spin J and parity π. The approximate scheme of transition states for even nuclei was proposed by Lynn [30]. This scheme was based on the account of the mass saddle-configuration asymmetry, which resulted in a lower $K^\pi=0^-$-band for a barrier B and in decreasing $K^\pi=2^+$-band of a barrier A.

This scheme is known only up to about 1.8 MeV above the fission threshold. Taking into account that fission thresholds for ^{239}Pu, ^{241}Pu and ^{235}U are equal to -1.6 MeV, -1.2 MeV and -0.6 MeV,

respectively, this approach is valid only near the thresholds for ^{239}Pu and ^{241}Pu and in the resolved level region for ^{235}U.

The problem of the nucleus level density at the fission point still remains unclear within the framework of the phenomenological approach to a fission process. As is mentioned by Lynn [13], from the double-humped fission barrier concept it follows that the density of single-particle states of actinides at the Fermi energy is substantially higher for fission deformation rather than for equilibrium one, i.e. the level density at the fission point at excitation energies within the discrete spectrum of transition states should be higher. The independent particle model suggests that at the excitation energies above the boundary of the discrete transition state spectrum, the level density at the fission point should be lower. However, the loss of the saddle-configuration symmetry can lead to increasing rotational states, that would compensate or even exceed this effect.

There are no direct experimental data for the level density at the fission point, except for fission cross sections themselves. The information on level density that can be obtained from σ_f is strongly affected by the fission barrier height, and vice versa the fission barrier heights obtained from experimental σ_f depend on the level density assumption. Therefore, in the high energy range where the scheme of transition states is unknown, to calculate $T_{fJ\pi}$ we used, as Lynn did [13], a simple formula for the transition state density which is similar to that of the constant-temperature model:

$$\rho_f(\varepsilon,J,\Pi) = (2J+1)\exp\left[-\frac{(J+1/2)^2}{2\sigma^2}\right] C_f \exp\left(\frac{\varepsilon}{\theta_f}\right) \qquad (25)$$

where σ, C_f and θ_f are the parameters of the continuous density of transition fissile nucleus states. These parameters are found from the experimental σ_f.

Thus, the "effective" fission transmission coefficient, $T_{fJ\pi}$, with allowance for discrete and continuous spectra of the transition fissile nucleus states can be written as:

$$T_{fJ\pi} = \sum_k P(E_{fk}, \hbar\omega_k) + \int_{E_f}^{\infty} d\varepsilon \rho_f(\varepsilon,J,\Pi) \cdot P(E_{fo}+\varepsilon,\hbar\omega) \qquad (26)$$

where $P(E_{fk}, \hbar\omega_k)$ and $P(E_{fo}+\varepsilon,\hbar\omega)$ are found from (24) and $\rho_f(\varepsilon,J,\Pi)$, from (25).

It is obvious that in this method the criterion for a correct account of the fission competition is the agreement between the calculated and experimental fission cross section σ_f.

Thus, the knowledge both of the approximate scheme of transition states up to about 1.8 MeV above the fission threshold and of the approximate fission barrier heights from the experiments on (d,pf) and (t,pf) reactions [48] as well as the use of the constant-temperature model for the level density at higher energies enabled to determine level density parameters and specified the transition state schemes and barrier heights based on the experimental data for σ_f for ^{239}Pu, ^{240}Pu, ^{241}Pu, ^{242}Pu and ^{235}U. It has appeared that about 0.2 MeV changes in E_f and about 10% changes in $\hbar\omega$ do not seriously affect the quality of the σ_f fitting provided that the relevant compensating changes are made for other parameters.

Owing to the fact that for actinides usually one peak of the fission barrier is higher than the other (except only ^{237}U, whose both peaks are the same) the effective fission transmission coefficient, $T_{fJ\pi}$, can be taken equal to the smaller of $T_{fJ\pi}^{(A,B)}$, which is quite satisfactory for calculation of neutron cross sections [13]. When both $T_f^{(A)}$ and $T_f^{(B)}$ are greatly less than 1 (subbarrier fission), formula (20) used to calculate σ_f becomes inapplicable and, therefore, the method described in the previous section has to be adopted.

The "effective" transmission, $T_{\gamma J\pi}(E)$, for radiative capture was calculated with allowance for possible cascade γ-quantum emission.

The transmission of a single γ-transition $T_{\gamma J\pi}(E,\varepsilon_\gamma)$ with emission of a γ-quantum having energy ε_γ from the $E+S_n$ excited state having a total moment J and parity π was calculated just as in the case of the neutron transmission:

$$T_{\gamma J\pi}(E,\varepsilon_\gamma) = \frac{2\pi\langle\Gamma_\gamma\rangle_{J\pi}(E,\varepsilon_\gamma)}{\langle D\rangle_{J\pi}(E+S_n)} = 2\pi f(E,\varepsilon_\gamma) \qquad (27)$$

The spectral factor $F(E,\varepsilon_\gamma)$ is usually given in the form proposed by Blatt and Weisskopf [49]. The collective giant resonance model is proved to better founded [50].

Total effective transmission for radiative capture can be obtained by all possible γ-transition summation. When only dipole γ-transitions are allowed for, we have:

$$T_{\gamma J\pi}(E) = 2\pi \int_0^{\frac{A}{A+1}E+S_n} d\varepsilon_\gamma \sum_{J_k=|J-1|}^{J+1} f(E,\varepsilon_\gamma)\rho(E+S_n-\Delta-\varepsilon_\gamma,J_k) \qquad (28)$$

where $\rho(E+S_n-\Delta-\varepsilon_\gamma,J_k)$ is the compound nucleus level density for excitation energy $E+S_n-\Delta-\varepsilon_\gamma$) and spin J_k.

The dependence of the level density upon parity was not allowed for since it can be probably ignored [25,51] in the case of deformed nuclei. The expressions obtained from the traditional Fermi-gas model, the Fermi-gas model involving collective modes and the superfluid nucleus model were used for the level density, $\rho(u,J)$.

When $T_{\gamma J\pi}(E)$ is calculated, in principle, it is necessary to allow for the available discrete spectrum of compound nucleus levels in the low excitation energy range. This would result both in the change of the integration limit in expression (28) and in the appearence of an extra summand that allows for γ-transitions from the continuous spectrum to the discrete one. However, the calculations have shown that the contribution of a discrete spectrum to the radiative width is very small and is not thus allowed for in further calculations.

Due to a large number of open channels, the partial width fluctuation effect ($S_{\alpha\alpha'}=1$) can be neglected in the excitation energy range corresponding to the continuous excitation spectrum of a nucleus-target. In this energy range the cross section $\sigma_{nn'}(E)$, can be written as:

$$\sigma_{nn'}(E) = \sum_0 \sigma_{nn'}(E,E_{q'}) + \sigma_{nn',\,cont}(E) \qquad (29)$$

where $\sigma_{nn'}(E,E_{q'})$ was calculated as by expression (2) with $S_{\alpha\alpha'}=1$ and an extra term $\alpha(E,J)$ in the denominator which takes into account the continuous competition; $\sigma_{nn',\,cont}(E)$ is the continuous spectrum excitation cross section and is defined as:

$$\sigma_{nn',\,cont}(E) = \frac{\pi}{k^2}\frac{1}{2(2i+1)} \sum_{\ell j} T_{\ell j}(E) \sum_J (2J+1) \times$$

$$\times \frac{\alpha(E,J)}{T_{comp} + \sum_{\ell'' j'' q''} T_{\ell'' o''}(E-\frac{A+1}{A}\varepsilon_{q''}) + \alpha(E,J)} \qquad (30)$$

$$\alpha(E,J) = \sum_{\ell' j'} \int_{E_{q',max}}^{\frac{A}{A+1}E} \sum_{i'} \rho(i',F')T_{\ell'} \qquad (31)$$

where $E_{q',max}$ is the energy, at which the continuous level spectrum starts.

In the case of the continuous level spectrum of a nucleus-target, the competition of fission due to inelastic scattering and radiative capture was allowed for by introducing "effective" transmissions:

$$T_{fJ\pi}(E) = (2J+1)\exp\left[\frac{-(J+1/2)^2}{2\sigma^2}\right] T_f(E) \qquad (32)$$

where $T_f(E)$ was deterrined by fitting the σ_f fission cross section calculated by the unique formalism to the experimental ones. The contribution of the $(n,\gamma f)$-reaction was allowed for in fission cross section calculations.

4. ANALYSIS OF DIFFERENT APPROACHES TO THE STATISTICAL THEORY

To our mind, the above method for neutron cross section calculations using the Hauser-Feshbach statistical model requires comparison with other models and clarifying the influence of the collective level density effects on neutron cross section calculations.

At low excitation energies, when the levels do not overlao, i.e. when the compound nucleus states are not completely statistically independent, there may appear correlations between inlet and outlet channels. Unfortunately, although this problem is very important, it has not been yet solved up to now. The use of the Moldauer approach [53,54] with the application of the parameter Q_α that depends on the statistical properties of the compound-nucleus states and varies within (0,1) also does not solve this problem since the choice of the correlation coefficient and its energy dependence is not sufficiently substantiated, and the parameter Q_α cannot be analytically calculated. Therefore, this approach is less applicable for neutron cross section evaluation of fissile nuclei.

The Tepel approach [46] allows for the correlation of the inlet and outlet elastic channels and can thus be successfully used in the case of the large number of channels having comparable contributions. However, we should bear in mind the restrictions typical for this approach.

When the Tepel approach [46] is used to calculate neutron cross sections, a specific combination of the decay channels and their transmission coefficient ratio should be taken into consideration. This approach can be adopted only either in the case of slightly differing channel transmissions or in the case of a combination of several weak and several strong channels provided that the total channel number is about 10. In the case of weak cross sections (for example, $\sigma_{n\gamma}$ and σ_{nn} for fissile nuclei), the neutron cross sections calculated by the Tepel formalism and those, by the Hauser-Feshbach (with correction for the width fluctuation) give the greatest discrepancy (10-30%). In this case the computer statistical calculations made by Moldauer [15] support the Hauser-Feshbach formalism.

If the number of the channels and of their freedom degrees is small and if a strong competing channel exists, then the Tepel approach can give incorrect results. When the number of open channels is large, the Tepel expression coincides with the Hauser-Feshbach formula. Moreover, both these approaches have a tendency to coincide at strong absorption ($T_{nr}\to 1$) and at decreasing fission competition.

Figure 19 gives the average ^{239}Pu $\langle\sigma_{nn}\rangle$ and $\langle\sigma_{n\gamma}\rangle$ 0^+ channel cross sections calculated by the Hauser-Feshbach and Tepel formalisms. In both approaches, for weak absorption ($T_n^{0+} \ll 1$) at 0.1 keV, the difference in $\langle\sigma_{nn}\rangle^{0+}$ reaches a factor 2.8 and at a transition to moderate absorption (E_n=100 keV, T_n^{0+} about 0.26) this difference is decreased to 1.6. The values of $\langle\sigma_{n\gamma}\rangle^{0+}$ are correlated in the same manner. In these two approaches, the difference between $\langle\sigma_n\rangle^{0+}$ calculations displays an opposite tendency, thereby varying from 10% at 0.1 keV to 25% at 100 keV. For the 1^+ state the difference in $\langle\sigma_{nn}\rangle^{1+}$ decreases to 20% within 0.1-100 keV, the difference in $\langle\sigma_{n\gamma}\rangle^{1+}$ varies from 17% at 0.1 keV to 10% at 100 keV and the one in $\langle\sigma_f\rangle^{1+}$, from 40 to 45%. The decrease of the differences

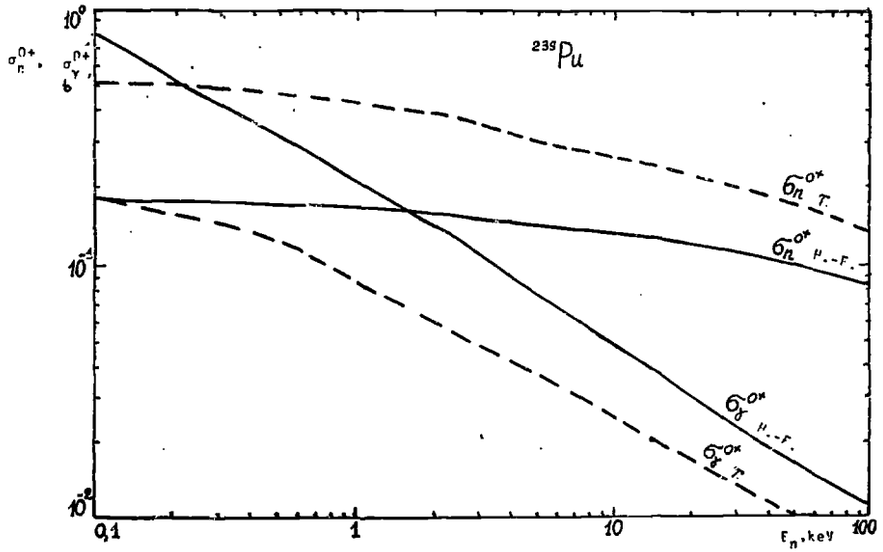

FIG. 19.
Comparison of the average ^{239}Pu σ_{nn}^{0+} and $\sigma_{n\gamma}^{0+}$ calculated using the Hauser-Feshbach formalism (solid line) and the Tepel formalism (dashed line)

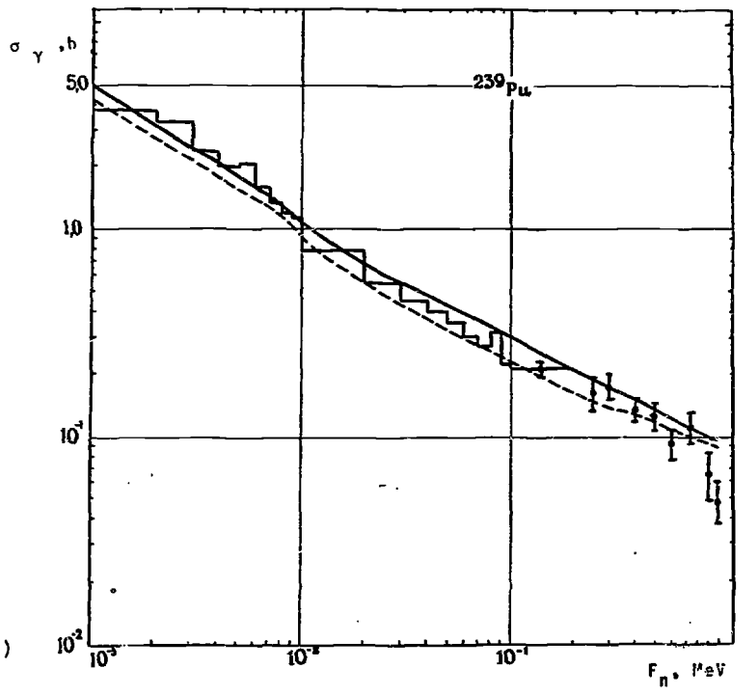

FIG. 20. Comparison of the calculated and experimental $\sigma_\gamma(^{239}Pu)$:
——present Hauser-Feshbach calculation; ----, calculation using the Tepel formalism; ⎍⎍⎍, evaluation of the experimental data.

in $\langle\sigma_{nn}\rangle^{1+}$ and $\langle\sigma_{n\gamma}\rangle^{1+}$, as compared to $\langle\sigma_{nn}\rangle^{0+}$ and $\langle\sigma_{n\gamma}\rangle^{0+}$ is caused by the substantial attenuation of the fission competition.

As compared to the Tepel formalism , the use of the Hofman formula [55] does not substantially change the results obtained although it takes into account the dependence of W_α not only on T_α but also on $\bar{T}$.

Figures 20 through 22 show ^{239}Pu $\sigma_{n\gamma}$, σ_f and $\sigma_{nn'}$ cross sections calculated by the Hauser-Feshbach approach with allowance for the fission competition and by the Tepel method. It is seen that

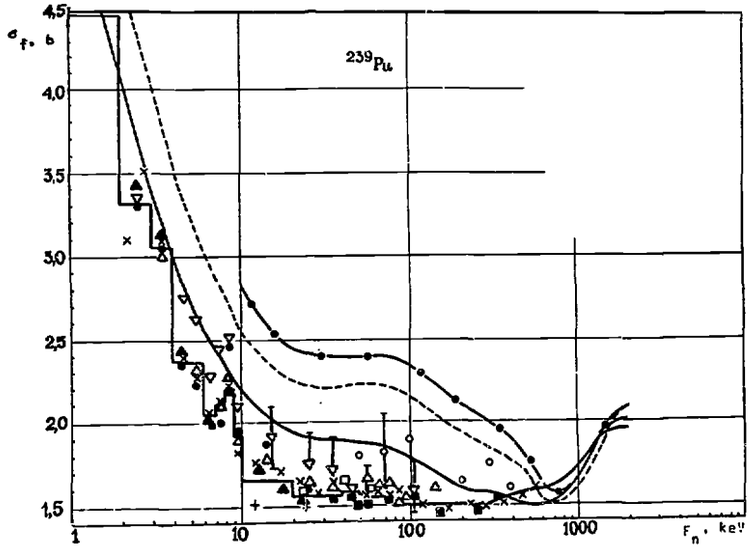

FIG. 21.

Comparison of the calculated and experimental $\sigma_f(^{239}Pu)$: _____, Hauser-Feshbach calculation with the S-factor; -----, Tepel calculation; -•-•-•-, Hauser-Feshbach calculation with no regard for the S-factor; ⎍⎍⎍, evaluated data

the fission cross sections calculated by the Tepel method are 15% higher and radiative capture cross sections are 15% lower within 1 keV-1 MeV than those calculated by the Hauser-Feshbach model, the latter being in a better agreement with experimental σ_f cross sections, and probably with $\sigma_{n\gamma}$. The difference in the inelastic scattering $\sigma_{nn'}$, (^{239}Pu) cross section is inconsiderable in both approaches. The same results are also obtained for other greatly fissile nuclei.

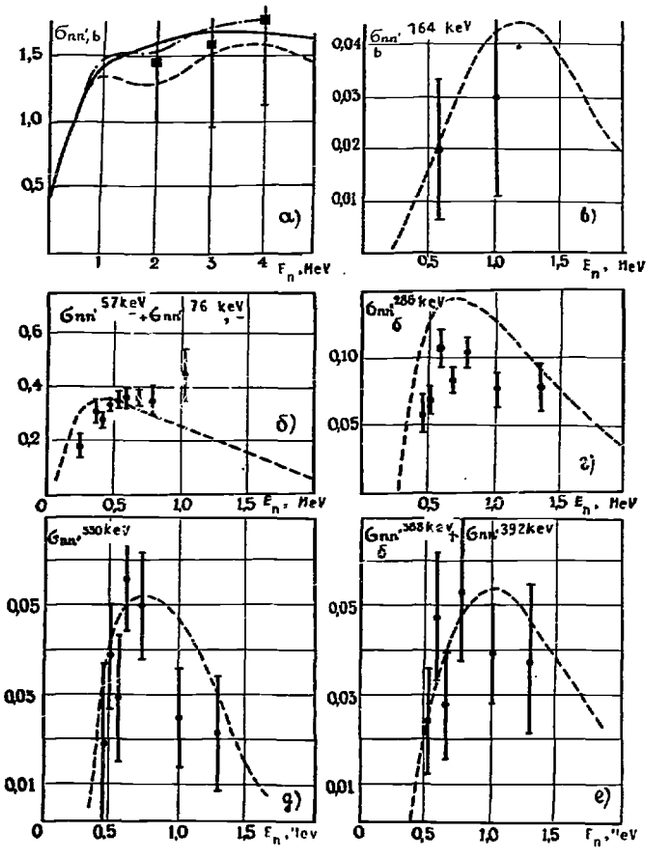

FIG. 22.

Comparison of the experimental $\sigma_{n,n'}$, (^{239}Pu) with those calculated by the statistical model : ----, statistical calculations; -.-.-, sum of compound and direct excitation

FIG. 5.

So, a conclusion may be made that within the framework of the above assumptions, the Tepel-Hofmann-Weidenmüller approach should not be used to calculate neutron cross sections of heavy strongly fissile nuclei up to 1 MeV, which is caused by the small number of decay channels and by the available strong competing fission channel with small ν_f. However, the present calculations (Fig. 23) show that already at 1.1 MeV, the neutron cross sections, calculated by the Hauser-Feshbach formalism with the S-factor and by the Tepel one, agree within 10% for $\sigma_{n\gamma}$, about 10% for σ_f and about 2% for $\sigma_{nn'}$. It should be noted that when the Tepel formalism was used, the sum of compound nucleus cross sections proves to be different from the one calculated by the optical model. With increasing energy, this difference due to neutron transmission modification for the inlet channel is however decreased and almost vanishes at $E_n > 1.1$ MeV. As above 1.1 Mev there are experimental σ_f (^{242}Pu) cross section data and fission transmissions T_f can be found with sufficient confidence (Fig. 24), while $\sigma_{n\gamma}$ in this energy range is much less than cross sections of other non-elastic processes, then the sum of elastic and inelastic compound nucleus cross sections calculated using the Hauser-Feshbach and Tepel formalisms proves to be the same. However, as compared to the Hauser-Feshbach formalism, the Tepel model takes into account the correlation of inlet and outlet elastic channels and more correctly calculates the elastic compound scattering cross section. This means that the Tepel formalism also gives better calculation of the inelastic scattering cross section in the energy range from 1.1 MeV to 2 MeV. Above 2 MeV, the use of both formalisms leads to the same results.

Above 1.1 MeV, the Tepel formalism was therefore employed, whose main difference from the Hauser-Feshbach model manifests itself in different expressions for inlet channel neutron transmission coefficients and in the extra factor in the formula for elastic scattering cross section:

$$\sigma_{nn'}(E_q) = \frac{\pi}{k^2}\frac{1}{2(2i+1)}\sum_{\ell jJ} V_{\ell j}(E)(2J+1) \times$$

$$\times \frac{\sum_{\ell' j' J} V_{\ell' j' J}\left(E-\frac{A+1}{A}E_q\right)}{V_{\gamma J\pi} + V_{fJ\pi} + \sum_{\ell'' j'' q'} V_{\ell'' j'' J} + \alpha(E,J)} \qquad (33)$$

$$\alpha(E,J) = \sum_{\ell' j' i'} \int_{E_{a_{max}}}^{\frac{A}{A+1}E} \rho(E',i') V_{\ell' j' J}\left(E-\frac{A+1}{A}E'\right)dE' \qquad (34)$$

$$\sigma_{nn'\,cont} = \frac{\pi}{k^2}\frac{1}{2(2i+1)}\sum_{\ell jJ} \times$$

$$\times \frac{V_{\ell jJ}(E)\cdot(2J+1)\alpha(E,J)}{V_{\gamma J\pi} + V_{fJ\pi} + \sum_{\ell'' j'' q''} V_{\ell'' j'' J} + \alpha(E,J)} \qquad (35)$$

$$\sigma_{nn'}(E) = \sum_q \sigma_{nn'}(E,E_q) + \sigma_{nn'\,cont} \qquad (36)$$

$$\sigma_{n\gamma} = \frac{\pi}{k^2}\frac{1}{2(2i+1)}\sum_{\ell jJ} V_{\ell jJ}(2J+1)\frac{V_{\gamma J\pi}}{V_{\gamma J\pi} + V_{fJ\pi} + V_{nJ\pi}} \qquad (37)$$

$$\sigma_f = \frac{\pi}{k^2}\frac{1}{2(2i+1)}\sum_{\ell jJ} V_{\ell jJ}(2J+1)\frac{V_{fJ\pi}}{V_{\gamma J\pi} + V_{fJ\pi} + V_{nJ\pi}} \qquad (38)$$

FIG. 7. Co
α(
wi
fi

where the modified transmission, $V_{\ell j}$, for an elastic neutron channel is :

$$V_{\ell j} = T_{\ell jJ}\left[1 + \frac{T_{\ell jJ}}{\sum_{\ell j} T_{\ell jJ}} (W_{\ell jJ} - 1)\right]^{-1} \qquad (39)$$

while $W_{\ell jJ}$ is calculated by the formula:

$$W_{\ell jJ} = 1 + 2\left[1 + \sqrt{T_{\ell jJ}}\right]^{-1} \qquad (40)$$

For other neutron channels as well as for those of fission and radiative capture $V_{\ell jJ}$ coincides with $T_{\ell jJ}$.

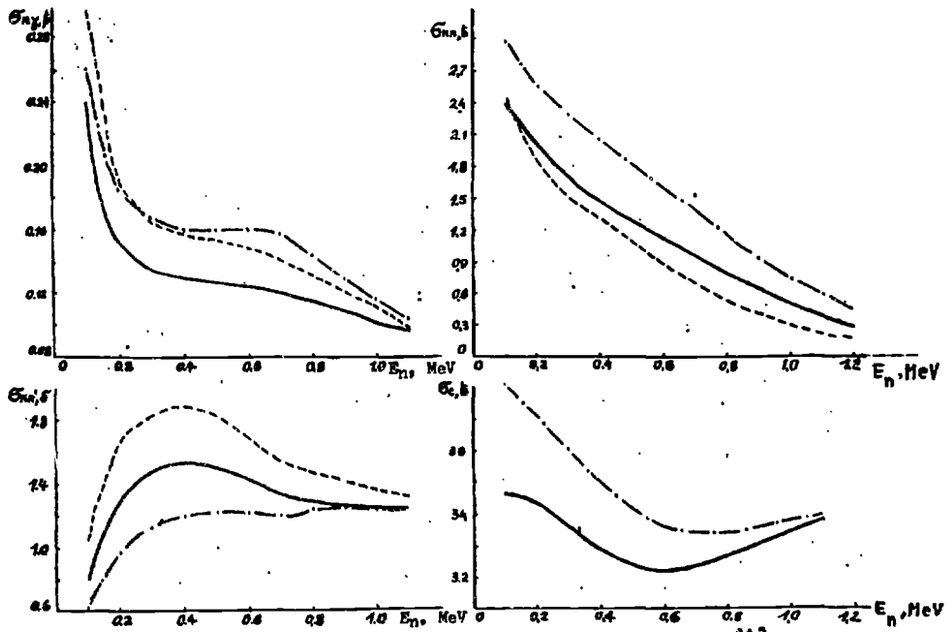

FIG. 23. Comparison of different approaches used to calculate ^{242}Pu radiative capture, elastic and inelastic scattering, and compound-nucleus cross sections (Fermi-gas model involving collective modes, spectral Lorentzian factor); ___, Tepel formalism; ----, Hauser-Feshbach formalism with no regard for the S-factor; -.-.-, Hauser-Feshbach formalism with allowance for the S-factor

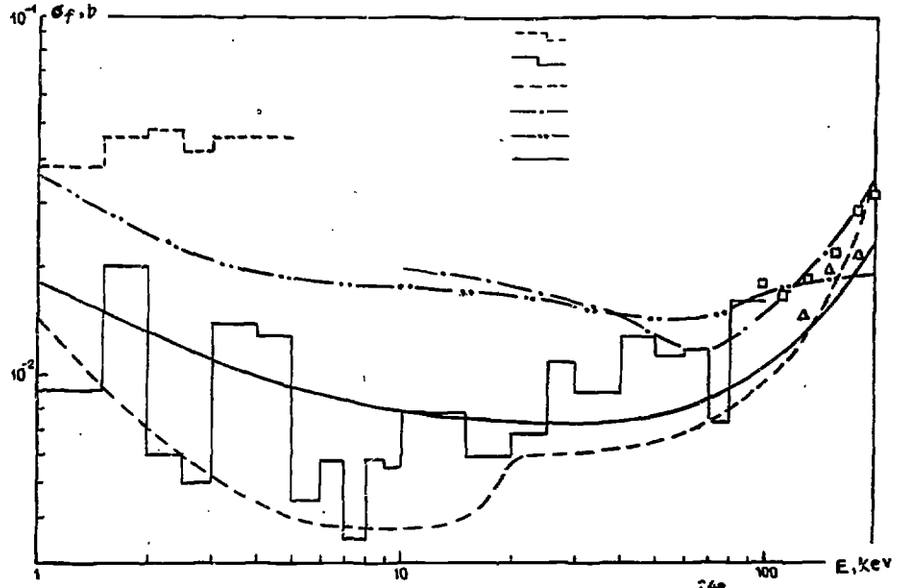

FIG. 24. Comparison of the experimental and calculated $\langle\sigma_f\rangle$ for ^{242}Pu below 200 keV: ⎍⎍, data of [44]; ⎍⎍, data of [45]; -----, evaluation data of [40]; -•-•-, calculation data from [41]; -••-••-••-, present calculation using the Lynn parameters [13]; ____, present calculation with E_A=5.94 MeV; $\hbar\omega_A$=0.8 MeV; E_B=5.64 MeV; $\hbar\omega_B$=0.52 MeV

Consequently, the Tepel formalism that allows for the correlation effect of inlet and outlet elastic channels is most suitable to calculate the cross sections in the case of a great number of channels whose contributions are comparable (for actinides it is implemented at E_n> 1.1 MeV).

It should be emphasized that the above method applied can correctly allow for the fission competition in calculations of neutron cross sections of other processes but it cannot predict the fission cross sections for nuclei, for which no experimental data are available since the nuclear level density in the energy range above the fission threshold should be fitted empirically to reproduce experimental σ_f cross sections. Nevertheless, this approach proves to be effective to evaluate fissile nucleus data.

A fission process is a complex phenomenon not yet sufficiently studied. Physics of this process is undoubtedly much more complex than it follows from the above semiempirical model. Even within

the framework of this approach, the level density at the fission point and the scheme of the transition states for even nuclei-targets are not yet clear. The main uncertainty in σ_f calculations is associated with the scheme of the transition nucleus states during the fission process and is especially high for even nucleus-target cross sections since for these nuclei a strong centrifugal barrier should be taken into account (when the barrier height varies in a similar manner, the greater change in σ_f is observed for the states with low orbital moments, as compared to those with high ones).

5. ALLOWANCE FOR THE (n,γf)-REACTION IN NEUTRON CROSS SECTION CALCULATIONS FOR FISSILE NUCLEI

In the case of fissile negative-threshold nuclei, it is of importance to allow for the (n,γf)-reaction in radiative capture cross section calculations.

In $\sigma_{n\gamma}$ calculations, the quantities $\bar{D}$ and $\bar{\Gamma}_\gamma$ are the most important parameters. This follows from the fact that the ratio $(2I+1)\frac{\bar{\sigma}_{n\gamma}}{\bar{S}_\gamma}$ where $\bar{S}_\gamma = \frac{2\pi\bar{\Gamma}_\gamma}{\bar{D}_{obs}}$ is approximately constant for all nuclei at the given neutron energy.

The correct level density model should be used to determine $\bar{D}$ and the appropriate level density parameter "a".

To calculate an average radiative width, $\bar{\Gamma}_\gamma$, one widely used the Blatt-Weisskopf factor [49]:

$$\bar{\Gamma}_\gamma(\varepsilon_\gamma,J) = C_\gamma A^{2/3}\varepsilon_\gamma^{2\ell+1}\,\bar{D}_J\,(u) \qquad (41)$$

However, this formula gives unsatisfactory prediction of the absolute value of $\bar{\Gamma}_\gamma$, so the constant C_γ is usually fitted using the experimental data.

For heavy deformed nuclei, a better agreement with the experimental photonuclear reaction cross sections is achieved, when the Lorentzian factor in the form of two lines is used [50]:

$$\bar{\Gamma}_\gamma(\varepsilon_\gamma,J) = \frac{8}{3}\frac{NZ}{A}\,\frac{e^2}{\hbar c}\,\frac{1.4}{m_p c^2}\sum_{i=1}^{2}\frac{\Gamma_{ig}\,\varepsilon_\gamma^4}{(\varepsilon_\gamma^2-E_{iG}^2)+(\Gamma_{ig}\varepsilon_\gamma)^2}\,\bar{D}_J(u) \qquad (42)$$

This formula is assumed to satisfactorily describe the energy dependence of Γ_γ for the nuclei being far from the closed shells [56].

The giant resonance parameters were chosen to be average for heavy nuclei [13]: E_{1G}=11 MeV, Γ_{1G}=2.9 MeV, E_{2G}=14 MeV, Γ_{2G}=4.5 MeV and then the calculated radiative widths $\Gamma_{\gamma J\pi}$ were normalized to the evaluated value of $\langle\Gamma_\gamma\rangle$ in the resolved resonance region.

The above expressions are valid when the emission of subsequent γ-rays is the only way to release the residual compound nucleus excitation after the first γ-quantum is emitted. Indeed, after the first γ-quantum is emitted the nucleus excitation may be released due to neutron emission and fission. The emittance of neutrons is possible only when the excitation energy, after the first γ-quantum is emitted, is larger than the neutron separation one.

Therefore, it is necessary to allow for the competition between (n,γn') and (n,γf) reactions and radiative capture to calculate radiative capture transmission coefficients using the cascade γ-ray emission theory [49].

It has appeared that allowance for the (n,γn')-reaction in radiative capture calculations is important for neutron energies that are higher than the average energy of the first cascade emitted γ-rays ($\bar{\varepsilon}_\gamma \sim 1$ MeV). Calculations show that at neutron energy of 0.5 MeV, allowance for this process in the case of ^{242}Pu reduces $\bar{\Gamma}_\gamma$ only by 0.5%.

It is of importance to allow for the (n,γf)-reaction in the case of fissile nuclei when the excited compound nucleus fission is possible after the first γ-quantum emission [57,58].

The authors of [57] obtained $\Gamma_{\gamma f} = 0.5 \bar{\Gamma}_{\gamma}$ for ^{239}Pu (i.e. $\Gamma_{\gamma} \approx$ 20 meV and Lynn [58] calculated the (n,γf)-process width, that proved to be $\Gamma_{\gamma f} \approx 3$ meV for the state 1^+ and $\Gamma_{\gamma f} \approx 4$-7 meV for the state 0^+

Since recently direct experimental data for the (n,γf)-process widths have appeared, it is of interest to make theoretical calculations of these widths using the developed statistical approach based on the self-consistent parameters. It is also of significance to analyse the effect of the (n,γf)-reaction on the energy dependences of $\bar{\Gamma}_{\gamma}$, $\sigma_{n\gamma}$, σ_{nF} and α.

The calculation of the (n,γf) width mainly implies the determination of the part of the spectrum of γ-rays that give the intermediate states lying above the appropriate fission thresholds. In this case, it is necessary to allow for the competition between fission and radiative capture widths in these states.

For negative fission threshold nuclei, the competition between the (n,γf)-reaction and radiative capture is possible in the cases when the residual nucleus excitation after the first γ-quantum is emitted, is less than the neutron binding energy provided $E-E_f > \varepsilon_{\gamma}$ where E_f is the fission threshold energy read out from the binding energy, i. e. for low fission threshold nuclei (^{239}Pu, E_f=-1.6 MeV, ^{241}Pu E_f= -1.2 MeV, ^{233}U E_f= -1.5 MeV) this competition is possible even for thermal neutron energies.

To allow for this effect, the spectral factor must be multiplied by $\dfrac{T_{\gamma}(E-\varepsilon_{\gamma})_{J\pi}}{T_{\gamma}(E-\varepsilon_{\gamma})_{J_k\pi} + T_f(E-\varepsilon_{\gamma})_{J_k\pi}}$ where $T_f(E-\varepsilon_{\gamma})_{J_k\pi}$ is the effective fission transmission coefficient at the excitation energy $E+S_n-\varepsilon_{\gamma}$.

Fission transmission coefficients were calculated by formula (23) and (24) while radiative capture transmission, by formula (28).

Since fission widths are the functions of spin and parity, the competition of the (n,γf)-reaction allowed for leads to a more pronounced dependence of the average radiative widths on spin and parity.

Calculations illustrate that the values of $\langle\Gamma_{\gamma}\rangle$ calculated with allowance for the (n,γf)-reaction for two forms of the spectral factor $f(E,\varepsilon_{\gamma})$, (41)-(42), slightly differ, only 5-10%.

A weak energy dependence of Γ_{γ} for both spectral factors up to 1 MeV, where experimental data for $\sigma_{n\gamma}$ are available, does not permit us to make a proper choice. However, the form of the spectral factor substantially affects the calculated $\langle\Gamma_{\gamma f}\rangle$ widths.

For ^{239}Pu the experimental values of $|\Gamma_{\gamma f}^{0+} - \Gamma_{\gamma f}^{1+}| < 4$ meV are obtained in [59], those of $\Gamma_{\gamma f}^{1+} = 4.1 \pm 0.9$ meV, in [60] and those of $\Gamma_{\gamma f}^{1+} = 6.1 \pm 2.9$ meV, in [61]. In our calculations, we used the spectral Weisskopf factor (formula (41)) and obtained $\langle\Gamma_{\gamma f}\rangle^{0+}$=9.3 meV and $\langle\Gamma_{\gamma f}\rangle^{1+}$=10.3 meV for ^{239}Pu, which is not consistent with the experimental data. When the spectral Lorentzian factor (formula(42)) was used, we obtained $\langle\Gamma_{\gamma f}\rangle^{1+}$=4.7 meV and $\langle\Gamma_{\gamma f}\rangle^{0+} - \langle\Gamma_{\gamma f}\rangle^{1+}$ = 5.6 meV, which agrees with the experimental data within their errors. Sums of the calculated widths $\langle\Gamma_f\rangle^{J\pi} + \langle\Gamma_{\gamma f}\rangle^{J\pi}$ for the states 0^+ and 1^+ for ^{239}Pu are equal to 2019 meV and 34.6 meV, respectively, which is consistent with the total experimental fission widths : $\langle\Gamma_F\rangle^{0+}$ = 2049 ± 200 meV and $\langle\Gamma_F\rangle^{1+}$ = 35.6 ± 2.0 meV. Note that the demand for the agreement between the theoretical and experimental fission widths $\langle\Gamma_F\rangle^{0+}$ and $\langle\Gamma_F\rangle^{1+}$ as well as $\langle\Gamma_{\gamma F}\rangle^{0+}$ and $\langle\Gamma_{\gamma f}\rangle^{1+}$ strictly specifies the fission threshold, especially, of semi-open channels and excess over the threshold of the states 0^+, 1^+ and 2^+.

The values of $\Gamma_{\gamma f}$ for ^{241}Pu were experimentally measured [62] and proved to be $\langle\Gamma_{\gamma f}\rangle^{2+}$ = 7 meV and $\langle\Gamma_{\gamma f}\rangle^{3+}$ = 2 meV. We used the spectral Lorentzian factor to calculate the (n,γf) widths for ^{241}Pu and obtained $\langle\Gamma_{\gamma f}\rangle^{2+}$= 4.95 meV and $\langle\Gamma_{\gamma f}\rangle^{3+}$=2.91 meV,

which is again better consistent with the experimental data than with those calculated by the Weisskopf factor when $\langle\Gamma_{\gamma f}\rangle^{2+}$ =10.44 and $\langle\Gamma_{\gamma f}\rangle^{3+}$ = 6.62 meV.

The above values of $\Gamma_{\gamma f}$ were calculated with regard only for El-transitions. If we assume that there exists some fraction of the Ml-transitions equal to $\frac{f(El)}{f(Ml)} \cong 6.8$ [63], then the calculation based on these Ml-transitions gives $|\Gamma_{\gamma f}^{0+} - \Gamma_{\gamma f}^{1+}|$ = 3 meV and $\Gamma_{\gamma f}^{1+}$ = 5.9 meV for ^{239}Pu, which also does not contradict the experimental data. With increasing contribution of the Ml-transitions [f(El)/f(Ml)→1], the value of $\Gamma_{\gamma f}^{1+}$ will grow, which results in a worse agreement between the theoretical and experimental data. No reasons are available now to consider that the contribution of the Ml-transitions for heavy nuclei is more than 10-20% of the El-transitions, although the contribution of the Ml-transitions for nuclei with medium A may be the large one [64].

Thus, a more strong dependence of the calculated widths $\langle\Gamma_{\gamma f}\rangle_{J^\pi}$ on the spectral factor, as compared to $\Gamma_{\gamma f}$, makes it possible to conclude that within the accuracy of the existing experimental data for $\Gamma_{\gamma f}$, the use of the spectral Weisskopf factor, on the whole, gives worse agreement with the experimental results for $\Gamma_{\gamma f}$ widths against the Lorentzian one, whereas the latter ensures satisfactory agreement with the experimental results for $\Gamma_{\gamma f}$.

As is expected, the regard for the (n,γf) and (n,γn')-reactions causes a change in the energy dependence of the radiative width, $\langle\Gamma_\gamma\rangle$, (Figs. 25 and 26). This change is extremely sharp above 1 MeV (at 1 MeV, when these processes are allowed for, $\langle\Gamma_\gamma\rangle$ decreases as much as 1.5 times. It is natural that this change in $\langle\Gamma_\gamma\rangle$ also affects the radiative capture cross section.

Figures 28 and 29 display comparison between the experimental data and our calculations of ^{239}Pu radiative capture cross sections.

These figures show that the (n,γf) and (n,γn')-processes must be allowed for to calculate $\sigma_{n\gamma}$ of strongly fissile nuclei with a negative threshold. At 1 MeV, the calculation results for $\sigma_{n\gamma}$ (^{239}Pu) with and without regard for a (n,γf)-process differ as much as 1.5-2.0 times. At 3 MeV, when the (n,γn')-reaction contributes much, this difference is of the order of several times.

A weak dependence of the calculated $\sigma_{n\gamma}$ cross sections on the spectral factor for strongly fissile nuclei up to 1 MeV does not enable to make a unique choice between the spectral Lorentzian and Weisskopf factors using the data for $\sigma_{n\gamma}$ alone. The results for $\sigma_{n\gamma}$ (^{239}Pu) calculated by both these spectral factors below 0.8 MeV are in good agreement with the experimental data both in absolute value and in the curve shape. In these calculations of σ_γ, the values of $\bar{\Gamma}_\gamma/D$ were not varied, as is usually done [28], but were obtained in the resolved resonance region and taken without any changes.

In the low energy range, where $\sigma_{n\gamma}$ is a considerable part of the nonelastic cross section, the (n,γf) -process may much contribute to the fission cross section $\sigma_F=\sigma_f+\sigma_{\gamma f}$. Calculations show that at 1 keV, the (n,γf)-reaction cross section contribution to σ_F is about 20%. With increasing energy, the (n,γf)-cross section contribution to σ_F decreases.

A change in $\sigma_{n\gamma}$ and σ_F with allowance for the (n,γf)--process also affects $\alpha = \frac{\sigma_{n\gamma}}{\sigma_F}$. So, calculations of α for ^{239}Pu with and without regard for this process differ by 25% at 1 keV, by about 15% at 40 keV, by about 20% at 0.3 MeV and by about 50% at 0.7 MeV. Below 100 keV, an increase in this difference with decreasing energy is caused by increasing contribution of $\sigma_{n,\gamma f}$ to σ_F. Above 100 keV, the competition between the (n,γf)-reaction and radiative capture is intensified.

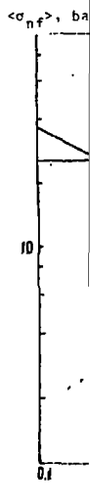

FIG. 12.

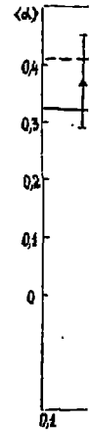

FIG. 13.

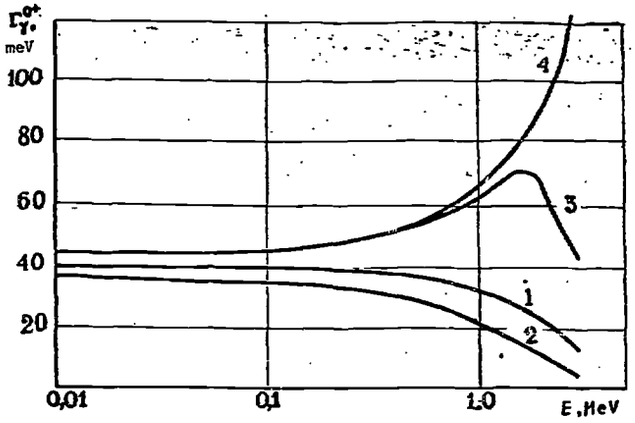

FIG. 25. Energy denendence of Γ_{γ}^{0+} for ^{239}Pu: 1, calculation with regard for (n,γf) and (n,γn')-reactions,Lorentzian spectral factor; 2, with regard for (n,γf) and (n,γn'),Weisskonf spectral factor; 3, with regard for (n,γn') alone, Lorentzian snectral factor; 4, without regard for (n,γf) and n,γn'), Lorentzian spectral factor

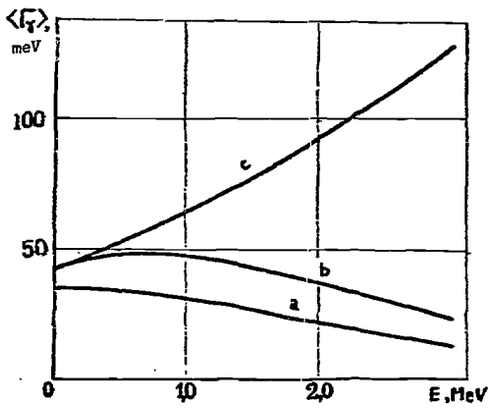

FIG. 26. Energy dependence of average radiative ^{241}Pu $\langle\Gamma_\gamma\rangle$ widths: a; 3^- channel width with regard for (n,γn') and (n,γf); b; 3^+ channel width with regard for (n,γn') and (n,γf); c; $3^{\pm}$ channel width without renard for (n,γn') and (n,γf)-reactions

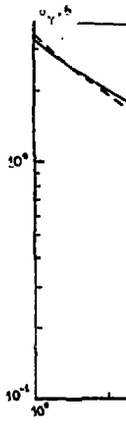

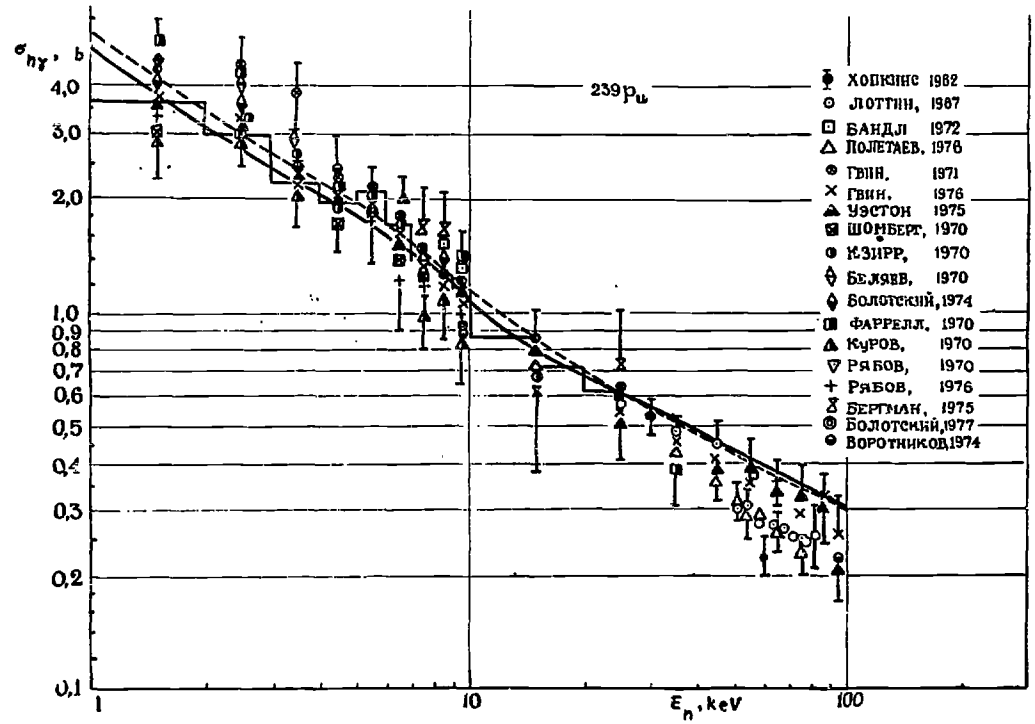

FIG. 27 Comparison of the experimental $\sigma_{n\gamma}$ for ^{239}Pu with those calculated by the statistical model (solid line, Lorentzian spectral factor) and from average resonance parameters (dashed line, energy-independent parameters; histogram, energy-dependent parameters $\langle \Gamma_n^0 \rangle$ and $\langle \Gamma_f \rangle_{J=1}^{\ell=0}$) with regard for the (n,γf)-reaction

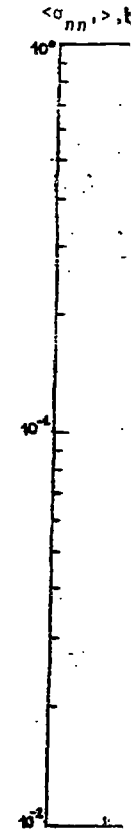

FIG. 17.

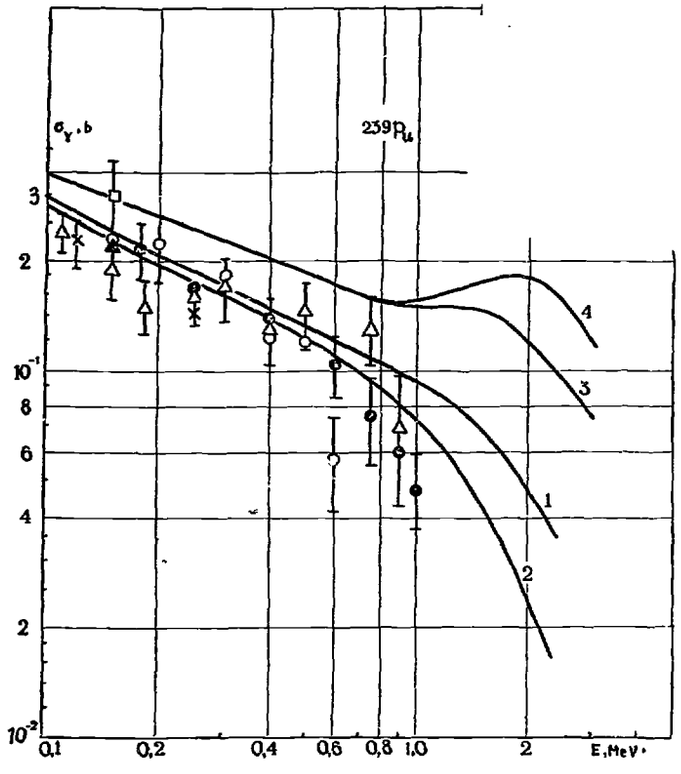

FIG. 28. Comparison of the experimental and calculated ^{239}Pu radiative capture cross sections: 1, calculation with regard for (n,γf) and (n,γn')-reactions, Lorentzian spectral factor in the form of two lines; 2, with regard for (n,γf) and (n,γn'), Weisskopf spectral factor; 3, with regard for (n,γn') alone, Lorentzian spectral factor; 4, without regard for (n,γ f) and (n,γn'), Lorentzian spectral factor.

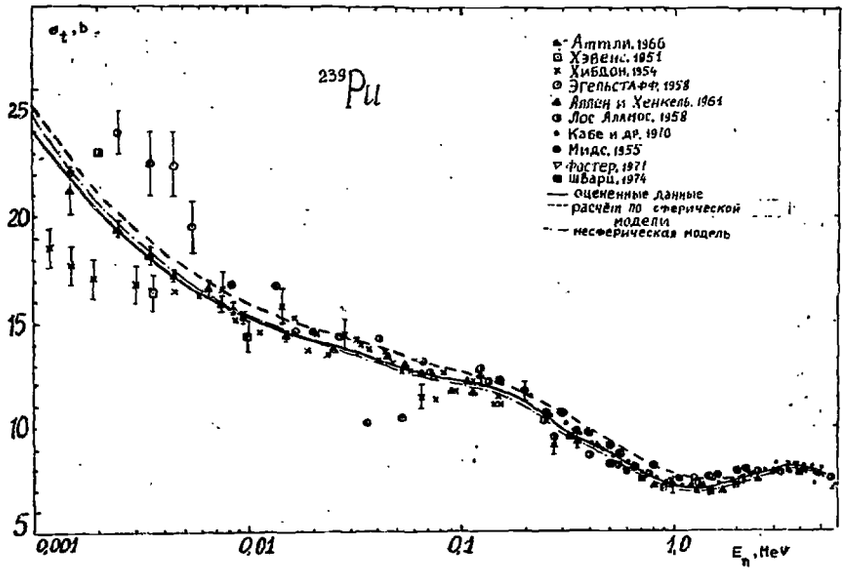

FIG. 29.

Comparison of the experimental and calculated $\sigma_t(^{239}Pu)$ cross sections: _____, evaluated data; -----, spherical model calculation; -.-.-, non-spherical model calculation

Below 100 keV, calculations of $\sigma_{n\gamma}$ in terms of the average parameters are sufficiently reliable. Besides, these allow for the cross section structure (Section 1). Figure 27 gives comparison of both methods for calculating $\sigma_{n\gamma}$ (^{239}Pu) below 100 keV, namely,the statistical approach with allowance for the fission competition (solid line) and the use of the average parameters in the

unresolved resonance region (dashed line). Above 20 keV, both curves coincide and below 20 keV, maximum difference between two curves is about 8%. Curves for $\sigma_{n\gamma}$ (^{239}Pu) within 1-100 keV are in a better agreement with the experimental data of Gwin [65] and Weston and Todd [66] (5-10%, within the experimental errors). In the case of such a strongly fissile nucleus, e. g. ^{239}Pu, the $\sigma_{n\gamma}$ calculation is mainly affected by the correct allowance for the fission competition and the difference in $\sigma_{n\gamma}$ calculations made with two spectral factors and different level density models proves to be small.

This method has been also adopted to calculate the remainder types of cross sections (Figs. 29 and 30). When predicting $\sigma_{nn'}$ by this method, it should be borne in mind that theoretical calculations are not completely specified due to a poor knowledge of the correlation properties of the resonance parameters. When the experimental data for σ_f are available and $\sigma_{n\gamma}$ is small in the fast neutron energy range, the reliable calculation of $\sigma_{nn'}$ is based on correct neutron transmission coefficients that, first of all, affect the value of the compound nucleus cross section. In the case of deformed nuclei, neutron transmission coefficients are most correctly calculated by the coupled channel method with carefully optimized non-spherical potential parameters to calculate more properly optical cross sections of the nucleus considered. However, the uncertainties in the partial cross sections calculated by the statistical model due to the use of the spherical optical potential can be, to a great extent, compensated by renormalization to the compound nucleus cross section calculated by the coupled channel method.

Our evaluation experience shows that $\sigma_{n\gamma}$ and $\sigma_{nn'}$ for strongly fissile odd nuclei can be successfully calculated by above method only if the fission competition (σ_f in this case must be found experimentally, at least, for some energies) is correctly allowed and neutron transmission coefficients are determined by the optical model involving carefully optimized potential parameters. Collective effects in level density should be allowed for in the case of even nuclei-targets.

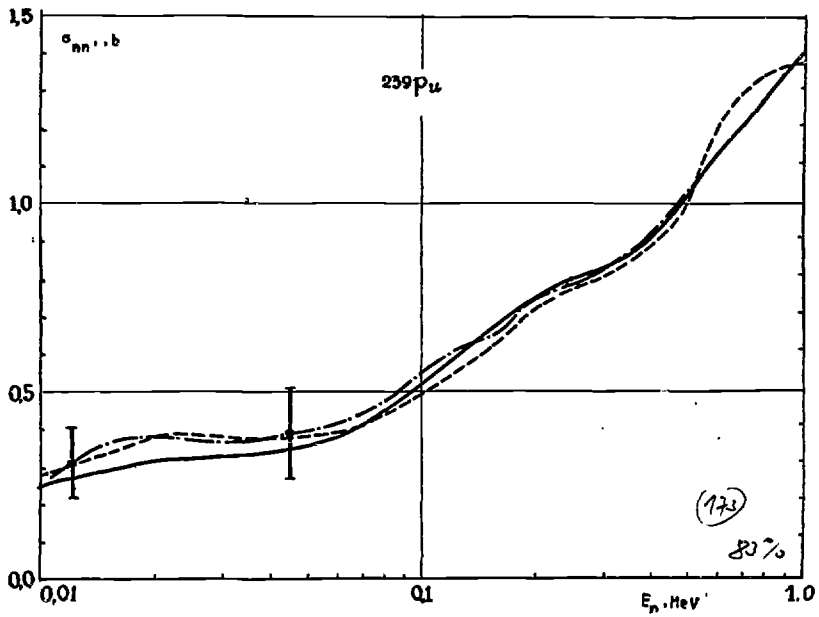

FIG. 30.
Comparison of the calculated and experimental $\sigma_{nn'}$,(^{239}Pu):_____, Hauser--Feshbach calculation; ----,calculation using the Tepel formalism; -•-•-, evaluation of the experimental data

6. EFFECT OF DIFFERENT LEVEL DENSITY MODELS ON ACTINIDE NEUTRON CROSS SECTION CALCULATION

At present the Fermi gas level density model is widely used for statistical theory calculations. The relations of this model are based on the complete mixing of collective freedom degrees in the excited nucleus and thus do not allow for the collective modes. Recently the authors of [51,67,68] have developed the semi-microscopic method for calculating level density that allows for vibrational and rotational modes. The statistical averaging methods are also widely used to calculate level densities, although within the framework of the adiabatic calculations of the collective effects still some problems remain unclear, namely, difference in collective unclear modes at different excitation energies, mixing of collective modes with single-particle ones, etc [72].

These problems may be solved by the microscopic methods for the direct modelling of the highly excited nucleus structure [73]. However, these methods appear to be very tedious and time consuming, especially at high energies, which hampers their application for nuclear data evaluation.

Therefore, we used the statistical method for averaging parameters of excited nuclei developed by Ignatyuk et al. [69,70,72] to clarify the effect of collective modes on calculations of the average neutron cross sections for heavy nuclei. These models allow for the existence of shell inhomogeneities in the single-particle level spectrum, the correlation of superconducting-type and coherent collective nature effects. We worked out a special computer program that permits calculation of level density and determination of the parameter "a" for the following models: traditional Fermi-gas model, Fermi-gas model with a back-shift over pairing energy, Fermi-gas model with the energy dependence a(E) used to allow for the shell effects [26], Fermi-gas model involving collective modes (rotational and vibrational), superfluid nucleus model that correctly allows for residual correlation interactions. The simple version of this model involving collective modes was proposed in [70].

The Fermi-gas model allows for the shell effects [26] through introducing the dependence of the parameter "a" on excitation energy and shell correction δW. The effect of the energy dependence of "a" is most substantial for nuclei near the filled nuclear shells. For the nuclei considered here, it is assumed that the value of shell nuclear corrections is relatively small and this effect can be thus ignored.

With the collective modes allowed for, the formula for the level density takes the form:

$$\rho(u,J) = K_{vib} \cdot K_{rot} \cdot \rho_{F.-g.}(u,J) \qquad (43)$$

The coefficients for the increase in level densities, K_{vib} and K_{rot}, due to rotational and vibrational modes and the factor σ^2, according to the adiabatic evaluation, are determined by [74,27]:

$$K_{rot} = F_{\perp} t \qquad (44)$$

$$K_{vib} = \exp(0.25a^{2/3}t^{4/3}) \qquad (45)$$

$$\sigma^2 = F_{\perp}^{2/3} F_{\parallel}^{1/3} t \qquad (46)$$

where $F_{\perp}$ and $F_{\parallel}$ are the perpendicular and parallel inertia moments and t is the excited nucleus temperature.

The superfluid nucleus model relations were taken from [74]. Unlike [74], we used K_{vib} in the form of (45) and did not allow for the energy dependence of the parameter "a" that can be neglected at small δW. As is shown in [74], the superfluid nucleus model formulas are valid not only for even-even nuclei but also, as is shown in [74], for odd-odd ones if the excitation energy

is defined as:

$$U=U_{even\text{-}even} + \begin{cases} \Delta_0 & \text{for odd nuclei} \\ 2\Delta_0 & \text{for odd-odd nuclei} \end{cases}$$

In the present work, Δ_0 is determined as $\Delta_0 = 12/\sqrt{A}$ MeV [27].

These level density models give different dependence of the level density on energy, which affects the value of the cross sections calculated by the statistical model.

The values of the level density parameter "a" calculated by different models with normalization to $\langle D \rangle_{obs}$ for ^{242}Pu, ^{243}Pu, ^{240}Pu, ^{238}U and ^{239}U are given in Table 1.

Table 1 VALUES OF THE PARAMETER "a" FOR DIFFERENT LEVEL DENSITY MODELS

Model	a, MeV^{-1}				
	^{238}U	^{239}U	^{240}Pu	^{242}Pu	^{243}Pu
Fermi-gas model	31.09	33.26	28.79	29.13	31.81
Back-shift Fermi-gas model	23.04 (Δ=0.83)	26.48 (Δ=0.40)	22.25 (Δ=0.75)	21.83 (Δ=0.82)	26.75 (Δ=0.32)
Fermi-gas model involving collective modes	19.10	20.07	17.66	17.74	19.25
Fermi-gas model involving energy dependence a(U) (at $U=S_n$)	31.09	33.26	28.79	29.13	31.81
Fermi-gas model with collective modes and a(U)	19.10	20.07	17.66	17.74	19.25
Superfluid nucleus model	52.02	59.68	44.69	45.31	57.05
Superfluid nucleus model involving collective modes	21.63	21.10	19.35	19.20	20.05

Table 1 illustrates that allowance for the energy dependence a(E) for actinides by the Fermi-gas model does not lead to a change in the parameter "a", which is natural, because this effect is most essential for the nuclei near the filled shells.

The value of "a" is observed to be very large when the superfluid nucleus model is used with no regard for the collective modes (probably, entropy decrease at $U=S_n$ is compensated due to a sharp increase in "a"). When the collective effects are taken into account the value of "a" is sharply decreased. When the values of "a" are calculated using the Fermi-gas and superfluid nucleus models, these values become close to each other and to the quasi-classical estimation ($\tilde{a}$=0.075A, for ^{243}Pu $\tilde{a}$=18.22 MeV^{-1}).

As the calculated fission cross sections are usually fitted to the experimental data, in statistical theory calculations the radiative capture cross section $\sigma_{n\gamma}$ proves to be most sensitive to the choice of one or another model. The choice of the model may be substantiated uniquely only for those nuclei, for which the experimental data for $\sigma_{n\gamma}$ are available over a wide energy range. From this point of view, the ^{238}U nucleus is most suitable and its radiative capture cross section was measured in a number of works. This nucleus is analysed to study the effect of different concepts of the level density on the energy dependence of $\sigma_{n\gamma}$ as well as the effect of the uncertainties in $\langle D \rangle_{obs}$ and $\langle \Gamma_\gamma \rangle$ on $\sigma_{n\gamma}$ calculation. The problem of the choice of the spectral factor will be considered, too.

Neutron transmission coefficients required for statistical model calculations were calculated by the coupled channel method with the non-spherical optical parameters carefully optimised with respect to the experimental data. S_0, S_1, σ_p were used as the inout experimental data at the energy of the order of several keV and σ_t in the region 2 keV to 15 MeV. Besides these data, we also used the most reliable experimental data for elastic scattering angular distributions [75,76] at 2.5 and 3.4 MeV where the contribution of the lower levels is clearly pronounced. It should

be noted, however, that despite the high accuracy of the experimental data [75] there exists a contradiction between the high value of the total cross section σ_t at 3.4 MeV and the comparatively small value of the differential elastic scattering cross section at small angles obtained in [75].

A careful optimization with regard for the above experimental data gives the following values of the non-spherical optical potential parameters for ^{238}U:

$V_R=(45.87-0.3\ E_n)$ MeV, $r_{0R}=1.256$ f, $a_R=0.626$ f

$W_D=(2.95+0.4\ E_n)$ MeV, $r_{0D}=1.260$ f, $a_D=0.555+0.0045\ E$

$V_{SO}=7.5$ MeV, $r_{SO}=1.2335$ f, $a_{SO}=0.62$ f

$\beta_{20}=0.216$, $\beta_{40}=0.080$

For ^{239}Pu:

$V_R=(46.10-0.3\ E_n)$ MeV, $r_{0R}=1.256$ f, $a_R=0.626$ f

$W_D=(3.0+0.4\ E_n)$ MeV, $r_{0D}=1.260$ f, $a_D=0.555+0.0045\ E$

$V_{SO}=7.5$ MeV

$\beta_{20}=0.214$, $\beta_{40}=0.080$.

The values of the obtained real and imaginary parts of the potential for ^{238}U are somewhat less (by 6% and 20%, respectively) than the appropriate parameters [75] which were determined by giving a great weight to their angular distributions of elastic and inelastic scattering neutrons.

This potential can be successfully used to calculate the strength functions S_0, S_1, σ_t, σ_n and angular distributions of elastically and inelastically scattered neutrons up to 10 MeV. Thus, it may be assumed that neutron transmission coefficients are calculated rather accurately.

In a number of works [77], a conclusion was made that the Weisskopf factor (formula (41)) in many cases can be successfully employed to calculate $\sigma_{n\gamma}$ but it does not ensure the agreement between the energy dependences of the radiation strength functions [78]. The use of the Lorentzian factor is physically more founded, but in this case the agreement with the experimental data for the energy dependence for $\sigma_{n\gamma}$ becomes worse, and calculated $\sigma_{n\gamma}$ values prove to be substantially higher than the experimental ones.

As radiative capture transmission depends on the compound nucleus level density, it may be assumed that the above discrepancy between theory and experiment is caused by the incorrectness of the model used (Fermi-gas model). This conclusion was made in [28] where ^{238}U neutron cross sections were calculated only up to 1 MeV, i.e. the fission competition was not allowed for and neutron transmission coefficients were calculated by the spherical model.

^{238}U neutron cross sections were calculated by the above mentioned formalism while above 1.3 Mev, by the Tepel formalism. The scheme of the ^{238}U levels was taken from [79].

There is a good agreement between the experimental (Fig. 31) and calculated cross sections for the discrete excited levels below 1.5 MeV which are not affected by the choice of the level density model.

Thus, the chosen parameters of the statistical model can be successfully used to calculate all neutron cross sections, except $\sigma_{n\gamma}$. The radiative capture cross section calculation is strongly affected by the type of the level density model, which allows the proper level density model to be chosen based on the comparison between the calculated and experimental data in the wide energy region.

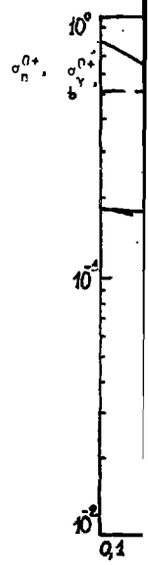

FIG. 19.
Compariso
Hauser-Fe

in $\langle\sigma_{nn}\rangle$
by the s
As
formula
although
T_α but a
Fig
tions ca
the fissi

Figure 32 shows comparison between the ^{238}U neutron capture cross sections calculated using the Lorentzian factor and different level density models, and the experimental $\sigma_{n\gamma}$ in the energy region from 0.1 to 3.0 Mev where non-compound radiative capture mechanisms can be neglected. This comparison witnesses that the best agreement between theory and experiment is achieved when the Fermi-gas model involving collective modes is used. The use of the superfluid nucleus model gives a discrepancy between theory and experiment in the energy range 1.2 - 3.0 MeV, and in the energy region up to 1.2 MeV the agreement is the same for the Fermi-gas model involving collective modes.

When the traditional Fermi-gas model is used, the greatest disagreement between theory and experiment is observed. The calculated $\sigma_{n\gamma}$ values are not substantially changed by introducing the energy dependence of the parameter "a" into the Fermi-gas model. So, at 3 MeV, this effect is no more than 4% and explained by a relatively small value of the ^{238}U and ^{239}U small corrections δW. In this case the energy dependence a(U) can be ignored in the superfluid nucleus model.

The use of the Weisskopf spectral factor does not give a better agreement between the calculated and experimental $\sigma_{n\gamma}$, as compared to the one achieved by means of the Lorentzian spectral factor and the Fermi-gas model involving the collective modes (Fig. 32, curve 4). Therefore, bearing in mind physical grounds of the Lorentzian factor, which is illustrated by the agreement of the calculated and experimental results for the radiative strength functions [78] and for the (n,γf)-reaction widths, it is advisable to use this spectral factor for statistical theory calculations.

It should be noted that the unique choice of the better model to calculate $\sigma_{n\gamma}$ may be substantially affected by the uncertainties in $\langle D \rangle_{obs}$ and $\langle \Gamma_\gamma \rangle_{obs}$ and by the neutron transmission coefficients (Fig. 35).

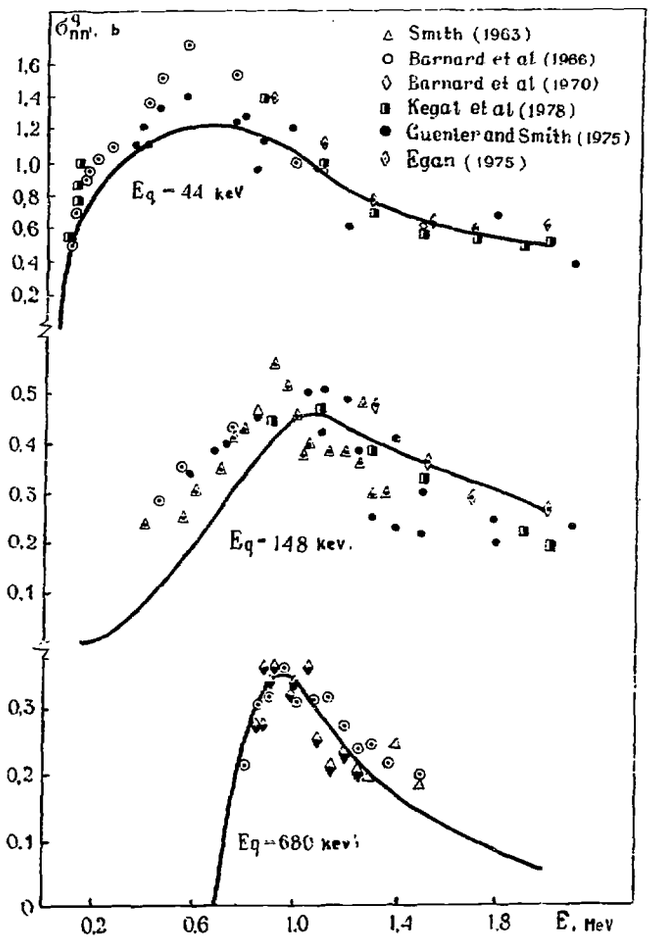

FIG. 31. Comparison of the calculated 44, 148 and 680 keV excitation level ^{238}U cross sections with the experimental ones

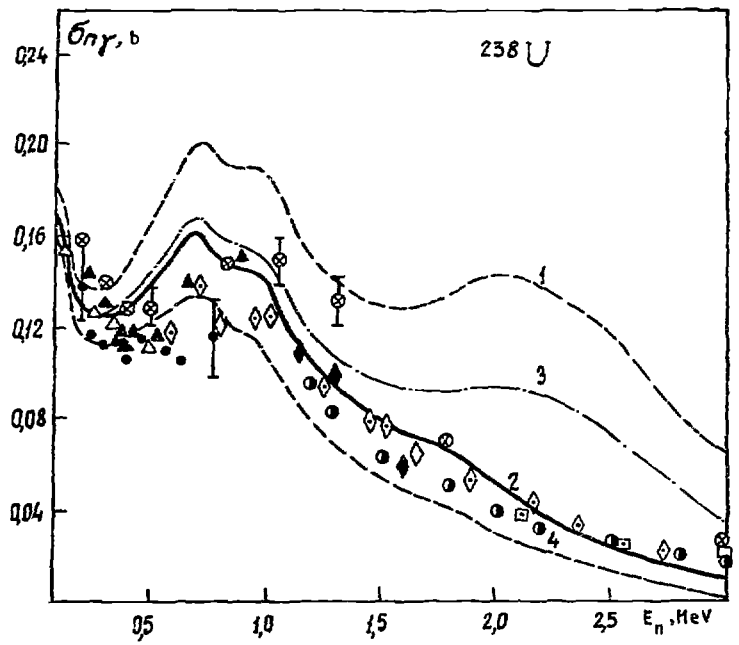

Fig. 32. Comparison of the ^{238}U $\sigma_{n\gamma}$ cross sections calculated by different level density models and the Lorentzian spectral factor with the experimental ones: 1, Fermi-gas model; 2, Fermi-gas model involving the collective modes; 3, superfluid model involving the collective modes ($\langle D\rangle_{obs}$=24.8 ev [83], $\langle\Gamma_\gamma\rangle_{obs}$=23.5 meV (ENDF/B IV)); 4, same as curve 2 but with the Weisskopf spectral factor

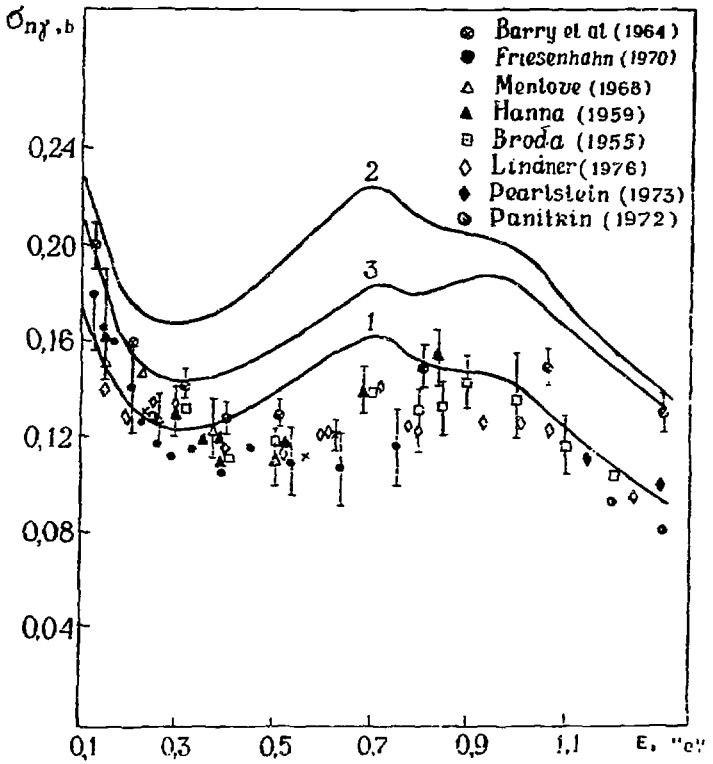

Fig. 33. The calculated ^{238}U $\sigma_{n\gamma}$ cross section for different $\langle D\rangle_{obs}$ and neutron transmission coefficients (Fermi-gas model involving the collective modes, Lorentzian spectral factor, $\langle\Gamma_\gamma\rangle_{obs}$=23.5 meV (ENDF/B-IV)): 1, $\langle D\rangle_{obs}$=24.8 ev [83], non-spherical potential; 2, $\langle D\rangle_{obs}$=17.7 ev (BNL-325,1973), non-spherical potential; 3, $\langle D\rangle_{obs}$=17.7 ev, spherical potential

The radiative ^{238}U capture width was normalized to $\langle\Gamma_\gamma\rangle_{obs}$ = 23.5 meV [80] which is consistent with 23.5 meV [81] and with 23.43 meV $\pm$ 0.11 meV_{stat} $\pm$ 0.70 meV_{system} [82]. The uncertainty in $\langle\Gamma_\gamma\rangle$, being equal to 4%, gives the same error in the calculated $\sigma_{n\gamma}$.

$\langle D\rangle_{obs}$ is characterized by the larger uncertainties that are associated with identifying s-and p-levels. According to the evaluation made in [83], $\langle D\rangle_{obs}$=24.78 $\pm$ 2.0 eV, which is much greater than $\langle D\rangle_{obs}$=20.8 $\pm$ 0.3 eV [84]. The reason of this difference lies in the fact that the weak levels which were assumed to be s-levels [84], in reality are p-levels as it was determined by Corvi et al. [85]. The difference in $\sigma_{n\gamma}$ due to two upper and lower values of $\langle D\rangle_{obs}$ is about 15%. Note that the present results for ^{238}U point to the high value of $\langle D\rangle_{obs}$=24.8 eV [83].

The existing uncertainties in $\langle\Gamma_\gamma\rangle$ and in $\langle D\rangle$ do not enable to explain such a strong difference between the experimental and calculated cross sections obtained using the traditional Fermi-gas model.

Figure 33 illustrates $\sigma_{n\gamma}$ affected by the values of neutron transmission coefficients that were obtained using the spherical and non-spherical models. The difference in $\sigma_{n\gamma}$ for these two cases depends on energy and varies from 5 to 20%.

This analysis shows that the use of the traditional Fermi-gas model for even-even nuclei gives a considerable difference between the experimental and calculated $\sigma_{n\gamma}$ cross sections for both spectral factors which cannot be attributed to the uncertainties of the parameters used.

The calculated $\sigma_{n\gamma}$ cross sections obtained by the superfluid nucleus model involving the collective modes and with the Lorentzian factor up to 1.5 MeV agree with the experimental data in the same manner, as in the case of the use of the Fermi-gas model involving the collective modes. However, some uncertainties in the parameters of the adopted version of the superfluid nucleus model, particularly phase transition energy, does not enable to state that the similar relationship between these two calculated curves will be valid for other nuclei. The $\sigma_{n\gamma}$ (^{242}Pu) calculations show that for this nucleus the $\sigma_{n\gamma}$ cross section calculated by means of the superfluid nucleus model involving the collective modes proves to be larger than the one calculated by the Fermi-gas model involving the collective modes. Note that the use of the superfluid nucleus model for calculation of $\sigma_{n\gamma}$ with the Weisskopf spectral factor leads to the greater values of $\sigma_{n\gamma}$, as compared to the Lorentzian spectral factor. The reverse is observed when the Fermi-gas model is used. The above uncertainty requires further investigation.

Therefore, the Fermi-gas model involving the collective modes and the Lorentzian spectral factor were used to calculate $\sigma_{n\gamma}$ (^{240}Pu and ^{242}Pu). Figure 34 displays $\sigma_{n\gamma}$ (^{242}Pu) calculated with different level density models. Note that in the energy range from the boundary of the discrete and continuous level spectra of a nucleus-target (1.5 MeV) to 2 MeV, the calculation leads to somewhat overestimated values of $\sigma_{n\gamma}$ because because the level density of the residual nucleus is underestimated in this range. This is clearly seen when the traditional Fermi-gas model is used.

If the calculated σ_f is fitted to the experimental data, then the choice of the model does not affect the value of the total inelastic scattering cross section. The difference in the level density of a nucleus-target, when different models are used, results both in a change of the relationship between the scattering cross sections in the discrete and continuous level spectra and in varying excitation cross sections of the discrete

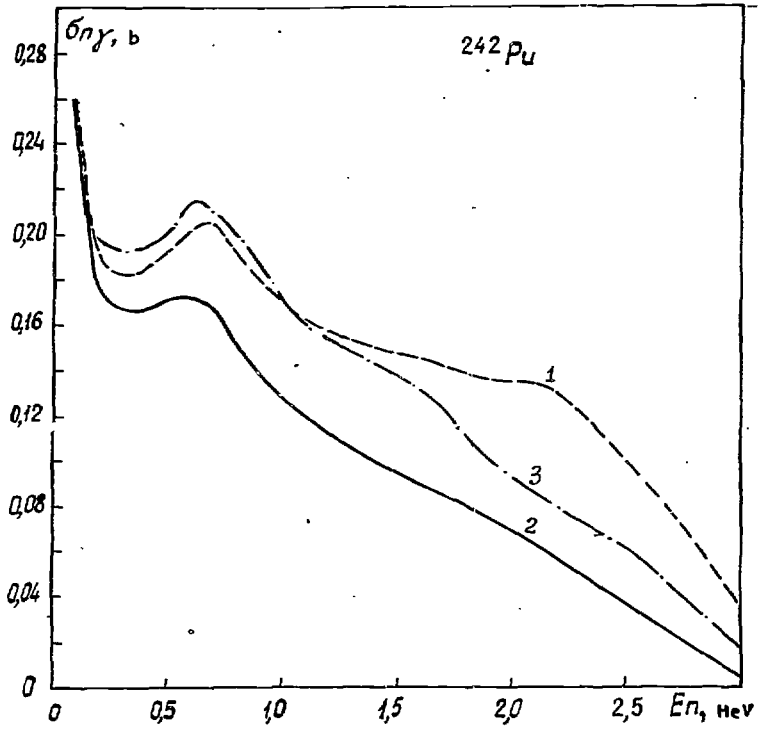

FIG. 34. ^{242}Pu radiative capture cross sections calculated using different level density models, non-spherical potential and the Lorentzian spectral factor: 1, Fermi-gas model; 2, Fermi-gas model involving the collective modes; 3, superfluid model involving the collective modes

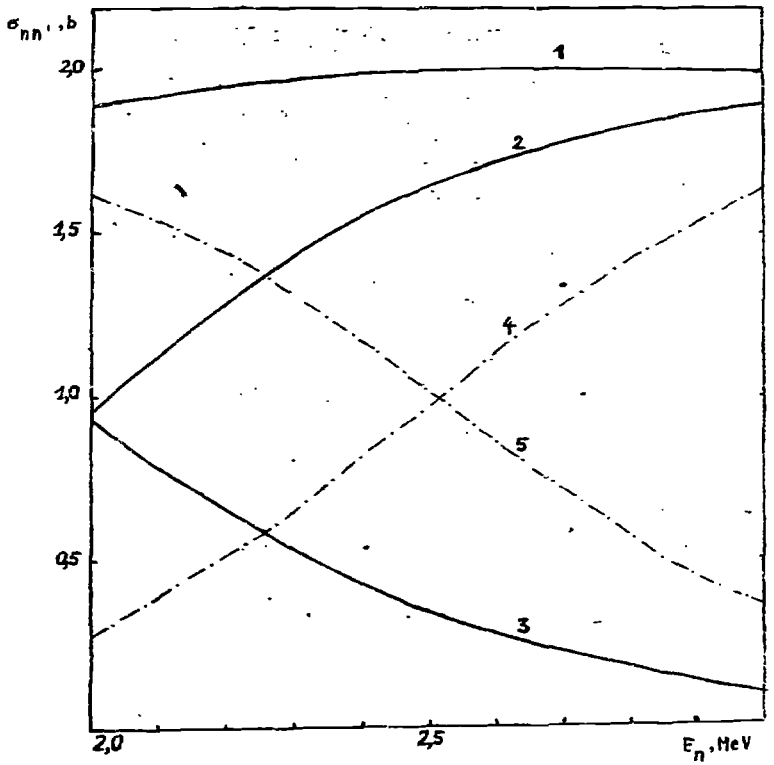

FIG. 35. Effect of the level density on $\sigma_{nn'}$ (^{242}Pu) calculation: curve 1, total $\sigma_{nn'}$; 2, $\sigma_{nn'}$ cont, Fermi-gas model involving collective modes; 3, $\sigma_{nn'}$ for discrete levels, Fermi-gas model involving collective modes; 4, $\sigma_{nn'}$ cont, Fermi-gas model; 5, $\sigma_{nn'}$ discr, Fermi-gas model

levels (Fig. 35). Hence, a conclusion may be drawn that the choice of a model may substantially affect the characteristics of the calculated spectrum of the scattered neutrons. Indeed, from the analysis of the experimental data on the neutron spectra for the nuclei with medium A it follows that smaller values of the parameter "a" are obtained than in the case of the Fermi-gas model used.

We assume that the conclusions of the present work can be adopted to calculate neutron cross sections for heavy nuclei that are not sufficiently studied experimentally.

Within the framework of the statistical approach, using the unique set of the parameters, the neutron transmission coefficients obtained by the non-spherical optical model, it is possible to calculate simultaneously compound neutron cross sections for fissile nuclei with an accuracy of about 5% in σ_t and σ_{nx}, about 15% in $\sigma_{n\gamma}$, about 20-30% in $\sigma_{nn'}$, and parametrize σ_f within about 10%. When experimental data for $\sigma_{n\gamma}$ and $\sigma_{nn'}$ are not available, these cross sections can be calculated by the method described within the same accuracy. The experimental data for σ_f, the average parameters $\langle\Gamma_\gamma\rangle$ and $\langle D\rangle$ and the scheme of the nuclear levels are the minimum information to calculate $\sigma_{nn'}$ and $\sigma_{n\gamma}$. The use of the non-spherical potential, the Lorentzian spectral factor and the Fermi-gas model involving the collective modes enables to obtain the self-consistent data for all neutron cross sections, including $\sigma_{n\gamma}$ (^{238}U) for even-even nuclei-targets over a wide energy range.

When the traditional Fermi-gas model is used, a considerable disagreement between the experimental and calculated $\sigma_{n\gamma}$ cross sections for even-even nuclei for both forms of spectral factors is observed, which cannot be explained by the uncertainties of the parameters adopted.

REFERENCES

[1] Hauser, W., and Feshbach, H., Phys. Rev., 1952, v. 87, p. 366.

[2] Feshbach, H., and Weisskopf, V., Phys. Rev., 1949, v. 76, p. 11.

[3] Moldauer, P.A., Proc. Intern. Symposium on Correlations in Nuclei, Hungary, 1973, p. 319.

[4] Lynn, J.E., Proc. Intern. Conference on the Interactions of Neutrons with Nuclei, Lowell, 1976, v. 2, p. 827.

[5] Lynn, J.E., Proc. Consultants Meeting on Nuclear Theory in Neutron Nuclear Data Evaluation, IAEA, Vienna, 1976, p. 325.

[6] Lane, A.M., and Lynn, J.E., Proc. Phys. Soc., 1957, v. A70, p. 557.

[7] Schmidt, J.J., KFK-T20, 1966.

[8] Dresner, L., ORNL-2659, 1959.

[9] Greehler, P., and Hutchins, B.A., Proc. Seminar on Physics of Fast and Intermediate Reactors, IAEA, 1962, v. 3, p. 121.

[10] Shaker, N.C., and Lukyanov, A.A., Phys. Letters, 1965, v. 19, p. 197.

[11] Antsipov, G.V., Konshin, V.A., and Maslov, V.M., Izv. AN BSSR, Ser. Fiz. Energ., 1979, No. 3, p. 25.

[12] Gradshtein, I.S., and Ryzhik, I.M., Tables of Integrals, Sums and Series of Products, Izd. Nauka, Moscow, 1971.

[13] Lynn, J.E., AERE-R7468, 1974.

[14] Kaiser, T., Gunter, H.P., et al., Nucl. Phys., 1978, v. A295, p. 141.

[15] Moldauer, P.A., Phys. Rev., 1976, v. C14, p. 764.

[16] Migneco, E., Theobald, J.P., Proc. Conf. on Neutron Cross Sections and Technology, Washington, 1968, v. 1, p. 527.

[17] Strutinsky, V.M., Nucl. Phys., 1967, v. A95, p. 420.

[18] Gai, E.V., Ignatyuk A.V., Rabotnov, N.S., and Smirenkin, G.N., Yadern. Fiz., 1969, v. 10, p. 542.

[19] Strutinsky, V.M., Bjørnholm, S., Proc. IAEA Symposium on Nuclear Structure, Dubna, 1968, p. 431.
[20] Hill, D.L., and Wheeler, J.A., Phys. Rev., 1953, v. 89, p. 1102.
[21] Tyapin, A.S., and Marshalkin, V.E., Yadern. Fiz., 1973, v. 18, p. 277.
[22] Tyapin, A.S., and Marshalkin, V.E., Voprosy Atom. Nauki i Tekhniki, ser. Yadern. Konstanty, 1976, vyp. 23, p. 105.
[23] Masterov, V.S., and Seregin, A.A., Yadern. Fiz., 1978, v. 27, p. 1464.
[24] Bondorf, J.P., Phys. Letters, 1970, v.B31, p. 1.
[25] Blokhin, A.I., and Ignatyuk, A.V., Proc. All-Union Conference on Neutron Physics, Kiev, 1976, v. 3, p. 3.
[26] Ignatyuk, A.V., Smirenkin, G.N., and Tishin, A.S., Yadern. Fiz., 1975, v. 21, p. 485.
[27] Ignatyuk, A.V., Istekov, K.K., and Smirenkin, G.N., Proc. Conference on Neutron Physics, Kiev, 1977, pt. 1, p. 60.
[28] Blokhin, A.I., Ignatyuk, A.V., Platonov, V.P., and Tolstikov, V.A., Voprosy Atom. Nauki i Tekhniki, ser. Yadern. Konstanty, 1976, vyp. 21, p. 3.
[29] Goldsmith, M., Nucl. Sci. Eng., 1973, v. 52, p. 461.
[30] Lynn, J.E., The Theory of Neutron Resonance Reactions, Oxford, Clarendon Press, 1968.
[31] Muradyan, G.V., Ustroev, G.I., Shchepkin, Yu.G., Adamchuk, Yu.V., Voskhanyan, M., and Prokofiev, L.Yu., Proc. 4th All-Union Conference on Neutron Physics, Kiev, 1977, pt.3, p. 119.
[32] Gwin, R., Silver, E.G., Ingle, R.W., and Weaver, H., Nucl. Sci. Eng., 1976, v. 59, p. 79.
[33] Weston, L.W., and Todd, J.H., Nucl. Sci. Eng., 1977, v. 63, p. 143.
[34] Hockenbury, R.W., Moyer, W.R., and Block, R.C., Nucl. Sci. Eng., 1972, v. 49, p. 153.
[35] Byers, D.E., Diven, B.C. et al., Proc. Conference on Nuclear Cross Sections and Technology, Washington, 1966, v. 2, p. 903.
[36] Pitterle, T.A., and Yamamoto, M., APDA-218/ENDF-122, 1968.
[37] Weston, L.W., and Todd, J.H., Nucl. Sci. Eng., 1978, v. 65, p. 454.
[38] Caner, M., and Yiftah, S., IA-1276, 1973.
[39] Young, T.E., and Reeder, S.D., Nucl. Sci. Eng., 1970, v. 40, p. 389.
[40] Caner, M., and Yiftah, S., IA-1275, 1973.
[41] Lagrange, Ch., and Jary, J., NEANDC(E) 198"L", INDC(FR)30/L, 1978.
[42] Hockenbury, R.W., Sanislo, A.J., Haushall, M.N., Proc. Conference on Neutron Cross Sections and Technology, Washington, 1975, v. 2, p. 584.
[43] Wisshak, K., and Käppeler, F., Nucl. Sci. Eng., 1978, v. 66, p. 363.
[44] Bergen, D.W., and Fullwood, R.R., Nucl. Phys., 1971, v.A163, p. 577.
[45] Auchampaugh, G.F., Farrell, J.A., and Bergen, D.W., Nucl. Phys., 1971, v.A171, p. 31.
[46] Tepel, J.W., et al., Phys. Letters, 1974, v. 49B, p. 1.
[47] Bohr, N., and Wheeler, J., Phys. Rev., 1939, v. 54, p. 426.
[48] Back, B.B., Hansen, O., Britt, H.C., and Garrett, J.D., Phys. Rev., 1974, v. C9, p. 1924.
[49] Blatt, J., and Weisskopf, V., Theoretical Nuclear Physics, 1954.
[50] Veyssière, A., Beil, H., Bergère, R., Carlos, P., and Leprêtre, A., Nucl. Phys., 1973, v. A199, p. 45.
[51] Soloviev, V.G., Stoyanov, Ch., and Vdovin, A.I., Nucl. Phys., 1974, v. A224, p. 411.
[52] Lynn, J.E., Proc. Advisory Group Meeting on Transactinium Isotope Nuclear Data, Karlsruhe, 1975, IAEA-186, p.201.
[53] Moldauer, P.A., Phys. Rev., 1964, v. 135, p. B642.
[54] Moldauer, P.A., Rev. Mod. Phys., 1964, v. 36, p. 1079.
[55] Hofmann, H.M., Richert, J., and Teoel, J.W., Ann. Phys., 1975, v. 90, p. 403.

[56] Voronov, V.V., and Soloviev, V.G., Proc. 4th All-Union Conference on Neutron Physics, Kiev, 1977, pt. 1, p. 41.
[57] Stavinsky, V.S., Shaker, M.O., Nucl. Phys., 1965, v. 62, p. 667.
[58] Lynn, J.E., Phys. Letters, 1965, v. 18, p. 31.
[59] Zen Chan Bom, Panteleev, I., and Tyan San Pan, Izv. AN SSSR, ser. Fiz., 1973, v. 37, p. 82.
[60] Ryabov, Y., Trochon, J., Shackleton, D., and Frehaut, J., Nucl. Phys., 1973, v. A216.
[61] Ivanov, K.N., Petrov, G.A., Petukhov, A.K., and Shcherbakov, O.A., Proc. 4th All-Union Conference on Neutron Physics, Kiev, 1977, pt. 3, p. 138.
[62] Simon, J., and Frehaut Jr., Proc. 3rd All-Union Conference on Neutron Physics, Kiev, 1976, v. 5, p. 337.
[63] Bollinger, L.M., and Thomas, G.T., Phys. Rev., 1972, v. 6C, p. 1322.
[64] Vtyurin, V.A., and Popov, Yu.P., Proc. 4th All-Union Conference on Neutron Physics, Kiev, 1977, pt. 3, p. 268.
[65] Gwin, R., Silver, E.G., Ingle, R.W., and Weaver, H., Nucl. Sci. Eng., 1976, v. 59, p. 79.
[66] Weston, L.W., and Todd, J.H., ORNL-4800, p. 4, Proc. Conference on Nuclear Cross Sections and Technology, 1975, v. 2, p. 627.
[67] Soloviev, V.G., and Malov, L.A., Nucl. Phys., 1972, v. A196, p. 433.
[68] Voronov, V.V., Komov, A.L., Malov, L.A., and Soloviev, V.G., Yadern. Fiz., 1976, v. 24, p. 504.
[69] Ignatyuk, A.V., Proc. Meeting on the Use of Nuclear Theory in Neutron Data Evaluation, Triest, 1976, v. 1, p. 211.
[70] Ignatyuk, A.V., and Shubin, Yu.N., Izv. AN SSSR, ser. Fiz., 1975, v. 37, p. 1947.
[71] Dossing, T., and Jensen, A.S., Nucl. Phys., 1974, v. A222, p. 493.
[72] Ignatyuk, A.V., Proc. 3rd International School on Neutron Physics, Alushta, 1978.
[73] Soloviev, V.G., Proc. Intern. Conf. on Interaction of Neutrons with Nuclei, Lowell, USA, 1976, v. 1, p. 421.
[74] Ignatyuk, A.V., Istekov, K.K., and Smirenkin, G.N., Yadern. Fiz., 1979, v. 29, p. 875.
[75] Haouat, G., Lachkar, J., Lagrange, Ch., Patin, Y., Sigand, J., and Shamu, R.E., NEANDC(E) 196"L", 1978.
[76] Haouat, G., Sigand, J., Lachkar, J., Lagrange, Ch., Duchemin, B., and Patin, J., NEANDC(E) 180"L", 1977.
[77] Fricke, M.P. et al., Proc. Intern. Conf. on Nuclear Data for Reactors, IAEA, 1970, v. 2, p. 265, p. 281.
[78] Bartholomew, G.A. et al., Advanced Nuclear Physics, 1974, v. 7, p. 232.
[79] Lambropoulos, P., Nucl. Sci. Eng., 1971, v. 49, p. 356.
[80] Abagyan, L.P., Korchagin, Zh.A., Nikolaev, M.N., and Nesterova, K.I., Sb. "Yadernye Konstanty", Atomizdat, 1972, vyp. 8, pt. 1, p. 121.
[81] Rahn, F., and Havens, W.W.,Jr., EANDC(US)-179/U, 1977.
[82] Poortmans, F. et al., Proc. Intern. Conference on the Interactions of Neutrons with Nuclei, Lowell, USA, 1976, p. 1246.
[83] De Saussure, G., Olsen, D.K., Perez, R.B., and Difilippo, F.C., Progress in Nuclear Energy, 1979, v. 3, p. 87.
[84] Rahn, F.J. et al., Phys. Rev., 1972, v. 6, p. 1854.
[85] Corvi, F., Rohr, G., and Weigmann, H., Proc. Conference on Nuclear Cross Sections and Technology, Washington, v. 2, p. 733.

EVALUATION AND PROCESSING OF NUCLEAR DATA

S. PEARLSTEIN
National Nuclear Data Center,
Brookhaven National Laboratory,
Upton, Yew York,
United States of America

ABSTRACT

The role a nuclear data evaluator plays in obtaining evaluated nuclear data, needed for applications, from measured nuclear data is surveyed. Specific evaluation objectives, problems, and procedures are discussed. The use of nuclear systematics to complement nuclear experiment and theory is described. Using the Evaluated Nuclear Data File (ENDF) as an example the formatting, checking, and processing of nuclear data is discussed as well as the testing of evaluated nuclear data in the calculation of integral benchmark experiments. Other important topics such as the Probability Table Method and interrelation between differential and integral data are also discussed.

1.0 Introduction

1.1 The Psychology of Evaluation

The process of evaluation involves decision making. The objectives of a nuclear data evaluator are to recommend values for nuclear data and also indicate the degree of confidence that can be placed in those recommendations. Often the experimental data being examined by the evaluator has quoted errors that are not realistic. Nevertheless, the evaluator is expected to estimate the most probably correct values of nuclear data. The evaluator is like a juror. From the evidence, no matter how contradictory it may be, the evaluator is supposed to get at the truth. As a juror's decision must be within the court of law, the evaluator's recommendation must be consistent with the best laws of physics. The evaluator need not be an expert in all phases of nuclear physics but where his knowledge is deficient he must be capable of incorporating the recommendations of other experts into his evaluation.

There is no prescribed college course for nuclear data evaluation as there is for nuclear physics, nuclear engineering, reactor physics, nuclear chemistry, etc. Evaluation is a combination of art and science. Evaluation used to be more art than science, since there was little data and the evaluator depended on nuclear systematics or just plain guesswork in order to recommend data for use in applications. Today, evaluation is more science than art. There is more data that can be considered and the evaluation is expected to be consistent with all of the observable facts. Sometimes observable facts and evaluations take on political importance. Good evaluations that can calculate observable facts from first principles are taken seriously by reactor designers and even play a role in international data exchange agreements. The evaluator through his recommendation can have an impact on nuclear power programs.

The evaluator must have the finest moral character. He must be uncorruptible. His recommendations must be supported by experimental and theoretical considerations and not be strongly influenced by values favored by particular nuclear applications.

The nuclear data base provided by the evaluator is important to both basic science and applied science. The basic scientist examines the nuclear data base and wants to know why the nuclear data are what they are. He seeks to explain

the systematics of nuclear data through an understanding of fundamental nuclear forces. For the basic scientist the nuclear data base must consist of hard facts confirmed by experiment. On the other hand, the applied scientist accepts nuclear data as they are and proceeds to apply them. However, gaps in the hard facts in the data base often prevent the applied scientist from finishing his work and he favors a data base complete in what he requires even if the gaps must be filled by approximate methods.

2.0 The Observable Facts

2.1 Deductive Conclusions

A configuration for measuring nuclear cross sections (probabilities) is a beam of projectiles incident on a sample of target nuclei with detectors to measure the reaction products or radioactivity of the residual nuclei. Conclusions are always inferred and never directly observed. For example, a neutron can be observed through the n-alpha reaction, capture gamma rays, proton recoil measurements, and induced radioactivity but not through the direct observation of a neutron. Because of the indirect methods that are used, the evaluator should closely examine the basis upon which the measurer drew his conclusions.

2.2 Inherent Averaging

All measured quantities are averaged to some degree. Neutron sources, even nominally monoenergetic ones, produce neutrons over a range of energy. As a result, the measured cross section may not apply to a single-valued energy. If the measurement is made at a certain angle with respect to the incident beam, the dimensions of the source and detector will cause an averaging over angle. For nonelastic processes, energy and angular averaging of the cross sections for the particles emitted will take place for the same reason. If the energy and angular averaging is small, the measurements are called differential. For some nuclear data, energy-averaged cross sections are deliberately obtained such as cross sections averaged over a 1/E (resonance integral), Maxwellian, polonium-beryllium, and Cf-252 spontaneous fission spectra. These are called integral measurements. More complex integral measurements are those that occur in reactor physics. The most important of these is criticality of a reactor assembly. When the neutron sources due to neutron producing reactions is exactly balanced by the neutron losses due to absorption and leakage the multiplication factor is unity to a high degree of precision, i.e., the multiplication factor is typically 1.000 plus or minus 0.002. Other measurements are sub-and supercriticality, reactivity coefficients, activations, and ratios of activations in the reactor spectrum. These integral measurements are difficult to interpret because there are a large number of nuclides and reactions as well as averaging over energy and angle but the measurements can be very precise when compared to differential data measurements.

2.3 Experimental Difficulties

When measuring nuclear cross sections, a number of experimental difficulties must be overcome. A common difficulty is shown in Figure 2.1. Measurements of neutron cross sections can be uniquely determined only if the sample consists entirely of the original nucleus or neighboring isotopes whose abundances and cross sections are well known and therefore can be used to correct the measurement.

Thick targets can give rise to erroneously large cross sections due to multiple scattering of the incident beam instead of a simple once-through-the-target reaction probability. Scattering of the incident beam can greatly increase the particle mean free path in the target, thus increasing the reaction probability.

The loss of energy of incident particles in the sample through elastic or inelastic scattering can also affect the cross section measurement if the cross section is strongly energy-dependent. If the energy of the incident particle is sharply lowered the measured cross section will include some reactions taking place at energies where the cross section may be very different than the cross section at the energy of the incident beam.

A well-known case of the effects of multiple scattering and energy degradation arises in the measurement of the high energy capture cross section, which is quite small. Neutrons with their energy degraded due to scattering are captured at much lower energies where the cross section is high. This problem can be avoided only by using very thin samples for the target or by performing extensive correction analysis.

Source characteristics are also important. The energies of particles from white sources (distributed over energy) are usually separated by time-of-flight measurements. The major uncertainties in the particle energy is caused by the finite width of the time channels in which the particles are produced and detected. Incident beams produced by charged particle reactions can be nominally monoenergetic but also have an energy spread due to accelerator and target properties. Furthermore, as the energy of the charged particle producing source reactions is increased, additional source reactions may be created that must be corrected for in the cross section measurements.

Ideally, the geometry of the measurement should be simple in order to facilitate analysis. Slab, cylindrical, and spherical geometries are the easiest to analyze. In practice, however, the experimental arrangement makes many compromises. Point or plain sources are only approximately realized and the detecting geometry is seldom ideal.

Hopefully, a cross section measurement will have a reasonable count rate for the events taking place. If the count rate is small, it will be difficult to obtain good statistical accuracy and maintain stable conditions for long periods of time. Conversely, large count rate experiments can be plagued by count rate losses due to successive events arriving at the detector before it has recovered.

The above discussion contains examples of the corrections that can be made in the analysis of any experiment. If a large correction is necessary, it does not necessarily mean that it is a poor experiment. It is the accuracy of the correction that is important. A large correction that can be accurately made can be preferable to smaller, less precise corrections.

2.4 Experimental Uncertainties

Every recommended number should have an uncertainty associated with that number. These uncertainties are called data covariances. Numbers without an assigned uncertainty have little scientific significance. They cannot be assumed to have zero error but can be taken only as an order of magnitude even if several digits are given. If the number is known better than to an order of magnitude, its degree of precision should be given. Data covariances can consist of random and systematic errors. The random errors are statistical in nature and can be reduced only by more, longer, or more efficient measurements. The systematic errors are usually inherent to measurements of a given type. They are difficult to identify and generally are apparent only when comparing measurements of one type with another. Correlations are also present and often important. Shape measurements with normalization at a single energy point is an example where uncertainties at one energy are correlated with uncertainties at another energy. Normalization of a measurement to a given standard will cause

the quoted uncertainties of a measurement to be correlated with the uncertainties in the measurement standard. The correlated uncertainties are important because the resultant uncertainity can be significantly different from the case where the uncertainties are considered to be statistically independent.

Many quoted errors are unreliable as evidenced by the fact that often the error bars from different measurements of the same quantity don't overlap. This means that the errors were incorrectly calculated or that all possible errors were not included. The evaluator must be prepared to reassign errors before determining a weighted result. When the evaluator has made his recommendation for nuclear data, he must also take responsibility for assigning the final covariances.

3.0 Evaluation Difficulties

3.1 Data Required

The types of data needed are determined by the application. Generally the objective is to solve for the transport of radiation through matter. This involves a vector characterization of the scattering, , disappearance and appearance of particles. Mathematically, this is expressed by the Boltzmann equation where the terms have their usual meaning

$$\frac{dn}{dt}(R,\Omega,E) = \frac{1}{v}\frac{d\phi}{dt}(R,\Omega,E) \qquad (3.1.1)$$

$$= -\Omega.\mathrm{grad}\phi(R,\Omega,E) - \sum_t(E)\phi(R,\Omega,E) + \iint\sum_s(\Omega'\to\Omega,E'\to E)\phi(R,\Omega',E')d\Omega'dE' + \int\sum_f(E'\to E)\phi(R,\Omega',E')d\Omega'dE' \qquad (3.1.2)$$

The application also determines what data are emphasized. With regard to the energy range of the data, an evaluation that is to be used for thermal reactor, fast reactor, and fusion reactor design will require data from very low energies up to 20 MeV. But an evaluation used only for thermal reactor design needs accurate data in the energy range below a few MeV. For criticality calculations the scattering, absorption, fission, and inelastic scattering cross sections are necessary to determine neutron balance. For radiation damage calculations, gas production cross sections such as those arising from the (n,p) or the (n,alpha) reactions are important. Neutron capture cross sections are important for activation analysis. For safeguards the delayed neutron yields and spectra are important to determine the signature for fissionable materials. For reactor emergency core cooling calculations the decay properties of radioactive nuclei are needed. For shielding calculations, total cross sections and the angular distribution of secondary particles are especially needed.

3.2 Gaps in Information

Sometimes the data needed are not directly observed or measured but must be derived. In other cases the measurements are incomplete and must be supplemented by theory. In Figure 3.1, the measurement and the analysis of elastic and inelastic neutron scattering from U-238 is shown. The energy resolution of the experiment is not capable of separating elastic scattering from inelastic scattering to the low-lying level at 44 keV. But an optical model calculation of the total scattering cross section in agreement with the measurements can provide the needed data for partial cross sections. There are also blind spots in the data caused by the difficulty in finding adequate neutron sources at certain energies. Examples of this are shown in Figures 3.2 and 3.3 where no data are given in the energy range 8-12 MeV for the krypton total cross section or the Ni-58 (n,2n) cross section, respectively. A frequent measurement difficulty is low signal strength, such as in the case of the measurement of the U-235 fission spectrum at very low and very high energies

where the data are not of sufficient statistical accuracy to precisely define the shape at very low or high energies.

The evaluator does not have an easy task. He is expected to provide a complete information base from incomplete and uncertain information. He is presented with differential and integral data without a sharp definition where one ends and the other begins. Both types are in the realm of observables that the evaluator must consider. Evaluated nuclear data and calculations using the data must be consistent with the best differential and integral data.

4.0 Nuclear Systematics

About 2000 nuclides are known. In detail cross sections are often complicated, yet many cross sections for a wide range of nuclides can be fit by models using relatively few parameters. Therefore, a simple unified understanding of nuclear reactions may yet be found. This section reviews some systematics of nuclear reactions that have been observed.

At low energies, the scattering cross section shows resonances. Between them it is flat and has the value that is given by potential scattering: $4\pi R^2$. Figure 4.1 shows that the nuclear radius required for optical model analysis as a function of mass number scatter around the curve $R=1.35A^{1/3}$ Fermis. At higher energies, the radius is very predictable: e.g., the experimental nonelastic cross section versus mass number are well approximated by the line $(1.2A^{1/3} + 2.1)$ Fermis (Fig. 4.2). For the description of resonances multilevel and single-level Breit-Wigner formulas and other approximations are used, as is shown in Figure 4.3 for the total and the capture cross section of Ti-48. The envelope containing the resonant cross sections is determined by the neutron wavelength. The systematic behavior of s- and p-wave neutron strength functions and total average s- and p-wave neutron radiation width versus A can be seen from Figure 4.4. The structure in the shape of these curves is associated with the closing of shells. Figure 4.5 shows experimental total, elastic, nonelastic, (n,2n), (n,p), and (n,alpha) cross sections for Co-59 as a function of incident neutron energy. As this element is monoisotopic and easy to handle as a sample and, moreover, has radioactive residual nuclei resulting from particle emission, the measurement record is more complete than it is for other nuclides. It can be seen that in the MeV region, the elastic cross section approximately equals the nonelastic cross section, which is generally true. In this case the charged particle cross sections are smaller than the (n,2n) cross section, the (n,alpha) cross section being less than that for (n,p).

In general, whenever a new channel opens, it rides on the coat tails and competes with the channels already open, and the envelope of the excitation function curves, i.e., the nonelastic cross section is almost constant. The sums of channels having the same origin, such as all (n,n'x) cross sections, will be part of the same envelope.

If one considers (n,2n) cross sections for various nuclei as a function of neutron energy (Fig. 4.6), one observes that the displacement of the excitation function curves is small (threshold between 12 and 14 MeV) and that the cross section increases as one goes from light to heavy nuclei. The (n,p) cross section for various nuclei (Fig. 4.7), on the other hand, decreases as one goes from light to heavy nuclei as the Coulomb barrier increases. The same tendency can be observed with (n,alpha) excitation functions (Fig. 4.8) where also the displacement of the curves for different masses increases as there is a larger increase in the Coulomb barrier. These general trends are even more impressively demonstrated by a plot (Fig. 4.9) of the ratio of peak charged particle cross sections to nonelastic cross sections at 14 MeV versus the

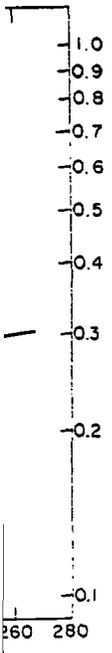

asymmetry parameter $\frac{N-Z}{N+Z}$. An exponential decrease with increasing $\frac{N-Z}{N+Z}$ is observed. The charged particle cross section peaks are shifted to higher energy with increasing asymmetry parameter as can be seen from Figure 4.10 so that 14 MeV cross sections can correspond to the rise, peak, or tail of the cross-section excitation curve.

With increasing Z and A (increasing asymmetry parameter) the magnitude of the (n,2n) cross section increases as neutron emission becomes more probable than charged particle emission because of the large proportion of neutrons in the nucleus and the Coulomb barrier for charged particles. The charged particle emission becomes very small and the (n,2n) cross section approaches the nonelastic cross section. For heavy nuclides elastic and inelastic scattering (n,2n), and fission are the principal cross sections.

In Figure 4.11, the same experimental data for Co-59 as in Figure 4.5 are displayed, but now they are compared with nuclear model calculations. By means of this comparison, a decision between two strongly differing sets of data for the (n,p) cross section (having the same symbol) can be made as well as predictions for cross sections for which no experimental data exist.

Figure 4.12 displays diffraction of monochromatic light through a circular aperture; an analogy by which the optical model has been developed to describe the diffraction of neutrons. In diffraction through an aperture, if the aperture size is increased while the frequency is kept constant the pattern begins to show more and more fringes. In an analogous manner, the number of diffraction peaks of the differential elastic cross section for 14 MeV neutrons increases with increasing mass number of the target nucleus, as is demonstrated in Figure 4.13. On the other hand, the same effect can be achieved by keeping the size of the aperture or mass of the target nucleus constant and decreasing the wavelength of light which corresponds to increasing the neutron energy.

This is shown for the case of Pb-208 in Figure 4.14. For the angular distribution of elastically scattered neutrons, an approximation based on Fraunhofer diffraction is displayed in Figure 4.15. It is a "universal" curve and is relatively accurate for predicting cross sections and location of diffraction peaks at forward angles. For the extrapolation of differential elastic cross sections to small angles, Wick's limit may be helpful. It is derived from the optical theorem and says

$$\frac{d\sigma_e(0^\circ)}{d\Omega} \geq \frac{\sigma_e^2}{4\lambda^2} \qquad (4.1.1)$$

where σ_e is the total elastic cross section. How Wick's limit agrees with experimental differential elastic cross sections is displayed in Figure 4.16 for the case of 14 MeV neutron scattering from natural chromium.

5.0 Evaluation Objectives

5.1 Consistency with Best Information Available

Experimental differential data is the starting point of an evaluation. The evaluation should be tested for consistency with good integral data experiments. Sometimes integral data can be used to support a particular differential data experiment from among a discrepant set of experiments. Each source of information should be carefully regarded. If necessary, one must rely on nuclear systematics or nuclear theory must be used to fill gaps in experimental data. The evaluated data should not be biased toward a particular application.

5.2 Good Documentation

Good documentation can take even longer than the evaluation procedure. The evaluator should aim at producing a document he would like to read. Each step of the evaluation procedure should be defined, e.g., the assignment of

uncertainties for weighting data, normalization of cross sections, etc. The documentation should be useful not only for physicists understanding the basis for data selection and programmers manipulating the data, but also for reactor licensing procedures.

5.3 Complete Data Base

The data base must contain all nuclear reaction data over the entire energy range expected by the cross section processing codes that are used. The detail to which it must be provided is, of course, determined by the applications considered.

5.4 Covariances

The data covariances, or degree of confidence that can be placed in the recommended data, should be clearly stated in the documentation and/or computerized file.

5.5 Convenient To Use

In order for evaluated data to be convenient to use, elaborate representations of data should not be employed. Also, many processing alternatives, e.g., interpolation schemes, should not be used or changed frequently unless necessary.

6.0 Evaluation Procedures

6.1 Adopt Measurement Standards

The ENDF/B (see Section 11) standards can be adopted. Frequently used standards are the hydrogen total and differential scattering, He-3(n,p), Li-6(n,alpha),B-10(n,alpha), C-12 differential elastic scattering, An-197(n,gamma), and U-235(n,f) cross sections. When reviewing measurements, normalization to the same standards should be performed before comparing data.

6.2 Critically Evaluate Each Piece of Promising Data and Recommend Data

Disqualification of data because of its age is not justified unless the method or apparatus used has become inferior to newer ones. Data must be compared on a consistent basis. Data should be evaluated using objective criteria with any personal bias eliminated. The nominal values given by the experiments should be averaged using the given uncertainty as weighting. If no consistency is achieved it may be necessary to revise the quoted errors. In the case of energy-dependent data, one set should be chosen as a reference and the ratios of the others to the reference set should be plotted to determine which measurements have similar shapes.

The consistency between internal error

$$(\Delta\sigma)^2 = \frac{1}{N}\sum_{n=1}^{N} (\Delta\sigma_n)^2 \qquad (6.2.1)$$

and external error

$$(\Delta\sigma)^2 = \frac{1}{N-1}\sum_{n=1}^{N} (\sigma_n - \bar{\sigma})^2 \qquad (6.2.2)$$

should be checked.

When situations do not follow standard procedures the evaluator must use his best judgement (common sense).

6.3 Fill Gaps

Gaps can be filled with the aid of nuclear models, nuclear systematics or free hand, if necessary.

6.4 Test Data

The data can be tested by use in calculations of integral benchmark experiments, calculation of resonance integrals, etc. Observe if the

disagreement between calculations and experiment can be correlated with particular cross sections or other features.

6.6 Review and Revise, If Necessary

Iteration of the whole procedure may be useful, especially when the calculation of integral benchmark experiments leads to disagreements between calculations and experiment. The choice of experimental differential data and assignment of errors should be reviewed. Finally, if the evaluation could be helped by better measurements, their specifications should be inserted in the international IAEA measurement request list WRENDA.

6.7 Evaluation Tools and Examples

The assembly of relevant experimental data is aided by performing a literature survey. For neutron data the IAEA index to neutron bibliography, CINDA (Fig. 6.1) is useful. By blocking of references to the same experiment, time can be saved because the first reference supersedes the others. One of the sources of information referred to in CINDA is the EXFOR library (Fig. 6.2). This is formatted information containing experimental data with a brief summary of the documentation of the article from which the data were taken. These data are available from the world data centers each serving a particular geographical area. However, assembling the pertinent data is only the first step.

A common problem is energy scales that do not agree for different measurements. Figure 6.3 shows the ENDF/B-IV and V curves for the U-235(n,f) cross sections together with experimental data. There is a knee in the curve at about 6 MeV, and the energy at which it appears strongly differs in the various experiments (Fig. 6.4).

Ratio measurements are generally more accurate than absolute magnitude measurements. Figure 6.5 displays measured fission cross section ratios and the relatively small scatter in the experimental data.

Nuclear model code calculations are useful for filling gaps in the data base but only after extensive comparisons with reference data and other codes. It is interesting to see that various statistical model codes did not a priori give the same results for the Cc-59 (n,d) cross section when tested in a code intercomparison in Spring 1977. As a result of additional code intercomparison, the calculated results 6 months later agreed much better with each other as well as with the experimental data. A number of optical model codes are in use that calculate elastic scattering and inelastic scattering from discrete levels. Examples of widely used codes are the following:

ABACUS II E. Auerbach, BNL-6592 (1969). Spherical Potential

JUPITOR T. Tamura, ORNL-4152 (1967). Deformed potential

When it is necessary to calculate nuclear reaction cross sections a number of statistical model codes are available. Examples of widely used codes are the following:

GNASH P.G. Young, E.D. Arthur, LA-6947, includes precompound.

HAUSER V F. Mann, HEDL-TME 78-83

THRES2 S. Pearlstein, JNE 27 (1973), limited applicability

The above codes and others are available from Nuclear Energy Agency Data Bank or the International Atomic Energy Agency Nuclear Data Section (see References).

7.0 Combining Differential and Integral Data

The uncertainties assigned to evaluated differential data should be included in the calculation of integral quantites in order to determine the confidence level that can be placed in the calculated results, e.g., effective multiplication factor, reaction rates, etc. However, the measured integral

parameters may also have experimental uncertainties of their own. As stated earlier, differential and integral data are observables that contain important information for use in predicting the behavior of nuclear systems. Revisions in integral as well as differential data may be required in order to achieve consistency. However, changes must be realistic and not violate in any way the physics of the measurements. Only integral benchmark experiments that are highly precise, free from systematic errors, and thoroughly documented should be used to test the consistency of evaluated nuclear data.

7.1 Least Square Fitting

Consider a set of parameters T_i, i=1,2...I, which can correspond to differential data, e.g., group cross sections, and a set of results R_n, n=1,2.....N which can correspond to integral data, e.g., criticality experiments.

In the method of least square fitting, it is required that the quantity

$$\psi^2 = \sum_{n=1}^{N} W_n (R_c - R_E)_n^2 \qquad (7.1.1)$$

is minimum. Here the subscripts C and E refer to calculated and experimental integral data. The quantity W is the weight assigned to each term and is usually taken as inversely proportional to the square of the assigned uncertainty which in the case of uncorrelated uncertainties is

$$W_n = \frac{1}{(\Delta R_n)^2} \qquad (7.1.2)$$

Minimizing ψ^2 requires that

$$\frac{d\psi^2}{dT_k} = 2 \sum_{n=1}^{N} W_n (R_c - R_E)_n \left(\frac{dR_c}{dT_k}\right)_n = 0 \qquad (7.1.3)$$

If we assume that a change in the differential quantity affects the calculated integral parameters in a linear way then we can expand R as

$$R_c = R_c (T_o) + \sum_{k=1}^{I} \frac{dR_c(T_o)}{dT_k} \, dT_k \qquad (7.1.4)$$

where T_o refers to an initial choice of parameters. Substitution in the previous equation produces the normal equations

$$\sum_{n=1}^{N} W_n \sum_{j=1}^{I} \frac{dR_c}{dT_j} \frac{dR_c}{dT_k} \, dT_j = \sum_{n=1}^{N} W_n \left[R_c(T_o) - R_E\right]_n \frac{dR_c}{dT_k} \qquad (7.1.5)$$

These are equivalent to a matrix equation of the form

$$A \cdot dT = R \qquad (7.1.6)$$

where A is an MxM square matrix and dT and R are Mx1 column vectors.

$$dT = A^{-1} \cdot R \qquad (7.1.7)$$

In cases where R is a linear equation in T, only one iteration is necessary to obtain the final answer. But in the nonlinear case, the initial parameter guesses are altered by dT and used as guesses for the next iteration until a convergence T is achieved. The covariances in the differential quantities are calculated by the equation

$$\langle dT_j \cdot dT_k \rangle = \left[A^{-1}\right]_{jk} \frac{\psi^2}{N-I} \qquad (7.1.8)$$

The covariances calculated for T apply to calculations of the integral quantities R and may be different from the covariances assigned to T before least squares fitting. Nonzero off-diagonal elements (j≠k) of the covariance matrix indicate correlations exist between the parameter uncertainties. The

correlation coefficient ≤ 1 is

$$\varepsilon_{jk} = \frac{\langle dT_j \cdot dT_k \rangle}{dT_j \cdot dT_k} \qquad (7.1.9)$$

where dT_j is the square root of the j row and j column diagonal element of the covariance matrix.

The assignment of uncertainties to integral measurements is very important.

To facilitate the discussion matrix symbols are used that are consistent with the primary reference (Dragt) used for this Section. It is useful to define the "sensitivity coefficients" to account for calculated integral quanties on differential data in the following way

$$G_{jk} = \frac{dR_j}{dT_k} \qquad (7.1.10)$$

where the subscripts j and k stand for particular integral data and differential data, respectively. The elements of G form the sensitivity matrix of order (NxI).

The accuracy of the differential data T can be expressed in a covariance matrix M of order (IxI) as

$$M = \left[\langle dT_j \cdot dT_k \rangle \right] \qquad (7.1.11)$$

If $\langle \Delta R \cdot \Delta R \rangle$ is the covariance of the two integral parameters, a covariance matrix V of order (NxN) similar to M may be defined to express the uncertainties in the integral data.

The uncertainty in the integral parameter R will depend upon the covariance of the differential parameter in the following way

$$dR^2 = \sum_{j=1}^{I} \sum_{k=1}^{I} \frac{dR}{dT_j} \frac{dR}{dT_k} \langle dT_j \cdot dT_k \rangle \qquad (7.1.12)$$

Then Eq. 7.1.5 can be written as

$$\left[\tilde{G} \cdot V^{-1} G \right] \cdot dT = \tilde{G} \cdot R \qquad (7.1.13)$$

or

$$dT = \left[\tilde{G} \cdot V^{-1} G \right]^{-1} \tilde{G} \cdot R \qquad (7.1.14)$$

The covariance matrix M' for differential data, using Eq. 7.1.13 can be written as

$$M' = \left[\tilde{G} \cdot V^{-1} G \right]^{-1} \frac{\psi^2}{N-I} \qquad (7.1.15)$$

which gives an estimate of the uncertainty in the differential data. The uncertainty in the integral data would then be given by

$$dR^2 = G \cdot M' \cdot \tilde{G} \qquad (7.1.16)$$

7.2 Dragt's Method

Dragt worked out a similar set of equations by assuming that all variables are normally distributed and that a linear relationship exists between the variations in the integral and differential quantities. If R' are the new calculated quantities and T' are the adjusted differential parameters, then this assumption implies

$$R_c' = R_c + G \cdot (T' - T) \qquad (7.2.1)$$

The vector T' and the final covariance matrix M' for differential data then are the solutions of the equations:

$$\left(M^{-1} + \tilde{G} \cdot V^{-1} \cdot G\right) \cdot (T' - T) = \tilde{G} \cdot V^{-1} \left(R_E - R_c\right) \qquad (7.2.2)$$

$$M' = \left(M^{-1} + \tilde{G} \cdot V^{-1} \cdot G\right)^{-1} \qquad (7.2.3)$$

The solution of these equations can be simplified by substituting

$$N = G \cdot M \cdot \tilde{G} \qquad (7.2.4)$$

which is the covariance matrix of the calculated integral parameters R . The Equations 7.2.2 and 7.2.3 may then be written as

$$(T' - T) = M \cdot \tilde{G} \cdot (N+V)^{-1} \cdot (R_E - R_c) \qquad (7.2.5)$$

$$M' = M - M \cdot \tilde{G} \cdot (N+V)^{-1} \cdot G \cdot M \qquad (7.2.6)$$

The inversion of a large matrix of order (MxM) in Equations 7.2.2 and 7.2.3 has been reduced to the inversion of a small matrix of order (NxN) in Equations 7.2.5 and 7.2.6. As the number of integral data N is much less than the number of differential parameters M this simplification is quite important from a computational point of view.

If all the integral experiments are uncorrelated, i.e., V is a diagonal matrix, the adjustment calculation can be performed without any matrix inversion at all. The fitted parameters should lie within the experimental limits of uncertainties. The adjustment of a particular parameter does not necessarily mean that the adjusted value of that parameter is more accurate. It may only mean that the whole set of adjusted parameters can predict the behavior of the system in a more consistent fashion and can be considered a parameterization of the system.

8.0 Probability Table Method

Tabulated cross sections versus energy in the resolved resonance region can require thousands of data points to describe resonance shapes. This requires large computer memory and a great deal of computer processing time. Therefore it is desirable to describe resonance region cross sections without having large tables in the data library. In ENDF the resonance parameters are given in the resolved resonance region. For one resonance one card contains all the necessary information. The cross section at a particular energy point can be calculated using suitable formulas. The U-235 fission cross section in the unresolved resonance region is shown in Fig. 8.1.

In the unresolved resonance region only the statistical distribution of resonance parameters is given. Sometimes it is possible to extrapolate the resolved resonance region parameters into the unresolved resonance region, provided they give the same average cross sections as observed in measurements.

In a reactor calculation detailed cross-sectional data are required in order to calculate energy self-shielding and Doppler broadening effects. Approximate methods are used. One such method consists in generating a ladder of resonance parameters using statistical models. More than one such ladder must be generated since it is not known what specific ladder corresponds to the actual data.

Another method is the use of the Probability Table Method, which consists in compiling a probability distribution of cross-sections against the cross section. For example in Fig. 8.2, the probability distribution of the fission cross section of U-235 has been plotted against the U-235 fission cross section

in the range of 80-200 eV. An alternate approach could be to plot the integrated probability against the cross section rather than the probability. By choosing a random number between 0 and 1 and entering the probability table an estimate of the cross section can be made. The probability tables can be plotted for each of the ladder of resonances. The same can be done for other energy ranges, temperature, etc. The main advantage of this method is that the computer has to handle fewer and smaller tables.

This method appears to be successful even if resonance cross sections are highly energy-correlated. A particular example would be the U-238 resonance region from 200 to 500 eV which shows some strong auto-correlations. However, calculations of capture rates using detailed cross section profiles are not statistically distinguishable from calculations using the Probability Table Method.

9.0 Multigroup Constants

9.1 Multigroup Solutions

The solution of Boltzmann's equation requires a description of the nuclear cross sections, material compositions, and spatial configuration. Cross sections describe nuclear reaction probabilities as a function of energy and direction of the incident particle. Although solutions that are continuous in energy and angle are possible using statistical sampling Monte Carlo methods, results from averaging over discrete ranges of energy and angle are commonly used. Cross sections averaged over discrete ranges are called multigroup constants.

The derivation of multigroup theory from Boltzmann's equation can be found in standard texts. Basically, the rate of change in particle density within each group is determined by the net difference between the rate of particle production and loss. A set of simultaneous equations results from writing multigroup balances at each spatial node of the configuration. The equations are solved by matrix inversion or relaxation methods.

9.2 Bondarenko Method

Ordinarily multigroup cross sections are problem dependent since multigroup cross sections are averaged over particle fluxes which in turn are determined by material composition and geometry. To avoid numerous recalculations of average cross sections, the Bondarenko method calculates energy averaged cross sections for an isotope over a range of cross sections representing that of the remaining isotopes in a mixture. A table of these values are stored and cross sections for individual cases are obtained by interpolation.

10.0 Benchmarks

10.1 Benchmark Analysis

A benchmark experiment is an integral experiment (see 2.2) that is carefully performed and documented sufficiently for detailed calculation. Cross section data, material compositions, and the geometry are used as input to reactor physics codes to calculate the parameters obtained by the integral experiment. If the methods of calculation are accurate and the systematic uncertainties of the integral experiment are negligble, the comparison of calculation with experiment can be used to determine the degree of confidence that can be placed in current nuclear technology for the applications considered.

A list of documented benchmark experiments is maintained by the Cross Section Evaluation Working Group (see References) in the U.S.A.

10.2 Reactor Physics Codes

Several computer codes used for cross section preparation and solution of reactor physics are in wide use and distributed by data centers. Unless a user has special energy group or angular approximation requirements, the prepared group libraries that are available can save time and money. A list of representative cross section processing and reactor physics codes is given in Appendix I. Generally, these codes are available from the IAEA or with their assistance from cooperating centers.

10.3 Benchmark Specifications and Results

Experimental integral benchmarks for fast reactor, thermal reactor, shielding, and dosimetry applications have been compiled by the U.S. Cross Section Evaluation Working Group. The specifications are reported in ENDF-202 and the comparisons between calculation and experiment are described in ENDF-230. For comparisons between calculation and experiment for benchmarks and other integral data, refer to reports appearing in Nuclear Science and Engineering and Transactions of the American Nuclear Society.

11.0 Evaluated Nuclear Data Systems

11.1 Formats and Procedures

Several widely used formats for evaluated data include UKNDL (United Kingdom), KEDAK (Karlsruhe), SOKRATOR (USSR), and ENDF (Brookhaven).

A well designed evaluated data system includes codes for format checking and standardization, physics checking, data correction, generation of infinite dilute cross sections, cross section integration over energy intervals, data plotting, data retrieval, data merging, and data listing. The best documented system is ENDF. Documents of general and specific interest and also reference guidelines for ENDF are given in Appendix II.

11.2 U.S. Evaluation System

In 1966, the U.S. formed the Cross Section Evaluation Working Group (CSEWG) consisting of representatives from over 20 federal, industrial, and university laboratories. The CSEWG structure consists of Evaluations, Data Testing and Applications, and Methods and Formats Committees reporting to an Executive Committee.

The Executive Committee consists of the CSEWG chairman, funding agency representatives, committee chairmen, three additional members appointed for limited terms by the CSEWG chairman in consultation with sponsors, and one member-at-large elected by CSEWG. The Executive Committee sets policy and gives final approval to recommendations by the other Committees.

The Evaluations committee would 1) recommend evaluation responsibilities, 2) schedule and oversee completion of individual evaluations, 3) selection of reviewers, 4) review physics contents, 5) recommend suitability of evaluations, 6) maintain a discrepancy list, 7) review requests for nuclear data, 8) recommend new nuclear data measurements, and 9) organize seminars, workshops, etc., to solve specific evaluation problems.

The Data Testing and Applications Committee would 1) recommend data testing responsibilities, 2) schedule and oversee completion of individual data testing, 3) review integral data experiments, 4) analyze integral data calculations, 5) select integral data benchmarks, maintain an integral data discrepancy list, 7) recommend suitability of evaluations, 8) collect needs of applied users, 9) recommend priorities for measurements based on discrepancies between calculation and integral experiments, and 10) organize seminars, workshops, etc., to solve specific data testing problems.

The Methods and Formats Committee would 1) develop ENDF formats for data and covariances, 2) develop ENDF utility codes, 3) develop ENDF processing codes, 4) recommend standard interfaces, 5) investigate analysis methods, and 6) orgenize seminars, workshops, etc., to solve specific methods and formats problems.

12.0 Acknowledgements

Although not individually identified, some material used in illustrating cross section analysis were provided by Mulki Bhat, Mundrathi Divadeenam, Said Mughabghab, and Gus Prince of Brookhaven National Laboratory. The list of example cross section processing and reactor physics codes was prepared by Phillip Rose of Brookhaven National Laboratory. Their help is very much appreciated.

During the lectures the help of the following people is gratefully acknowledged:

1. M. Anwar, S.K. Gupta, and C.C. Madueme for their assistance on Sections 1, 2, and 3 and S.K. Gupta and A. Waheed for their leading of the afternoon workshop discussion on (n, n'γ) and (n,γn').
2. O. Harouna and B. Strohmaier for their assistance on Sections 4, 5, and 6.
3. K. Stankiewicz, K. Morstin, and J. Rama Rao for their workshop presentations on ENDF formats for File 2, 4, and 5, respectively.
4. I.A. Azhar and B. Osmera for their assistance on Sections 7 and 8.
5. A.K. Ahafia for his presentation on the evidence for the existence of the neutron.

Finally, I wish to acknowledge the keen attention given to the Trieste Winter College on Nuclear Physics and Reactors by the course directors, M.K. Mehta and J.J. Schmidt.

13.0 References

13.1 Neutron Physics

1. D.J. Hughes, File Neutron Research, Addison-Wesley, Reading, Mass. 1953.
2. K.H. Beckurts and K. Wirtz, Neutron Physics-Springer Verlag, 1964.
3. S.F. Mughabghab, et al. Neutron Cross Sections, Vol. 1, Resonance Parameters, Third Edition (Introduction), BNL-325 (1978).

13.2 Specific Neutron Data

(n,2n)

1. M. Caner, M. Segev, and S. Yiftah, Nucl. Sci. Eng. 59 (1976) 395.

fission ratios

1. J.W. Behrens, R.S. Newbury, and J.W. Morgana, Nucl. Sci. Eng. 66 (1978) 433.

13.3 Nuclear Systematics

1. S. Pearlstein, Nucl. Sci. Eng. 49 (1972) 162.
2. S. Pearlstein, J. Nucl. Energy 27 (1973) 81.
3. S. Pearlstein, Washington Conference, March 1975, p. 331.
4. S. Pearlstein, Nucl. Sci. Eng. 68 (1978) 55.
5. I. Angeli and J. Csikai, Nucl. Phys. A158 (1970) 389.

13.4 Covariances

1. F.G. Perey, Neutron Physics and Nuclear Data, Harwell, September 1978, p. 104.
2. C.Y. Fu, D.M. Hetrick, and F.G. Perey, Knoxville Conference, October 1979.

13.5 Data Adjustment

1. P. Greebler and B.A. Hutchins, Physics of Fast and Intermediate Reactors, IAEA, Vienna 1962, Vol. 3, p. 121.
2. J.B. Dragt, J.W.M. Dekker, H. Gruppelaar, and A.J. Hansen, Nucl. Sci. Eng. 62 (1977) 117.
3. W.P. Pönitz, Neutron Standards and Flux Normalization, AEC Symposium Series 23, 1970, p. 331.
4. Y. Chao, Nucl. Sci. Eng. 72 (1979) 1.

13.6 Group Constants

1. I.I. Bondarenko (Editor), Group Constants for Nuclear Reactor Calculations, Consultants Bureau, N.Y. (1964).

13.7 Probability Table Method

1. L.B. Levitt, Nucl. Sci. Eng. 49 (1972) 450.
2. J.M. Otter, R.C. Lewis, and L.B. Levitt, U3R, "A Code to Calculate Unresolved Resonance Cross Section Probability Tables," AI-AEC-13024, Atomics International (1972).
3. S. Pearlstein, Nucl. Sci. Eng. 58 (1975) 354.
4. S. Pearlstein, Nucl. Sci. Eng. 68 (1978) 10.

13.8 Bibliography

1. CINDA, an Index to the Literature on Microscopic Neutron Data, International Atomic Energy Agency, Vienna.
2. Burrows, T.W., et al. The Bibliography of Integral Charged Particle Nuclear Data, Third Edition. BNL-NCS-50640, April 1979.
3. Burrows, T.W. and Holden, N.E. A Source List of Nuclear Data Bibliography, Compilations, and Evaluations. BNL-NCS-50702, Second Edition, October 1978.
4. S. Pearlstein, Adv. Nucl. Science and Tech. 8 (1975) 115.
5. The Evaluation of Neutron Nuclear Data, Proceedings of a Panel, Vienna, 1971, IAEA-153.

13.9 Nuclear Reaction Data Centers

1. National Nuclear Data Center, Brookhaven National Laboratory, Bldg. 197D, Upton, N.Y. 11973
2. European Nuclear Energy Agency Data Bank , Neutron Data Compilation Center (Nuclear Energy Agency) P.O. No. 9, 91190 Gif-sur-Yvette, France.
3. Nuclear Data Section (International Atomic Energy Agency) Wagramerstrasse 5, A-1400 Vienna, Austria.
4. Center Po Jadernym Dannym (USSR), Institute of Physics and Energy, Obninsk, USSR.
5. Karlsruhe Charged Particle Group, Kernforschungszentrum, D-7500 Karlsruhe, Germany.
6. Centre Po Atomn. i Jadernym Dannym, Kurchatov Inst. Moscow, USSR.

APPENDIX I

EXAMPLE CROSS-SECTION PROCESSING AND REACTOR PHYSICS CODES

February 1980

Spectrum Calculations by Contents, etc.

FORM-Thermal (Fast x-sects) Fortran version of MUFT systems
HAMMER-Thermal lattice contains THERMOS
LASER-Thermal lattice EPRI-CELL
MC**2-LMFBR (ANL) calculated spectrum (P_1B_1 and consistent P_1+B_1) used for weighting and constructing gp x-sects
NJOY(MINX)-General but geared for LMFBR (LASL)
RAHAB-Thermal lattice (SRL) good for D_2O systems
SUPERTOG-Fast group constants. General systems.
TEMPEST-(Thermal-x-sects) Thermal systems.
THERMOS-Thermal lattice Integral Transport Solution (In Hammer)
WIMS-Thermal lattice
IDX-Benchmark calculation (will process X-sections to ANISN format)
AMPX-General (ORNL)
GGTC-ENEL-Thermal multigroup x-sects
ETOG-Thermal analysis (Fast x-sects) Produces HAMMER Library etc.also ETOM (ETOE)
FLANGE-Thermal scattering matrices
LITHE-Thermal (Processes thermal x-sects for HAMMER uses FLANGE output)
SPHINX-Similar to IDX uses 'CCCC' format transport calculation
PUPX-Handles data for IDX code
ETOX-Fast cross sections similar to ETOG but geared for LMFBR systems

Static Design

ANISN-General ID transport ORNL
DOT-2+3D transport ORNL
DTF-Similar to ANISN
PERT-Perturbation code uses ANISN output etc.
VENTURE-3D system ORNL-LMFBR
TWOTRAN-2D Transport LASL
2DB(2DF)-2D diffusion LMFBR cores
PDQ-7(TRITON,SQUID)-2-3D diffusion Thermal cores
EXTERMWATOR-2D diffusion x-y R-z R-θ searches
CITATION-3D system ORNL-LMFBR
TRIDENT-2D Transport X-Y, R-Z general anistropic scattering
ONETRAN-General ID transport LASL

Dynamic Design

RAUM-ZEIT-(old)
SYNTH-3D-3D transient space-time synthesis
FRAP-T3-Light Water Reactor transient response
RECAP series-Dynamic response for light water systems
BOIL-1-Meltdown sequence
NATRANSIENT-Pressure transients in LMFBR's

Monte Carlo Codes (Static & Transient Design)

VIM-Fast and thermal analysis
RECAP-Thermal lattices
SAM-CE-Fast and thermal analysis--shielding applications FUSION
KENG-Criticality hazards

Shielding

SAM-CE-(see above) DOT (see before)
MORSE-γ Shielding Monte Carlo
ISOSHLD-3-General purpose shielding analysis
GAMLEG-γ cross sections
GAMSOURCE-γ ray source from neutron capture
QAD-Paint kernel shielding calculations (LASL)
RADHEAT-Coupled n+γ,calculates transport and energy deposition
LAPHANO-Calculates γ source from n

Depletion & Fuel Management

ORIGEN-Fission product decay heat
REBUS-Fuel management
CINDER-Fission product decay heat
2DB-In depletion mode
ORSIM-Fuel management
HYACINTH-Heavy isotope inventory with depletion
RICE-CEGB-Actinide and fusion product inventory of irradiated fuel
LEOPARD-A spectrum-dependent nonspatial depletion code (thermal analysis)
DTF-BURN-Depletion using DTF code
NUCY-Depletion package can be adopted to ANISN, etc.

Fusion

MACK-IV-Nuclear response functions important to the neutronics analysis of nuclear and fusion systems. Mostly nuclear heating from kernal factors.
HETC-High energy nucleon-meson transport code package
See other packages for static design.

Some References

DTF	LA-3373, LA-3267, NAA-SR-10951
OGRE	ORNL-3805
QAD	LA-3573
ISØSHLD	BNWL-236, HW-83784
ANISN	K-1693 (ORNL)
DOT	ORNL-TM-4280
SAM-C	UNC-5157, MAGI-6701, EPRINP-1042
MORSE	ORNL-4585
2DB	BNWL
HETC	ORNL-4744
TWØTRAN	LA-4600, LA-4848, LA-4774, LA-4432, LA-4058
ORIGEN	ORNL-4628
TRIPLET	(2D Triangular mesh discrete ordinates) LA-5428-MS
IDX	BNWL-954
ETOX	BNWL-1002
NJOY	LA-7584-M
MINX	LA-6486-MS
FLANGE	DP-1278, ENDF-152
ETØG	WCAP-3845-1
HAMMER	DP-1064 (SRL)
THERMOS	BNL-5826
MC^2	ANL-8144
VENTURE	ORNL
CITATION	ORNL

NEA-DATA BANK

Library	Comments	Application
5.1	LIB-IV "CCCC" Format	LMFBR
5.2	26 gp ARAMCO	General
5.3	Benjamin - SRL library	Actinide depletion
5.4	460 gp ENDF/B-IV Thermal	Thermal Reactors
5.5	SAND-II	Dosimetry
5.6	-	-
5.7	-	-
5.8	-	-
5.9	-	-
5.10	ENDL 175 gp library	Fusion
5.11	-	-

APPENDIX II

ENDF DOCUMENTS of GENERAL INTEREST

ENDF-102	BNL-NCS-50496	GARBER, D.	DATA FORMATS AND PROCEDURES FOR THE EVAL. NUCLEAR DATA FILE
ENDF-110	BNL-50300	OZER, O.	DESCRIPTION OF THE ENDF/B PROCESSING CODES AND RETRIEVAL SUBROUTINES
ENDF-201	BNL-17541	GARBER, D.	ENDF/B SUMMARY DOCUMENTATION
ENDF-202	BNL-19302	ALTER, H.	CROSS SECTION EVAL. WORKING GROUP BENCHMARK SPECIFICATIONS
ENDF-210	ANCR-1157	REICH, C.W.	RADIOACTIVE-NUCLIDE DECAY DATA FOR ENDF/B
ENDF-216	BNL-NCS-50446	MAGURNO, B.A.	ENDF/B-IV DOSIMETRY FILE
ENDF-223	LA-6116-MS	ENGLAND, T.R.	ENDF/B-IV FISSION-PRODUCT FILES: SUMMARY OF MAJOR NUCLIDE DATA
ENDF-225	BNL-NCS-50464	MAGURNO, B.A.	ENDF/B-IV CROSS SECTION MEASUREMENT STANDARDS
ENDF-230	BNL-NCS-21118	BOHN, E.	BENCHMARK TESTING OF ENDF/B-IV
ENDF-243	BNL-NCS-50545	ROSE, P.F.	ENDF/B FISSION PRODUCT DECAY DATA
ENDF-244	LA-6518-MS	HALE, G.M.	LIGHT ELEMENT STANDARD CROSS SECTIONS FOR ENDF/B-IV
ENDF-249	ORNL-TM-5938	PEREY, F.G.	DATA COVARIANCE FILES FOR ENDF/B-V
ENDF-265	BNL-NCS-24853	WEISBIN, C.R.	SENSITIVITY COEFFICIENT COMPILATION FOR CSEWG DATA TESTING BENCHMARKS

APPENDIX II cont.

ENDF DOCUMENTS OF SPECIFIC TOPIC

ENDF-152	DP-1278	HONECK, H.C.	FLANGE II (VERSION 71-1) A CODE TO PROCESS THERMAL NEUTRON DATA FROM AN ENDF/B TAPE
ENDF-218	ORNL-TM-4847	WEISBIN, C.	CROSS SECTION AND METHOD UNCERTAINTIES: THE APPLICATION OF SENSITIVITY ANALYSIS TO STUDY THEIR RELATIONSHIP IN RADIATION TRANSPORT BENCHMARK PROBLEMS
ENDF-237	LA-6486-MS	WEISBIN, C.	MINX: A MULTIGROUP INTERPRETATION OF NUCLEAR CROSS SECTIONS FROM ENDF/B
ENDF-238	ANCR-1322	GRIMESEY, R.A.	ETOP 14: A FORTRAN CODE TO PROCESS ENDF/B DATA INTO THE 68-GROUP PHROG LIBRARY FORMAT
ENDF-239	ANL-8144	HENRYSON, H.	MC^2-2: A CODE TO CALCULATE FAST NEUTRON SPECTRA AND MULTIGROUP CROSS SECTIONS
ENDF-251	HEDL-TME-77-54	MANN, F.	HEDL EVALUATION OF ACTINIDE CROSS SECTION FOR ENDF/B-V
ENDF-266	TREE-1259	HARKER, Y.D.	FISSION PRODUCT AND REACTOR DOSIMETRY STUDIES AT COUPLED FAST REACTIVITY MEASUREMENTS FACILITY
ENDF-269	GA-8774	KOPPEL, J.U.	REFERENCE MANUAL FOR ENDF THERMAL NEUTRON SCATTERING DATA
ENDF-272	LA-7584-M	MACFARLANE, R.	THE NJOY NUCLEAR DATA PROCESSING SYSTEM: USER'S MANUAL

REFERENCE GUIDELINES FOR ENDF/B

Case I: Use of ENDF/B evaluations in a secondary manner, where many elements are used together, or other cases where NO CONCLUSIONS ARE DRAWN CONCERNING QUALITY OF EVALUATIONS. In this case we propose the following form for ENDF/B-V.

> "ENDF/B Summary Documentation, BNL-NCS-17541 (ENDF-201), 3rd Edition (ENDF/B-V), edited by R. Kinsey, available from the National Nuclear Data Center, Brookhaven National Laboratory, Upton, N.Y. (July 1979)."

Case II: Use of ENDF/B evaluations in a direct manner, for example comparing measured results with evaluated results, or ANY CASE WHERE CONCLUSIONS ARE DRAWN ABOUT AN EVALUATION FOR A PARTICULAR MATERIAL. We propose, for ^{12}C from ENDF/B-V as an example:

> "ENDF/B data file for ^{12}C (MAT 1306,MOD 1), evaluation by C.Y. Fu and F.G. Perey (ORNL), BNL-NCS-17541 (ENDF-201), 3rd Edition (ENDF/B-V), edited by R. Kinsey, available from the Brookhaven National Laboratory, Upton, N.Y. (July 1979)."

Case III: Use of ENDF/B evaluations to generate a multigroup library. In this case we propose that the report describing the library contain a table which includes the following information for each evaluation:

Material	MAT,MOD	Authors	Institution

This table may contain in addition other useful information concerning the multigroup library. Finally, a general reference should be given of the type described in Case I.

As shown in Cases II and III, a correct reference would contain the material name, MAT number, author list and institution(s), along with a reference to the Summary Documentation. In addition, for ENDF/B-Version V, updates will be allowed to the evaluations prior to the release of ENDF/B-VI. Thus, references to ENDF/B-V evaluations should also contain the appropriate MOD number, which serves to define the current status of an evaluation. All of this information is readily available in File 1 of each evaluation. The only exception to the above cases would be where a published document, prepared by the authors of the evaluation, is available. This document should then be referenced directly.

	N−2	N−1	N	N+1
Z	n, 3n	n, 2n	Original Nucleus n, n	n, γ
Z−1	n, nt n, tn	n, t n, nd n, dn	n, d n, np n, pn	n, p
Z−2	n, αn n, nα	n, α n, He^3 n n, n He^3	n, He^3 n, pd n, dp	

Fig. 2.1

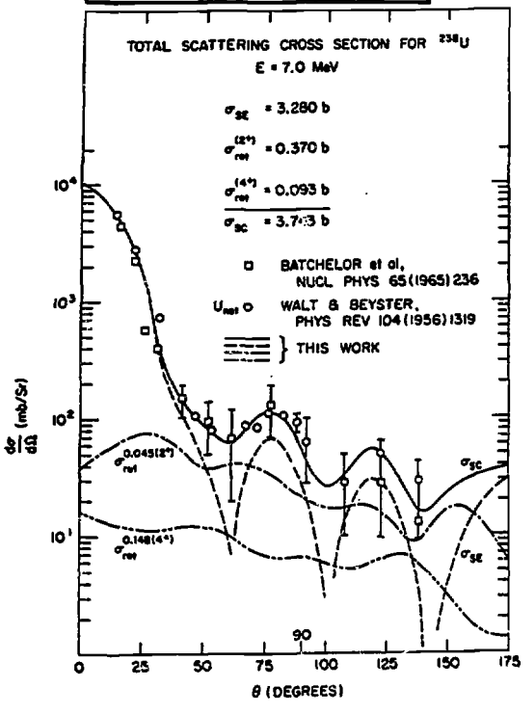

Fig. 3.1

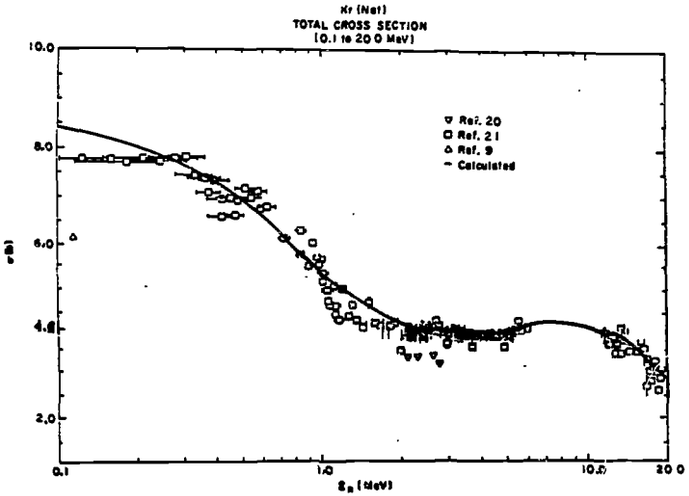

Fig. 3.2

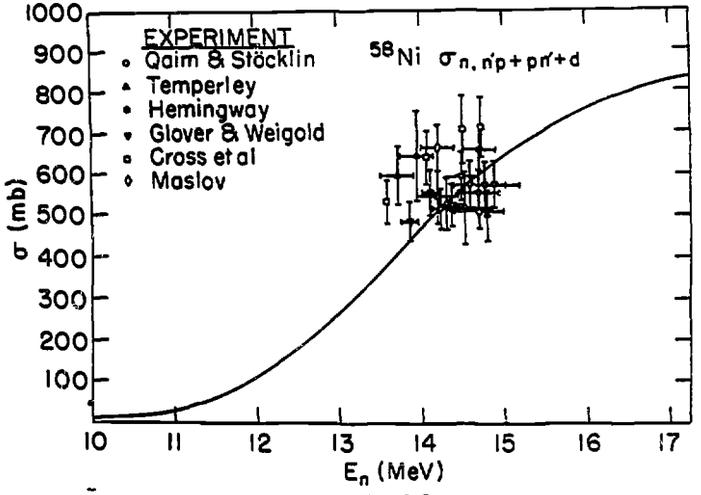

Fig. 3.3

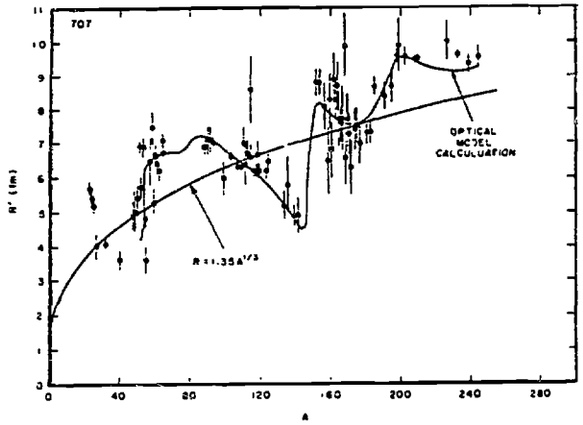

Variation of R' with A. The solid curve is based on the vibrational rotational optical model with parameters $V_0 = 43.5$ MeV, $r_{op} = 1.35$ fm, $V_{so} = 8$ MeV and surface absorption $W_D = 5.4$ MeV.

Fig. 4.1

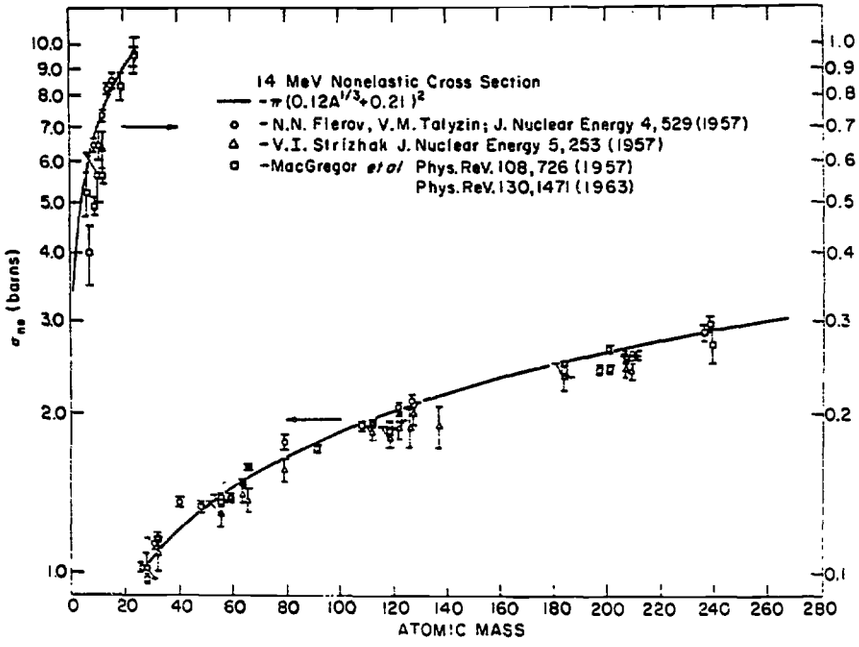

Fig. 4.2

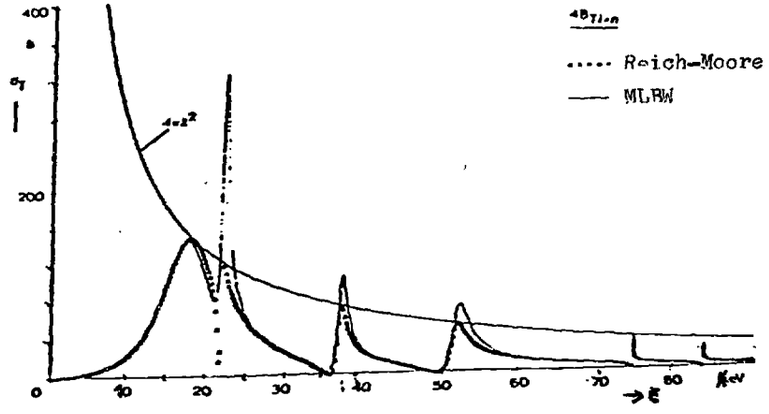

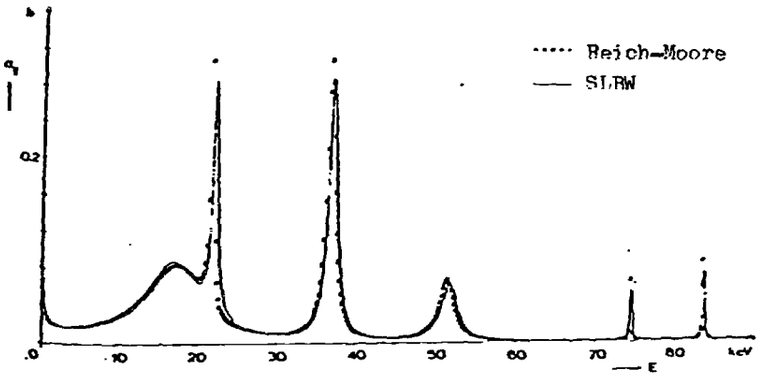

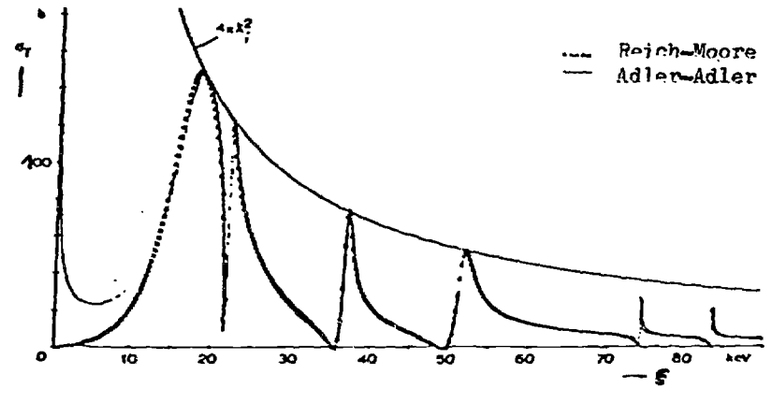

Illustration of inadequacy of approximations admitted by ENDF conventions for a medium-mass nucleus, ^{48}Ti. The Reich-Moore values are exact (parameters from /18/). The unitarity limit $4\pi\lambda^2$ is seriously violated by MLBW, less by Adler-Adler. Both these approximations are useless for capture cross section calculation here.

Fig. 4.3

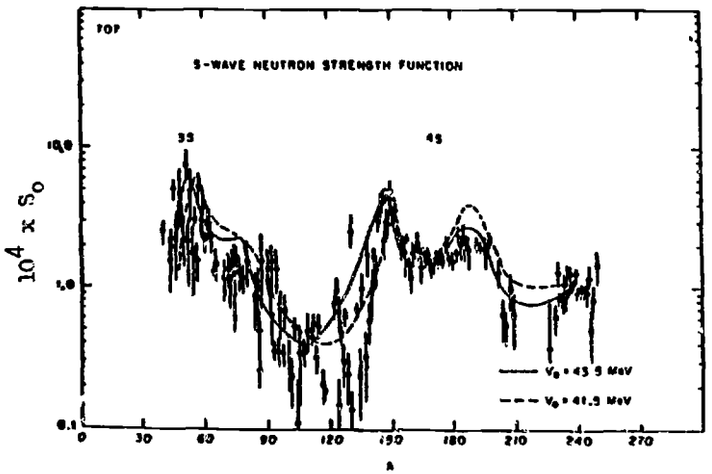

s-Wave neutron strength function. The parameters of the optical potential are the same as in Figure 1.

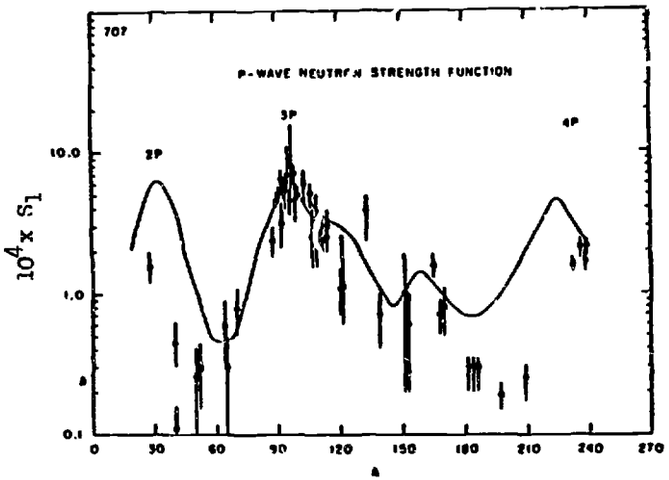

Experimental values of p-wave strength functions compared with predictions of the optical model.

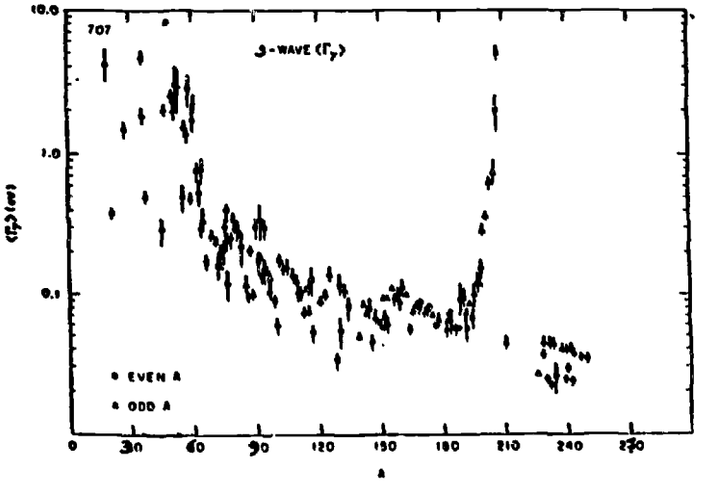

s-Wave radiation widths.

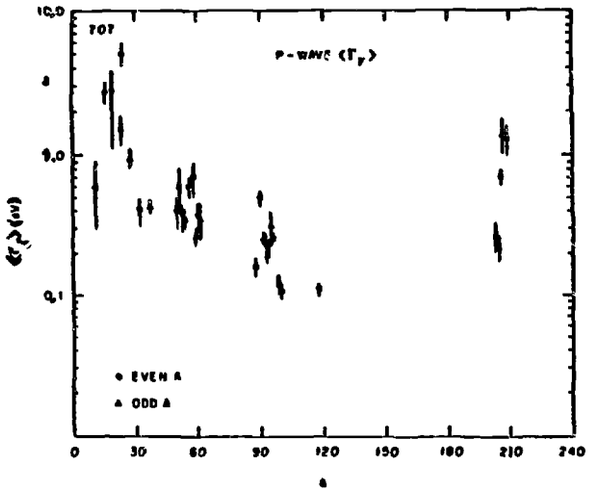

p-Wave radiation widths.

Fig. 4.4

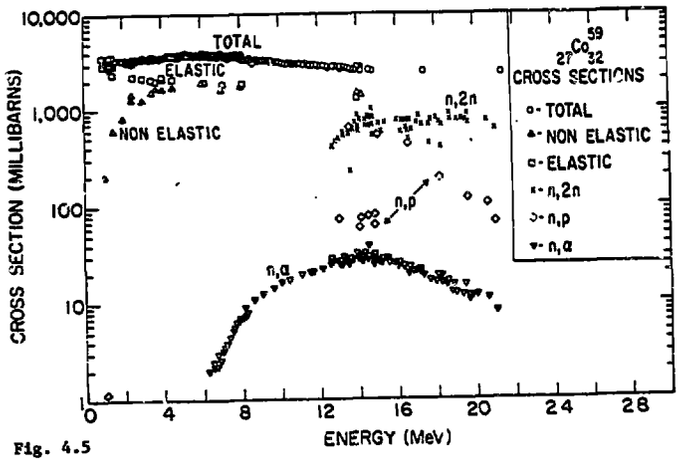

Fig. 4.5

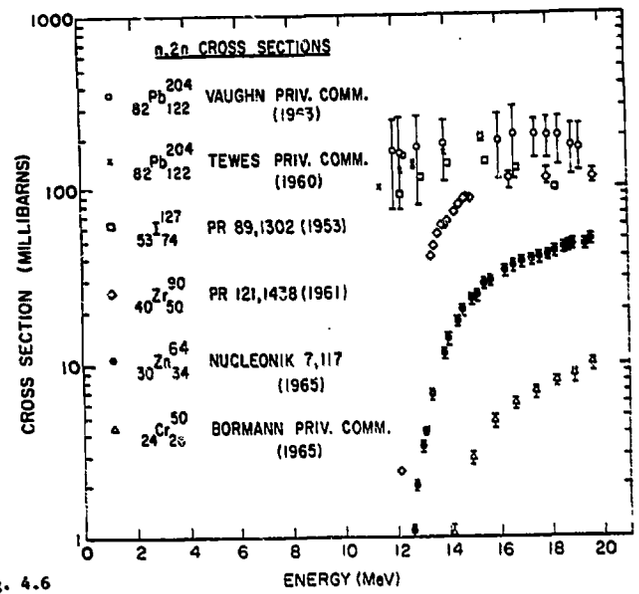

Fig. 4.6

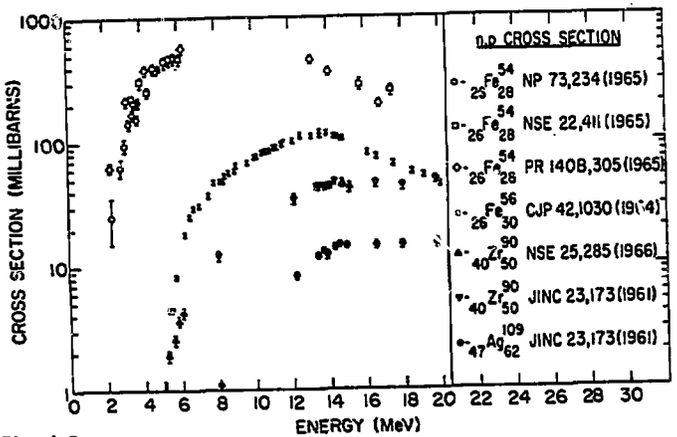

Fig. 4.7

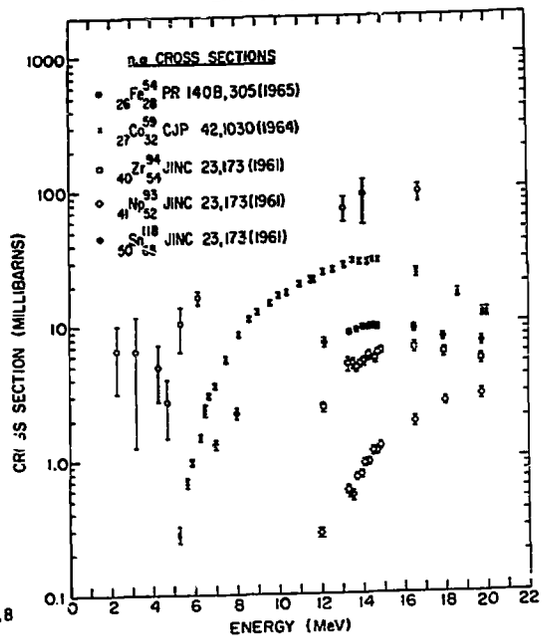

Fig. 4.8

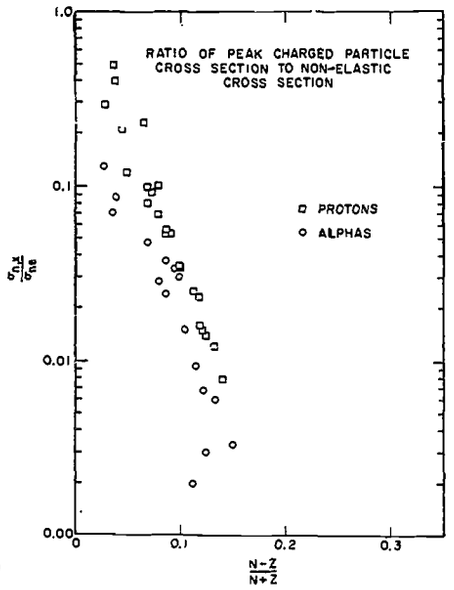

Fig. 4.9

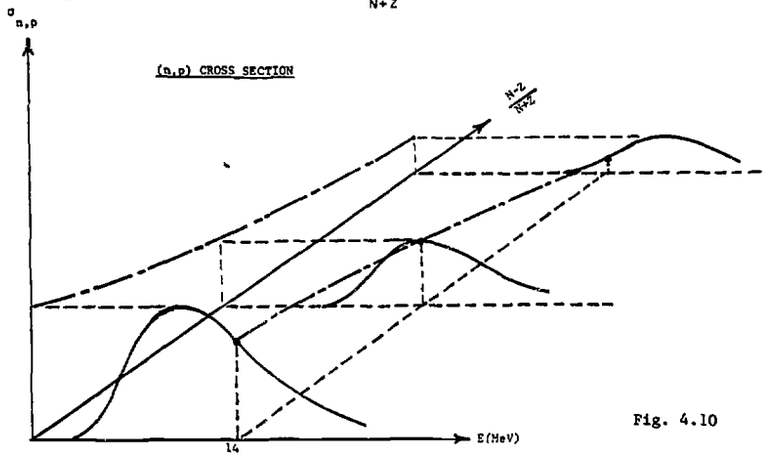

Fig. 4.10

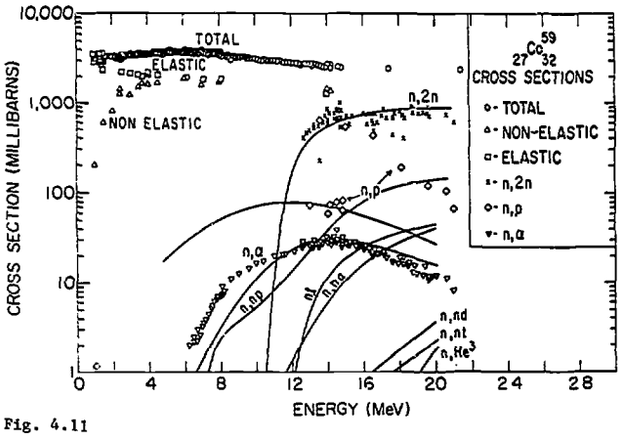

Fig. 4.11

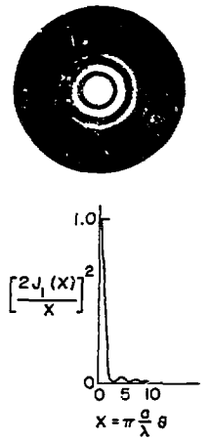

Fig. 4.12
DIFFRACTION THROUGH CIRCULAR APERTURE

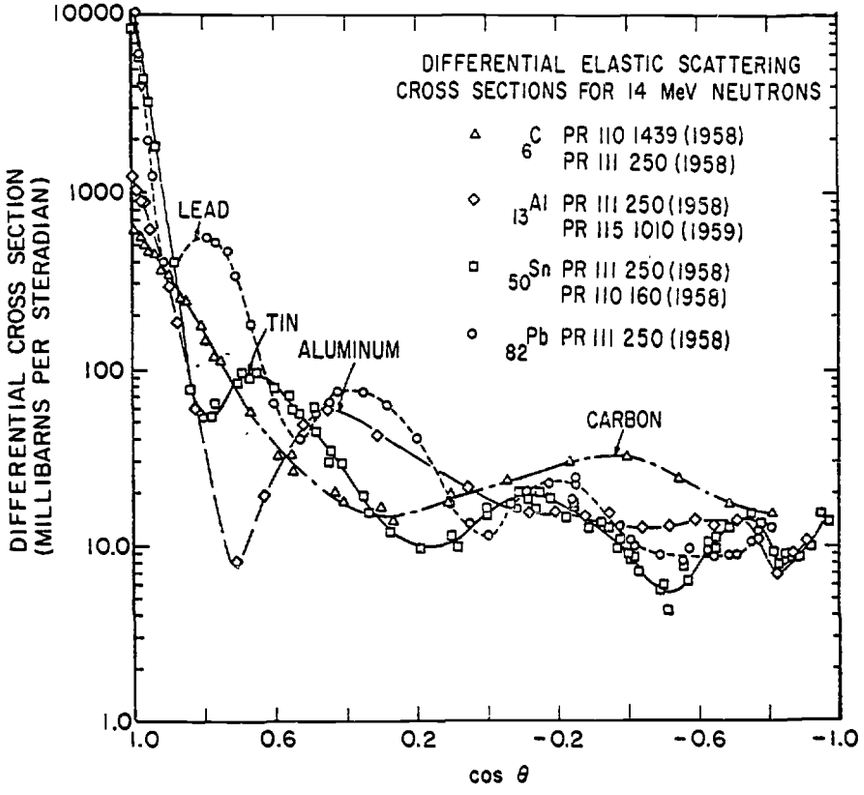

Fig. 4.13

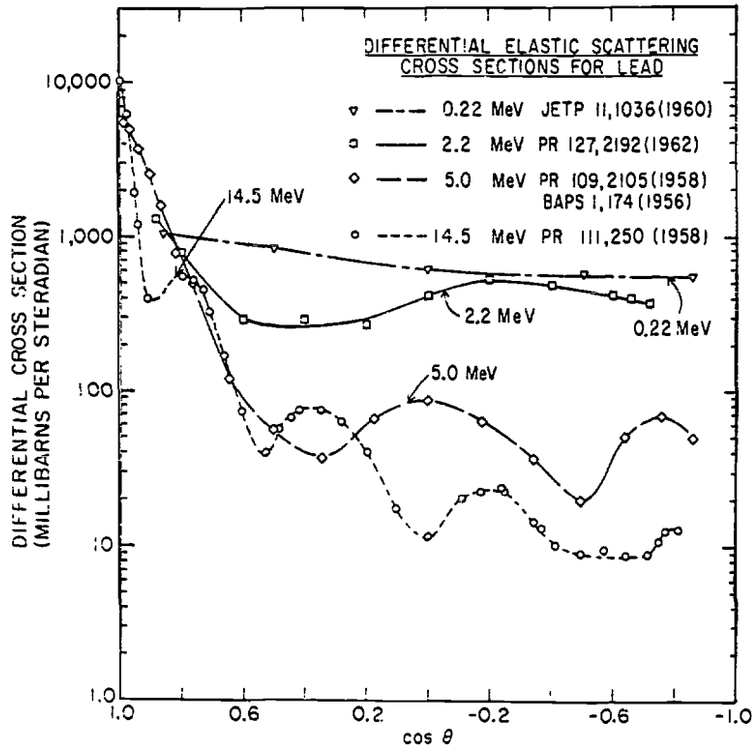

Fig. 4.14

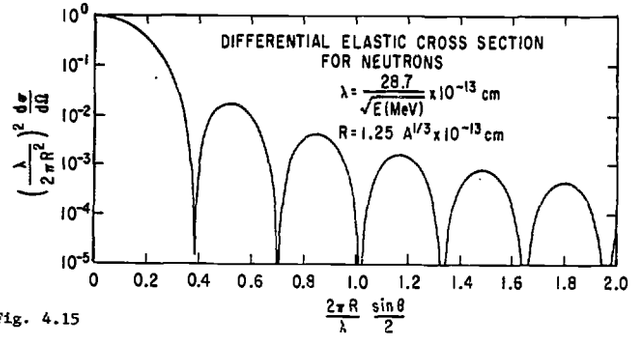

Fig. 4.15

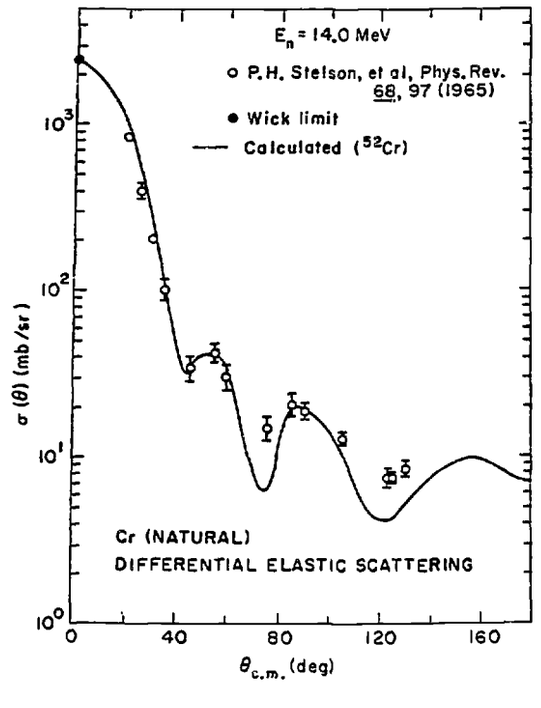

Fig. 4.16

92 Uranium 235

Quantity	Energy (ev) Min	Max	Lab	Type	Documentation Ref	Vol	Page	Date	Author, Comments
Fission	2.7+5		MHG	Expt	Abst	ANS	21 503	Jun 75	Robertson+CS=1.32B +-2PC.REL NBS-2
Fission	Fast		DOU	Expt	Prog	UKNDC(75)P71		Jul 75	Davies+ IRRADIATION PFR SMALL SAMPLE
Fission	Maxwl		ILL	Expt	Jour	NP/A	247 74	Jul 75	Clerc+ MEASURED Z-DIST OF FP,TBL
Fission	Maxwl		SRC	Expt	Prog	UKNDC(75)P71		Jul 75	Alam+ BETA ENERGY EMITTED AFTER FISS
Fission	Pile		WIN	Expt	Prog	UKNDC(75)P71		Jul 75	Taylor+BETA ENERGY AFTER FISS
Fission	9.6+5		MHG	Expt	Jour	ANE	2 637	Sep 75	Gilliam+ CS(964KEV) = 1.21+-0.025 B
					Conf	75Wash.	634	Mar 75	- +CS=1.21B+-2.1PCT.NA-BE NEUTS
					Abst	ANS	15 946	Nov 72	- + SUPERSEDED
	9.6+5				Data	EXFOR	10314.002	Feb 76	1 PT. 964 KEV
Fission	5.3+6	1.0+7	ANL	Expt	Jour	NSE	58 255	Oct 75	Meadows.TBL,GRPH 238/235U NF RATIO
Fission	1.5+7		BRC	Expt	Abst	ANS	22 664	Nov 75	Cance+ 14.6MEV.CFD OTHER EXPT,ENDF
Fission	9.6+5		MHG	Expt	Jour	ANE	2 637	Nov 75	Gilliam+ ABSOL EXPT NA-BE SOURCE
Fission	4.0+1	2.0+2	BNL	Theo	Jour	NSE	58 354	Dec 75	Pearlstein.PROB TABLE METHOD.GRPHS
Fission	Maxwl		IBJ	Expt	Jour	NP/A	255 387	Dec 75	Piasecki+P.D.T.ALF EMISSION MEASURED
Fission	8.0+5	4.0+6	LRL	Expt	Jour	NSE	58 371	Dec 75	Czirr+ TBLS,GRPHS.REL NP SCATTERING
	8.0+5	2.0+7			Prog	ERDA-NDC-2	70	May 75	- +REL.TO N-P SCAT.NDG.
					Conf	75Wash.	615	Mar 75	Sidhu+TABLE,GRAPH.REL TO N-P SCATT.
	7.3+5	2.0+7			Data	EXFOR	10428.002	May 75	88PTS,SIGMA
Fission	0.0+0	1.0+7	CAI	Theo	Jour	AKE	27 1 47	76	El Nadi+ QUASI-MOLECULAR MODEL
Fission	2.0-2	2.0+5	ORL	Expt	Jour	NSE	59 79	Feb 76	Gwin+ TBLS,GRPHS AVG CS

Fig. 6.1

```
ENTRY           10900     790830          5                    10900000000001
SUBENT       10900001     790830                               10900001     1
BIB                14         44                               10900001     2
INSTITUTE  (1USAANL)                                           10900001     3
REFERENCE  (J,BAP,24,631,7904)                                 10900001     4
           (A,SMITH,7904)                                      10900001     5
AUTHOR     (D.L.SMITH,J.W.MEADOWS)                             10900001     6
TITLE      CROSS SECTION MEASUREMENT FOR THE CR-52(N,PROTON)V-52 10900001    7
            REACTION NEAR THRESHOLD                            10900001     8
FACILITY   ARGONNE FAST NEUTRON GENERATOR                      10900001     9
N-SOURCE   (D-D) DEUTERONS ON DEUTERIUM GAS                    10900001    10
SAMPLE     SOLID CHROMIUM CYLINDER, MASS OF 86.76-GRAMS APPROX 10900001    11
            10-CM FROM NEUTRON SOURCE.                         10900001    12
DETECTOR   (GELI) TRUE COAXIAL GERMANIUM-LITHIUM DETECTOR IN   10900001    13
            MASSIVE SHIELD. VOLUME IS APPROX 100-CC. LOCATED   10900001    14
            APPROX 100-CM FROM SAMPLE, 90-DEG FROM BEAM.       10900001    15
           (FISCH) U-238(93.90-PERCENT),U-233(6.09-PERCENT),   10900001    16
            U-235(0.01-PERCENT) FISSION CHAMBER FOR NEUTRON FLUX 10900001  17
            MEASUREMENT.                                       10900001    18
DECAY-DATA (23-V-52,3.75MIN,DG,1434.)                          10900001    19
MONITOR    (92-U-235(N,F),,SIG) FROM ENDF/B-IV                 10900001    20
METHOD     (ACTIV). ENERGY SCALE OF ACCELERATOR CALIBRATED USING 10900001  21
            PROTON BEAM AND OBSERVING REACTION THRESHOLDS FOR   10900001    22
            PROTONS ON LI-7, B-11, AND AL-27. CRYSTAL CONTROLLED 10900001  23
            DELAY CIRCUIT USED TO INTRODUCE A DELAY TO ALLOW   10900001    24
            SCATTERED NEUTRON BACKGROUND TO DIE AWAY.          10900001    25
CORRECTION CORRECTED FOR GEOMETRY, NEUTRON SOURCE CHARACTERISTICS, 10900001 26
            ABORPTION AND MULTIPLE SCATTERING OF NEUTRONS,     10900001    27
            ABSORPTION OF GAMMAS, TARGET THICKNESS, AND DECAY  10900001    28
            HALF-LIFE.                                         10900001    29
ERR-ANALYS SOURCE OF ERRORS IN MEASURED RATIO INCLUDE-         10900001    30
           -DETERMINATION DETECTOR COUNTS, 2-16 PERCENT        10900001    31
           -GEOMETRIC EFFECTS, 3-PERCENT                       10900001    32
           -NEUTRON SOURCE CHARACTERISTICS, 3-PERCENT          10900001    33
           -GAMMA-RAY DETECTOR EFFICIENCY, 4-PERCENT           10900001    34
           -MASS OF URANIUM DEPOSIT, 1-PERCENT                 10900001    35
           -GAMMA RAY ABSORPTION IN CHROMIUM, 2-PERCENT        10900001    36
           -NEUTRON ABSORPTION IN CHROMIUM, 2-PERCENT          10900001    37
           -NEUTRON MULTIPLE SCATTERING IN CHROMIUM, 2-PERCENT 10900001    38
           -HALF LIFE AND DUTY CYCLE, 2-PERCENT                10900001    39
           -BACKGROUND EFFECTS, 1-4 PERCENT                    10900001    40
           -GAMMA DECAY BRANCHING FACTOR, 1-PERCENT            10900001    41
          TOTAL RMS ERROR, 8-18 PERCENT                        10900001    42
          SYSTEMATIC ERROR, APPROX 8-PERCENT                   10900001    43
          ERROR IN U-238 FISSION CROSS SECTIONS ASSUMED TO BE  10900001    44
           APPROX 5-PERCENT.                                   10900001    45
HISTORY    (790412C)                                           10900001    46
ENDBIB             44                                          10900001    47
COMMON              1          3                               10900001    48
Q-VAL                                                          10900001    49
MEV                                                            10900001    50
 -3.195                                                        10900001    51
ENDCOMMON           3                                          10900001    52
ENDSUBENT          51                                          10900001999999
SUBENT       10900002     790830                               10900002     1
BIB                2          5                               10900002     2
REACTION   1((24-CR-52(N,P)23-V-52,,SIG)/(92-U-238(N,F),,SIG)) 10900002     3
           2(24-CR-52(N,P)23-V-52,,SIG)                        10900002     4
```

Fig. 6.2

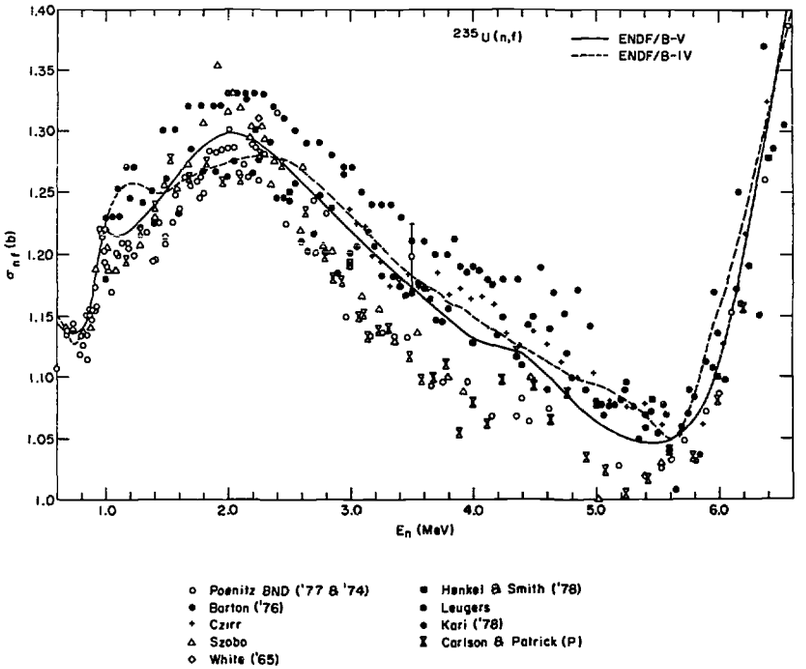

Fig. 6.3

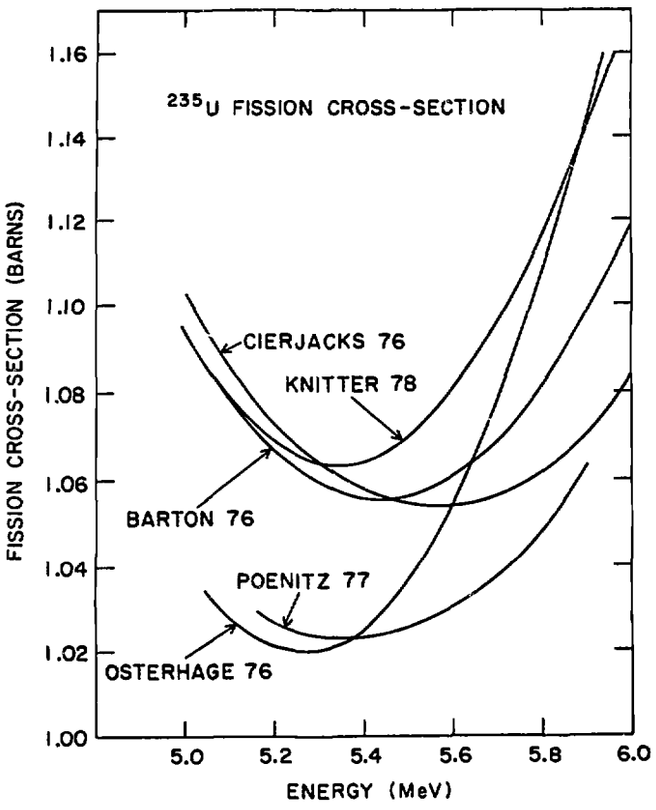

Fig. 6.4

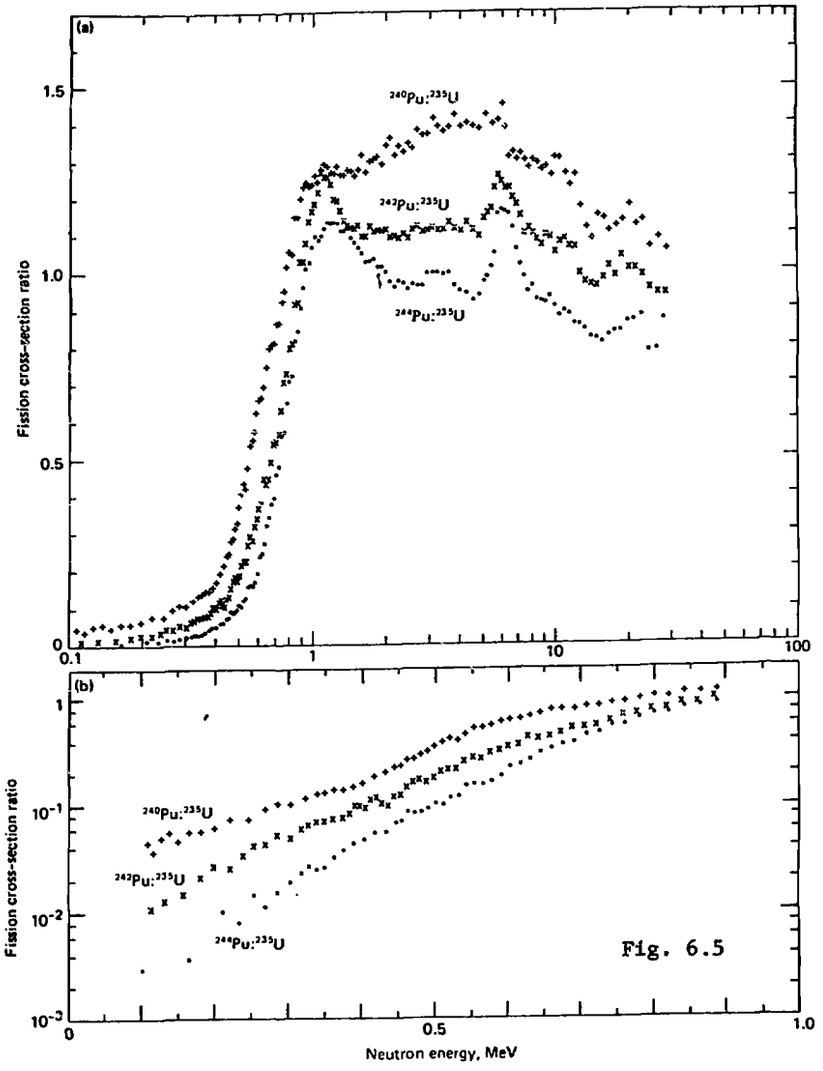

Fig. 6.5

Present measurements of the $^{240}Pu:^{235}U$, $^{242}Pu:^{235}U$, *and* $^{244}Pu:^{235}U$ *fission cross-section ratios (a) over the neutron-energy range from 0.1 to 30 MeV, and (b) from 0.1 to 0.9 MeV.*

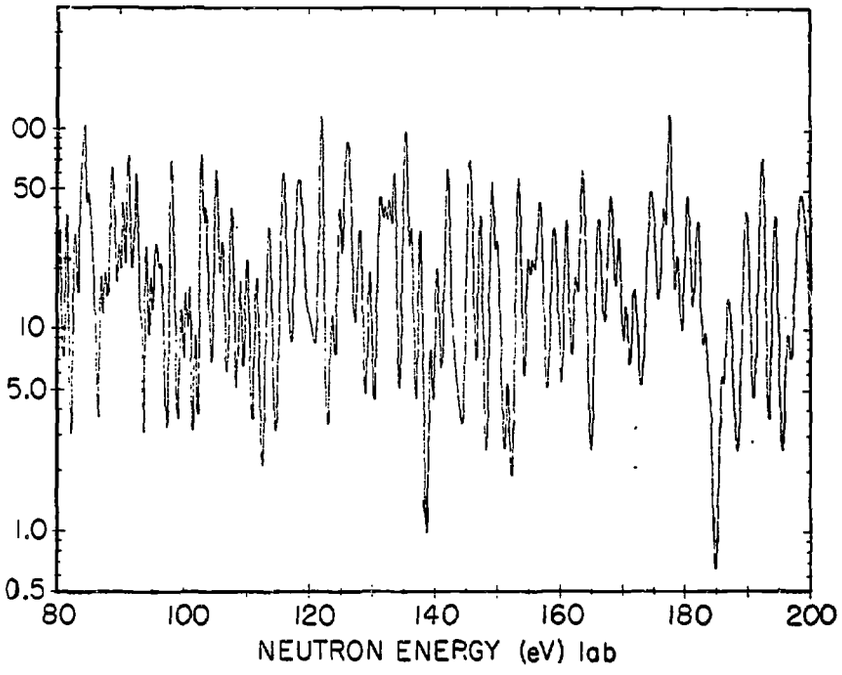

Fig. 8.1 ^{235}U FISSION CROSS SECTION
80-200 eV
R. B. PEREZ et al
Nuc. Sci. and Eng. 52 (1973) 46 -72

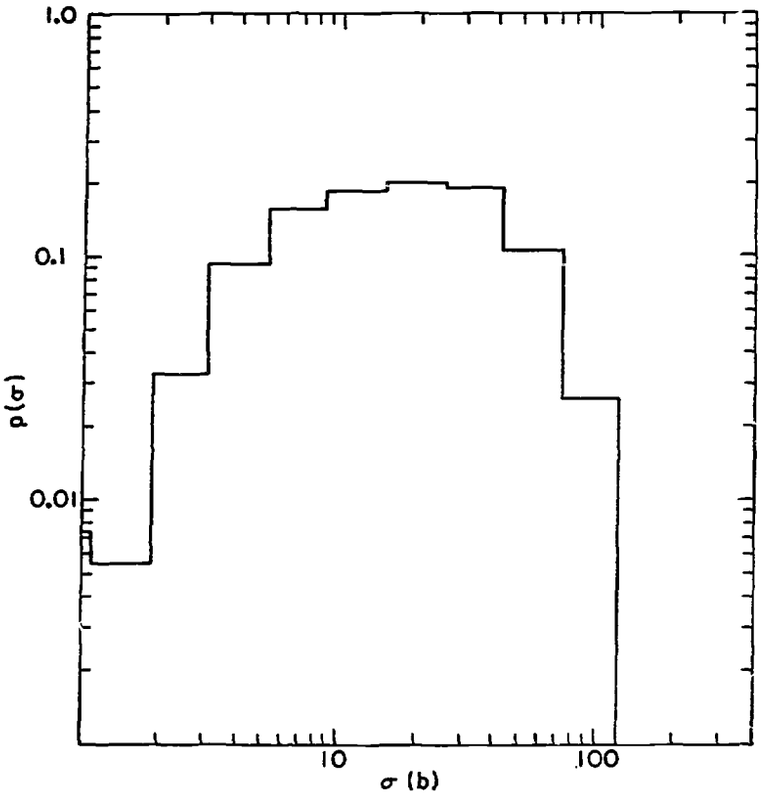

Fig. 8.2 PROBABILITY TABLE
^{235}U FISSION CROSS SECTION
80-200 eV

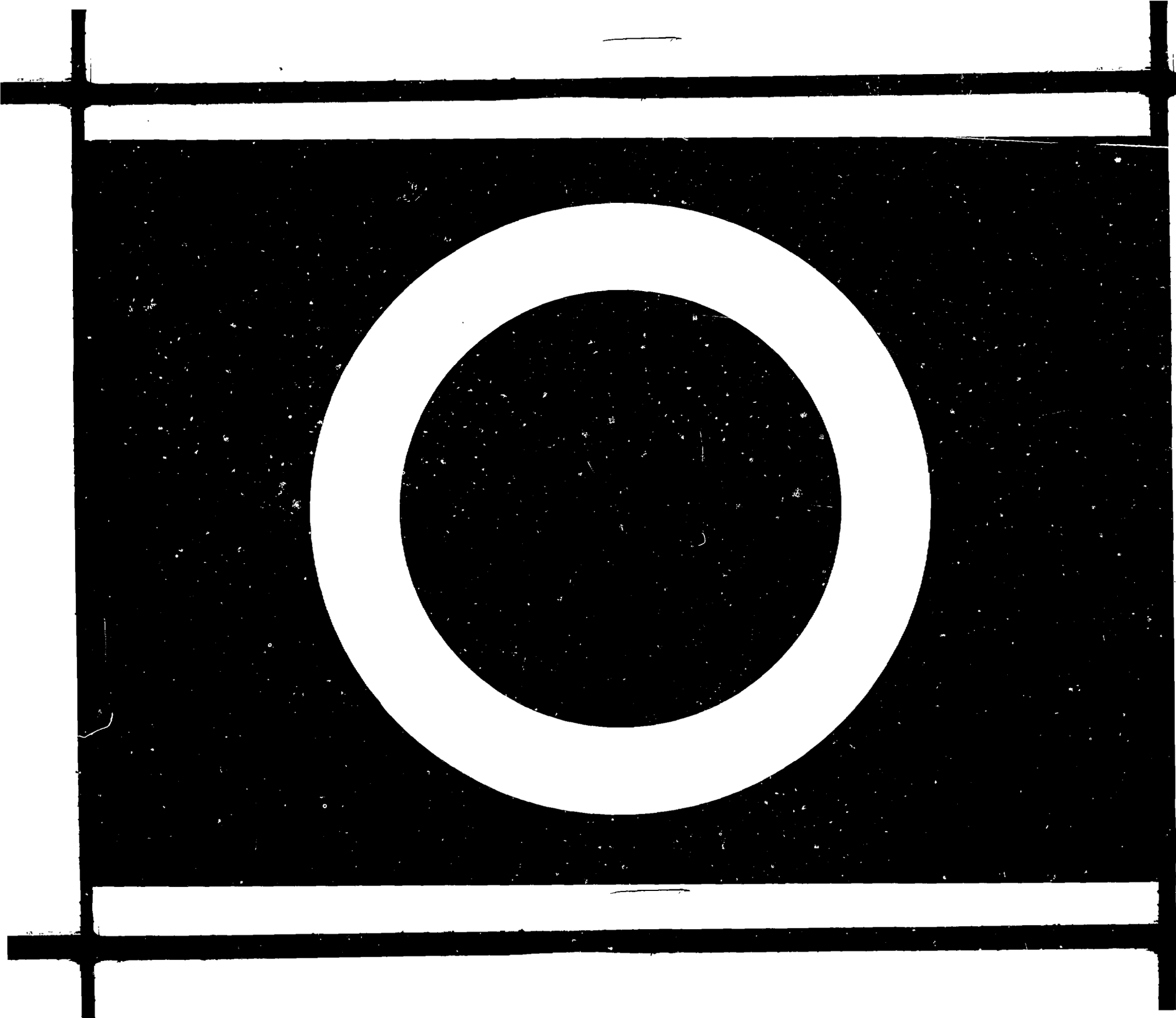

Spec

FORM
HAMM
LASE
MC**

NJOY
RAHA
SUPE
TEMP
THER
WIMS
IDX-
AMPX
GGTC
ETOG
FLAN
LITH
SPHI
PUPX
ETOX

Sta

ANI
DOT
DTF
PER
VEN
TWO
2DB
PDQ
EXT
CIT
TRI
ONE

EXPERIMENTAL TECHNIQUES AND THEORETICAL MODELS FOR THE STUDY OF INTEGRAL 14 MeV NEUTRON CROSS SECTIONS

J. CSIKAI
Institute of Experimental Physics,
Kossuth University,
Debrecen, Hungary

ABSTRACT. Owing to technical reasons, most of the data for fast neutron-induced reactions were measured at 14 MeV and the free parameters in nuclear reaction models have been determined at this energy. The discrepancies between experiment and theory are often due to the unmeasured or unreliable experimental data; therefore, it is important to survey the present techniques used for the measurement of total, elastic, nonelastic and partial nonelastic [(n,xn); (n,x charged); (n,f); (n,γ)] cross sections for 14 MeV neutrons. Systematics in the data as well as theoretical and semi-empirical models are also outlined.

INTRDDUCTION

It is well known that the large cross section of the $^{3}H(d,n)^{4}He$ reaction permits high yields of fast neutrons to be obtained even at low energy, e.g. at 150-200 keV. Such a device is inexpensive, easy to install and operate. Therefore, in addition to nuclear physicists, there are a number of groups of scientists who use small neutron generators in nuclear technology. The approximate distribution of these accelerators among various institutions [1] is: hospitals and medical centres 1 %, research laboratories 34 %, universities 32 % and industry 33 %. During the last decade, the IAEA has promoted neutron research in several developing countries by providing neutron generators to be used in fundamental and applied research. The fast neutron data have played an important role in nuclear technology since about 40 years, when Barschall and others [2, 3, 4] reported measurements of cross sections for the elastic and inelastic scattering of neutrons by various materials. In these experiments neutrons between 2 and 3 MeV were obtained from the $^{2}H(d,n)^{3}He$ reaction, which is still commonly used. Around 1950 the tritium was available as a target material [5] to produce 14 MeV neutrons by the D-T reaction with high yields, resulting in a large development in the use of small accelerators. Barschall and his co-workers used metal tritide targets in 1949 to measure the angular distribution of neutrons scattered by protons [6], deuterons [7] and tritons [8] and to determine the total cross sections [9] for the elements from H to U. From this time physicists in many laboratories have dealt with the measurements of cross sections for D-D and D-T neutrons.

As indicated in the latest WRENDA list issued by the IAEA [10] there is still a large number of requests for fast neutron cross section measurements.

Recent studies on fusion reactors show that the D-T reaction will probably be used to release the thermonuclear energy in the D-T-Li fuel cycle. In the D-T fusion about 80 % of the total energy is carried off by the 14 MeV neutrons; therefore, the investigations on the interaction of fast neutrons with structural materials are of primary importance for the design of the reactor. Because intense 14 MeV neutron sources are not available at present for the engineering testing of the working conditions of fusion reactors, neutron data are needed for the calculations of the tritium breeding, radiation damage effects, radiation shielding, neutron multiplication, isotope production, energy deposition in the first wall and superconducting

magnet, fission reaction and fissile fuel breeding in the fusion-fission hybrid systems, etc. [11, 12, 13].

An IAEA Advisory Group Meeting in 1978 has discussed the status of nuclear data for fusion reactor technology and formulated recommendations for future activities to improve the accuracy of 14 MeV cross sections and to coordinate research programmes with the aim of completing the data needed for applications and also for checking nuclear model calculations [14]. Considering the D-T burning systems, about one third of the elements are conceived as structural materials, so it is worth-while to survey the status of integral 14 MeV neutron cross sections and the present techniques and theoretical models for the study of these data.

1. OUTPUT CHARACTERISTICS OF NEUTRON GENERATORS

The details on D-T generators, as well as on their installation, operation and hazards can be found e.g. in Refs. [15, 16, 17]. A survey of commercially available neutron generators is given in Ref. [18]. The cross section of the $^{3}H(d,n)^{4}He$ reaction as a function of bombarding deuteron energy has a broad resonance at E_d=109 keV, therefore, the thick-target neutron yield increases rapidly up to about E_d=200 keV. As shown in Fig. 1 the yield increases by a factor of four between 100 and 200 keV and only about 50 % excess can be achieved when the 200 keV deuteron energy is doubled [19]. According to the yield curve, 1 mA of 200 keV atomic deuteron beam on a fresh tritium target produces about $2x10^{11}$n/s. Typical D-ion currents both for home-made and commercially available D-T generators are a few mA, producing neutrons in the order of 10^{11}n/s.

Yields much above 10^{11}n/s need high beam currents, dissipating about 100 kW power in the target. Using 0.5 A ion current a neutron source strength of $8x10^{12}$n/s was achieved in D-T reaction at 80 kW power (see Ref. [16]). Various methods to obtain high source strengths have been described by Barschall[16].

The maximum yield from neutron generators, in addition to the beam current, is determined by the target construction and a number of different stationary and rotary target systems have been developed. The type and geometry of structural materials around the target and the design of a target with a long life time are playing very important roles in the cross section measurements. In low-voltage generators the most common targets are deuterium or tritium absorbed in thin metal layers. Besides titanium and zirconium, Er, Sc, Y and U are also used to produce intermetallic compounds with deuterium or tritium. A thin layer of Ti or Zr is evaporated onto Al, Cu, Ag and W backing metal. Theoretically, the ratio of tritium to titanium atoms is about 1.9:1, but in the case of commercial targets it is about 1.5:1. Rare earth targets have a much higher thermal stability than Ti. The lifetime of a target can be represented by the following ratio [20]:

$$\text{Target lifetime} = \frac{\text{Ion current (mA)x Hours to half yield}}{\text{Target area (cm}^2\text{)}}$$

The average target life for Ti-T is about 2.7 mA·h/cm^2, the maximum being 4 mA·h/cm^2 for stationary targets. For Ti-T targets, by the time the 14 MeV neutron yield reaches one half of its initial value, the deuteron build-up achieves saturation and the yield of 3 MeV neutrons is about 1 % of the D-T output. In the first D-T generator built by Graves et al. [21] metal tritide target was used. Nowadays various suppliers (Amersham UK, ORNL USA, CEA France, IRE Belgium, SORIN Italy, Techsnabexport USSR, Metronex Poland, International Engineering Service Austria) sell metal tritide targets for DT generators, mostly with Ti layers from 0.2 to 4 mg/cm^2 thickness with different backing materials. Targets with dimension up to 50 cm diameter and thickness from micrograms to milligrams per cm^2 can be manufactured. In addition to disks, rectangular strips, annuli and other geometrical

shapes of targets are commercially available. In the case of large target surface, strong backing materials are needed to withstand pressure differences. These backings are prepared from copper alloys (Amzirk: 0.15 % Zr in Cu, Glid-Cop: Al_2O_3 in Cu).

Targets should be stored for short periods only, in dry and inert atmosphere, to ensure that the titanium layer remains adherent.

Using a 22 cm diameter rotating target, 16 mA of 400 keV deuterons produced a neutron yield of 4×10^{12} n/s that decreased 10-20 % in 50 hours for a 1 cm diameter spot [22] which corresponds to about 1600 mA·h/cm^2 lifetime.

In addition to the solid targets, tritium gas as well as an implanted mixed beam of ^{2}H and ^{3}H have been used as targets to produce 14 MeV neutrons. Figure 2 plots the neutron yields of various targets against the deuteron energy [23, 24].

According to the evaluation of Paulsen and Liskien [25] for the differential cross sections, the yield of neutrons from D-T reaction depends on emission angle in the laboratory system, but the anisotropy is less than 15 % between the forward and backward directions at E_d=200 keV. The energy of neutrons in the c.m. system emitted in D-T reaction is 14.1 MeV. In laboratory system the neutron energy depends on the bombarding deuteron energy and on the emission angle as shown in Fig. 3. If E_d=200 keV, the angular variation of energy is E_n~2 MeV; this variation is especially accentuated around 90°.

The excitation functions for many threshold reactions vary significantly around 14 MeV, thus the cross section depends on the position and the dimension of the sample. This may be one reason of the large spread in the data published by different authors.

The inconsistencies of the data may be caused by the unnormalized neutron energy. For normalization, the angular interval from 93° to 103° seems to be acceptable in which the energy spread of neutrons does not exceed a few ten keV, resulting in negligible errors in the cross sections [26]. The energy spread of neutrons at a definite angle arises mainly from the stopping and scattering of deuterons in the target. The spread caused by stopping is indicated in Fig. 3, as function of the angle, for different deuteron energies. The large energy spread ($\Delta E \sim 0.45$ MeV) in forward and backward directions raises several problems in measuring rapidly varying excitation functions [26]. This is the reason why physicists should take the target arrangements and through it the spectra of emitted neutrons into consideration before measuring the cross sections. Fig. 2

Most recently Raics [27] has given the following simple formula (based on the reaction kinematics) for the calculation of the laboratory neutron energy (E_n) versus deuteron energy (E_d) and emission angle (ϑ) for thick Ti-T target:

$$E_n(E_d,\vartheta) = 1.94 \cdot 10^{-4} E_d^{3/2} \cos^3\vartheta + 0.162 E_d \cos^2\vartheta + (9.52 \cdot 10^{-4} E_d^{3/2} + 67.42 E_d^{1/2}) \cos\vartheta + 0.397 E_d + 14049.51 \qquad (1)$$

were E_n and E_d are in keV. Using this formula such quantities as $\partial E_n/\partial E_d$ and $\partial E_n/\partial \vartheta$ as well as the anisotropy factor can be given in a simple way. In the knowledge of the stopping cross section $\varepsilon(E_d) = (dE_d/dx)/N$ and the D-T reaction cross section $\sigma(E_d)$ the energy distribution of emitted neutrons $S(E_n, E_d)$ at a given angle can be calculated. Fig. 4/a shows the "stopping spectra" of neutrons for five different angles at E_d=175 keV. The resultant spectrum $S(E_n)$ that will reach the sample, depends on the source-sample geometry, too. If the dimension of the sample covers a $\vartheta^o \pm \Delta\vartheta$ angle interval which corresponds to a change in neutron energy $E_n^o \pm \Delta E_n$, then the average energy $\langle E_n \rangle$ for the surface of the sample far from a point source is: Fig. 3

$$\langle E_n \rangle = \int_{E_n^o - \Delta E_n}^{E_n^o + \Delta E_n} N(E_n)\, \Phi(E_n)\, E_n dE_n \Big/ \int_{E_n^o - \Delta E_n}^{E_n^o + \Delta E_n} N(E_n)\, \Phi(E_n)\, dE_n \qquad (2)$$

where $N(E_n)$ is the number of target atoms in the unit angle interval at ϑ^o direction. The spectrum of impinging neutrons on the sample is $S(E_n)=S(E_n,E_d)_\vartheta\ N(E_n)\ \Phi(E_n)$,

where $\Phi(E_n)$ is the flux density. Curves of $S(E_n)$ are given in Fig. 4/b for a typical geometrical arrangement shown in Fig. 5 (the diameter of the sample is 19 mm, the distance from the source is 7 cm, the diameter of the beam is 14 mm). In Table I neutron energies and the relative yields as a function of angle as well as the energy spreads, including the effect of multiple scattering of deuterons, are summarized for the geometry shown in Fig. 5. The relatively large spread at 90^o is caused by the effect of finite angular interval used for the irradiation.

Table I.

Neutron energies vs. emission angle for D-T reaction at E_d=175 keV and $\sigma_{n,\alpha}$ for ^{27}Al and $\sigma_{n,2n}$ for ^{93}Nb

Angle	Average energy (MeV)	Relative intensity	$^{27}\sigma$(mb) Al(n,α)	$^{93}\sigma$(mb) Nb(n,2n)
0	14.80±0.17	1.07	110.3	↑
30	14.70±0.15	1.06	111.5	
60	14.45±0.12	1.03	117.0	464±3 %
90	14.12±0.08	1.00	120.4	↓
120	13.75±0.10	0.97	123.5	
150	13.52±0.12	0.95	125.5	
180	13.41±0.13	0.94		

The energy spread of neutrons depends also on the ratio of atomic and molecular ions. The energy of the latter is half of the former; therefore, they produce much less neutrons. According to the problems mentioned above in the cross section meesurements the neutron energy must be specified more definitely then "14 MeV" and it is advisable to determine the spectrum experimentally for the given source-sample arrangement. One should pay special attention to the role of secondary neutrons produced in the target holder or in the surrounding materials if cross sections for low threshold reactions are measured; e.g. (n,γ), (n,n'γ), (n,p), etc. Because of the large amount of structural materials around the target the sealed-tube generetor and the intense D-T sources [16, 75] (see Fig. 8) have serious limitations in the cross section measurements but not in the field of applications. By these equipments, however, the primary neutron spectrum to be expected from a D-T plasma of a few ten keV temperature can be simulated. Liskien [28] has pointed out that the 14.1 MeV line is strongly broadened and hes a width of about 2 MeV if neutrons with at least 5 % of the maximum intensity are included (see Fig. 6).

2. MEASUREMENTS OF NEUTRON FLUX AT THE SAMPLE

The quantity that one should measure for the determination of cross sections by an absolute method is either the flux density or the fluence (the time integral of the flux density). For D-T reactions the neutron flux can be measured to an absolute accuracy of about 1 % using the associated particle method (APM) [29, 30, 31]. By detecting the alphe particles within a well defined recoil solid angle, the neutron flux in the respective interval can be determined and - with a knowledge of the angular distribution - the total yield of the source as well. Figure 7 shows a spectrum obtained by a thin (~5mg/cm^2) CsI(Tl) APM detector [32, 33]. The APM has definite adventage when electronic collimation is needed; in this case alpha particles should be counted in coincidence with the neutron-induced events. The cross section for the $^{27}Al(n,\alpha)^{24}Na$ reaction was measured with an accuracy of 0.7 % by Vonach et al. [34, 35] besed on the APM without coincidence counting.

There are a number of fluence monitors for routine use, e.g. the charged particles emitted by a monitor foil or the induced radioactivity can be converted to fluence if the cross section is known.

The choice of standard reference data has a great importance; at 14 MeV the n-p elastic scattering, the $^{27}Al(n,\alpha)^{24}Na$ and $^{93}Nb(n,2n)^{92m}Nb$ cross sections are widely used. The advantages of $^{93}Nb(n,2n)^{92m}Nb$ reaction are that the excitation function has a flat shape around 14 MeV and the slow neutrons do not contribute to the activity because of the high threshold. The dashed line indicated in the insert part of Fig. 9 was measured in the geometry shown in Fig. 5, while the absolute data were taken from the literature obtained by moderation [36, 37] and activation [38, 39, 40] methods (see Ref. [41]). According to the evaluation of Nethaway [41] the peak cross section in the 14.0 to 14.6 MeV range is 464 mb, with an uncertainty of about 3 %. Our relative measurements show that the change in the cross section of $^{93}Nb(n,2n)^{92m}Nb$ reaction is within ±5 % for the 13.5-14.8 MeV interval. These cross section curves can be accepted as standards in relative measurements or to determine the neutron flux density.

The elastic stattering of fast neutrons renders it possible to measure the neutron fluence at the position of the sample with a high accuracy by detecting the proton recoils using a counter telescope [42, 43].

Fragments from a thin layer of ^{238}U placed in an ionization chamber is a convenient fast neutron monitor. Using a gas flowing chamber with a uranium layer shown in Fig. 5 the fluence observed by the sample can be measured. In the fission chamber 0.2 mg/cm^2 of ^{238}U layer is used to separate the pulses from the background.

The physical bases of the methods mentioned above with many others for the flux density and fluence measurements are discussed in detail in Ref. [44].

3. EXPERIMENTAL TECHNIQUES FOR TOTAL, ELASTIC AND NONELASTIC CROSS SECTION MEASUREMENTS

The total cross sections for 14 MeV neutrons is usually determined by the simple transmission method, which requires to measure only the relative neutron flux with (I) and without (I_o) sample. The sample must completely shadow the detector from the direct beam of neutrons. A typical arrangement is that the distance between the source and detector is about 100-150 cm placing the sample at a half-distance. The transmission is given by

$$T=I/I_o=\exp(-nt\sigma_T)$$

from which we have

$$\sigma_T=\frac{1}{nt}\ln\frac{1}{T} \qquad (3)$$

where n and t are the number of nuclei per cm^3 and the total sample thickness, respectively. The expression for the relative error of σ_T

$$\left|\frac{\Delta\sigma_T}{\sigma_T}\right|=\left|\frac{1}{\ln T}\cdot\frac{\Delta T}{T}\right|$$

shows that the optimum thickness of sample is if T=0,5. It is easy to fulfil this requirement for samples prepared from natural elements but not for separated isotopes. Corrections for in-scattering, background and hardening are discussed in detail by Miller [45].

Dukarevich and Dyumin [46] developed an α-n coincidence technique with a time resolution of 4ns to measure total neutron cross sections using small samples of separated isotopes. The angular width of neutron beam was about 1.5°. The weights of the specimens having different enrichments were a few grammes. Such investigations can yield information on the existence of isotopic, nuclear deformation and shell effects on the total cross sections, which data are of great interest up to now. The use of

oriented nuclear targets to study the effect of deformation (see Ref. [47, 48]) is beyond the possibilities of small laboratories.

The elastic scattering cross section σ_{EL} can be measured by detecting the recoil nucleus or the scattered neutrons. Most of the σ_{EL} data have been determined by measuring the energy spectra of scattered neutrons. To eliminate the contribution from neutrons inelastically scattered through the low-lying states of the nucleus, time-of-flight (TOF) spectrometers are preferred because of their good resolution. Cylindrical, ring and flat plate experimental geometries (see Fig. 10) are the most commonly used for measuring neutron scattering [49]. Recently, the scattered neutrons are detected by an NE-213 liquid scintillator coupled to an XP 1040 photomultiplier tube. The pulse width is about 1-2 ns and the total resolution including pulse width, target, sample and scintillator time spreads and electronic resolution is 2-3 ns for 14 MeV neutrons [50]. A typical arrangement of a TOF spectrometer to measure the elastic and inelastic cross sections is shown in Fig. 11. In addition to the α-n coincidence method, pulsed neutron generators with bunching and time pick-off systems are used. The details of these techniques are presented by Seeliger [51] at this course.

The relation between the differential cross section $\sigma(\theta)$ and the neutron flux scattered by a small sample into the unit solid angle at θ is

$$\sigma(\theta)=\Phi_s r^2 / \Phi_{in} N \qquad (4)$$

where Φ_s, Φ_{in}, r and N are the scattered flux, the incident flux at the sample, the distance between the sample and the detector, and the number of nuclei in the sample, respectively. Since eq.(4) contains only the ratio of the scattered and incident fluxes it is convenient to use the same detector to measure both fluxes. If S, I and B are the counting rates for Φ_s, Φ_{in} and for the background, respectively, eq.(4) becomes

$$\sigma(\theta)=(S-B) r^2/IN \qquad (5)$$

This equation supposes that the detector sensitivity is the same for both the source and the elastically scattered neutrons. However, in general the sensitivity depends on neutron energy; therefore, correction is needed to the ratio (S-B)/I for this effect.

The integrated elastic scattering cross section can be obtained from

$$\sigma_{EL} = 2\pi\int_0^{\pi}\sigma(\theta)\sin\theta \, d\theta \qquad (6)$$

Corrections to the experimental data are discussed in detail by Walt [52] and Kammerdiener [49]. A typical time-of-flight spectrum produced by 14 MeV neutrons in a sulphur sample at $\theta=44,6^{o}$ is shown in Fig. 12. Angular distributions for neutron scattering to the ground state and to the first excited state (2.24 MeV) in ^{32}S measured at 14.1 MeV [53] are presented in Fig. 13.

The nonelastic cross section is defined as $\sigma_T-\sigma_{EL}$, which means that σ_{NE} includes all neutron interactions other than elastic scattering. The components of σ_{NE} are inelastic scattering, capture, reactions and fission. At 14 MeV the main processes are: (n,n'γ), (n,2n), (n,p), (n,d), (n,α) and (n,f). The cross sections for (n,t), (n,^{3}He), (n,γ) and for charged particle emission following inelastic neutron scattering are very low except for light nuclei. The determination of the nonelastic cross section can be performed directly using the sphere transmission method or indirectly either by summing the reaction cross sections or by measuring σ_T and σ_{EL}.
The first measurements with 14 MeV neutrons and threshold activation detectors were made by Gittings et al. [54] using the sphere transmission method. In the fifties several groups [55, 56, 57, 58] have measured the σ_{NE} values at 14 MeV. The principle of the sphere transmission method is very simple: an isotropic point-source of neutrons is surrounded by a thin spherical shell of the absorber, and an ideal isotropic detector - which counts the primary and elastically scattered

neutrons with equal efficiency but insensitive to inelastically scattered neutrons - is placed at a large distance from the sphere. In this case the relation between the transmission and the nonelastic cross section is the following:

$$T=\exp[-\Sigma(r_2-r_1)] \qquad (7)$$

where r_2-r_1 is the thickness of the sphere, $\Sigma=N\sigma_{NE}$ is the macroscopic nonelastic cross section in cm^{-1}. If the thickness of the shell is small, then

$$T=1-N\sigma_{NE}t \text{ and } \sigma_{NE}=\frac{1-T}{Nt} \qquad (8)$$

where $t=r_2-r_1$.

In actual practice the isotropic detector is placed inside the spherical shell to a large distance from the source and the data are analysed using Bethe's method [59, 60]. Corrections for finite thickness of the sample, finite source-detector distance, finite detector size, absorption in the source, nonisotropic detector and source, elastic energy loss, one should consider if σ_{NE} values are determined by the sphere method [61]. These correction factors require the knowledge of additional nuclear data like total and differential elastic scattering cross sections. Recently Chatterjee and Ghose [62] have reported a new technique in which the sphere-transmission data alone are sufficient for the determination of the nonelastic cross sections. It would be worth-while to use this method to complete the σ_{NE} data at 14 MeV.

4. IRRADIATION AND MEASURING ARRANGEMENTS USED FOR THE DETERMINATION OF PARTIAL NONELASTIC CROSS SECTIONS

The techniques used for the determination of reaction cross sections can be divided into three groups, namely activation, accumulation and spectrum methods. The latter is rather difficult because it needs the measurement of the spectrum and angular distribution of emitted particles in a high background. In this case the cross sections are obtained by integration over the secondary neutron spectrum and over the emission angles. Recently a charged-particle magnetic-quadrupole spectrometer has been constructed for H and He to increase the solid angle at large source-to-detector separation and to suppress the background caused by other charged particles [63]. The improvement in the spectrum methods for the emitted charged particles and neutrons has been surveyed by Qaim [64, 65]. The accumulation method is simple because only the emitted particles should be collected. In the case of fission, the fragments are recorded by a track detector, while for (n,α) and (n,p) reactions the accumulated He and H gases can be measured by gas mass spectrometer [66]. The relative emission of ^3He and ^4He is being investigated by Wu et al. [67] at Jülich using a quadrupole mass spectrometer. In the case of (n,t) reactions, the accumulated tritium can be separated by vacuum extraction or oxidization techniques and measured through its beta decay [68, 69]. This method is applicable for other radioactive gaseous products, e.g. the ^{37}A content produced in $^{40}Ca(n,\alpha)$ and $^{39}K(n,t)$ [70] reactions was measured by its soft radiation. The spectrum integration, mass spectrometric, radiochemical separation, accumulation techniques used for the determination of integral cross sections will be discussed in more detail by Qaim, Seeliger and Vonach at this course.

For the determination of total neutron emission cross section σ_{nM}, the absorption methods have some advantages in comparison with the spectrum integration and are used to check the differential data.

By definition

$$\sigma_{nM}=\sigma_{n,n'}+2\sigma_{2n}+3\sigma_{3n}+\sigma_{n\ charged}+\bar{\nu}\sigma_f \qquad (9)$$

includes all processes in which neutrons are emitted weighted

by the number of secondary neutrons. The disappearance cross section σ_D measures those reactions in which a neutron is converted to some other particle.

Neutrons having different energies are slowed down and finally absorbed in the surrounding medium (manganese-bath, boron-bath, liquid scintillator tank [71]). In practice the D-T target is placed in the middle of a large vessel containing aqueous solution of $MnSO_4$. One can determine the number of excess neutrons related to the source neutrons by measuring the flux distributions with and without a spherical sample around an isotropic neutron source, i.e.:

$$\frac{n_e}{n_{14}} = \frac{\int_R^\infty \varphi_{th}^{(normalized)}(r) r^2\, dr - \int_R^\infty \varphi_{th}^{o}(r) r^2\, dr}{\int_R^\infty \varphi_{th}^{o}(r) r^2\, dr} \qquad (10)$$

where R is the radius of the sample. The sample must be thick enough in order to obtain considerable difference in eq. (10), which leads also to a definite depression in the primary flux. This effect can be corrected by normalization measuring the relative fluxes at so large distance from the source, where only the primary neutrons are present. For this aim the activation foil method can be used, while, for the measurement of the integrated fluxes the manganese-bath is advisable: after irradiation the solution is stirred and a definite volume is taken out to measure the activity of ^{56}Mn. Relative measurements are needed only to determine the average activites <A> with and without sample, i.e.:

$$\frac{n_e}{n_{14}} = \frac{\langle A_s^n \rangle - \langle A \rangle}{\langle A \rangle}$$

where $\langle A_s^n \rangle$ is the normalized activity with sample.

 Corrections are needed also for the absorption of slow neutrons by the sample. Using relations given in Refs. [72, 73] we have the following equation for the neutron emission cross section:

$$\sigma_{nM} = \frac{n_e}{n_{14}} \cdot \frac{\sigma_{NE}}{e^{\sigma_{NE} NS} - 1} \qquad (11)$$

where S is the thickness of the sample. If S in small eq. (11) becomes

$$\sigma_{nM} = \frac{n_e}{n_{14}} \cdot \frac{1}{NS} \cdot \qquad (12)$$

Using the water-bath method the $\sigma_{n,2n}$ value for bismuth was determined [72].

Recently the activation technique has been improved [64] by application of separated isotopes as targets, quick radiochemical separations and high-resolution counting systems (Ge(Li), HPGe, Si(Li), etc.). Considerable progress has been made in the knowledge of decay data for the radioactive products from fast neutron reactions. Following the notation of Smith [74] the relation between the reaction cross section, the reaction rate and the detector counts for a sample irradiated with a constant flux of monoenergetic neutrons is given by the formulas:

$$R = F\, N\, G_n \eta_n \sigma \qquad (13)$$

$$C = b\varepsilon G_r \eta_r\, R(1-e^{-\lambda t_E}) \cdot e^{-\lambda(t_w+t)} \qquad (14)$$

where R=reaction rate, F=neutron fluence, N=number of atoms in the sample, G_n=geometric factor for neutron irradiation, η_n=neutron absorption and scattering factor, σ=cross section, C=detector

Table II.

scattering factor, λ=decay constant, t_-=irradiation

Table II.

Limits to the sensitivity of cross section measurements at 14 MeV assuming that gamma-ray activity is measured

Parameter	Limit
Neutron intensity	3-5 % at F~10^{10}n $s^{-1}sr^{-1}$
Sample size	<2×10^{23} atoms
Counting rate	C~1 count/s; 1-3 %
Detector efficiency, $E_\gamma \lesssim 1$ MeV	ε~0.05 for Ge(Li)
Irradiation time	$\lambda t_E < 0.1$, $t_E(max) \sim 10^5$s
Cooling time	$\lambda t_w \ll 1$
Counting time	$t_c \lesssim T_{1/2}$; $Ct_c > 10^3$ for 6~3%
Neutron-energy definition	~100 keV around 14 MeV
Angular-distribution effects	13 %, 0^o to 180^o interval
Secondary-neutron reactions	% depends on the threshold
Absolute fluence	~3 % for APM
Standard cross sections	≳1 % for $^{27}Al(n,\alpha)$
	≳3 % for $^{93}Nb(n,2n)$
	≳5 % for $^{238}U(n,f)$
Calibration of Ge(Li) detector	~2-3 %
Decay data	?, variable
Effect of the geometry	~1 %
Absorption and scattering	<1 %
Total uncertainty using eqs. (13, 14)	≳5-10 %

count rate at time t, b=factor to account for mass yields, decay branching, isotopic abundance, etc., ε=radiation detection efficiency, G_r=geometric factor for measurement, η_r=decay radiation absorption and scattering factor, λ=decay constant, t_E=irradiation time, t_w=cooling time. Smith [74] discussed some details associated with the accurate measurement of cross sections, using the activation method. The effects of various parameters mentioned above were studied. In Table II. the practical limits of each parameters are summarized.

Errors from sample attenuation, neutron flux normalization, nuclear recoil effect, interfering reactions are discussed e.g. in Refs. [15, 26].

The removal cross section is useful for calculating the attenuation of fast primary neutrons in shielding materials and in the samples used for the cross section measurements. The flux of primary neutrons from a point source is

$$\Phi(r) = \frac{Q}{4r^2\pi} \exp\left[-\Sigma(r-r_o)\right]$$

where Σ is the macroscopic removal cross section, Q is the source strength, and $d=r-r_o$ is the total thickness of sample traversed. Typical experimental arrangement used for the measurements of Σ or the relaxation length $1/\Sigma=\lambda$ of primary neutrons is shown in Fig. 14. Using the activation method, the value of ln (activity xr^2) plotted against d results in a straight line with a slope of Σ from which the microscopic cross sections for different geometries can be determined. For iron the slab and cylindrical geometries gave almost identical results [150] and the cross section was found to be 1.42±0.015 b at 14 MeV. Using copper as threshold foil detector and monitor we have determined [76] the removal cross sections for samples indicated in Table III.

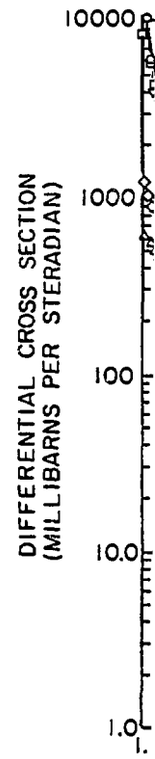

Fig. 4·13

Table III.

Removal cross sections for 14 MeV neutrons

Sample	$\Sigma(cm^{-1})$	λ(cm)	σ(barn)
Graphite ($1.7\ g/cm^3$)	0.0627±0.0027	15.95±0.70	0.74±0.03
Fe (0.3 % C)	0.1214±0.0012	8.24±0.08	1.43±0.02
Pb	0.0850±0.0040	11.76±0.55	2.58±0.12
Al (97% Al) (3% Mg.Si)	0.0651±0.0030	15.36±0.70	1.12±0.06
Paraffin	0.0674±0.0026	14.84±0.60	-

5. PRESENT STATUS OF 14 MeV NEUTRON CROSS SECTION DATA

The majority of the recent fast neutron cross section data has been determined for D-T neutrons in the interval of 13.5-15 MeV and similarly to the earlier measurements, in most cases the activation method was used. Haight [77] has given a review on the neutron data for incident energies between 10 and 40 MeV. A plot of the number of cross section vs. atomic number of the target shows that for differential elastic scattering and neutron emission the data are very scanty in the interval of $55 \leq Z \leq 70$ (see Figs. 15 and 16).

a/ TOTAL NEUTRON CROSS SECTION

Among fast neutron data the total cross sections are the most complete and accurate, so they give reliable information on the average properties of nuclei. The σ_T values measured by different authors are approximately consistent with the given errors. Although there are some exceptions, on average the inconsistency does not exceed 1 %. There are no data at 14 MeV for the following elements: Ru, Rh, Po, At, Rn, Fr, Ra, Ac, Pa and for most of the stable isotopes. The white neutron sources based on cyclotrons, electron linacs and tandem generators have been used in the last decade for the measurements of $\sigma_T(A,E)$ (see Refs. in [77]). Some work on the determination of σ_T for the isotopes of Ti, Ni, Cr, Cu, Zn, Ag, Cd, In, Sn, Sb, Te, Nd, Sm and Gd elements has been done at 14.2 MeV by Oukarevich et al. [78, 79, 80]. They found, in agreement with the prediction of the "black nucleus" formula $\sigma_T = 2\pi(R+\lambda)^2$ that for a given element the cross section increases smoothly with increasing atomic weight of its isotopes.

The $\sigma_T(A)$ data at Z=const. can be approximated by straight lines with an average slope of $\Delta\sigma \approx 2.3 \cdot 10^{-2}\ \Delta A$ barn.

In our earlier investigation [81] it was found that the ratio of $\sigma_T^{exp}/2\pi(R+\lambda)^2$ shows a sinusoidal form as a function of $A^{1/3}$ and can be well described by the following empirical expression (dashed curve in Fig. 17):

$$\frac{\sigma_T^{exp}}{2\pi(R+\lambda)^2} = 1.021 - 0.104 \cos(2.18\ A^{1/3} - 1.25) \qquad (15)$$

where $R = r_o A^{1/3}$, $r_o = 1.4$ fm and $\lambda = 1.22\ (A+1)/A$.

The good fit of this empirical analytical formula to the experimental data for A>27, independent of the fact that the elements are monoisotopic or not, suggests that if any systematic trend in σ_T exists, its magnitude does not exceed a few per cent and so eq. [15] can be used for the calculation of unknown data. This conclusion is supported by the measurements for the isotopic dependence of total cross sections [78] where the relative change of σ_T for $\Delta A = 1$, varies from Ni to Te in the interval of 0.8 to 0.4 %. Expression (15) could be interpreted quantitatively by a semiclassical optical picture (SOM)

[82, 83] with reasonable values of the nuclear radius parameter r_o, potential depth and surface thickness. The general formulae for the total, elastic and nonelastic cross sections are as follows [84]

$$\sigma_T = 2\pi\lambda^2 \sum_{\ell=o}^{\infty}(2\ell+1)\,(1-\mathrm{Re}\,\eta_\ell) \qquad (16)$$

$$\sigma_{EL} = \pi\lambda^2 \sum_{\ell=o}^{\infty}(2\ell+1)\,|1-\eta_\ell|^2 \qquad (17)$$

$$\sigma_{NE} = \pi\lambda^2 \sum_{\ell=o}^{\infty}(2\ell+1)\,(1-|\eta_\ell|^2) \qquad (18)$$

where $\eta_\ell=\exp(i\Delta_\ell)$, Δ_ℓ being the phase shift between the wave traversing the nucleus and that going around. Assuming $\eta_\ell=o$ for $\ell\le\ell_{max}=R/\lambda$ and $\eta_\ell=1$ for $\ell>\ell_{max}$, then we get the black nucleus formulae which can reproduce the data of σ_T, σ_{EL} and σ_{NE} with accuracies of about 10 %, 20 % and 10 %, respectively, at 14 MeV. Let us suppose as a second approximation that $\eta_\ell=\eta=\varsigma\exp(i\delta)$ for $\ell\le\ell_{max}=R/\lambda$ and $\eta_\ell=1$ for $\ell>\ell_{max}$ where $\varsigma=\exp(-\mathrm{Im}\,\Delta)$ and $\delta=\mathrm{Re}\,\Delta$, than we have

$$\sigma_T=2\pi\lambda^2\underbrace{\sum_{\ell=o}^{\ell_{max}}(2\ell+1)}_{(\ell_{max}+1)^2}\underbrace{(1-\mathrm{Re}\,e^{i\Delta})}_{e^{-\mathrm{Im}\Delta}\cos\mathrm{Re}\Delta}=$$

$$=2\pi(R+\lambda)^2(1-e^{-\mathrm{Im}\Delta}\cos\mathrm{Re}\Delta)=$$

$$=2\pi(R+\lambda)^2(1-\varsigma\cos\delta) \qquad (19)$$

$$\sigma_{EL}=\pi(R+\lambda)^2(1+\varsigma^2-2\varsigma\cos\delta) \qquad (20)$$

$$\sigma_{NE}=\pi(R+\lambda)^2(1-\varsigma^2) \qquad (21)$$

For $\varsigma\neq o$, an oscillating term appears in the total cross section, caused only by the elastic scattering process. The phase shift in the optical model formula for σ_T can be determined from the solution of the Schrödinger equation if the potential parameters are known. This formula is accurate but not simple and computer is necessary for the calculations, however, the data for σ_T can be reproduced within their 1-2 % error limits. The nuclear Ramsauer effect used successfully by Peterson [85] for the location of maxima and minima in neutron total cross sections is another way for the determination of the phase shift. Both the phase shift and the phase constant 1.25 in eq. (15) can be explained by assuming that the nucleus has a surface thickness t in which the index of refraction n changes. The physical picture and the meaning of symbols used in this model are given below. The phase shift δ takes the form:

$$\delta=(n2R-2R)/\lambda-2t(n-\bar{n})/\lambda=(n-1)\,2r_oA^{1/3}/\lambda-2t(n-\bar{n})/\lambda=$$
$$=\delta'-r=\mathrm{const.}\,A^{1/3}-r \qquad (22)$$

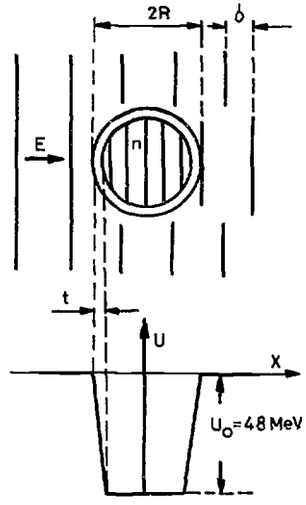

where

$$n=\left(\frac{E_n+U}{E_n}\right)^{1/2}, \quad U=V+iW,$$

and $\bar{n}$ is an average value of the index of refraction within the surface layer.

ENTRY
SUBENT
BIB
INSTITUT
REFERENC

AUTHOR
TITLE

FACILITY
N-SOURCE
SAMPLE

DETECTOR

DECAY-DA
MONITOR
METHOD

CORRECTI

ERR-ANALY

HISTORY
ENDBIB
COMMON
Q-VAL
MEV
-3.195
ENDCOMMON
ENDSUBENT
SUBENT
BIB
REACTION

Fig. 6.2

The good fit of the calculated curve to the experimental data suggests that n is independent of A. The frequency constant in the empirical expression (15) is 2.18 resulting in a value of n=2.015. Taking into account the surface thickness in the nuclear radius, r_o=1.26 fm was found from the σ_T data. Using this r_o, from the observed frequency we get a potential depth of U_o=46 MeV and t=1.6 fm. From the amplitude of the oscillation which is almost constant for medium and heavy nuclei (see Fig. 17) the imaginary part of the optical potential can be determined. The 14 MeV data support the existence of an imaginary potential with strong surface and weak volume absorption. The first term in eq. (22) is proportional to $A^{1/3}$, while r is constant for a given n and t. Expression of the form

$$\sigma_T = 2\pi(R+\lambda)^2[a - p\cos(qA^{1/3} - r)] \qquad (23)$$

is a good approximation to reproduce the mass number and energy dependence of total cross section [83], where a, p, q and r are energy-dependent parameters. Using this simple model the energy dependence of total cross sections can be calculated in the interval of 3-30 MeV. It was found that the calculated and experimental values for Bi are in agreement within a few percent.

b/ ELASTIC SCATTERING CROSS SECTIONS

Most of the elastic scattering cross sections σ_{EL} have been determined by measuring the energy of scattered neutrons. Because of experimental difficulties (poor energy resolution, background, incomplete knowledge of the energy dependence of the neutron detection efficiency), integrated σ_{EL} data were determined from direct measurements only for 26 elements at 14 MeV. Recently using neutron T.O.F system

[86] in Bruyères-le Châtel the angle-integrated elastic and inelastic cross sections, as well as the angular distribution for elastic and inelastic scattering from carbon were measured [50]. The angle-integrated cross sections in the energy range from 8 to 14.5 MeV show significant disagreements with the ENDF/B-III. and-IV. evaluations based on the very scarce data. The new differential elastic cross sections for Be at 14.2 MeV measured in LASL [87] are in good agreement with the ENDF/B-IV. evaluation. A number of σ_{EL} were derived by subtracting the measured nonelastic σ_{NE} from the total cross sections $\sigma_{EL}=\sigma_T-\sigma_{NE}$. In Fig. 18 the 14 MeV σ_{EL} data divided by their "black-nucleus" values are plotted as a function of $A^{1/3}$. The dashed curve shows the result of calculations using the semiclassical model with the same parameter values as determined from the total cross sections (see eq.(20)). Unknown σ_{EL} values for A≥15 may be calculated with the simple analytical expression

$$\sigma_{EL} = \pi(r_o A^{1/3} + \lambda)^2[1.03 - 0.208\cos(2.18\,A^{1/3} - 1.25)] \qquad (24)$$

Eq. (24) is very useful in normalizing angular distributions. The integrated σ_{EL} and differential $\sigma_{EL}(\theta)$ elastic scattering cross sections can be reproduced within a few per cent by the nuclear optical models [88]: however, these models need a number of adjustable parameters depending on energy and/or mass number and the calculations require at least medium-sized computers.

As there are no measurements for the differential elastic scattering cross sections of about 30 % of the elements, while for the remaining nuclei significant deviations are present in the shapes and absolute values of the $\sigma_{EL}(\theta)$ function, any conclusion concerning the potential form and the values of the parameters is rather uncertain. It was shown that the semiclassical model can be used to describe not only total and integrated elastic but also differential

elastic and nonelastic neutron cross sections in a wide range of mass numbers, using the same parameter sets for each nucleus.

The general expression for the differential elastic scattering cross section is

$$\sigma_{EL}(\Theta)=\left|\frac{\lambda}{2i}\sum_{\ell=0}^{\infty}(2\ell+1)(1-\eta_\ell)P_\ell(\cos\Theta)\right|^2. \qquad (25)$$

Applying the same assumptions and notations as before, this gives [89]

$$\sigma_{EL}(\Theta)=\left(\frac{\lambda}{2}\right)^2[a+p^2-2p\cos(qA^{1/3}-r)]\left|\sum_{\ell=0}^{\ell_{max}}(2\ell+1)P_\ell(\cos\Theta)\right|^2. \qquad (26)$$

The mass number dependence of $\sigma_{EL}(\Theta)$ at 14 MeV is:

$$\sigma_{EL}(\Theta)=\left(\frac{\lambda}{2}\right)^2[1.03-0.208\cos(2.18\,A^{1/3}-1.25)]\cdot\left|\sum_{\ell=0}^{\ell_{max}}(2l+1)P(\cos\Theta)\right|^2 \qquad (27)$$

where $\ell_{max}=\frac{r_o(A)\,A^{1/3}}{\lambda}$. Figure 19 show experimental and calculated scattering cross sections for ^{56}Fe, ^{181}Ta and ^{209}Bi. Normalizing constants were not used. The dashed line shows the sum of the shape elastic scattering and a constant background of 10 mb/sr. Using Eq. [27] the forward peaks are fairly well reproduced in a wide range of mass numbers both in form and in absolute values, while there are deviations at some of the remaining peaks especially for the heavy nuclei. It should be noted however, that no free perameters were used in the calculations.

Pearlstein [90] has also given a simple method for the calculation of differential elastic scattering cross sections of 14 MeV neutrons, using a Bessel function expansion as suggested by the diffraction model. The $\sigma_{EL}(\Theta)$ values can be estimated for $12\leq A\leq 238$ mass numbers.

c/ NONELASTIC CROSS SECTIONS

The neutron nonelastic cross section σ_{NE} is equal to that of the $\sigma_T-\sigma_{EL}$. Using a more complete data set for σ_T, σ_{EL} and σ_{NE} at 14 MeV the reduced σ_{NE} values are plotted in Fig. 20 as a function of mass number. It can be seen that there are no data for about half the elements; the existing data, however, show a decrease with increasing mass number A which means that r_o is A-dependent. Since 1970 no new data have been published for σ_{NE}. The nonelastic cross sections can be calculated by the expression [82, 83]

$$\sigma_{NE}=\pi[r_o(A)\cdot A^{1/3}+\lambda]^2(1-\varrho^2) \qquad (28)$$

where at 14 MeV $r_o(A)=1.21+\frac{4.0}{A^{2/3}}-\frac{15}{A^{4/3}}$ fm, and $\varrho=0.104$ from eq. (15).

The energy dependence of σ_{NE} around 14 MeV is smooth and no additional tendency, e.g. isotopic effect can be observed in the data within their relatively high limits of errors.

The semiclassical optical model is capable to describe the σ_T, σ_{EL}, $\sigma_{EL}(\Theta)$ and σ_{NE} data above 10 MeV for $14\leq A\leq 238$ interval. The cross sections are given as closed analytical expressions of the optical parameters; this renders possible both the quick estimates of unmeasured cross sections and the analytical operations [89].

Considering the fact that the total, elastic and nonelastic cross sections at 14 MeV can be well described both by exact or simplified optical models and by empirical expressions with an accuracy of 1-2 %, further accurate measurements are needed first of all for the $\sigma_{EL}(\Theta)$ function for which the agreement is rather poor.

Fig. 8

d/ PARTIAL NONELASTIC CROSS SECTIONS

14 MeV neutrons can give rise to about 1800 reactions on the 290 stable or long half-life isotopes leading to radioactive residual nuclei. In this number the reactions (n,p), (n,α), (n,2n), (n,3n), (n,γ), (n,np), (n,d), (n,nα), (n,^{3}He), (n,t), (n,nt), and (n,n'γ) were taken into account. These reactions give rise to about 600 different radioactive isotopes, i.e. a given isotope on the average can arise from three different interfering reactions. The number of known fission products in $^{238}U(n_{14},f)$ is about 450, from which 363 have a cumulative yield higher than 0.1 %, with half-lives ranging from 10^{-1} to 10^{9} s.

There are a few compilations and surveys of the available 14 MeV neutron reaction and fission cross sections based on recent publications [64 , 73, 91-98] which were used in this review.

In spite of the simplicity of measuring activation cross sections, there are considerable disagreements between published data; therefore, more accurate trends can be revealed from the data measured by the same author because of the higher relative accuracy.

The activation cross sections for (n,2n), (n,p) and (n,α) reactions vs. target proton number Z at 14 MeV are plotted in Figs. 21 a-e, 22 a-e, 23 a-d respectively. The deadline date for the literature survey for points was 1969, while the crosses represent the modern data. In these Figures the target mass numbers and the half-lives (<1y) of the residual nuclei (in parenthesis) are indicated above the experimental points. The numbers shown above the question marks denote the mass numbers of those nuclides for which data are not available. As in most cases the differences between the data relating to the same nuclide considerably exceed the errors given in the references, the error limits are not indicated. As it can be seen the spread is significant in the modern data, too. The main sources of errors are as follows: interfering reactions caused by impurities in the samples; half-life data; abundance of the radiation detected; converting counting into disintegration rate; efficiency of the separation technique; absolute neutron flux and its variation in time; energy and energy spread of neutrons; cross section of monitor reaction; escape of residual nuclei by nuclear recoil or diffusion. A few among these sources can be eliminated oy using the arrangement given in Fig. 5 for irradiation. The fission on depleted ^{238}U layer can serve as flux monitor and standard cross section. Dacay data including decay schemes can be found in Refs. [99-108].

e) (n,n') AND (n,2n) CROSS SECTIONS

The ratios of $\sigma_{n,2n}$ and σ_{NE} values plotted against the target neutron number at 14 MeV show that the (n,2n) cross sections give about 80 % of σ_{NE} above N=60; therefore, by the study of the (n,2n) reaction one can get information on those properties of nuclei which are dominant in nuclear reactions.

According to a recent survey by Bödy [109] (n,2n) cross sections have been measured at 14 MeV for about 30 % of the stable nuclei. The observed N-Z dependence in the (n,2n) cross sections [110] provides a possibility to estimate unknown values for isotopes and elements. On the basis of measured and estimated data, recommended values of (n,2n) cross sections at 14.7 MeV were given for 114 nuclides from experimental data, for 137 nuclides from N-Z systematics and for 71 elements from the averaging of $\sigma_{n,2n}$ over isotopic abundances [111].

In addition to the activation technique a new method based on pulsed sources and a large liquid scintillator to detect neutrons [112] is used for the measurement of $\sigma_{n,2n}$ [113]. Fréhaut et al. [113] obtained higher $\sigma_{n,2n}$ values for

heavy nuclei than those measured by activation method. Using this scintillator-tank method the $\sigma_{n,2n}$ values obtained by Veeser et al. [114] at 14 MeV for a number of nuclides are in good agreement with our recommended values, except for ^{103}Rh. The (n,2n) cross sections for elements have been measured for FRT-structural materials in LASL by spectrometric method [115]. Results at 14.7 MeV are in good agreement with the recommended values [111] except for Ti at which the deviation is about 50 %. There is, however, considerable spread among existing old and new (n,2n) data in the 13 to 15 MeV region determined by the activation method. The discrepancies are attributed to the accepted decay schemes and insufficient energy resolution of the detectors in the past [116].

The plot of (n,2n) cross sections (Figs. 21 a-e) enables the following rough trends to be established: a) In the mass number region 19<A<40 the cross section decreases from 50 mb to 4-5 mb, b) at A~48 it rises rapidly to ~1000 mb and shows a trend of increasing slowly up to a maximum value of ~2000 mb for the heaviest nuclei, c) in the region 48<A<100 strong local fluctuations exist. The trends in (n,2n) reaction cross sections have been investigated by several authors [117] and both isotopic and isotonic as well as odd-even effects have been observed.

Taking into account the differences of σ_{NE} and $\sigma_{n,2n}$ as well as the values of partial cross sections at 14 MeV, for $\sigma_{n,n'}$ in average a few hundred mb can be expected. So, in first approximation for A≥100, $\sigma_{NE} \simeq \sigma_{n,2n'} + \sigma_{n,n'}$, around 14 MeV, i.e. the difference $\sigma_{NE} - \sigma_{n,2n}$ is due to the inelastic scattering and the same trends in opposite direction should appear in $\sigma_{n,n'}$ as in $\sigma_{n,2n}$. Very few data are available for the total inelastic scattering cross sections because the direct measurements by the angle-integrated neutron spectra are difficult. Using the simple activation method a lower limit for $\sigma_{n,n'\gamma}$ process can be given for nuclei that have low-lying isomeric states. According to the few data available, the σ_n^m, values lie in the interval of 100 to 600 mb. As $\sigma_{n'} = \sigma_{n'}^g + \sigma_{n'}^m$, from the calculation of isomeric cross section ratio in the knowledge of $\sigma_{n'}^m$, the value of $\sigma_{n'}^g$, can be estimated. Another way is to measure the neutron emission cross section σ_{nM}. At 14 MeV $\sigma_{n',charged}$ can in most cases be neglected or in some cases can be measured by activation method. Systematic measurements were carried out in Dresden for σ_{nM} [118]. It is assumed that in the case of vibrational even-even nuclei following inelastic scattering, the excited states decay through the 2^+ state, and so by measuring the number of gammas from the $2^+ \to 0^+$ transitions the total inelastic scattering cross section can be determined. Koopman [119] has given the results for $\sigma_{n,n'}(2^+ \to 0^+)$ in comparison with that obtained from $\sigma_{NE} - \Sigma\sigma_{i \neq n,n'}$. The agreements between the data are satisfactory except for ^{110}Cd and ^{116}Cd.

Several semi-empirical and empirical formulae are available for the estimation of $\sigma_{n,2n}$ at 14 MeV [117], among these, the expression given by Pearlstein [120] shows the best approximation [111]. Kumabe [121] calculated (n,2n) cross sections at 14.7 MeV in the region of rare-earths taking into account both statistical and precompound effects. His results show good agreement with Qaim's experimental values [122]. According to our investigations [123] the excitation functions of (n,2n), (n,t), (n,α) and (n,p) reactions can be well described by the Hauser-Feshbach model [124, 125, 126].

The angle-integrated cross section, $\sigma_{\alpha,\alpha'}$, for a reaction α-α' averaged over compound nucleus fluctuations, without width-fluctuation correction, may be written

$$\sigma_{\alpha,\alpha'} = \pi\lambda^2 \sum_{J,\pi} \frac{(2J+1)}{(2\ell+1)(2i+1)} \frac{\sum_{s\ell}^{J} T_{\alpha s\ell} \sum_{s'\ell'}^{J} T_{\alpha' s'\ell'}}{D(J,\pi)} \qquad (29)$$

where I and i are the spin values of the incident particles, J and π are the angular momentum and parity of the com-

pound nucleus, respectively, while the denominator is

$$D(J,\pi)=\sum_{\alpha,s,\ell}\left[\sum_{I'\pi'}\int_{E_d}^{E_m}\rho(E_x,I',\pi')T^J_{\alpha,s,\ell}dE_x+\sum_{E_x=0}^{E_d}T^J_{\alpha,s,\ell}\right]. \quad (30)$$

In eq. (30), the sum from E_x=0 to E_d is over known discrete levels of residual nuclei, and the integral is for continuum states up to the highest excitation energy. The level density parameter a in the back-shifted formula used in this calculation was taken from the literature for (n,n'), (n,α) and (n,p) processes. The actual value of a in the neutron channel has been determined from the fit of the calculated (n,α) excitation function to the experimental data. The value of a_n has been changed only within its limit of error. The fit to the (n,α) reaction is favourable because the transitions to the known levels give the greatest part of the cross section up to 16 MeV, so the inaccuracy in a_α does not cause any considerable error in the determination of the level density parameter a_n for the neutron channel.

Holub et al. [127] calculated the (n,2n) cross sections for 6 MeV excess energy and the excitation functions from threshold to 20 MeV. The influence of the level density parameter and the inverse particle reaction cross sections on the evaporation model was tested. The systematic discrepancies between experimental data and evaporation calculations have led to the conclusion that preequilibrium emission is present in the (n,2n) reaction at high energies, in agreement with the results of Veeser et al. [114].

Most recently Qaim et al. [128] found that at 14.6 MeV neutron energy the strong reaction channels can be well described by the Hauser-Feshbach model, while for the (n,t) and (n,^{3}He) processes the measured cross sections are much higher than the calculated data.

For the analysis of neutron emission spectra from 14 MeV neutron reactions, Pearlstein [129] has used the nuclear model code ALICE, developed by Blann [130] and a global set of input nuclear constants. Over 70 % of the cases the calculated spectra can be fit to within 30 % of experimental values in the range Na to Bi.

f) (n,p) AND (n,α) CROSS SECTIONS

The plot of (n,p) cross sections vs. proton number of the target nucleus (Figs. 22 a-e) shows an increasing trend up to Z~16, from $\sigma_{n,p}\leq$10 mb to ~300 mb. In the region 16≤Z≤24 a broad maximum can be observed, then $\sigma_{n,p}$ gradually decreases to 2-3 mb for the heaviest elements. The $\sigma_{n,\alpha}$ values (Figs. 23 a-d) generally decrease from ~100 mb to ~1 mb from the lightest nuclei to the heaviest elements. Two definite maxima can be seen, one in the region from Na to Cl($\sigma_{n,\alpha}\geq$100 mb), the other in the rare-earth region ($\sigma_{n,\alpha}$ ~100 mb). At N=50 the $\sigma_{n,\alpha}$ data are considerably higher than for the neighbouring nuclides. Gardner and Yu-Wen [131] have given a relationship for the isotopic dependence of $\sigma_{n,\alpha}$.

The (n,p), (n,α) as well as the hydrogen and helium producing cross sections for FRT related structural materials were measured for a number of nuclei during the last years [109, 132-138]. Molla and Qaim [132] have determined the $\sigma_{n,p}$ data at 14.7 MeV for 48 nuclides of 19 elements using the activation method. In the cross sections, from the systematic mesurements and from the evaluation of literature data, they found a strong dependence on (N-Z)/A in the case of medium and heevy nuclei supporting the prediction of an earlier formula given by Levkovskii [139] for the interval 12≤A≤150:

$$\sigma_{n,p}=45.2(A^{1/3}+1)^2\ e^{-33(N-Z)/A}\ \text{mb}. \quad (31)$$

The (N-Z)/A dependence of $\sigma_{n,p}$ and $\sigma_{n,\alpha}$ is confirmed by recent data indicated in Fig. 24[97].

Haight et al. [134, 136, 137] have used a Magnetic Quadrupole Spectrometer (MQS) [140] for the measurement of the spectra of proton and alpha particles from 14 MeV neutron-induced reactions. The agreement between the results obtained at Livermore by MQS and Jülich by activation for ^{48}Ti, ^{58}Ni and ^{65}Cu is satisfactory. Fig. 25 shows a typical angle-averaged proton spectrum from ^{48}Ti.

It was shown by Qaim and Stöcklin [141] that the contribution of (n,np) and (n,nα) reactions to the production of hydrogen and helium at 14 MeV are not negligible. The limited number of data shows, as a gross trend, the (N-Z)/A dependence [64]; however, further measurements are needed to observe any fine structure and to understand the reaction mechanisms.

Reaction mechanisms in fast neutron-induced reactions have been discussed in detail by Cindro [142]. The compound nucleus emission is able to account for the $\sigma_{n,\alpha}$ in the region $20 \leq A \leq 80$, while for the explanation of the alpha emission from heavy nuclei both preequilibrium and direct effects should be taken into account. The fine structure in the angle-integrated alpha spectra was described by dispersion theory [143]. The excitation functions of (n,p) and (n,α) reactions can be satisfactorily described [123] by the Hauser-Feshbach model (see e.g. Figs. 26 and 27). Pearlstein [144] has given an empirical model based on statistical theory to calculate reaction cross section curves for medium mass nuclei. He obtained fair agreement between calculated and measured (n,2n), (n,α) and (n,p) cross sections at 14 MeV.

g) (n,t), (n,^{3}He) AND (n,2p) CROSS SECTIONS

The study of (n,t) and (n,^{3}He) reactions may add to our understanding of the emission of the three-nucleon structures ^3H, ^3He and to obtain important data for the tritium and helium concentration build-up in fission reactors and thermonuclear devices.

The cross sections for (n,t) and (n,^{3}He) reactions at 14 MeV have been recently investigated by the activation and tritium beta counting techniques mainly at Jülich [145], Debrecen [69, 123] and Zagreb [146].

Values of (n,^{3}He) reaction cross sections measured in Zagreb [135] are much higher than those (~1-100μb) obtained in Jülich and Debrecen. Qaim [64] has given the following empirical formula to predict the unknown data for medium and heavy nuclei:

$$\sigma_{n,^3He} = 0.54\,(A^{1/3}+1)^2 \exp\,[-10(N-Z)/A]\,\mu b \qquad (32)$$

The same formula is valid for $\sigma_{n,t}$, but the constant factor is 4.52 instead of 0.54 [64].

The (n,t) cross sections for very light nuclei are relatively large (~100 mb), while for medium and heavy nuclei they lie in the ~10-100μb region. Extensive investigations were carried out for the determination of tritium production rates in the model Li blanket [13, 152], and also for Li isotopes [147].

Qaim and Stöcklin [145] found that a maximum appears in the $\sigma_{n,t}$ values at Z=26, and an (N-Z)/A dependence exits for Z>22. According to our earlier results, a strong decreasing tendency with increasing atomic number can be found in $\sigma_{n,t}$ data, on which deviations arising from individual properties of nuclei are superimposed [69]. The Hauser-Feshbach model calculation can reproduce both the shape and the magnitude of (n,t) excitation functions [123]. As can be seen in Fig. 28 the cross sec-

tion curves change significantly around 14 MeV especially for even nuclei; this may be a reason of the large spread in the literature data. Similarly to Qaim's observation we also found the (N-Z)/A dependence for odd target nuclei, but the $\sigma_{n,t}$ data are higher than for even nuclei by one order of magnitude. For even nuclei the triton energy is less by about 2 MeV than that for odd ones, which may be a reason of the separation of the cross sections in Fig. 29. The formula given by Qaim [64] for the calculation of $\sigma_{n,t}$ values does not contain a term for the odd-even effects.

The study of the (n,2p) reaction can yield information on such properties of nuclear transformation that cannot be obtained with charged particles [146], e.g. on the sub-Coulomb barrier reactions which lead to two holes and one particle in the proton and neutron configurations, respectively. LULIC et al. [148] used a simple model for the calculation of the ratio $R=\sigma(n,2p)/\sigma(n,pn)$. They supposed that R is proportional to the Coulomb barrier penetration factor for protons emitted from the product B of the A(n,p)B reaction, and to a factor which takes into account the level density and the neutron and proton separation energies in the nucleus B. According to this model the R values range from 10^{-3} to 10^{-6}. Our calculations for high threshold reactions show the very strong effect of the Coulomb barrier penetration factor on the cross sections [123]. Taking into account the facts mentioned above and the experimental data for the (n,pn) cross sections, only a few microbarns can be expected for the (n,2p) reactions instead of the (10-50) μb value given by LULIC et al.[148]. Our present value for the (n,2p) cross section for ^{141}Pr is in agreement with the theoretical expectation [149]. Further measurements are needed, however, to clear up the systematics in the data.

h) (n,γ) CROSS SECTIONS

For the determination of (n,γ) cross sections at 14 MeV two methods are used: the activation technique σ_{act} and measurements of prompt gamma-ray spectra σ_{int}. The σ_{act} values from earlier measurements were higher by a factor of ten than σ_{int}, because of the presence of scattered neutrons. The measurements for σ_{act} have been repeated with improved methods, eliminating the effects of secondary neutrons, and good agreement was found between σ_{act} and σ_{int}. Results indicated in Fig. 30 [150] show that $\sigma_{n,\gamma}$ is ~1 mb in a wide range of mass number, and that data are scanty especially for light nuclei. The A-dependence of the cross section is in qualitative agreement with the expectation of the direct-semidirect model [150]. The magnitude of the γ-ray cascade through unbound levels could be determined from the difference of $\sigma_{act} - \sigma_{int}$, which requires further precise activation (n,γ) measurements. Most recently Budnar et al. [151] measured prompt γ-ray spectra and integrated cross sections of the radiative capture of 14.6 MeV neutrons for 28 elements using a telescopic scintillation pair spectrometer. The integrated cross sections have a saturation value of about 1 mb at A~60. Additional measurements should be performed to clarify the effect of closed neutron shells.

i) (n,xγ) CROSS SECTIONS

During the last years there have been measurements at 14 MeV for neutron-induced gamma-ray production cross sections and spectra. In such experiments pulsed beam end T.O.F methods are used and the time spectrum of gammas is detected by plastic or NaI(Tl) scintillators. Gamma-ray production cross sections were measured at 14.2 MeV by Drake et al. [153] for 20 samples ranging from Be to Pu, including elements that are of interest for CTR programs. Cox et al. [154, 155] have

measured the gamma-rays associated with scattering of 14 MeV neutrons in extended samples of possible fusion reactor materials. Fig. 31 shows a typical example for the shape of a spectrum measured for ^{27}Al [77]. The discrepancies in the results indicate the difficulties of such measurements. It would be important to obtain data for standard $\sigma_{n,x\gamma}$ values and spectrum at 14 MeV neutron energy.

j) FISSION BY 14 MEV NEUTRONS

Fast neutron fission cross sections for ^{233}U, ^{235}U, ^{238}U and ^{239}Pu have been reviewed in detail by Poenitz and Guenther [156], and Lapenas [96]. The deviations in $\sigma_{n,f}$ values measured by different authors around 14 MeV are related to the energy dependence of the fission cross section near the (n,2nf) threshold as the bombarding energy is not always well defined. At 14 MeV the change in $\sigma_{n,f}$ is especially marked for ^{235}U, while for ^{239}Pu it is negligible.

Most recently Cance and Grenier [157] measured the absolute neutron fission cross sections of ^{235}U and ^{239}Pu around 14 MeV. In disagreement with earlier observations no significant energy dependence was found for ^{235}U in the interval 13.9 to 14.6 MeV and the results for ^{239}Pu are 12 % lower than the old data. Further measurements are needed around 14 MeV with good energy resolution to solve these questions.

As for the fission yields at 14 MeV, data for $^{234,236}U$ and ^{240}Pu are incomplete and it is necessary to extend the measurements over the ^{231}Pa, $^{236,237}Np$ and $^{242,244}Pu$ isotopes. More accurate data are needed for the wings and valleys of the mass distributions.

In order to study the fine structures, the present 5-10 % errors in the determination of yields in the peaks should be reduced as low as 2-3 %. In the case of independent yields the data are not sufficient even for ^{232}Th, $^{233,235,238}U$ and ^{239}Pu, which makes the conclusion on the charge distribution, polarization and dispersion, as well as on odd-even effects rather uncertain at 14 MeV [158]. The present status of fission yield data has been surveyed by Cuninghame [159].

For the determination of mass distribution of fission products, in addition to the earlier radiochemical and mass spectrometric methods, nowadays the on-line isotope separation technique and the gamma-spectrometric method [160] are applied at 14 MeV. The determination of both independent and cumulative yields using Ge(Li) detectors is more accurate because the method is fast and several gamma lines can be used for the identification of fragments for the same isotope [161].

According to a present investigation of Daróczy [161, 165, 166] the main advantages of the Ge(Li) technique are as follows: mass yields ≥0.5 % can be determined, i.e. in the $82 \leq A \leq 152$ region for fast neutron-induced fission; among these about 40-50 cumulative yields can be evaluated on the bases of the known nuclear data; the accuracy is about 1-3 % for fragments having a few γ-lines with intensities higher than 10 % (e.g. ^{132}Te, ^{140}Ba), and so they can be used as standards in relative measurements; the method is also applicable for fragments having short half lives; the necessary equipments are available even for small laboratories to study the nuclear fission.

The angular distribution of fission fragments can yield information on the states at the saddle point. It is expected by theory that the anisotropy parameter $R=W(0^o)/W(90^o)$ has maxima at the (n,f), (n,n'f) and (n,2nf) thresholds. The existence of the maximum at the (n,2nf) threshold could not be settled as yet because of the great spread and error in the experimental data around 14 MeV. The solid state track detector technique is a very simple method to measure the angular distributions for all fragments [162, 163, 164]. and also for the determination of fission cross sections. The difficult

microscopy work can be eliminated by the application of the jumping spark counter [167] for scanning. Schematic drawing of such an experimental arrangement for irradiation is shown in Fig. 32 [163].

ACKNOWLEDGEMENTS

The author is indebted to Dr. Z.T.Bődy and Mr. I.Szalóky for their willing assistance in a part of the compilation of data.

REFERENCES

[1] DICKSON, H., ROBERTS, E. Jr., BUTLER, Hal M., CLOUTIER, R.J., SMITHWICK, G., WATSDN, E.E., HAYWOOD, F.F., BERGER, J.D., The Use of Small Accelerators Proc. Conf. Oak Ridge, (1970), Rep. CONF-700322, p. 441.
[2] BARSCHALL, H.H., KANNER, M.H., Phys. Rev. 58 (1940) 590.
[3] BARSCHALL, H.H., LADENBURG, R., VAN VOORHIS, C.C., Phys. Rev. 59 (1941) 917.
[4] BARSCHALL, H.H., LADENBURG, R., Phys. Rev. 61 (1942) 129.
[5] BARSCHALL, H.H., Physics Today. 22 (1969) No. 8. p. 54.
[6] BARSCHALL, H.H., TASCHEK, R.F., Phys. Rev. 75 (1949) 1819.
[7] COON, J.H., TASCHEK, R.F., Phys. Rev. 76 (1949) 710.
[8] COON, J.H., BOCKELMAN, C.K., BARSCHALL, H.H., Phys. Rev. 81 (1951) 33.
[9] COON, J.H., GRAVES, E.R., BARSCHALL, H.H., Phys. Rev. 88 (1952) 562.
[10] MUIR, D.W., WRENDA 79/8D, INDC SEC-73/URSF, IAEA, Vienna (1979).
[11] STEINER, D., Nucl. Sci. Eng. 58 (1975) 107.
[12] STEINER, D., TOBIAS, M., Nuclear Fusion 14 (1974) 153.
[13] QAIM, S.M., WÖLFLE, R., STÖCKLIN, G., J. of Radioanal. Chem. 30 (1976) 35.
[14] IAEA Advisory Group Meeting on Nuclear Data for Fusion Reactor Technology, Vienna, 11-15 December 1978, INDC(NDS)-101/LF (1979).
[15] NARGOLWALLA, S.S., PRZYBYLOWICZ, E.P., Activation Analysis with Neutron Generators, Wiley, New York (1973).
[16] BARSCHALL, H.H., 14 MeV d,t Sources, UWFDM-331, Univ. of Wisconsin (1979).
[17] CSIKAI, J., Atomic Energy Review 11 (1973) 415.
[18] SHOPE, L.A., Sandia Corp. Report SC-TM-66-247 (1966).
[19] Nucleonics 23 4 (1965) 60 J.
[20] SMITH, D.L.E., Accelerator Targets Designed for the Production of Neutrons, Rep. EUR-3895 d-f-e (1968) 5.
[21] GRAVES, E.R., RADRIGUES, A.A., GOLDBLATT M., MEYER, D.I., Rev. Sci. Instrum. 20 (1949) 579.
[22] BOOTH, R., GOLDBERG, E., BARSCHALL, H.H., Br. J. Radiol. 47 (1974) 737.
[23] KELSEY, C.A., SPALEK, G.C., DELUCA, P.M., CHENEVERT, G.M., McCULLOUGH, E.C., NICKLES, R.J., Proc. Symp. Neutron Dosimetry in Biology and Medicine, Neuherberg/München (1972) 818.
[24] HILLIER, M., LOMER, P.D., STARK, D.S., WOOD, J.D.L.H., Accelerator Targets, Designed for the Production of Neutrons, Rep. EUR-3895 d-f-e (1968) 125.
[25] PAULSEN, A., LISKIEN, H., Rep. EANDC E-144 "L" CBNM (1972); Rep. EANDC E-143 "L" CBNM (1971). Nuclear Data Tables 11 (1973) 569.
[26] CSIKAI, J., BUCZKÓ, M., BŐDY, Z., DEMÉNY, A., Atomic Energy Review 7 (1969) 93.
[27] RAICS, P., Thesis, Kossuth University Debrecen (1978).
[28] LISKIEN, H., Advisory Group Meeting on Nuclear Data for Fusion Reactor Technology, Vienna 11 to 15 December (1978) IAEA-TECDOC-223, p. 185.
[29] BARSCHALL, H.H., RDSEN, L., TASCHEK, R.F., Rev. Mod. Phys. 24 (1952) 1.
[30] BENVENISTE, J., ZENGER, J., Rep. UCRL-4266 (1954).
[31] LARSSON, K.E., Ark. Fysik 7 1954 323; 9 (1955) 293; 603.
[32] HREHUSS, G., BORBÉLY, I., Nucl. Instrum. Methods 34 (1965) 37.
[33] NAGY, S., Thesis, University of Debrecen (1970).

[34] VONACH, H., HILLE, M., STENGL, G., BREUNLICH, W., WERNER, E., Z. Physik 237 (1970) 155.
[35] MANNHART, W., VONACH, H., Z. Physik A272 (1975) 279.
[36] VEESER, L.R., ARTHUR, E.D., YOUNG, P.G., Phys. Rev. C16 (1977) 1792.
[37] FREHAUT, J., MOSINSKI, G., Nuclear Cross Sections and Technology, NBS Washington (1975) 855.
[38] PRESTWOOD, R.J., BAYHURST, B.P., Phys. Rev. 121 (1961) 1438.
[39] PAULSEN, A., WIOERA, R., Z. Physik 238 (1970) 23.
[40] NETHAWAY, O.R., J. Inorg. Nucl. Chem. 40 (1978) 1285.
[41] NETHAWAY, O.R., Preprint UCRL-80097, LLL (1977).
[42] JOHNSON, C.H., Recoil telescope detectors, Fast Neutron Physics, Interscience, New York (1960) p. 247.
[43] BARTON, O.M., DIVEN, B.C., HANSEN, G.E., JARVIS, G.A., KOONTZ, P.G., SMITH, R.K., Nucl. Sci. Eng. 60 (1976) 369.
[44] MARION, J.B., FOWLER, J.L., Fast Neutron Physics, Part I., Interscience, New York (1960).
[45] MILLER, Oan W., in Fast Neutron Physics, Part II., I Interscience, New York (1960) 985.
[46] DUKAREVICH, Yu. V., OYUMIN, A.N., Pribory i tekhnika experimenta, No.5 (1961) 34.
[47] MARSHAK, H., RICHAROSON, A.C.B., TAMURA, T., Phys. Rev. 150 (1966) 996.
[48] MARSHAK, A., LANGSFORD A., TAMURA, T., WONG, C.Y., Phys. Rev. C2 (1970) 1862.
[49] KAMMERDIENER, J.L., UCRL-51232, LLL (1972).
[50] HAOUAT, G., LACHKAR, J., SIGAUD, J., PATIN, Y., COCU, F., Nucl. Sci. Eng. 65 (1978) 331.
[51] SEELIGER, D., Course of Nuclear Theory for Applications, Trieste, ICTP (1980), these Proceedings.
[52] WALT, M., in Fast Neutron Physics, Part II., Interscience, New York (1960) 1033.
[53] CLARKE, R.L., CROSS, W.G., Nucl. Phys. 53 (1964) 177.
[54] GITTINGS, H.T., BARSCHALL, H.H., EVERHART, G.G., Phys. Rev. 75 (1949) 1610.
[55] TAYLOR, H.L., LONSJO, O., BONNER, T.W., Phys. Rev. 100 (1955) 174.
[56] FLEROV, N.N., TALYZIN, V.N. Soviet J. At. Energy 4 (1956) 617.
[57] MacGREGOR, M.H., BALL, W.P., BOOTH, R., Phys. Rev. 108 (1957) 726.
[58] BALL, W.P., MacGREGOR, M.H., BOOTH, R., Phys. Rev. 110 (1958) 1392.
[59] BETHE, H.A., Los Alamos Laboratory Report No LA-1428 (1952)
[60] BETHE, H.A., BEYSTER, J.R., CARTER, R.E., J. Nucl. Energy 3 (1956) 207.
[61] ALLEN, R.C., CARTER, R.E., TAYLOR, H.L., in Fast Neutron Physics, Part II., Interscience, New York (1963) 1429.
[62] CHATTERJEE, A., GHOSE, A.M., Phys. Rev. 161 (1967) 1181.
[63] GRIMES, S.M., HAIGHT, R.C., ANDERSON, J.O., Nucl. Sci. Eng. 62 (1977) 187.
[64] QAIM, S.M., in Proc. Int. Conf. on Neutron Physics and Nuclear Data for Reactors and other Applied Purposes, Harwell, U.K., 25 to 29 Sept. 1978.
[65] QAIM, S.M., Nucl. Cross Sections and Technology, Vol. II. NBS-SP 425, p. 664 (1975).
[66] FARRAR, IV.H., KNEFF, D.W., BRITTEN, R.A., HEINRICH, R.R., BNL-NCS-50681, p. 175 (1977).
[67] WU, C.H., WÖLFLE, R., QAIM, S.M., Nucl. Phys. A329 (1979) 63.
[68] QAIM, S.M., WÖLFLE, R., STÖCKLIN, G., J.Inorg. Nucl. Chem. 36 (1974) 3639.
[69] BIRÓ, T., SUDÁR, S., MILIGY, Z., DEZSŐ, Z., CSIKAI, J., J.Inorg. Nucl. Chem. 37 (1975) 1583.
[70] QAIM, S.M., RUSHEEO, A., STÖCKLIN, G., WÖLFLE, R., Int. J. appl. Radiat. Isotopes 28 (1977) 585.
[71] BECKURTS, K.H., WIRTZ, K., Neutron Physics, Springer-Verlag, Berlin (1964).
[72] FEICHT, E., VONACH, H., Nukleonik 10 (1967) 58.
[73] HEUSCH, C.A., Nukleonik 2 (1960) 228.
[74] SMITH, D.L., ANL/NDM-23, (1976).

[75] SCHMIDT, K.A., DOHRMAN, H., Atomkernenergie 27 (1976) 158.
[76] CSIKAI, J., BOUFRAQUECH, A., to be published
[77] HAIGHT, R.C., Review of Neutron Data: 10 to 40 MeV, Preprint UCRL-79453, LLL (1977).
[78] DURAKEVICH, Yu.V., DYUMIN, A.N., KAMINKER, D.M., Nucl. Phys. A92 (1967) 433.
[79] DYUMIN, A.N., KAMINKER, D.M., POPOVA, G.N., SMOLIN, V.A., Izv. Akad. Nauk SSSR., Ser. Fiz., 36 (1972) 852.
[80] DYUMIN, A.N., EGOROV, A.I., POPOVA, G.N., SMOLIN, V.A., Acad. of Sci. USSR, Leningrad Nuclear Physics Institute, N14 (1973).
[81] ANGELI, I., CSIKAI, J., NAGY, J.L., SCHARBERT, T., SZTARICSKAI, T., Acta Phys. Hung. 30 (1971) 115.
[82] ANGELI, I., CSIKAI, J., Nucl. Phys. A158 (1970) 389.
[83] ANGELI, I., CSIKAI, J., Nucl. Phys. A170 (1971) 577.
[84] BETHE, H.A., MORRISON, P., Elementary nuclear theory Wiley, New York, (1956) p. 177.
[85] PETERSON, J.M., Phys. Rev. 125 (1962) 955
[86] LACHKAR, J.C., McELLISTREM, M.T., HAOUAT, G., PATIN, Y., SIGAUD, J., COCU, F., Phys. Rev. C14 (1976) 933.
[87] ORAKE, D.M., AUCHAMPAUGH, G.F., ARTHUR, E.D., RAGAN, C.E., YOUNG, P.G., Nucl. Sci. Eng. 63 (1977) 401.
[88] HODGSON, P.E., Ann, Rev. Nucl. Sci. 17 (1967) 1.
[89] ANGELI, I., CSIKAI, J., NAGY, P., Nucl. Sci. Eng. 55 (1974) 418.
[90] PEARLSTEIN, S., Nucl. Sci. Eng. 49 (1972) 162.
[91] TSUKADA, K., JAERI 1252 (1977)
[92] QAIM, S.M., Handbook of Spectroscopy, Vol III, CRC (to be published).
[93] Fission Product Nuclear Data FPND - 1977, Vol I. IAEA-213 (1978).
[94] NESTEROV, B.V., Yadernye Konstanty 27 (1977) 45.
[95] IGARASI, S., KANDA, Y., MATSUNOBU, H., MURATA, T., OHSAWA, T., KIKUCHI, Y., JAERI-memo 6315 (1975).
[96] LAPENAS, A.A., Izmerenye spektrov neytronov aktivationnym metodom, Izdatelstvo Z natne, Riga (1975).
[97] QAIM, S.M., STÖCKLIN, G., Proc. Neutron Data of Structural Materials for Fast Reactors, Geel, Belgium 5-8 Dec. (1977).
[98] Progress in Fission Product Nuclear Data, Ed. by G. LAMMER, INDC (NDS)-95/G+P, (1978); INDC (NDS)-86/G+P (1977).
[99] LEDERER, C.M., SHIRLEY, V.S., editors, Table of isotopes, (seventh ed., J.Wiley , N.Y, 1978).
[100] Current numbers of the journal Nuclear Data Sheets (Acad.Press. N.Y, London)
[101] BLACHOT, J., FICHE, C., Gamma-ray and half-life data for the fission products, At. Data Nucl. Data Tables 20 (1977) 241; CEA-Report (1979).
[102] GUSEV, N.G., DMITRIEV, P.P., Kvantovoe izluchenie radioaktivnykh nuklidov Moskva, Atomizdat, (1977).
[103] MARTIN, M.J., Nuclear decay data for selected radionuclides, ORNL-5114 (1976)
[104] BOWMAN, W.W., MacMURDO, K.W., Radioactive-decay gammas, At. Data Nucl. Data Tables 13 (1974) 13.
[105] ERDTMANN, G., SOYKA, W., Die γ-linien der Radionuclide, Jül-1003-AC Kernforschungsanlage, Jülich, (1973).
[106] DYER, F.F., BATE, ..C., DECAYGAM: Radioactive decay gamma-ray spectra compilation, RSIC Data Library Collection, DLC-19 ORNL (1973).
[107] GUNNINK, R., NIDAY, J.B., ANDERSON, R.P., MEYER, R.A., Gamma-ray energies and intensities, UCID 15439 LRL, Univ. of Col, Livermore (1969).
[108] KOLOBASHKIN, V.M., RUBTSOV, P.M., ALEKSANKIN, V.G., RUZHANSKII, P.A., Beta-izluchenie iroduktov deleniya, Sirovochnik, Moskva, Atomizdat, (1978).
[109] BÖDY, Z.T., private communication.
[110] CSIKAI, J., PETŐ, G., Phys. Lett. 20 (1966) 52.
[111] BÖDY, Z.T., CSIKAI, J., Atom. Energy Rev. 11 (1973) 153.
[112] FREHAUT, J., Nucl. Instr. Methods 135 (1976) 511.

[113] FREHAUT, J., HOLUB, E., CALES, M., MOSINSKI, G., CEA-N-1998 [135] GRIMES, S.M., private communication.

[113] FREHAUT, J., HOLUB, E., CAMES, M., MOSINSKI, G., CEA-N-1998 (1977).
[114] VEESER, L.R., ARTHUR, E.D., YOUNG, P.G., Phys. Rev. 16 (1977) 1792.
[115] AUCHAMPAUGH, G.F., DRAKE, D.M., VEESER, L.R., BNL-NCS-50681 (1977).
[116] PAULSEN, A., LISKIEN, H., WIDERA, R., Atomkernenergie 26 (1975) 34.
[117] CHATTERJEE, S., CHATTERJEE, A., Nucl. Phys. A125 (1969) 593.
[118] HERMSDORF, D., MEISTER, A., SASSONOFF, S., SEELIGER, D., SEIDEL, K., SHAHIN, F., ZfK-277 U, Rossendorf (1975).
[119] KOOPMAN, R.P., thesis, University of California at San ... (1977).
[120] PEARLSTEIN, S., Nucl.Sci.Eng. 23 (1965) 238.
[121] KUMABE, I., J. Nucl.Sci.Techn. 14 (1977) 460.
[122] QAIM, S.M., Nucl. Phys. A224 (1974) 319.
[123] CUDÁR, S., CSIKAI, J., Proc. Int. Conf. on Neutron Physics and Nuclear Data for Reactor and other Applied Purposes, Harwell 25 to 29 Sept. p. 128. (1978). Nucl.Phys. A319 (1979) 157.
[124] HAUSER, W., FESHBACH, M., Phys. Rev. 87 (1952) 366.
[125] VOGT, E., The statistical theory of nuclear reactions, Advances in Nucl.Phys. 1 (1968) 261.
[126] FU, C.Y., Atomic Data and Nuclear Data Tables 17 (1976) 128.
[127] HOLUB, E., CINDRO, N., BERSILLON, O., JARY, J., Z. Physik A289 (1979) 421.
[128] QAIM, S.M., KLAPDOR, H.V., REISS, H., to be published.
[129] PEARLSTEIN, S., BNL-NCS-24066 (1978).
[130] BLANN, M., Annual Rev. of Nucl. Sci. 25 (1975) 123.
[131] GARDNER, D., YU-WEN, Yu., Nucl.Phys. 60 (1974) 49.
[132] MOLLA, N.I., QAIM, S.M., Nucl. Phys. A283 (1977) 269.
[133] HAIGHT, R.C., GRIMES, S.M., ANDERSON, J.D., Nucl.Sci.Eng. 63 (1977) 200.
[134] GRIMES, S.M., HAIGHT, R.C., ANDERSON, J.D., Phys. Rev. C17 (1978) 408.
[135] GRIMES, S.M., private communication.
[136] HAIGHT, R.C., GRIMES, S.M., Preprint UCRL-80235 (1977).
[137] GRIMES, S.M., HAIGHT, R.C., ANDERSON, J.D., ALVAR, K.R., BORCHERS, R.R., Preprint UCRL-79454 (1977).
[138] SAILER, K., DARÓCZY, S., RAICS, P., NAGY, S., Neytronnaya Fizika I. 246. Kiev (1977).
[139] LEVKOVSKI, V.N., JETP. 45 (1963) 305 .
[140] ALVAR, K.R., BARSCHALL, H.H., BORCHERS, R.R., GRIMES, S.M., HAIGHT, R.C., Nucl.Instr. Methods 148 (1978) 303.
[141] QAIM, S.M., STÖCKLIN, G., Proc. 8th Symp. Fusion Technology, Noordwijkerhout, June 1974, EUR 5182e, p. 939 (1974).
[142] CINDRO, N., Acta Phys. Slovaca 25 (1975) 158.
[143] GLOWACKA, L., JASKOLA, M., TURKIEWICZ, J., ZEMO, L., KOZLOWSKI, M., OSAKIEWICZ, W., Nucl. Phys. A244 (1975) 117; ibid A262 (1976) 205.
[144] PEARLSTEIN, S., J. of Nucl. Energy 27 (1973) 81.
[145] QAIM, S.M., STÖCKLIN, G., Nucl. Phys. A257 (1976) 233.
[146] DIKSIC, M., STROHAL, P., SLAUS, I., J. inorg.nucl.Chem. 36 (1974) 477.
[147] EXFOR MASTER-FILE INDEX, IAEA Vienna .
[148] LULIC, S., STROHAL, P., SLAUS, I., Nucl. Phys. A154, (1970) 273.
[149] CSIKAI, J., CHOUAK, A.K., Radiochimica Acta, 26 (1979) 135.
[150] BERGQVIST, I., POTOKAR, M., LUNDFD6/ NFFR-3023 /1-19
[151] BUDNAR, M., CVELBAR, F., HODGSON, E., HUDOKLIN, A., IVKOVIC, V., LIKAR, A., MIHAILOVIC, M.V., MARTINCIC, R., NAJZER, M., PERDAN, A., POTOKAR, M., RAMSAK, V., INDC YUG-6/L, IAEA, Vienna 1979 .
[152] FRITSCHER, U., KAPPLER, F., RUSCH, D., Nucl.Instr. Methods 153 1978 563.
[153] DRAKE, D.M., ARTHUR, E.D., SILBERT, M.G., Nucl. Sci. Eng. 65 1978 49.
[154] COX, A.J., POURMANSOORI, M., Int. J. of Appl. Rad. and Isotopes 28 1977 235.

[155] CONNEL, K.A., COX, A.J., Int. J. of Appl. Rad. and Isotopes, 20 1975 71.
[156] POENITZ, W.P., GUENTHER, P.T., Proc. NEANDC/NEARCRP Specialist Meeting on Fast Fission Cross Sections, ANL-76-90. 1976 .
[157] CANCE, M., GRENIER, G., Nucl. Sci.Eng. 68 1978 197.
[158] DARÓCZY, S., private communication.
[159] CUNINGHAME, J.G., FPND in 1977, AERE-R 8753.
[160] DARÓCZY, S., GERMÁN, E., RAICS, P., NAGY, S., CSIKAI, J., Soviet National Conf. on Neutron Physics, Kiev, 3 1973 323.
[161] DARÓCZY, S., CSc. Thesis, Debrecen, 1979 .
[162] CSIKAI, J., NAGY, S., J. Nucl. Energy 21 1967 375.
[163] ABEGG, R., WAGNER, R., Phys.Rev. C15 1977 1171.
[164] BARUTCUGIL, E., JUHÁSZ, S., VÁRNAGY, M., NAGY, S., CSIKAI, J., Nucl. Phys. A173 1971 571.
[165] DARÓCZY, S., RAICS, P., NAGY, S., ATOMKI Közl. 18 317 1976 Proc.Symp. Fast Neutron Interactions and the Problems of High Current Neutron Generators, 27-30 Aug. 1975, Debrecen
[166] DARÓCZY, S., NAGY, S., RAICS, P., HAMVAS, I., Proc. 7th Int. Symp. on the Interaction of Fast Neutrons with Nuclei, 147. 21-25 Nov. 1977, Gaussig, GDR; ZfK-376,1978 .
[167] VÁRNAGY, M., VASVÁRY, L., GYARMATI, E., JUHÁSZ, S., SCHARBERT, T., SZTARICSKAI, T., Nucl. Instr. and Meth. 141 1977 489.

LEGEND FOR FIGURES

Fig. 1. Cross section of the $^{3}H(d,n)^{4}He$ reaction and the total neutron yield as a function of deuteron energy.
Fig. 2. Total neutron yields for various target compositions.
Fig. 3. The energy and energy spread of neutrons versus angle for D-T reaction.
Fig. 4. Energy spectra of neutrons for five different angles at E_d=175 keV.
Fig. 5. Scattering-free arrangement for irradiation around 14 MeV.
Fig. 6. Energy spectra of neutrons from a D-T plasma of temperature T=10, 20 and 30 keV.
Fig. 7. Charged particle spectrum in an APM system.
Fig. 8. Scheme of an intense neutron generator based on mixed beam of T and D (see Ref.[75]).
Fig. 9. Excitation function for the $^{93}Nb(n,2n)^{92m}Nb$ reaction.
Fig.10. Experimental geometries for measuring neutron scattering.
Fig.11. Scheme of the arrangement of a TOF spectrometer.
Fig.12. The TOF spectrum for sulphur measured at 14.1 MeV.
Fig.13. The differential cross sections for elastic and inelastic scattering of neutrons from S.
Fig.14. Geometrical arrangement for the measurements of removal cross sections.
Fig.15. Number of data points vs. atomic number for σ_T, $\sigma_{EL}(\theta)$ and σ_{nM} for E_n between 10 and 40 MeV.
Fig.16. Number of data points vs. atomic number for H and He producing reactions, and all other partial non-elastic reactions.
Fig.17. 14 MeV neutron total cross sections.
Fig.18. 14 MeV integrated elastic scattering cross sections.
Fig.19. Experimental and calculated (dashed curve) differential elastic scattering cross sections.
Fig.20. 14 MeV nonelastic cross sections.
Fig.21. a-e. Activation cross sections for (n,2n) reactions at 14 MeV.
Fig. 22. a-e. Activation cross sections for (n,p) reactions at 14 MeV.
Fig. 23. a-d. Activation cross sections for (n,α) reactions at 14 MeV.

Fig. 24. Dependence of (n,2n), (n,p) and (n,α) cross sections on asymmetry parameter [97].

Fig. 25. Angle-averaged proton spectrum from ^{48}Ti measured with MQS [136] at 15 MeV.

Fig. 26. Hauser-Feshbach model calculation for $^{27}Al(n,\alpha)$ reaction (points are from experiments).

Fig. 27. Measured and calculated excitation functions for $^{27}Al(n,p)$ reaction.

Fig. 28. Measured and calculated excitation functions for (n,t) reactions.

Fig. 29. Dependence of $\sigma_{n,t}$ on (N-Z)/A (full points for even nuclei, open circles for odd target nuclei).

Fig. 30. 14 MeV corrected σ_{act} and σ_{int} (n,γ) cross sections [150].

Fig. 31. $\sigma_{n,x\gamma}$ values as a function of E_γ for ^{27}Al near 14 MeV [77].

Fig. 32. Experimental arrangement for the measurement of angular distributions of fragments.

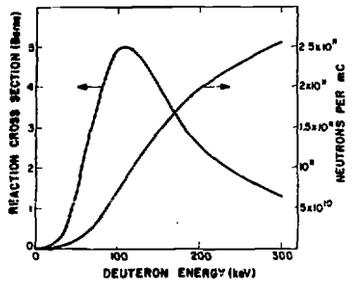

Fig. 1. Cross section of the $^{3}H(d,n)^{4}He$ reaction and the total neutron yield as a function of deuteron energy

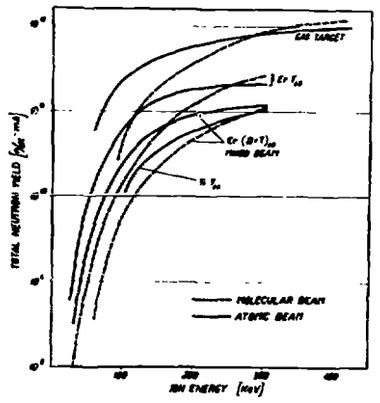

Fig. 2. Total neutron yields for various target compositions

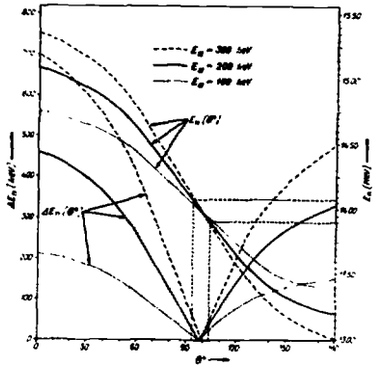

Fig. 3. The energy and energy spread of neutrons versus angle for D-T reaction

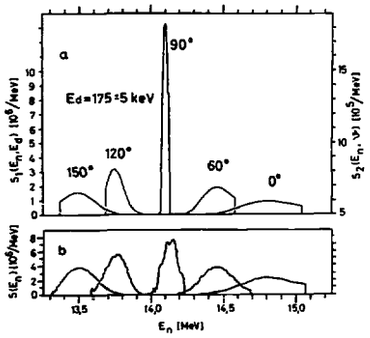

Fig. 4. Energy spectra of neutrons for five different angles at E_d=175 keV

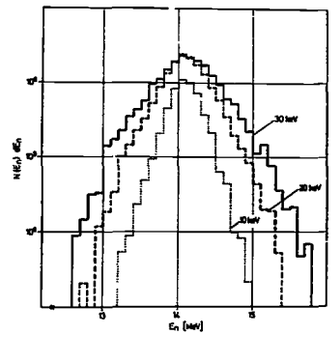

Fig. 6.
Energy spectra of neutrons from a D-T plasma of temperature T=10, 20 and 30 keV

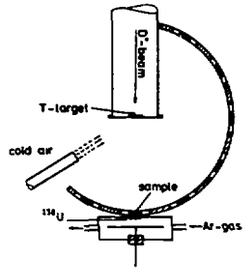

Fig. 5. Scattering-free arrangement for irradiation around 14 MeV

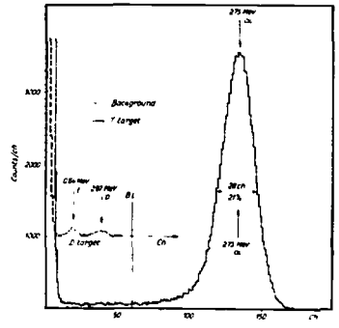

Fig. 7.
Charged particle spectrum in an APM system

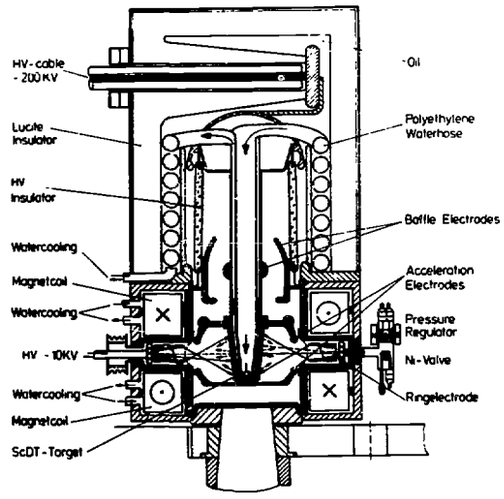

Fig. 8.
Scheme of an intense neutron generator based on mixed beam of T and D (see Ref. [75]).

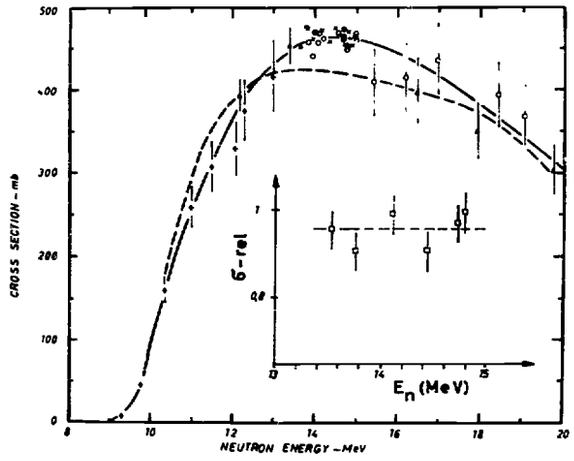

Fig. 9. Excitation function for the $^{93}Nb(n,2n)^{92m}Nb$ reaction

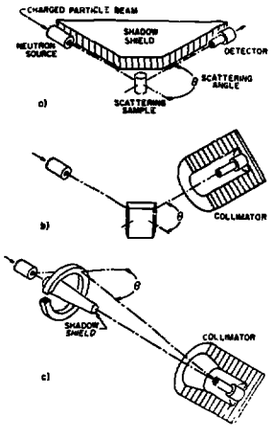

Fig. 10. Experimental geometries for measuring neutron scattering

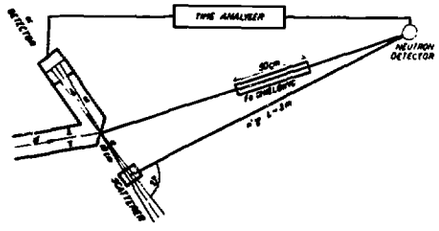

Fig. 11. Scheme of the arrangement of a TOF spectrometer

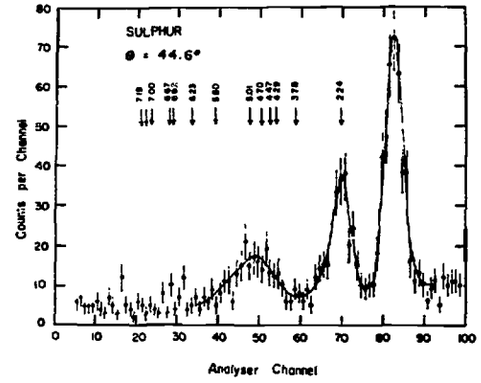

Fig. 12. The TOF spectrum for sulphur measured at 14.1 MeV

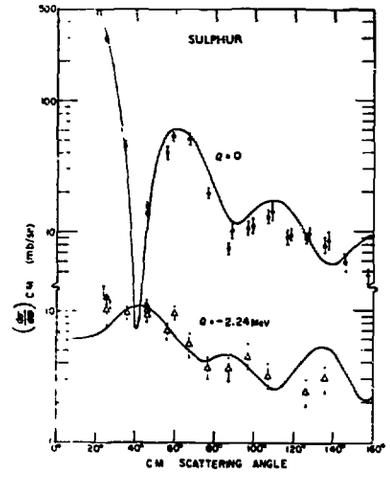

Fig. 13. The differential cross sections for elastic and inelastic scattering of neutrons from S

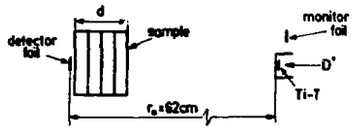

Fig. 14. Geometrical arrangement for the measurements of removal cross sections

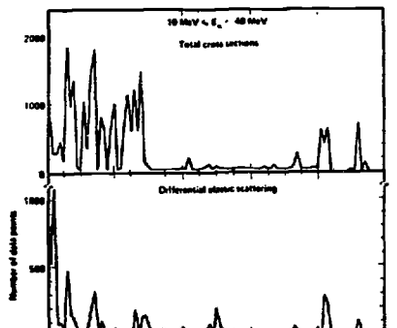

Fig. 15. Number of data points vs. atomic number for σ_T, $\sigma_{EL}(\Theta)$ and σ_{nM} for E_n between 10 and 40 MeV

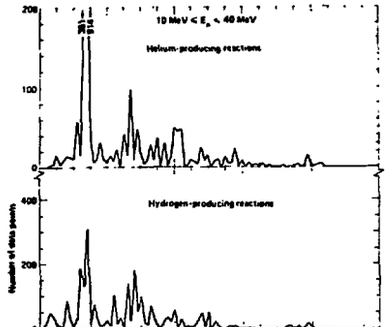

Fig. 16. Number of data points vs. atomic number for H and He producing reactions, and all other partial nonelastic reactions

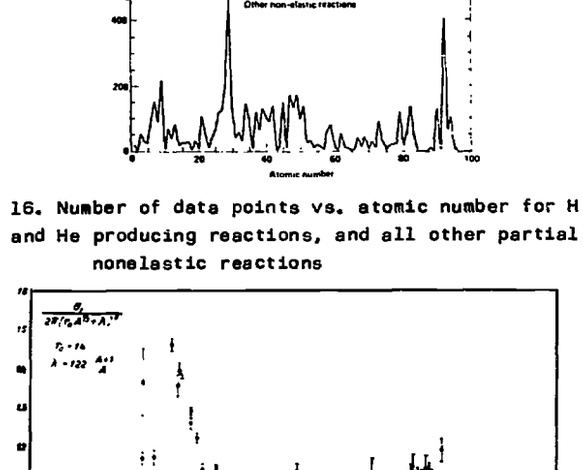

Fig. 17. 14 MeV neutron total cross sections

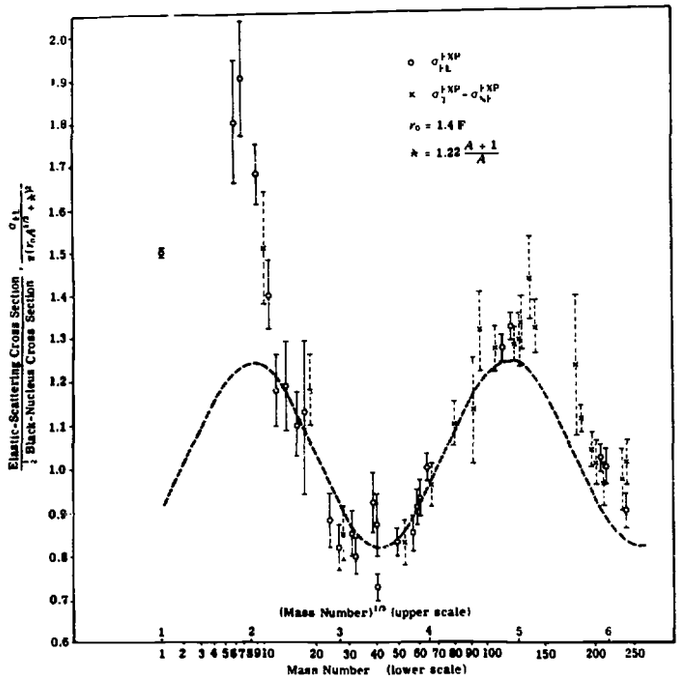

Fig. 18. 14 MeV integrated elastic scattering cross sections

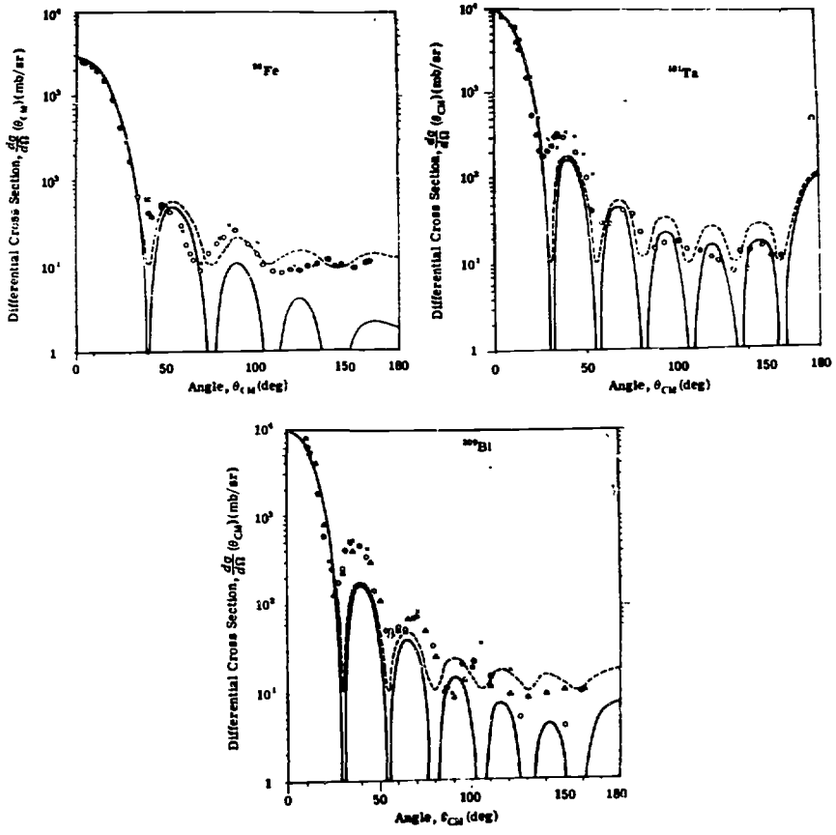

Fig. 19. Experimental and calculated (dashed curve) differential elastic scattering cross sections

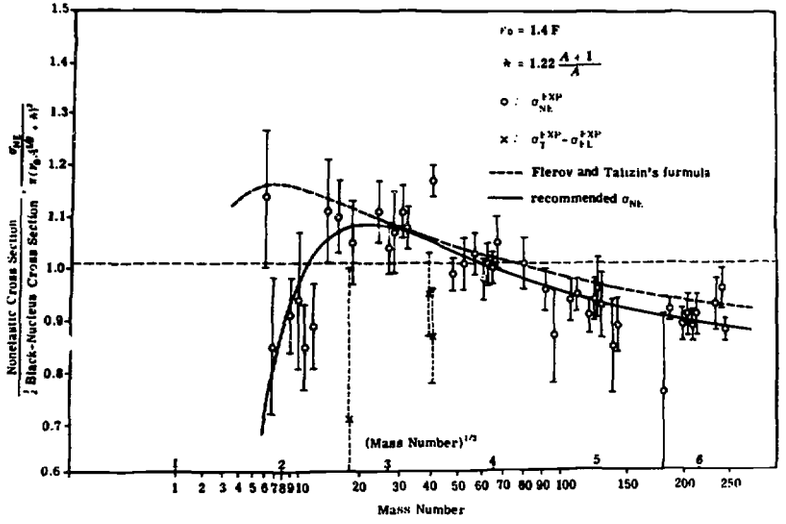

Fig. 20. 14 MeV nonelastic cross sections

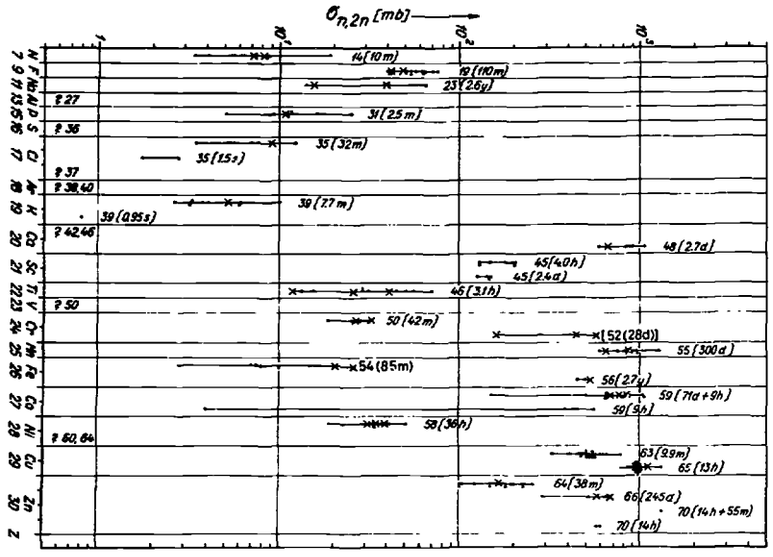

Fig. 21. a-e. Activation cross sections for (n,2n) reactions at 14 MeV

Fig. 21. b.

Fig. 21.c.

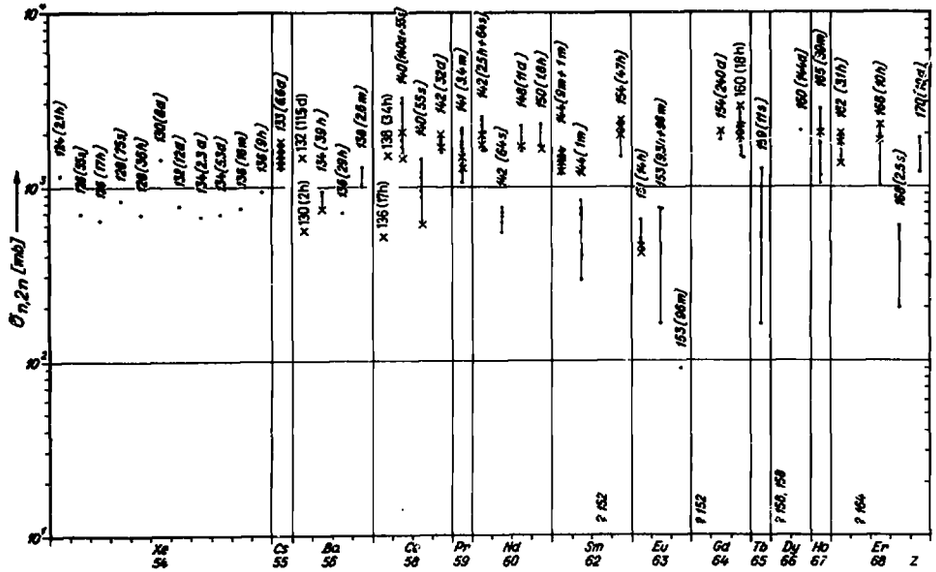

Fig. 21. d.

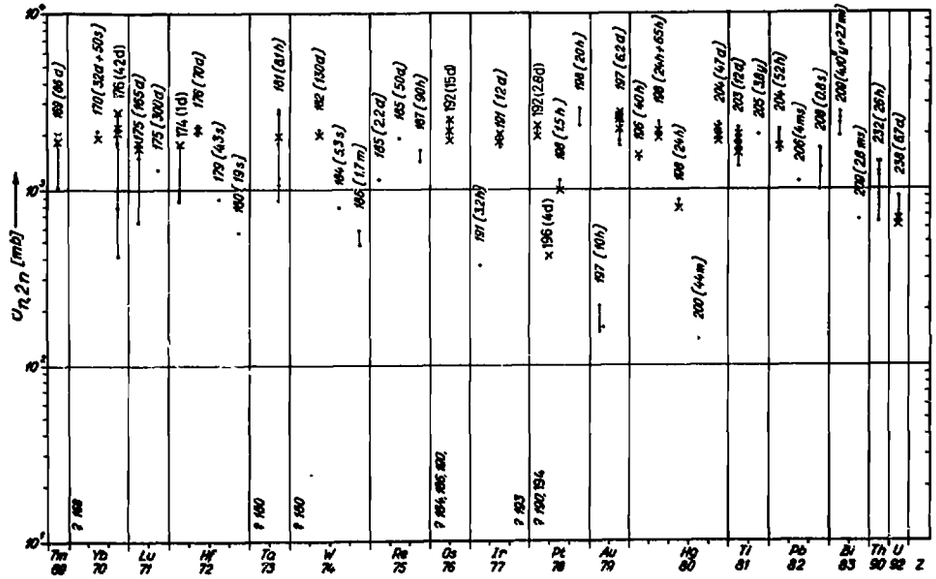

Fig. 21. e.

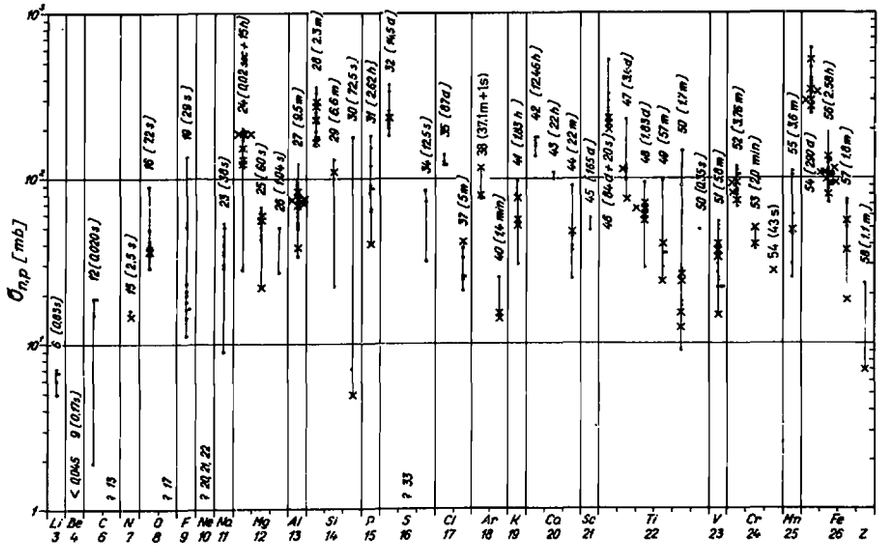

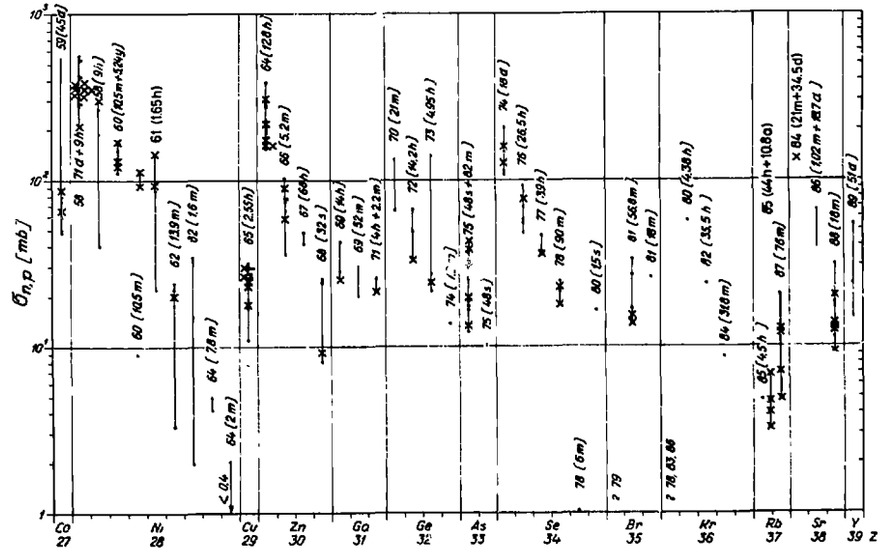

Fig. 22. a-e. Activation cross sections for (n,p) reactions at 14 MeV

Fig. 22. b.

Fig. 22. d.

Fig. 22. c.

[34] [35] [36] [37] [38] [39] [40] [41] [42] [43] [44] [45] [46] [47] [48] [49] [50] [51] [52] [53] [54]

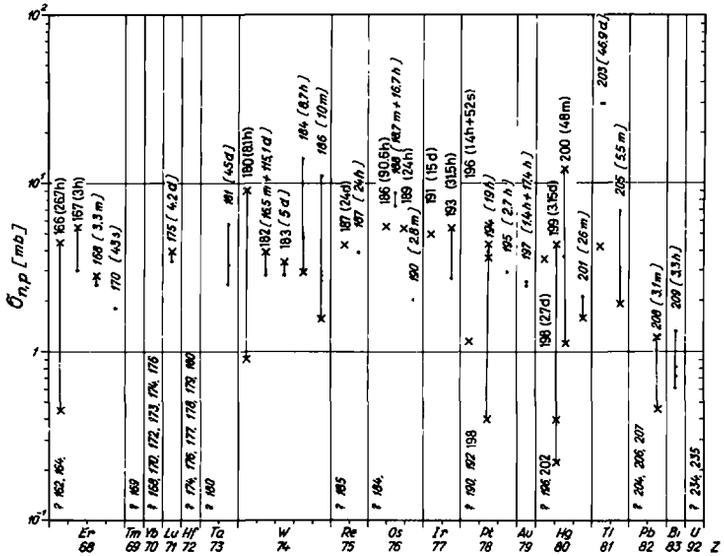

Fig. 22. e.

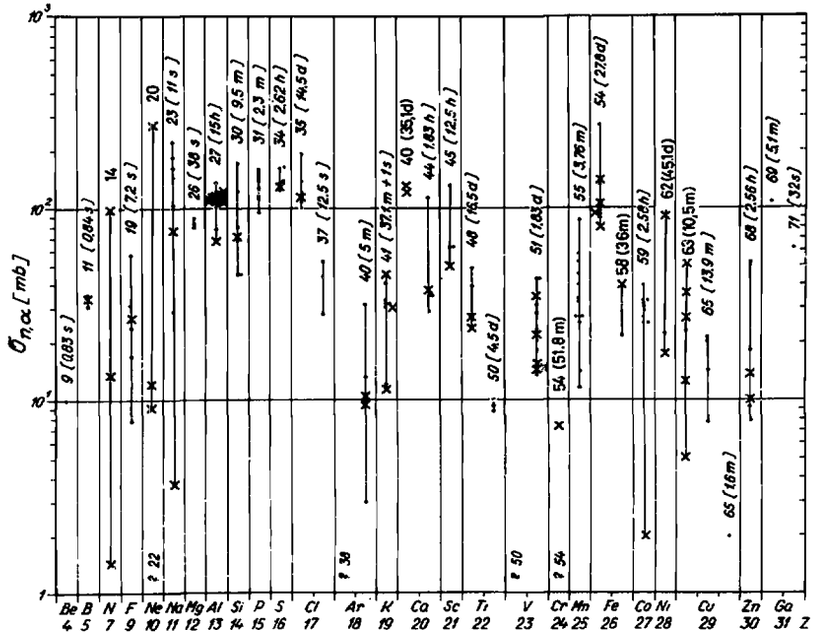

Fig. 23. a-d. Activation cross sections for (n,α) reactions at 14 MeV

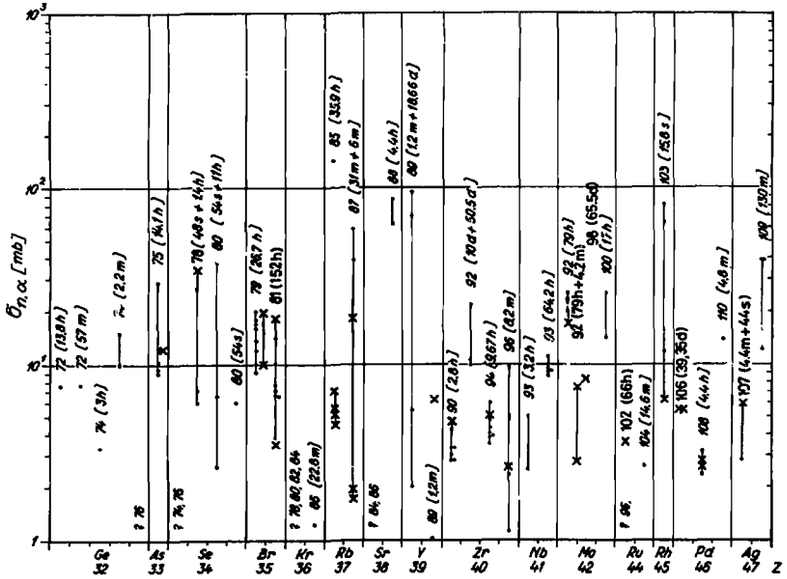

Fig. 23. b.

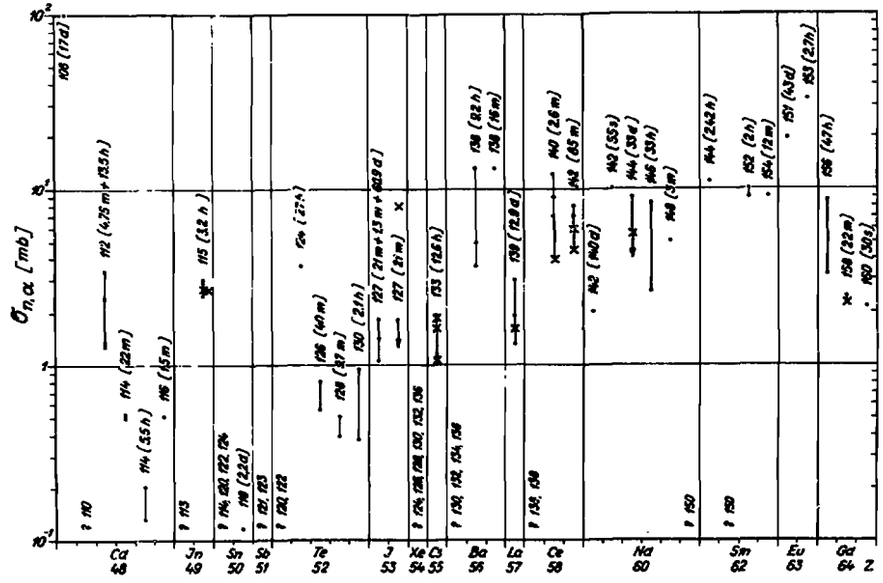

Fig. 23. c.

[113] FRE
(19
[114] VEE
(19
[115] AUC
(19
[116] PAU
(19
[117] CHA
[118] HER
SEI
[119] KOC
(19
[120] PEA
[121] KUM
[122] QAI
[123] CUD
and
Har
(19
[124] HAU
[125] VOC
Adv
[126] FU,
[127] HOL
A26
[128] QAI
[129] PEA
[130] BLA
[131] GAR
[132] MOL
[133] HAI
63
[134] GRI
(19

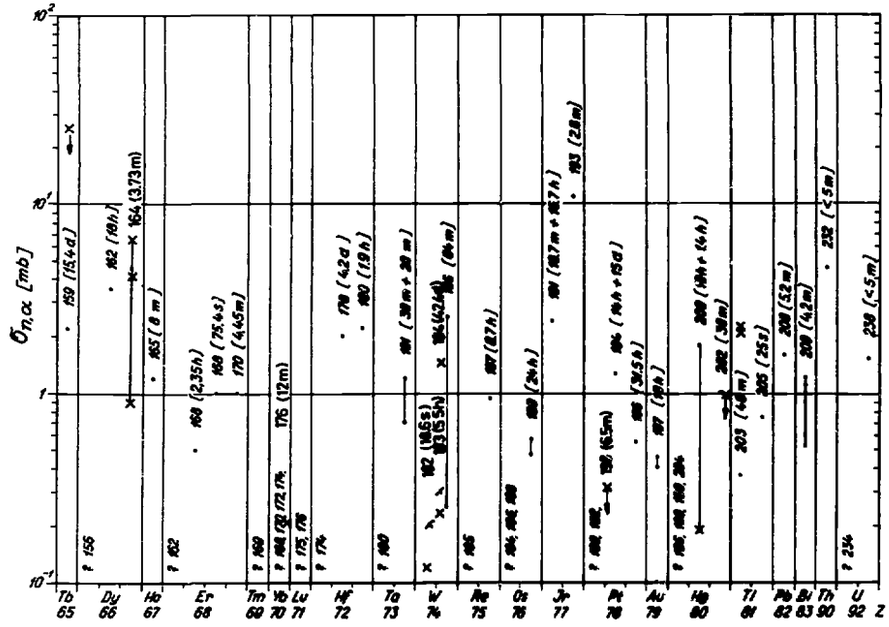

Fig. 23. d.

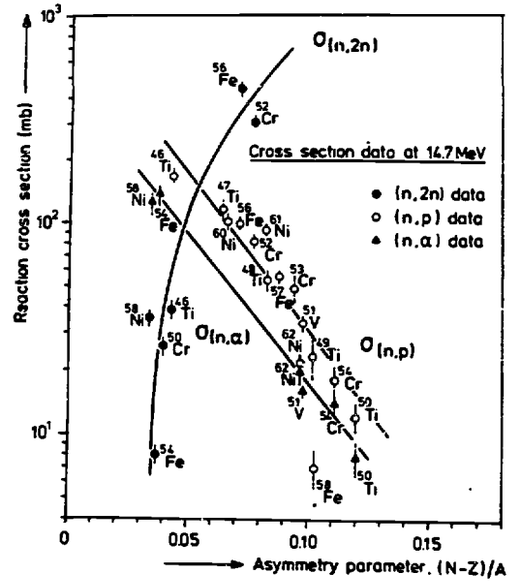

Fig. 24. Dependence of (n,2n), (n,p) and (n,α) cross sections on asymmetry parameter [97]

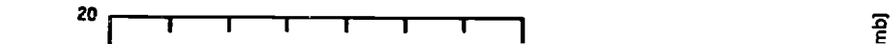

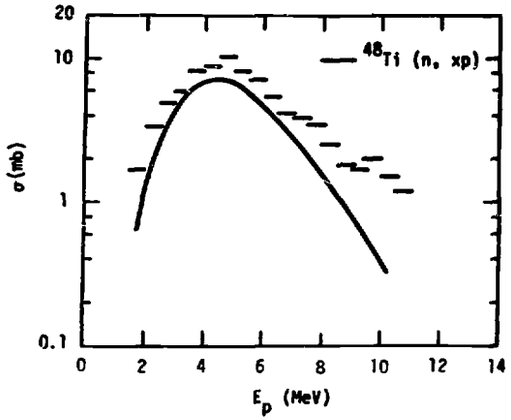

Fig. 25. Angle-averaged proton spectrum from ^{48}Ti measured with MQS [136] at 15 MeV

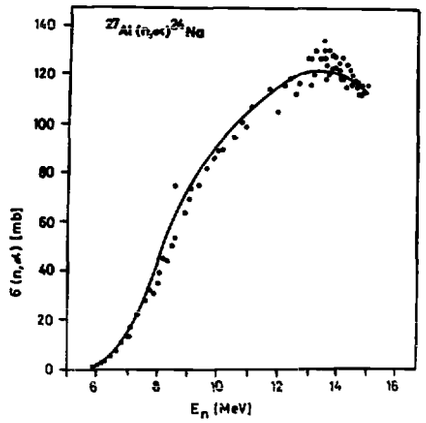

Fig. 26. Hauser-Feshbach model calculation for ^{27}Al(n,α) reaction (points are from experiments)

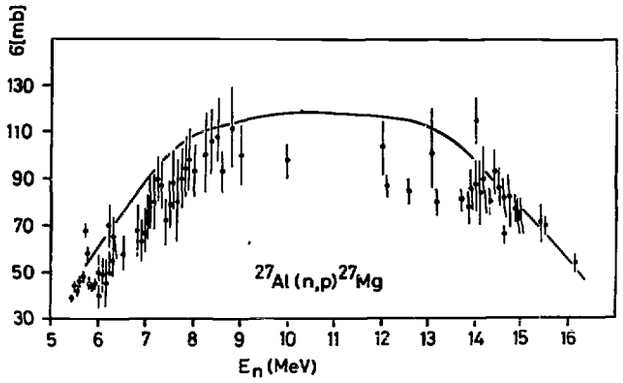

Fig. 27. Measured and calculated excitation functions for ^{27}Al (n,p) reaction

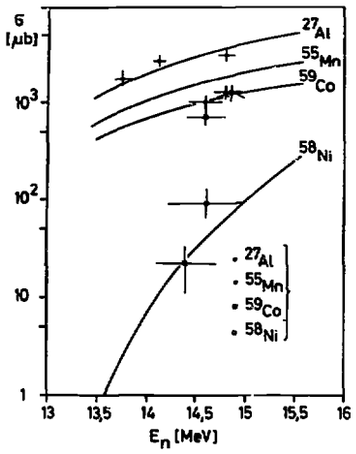

Fig. 28. Measured and calculated excitation functions for (n,t) reactions

Fig. 1

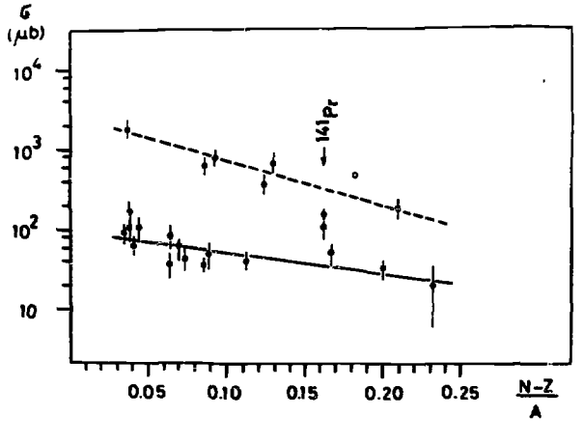

Fig. 29. Dependence of $\sigma_{n,t}$ on (N-Z)/A (full points for even nuclei, open circles for odd target nuclei)

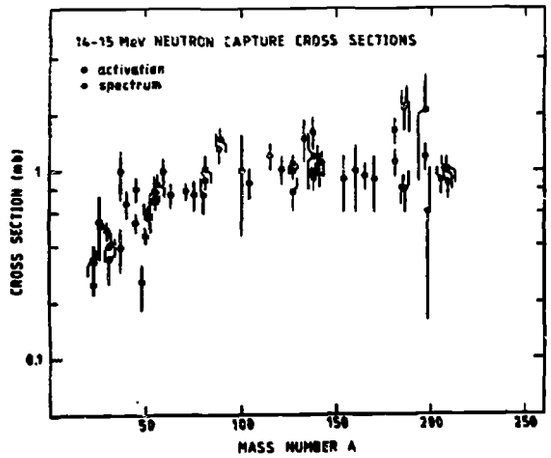

Fig. 30. 14 MeV corrected σ_{act} and σ_{int} (n,γ) cross sections [150]

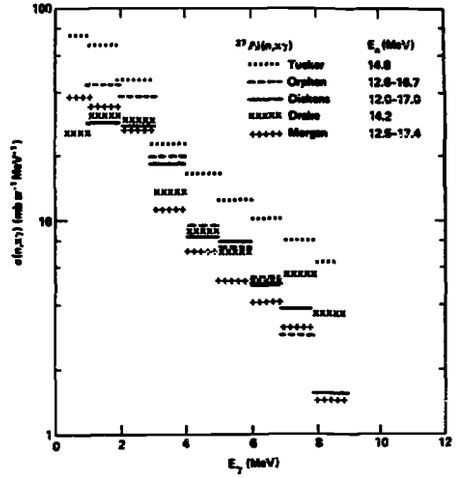

Fig. 31. $\sigma_{n,x\gamma}$ values as a function of E_γ for ^{27}Al near 14 MeV [77]

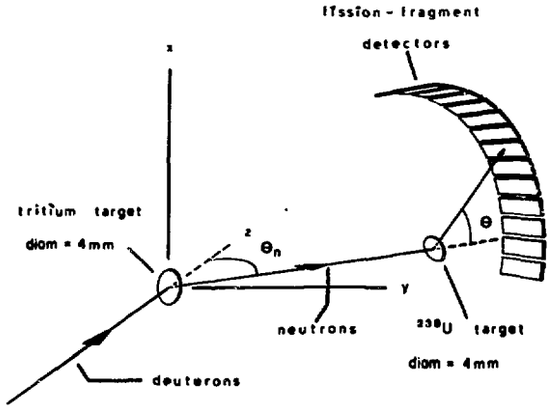

Fig. 32. Experimental arrangement for the measurement of angular distributions of fragments

SOME REMARKS ON EXPERIMENTAL TECHNIQUES FOR THE STUDY OF SECONDARY PARTICLE SPECTRA AND ANGULAR DISTRIBUTIONS EMANATING FROM 14 MeV NEUTRON – INDUCED NUCLEAR REACTIONS

D. SEELIGER
Dresden Technical University,
Dresden,
German Democratic Republic

Abstract:

Neutron time-of-flight spectroscopy is widely used for experimental investigations of neutron emission from neutron-induced reactions at 14 MeV incident energy. The paper contains some recommendations in connection with the design of pulsed-beam time-of-flight spectrometers at DT-generators in developing countries.

I. Experimental Techniques

1. Time-of-flight spectroscopy at DT-Neutron Generators

The main advantage of the $T(d,n)^4He$ reaction as a source of monoenergetic neutrons is its high cross section at low deuteron energy, which typically is between 120 keV and 250 keV. Moreover, the reaction yield is almost isotropic (within about 3 %) and neutron energy only weakly depends on the emission angle. Counting the associated α-particles, a both absolute and precise monitoring of the neutron flux is possible.

DT-generators usually are equipped with a Cockroft-Walton type high voltage power supply and a RF-ion source. The mixed-ion beam obtained from these sources is analyzed magnetically after acceleration, resulting in a deuteron current between 10 μA and 1 mA at the target. With thick tritium targets (1...10 Curie of tritium absorbed in the titanium or zirconium occlusion layer on a 0.2...0.5 mm air-cooled or water-cooled copper backing) averaged neutron intensities of $10^9...10^{11}$ neutrons per second can be generated. The mean target life-time typically is in the order of 20 h...100 h of operation.

On the one hand, small neutron generators of this type are comparatively inexpensive and easy to operate. On the other hand, they are rather useful for fundamental as well as applied nuclear research. Therefore in a great number of laboratories such devices are succesfully used since many years [1,2].

More advanced devices of DT-generators are equipped with high current duoplasmatron ion sources and high power rotating targets, which allow neutron yields between 10^{12} and 10^{14} neutrons per second. But the number of existing devices of that type is still rather limited [3,4].

For the overwhelming number of investigations of neutron emission reaction channels time-of-flight spectrometers are preferred, due to their high efficiency and good energy resolution [2]. In some cases also with proton recoil scintillation spectrometers useful physical information with comparatively weak energy resolution has been obtained [5].

The energy resolution of a non-relativistic time-of-flight spectrometer

$$\delta_E [\%] = 2{,}8 \sqrt{E [\mathrm{MeV}]} \; \frac{\Delta t [\mathrm{ns}]}{L [\mathrm{m}]} \qquad (1)$$

is determined by the overall time-spread Δt [ns] and the length of the flight path L [m]. The full time spread is composed of

the independent partial uncertainties Δt_i

$$\Delta t = \left(\sum_i \Delta t_i^2 \right)^{1/2} \qquad (2)$$

amongst which the main contributions are due to

Δt_I – the time spread of the 'start' moment, (e.g. the width of the ion pulse for the beam pulsing method or the time spread for the detection of associated α-particles);

Δt_D – the spread of the 'stop' moment, which is determined by the time resolution of the neutron detector, and

Δt_G – the time spread, which is caused by 'geometric' uncertainties of the flight path.

At present both of the two methods for determination of the 'start' moment are widely used: The so-called 'associated particle method' can be used at low source intensities only ($10^6 \ldots 10^8$ neutrons per second), due-to the limitations by random coincidences. This results in very long running time for most of the experiments. But there are also some advantages connected with this method: The time resolution of the order of 1.0...1.5 ns for the best cases is completely independent of the parameters of the neutron generator, such as the stability of the high-voltage power supply and others. Based on the associated-particle method, fast neutron TOF-spectrometry depends on the disposal of high-quality nanosecond detector electronics equipment only. Using this method, the background TOF-spectra are not time-depending and, therefore, the background-line can be determined with high precision. Finally, the formation of a well-defined coincident neutron cone makes possible experimental arrangements without a heavy shielding of neutron detectors. For these reasons, especially if the running of the DT-generator is not time-limited, the associated particle method seems to be a very useful tool for fast neutron spectroscopy. This is true, particularly if a specific reaction channel for a small number of cases has to be investigated with high precision.

Compared with that, the main advantage of the pulsed-beam method consists in the much higher neutron intensity, which in principle can be applied for experiments. However, one has to pay for this advantage:

- The background-line becomes time-depending;
- neutron detectors have to be located in heavy collimators;
- and some of the neutron generator parameters must be controlled strongly, since they influence the overall time resolution and stability of the TOF-spectrometer.

But no doubt, for systematic investigations of many nuclei the pulsed-beam method is favoured.

In the review paper [6] the existing methods for nanosecond ion beam pulsing are discussed in detail. The following conclusions can be drawn from this paper: In relation to the 120...200 keV DT-generators, the most reasonable (but the only possible one!) solution for a nanosecond beam-pulsing system consists of the combination of RF-deflection with RF-klystron bunching of the ion beam. By the last method, the monoenergetic deuteron beam with the velocity v_o and kinetic energy E_o is modulated with the harmonic energy spread $E_m \cdot \sin \omega t$ in a narrow modulation gap. This velocity modulation leads to the collection of a definite part of the whole ion beam (e.g. ions crossing the modulation gap during a definite phase interval $\Delta\phi_o = \Delta\omega t_o$ of the modulation voltage) into very intense short burst after drifting to the 'focus' distance x_s from the modulation gap.
The focus distance

$$x_s = \frac{2 v_o}{\alpha \cdot \omega} \qquad (3)$$

depends on the frequency ω, velocity v_o and the so-called modulation factor $\alpha \equiv \frac{E_m}{E_o}$. For klystron bunching of a 150 keV monoenergetic deuteron beam with the bunching frequency of 5 M c, as shown in fig. 1, the following characteristics can be obtained theoretically: Ions, passing the modulation gap within a time interval $\Delta t_o = 45$ ns, e.g. 22,5 % of the total amount of deuterons, can be collected within the time interval $\Delta t_s = 1$ ns at the target. The somewhat broadened initial time interval $\Delta t_o = 60$ ns, e.g. 30 % of the beam, contributes to an $\Delta t_s = 2$ ns ion burst at the target. The corresponding compression factors $\frac{\Delta t_o}{\Delta t_s}$ amount to 45 and 30, respectively [7]. But such high bunching factors cannot be obtained practically. As it was shown (see f.i. [8]), bunching factors obtained experimentally are limited by the energy spread ΔE_o of the ions before klystron bunching. The maximum compression factor is given by

$$\frac{\Delta t_o}{\Delta t_s} = \frac{\Delta E}{\Delta E_o} \quad , \qquad (4)$$

where ΔE is the energy spread introduced by the klystron bunching, e.g. approximately $\Delta E \approx E_m$. Having in mind, that even for a well stabilized high voltage power supply the beam energy spread is at least of the order of $\Delta E_o = 500$ eV, modulation amplitudes E_m should be higher than 5 keV. Practically modulation factors of $\alpha = 0.05...0.1$ are used, which correspond to modulation amplitudes $E_m = 7.5...15$ keV for a 150 keV deuteron beam. In this case according to eq. (4) compression factors up to $\frac{\Delta t_o}{\Delta t_s} = 15...30$ are possible.

For practical design of pulsing systems for DT-generators the following conclusions can be drawn:

- In order to preserve the main advantage of the pulsed beam method, e.g. the maximum average intensity for a requested pulse width Δt_s, it is necessary to choose the pulse width Δt_o by beam deflection in accordance with eq. (4). If Δt_o is smaller, beam intensity is lost without any benefit. If Δt_o is higher than predicted by eq. (4), the requested Δt_s cannot be achieved.
- Introduction of a modulation amplitude in the order of E_m 7,5...15 keV immediately after the ion source, where the total kinetic energy of the ions is of the same order of magnitude, is impossible due to the requirements of ion optics. Therefore, in systems, introducing velocity modulation before acceleration, much smaller modulation amplitudes E_m have to be used. The apparent advantage of using a low power RF-generator is paid by the decrease of the maximum compression factor, resulting finally in a loss of average neutron intensity.
- Sometimes, beam deflection and klystron bunching electrodes are supplied with different RF-voltages. From eq. (3) it's evident, that using instead of ω the frequency $2k\omega$ (with $k = 1,2...n$) the focus distance x_s is preserved with $\frac{E_m}{2k}$ of the modulation amplitude. In this case it is necessary to shorten the incident ion pulses to $\frac{\Delta t_o}{2k}$ by means of the beam deflection, e.g. to preserve constant the compressible phase interval $\Delta \phi_o = \omega \Delta t_o = \frac{\Delta t_o}{(2k)} \cdot (2k\omega)$ for the new bunching frequency $2k\omega$. In this case again the apparent advantage of using a smaller RF-generator is paid by the loss of target intensity (by a factor $\frac{1}{2k}$, if other parameters like Δt_s, x_s, E_o, ΔE_o and beam loss along the drift path are considered to be constant!).

And so we conclude, that for low energy DT-generators (for other accelerators the situation is quite different!) from the point of view of a maximum pulsed neutron intensity the best solution consists in post-acceleration klystron bunching of the deuterons with a modulation factor $\alpha = 0.05...0.1$, combined with a beam deflection at the same frequency before or after acceleration.

Fig.

Fig.

The frequency ω used is determined by the dynamical range Δt_F of the TOF-spectrometer

$$\Delta t_F \leq \frac{2\pi}{\omega} . \qquad (5)$$

DT-generators of this type should be equipped with

- stabilisation of acceleration voltage,
- ion beam analysis by magnetic deflection,
- quadrupole lenses, to minimize the loss of beam intensity during the ion transport to the target,
- and, finally, enough laboratory space for the x_s = 2...3 m drift distance is required.

The necessary RF-generator represents a comparatively simple electronic circuit, which easily can be constructed even in a small laboratory in developing countries. If requirements, mentioned above, partially cannot be fulfilled, an alternative system (e.g. using klystron bunching before acceleration or bunching with 2k-fold frequency) may be more suitable for practical purposes, though these arrangements are less effective in respect of the neutron intensity. As an example in figs. 2 and 3 the principal schemes of the ion tract and pulsing system of a pulsed DT-generator are shown. This generator over more than 15 years is used for TOF-spectroscopy in Dresden.

References

1	Csikai, J.	Use of small Neutron Generators in Science and Technology Atomic Energy Review, 11 (1973) 415
2	Lescenko, B.	Fast Neutron Spectroscopy by the Time-of-Flight Method Kiev, 1978
3	Tsukada, K.	Neutron Sources for the Medical Use; IAEA Consultants' Meeting on Neutron Source Properties Debrecen, Hungary, March 1980 INDC(JAP)-49/L, 1980
4	Barshall, M.H.	14 MeV(d,t)-Sources UWFDM-331, Univ.of Wisconsin(1979)
5	Morgan, G.L., Love, T.A., Perey, F.G.	Nucl.Instr.a.Methods 128 (1975)125
	Morgan, G.L., Perey, F.G.	Nucl.-Sci. Eng. 61 (1976) 337
6	Lehmann, D., Seeliger, D., Sgonina, A.	Nanosekunden-Pulsung stationärer Teilchenbeschleuniger ZfK - 268 (1974)
7	Seeliger, D., Trützschler, K.	Nucl. Instr.a.Methods, 66 (1968) 157
8	Marion, J.G., Fowler, J.L.	Fast Neutron Physics, part. I Intersc.publ., N.I. - London, 196

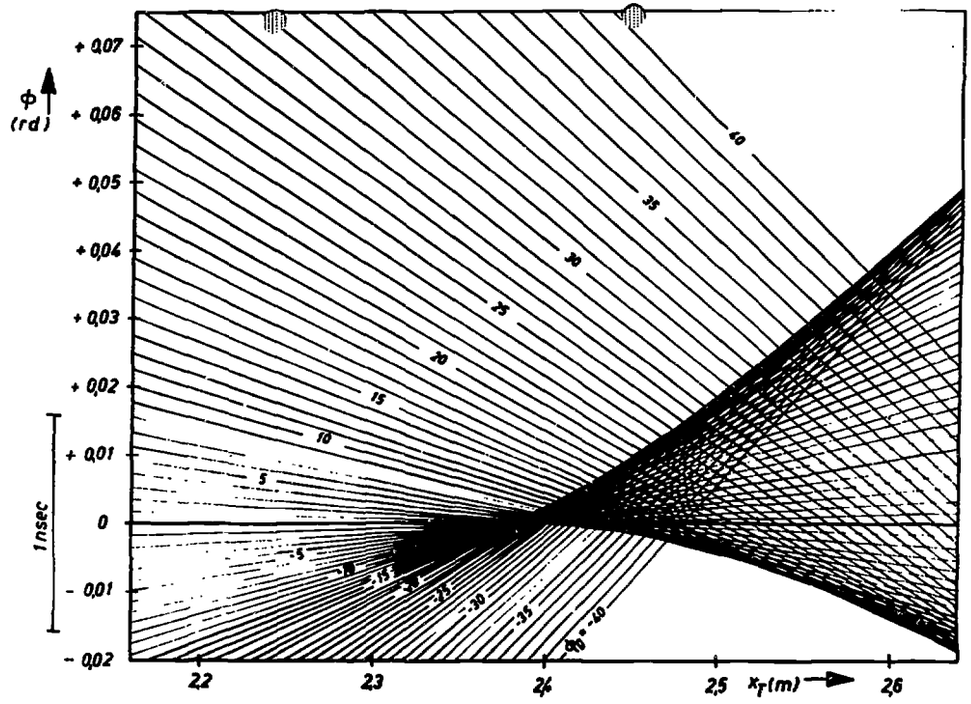

Fig.1

Phase bunching for 15o keV deuterons with modulation factor α = o.1 at ω = 1·1o^7 s^{-1} ; $\phi = \omega t_s$ as a function of the drift distance x_T for different initial phases $\Phi_o = \omega t_o$.

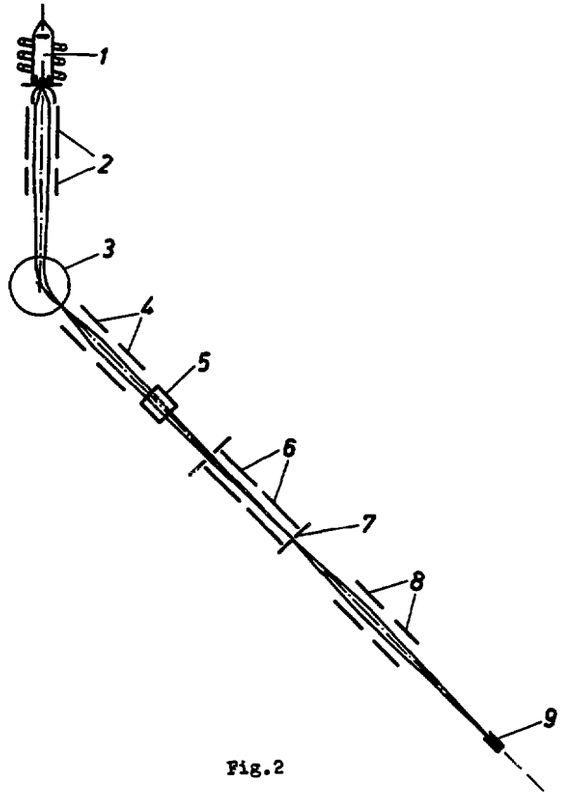

Fig.2

Principal scheme of the ion tract of a pulsed-beam DT - generator [7] ; 1 - ion source; 2 - acceleration electrodes; 3 - deflecting magnet ; 4 - quadrupole lenses; 5 - RF-deflection plates; 6 - klystron bunching electrodes; 8 - quadrupole lenses; 9 - target.

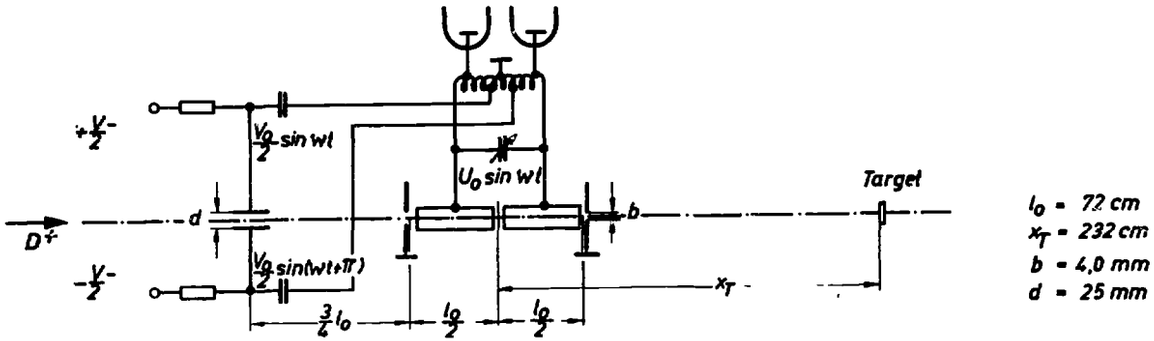

Fig.3 Pulsing system of a DT- generator using one 5Mc RF-generator[7].

INTEGRAL CROSS-SECTION MEASUREMENTS FOR INVESTIGATING THE EMISSION OF COMPLEX PARTICLES IN 14 MeV NEUTRON-INDUCED NUCLEAR REACTIONS

S.M. QAIM
Institut für Chemie 1 (Nuklearchemie),
Kernforschungsanlage Jülich GmbH,
Jülich, Federal Republic of Germany

ABSTRACT

Some of the off-line techniques used for the determination of integral cross-section data are reviewed and, as a critical check, some typical data sets are compared. The systematic trends reported in the cross-section data for (n,d), (n,t), (n,^{3}He) and (n,α) reactions are discussed. A brief discussion of the possible reaction mechanisms is given. Some of the applications of the data are outlined.

1. INTRODUCTION

In the interactions of 14 MeV neutrons with nuclei radiative neutron capture has low probability but the emission of both neutrons and protons is highly favoured. In addition the emission of complex particles like ^{2}H, ^{3}H, ^{3}He and ^{4}He is also energetically possible. However, with the exception of ^{4}He, in general the emission of complex particles has not been investigated in great detail, mainly due to the relatively low cross sections of such processes [cf. 1]. Such investigations are, however, of great significance for enhancing our understanding of nuclear theory and for practical applications. Integral cross-section measurements play an important role in the study of such reactions and this review gives a summary of the information available in this field.

2. EXPERIMENTAL TECHNIQUES

In general three techniques are commonly used for measuring integral cross sections of reactions involving the emission of complex particles.

- On-line particle detection
- Activation technique
- Mass spectrometry

The on-line particle detection technique involves identification and measurement of the energy and angular distributions of the emitted complex charged particles (^{2}H,^{3}H,^{4}He) and yields differential data. Integration of the cross section over the angular range gives the integral cross section. Several types of counter telescopes have been used for studying charged particles and the subject is treated in detail by Vonach [2].

2.1 Activation Technique

This is a relatively simple technique and involves an off-line identification and radiometric determination of the radioactive reaction product. In the special case of (n,t) reactions the technique has been applied in two variations, namely, identification of the activation products and estimation of the formed tritium by β$^-$-counting in the gas phase.

Several of the steps involved in the precise measurement of the cross sections by the activation technique have been discussed by Csikai [3]. In this review only those aspects are emphasized which are relevant to the study of the rather low-yield reactions.

2.1.1 Sample preparation for irradiations

The chemical form of the substance to be irradiated should be well defined. As has been discussed in several publications from Jülich [cf. 4-10], in investigations of low-yield reactions it is most essential that high purity materials be irradiated since many of the activation products under investigation may also be formed via interfering reactions on impurities, thereby giving rise to erroneous results. In this context both isotopic and non-isotopic impurities are undesirable. It has been found, for example, that in the 14.6 MeV cross-section measurement of the reaction ^{60}Ni(n,t)^{58}Co, if target nickel contains 10 ppm cobalt impurity, the interfering reaction ^{59}Co(n,2n)^{58}Co will give rise to ∿ 20% of the ^{58}Co activity. Similarly if the target isotope ^{60}Ni is 99.8% enriched with ^{58}Ni isotopic impurity of 0.2%, the interfering reaction ^{58}Ni(n,p)^{58}Co will contribute about 12% of the ^{58}Co activity. The interference from non-isotopic impurities can be suppressed by using > 99.999% pure materials and that from the isotopic impurities by using highly enriched isotopes.

Whenever possible thin samples should be used since thick samples cause the production of low-energy secondary neutrons. In general the Q-values of the low-yield reactions are highly negative and the effect of secondary neutrons is therefore negligible. However, if the investigated activation product is the same as that formed in an (n,γ) reaction on some isotopic or non-isotopic impurity, the measured reaction cross section will be erroneous since the low-energy neutrons have rather high cross sections for the (n,γ) reaction. In investigations of (n,t) reactions by tritium counting the interference due to secondary neutrons must be taken into account, especially if the

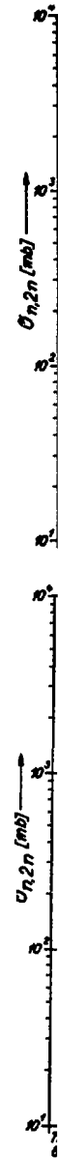

irradiated sample contains lithium impurity for which the (n,t) cross section is particularly high.

2.1.2 Choice of E_n and neutron flux measurement

It is known that the energy of the neutrons produced in a dt neutron generator ranges between 13 and 15 MeV, depending on the energy of the deuterons incident on the tritium target and the emission angle of neutrons. A typical irradiation facility at a 300 keV dt neutron generator is shown in Fig. 1. The energy and energy spread of the neutron incident on the sample can be calculated [cf. 11] by taking into account the angle of emission and scattering in the intervening medium. From the energy profile of the neutron flux in various groups it is estimated that the energy of 90% neutrons reaching the sample is 14.7±0.3 MeV. Since in investigations of nuclear reactions with low cross sections, with a view to obtaining reasonably reliable counting statistics, it is necessary to irradiate rather thick samples at angles of 0-40°, the resulting neutron energy is 14.6±0.4 MeV.

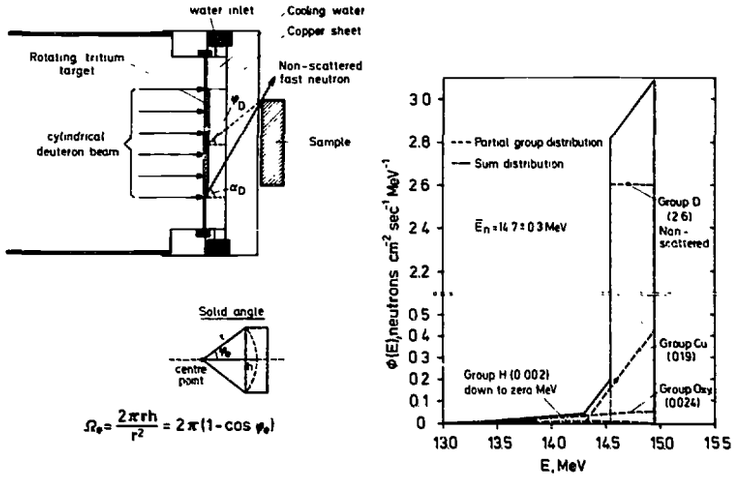

Fig. 1 Experimental set-up for irradiations at a 300 keV dt neutron generator and energy profile of the neutron flux.

The neutron flux can generally be measured accurately by the associated particle technique. However, in the case of thick samples it may not give the neutron flux effective in the thick target, unless some Monte Carlo type calculations are done to take into account the size and thickness of the sample. As an alternative the use of an internal standard reaction with a well-known cross section may be very advantageous. In investigations of (n,t) and (n,^{3}He) reactions, for example, (n,p) and (n,α) reactions, respectively, on the same target nucleus have been employed as internal monitor reactions [4,6,8,9].

2.1.3 Radiochemical separations

The activation products of strong reaction channels can often be identified non-destructively, mainly through the use of high-resolution counters. In the case of low-yield reaction products, however, in order to identify the weak activities it is important to separate them chemically from the strong matrix activities. Such chemical separations are often straightforward but they do demand a good knowledge and skill of radiochemical techniques, especially when dealing with carrier-free materials.

The more commonly used radiochemical methods of separation include processes like precipitation, coprecipitation, adsorption on preformed precipitates, solvent extraction, ion-exchange chromatography, high-pressure liquid chromatography, gas extraction, etc. A summary of the radiochemical methods used at Jülich for the determination of nuclear data is given elsewhere [12,13]. The latter two separation methods, viz. high pressure liquid chromatography and gas extraction, proved to be of special advantage. The high-pressure liquid chromatography (HPLC) is virtually an efficient column chromatographic technique which makes use of high pressure to accelerate the separation. It facilitated rapid separation of the rare earths [14] and allowed accurate measurement of the (n,p), (n,^{3}He) and (n,α) reaction cross sections [9,15]. The gas extraction technique [5] is ideal for those cases where the activation product is a very soft β^- emitting gaseous product like ^{3}H or ^{37}Ar [16]. It has been applied extensively to studies on (n,t) reactions [cf. 5,7,12,13,17,18].

2.1.4 Sample preparation for counting

Radiochemical techniques not only allow separation of the transmutation products from strong matrix activities but also facilitate preparation of thin sources for β^- counting or X-ray spectroscopy. Typical examples are furnished by investigations on the reactions ^{58}Ni(n,α)^{55}Fe and ^{50}Cr(n,n'p)^{49}V [19]. Since both ^{55}Fe and ^{49}V are long-lived, gramme quantities of

Ni and Cr target samples must be irradiated. Due to high self-absorption effects, however, the products ^{55}Fe and ^{49}V, both of which decay exclusively by EC and thereby emit 5.9 and 4.5 keV X-rays, respectively, cannot be accurately determined. Use of carrier-free radiochemical separations for V and Fe, and preparation of thin ^{49}V and ^{55}Fe sources, eliminate this difficulty.

2.1.5 Measurement of radioactivity

High resolution counting methods are essential for an unambiguous identification of the activation products. In recent years Ge(Li) detector γ-ray spectroscopy has superseded almost all the other methods of counting. There is, however, still considerable scope of the application of soft X-ray spectroscopy, such as applied in the detection of ^{49}V and ^{55}Fe [19], since cross-section data for many of the light mass nuclei are not known. The use of non-specific ß⁻ counting should in general be avoided. If, however, no other radiation is emitted, use should be made of low-background anticoincidence ß-proportional counters [cf. 4,6,8,9]. Chemical separation, preparation of thin source and a stringent test of half-life are most essential.

2.1.6 Calculation of cross section

The count rate is converted into decay rate by applying the usual corrections like those for decay, γ-ray branching, counting efficiency, geometry, absorption, etc. and the cross section is calculated using the well-known activation equation. It should be pointed out that many of the older cross sections are in error because of the use of erroneous decay data. It is therefore recommended that in each case two or three strong γ-rays with well-defined branching ratios should be used for cross section work. Furthermore, a check of the half-life of the product should be carried out. It is also essential to give enough details of the data used so that a renormalization, if necessary, may be carried out at a later date.

2.1.7 Advantages and limitations of the activation technique

The advantages of the activation technique are:
- Simplicity
- High sensitivity, especially in combination with specific radiochemical separations and low-level methods of counting. In the case of (n,^{3}He) reactions cross sections of the order of 1 µb have been measured [8,9].
- It is possible to distinguish between (n,x) and (n,n'x) processes since they lead to different activation products. In contrast, in on-line detection of emitted charged particles the contributions of (n,x) and (n,n'x) processes can be analysed only by an elaborate theoretical analysis.
- Cross sections for transitions leading to the formation of closely spaced nuclear levels with measurable half-lives can be determined. Due to resolution problems such isomeric cross sections cannot be easily determined by an analysis of the emitted particle spectrum.

The limitations of the activation technique are:
- It is not applicable in the case of stable reaction products.
- It yields only integral data and hence the information extractable on the reaction mechanisms is rather small.
- It involves measurement of the activation product, irrespective of its mode of formation. Therefore, if proper care is not taken, the interfering reactions may lead to erroneous results.

2.2 Mass Spectrometry

This method involves an off-line identification of the generally stable or very long-lived reaction product via its mass. Cross sections for the formation of some medium and heavy mass products via (n,γ) reactions during long irradiations in nuclear reactors have been determined using a magnetic mass spectrometer [cf. 20]. However, as far as nuclear reactions involving the emission of complex particles are concerned, the method has been applied exclusively to the estimation of light mass gaseous products ^3He and ^4He; in cross-section work the detection of ^1H, ^2H and ^3H by mass spectrometry has so far not been attempted.

The mass spectrometric determination of helium isotopes has been carried out so far mainly at Rockwell International, California [cf. 21,22] and Jülich [10]. Whereas at Rockwell International the produced ^4He was heated out of the irradiated material, spiked with ^3He and measured using a high sensitivity magnetic mass spectrometer in a static mode, in our Institute relative measurements of ^3He and ^4He, both produced in fast neutron-induced reactions, were carried out in a dynamic mode using a quadrupole mass spectrometer.

Mass spectrometry constitutes a sensitive method for the detection of light mass stable gaseous products and about 10^8 atoms can be detected [21,22]. The dynamic range of the system is generally > 10^7, which means that the intensity ratios of $1:10^7$ for neighbouring masses can be well distinguished [10]. The technique has proven to be very useful for estimating total helium gas production in various structural materials [cf. 22]. In recent years it has gained considerable sophistication and has found application even in passive neutron dosimetry [cf. 23].

Similar to the activation technique the mass spectrometric method has the disadvantage of yielding only integral cross-section values so that little information on the reaction mechanism is obtained. Furthermore, no distinction is made between (n,x) and (n,n'x) type reactions, the measured cross

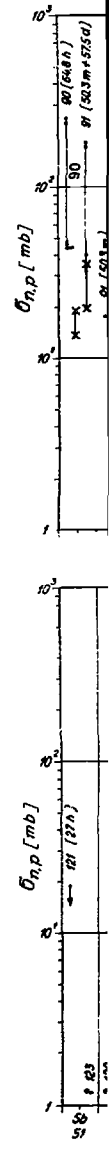

section being a sum of all the helium emitting reactions. On the other hand, in contrast to the activation technique, mass spectrometry can be applied even in those cases where the transmutation products are stable.

3. CROSS-SECTION DATA AND SYSTEMATICS

3.1 Comparison of Cross-Section Data obtained by various Techniques

The (n,t) reaction on very light nuclei has been investigated using both particle detection with counter telescopes [cf. 24,25] and the activation technique in combination with tritium counting. The results are more or less in agreement. In the medium and heavy mass regions so far both the (n,t) and (n,^{3}He) reactions have been investigated exclusively by the activation technique so that a comparison with other techniques is not possible. The cases of (n,d) and (n,α) reactions are discussed below.

Since integral cross-section data of 14 MeV neutron-induced reactions obtained via the three techniques mentioned above incorporate varying contributions from side reactions, some adjustments in the data are necessary before a comparison can be made. We present in Table I the results for a few typical cases.

Table I. Comparison of some data sets obtained by various techniques

Activation and Radiochemistry (KFA Jülich)		Quadrupole Spectrometer (LLL, Calif.)		Mass Spectrometer (Rockwell Int., Calif.)	
^{58}Ni(n,p)^{58}Co	375±22	^{58}Ni(n,xp)	1000±120		
^{58}Ni[(n,n'p)+(n,d)]^{57}Co	526±45	^{58}Ni(n,d)	14± 16		
Total:	901±67 mb		1014±136 mb		
^{58}Ni(n,α)^{55}Fe	125±15	^{58}Ni(n,xα)	106±17	^{58}Ni(n,xα)	116±8
^{58}Ni(n,n'α)^{54}Fe*	< 10				
Total:	125±15 mb		106±17 mb		116±8 mb
^{51}V(n,α)^{48}Sc	16±2	^{51}V(n,xα)	17±2	^{51}V(n,xα)	18±2
^{51}V(n,n'α)^{47}Sc	2±0.5				
Total:	18±2.5 mb		17±2 mb		18±2 mb

* Value from systematics.

In general it seems that the recent results obtained by the three techniques are in agreement within the limits of experimental errors.

3.2 Systematic Trends in Integral Cross-Section Data

Miljanic and Valkovic [26] surveyed the cross-section data for (n,d) reactions on the light nuclei ^{3}He, ^{6}Li, ^{7}Li, ^{10}B, ^{11}B, ^{14}N, ^{15}N, ^{16}O and ^{19}F. In recent years extensive studies on nuclei in the medium mass region have been carried out at Livermore [cf. 27-29]. The trend based on the integrated (n,d) data reported from Livermore is shown in Fig. 2. For comparison

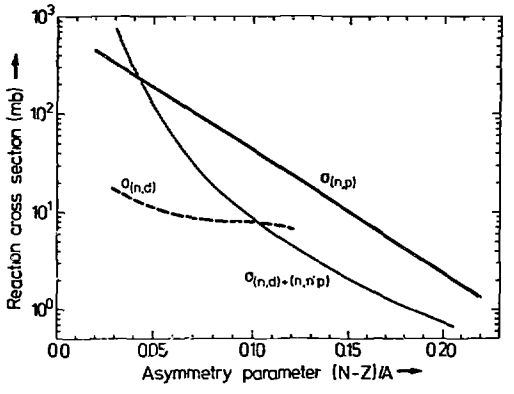

Fig. 2

Systematics of (n,d) and [(n,d)+(n,n'p)+(n,pn)] reaction cross sections at 14.7 MeV. The trend in the [(n,d)+(n,n'p)+(n,pn)] reaction cross sections is based on radiochemical measurements done at Jülich, that in the (n,d) cross sections on magnetic quadrupole spectrometric measurements carried out at Livermore.

the trend in the [(n,d)+(n,n'p)+(n,pn)] cross sections based on the data measured at Jülich [30-32] is also shown. It is

For medium and heavy mass nuclei it was observed that the (n,t) cross section decreases rather slowly with (N-Z)/A of the

the trend in the [(n,d)+(n,n'p)+(n,pn)] cross sections based on the data measured at Jülich [30-32] is also shown. It is apparent that for nuclei with A $\gtrsim$ 30 the (n,d) cross section is small compared with the [(n,d)+(n,n'p)+(n,pn)] cross section. The sequential emission of a neutron and a proton is therefore more favoured than the emission of a bound deuteron. In the medium mass region, however, the (n,d) cross section almost approaches the sum of the (n,d), (n,n'p) and (n,pn) cross sections.

The (n,t) cross section for very light nuclei is exceptionally large [cf. 24,25]. First systematic studies on (n,t) reactions in the medium and heavy mass regions were carried out at Jülich [4-7]. The trends in broad terms are shown in Fig. 3. At 14.6 MeV, in general the (n,t) cross section decreases as a function of Z. The proposed rising part of the curve is due to nuclear structure effects; our Hauser-Feshbach calculations have shown (see below) that in this mass region the (n,t) reaction proceeds mainly via statistical processes, whereas in other mass regions non-statistical processes are important.

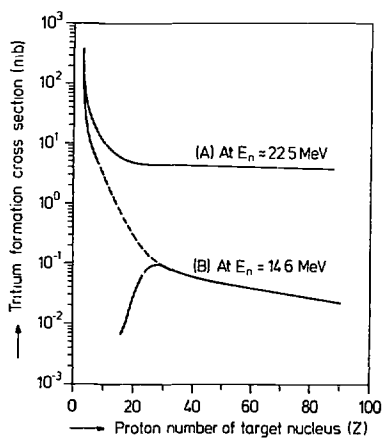

Fig. 3 Trends in tritium formation reaction cross sections. (A) With break-up neutron spectrum (E_n = 11.5-43.5 MeV; I_{max} at 22.5 MeV; FWHM = 15.8 MeV). (B) At E_n = 14.6 MeV [7].

For medium and heavy mass nuclei it was observed that the (n,t) cross section decreases rather slowly with (N-Z)/A of the target nucleus. The cross section can be described by a phenomenological formula [6],

$$\sigma(n,t) = 4.52(A^{1/3}+1)^2 \cdot \exp[-10(N-Z)/A]\,\mu b.$$

Measurements at Debrecen [17,18] on seven odd mass target nuclei gave cross-section values which are by an order of magnitude higher than the trend described above. This suggests the existence of an odd-even effect in the (n,t) cross section at 14.6 MeV for medium and heavy mass nuclei [18], somewhat similar to that for light nuclei at higher incident neutron energies [7]. In the above formula therefore an extra term should be included to take into account the odd-even effect.

Systematic studies on (n,^{3}He) reactions have been carried out mainly at Jülich [8,9]. Similar to (n,t) cross sections, a phenomenological formula has been developed to predict unknown (n,^{3}He) cross sections.

$$\sigma(n,{}^3He) = 0.54(A^{1/3}+1)^2 \cdot \exp[-10(N-Z)/A]\,\mu b.$$

The trend in (n,^{3}He) cross sections is similar to that for (n,t) cross sections; in absolute terms, however, the (n,^{3}He) cross section is by an order of magnitude smaller than the (n,t) cross section.

The gross trends in the cross sections for the four (n,charged particle) reactions investigated in rather more detail, viz. (n,p), (n,t), (n,^{3}He) and (n,α) are shown in Fig. 4. The (n,t) and (n,^{3}He) cross sections have been multiplied by a factor of 10^3 to facilitate visual comparison.

The decrease in cross section as a function of the asymmetry parameter (N-Z)/A is a characteristic feature of all the reactions in which charged particles are emitted. The (n,p) and (n,α) reactions constitute rather strong reaction channels in the light mass region. The strong decrease in their cross sections as a function of (N-Z)/A is due to the increasing competition from (n,n'γ) and (n,2n) processes. The decrease of both the (n,t) and (n,^{3}He) cross sections with (N-Z)/A is much less pronounced. Apparently the emission of ^{3}H and ^{3}He particles in the medium and heavy mass regions at incident neutron energies very near the grazing thresholds of the two reactions is relatively independent of the emission of other particles, such as n, p and α, and possibly entails substantial contributions from direct processes.

4. REACTION THEORIES AND CALCULATIONS

The differential cross-section data on the emission of deuterons, tritons and α-particles in 14 MeV neutron-induced reactions on very light nuclei have been interpreted in the light of several direct reaction theories [cf. 24-26,33,34]. The (n,d) reaction seems to proceed via direct processes in other mass regions as well [cf. 35,36]. For α-emission in the

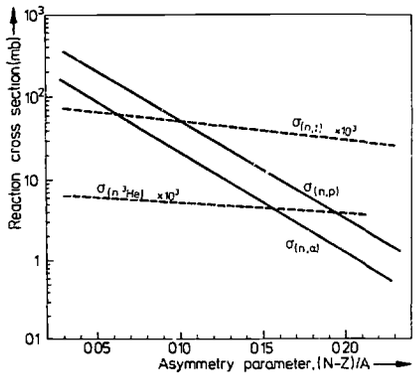

Fig. 4 Gross trends in some (n,charged particle) reaction cross sections at 14.6 MeV [9].

medium mass region multi-step Hauser-Feshbach analysis has been quite successful [cf. 28,29] whereas in the heavy mass region direct effects play an important role [cf. 37].

Attempts to interpret the integral cross-section data, i.e. those obtained by off-line methods described above, have in general been limited to the use of the statistical model. The (n,α) cross section in the mass region $20<A<80$ is described successfully by the statistical model [cf. 38]. In contrast, the (n,d), (n,t) and (n,^{3}He) reactions in the medium and heavy mass regions constitute special cases since their Q-values are highly negative. A schematic representation of the energy scale involved in those reactions is shown in Fig. 5. Most of the transitions occur to the discrete states of the product nucleus. The total width for the decay of the compound nucleus into all open channels must therefore be split into two parts, thus replacing the summation over transmission coefficients of discrete levels by an integration over level densities at the beginning of the continuum region. Another important factor is the choice of the optical model parameters; in general for low energy tritons and ^{3}He-particles such parameters are not known with high accuracies. Despite these limitations recently Sudar and Csikai [18] calculated (n,t) cross sections for several target nuclei and Qaim et al [39] gave an analysis of (n,t), (n,^{3}He) and (n,d) reaction cross sections in the mass region 27 to 59. It was concluded by Qaim et al [39] that the (n,t) reaction on target nuclei in the (2S,1d) shell seems to proceed predominantly via statistical processes; for heavier nuclei non-statistical contributions become important. In the case of (n,d) and (n,^{3}He) reactions non-statistical contributions appear to be significant for all the nuclei.

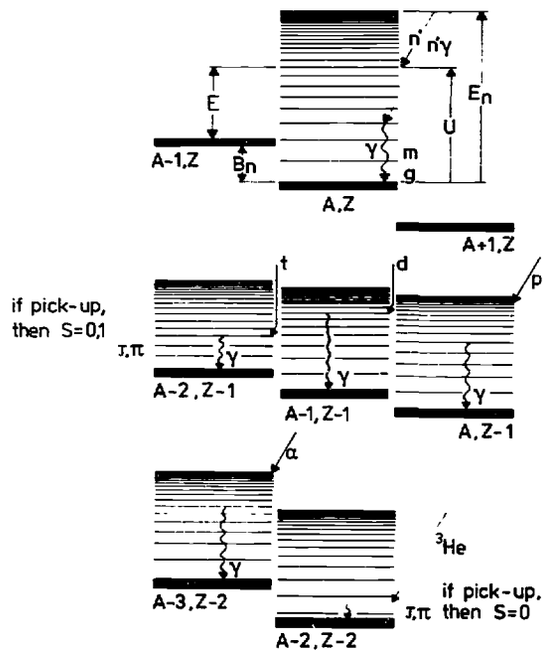

Fig. 5 Schematic representation of the energy scheme of (n,n'), (n,2n), (n,p), (n,d), (n,t), (n,^{3}He) and (n,α) reactions.

5. PRACTICAL APPLICATIONS

In addition to their importance for an understanding of nuclear theory, studies of neutron-induced nuclear reactions involving the emission of complex particles are of value in reactor technology, especially for design calculations in fusion reactor technology (FRT). Some of the areas demanding such studies are discussed below.

5.1 Tritium Breeding

Most of the recently developed FRT-concepts are based on a dt burner and aim at self-breeding of tritium via (n,t) reactions on lithium. An accurate knowledge of the cross sections of the two tritium producing reactions $^{6}Li(n,t)^{4}He$ and $^{7}Li(n,n't)^{4}He$ is therefore most essential. The excitation functions of those reactions, taken from the ENDF/B IV file, are shown in Fig. 6. Whereas the cross-section data for the $^{6}Li(n,t)^{4}He$ reaction are known with adequate accuracy, there are some discrepancies in

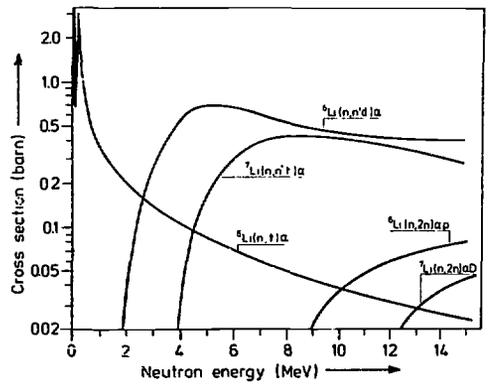

Fig. 6 Excitation functions of tritium producing and some competing reactions on ^{6}Li and ^{7}Li.

the case of the $^{7}Li(n,n't)^{4}He$ reaction. A recent measurement at Harwell [40] gives $^{7}Li(n,n't)^{4}He$ cross-section values which, in the energy range of 5.5 to 14 MeV, are lower than the ENDF/B IV values by about 25%. If true, this will adversely affect the tritium breeding ratio in a blanket. A careful measurement of the excitation function is therefore underway at Argonne and as a Geel-Jülich collaboration.

For estimating neutron losses in the blanket it is also essential to know the cross sections of the competing non-tritium producing reactions. As can be seen in Fig. 6, cross sections for some of the non-tritium producing reactions have been determined. Further investigations, however, are necessary.

5.2 Radiation Damage

Radiation damage in metals originates from two sources, viz. displacement of atoms from their normal lattice sites and the formation of foreign atoms via nuclear transmutations. As far as the displacement damage is concerned, even with 14 MeV neutrons the major contribution is furnished by (n,n), (n,n') and (n,2n) processes. Nuclear transmutations give rise to foreign elements, and more seriously, to hydrogen and helium gas production via (n,xp) and (n,xα) reactions. The latter is normally not a very serious phenomenon at relatively low neutron energies but is expected to be one of the major sources of radiation damage in the case of fast neutrons such as those anticipated in a fusion reactor.

The radiation damage effects manifest themselves in phenomena such as bulk swelling, radiation-enhanced creep, radiation-enhanced self diffusion and gas-produced embrittlement. For an interpretation of the radiation damage effects at 14 MeV a knowledge of the (n,p), (n,n'p), (n,d), (n,α) and (n,n'α) cross-section data is essential [41].

5.3 Activation and Nuclear Heating

Activation of reactor components constitutes a serious problem in reactor technology. An estimation of the induced radioactivity is essential to assess the practical problems associated with plant maintenance, radioactive waste disposal and reactor safety. It also enables one to calculate nuclear afterheat. Cross sections of all the energetically possible reactions leading to the formation of radioactive products, especially long-lived radioisotopes, are needed.

The energy and momentum balance calculations necessary for estimating KERMA (kinetic energy released in matter) factors

for nuclear heating calculations require an accurate knowledge of individual reaction cross sections, Q-values and energy and angular distributions of emitted particles and photons. Since local energy deposition is sensitive to charged-particle producing reactions, data needs for those reactions are imminent.

CONCLUSIONS

Activation technique in combination with radiochemical separations constitutes a very sensitive method for measuring integral cross sections of fast neutron-induced nuclear reactions. It is of special significance for studying the emission of complex particles. Mass spectrometry has also been used successfully for estimating helium isotopes. The recent data obtained by on-line particle detection as well as off-line activation and mass spectrometric methods are in good agreement. The cross sections of all the (n,charged particle) reactions decrease with increasing Z and (N-Z)/A. In complex particle emission both statistical and non-statistical processes are involved. The cross-section data are of practical importance for design calculations in fusion reactor technology.

REFERENCES

[1] S.M. Qaim, Proc.Int.Conf.Neutron Physics and Nuclear Data for Reactors and other Applied Purposes, Harwell, September 1978, (NEA, Paris, 1979) p. 1088
[2] H. Vonach, these Proceedings
[3] J. Csikai, these Proceedings
[4] S.M. Qaim and G. Stöcklin, J.Inorg.Nucl.Chem. 35 (1973) 19
[5] S.M. Qaim, R. Wölfle and G. Stöcklin, J.Inorg.Nucl.Chem. 36 (1974) 3639
[6] S.M. Qaim and G. Stöcklin, Nucl.Phys. A257 (1976) 233
[7] S.M. Qaim and R. Wölfle, Nucl.Phys. A295 (1978) 150
[8] S.M. Qaim, J.Inorg.Nucl.Chem. 36 (1974) 239
[9] S.M. Qaim, Radiochimica Acta 25 (1978) 13
[10] C.H. Wu, R. Wölfle and S.M. Qaim, Nucl.Phys. A329 (1979) 63
[11] E. Ricci, J.Inorg.Nucl.Chem. 27 (1965) 41
[12] S.M. Qaim, R. Wölfle and G. Stöcklin, J.Radioanalyt.Chem. 21 (1974) 395
[13] S.M. Qaim, R. Wölfle and G. Stöcklin, J.Radioanalyt.Chem. 30 (1976) 35
[14] S.M. Qaim, H. Ollig and G. Blessing, Radiochimica Acta 26 (1979) 59
[15] S.M. Qaim, Radiochem.Radioanalyt.Letters 25 (1976) 335
[16] S.M. Qaim, A. Rusheed, G. Stöcklin and R. Wölfle, Int.J.appl. Radiat.Isotopes 28 (1977) 585
[17] T. Biro, S. Sudar, Z. Miligy, Z. Dezsö and J. Csikai, J.
[18] S. Sudar and J. Csikai, Nucl.Phys. A319 (1979) 157
[19] R. Wölfle and S.M. Qaim, Radiochimica Acta 27 (1980) 65
[20] H. Michael, A. Neubert and H. Nickel, Int.J.appl.Radiat. Isotopes 25 (1974) 183
[21] H. Farrar IV, W.N. McElroy and E.P. Lippincott, Nucl.Techn. 25 (1975) 305
[22] D.W. Kneff, B.M. Oliver, M.M. Nakata and H. Farrar IV, Proc.Symp.on Neutron Cross Sections from 10 to 50 MeV, Brookhaven, May 1980, BNL-NCS-51245 (1980)
[23] D.W. Kneff, H. Farrar IV, L.R. Greenwood and M.W. Guinan, Proc.Symp.on Neutron Cross Sections from 10 to 50 MeV, Brookhaven, May 1980, BNL-NCS-51245 (1980)
[24] D. Rendic, in Few Body Problems, Light Nuclei and Nuclear Interactions, Vol. 2 (Gordon and Breach, N.Y. 1968) p. 485
[25] D. Miljanic, V. Valkovic, D. Rendic and M. Furic, Nucl. Phys. A156 (1970) 193
[26] D. Miljanic and V. Valkovic, Nucl.Phys. A176 (1971) 110
[27] S.M. Grimes, R.C. Haight, J.D. Anderson, K.R. Alvar and R.R. Borchers, Proc.Symp.Neutron Cross Sections from 10 to 40 MeV, Brookhaven, May 1977, BNL-NCS-50681 (1977) p. 297
[28] S.M. Grimes, R.C. Haight and J.D. Anderson, Phys.Rev. C17 (1978) 508
[29] S.M. Grimes, R.C. Haight, K.R. Alvar, H.H. Barschall and R.R. Borchers, Phys.Rev. C19 (1979) 2127
[30] S.M. Qaim and G. Stöcklin, Proc. 8th Symp.Fusion Technology, Noordwijkerhout, June 1974, EUR 5182e (1974) p. 939
[31] S.M. Qaim and N.I. Molla, Proc. 9th Symp.Fusion Technology, Garmisch-Partenkirchen, June 1976, EUR 5602 (1976) p. 589
[32] S.M. Qaim and G. Stöcklin, Proc.Specialist Meeting on Neutron Data of Structural Materials for Fast Reactors, Geel, December 1977 (Pergamon-Press, London, 1979) p. 327
[33] M. Brendle, R. Enge and G. Steidle, Z.Physik A285 (1978) 293
[34] M. Mörike, G. Staudt and F. Weng, Z.Physik A287 (1978) 211
[35] E. Rosario-Garcia and R.E. Benenson, Nucl.Phys. A275 (1977) 453
[36] D.C. Palmer, D.R. Maxson and J.R. Bading, J.Phys.G.: Nucl. Phys. 3 (1977) 1363
[37] L. Glowacka, M. Jaskola, J. Turkiewicz, L. Zemlo, M. Kozlowski and W. Osakiewicz, Nucl.Phys. A244 (1975) 117
[38] N. Cindro, Acta Phys. Slovaca 25 (1975) 158
[39] S.M. Qaim, H.V. Klapdor and H. Reiss, Phys.Rev. C21 (1980) in press
[40] M.T. Swinhoe and C.A. Uttley, NEANDC(E) 202 U Vol. 8, INDC(UK) 31/LN (1979) p. 54, and private communication
[41] S.M. Qaim, Proc. of the Advisory Group Meeting on Nuclear Data for Fusion Reactor Technology, Vienna, December 1978, IAEA-TECDOC-223 (1979) p. 75

EXPERIMENTAL METHODS FOR INVESTIGATION OF (N, P) AND (N, α) SPECTRA AND ANGULAR DISTRIBUTIONS

H. VONACH
Institut für Radiumforschung und Kernphysik,
Österreichische Akademie der Wissenschaften,
Vienna, Austria

ABSTRACT

The various methods for investigation of angular and energy distributions of charged particles from neutron induced nuclear reactions are reviewed. The design of counter telescopes and multi-telescope systems for this purpose is discussed and the properties of a number of such measuring systems designed in the last decade are compared in detail.

1. Outline of the general problems

Energy and angular distributions of charged particles from (n,p) and (n,α) reactions have been investigated since about 25 years, nevertheless there is still a lack of adequate results for many nuclei, especially in the region of A > 70, and very few measurements have been done at all for neutron energies other than 14-15 MeV. This is due to specific experimental difficulties which can be discussed most easily by looking at Fig. 1 showing schematically an experimental setup for such measurements.

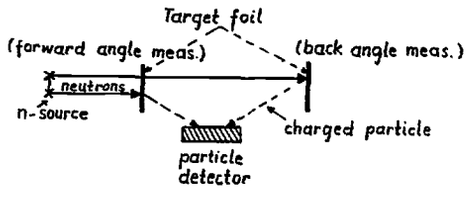

Fig. 1. Basic experimental set-up for study of charged particle spectra from neutron-induced reactions

The two main problems are:

1) Very low event rate because of
   a) necessity of rather thin target foils in order to get reasonable energy resolution, as the charged particle spectra extend to rather low energies (1-2 MeV p, 2-3 MeV α) in many cases
   b) rather small production cross-sections ($\sim$ 1-100 mb)
   c) either a rather large source-target distance is necessary if a shielded detector is used or only rather small neutron source strengths are permitted in case of unshielded detectors.

   Due to these circumstances the ratio of detected charged particles to the number of source neutrons amounts to 10^{-11} - 10^{-14}.
2) The background from neutron-induced events in the detector due to (n,n'γ), (n,p) and (n,α) reactions in the detector material itself and its surrounding is much higher than the true events rate (for an unshielded detector by a factor of 10^3-10^6) necessitating the use of special techniques for background suppression and an efficient shielding of the detector. In general the conditions for low background and for high event rate are contradicting each other.

   Thus the design of an experimental system for the study of charged particle spectra amounts essentially to optimization of the event rate at a given energy resolution and background level.

2. Early approaches

The first studies of charged particle spectra used nuclear emulsions as charged particle detectors [1-4]. Although p/α discrimination is possible by means of special development techniques [2] and efficient background reduction can be achieved by careful inspection of the tracks (e.g. for the criteria of origin at the surface and track direction), the method was abandoned because of the very time-consuming scanning work as soon as electronic detection techniques became comparable in quality about 15 years ago.

Essentially three types of measuring systems were used which are shown schematically in Fig. 2. In the simplest systems (Fig. 2a) a CsI scintillation crystal shielded against the source neutrons by about 20 cm of brass was used [5,6]. As both Cs and I have very low (n,p) and (n,α) cross-sections and in addition CsI has excellent pulse-shape properties which allow γ-p-α discrimination down to about 1 MeV proton energy, successful measurements were possible with this very simple system for (n,α) cross-sections in the 100 mb range. Lateron Bormann[7] achieved a further background reduction measuring the associated α-particles corresponding to the neutron cone hitting the target foil and rejecting all events not coincident with a corresponding associated α-particle.

In this way (n,α) reactions with cross-sections as low as 5 mb could be measured (Fig. 2b).

Most of the measurements, however, have used a third approach, the so-called counter telescope [8-19] as shown in Fig. 2c.

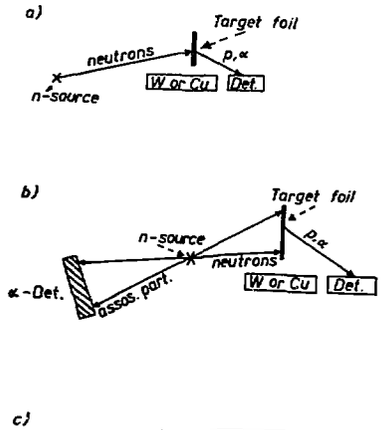

Fig. 2. Main types of experimental systems for study of (n,p) and (n,α) charged particle spectra
(a) shielded CsI detector
(b) shielded CsI detector + assoc. part. coincidence
(c) counter telescope

In this system the charged particles emitted by the target foil traverse at first one to three thin so-called $\frac{dE}{dx}$ detectors, mostly proportional counters until they are finally stopped in an E detector thick compared to their range. No shielding is used in most cases. Background reduction and particle identification is achieved by demanding coincidences between the E and the dE/dx counters and reaccepting only pulses located in the appropriate regions of the $E - \frac{dE}{dx}$ plane.

Finally it is to be mentioned that simple unshielded Si-detectors have been used for the study of the high energy parts of the α-spectra from heavy nuclei, which due to the large positive Q-values are well above the highest α-energies produced by (n,α) reactions in the Si-detector itself [20-22].

Though rather different in their designs the results achieved with the above systems are rather similar as to quality. All of them suffer from extremely low event rates. Even with modest energy and angular resolution (see table 3) typical true event rates were ∿ 0.01 sec^{-1} and background remains a problem.

Higher count-rates and thus measurements with good statistical accuracy have been obtained for these nuclei which are constituents of charged particle detectors like Na, Si, K, Cs and I.

In these cases the target served simultaneously as charged particle detector. In this way the count rates are increased by 2-3 orders of magnitude compared to systems discussed before, but of course only angle integrated energy spectra are obtained [7, 23-30] except for Si where by means of coincidences between two Si-detectors also angular distributions could be measured [30].

3. The classical telescope

As mentioned in the previous section, the standard method for the study of (n,α) and (n,p) spectra in the last two decades has been the use of the counter telescope [8-19] and it is the basis of the more recently developed system to be discussed in the next section. Therefore I will discuss this instrument in some detail in this section. As an example Fig. 3 shows one of the more sophisticated designs, the telescope developed by Shirato and Koori [12].

Charged particles from the target foil traverse two (or in the case of Fig. 3 three) dE/dx detectors and are finally stopped in a detector thick compared to their range, mostly a Si-detector or CsI scintillator. True events are identified by a triple coincidence between the proportional counters and the final E-detector and particle identification is done by means of the relations between the E and dE/dx detectors respectively. A further reduction in background is achieved in some designs (like that of Fig. 3) by means of a so-called veto counter behind the target foil operated in anticoincidence to eliminate charged particles originating in the E-counter and traversing the telescope backwards.

Table 1 summarizes the most important properties of a number of such telescopes reported in the literature.

Concerning the choice of the different design parameters (see table) the following can be said:

a) Choice of E-detector: No clear preference can be given to either the Si surface-barrier or CsI scintillation detectors. On the one hand CsI has much smaller (n,p) and (n,α) cross-sections than Si (see table 2), and allows pulse shape discrimination between photons, protons and α-particles down to energies as low as 1 MeV protons, on the other it shows a non-linear pulse-height response for α-particles and has a much lower energy resolution than a Si-detector. This advantage, however, cannot be exploited in most cases as for intensity reasons rather thick targets have to be used which limit the energy resolution to about the value obtainable with CsI anyway. For the study of α-spectra Si-detectors have the additional advantage that the effective counter thickness can be adjusted very easily to the maximum α-range by proper bias setting. Thus so far mostly CsI crystals have been used for measurements of proton spectra whereas in the study of α-spectra there is a definite trend to the use of Si-detectors.

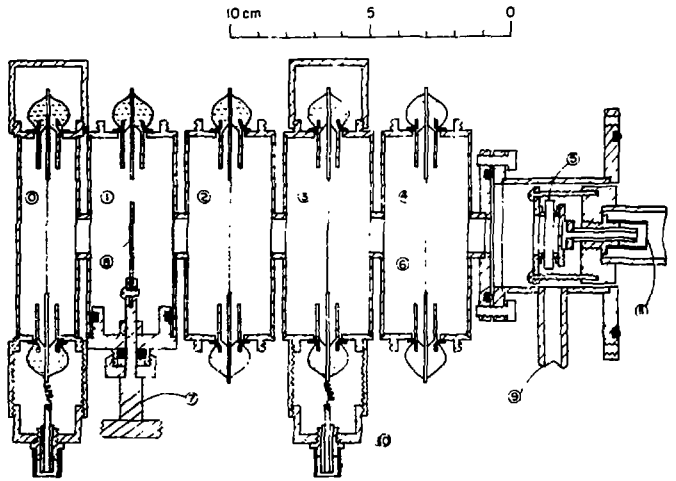

Fig. 3. Counter telescope designed by Shirato and Koori (12): Vertical cross-section of the tandem dE/dx - E-counter-telescope. (0) Anticoincidence proportional counter. (1) Target room for the solid target shown as (8) or a proportional counter for the gas target. (2) - (4) dE/dx proportional counters. (5) Lithium-drifted silicon detector. (6) Counter wire of stainless steel 0.015 cm in dia. (7) Target wheel. (9) Gas filling tube. (10), (11) BNC-connectors. (Fig. 1 of ref. 12)

b) Choice of $\frac{dE}{dx}$ detector: Proportional counters have been used in most cases as they are inexpensive and can easily be adjusted to any telescope geometry; gas pressures of about 100-200 mbar and counter dimensions of a few cm are generally used as this results in an energy loss sufficient to separate p, d and α-particles in the $\frac{dE}{dx}$ spectrum and low enough to transmit also the low energy parts of the particle spectra.
Pure CO_2, mixtures of Ar with about 5 to 10% CO_2 or CH_4 and in one case Xe have been successfully used. As charged particles produced in the counter gas by neutron induced reactions near the target foil cannot be distinguished by the telescope from true events, (n,p) and (n,α) cross-sections and Q-values are very important for the choice of the counter gas. These values are summarized in table 2 together with the same data for the nuclei used in the E-detectors. As the table shows CO_2 is a very good choice for investigation of protons due to the highly negative (n,p) Q-values, but it does produce an appreciable α-background at lower energies, CH_4 produces a rather large proton background whereas Ar + some % CO_2 probably gives the lowest overall background.

The main drawback of the proportional counters is their bad time resolution which makes it necessary to use coincidence resolving times of 0.5 - 1 μsec in most designs and chance coincidences are therefore one of the factors limiting the maximum admissible neutron flux.

An improvement in this respect is possible by decreasing the telescope dimensions thereby reducing the drift times in the proportional counters. Using this approach the University of Tübingen group succeeded in achieving practically 100% efficiency with a coincidence resolving time of only 0.1 μsec [15].

A further reduction of the resolving time to about 0.02 μsec can be obtained if the proportional counters are replaced by parallel plate avalanche counters [16]. However, in the present design considerable additional background is produced by the electrode foils needed for the counters and it is mainly useful for studies of the high energy parts of the α-spectra above the $^{16}O(n,\alpha_o)$ energy.

Recently also thin (30 μ) solid state detectors of sufficient size (up to 300 mm^2) have also been used successfully as dE/dx detectors in the Ohio State Univ. Triplett quadrupole spectrometer [41]. In this way the time resolution can also be very much improved (to a few nsec), however, due to its price and sensitivity the use of such detectors will probably be restricted to shielded telescope systems.

c) Wall materials and background: The wall materials for all parts of the telescope have also to be chosen for minimum proton and α-production cross section. Either graphite (essentially no proton emission) or heavy elements like Pb, Ta or Au have been used. The optimum solution is probably graphite covered with a gold foil just thick enough to absorb the rather low energy α-particles from the $^{12}C(n,\alpha)$ and $^{12}C(n,n'3\alpha)$ reactions. As backing of the target itself even such a graded backing may produce background problems if (n,p) and (n,α) reactions on heavy elements are to be investigated and in this case the use of a self-supporting target foil and a veto counter (see Fig. 3) behind it is the best solution.
d) Energy and angular resolution: In order to achieve even count-rates of 10^{-2} sec^{-1} in general solid angles of 50 - 100 msr and target thickness of some mg/cm^2 have to be used resulting in a typical angular resolution of 15-20° and energy resolution of 0.5 - 1 MeV.
e) Maximum admissible neutron source strength: Admissible single count-rates (in order to keep pulse-pile up in tolerable limits) in both the dE/dx and E-detectors and background due to chance coincidences limit the maximum neutron flux at the telescope position to about 10^5-10^6 n/sec (see table 1); details on which effects actually limit the admissible neutron source strength are not given in most papers.
f) Background: In all telescopes there are about 4 sources of background of comparable magnitude:
   A) charged particles produced by (n,p) and (n,α) reactions in the backing of the target foil;
   B) charged particles produced in the gas of the first proportional counter;
   C) random coincidences between pulses in the dE/dx and E-counters (mostly between pulses from the E-counter and genuine double coincidences between the dE/dx counters);
   D) charged particles produced in the E-detector traversing the telescope backwards.

Minimization of background sources has already been discussed, the number of chance coincidences can be minimized (apart from achieving the smallest possible coincidence resolving time as discussed above) by minimization of the single count-rates in all detectors by careful selection of all construction materials and use of the smallest possible detector volumes. Chance coincidences are a large problem for measurement of proton spectra as both low energy thresholds in the dE/dx detectors (because of the smaller dE/dx of protons) and thick E-detectors (because of the larger proton range) have to be used than in the case of α-particles. Few quantitive information on the various sources of background is given in most papers, some can be found in ref. [8,9].

4. Recent developments

All experimental set-ups discussed as yet can only produce very low count-rates necessitating very long running times (∼ 1000 hours per experiment). Such running times are possible if relatively cheap neutron generators can be used e.g. in 14 MeV neutron experiments. For measurements at other neutron energies, however, where more expensive accelerators in the MeV range are necessary, the cost of beam time would be excessive and therefore up to now very few (n,p) and (n,α) spectra measurements have been performed at energies other than 14 MeV except for these favourable special cases (Na, Si, Cs, I) where the detector material itself can be used as target [23-27]. In addition also at 14 MeV especially the low energy parts of the p- and α-spectra were only very poorly known.

In order to improve this situation some new approaches were followed in the last years which led to a considerable progress both in the achievable event rate and in background reduction.

a) The Livermore quadrupole spectrometer [31]:
   A schematic view of this set-up is given in Fig. 4. Charged particles produced in the target foil by (n,p) and (n,α) reactions are focussed by means of a magnetic quadrupole doublet or triplet on a counter telescope at a distance of about 2.5 m. This results in a drastic reduction of background for two reasons:
   1) Due to the focussing effect of the quadrupoles the effective solid angle of the telescope is about a factor 100 higher for charged particles than for the neutrons the intensity of which decreases simply proportional to $1/r^2$.
   2) Because of the large distance of the detector from the neutron source the whole telescope can be well shielded by shadow-bars several mean free paths thick (see Fig. 4.).

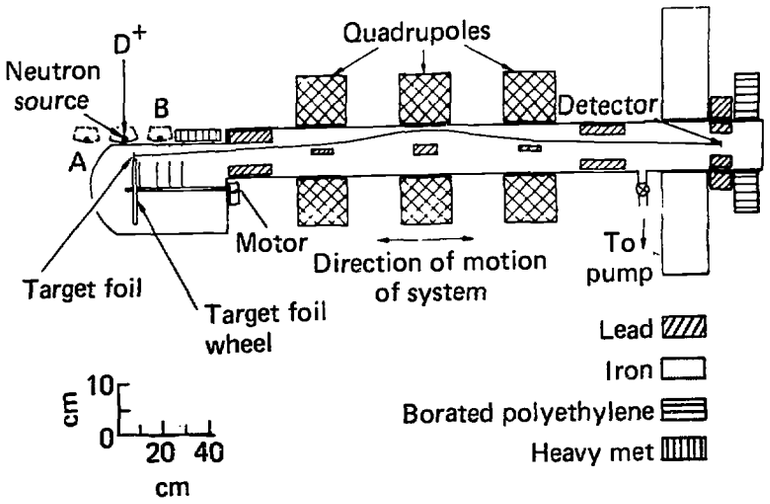

Fig. 4. Livermore quadrupole spectrometer
A typical trajectory of a charged particle from a neutron-induced reaction is shown. The entire system can be moved parallel to its axis so that charged particles emitted at different angles with respect to the incident neutron direction can be observed. Position A of the neutron source corresponds to reaction angles greater than 90° (Fig. 1 of ref. 34)

Because of these features a very close neutron source to target distance (5-10 cm) and a neutron source strength of $\sim 2.5.10^{11}$ n/sr that is about a factor of 2000 more than with conventional counter telescopes can be used while at the same time preserving a much lower background than in conventional set-ups.

These advantages are, however, partially compensated by two draw-backs:

1) The acceptance angle of the quadrupoles (see table 3) is much smaller than the solid angles achievable in conventional telescopes.
2) The quadrupole system is momentum selective and acts as an energy band pass filter and only particles within a rather narrow energy band (FWHM $\sim$ 35%) centered around the momentum selected by the particular quadrupole current setting are transmitted to the telescope. Thus

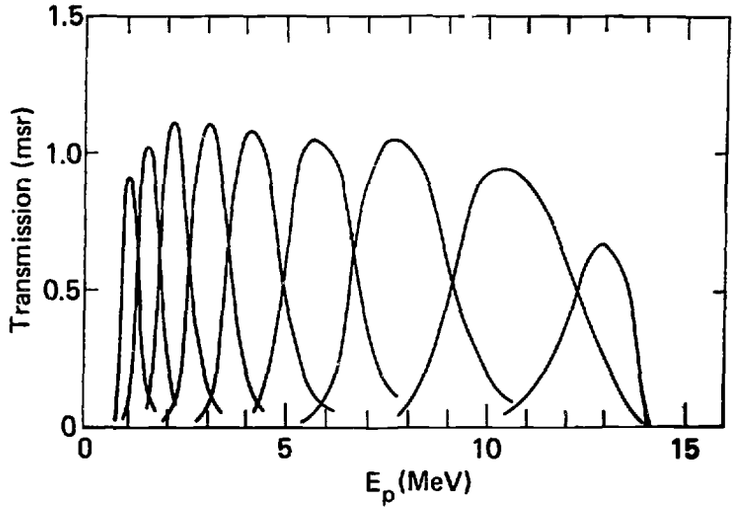

Fig. 5. Measured transmission of protons for some magnet current set-ups. The transmissions are expressed as effective solid angles for accepting protons emitted from the target foil. (Fig. 2 of ref. 34).

all data have to be corrected for this transmission function (see Fig. 5) and several (7-9) measurements at different quadrupole current settings are necessary to cover one full proton or α-particle spectrum

The discussed draw-backs compensate to a large part for the intensity gain because of the higher admissible neutron source strength.

However, in total a net gain of about a factor of 10 in count-rate could be achieved compared to conventional telescopes combined with somewhat better angular resolution and lower background especially for low energy α-particles and protons. It has up to now been successfully used for (n,p), (n,d) and (n,α) spectra and cross-section measurements on about 15 isotopes in the mass-range 27 - 93 [32-34] and it has for the first time opened the possibility for a reliable measurement of the low energy parts of the charged particle spectra due to (n,n'p) reactions. Fig. 6 shows an example of this.

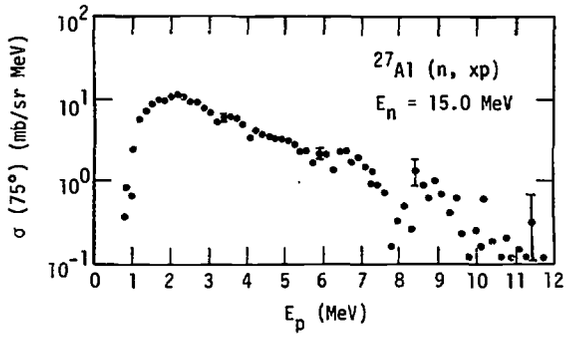

Fig. 6. Proton spectrum from the ^{27}Al(n,xp) reaction at 75°. (Fig. 3 from ref.32).

b) The Tübingen four fold telescope [35]:
By means of a very compact design the University of Tübingen has succeeded to combine four of their larger solid angle telescopes into one rather small reaction chamber as shown in Fig. 7.

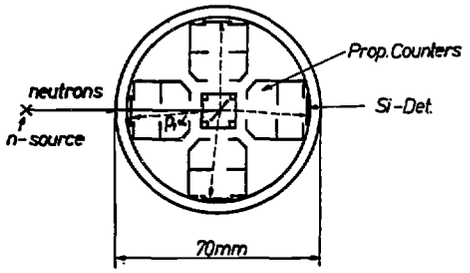

Fig. 7. The University of Tübingen four fold telescope (schematic) (Fig. 2 from ref. 35).

c) The Geel multi-telescope [36]:
This system (Fig. 8) consists of a target foil in the center of a reaction chamber containing four proportional counters and 5 Si-detectors. By imposing suitable coincidence conditions the system can be operated as 5 independent counter telescopes set at fixed reaction angles of 16.1, 52.5, 79.8, 105.4 and 141°. Because of the very compact design a large solid angle (∿ 100 msr/telescope), a tolerable energy loss in the gas (0.5-1 MeV for 4 MeV α-particles) and good time resolution (0.2-0.5 μsec) is achieved. The Si-detectors and partially also the proportional counters are shielded against the source neutrons by 20 cm of brass. This necessitates a neutron-source target distance of 30 cm, on the other hand it allows the use of much higher source strength (see table 3) and thus the system as a whole allows a count-rate of about one order of magnitude larger than conventional telescopes. It has so far been successfully used to measure the ^{58}Ni(n,α) spectra,angular distributions and integrated cross-sections for incident neutron

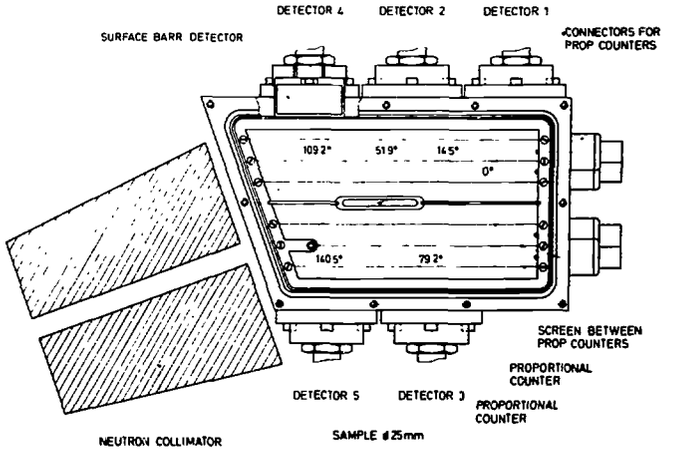

Fig. 8. The Geel multitelescope (A. Paulsen, priv. comm.)

energies of 5-10 MeV with measuring times of about 1 day/ incident neutron energy point. Fig. 9 shows an example of their data. Though designed specifically for study of α-particles it is certainly also very well suited to the study of protons from neutron-induced reactions.

d) The Vienna multiwire telescope [37] :
In this design (fig. 10) a combination of a small multiwire proportional counter and a scintillator is used, which allows simultaneously the measurement of the energy and angular distributions of charged particles of neutron-induced nuclear reactions and the determination of the background.
In a cylindrical chamber (20 cm diameter, 12 cm height) 32 counting wires are arranged around a central scintillator shielded from the source neutrons by about 30 cm of tungsten. The thin target foil is laid in a semicircle along the chamber wall outside the counting wires. A graded shield, consisting of a graphite ring and a gold foil is put behind the target foil as well as on the other half of the chamber to reduce background from the construction materials.
The origin of the charged particle is traced back by a coincidence between the central crystal and one of the counting wires. As the direction of the incoming neutrons is known, the reaction angle can be derived. On the average the angular resolution is 13 degrees at FWHM.
The energy resolution is mainly determined by the thickness of the target, the pressure of the filling gas, the distribution of path lengths in the chamber and the properties of the scintillator. The resolution varies between 0.5 and 1 MeV, depending on the energy, the type of the particle and the target thickness necessary for sufficient count-rate.
The central scintillator is a CsI(Tl) crystal (1 inch diameter, 1 mm height) and has good pulse shape properties for particle identification. Charged particles up to an energy of 20 MeV are stopped.
The proportional chamber is operated with a mixture of 90% argon and 10% CH_4 at a pressure of approximately 100 mbar, a voltage of 700 V and uses 20 μ gold coated tungsten wires as counting wires.
Fig. 11 shows the block diagram of the associated electronics. Each wire produces both an analog and a logical signal (Time-out). The logical signals are fed to an address logic, which transforms them to a bit address characterizing the different counting wires, simultaneously they are used as timing signals to identify the coincidences between the proportional counter and the scintillator pulses. The analog pulses from the proportional counters are at first combined in 4 summing amplifiers summing 8 preamplifier outputs each. The output of these

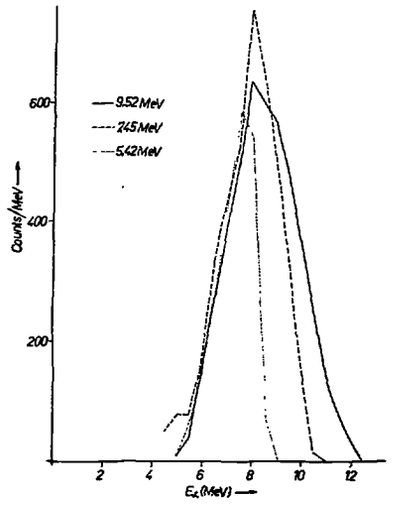

Fig. 9. Energy spectra from nat. Ni (3 mg/cm^2) at 79° and various neutron energies as measured with the Geel multitelescope (A. Paulsen, priv. comm.)

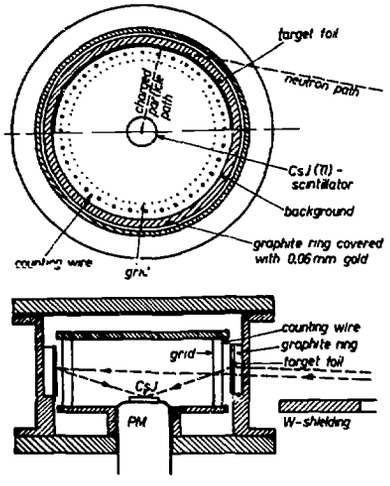

Fig. 10. The Vienna multiwire telescope a) top view b) side view

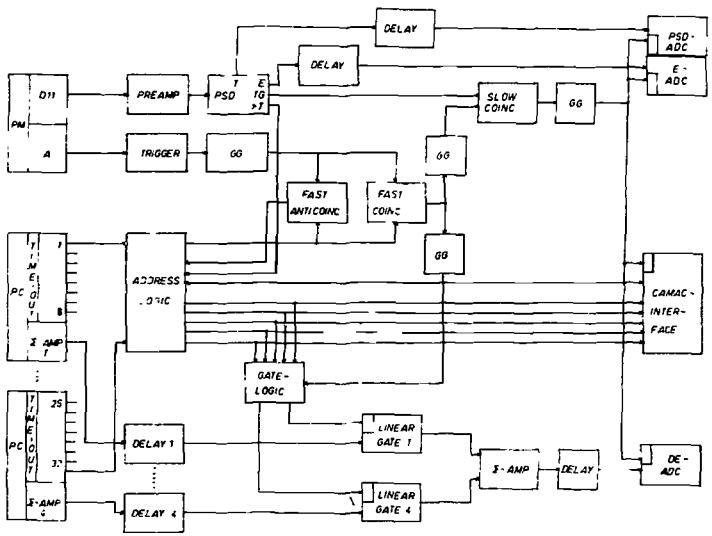

Fig. 11. Block diagram of the electronics for the multiwire proportional-counter-scintillator system.

summing amplifiers are fed into linear gates, which are opened in case of coincidence with the scintillator and eventually all proportional counter signals are combined in a final summing amplifier. By means of this arrangement 4 times higher counting rates can be admitted to the proportional counter outputs (DE signals) in one summing amplifier. The CsI scintillator is used to produce a timing signal, an energy (E) signal and a pulse-shape-signal (PSD) which allows to discriminate between photons, protons and α-particles.
Finally for each valid event the E, PSD and DE signals and the wire address are stored sequentially in an on-line computer enabling simultaneous measurement of the energy and angular distribution of all kinds of charged particles emitted by the investigated target. Particle identification is done both by means of PSD information in the CsI scintillator and the dE/dx information of the proportional counters.

5. Comparison of presently existing systems, their possible further developments and applications to neutron energies different from 14 MeV

In order to see the possibilities resulting from the new developments more clearly the main properties of the discussed systems are summarized in table 3 and compared both with each other and with the conventional systems used up to a few years ago. In the table we compare the count-rates achievable for one specific example.
a) under the assumption that each system can be used with its specific maximum admissible neutron source strength (this would be the realistic situation for 14 MeV neutron energy)
and
b) for the case that the neutron source output is restricted to values lower than 10^9 n/cm²sr (which is the experimental situation for most neutron energy regions except the 14-15 MeV range).
As the table shows, for 14 MeV both the quadrupole spectrometer and the multitelescope and multiwire telescope do achieve an event rate of about one order of magnitude higher than all previous systems, comparable background measurements are at present not yet available but it appears that probably in this respect the quadrupole spectrometer (at least if used with the low area Si-Si telescope) is superior to the multi-detector systems. Thus at present the combination of the Livermore quadrupole spectrometer with the Livermore intense neutron generator is probably the most powerful system for study of charged particle spectra at 15 MeV, although the difference to the multi-detector systems which do not need the extremely high neutron flux is not very large except for lowest charged particle energies.

For other neutron energies, however, it has to be kept in mind, that at present and in near future neutron source strength will be restricted to $< 10^9$ n/sr. If this feature is used to calculate the event rates (Z_2 in table 3) it becomes obvious that the quadrupole spectrometer in its present form loses its merits and produces event rates even lower than simple counter telescopes even for the large solid angle version. The multidetector systems on the other hand retain their superiority and can be expected to enable (n,p) and (n,α) energy and angular distribution studies in the whole energy range of about 5 - 20 MeV with event rates of about 0.1 sec^{-1}.

It seems, however, possible to design an achromatic large solid magnetic charged particle transport system and combine this with a conventional telescope. Such a system would retain the main advantage of the quadrupole spectrometer, the very low background (because of the large distance of the telescope and the neutron source) and at the same time an increase of the count rate by a factor

of about 100 against even the high solid angle version of the Livermore quadrupole spectrometer. Such an instrument would at equal source strength produce about equal count-rates as the multi-telescope and operate at much more favorable background conditions.

The simplest way to implement such a achromatic large solid angle magnetic transport system would be 1 - 2 m superconducting solenoid with a field of about 50 KG and diameter of 10 cm similar to that used in the myon channel at SIN [40].

Literature

1. D.L. Allan, Nucl. Phys. 6, 464 (1958)
2. W. Patzak and H. Vonach, Nucl. Phys. 39 (1962) 325
3. M. Cevolani et al., Nuov. Cim. 16 (1960) 950
4. C.J.D. Jarvis, W.R. Dixon and R.S. Storey, Nucl. Phys. 44 (1963) 680
5. U. Seebeck and M. Bormann, Nucl. Phys. 68 (1965) 387
6. H. Palme, Thesis,Univ. of Vienna,1970
7. M. Bormann et al., Nucl. Phys. A186 (1972) 65
8. R.N. Glover, K.H. Purser and E. Weigold, Nucl. Instr. Meth. 10 (1961) 343
9. L.G. Kuo, M. Petravic and B. Turko, Nucl. Instr. Meth. 10 (1961) 53
10. W.N. McDicken and W. Jack, Nucl. Phys. 88 (1966) 457
11. T. Knellwolf and J. Rossel, Helv. Phys. Acta 39 (1966) 379
12. S. Shirato and N. Koori, Nucl. Instr. Meth. 57 (1967) 325
13. M. Irfan and W. Jack, Proc. Phys. Soc. 81 (1963) 800
14. D.R. Maxson, R.D. Murphy and M.R. Zatzick, Nucl. Phys. A110 (1968) 609
15. M. Brendle, M. Mörike, G. Staudt and G. Steidle, Nucl. Instr. Meth. 81 (1970) 141
16. H. Brede, Z. Physik 254 (1972) 364
17. I. Sick et al., Helv. Phys. Acta 41 (1968) 573
18. R.R. Wagner and R.A. Peck, Nucl. Phys. A110 (1968) 81
19. I.M. Turkiewicz et al., Nucl. Phys. 77 (1966) 276
20. M. Jaskola et al., Nucl. Phys. 53 (1964) 270
21. M. Jaskola et al., Nucl. Phys. A110 (1968) 11
22. A. Augustyniak et al., Proc. 8th Int. Symp. on Interaction of Fast neutrons with Nuclei, 1979, Gaussig, DDR
23. G. Wölfer and M. Bormann, Z. Physik 194 (1966) 75
24. C.M. Bartle, Nucl. Instr. Meth. 124 (1975) 547
25. R.G. Miller and R.W. Kavanagh, Nucl. Instr. Meth. 48 (1967) 13
26. D.W. Mingay, J.F.P. Sellshop and P.M. Johnson, Nucl. Instr. Meth. 94 (1971) 497
27. P. Plischke, W. Scobel and M. Bormann, Z. Physik A281 (1977) 245
28. P. Forti, E. Gadioli and A. Marini, Nuov. Cim. 41 (1966) 244
29. B. Leroux et al., Nucl. Phys. 67 (1965) 333
30. H. Morgenstern, D. Hilscher and I. Scheer, Nucl. Phys. 83 (1966) 369
31. K.R. Alvar, H.H. Barshall, R.R. Borchers, S.M. Grimes and R.C. Haight, Nucl. Instr. Meth. 148 (1978) 303
32. S.M. Grimes, R.C. Haight and I.D. Anderson, Nucl. Sci. Eng. 62 (1977) 187
33. S.M. Grimes, R.C. Haight and I.D. Anderson, Phys. Rev. C17 (1978) 508
34. S.M. Grimes et al., Preprint UCRL-81802 (1978), Phys. Rev. C (in press)
35. M. Mörike, B. Schilling and G. Staudt, Nucl. Instr. Meth. (to be submitted)
36. A. Paulsen, priv. comm.
37. C. Derndorfer, R. Fischer, P. Hille, G. Stengl and H. Vonach, Nucl. Instr. Meth. (to be published)
38. Handbook on Nuclear Activation Cross-Section, IAEA Technical Report Series Nr. 156, Vienna 1974
39. BNL 325, 3rd Edition Vol. II, Brookhaven 1976
40. G. Vecsey, I. Horvath and J. Zellweger, 5th Int. Conf. on Magnet Technology, Rome 1975
41. P. Grabmayr, priv. comm.

Table 1 Comparison of characteristic parameters of various counter telescopes used in the study of (n,p) and (n,α) reactions

Ref.	8	9	10	11	12	13	14	15	16	18
Components	P.C.-P.C. -Sz + assoc. part.coinc.	PC-PC -Sz + Veto. C.	PC-PC -Si	PC-PC -Si	PC-PC -PC-Sz + Veto	PC-Sz	PC-PC - Si	PC-PC - Si	PPC-PPC - Si + PPC Veto	PC-PC CsJ
Prop. Counter										
counting-gas	90% Ar + 10% CO_2	CO_2	Ne + 4% CH_4	CO_2	Ar + 5% CO_2	Ar + 10% C_3H_3	Ar + 5% CO_2	CO_2	CO_2	Ar + 5% CO_2
pressure (mb)	150	60-140	300-1000	25	80-180	120	140	200	100	220
length traversed by part (mm)		40/120	15/15	20/88	30/30/30	10	30	12.5/12.5	10/10	40/40
wall material	C	C	Au	C	Au	C + 50 μPb	Pb	Ta(C + 12μAu)	Plexi	Pb
E-counter										
Kind	NaJ	CsJ	Si	Si	Si	CsJ	CsJ	Si	Si	CsJ
Thickness (mm)		2		0.145	2	90mg/cm^2	0.14	$R_{\alpha Max}$	$R_{\alpha Max}$	1.2
effect.area(cm^2)	5	10	1.13	4.5	1.13		4.0	0.5	0.5	1.0
En.resolution	5.5% for 14 MeV P	3% for 13MeV P		0.13MeV f. 8.8 MeVα	3.3% f. 14MeV P	8% for 10MeVα	∿1MeV f. 12MeVα	0.1MeV f. 5.5 MeV α	0.13 f. 5.5 MeV α	
Geometry										
source-target dist. (cm)	13.1	10	10	5-10	11.2	0.4-7.0	70-100	5.0-6.5	7.6	8
Target area(cm^2)	5	3	2	7	1.2	1.8	3	0.5	0.5	2

Table 1 Cont.

solid angle of telescope (msr)	22	19	70	20	5	110	27	70	70	5
total angular resolution (FWHM)	8-14°	∿15°	∿18°	15-20°	5°	100°	∿17°	∿16°	∿16°	6-14°
Misc.										
Max.admissible n-source stren. (n/sr.sec)	6.10^7	$\sim 10^8$	4.10^8			4.10^7		$\sim 10^8$	4.10^8	8.10^7
time resolution (μSec)	1.2	1.0		∿2	∿ 0.5	2.5		0.1	0.02	
$E_{min\ \alpha}$								∿2 MeV	∿3 MeV	
$E_{min\ p}$	2 MeV	2 MeV			∿2 MeV					2 MeV
actually meas. part.-spectra	p,d	p,d,α	α with E>8MeV	α	p,d,α	α	α	α	α	p,d
σ_{min} (mb/srMeV)	0.1-0.3 f. prot.					0.04-0.1 α				
shielding	no	no	6cm W 50% backg.	no	no	no	no	no	no	no
background	detailed inf.given	detailed inf.given ∿0.1/sec P above 15 MeV at 10^8 n/s	reduction no inf.	no inf.	qualit. inf.	no inf.		qualit. inf.	qualit. inf.	no inf.

PC = proportional counter
Sz = szintillation crystal
PPC = parallel plate avalanche counter

Table 2 14 MeV cross-sections and Q-values for the main constitents of the E and $\frac{dE}{dx}$ detectors in counter telescopes

Nuclide	Q(n,p) (MeV)	σ(n,p) (mb)	Ref.	Q(n,α) (MeV)	σ(n,α) (mb)	Ref.
^{1}H	0	690	39	-	-	-
^{12}C	- 12.7	< 1	39	- 5.7 (-8.2 f.(nn'3α))	∿ 70 (nn'3α)∿ 150	39
^{16}O	- 9.6	40	38	- 2.2	300	39
^{40}Ar	- 6.8	16	38	- 2.5	10	38
Xe	+ 0.6 - -3.4	2 - 7	38	+ 2 - + 7	< 2*	
^{28}Si	- 3.9	230	38	- 2.7	∿ 180	26
^{29}Si	- 2.9	120	38	0.0	probably ∿ 100*	
Cs	+ 0.1	∿ 5	38	+ 4.4	∿ 1 mb	38
J	+ 0.4	∿ 10	38	+ 4.3	∿ 1 mb	38

* own estimate from systematics

Table 3 Comparison of different contemporary systems for study of neutron-induced charged particle emission

SYTEM	source-target dist. R (cm)	target area F_2 (cm^2)	solid angle (msr)	max.n-source strength (n/sr)	ang. res. (FWHM, degrees)	n-shield	M**	Z_1 (sec^{-1})	Z_2 (sec^{-1})
typical counter telescope [15]	6.5	0.5	70	10^8	$\sim 20^o$	none	1	0.0066	0.0066
shielded CsJ detector [7]	20	8	100	5.10^7	$\sim 25^o$	10 cm Pb + 9cm brass	1	0.0080	0.0080
Tübingen four fold telescope [35]	6.5	0.5	280	10^6	$\sim 20^o$	none	1	0.0264	0.0264
Livermore quadrupole spectr. [31]	5 - 10	3	0.3 a) 2.5 b)	$2.5.10^{11}$			8 a) 6 b)	0.039 a) 0.432 b)	0.00016 a) 0.00172 b)
Geel multitelescope [36]	30	5	500	10^9	$\sim 15-30^o$	$\sim$20cm brass	1	0.220	0.220
Vienna multiwire telescope [37]	50	100	14	10^9	$\sim 13^o$	$\sim$30cm W	1	0.050 *)	0.050 *)

a) small area detector system b) large area detector system

*) in comparison of this number with the count rates of the other systems it has to be kept in mind that in the Vienna multiwire telescope the background spectrum is measured simultaneously with the target spectrum whereas in all other systems separate background measurements are necessary, thus for comparison of measuring times for experiments the Vienna values should be multiplied by about a factor of two.

**) M = number of measurements necessary for one full energy spectrum.

$Z_1 = \frac{N_{n\,max.}}{R^2} \cdot \frac{F.\Omega}{M} \cdot 10^{-6}$ = count rate for σ = 30 mb, A = 90 target thickness 5 mg/cm^2 and operation at max. admissible neutron source strength

$Z_2 = \frac{N_{n\,max.}}{R^2} \cdot \frac{F.\Omega}{M} \cdot 10^{-6}$ = count rate for same conditions except for assumption that a max. neutron source strength is limited to $N_{n\,max.}$ either by max. admissible value of system to $N_{n\,max.}$ and by source properties to $< 10^9$ n/sr; $N_{max.}$ being the smaller of the two values

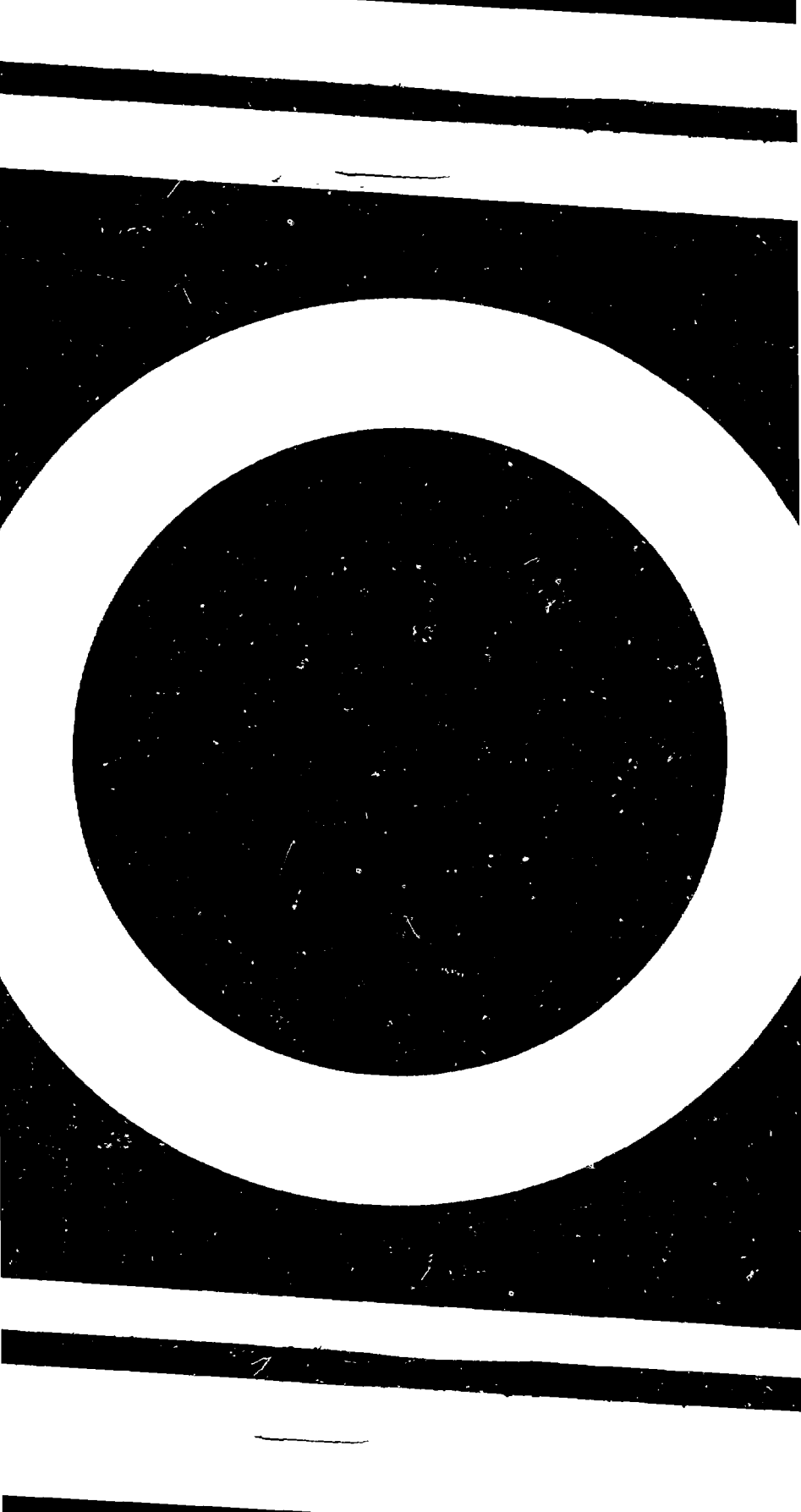

PROGRAMME SCHEDULE

Interregional Advanced Training Course on Applications of Nuclear Theory to Nuclear Data Calculations for Nuclear Reactor Design

ICTP Trieste, 28 January - 22 February 1980

Week 1: 28 January - 1 February 1980

I. Reaction Mechanisms for Fast Neutron-Nuclear Interactions

Invited lectures

- Statistical theory of neutron-nuclear reactions (P.A. Moldauer, Argonne, USA - 5 lectures)
- Recent results in the theoretical description of pre-equilibrium processes (E. Gadioli, Milan, Italy - 2 lectures)
- Developments and applications of multi-step Hauser-Feshbach/pre-equilibrium model theory (C.Y. Fu, Oak Ridge, USA - 5 lectures)

Special Seminars

- Analytical solution of the exiton model master equation (S.K. Gupta, BARC, Bombay, India)
- A unified model of pre-equilibrium decay (J. Rama Rao, Varanasi, India)

Afternoons: Workshops on current problems in the understanding of fast neutron-nuclear reaction mechanisms and on nuclear data calculations with new nuclear model codes

Week 2: 4 - 8 February 1980

II. Nuclear Fission

Invited lectures

- A critical review of some aspects of the theory of fission (H.C. Pauli, Heidelberg, Fed. Rep. of Germany - 5 lectures)
- Theory and phenomenology of neutron-induced fission cross-sections (H. Weigmann, Geel, Belgium - 5 lectures)
- Applications of the nuclear theory to the computation of neutron cross-sections for actinide isotopes (V. Konshin, Minsk, USSR - 5 lectures; in the absence of Dr. Konshin presented by V.S. Ramamurthy, Bhabha Atomic Research Centre, Bombay, India)

Special Seminars

- A semi-empirical nuclear level density formula with the inclusion of shell effects (V.S. Ramamurthy, S.K. Kataria, BARC, Bombay, India)
- Elementary excitations in nuclei (E.O. Civitarese, La Plata, Argentina)

Afternoons: Workshops on current problems in nuclear fission theory and in the parameterization of the double-humped fission barrier for neutron cross section calculations

Week 3: 11 - 15 February 1980

III. Nuclear Data Evaluation and Processing of Nuclear Data
(S. Pearlstein, Brookhaven, USA - 10 lectures)

Special Seminars

- Simple parameterization of optical model reaction cross sections for neutrons and charged particles (S.K. Gupta, BARC, Bombay, India)
- An interactive system for evaluation of nuclear data (M. Collin, Bruyères-le-Chatel, France)

Afternoons: Workshops on formatting, checking, processing and testing of evaluated nuclear data with examples and exercises on the US ENDF/B library

Week 4: 18 - 22 February 1980

IV. 14 MeV Neutron Cross-Sections in Experiment and Theory

Invited lectures

- Experimental techniques and theoretical models for the study of integral 14 MeV neutron cross-sections (J. Csikai, Debrecen, Hungary - 3 lectures)
- Some remarks on experimental techniques for the study of secondary particle spectra and angular distributions emanating from 14 MeV neutron-induced nuclear reactions (D. Seeliger, Dresden, German Democratic Republic - 3 lectures)
- Integral cross-section measurements for investigating the emission of complex particles in 14 MeV neutron-induced nuclear reactions (S.M. Qaim, Juelich, Fed. Rep. of Germany - 2 lectures)
- Experimental methods for investigation of (n,p) and (n,α) spectra and angular distributions (H.K. Vonach, Austria - 2 lectures)

Special Seminar

- Introductory remarks on a planned IAEA Interregional Technical Assistance Project in the field of nuclear data (J.J. Schmidt, IAEA, Vienna, Austria)

Afternoons: Workshops with the task to develop the scientific and technical basis of a planned IAEA Interregional Technical Assistance Project in the field of nuclear data.

FACULTY AND PARTICIPANTS

DIRECTORS

SCHMIDT, J.J.
Nuclear Data Section
International Atomic Energy Agency
P.O. Box 100
A-1400 Vienna
Austria

MEHTA, M.K.
Nuclear Physics Division
Bhabha Atomic Research Centre
Bombay 400 085
India

FONDA, L.
International Centre for
Theoretical Physics
Strada Costiera 11
P.O. Box 586
I-34100 Trieste
Italy

LECTURERS

CSIKAI, J.
Institute of Experimental Physics
Kossuth Lajos University
P.O. Box 105
H-4001 Debrecen
Hungary

GADIOLI, E.
Instituto di Fisica
Universita di Milano
Via Celoria 16
I-20133 Milan
Italy

FU, C.Y.
Engineering Physics Division
Oak Ridge National Laboratory
P.O. Box x
Oak Ridge, Tennessee 37830
U.S.A.

MOLDAUER, P.A.
Applied Physics Division
Argonne National Laboratory
9700 South Cass Avenue
Argonne, Illinois 60439
U.S.A.

PAULI, H.C.
Max-Planck Institut fuer
Kernphysik
Saupfercheckweg 1
D-6900 Heidelberg 1
Fed. Rep. of Germany

PEARLSTEIN, S.
Bldg. 197D
National Nuclear Data Center
Brookhaven National Lab.
Upton, New York 11973
U.S.A.

QAIM, S.M.
Inst. fuer Chemie I
(Nuklearchemie)
Kernforschungsanlage Juelich
GmbH
Postfach 1913
D-5170 Juelich 1
Fed. Rep. of Germany

RAMAMURTHY, V.S.
Nuclear Physics Division
Bhabha Atomic Research Centre
Trombay
Bombay 400 005
India

SEELIGER, D.
Sektion Physik
Technische Universitaet Dresden
Mommsenstrasse 13
DDR-8027 Dresden
German Democratic Republic

VONACH, H.K.
Institut fuer Radium-
forschung und Kernphysik
Boltzmanngasse
A-1090 Vienna
Austria

WEIGMANN, H.
EURATOM-BCMN
Steenweg naar Retie
B-2440 Geel
Belgium

P A R T I C I P A N T S

ABBATE, M.J.
Centro Atomico Bariloche
8400 S.C. de Bariloche
Rio Negro
Argentina

AHAFIA, A.K.
Department of Physics
University of Science and Technology
Kumasi
Ghana

ALLEY, S.R.
KANUPP
P.O. Box 3183
Karachi - 29
Pakistan

AMUSA, A.
Department of Physics
University of Ile-Ife
Ile-Ife
Nigeria

ANWAR, M.
Pakistan Institute of Nuclear Science and Technology
P.O. Nilore
Rawalpindi
Pakistan

ANZALDO-MENESES, A.M.
Kernforschungszentrum
INR
Postfach 3640
D-7500 Karlsruhe 1
Fed. Rep. of Germany

AUGUSTYNIAK, W.
Institute of Nuclear Research
Hoza 69
Warsaw
Poland

AYOUB, N.
Department of Physics
Faculty of Science and Arts
Yarmouk University
Irbid
Jordan

AZHAR, I.A.
Pakistan Institute of Nuclear Science and Technology
P.O. Nilore
Rawalpindi
Pakistan

BAK, H.-I.
Department of Nuclear Engineering
College of Engineering
Seoul National University
Seoul
Korea

BURZYNSKI, S.
Institute of Nuclear Research
00-681 Hoza 69
Warsaw
Poland

CAPLAR, R.
Inst. "Ruder Boskovic"
P.O. Box 1916
Bijenicka cesta 54
YU-41001 Zagreb
Yugoslavia

CHEON, I.-T.
Department of Physics
Yonsei University
Seoul 120-00
Korea

CHO, S.-W.
Korea Atomic Energy Research Institute
P.O. Box 7
Cheong Ryang
Seoul
Korea

CHOUAK, A.
Département de Physique
Faculté de Physique
Rabat
Morocco

CIVITARESE, E.O.
Department of Physics
UNLP
49 y 115, C.C. 67 (1900)
La Plata
Argentina

COLLIN, M.
Commissariat à l'Energie Atomique
Service de Physique Neutronique et Nucléaire
B.P. 561
F-92542 Montrouge Cedex
France

DAVIDOVICH, N.E.
Laboratorio Teorica e Calcolo Reattori
CNEN-CSN Casaccia
S.P. Anguillarese
km 1+300
I-00100 Roma
Italy

DE VILHENA, M.T.
Nuclear Engineering Department
UFRGS
Praca Argentina s/n
900.000 - Porto Alegre - RS
Brazil

DIAS, H.
Divisao de Estudos Avancados
Centro Tecnico Aerospacial
Instituto de Atividades Espaciais
12200 - Sao José dos Campos - SP
Brazil

DUMITRESCU
Central Institute of Physics
Institute of Physics and Nuclear Engineering
Department of Fundamental Physics
P.O. Box 5206
Bucharest
Romania

ELBERN, A.W.
Departamento de Engenharia Nuclear
UFRGS
Praca Argentina s/n
90.000 - Porto Alegre - RS
Brazil

GALLARDO, J.I.L.
UPIICSA-IPN
Apartado Postal 92-054
Mexico 9, D.F.
Mexico

GAZDY, B.
Institute of Physics
Technical University of Budapest
Budafoki ut. 8
H-1521 Budapest
Hungary

GOUMRY, N.
Physics Department
Faculty of Science
Jordan University
Amman
Jordan

GUPTA, R.K.
Physics Department
Panjab University
Chandigarh - 160014
India

GUPTA, S.K.
Nuclear Physics Division
Bhabha Atomic Research Centre
Bombay 400 085
India

HALLAK, A.
Department of Physics
University of Jordan
Amman
Jordan

HAROUNA, O.
University of Niamey
Niamey
Niger

HUSSAIN, F.I.
Department of Physics
Faculty of Science
University of Garyounis
P.O. Box 9480
Benghazi
Libya

IMSALLIM, M.
Department of Physics
Faculty of Science
University of Garyounis
P.O. Box 9480
Benghazi
Libya

JAHN, H.
Kernforschungszentrum
D-75 Karlsruhe 1
Fed. Rep. of Germany

JINDEEL, T.
Institute of Nuclear Research
Iraq Atomic Energy Commission
Baghdad
Iraq

KATARIA, S.K.
Modular Laboratories
Nuclear Physics Division
Bhabha Atomic Research Centre
Bombay
India

KHADKIKAR, S.B.
Physical Research Laboratory
Navrangpura
Ahmedabad - 380009
India

KHALIQUZZAMAN, M.
Atomic Energy Centre
P.O. Box 164
Ramna
Dacca
Bangladesh

KHAN, A.M.
Physics Department
University of Dacca
Dacca - 2
Bangladesh

KHAN, Z.A.
Department of Physics
Aligarh Muslim University
Aligarh 202001
India

KRISTIAK, J.
Institute of Physics
Academy of Sciences
89830 Bratislava
Czechoslovakia

KRISZTINKOVICS, F.
Institute of Physics
Technical University of Budapest
H-1531 Budapest
Hungary

KRIVEC, R.
Institute "Jozef Stefan"
Jamova 39
Ljubljana
Yugoslavia

KUSNO, D.
Department of Physics
FIPIA-UI
University of Indonesia
Salemba 4
Jakarta
Indonesia

Madueme, G.C.
Department of Physics
University of Ife
Ile-Ife
Nigeria

MAHMUD, Y.
Faculty of Science
University of Jordan
Amman
Jordan

MAINO, G.
CNEN
Via Mazzini 2
Bologna
Italy

MAQUEDA, E.E.
Comision Nacional de Energia Atomica
Avda. del Libertador 8250
1429 Buenos Aires
Argentina

MARCINKOWSKI, A.
Institute of Nuclear Research
Hoza 69
00-681 Warsaw
Poland

MEDJADI, D.-E.
Centre des Sciences et de la Technologie Nucléaire
Bd. Frantz Fanon
B.P. 1017
Alger-Gare
Algeria

MEDRANO, G.
INTESCA
Division de Energia
Orense 70
Madrid 27
Spain

MENAPACE, E.
CNEN
Via Mazzini 2
Bologna
Italy

MORSTIN, K.
Institute of Physics and Nuclear Techniques
University of Mining and Metallurgy
ul. Mickiewicza 30
Krakow
Poland

NADJAKOV, E.G.
Laboratory of Nuclear Reactors
Joint Institute for Nuclear Research
141980 Dubna
U.S.S.R.

OLIVEIRA, E.C.
Centro Tecnico Aerospacial
Instituto de Atividades Espaciais
12200 Sao José dos Campos - SP
Brazil

OSMAN, A.M.
Department of Physics
University of Cairo
Cairo
Egypt

OSMERA, B.
Institute of Nuclear Research
250 68 Rez
Czechoslovakia

OUICHAOUI, S.
Centre des Sciences et de la Technologie Nucléaires
B.P. no. 1017
Alger
Algeria

POLJSAK, M.
Institute "Jozef Stefan"
University of Ljubljana
Jamova 39
P.O. Box 199
YU-61001 Ljubljana
Yugoslavia

[illegible]I, H.
Department of Physics
Peking University
Peking
People's Republic of China

RAICS, P.
Institute of Experimental Physics
L. Kossuth University
Bem tér 18/A
P.O. Box 105
Debrecen
Hungary

RAMAMURTHY, V.S.
Nuclear Physics Division
Bhabha Atomic Research Centre
Trombay
Bombay 400 005
India

RAMA RAO, J.
Department of Physics
Banaras Hindu University
Varanasi - 221005
India

RAM RAJ
Physics Department
Kurukshetra University
Kurukshetra - 132 119
India

REICH, S.L.
Comision Nacional de Energia Atomica
Avda. del Libertador 8250
1429 Buenos Aires
Argentina

RIBANSKY, I.
Institute of Physics
Slovak Academy of Sciences
89930 Bratislava
Czechoslovakia

SEHGAL, M.L.
Experimental Nuclear Physics
Physics Department
Aligarh Muslim University
Aligarh
India

SHARMA, S.K.
Department of Physics
Indian Institute of Technology
IIT Post Office
Kanpur 208016, U.P.
India

SIM, K.-S.
Department of Physics
Chung-Ang University
Kwanak-Ku Heugsuk Dong 221
Seoul 151
Korea

STANKIEWICZ, K.
Institute of Nuclear Research
Computing Centre CYFRONET
05-400 Otwock - Swierk
Poland

STRATAN, G.
Institute of Physics and Nuclear Engineering
Department of Fundamental Physics
P.O. Box 5206
Bucharest-Magurele
Romania

STROHMAIER, B.
Institut fuer Radiumforschung
und Kernphysik
Universitaet Wien
Boltzmanngasse 3
A-1090 Vienna
Austria

THAKUR, J.
Department of Physics
Patna University
Patna 800 005
India

UHL, M.
Institut fuer Radiumforschung
und Kernphysik
Universitaet Wien
Boltzmanngasse 3
A-1090 Vienna
Austria

UNGKITCHANUKIT, A.
Department of Physics and
Mathematics
Mahidol University
Rama 6 Road
Bangkok 4
Thailand

VENTURA, A.
CNEN
Via Mazzini 2
Bologna
Italy

WAGHMARE, Y.R.
Physics Department
Indian Institute of Technology
Kanpur - 208016
India

WAGIRAN, H.
Physics Department
University of Technology
Jalan Gurney
Kuala Lumpur
Malaysia

WAHEED, A.
Nuclear Physics Division
PINSTECH
P.O. Nilore
Rawalpindi
Pakistan

YOUNIS, A.M.
Faculty of Science
University of Garyounis
P.O. Box 9480
Benghazi
Libya

YOUSSEF, M.A.
Department of Physics
Faculty of Science
University of Garyounis
P.O. Box 9480
Benghazi
Libya

YOUSSEF, M.I.
Physics Department
Faculty of Science
Mansoura University
Mansoura
Egypt

ZHONG, Y.-S.
Department of Physics
Peking University
Peking
People's Republic of China